Under Contract
DTFR 53-92-C-00003

MAGLEV SYSTEM CONCEPT DEFINITION

FINAL REPORT – VOLUME I
Book 2 of 2

Prepared for

U.S. Department of Transportation
Federal Railroad Administration

September 30, 1992

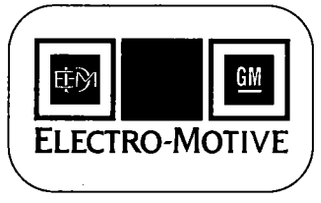

Under Contract
DTFR 53-92-C-00003

MAGLEV SYSTEM CONCEPT DEFINITION

FINAL REPORT – VOLUME I
Book 2 of 2

Prepared for

U.S. Department of Transportation
Federal Railroad Administration

September 30, 1992

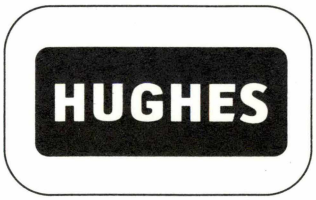

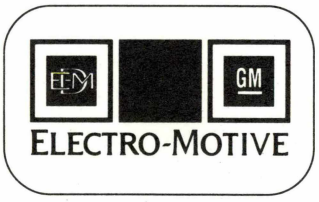

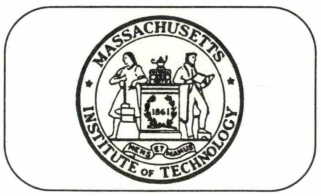

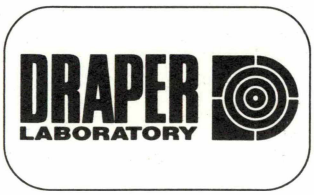

MAGLEV System Concept Definition Report
Final Report

TABLE OF CONTENTS

TABLE OF CONTENTS (Cont'd)

TABLE OF CONTENTS (Cont'd)

TABLE OF CONTENTS (Cont'd)

TABLE OF CONTENTS (Cont'd)

Section C

Page

TABLE OF CONTENTS (Cont'd)

Section C

Page

TABLE OF CONTENTS (Cont'd)

TABLE OF CONTENTS (Cont'd)

TABLE OF CONTENTS (Cont'd)

TABLE OF CONTENTS (Cont'd)

TABLE OF CONTENTS (Cont'd)

TABLE OF CONTENTS (Cont'd)

TABLE OF CONTENTS (Cont'd)

TABLE OF CONTENTS (Cont'd)

TABLE OF CONTENTS (Cont'd)

TABLE OF CONTENTS (Cont'd)

ILLUSTRATIONS

ILLUSTRATIONS (Cont'd)

ILLUSTRATIONS (Cont'd)

ILLUSTRATIONS (Cont'd)

ILLUSTRATIONS (Cont'd)

ILLUSTRATIONS (Cont'd)

ILLUSTRATIONS (Cont'd)

ILLUSTRATIONS (Cont'd)

ILLUSTRATIONS (Cont'd)

ILLUSTRATIONS (Cont'd)

TABLES

APPENDICES

Appendix

C. PARAMETRIC PERFORMANCE REPORT

1. Vehicle

1. VEHICLE

1.1 INTRODUCTION

This section discusses the baseline vehicle design and tradeoffs that were made during concept development. Figure C1-1 is a complete general arrangement drawing of the vehicle. Also included in this section is the Baseline Vehicle Specification Sheet which details all major vehicle parameters that may be useful in discussions relating to the Bechtel concept.

While this part of the report provides a detailed view of the vehicle, some topics have been discussed in other report sections, including:

Superconducting Magnet Design – Part B

Cryogenics System – Part B

Magnetic Fields – Part F

On-Board Control and Communication System – Part C4

Ride Quality – Part C6

Vehicle Reliability and Failure Modes – Part C7

BASELINE VEHICLE SPECIFICATION SHEET

Vehicle Width	4.1 m Cabin Window to Cabin Window 6.032 m Tip of Plane to Tip of Plane	
Vehicle Length	36.129 m	
Vehicle Height	5.080 m	
Vehicle Frontal Area	15.7 m^2	C_d=0.1
Vehicle Skin Area	660 m^2	C_d=0.004
Vehicle Overall Center of Mass	1155 mm Above Top of Guideway	
Vehicle Carbody Center of Mass	1883 mm Above Top of Guideway	
Vehicle Bogie Center of Mass	280 mm Below Top of Guideway	
Overall Vehicle Mass	63,349 kg	
Sprung Fixed Mass	26,686 kg	
Sprung Variable Mass	14,800 kg	
Unsprung Mass	21,628 kg	

First Class Section 16 seats 2+2 seating
- Seat Pitch (965 mm) 38"
- Seat Width 20" (508 mm)
- Aisle Width 36.7" (932 mm)

Coach Class Section — 90 seats 3+3 seating
- Seat Pitch 31" (787 mm)
- Seat Width 18" (460 mm)
- Aisle Width 23.4" (932 mm)

Full ADA Compliance

Monocoque Vehicle Construction

LSM Propulsion System

Electro-Dynamic Suspension Flux Cancelling Design

Top Operational Speed 500 kps
Minimum Operational Speed Levitated 10 kph

Unidirectional Vehicle Option @ Full Speed

Remote Computer Controlled

Number of Bogies Six

Four meter long bogies with one meter inter-spacing connected to carbody by modified watts linkage. Each bogie with four parking brake guidance wheels and four air bearings per bogie. Four internal air tanks 100 PSI maximum pressure.

Two Magnets/Bogie – Octopole Design, Liquid Helium Cooled

Eight 1.5 m^2 Aerodynamic Speed Brakes per Vehicle, 4 Fore/4 Aft, Provides 0.2g Deceleration @ 139 m/s (500 kph)

One 13 m^2 (4.11 m Diameter) Emergency Parachute with Mortar Deployment mechanism, provides 0.2g Deceleration @ 139 m/s (500 kph), 0.8 C_D Chute

Fire Extinguishing System–2 Automatic Halon Spheres (Aircraft Style), 12 Portable Cabin Extinguishers (10 CO_2, 2 Halon)

Three Cabin Attendants per Vehicle

Four Evacuation Slides, One per Door, 12 m (40 ft) Maximum Deployable Height, 55° Angle when Deployed

Four Inter-vehicle Emergency Ramps/Vehicle, One Stored by Each Door

Four Evacuation Tubes, One per Door

Four Levitation Planes/vehicle, 1.0 m^2 Surface Area/Plane
0.9 Hz Reaction Rate

Two Emergency Coupling Areas/Vehicle, 1 Fore, 1 Aft

Full Vehicle Speed Operation to 40 mph Steady State Crosswind, Reduced Vehicle Speed to 60 mph Steady Crosswind, Capable of Withstanding 120 mph Crosswind when Stopped

Hydraulics System
2 Motor Driven Pumps, Output 3000 PSI
2000 PSI System Working Pressure
816 mm Diameter Main Supply Line
114 Liters/min (30 gpm) Total Flow
Three Accumulators

71 Liter (18.7 Gallon) Central
36 Liter (9.4 Gallon) Fore
36 Liter (9.4 Gallon) Aft
65 kW (87 hp) Total Energy Usage by System

Air System
2 Motor Driven Air Compressors, 3 kW Each
100 PSI Maximum Working Pressure
3.5 Normal Cycles Air Tank Capacity
Recharge Empty Tanks in 13 minutes

Water Tank
Two 100L Water Tanks
One 100L Waste Water Tank

On-board Power
440V 3-phase 186 kW 400 Hz Supply
60 Hz 110V Single Phase Available
186 kW Power Output, Derived from Two 93 kW Fuel Cells
Methanol Reforming, Proton Exchange Membrane Style
785L Methanol Capacity, 80°C Operating Temperature
Eight Hours Capacity @ 250 kW Output Rating
Normal Power Load 186 kW
Essential Power Load 42 kW
Emergency Power Load 5 kW

Two 252 ampere-hour Banks Battery, 20 Cells/Bank
230 kg/Bank

HVAC
79 kW Heating Coils
94 kW Air Conditioning
15 CFM Fresh Air/Person

Emergency Control Station Provided with Integral
On-board Controller
Communications to Wayside
2 Radio Transponders operating via Lossycoax
2 Radio Transponders operating via Beacon System
2 Radio Transponders operating via Propulsion Windings
1 Cellular Telephone System
1 Emergency Voice Radio System

Primary Suspension-Magnetic
1.25 g Restoring Force for 1 cm Deflection from Nominal

Tilt Capability
15° Guideway 15° Vehicle Max

Tilting Actuators
Four per Vehicle
Maximum Stroke +481 mm/-427 mm

Peplar Index
1.88 @ 134 m/s

Carbody Aerodynamic Boat Tailing at Rear 22°

Lightning Protection Supplied via Flying Wire System

Cryogenic System – Transient Shield
Operating Temperature 4.2K
Operating Pressure 1.3 Atmospheres
Tank Capacity 8,800 L (2,330 Gallons)

Secondary Suspension
Semi-Active
Two Lateral Actuators per Bogie
Four Vertical Actuators per Bogie

Switch Speed
Up to 200 kph

Bogie Gap
0.05 m Outer Shell of Cryostat to Outer Shell of Guideway
0.10 m Top of Guideway to Bottom of Bogie

Effective Magnet Length
24 m Resulting in 2,639 kg/m
Effective Guideway Length of Magnet Acting
29 m Resulting in 2,184 kg/m

Minimum Radius of Curvature 400 m @ 52 m/s (187 kph)

Inner Passenger Cabin Noise
70 dBA Max @ 500 kph

Four Type A Aircraft Doors per Vehicle

Two Cargo Doors per Vehicle

Two Equipment Access Doors per Bogie

Air Bearings
Zero Speed Levitation Device
Four Per Bogie, Each 21" Diameter
Each Bogie Maximum Air Bearing Lift 303kN (68,000 lbs)

Two Lavatories per Vehicle
One Handicapped Accessible Located in First Class Cabin

Two Galleys per Vehicle

0.5" H_2O Cabin Pressurization

0.2 g Thrust Maximum

Pitch Rate	3°/second	
Yaw Rate	1°/second	
Roll Rate	5°/second	Roll Acceleration 15°/sec^2

1.2 STRUCTURAL DESIGN CONSIDERATIONS

1.2.1 Size Considerations

Overview

Vehicle size is a complex issue, in which a balance must be struck between a long narrow vehicle and a short wide one. Aerodynamics determine external vehicle size and shape while needs of passengers are the major consideration in internal vehicle design. These factors must be constantly weighed when determining optimum vehicle size.

Design Parameters

For the Bechtel Team concept the following factors were considered:

- The system must be capable of carrying 4,000 passengers per hour initially, expandable to 12,000 passengers per hour maximum. (Government requirement)
- The system should be designed to use as many existing rights-of-way as possible.
- The system should allow for efficient loading and unloading of passengers. (Bechtel Team Requirement)
- The system should allow for passenger baggage, both checked and carry-on. (Bechtel Team requirement)
- The system should allow for cargo vehicles or mixed cargo/passenger configurations. (Bechtel Team Requirement)
- The system should provide aircraft like service. (Government recommendation)
- The vehicle should be energy-efficient in design. (Good design practice)
- The vehicle should be easy to manufacture and cost-effective. (Good design practice)

Vehicle Design

The foremost requirement is that the system must be capable of carrying 4,000 passengers per hour initially and expandable to 12,000 passengers per hour. This requirement determines whether or not the final design is a multiple or single vehicle concept. To determine the required vehicle size, information must be obtained on the possible safe headway. The electromagnetic propulsion system only allows one vehicle per zone at full speed. Since maglev zones are typically 4.2 km in size (see linear synchronous motor design section), a vehicle traveling at full speed, 139 m/s (500 kph), would traverse a zone approximately every 30 seconds. Thus, at maximum vehicle speed maximum vehicle capacity is reached with one vehicle passing a fixed point (a particular zone)

every 30 seconds. Therefore, to accommodate 12,000 passengers per hour with 120 vehicle passings per hour, each vehicle must carry at least 100 passengers (12,000 / 120 = 100). One vehicle per block operations requires that the vehicle can operate safely at a 30-second headway. The calculations in the vehicle braking section show that a vehicle can safely stop within 3.3 kilometers using its on-board braking systems coupled with its inherent aerodynamic and electromagnetic drag. This shows that a 100-passenger single vehicle is capable of meeting passenger density requirements. If only 4,000 passengers per hour are required, then there will be only one vehicle per three zones, i.e. there is a 90-second headway. Therefore, the initial control and propulsion system has room for refinement from initial deployment until the system reaches maximum capacity.[1]

Another important consideration was using as many existing rights-of-way as possible in the system design. The General Accounting Office report on rights-of-way specifies three main available rights-of-way which may be used in a final maglev systems alignment: interstate highway, railroad, and utility. The most usable rights-of-way are those around existing interstate highways. The railroad rights-of-way also may make good routes; however, there may be difficulties using these if the track is still operational. Finally, utility rights-of-way can be utilized; however, utility rights-of-way are often narrow and are in less optimum terrain. Since the interstate highway right-of-way is the most likely to be utilized, its characteristics are important in a maglev systems design. Typically, interstate highways use curve radii of a few thousand feet (600-900 meters or less in some areas). For a maglev system to follow these tight turn radii it must also be able to negotiate tight turns at an appreciable speed. Some highways even make turns as tight as 400 meters in urban areas.

Tight turns affect a maglev vehicle's design in different ways depending on its "bogie" support arrangement. A bogie is a railroad term (usually used outside of the United States) referring to the device which holds the wheel and axles and attaches to the rest of the locomotive carbody. The existing JNR MLU-002 maglev system plans on using two magnet bogies, one at each end of the passenger car. This is a concentrated bogie arrangement. It has the advantage of allowing for tighter turns and lower overall cabin fields but sacrifices this for higher fields in the cabin near the bogie. The Transrapid EMS system uses a distributed magnet arrangement, where the magnet bogie is actually more part of the carbody than a separate entity. This arrangement has the advantage of lower distributed magnetic fields for lift and guidance but requires a complex

[1]Footnote to Reader: This discussion is primarily for illustration. Performance calculations of our baseline system on the Hypothetical Route (Severe Segment Test) governs our baseline concept definition.

articulation mechanism to allow the magnets to have lateral movement needed for tight turn negotiation.

Due to the magnetic fields and other electromagnetic concerns (see the sections on the electromagnetic system) the Bechtel Team has centered on a distributed magnet bogie arrangement. This arrangement requires that each bogie be able to move laterally to accommodate tight turn negotiation. This is accomplished by a simple Watts-linkage mechanism described in the bogie and attachment structure sections of this report.

Since a distributed bogie arrangement was selected, a tradeoff had to be made on the length of the vehicle section. With an extremely long but narrow vehicle the end-most bogies must translate through a significant distance in turns as tight as 400 meters. A shorter and wider vehicle has the advantage of using fewer bogies, each requiring less lateral translation; however, its aerodynamic drag and weight per bogie is higher. CAD analysis showed that acceptable lateral translations (under 12 centimeters, or five inches) if the overall distributed bogie length is less than or equal to 30 meters. Therefore, it was desirable to keep the overall vehicle length to approximately 35 meters.

The system should allow for efficient loading and unloading of passengers, a Bechtel Team requirement. This is important since high utilization of vehicles is desirable to minimize capital and overall vehicle maintenance costs. Aircraft are typically loaded and unloaded through one door only where other systems (such as rapid transit systems) usually use multiple doors for more rapid passenger embarkment/disembarkment. The Bechtel Team vehicle integrators felt that four doors per vehicle was a reasonable compromise between vehicle structural strength (since doors lower structural strength) and efficient passenger loading/unloading. Two doors were placed on each side, allowing one side to be used for disembarkment and one side for embarkment. The doors were placed at the one-quarter and three-quarter positions in the cabin, since two lines would form at each exit and thereby speed disembarkment.

Another Bechtel Team requirement is the provision of facilities to accommodate passenger baggage, both checked and carry-on. This is necessary since maglev systems will typically operate in the range of short-haul aircraft, 500-1000 kilometers (300-600 miles), where baggage consists of carry-on bags, some checked baggage, and some other freight such as mail and air freight packages. The two existing maglev systems, Transrapid and JNR, are multiple vehicle configurations where baggage is relegated to separate cars or is treated as carry-on only. The Bechtel Team felt that a U.S. maglev vehicle should provide for both carry-on and checked

baggage in configurations and quantities similar to aircraft. To this end the maglev cabin must have overhead bins and the vehicle should allocate some space for checked baggage. It was felt that capacity for one checked bag per passenger was adequate.

The Bechtel Team also felt that the system should allow for cargo vehicles or mixed cargo/passenger configurations. Since cargo-carrying capacity and the profit that it produces can significantly help to offset system operating costs, a mixed mode vehicle configuration is possible for initial maglev applications. To accommodate this, the maglev vehicle was designed with containerized cargo capability. This capability is normally used for passenger baggage only, but in mixed-use vehicles, where more of the cabin is devoted to cargo rather than passenger seats this capability serves two purposes. The weight of the cargo carried is of more concern than the volume in maglev systems since most cargo is denser than human beings. This was not considered a concern since most cargo carriers are used to keeping track of and balancing weight loads on other vehicle systems.

To facilitate acceptance of maglev as a transportation system it was generally recognized that the maglev system should provide aircraft like service, at a minimum. Aircraft-like was defined by the Bechtel Team as providing both carry-on and checked baggage facilities, lavatories, food and beverage service, and possibly other features such as on-board phones and radio/video capabilities. These capabilities require a cabin arrangement similar to that of modern short-haul passenger aircraft. This was also advantageous since most of the items used in the aircraft cabin are commercially available, and designed for low weight and low power operation.

The vehicle should be energy efficient in design, a consideration that centered around vehicle aerodynamics. Since a single vehicle design was chosen, consideration was made regarding the seating arrangement. High speed trains typically have a 2+2 seating arrangement (often resulting from vehicle width restrictions from the track gauge.) Modern short-haul aircraft typically utilize 2+3 (McDonnell Douglas) or 3+3 seating arrangements (Boeing). Maglev vehicles must tradeoff vehicle cross sectional area for vehicle length. As stated before, due to tight turn negotiation considerations, the overall vehicle length should be about 35 meters or less. It was determined that with 3+3 seating, a 120-passenger vehicle could be designed meeting length criteria. This would allow for some business class passengers (one section of 16 passengers) resulting in a 106-passenger vehicle that is still capable of meeting passenger density requirements. If the Bechtel Team desire for tight turn negotiation was relaxed, then a 2+3 seating arrangement would be re-evaluated for its slight aerodynamic advantage; however, this also results in a vehicle whose center of mass through the cross section is not as easily balanced which may also effect ride quality, and

the parking brake design due to different vehicle overturning criteria. For a detailed discussion of vehicle aerodynamics see the section on wide vs. narrow bodied vehicles and its impact on aerodynamic drag within this report.

The final good design practice considered is that the vehicle should be easy to manufacture and cost effective. The Bechtel Team's vehicle integrators attempted to make the vehicle modular in design which allows for separate component assembly with a final integration step of major components and systems. For example, the inner tilting coach is actually four equal sections which are joined together via bulkheads for structural strength. Considerations such as these will continue to drive the design in the detailed design stage.

Conclusion

The vehicle size design was most heavily driven by the tight turning considerations and passenger service requirements (4,000-12,000 baggage laden passengers per hour transported in aircraft-like conditions). One advantage of the resulting design is that it allows for various cabin arrangements including narrower 2+2 seating if desired (with different passenger service rates). In fact, a vehicle meeting the requirements of the AAR Plate C Railroad Clearance Diagram could also be designed, as shown in Figure C1-2. These capabilities results from the universality and simplicity of the box beam design.

1.2.2 Weight

Abstract

Key to the development of a cost-effective system is minimizing the cost of the guideway and its support systems. By identifying and minimizing the weight of the vehicle, cost-effective guideway and propulsion systems are possible.

Key Requirements

There are no direct requirements in the contract regarding vehicle weight; however, weight has an important impact on guideway civil structure and propulsion system design.

Approach Used

Our goal is a vehicle that weighs less than 2 tonnes per meter because of its cost impact on guideway civil structure and propulsion systems.

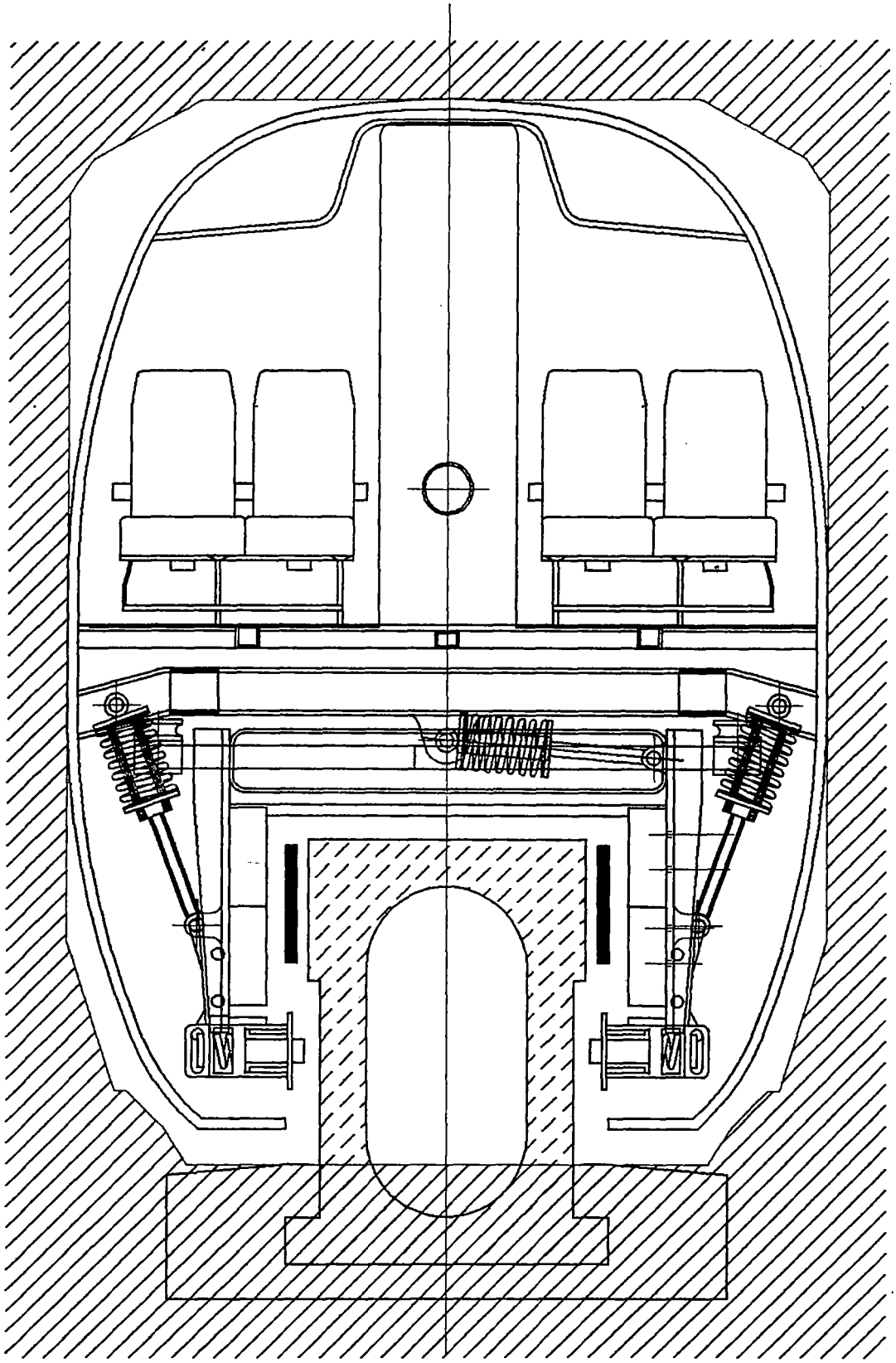

Figure C1-2 Variation on baseline concept vehicle meeting AAR Plate C clearance requirements

Description

Considerable work has been completed to identify the components of the vehicle weight and to develop methods to minimize them. A summary of single vehicle weight is shown in Table C1-1. Figure C1-3 shows vehicle weight broken down by subsystems.

A summary of cargo vehicle weight is shown in Table C1-2. Payload efficiencies of various cargo vehicles are shown in Figure C1-4.

Weight estimates were made by extrapolating weights of existing structures. Where no comparison was possible, components were carefully identified to estimate the weight accurately.Benefits/Risk Summary

With our box-beam guideway structure an extremely cost-effective maglev system can be built provided the weight of the vehicle is minimized. Our vehicle weighs approximately 2 tonnes per meter which allows us to use an inexpensive guideway design.

1.2.3 Basic Body Design

Abstract

The vehicle's main outer structure must have high strength and low weight. Low weight is necessary to achieve high magnetic braking and acceleration. High strength is required to transmit all aerodynamic forces associated with a 139 m/s (500 kph) vehicle to its bogies.

Key Requirements

Critical elements include mass, aerodynamic drag, aerodynamic noise, geometry, and safety as affected by vehicle shell design. The tilt concept will also have a major effect on these elements.

Approach Used

The team has based its design on a monocoque type structure, using high strength aluminum for the skin and structural members. A separate internal tilting coach is used to greatly reduce aerodynamic noise while having minimal impact on mass and overall aerodynamic drag.

Table C1-1
Summary of Single Vehicle Weight

DESCRIPTION	MASS kg (each)	QUANTITY	SINGLE VEHICLE INDIVIDUAL MASS TOTAL	SPRUNG MASS TOTAL	UNSPRUNG MASS TOTAL	AGGREGATE MASS TOTAL
ASSEMBLED VEHICLE TOTAL						63,349
PAINTING	23	1	23	23		23
VEHICLE ASSEMBLY COMPLETE						12,298
BASIC BODY	8,500	1	8,500	8,500		
AERODYNAMIC BRAKES	125	8	1,000	1,000		
HYDRAULICS SYSTEM	770	1	770	770		
AIR SUPPLY SYSTEM FOR AIR BEARINGS	41	1	41	41		
AIR PIPING FOR AIR BEARINGS	2	150	273	273		
CARGO DOORS, BOTH SIDES	50	4	200	200		
EMERGENCY COUPLING AREA	500	1	500	500		
EMERGENCY PARACHUTE	40	1	40	40		
EMERGENCY EVACUATION SLIDES	100	4	400	400		
INSULATION–SPRAY ON	200	1	200	200		
WINDOWS	7	40	272	272		
FIRE EXTINGUISHER SYSTEM						
FIRE EXTINGUISHING AGENT SPHERES	6	6	37	37		
FIRE EXTINGUISHER PIPING	10	1	10	10		
SMOKE AND FIRE DETECTORS	0	4	2	2		
CO2 & HALON PORTABLE EXTINGUISHERS	5	12	54	54		
GUIDANCE CONTROL SURFACE	23	2	45	45		45
LEVITATION CONTROL SURFACE	23	4	91	91		91
ENVIRONMENTAL CONTROL SYSTEM	1,020	1	1,020	1,020		1,020
INNER COACH	4,500	1	4,500	4,500		4,500
SEATS–COACH CLASS	28	30	830	830		2,471
SEATS–BUSINESS CLASS	42	8	340	340		
WINDOWS	2	40	91	91		
GALLEY	136	2	272	272		
GALLEY CART	10	6	60	60		
LAVATORY	136	2	272	272		
WATER SUPPLY TANK	100	2	200	200		
WASTE WATER STORAGE TANK	100	1	100	100		
PASSENGER COMMUNICATIONS & ENTERTAINMENT SYSTEM	1	106	106	106		
LIGHTING	5	44	200	200		
VEHICLE CONTROL SUBYSYSTEM				0		184
COMMUNICATIONS SET	10	1	10	10		
COMPUTER SUITE & MANUAL CONTROL SUBSYSTEM	9	1	9	9		
CONTROL SENSORS	50	1	50	50		
INTERFACE CABLING	115	1	115	115		
SECONDARY SUSPENSION SUBSYSTEM						22,050
LATERAL ACTUATORS & SENSORS	55	6	332	166	166	
VERTICAL ACTUATORS, SENSORS & POWER SUPPLY	8	24	181	90	90	
BOGIE LINKS	218	6	1,306	653	653	
TILTING ACTUATORS & MECHANISM	1,000	1	1,000	1,000		
MAGNET BOGIE SUBSYSTEM	1,205	6	7,230		7,230	
AIR BEARINGS & AIR BLADDERS	76	6	457		457	
SUPERCONDUCTING MAGNET SUBSYSTEM	962	12	11,544		11,544	
MECHANICAL BRAKING SUBSYSTEM						1,176
BRAKING ACTUATOR SUBSYSTEM	23	24	544	544		
BRAKE PADS	5	24	109	109		
WHEELS	22	24	522	522		
CRYROGENIC REFRIGERATION SUBSYSTEM						2,572
HELIUM & STORAGE DEWAR	2,333	1	2,333	2,333		
CRYOGENIC PUMP	1	1	1	1		
COOLANT DISTRIBUTION LINES	7	32	238	238		
FUSELAGE ELECTRICAL POWER SUBSYSTEM				0		2,148
BATTERY	230	1	230	230		
UNINTERUPTABLE POWER SUPPLY	15	2	29	29		
POWER DISTRIBUTION & CONTROL EQUIPMENT	400	1	400	400		
FUEL CELL SYSTEM & 8 HOURS OF FUEL	1,487	1	1,487		1,487	
VARIABLE FACTORS						14,772
PASSENGER LOAD	77	106	8,191	8,191		
PASSENGER SERVICE PERSONNEL LOAD	77	3	232	232		
WATER	1	114	114	114		
FOOD	0.5	106	48	48		
Misc. CONSUMABLES	10	1	10	10		
CARRY ON BAGGAGE	20	106	2,168	2,168		
BAGGAGE CONTAINERS	159	4	636	636		
CHECKED BAGGAGE	32	106	3,373	3,373		
			TOTALS=>	41,721 SPRUNG MASS	21,628 UNSPRUNG MASS	63,349

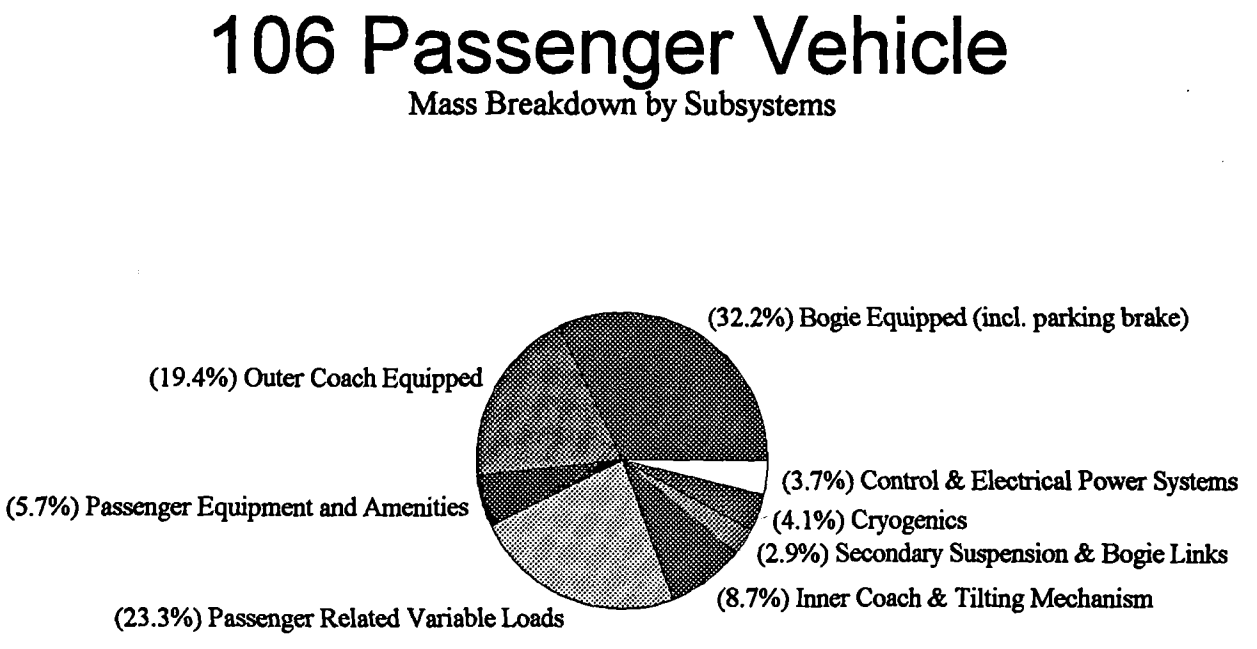

Figure C1-3 Vehicle weight breakdown by subsystem

Table C1-2
Summary of Cargo Vehicle Weight

DESCRIPTION	MASS kg (each)	QUANTITY	EMPTY CARGO VEHICLE INDIVIDUAL MASS TOTAL	SPRUNG MASS TOTAL	UNSPRUNG MASS TOTAL	AGGREGATE MASS TOTAL
ASSEMBLED VEHICLE TOTAL						37,849
PAINTING	23	1	23	23		23
VEHICLE ASSEMBLY COMPLETE						37,826
BASIC BODY	8,500	1	8,500	8,500		
AERODYNAMIC BRAKES	125	8				
HYDRAULICS SYSTEM	770	1	770	770		
AIR SUPPLY SYSTEM FOR AIR BEARINGS	41	1	41	41		41
AIR PIPING FOR AIR BEARINGS	2	150	273	273		273
CARGO DOORS, BOTH SIDES	50	4	200	200		
EMERGENCY COUPLING AREA	500	1	500	500		
EMERGENCY PARACHUTE	40	1	40	40		
EMERGENCY EVACUATION SLIDES	100	4				
INSULATION--SPRAY ON	200	1				
WINDOWS	7	40	272	272		
FIRE EXTINGUISHER SYSTEM						
FIRE EXTINGUISHING AGENT SPHERES	6	6	37	37		
FIRE EXTINGUISHER PIPING	10	1	10	10		
SMOKE AND FIRE DETECTORS	0	4	2	2		
CO2 & HALON PORTABLE EXTINGUISHERS	5	12	54	54		
GUIDANCE CONTROL SURFACE	23	2				
LEVITATION CONTROL SURFACE	23	4				
ENVIRONMENTAL CONTROL SYSTEM	1,020	1				
INNER COACH	4,500	1				0
SEATS--COACH CLASS	28	30				
SEATS--BUSINESS CLASS	42	8				
WINDOWS	2	40				
GALLEY	136	2				
GALLEY CART	10	6				
LAVATORY	136	2				
WATER SUPPLY TANK	100	2				
WASTE WATER STORAGE TANK	100	1				
PASSENGER COMMUNICATIONS & ENTERTAINMENT SYSTEM	1	106				
LIGHTING	5	44				
VEHICLE CONTROL SUBYSYSTEM						184
COMMUNICATIONS SET	10	1	10	10		
COMPUTER SUITE & MANUAL CONTROL SUBSYSTEM	9	1	9	9		
CONTROL SENSORS	50	1	50	50		
INTERFACE CABLING	115	1	115	115		
SECONDARY SUSPENSION SUBSYSTEM						21,050
LATERAL ACTUATORS & SENSORS	55	6	332	166	166	
VERTICAL ACTUATORS, SENSORS & POWER SUPPLY	8	24	181	90	90	
BOGIE LINKS	218	6	1,306	653	653	
TILTING ACTUATORS & MECHANISM	1,000	1				
MAGNET BOGIE SUBSYSTEM	1,205	6	7,230		7,230	
AIR BEARINGS & AIR BLADDERS	76	6	457		457	
SUPERCONDUCTING MAGNET SUBSYSTEM	962	12	11,544		11,544	
MECHANICAL BRAKING SUBSYSTEM						1,176
BRAKING ACTUATOR SUBSYSTEM	23	24	544	544		
BRAKE PADS	5	24	109	109		
WHEELS	22	24	522	522		
CRYROGENIC REFRIGERATION SUBSYSTEM						2,572
HELIUM & STORAGE DEWAR	2,333	1	2,333	2,333		
CRYOGENIC PUMP	1	1	1	1		
COOLANT DISTRIBUTION LINES	7	32	238	238		
FUSELAGE ELECTRICAL POWER SUBSYSTEM				0		2,146
BATTERY	230	1	230	230		
UNINTERUPTABLE POWER SUPPLY	15	2	29	29		
POWER DISTRIBUTION & CONTROL EQUIPMENT	400	1	400	400		
FUEL CELL SYSTEM & 8 HOURS OF FUEL	1,487	1	1,487		1,487	
VARIABLE FACTORS						0
PASSENGER LOAD	77	106				
PASSENGER SERVICE PERSONNEL LOAD	77	3				
WATER	1	114				
FOOD	0.5	106				
Misc. CONSUMABLES	10	1				
CARRY ON BAGGAGE	20	106				
BAGGAGE CONTAINERS	159	4				
CHECKED BAGGAGE	32	106				
			TOTALS=>	16,221 SPRUNG MASS	21,628 UNSPRUNG MASS	37,849

Trend of Payload Efficiencies

For Various Cargo Vehicles Capable of Speeds in Excess of 320 kph (200 mph)

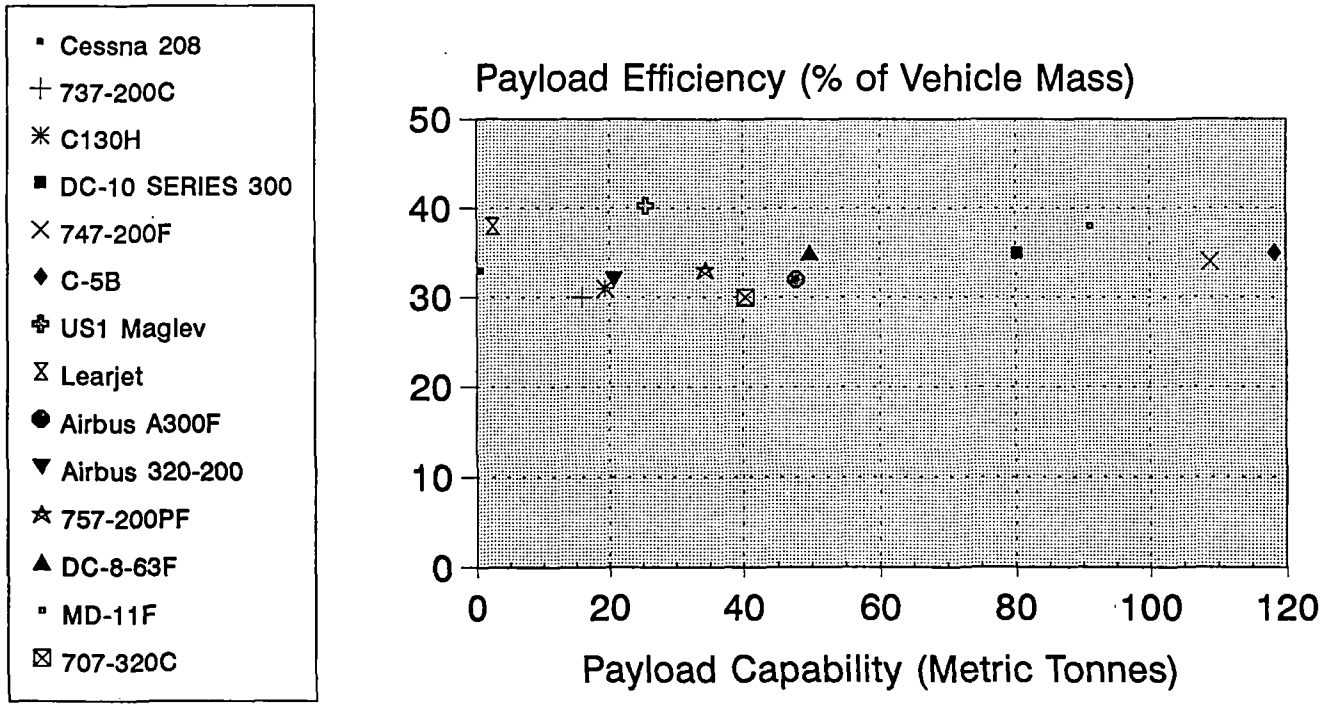

RLP 9/10/92

Figure C1-4 Relative efficiency of cargo vehicle configuration

Description

Three structure types were considered for the vehicle construction with monocoque being clearly superior in meeting the key requirements.

An underframe buff beam design typically used on freight locomotives has a very high weight-to-strength ratio but has low manufacturing costs and is easily adaptable to high strength collision, post type collision protection.

A space frame design typical of passenger locomotives has a relatively high weight-to-strength ratio, is adaptable to high strength collision, fast type collision protection, and is higher cost than an underframe buff beam.

A monocoque design typical of rockets and airplane fuselages utilizes the outer skin as a structural member to carry a major portion of the loads. This type of construction has the lowest weight-to-strength ratio of the three types and is more amenable to energy-absorbing controlled deformation type collision protection. Manufacturing costs are higher for monocoque construction are proven and well understood.

High strength aluminum, the proven choice of the airline industry, will be the basic construction material. We are evaluating high strength composites to replace aluminum where stiffness and strength tradeoffs will allow cost or weight advantages.

Analysis of structural integrity from bending modes, high stress points, panel vibration, and buff loading was calculated with ANSYS Finite Element Modeling Program (see Figure C1-5).

To prevent passenger discomfort from passing vehicles and while entering and exiting tunnels, the vehicle interior will be pressurized to 0.5 psi.

Benefits/Risk Summary

Choosing the monocoque construction for the vehicle structure incorporates known and proven technology to yield a low weight, high strength vehicle which can be manufactured reliably at moderate cost.

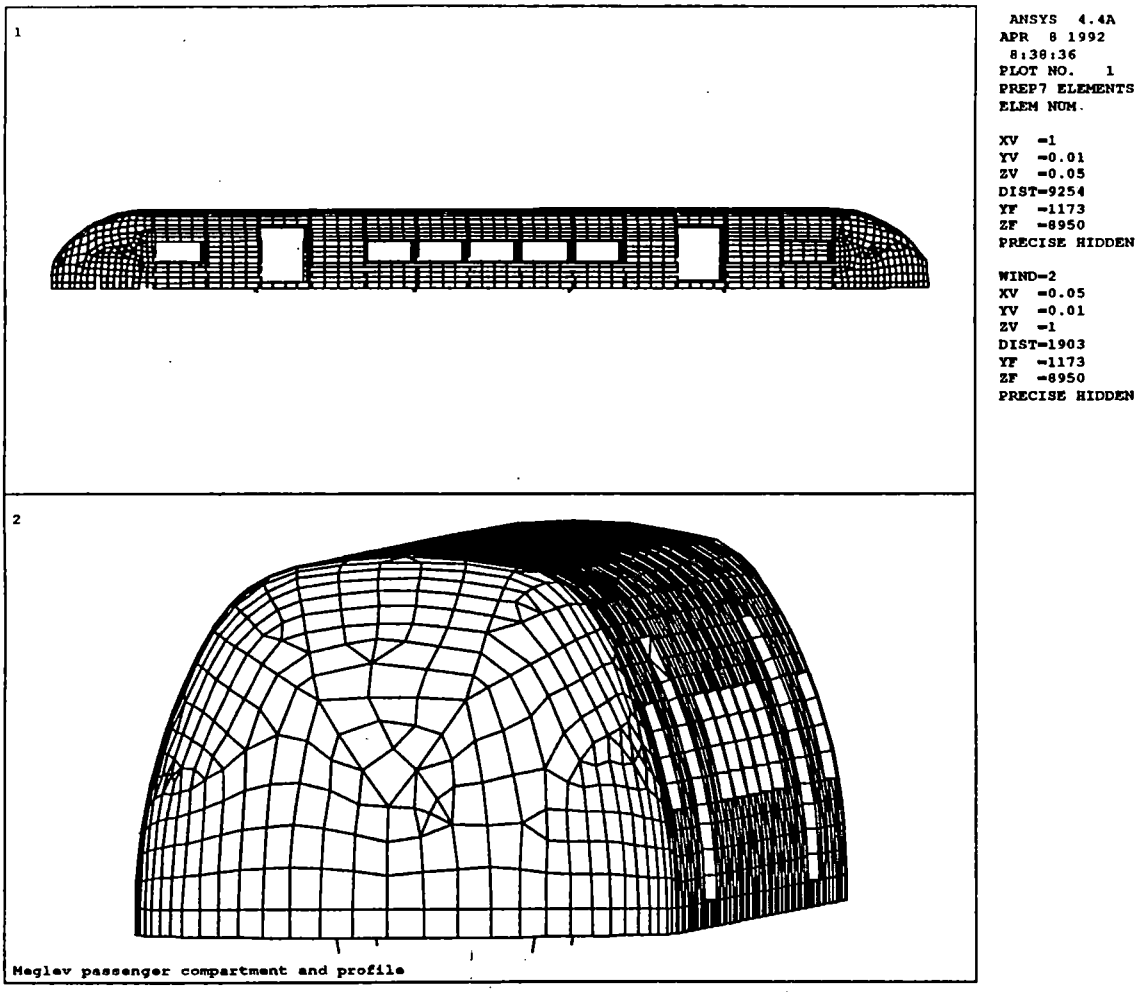

Figure C1-5 Analysis of structural integrity

1.2.4 Crashworthiness

Key Requirements

Although the best crashworthiness protection is to avoid collisions, controlled energy absorption through energy management will drive vehicle design to effective crashworthiness at slow speeds.

The key requirements for crashworthiness need to be defined in a later design phase and should include maximum passenger g loading during an agreed-upon closing speed front-end to rear-end maglev-to-maglev vehicle collision.

Approach Used

The Bechtel Team has chosen a controlled energy absorption, mass shedding concept. Energy management will be the process used to develop and refine the concept.

Description

Crashworthiness may have to be redefined for use with maglev vehicles. Experience with high speed rail has shown that total system design can reduce vehicle-to-large-object collisions to virtually zero. Expanding on high speed rail's lessons by eliminating the operator (and thus operator error) as well as using a magnetic wave propulsion system, which prevents a trailing vehicle from overtaking a lead vehicle, will make maglev inherently safer than high speed rail. The only scenario considered here is low speed front- to-rear, vehicle-to-vehicle collisions.

Locomotives with 5,000 to 10,000 ton trains trailing them have no alternative, but to deflect and/or destroy the object they are hitting. They accomplish this with "snow plows," high strength collision posts, thick high strength steel nose plates and 500,000 g buff capability. In the maglev system, it is not acceptable to destroy the object being hit (another maglev vehicle) nor attempt to deflect it.

Energy management is a concept where the energy involved in a collision is managed on a time and acceleration loading basis from the passenger point of view. In a collision of known velocity and impact angle, a profile of loading on the passenger body with respect to time on a microsecond basis can be generated. An evaluation of loading and duration on various body parts can be completed to determine at what point in the collision fatal injuries may occur. The structure is then modified to reduce the peak acceleration forces or their duration. This is accomplished by adding energy absorbing members in selected spots or shedding mass (as is sometimes done by shearing

engine mounts earlier in the crash to remove its momentum from the carbody). Special structural finite element programs such as DYNA3D and PAM CRASH are seen on super computers to analyze the structure collapse in extremely small time increments (every 10 or 15 ms).

Maglev vehicles, with their well defined crash parameters, are ideal for energy management analysis. After the initial structural design is established, and a maximum impact closing speed goal is agreed upon, collision analysis may begin on super computer. An iterative process of structural changes and analysis of g load and duration on passengers will yield the ultimate design.

The concept can be pushed further by making the system active and intelligent. Upon detecting that a collision is imminent, the involved vehicles may shed their checked baggage at high speed (automotive type air bags to drive baggage containers out loading doors). This will not only lower vehicle mass but will provide valuable additional crush space for energy absorption. Computers will also be able to analyze the vehicle location (lead or trail) and determine which bogies it might want to shed.

The crashworthiness design process will be both lengthy and costly. An agreement between regulators and builders as to the initial closure speed goal for survivability is a must. That decision should be based on likelihood of such a collision, realistic attainability, and cost of attainability.

Assumptions:

1. Maglev vehicles may collide with other maglev vehicles in front-end to rear-end collisions.
2. Mass of both vehicles is essentially equal.
3. Seated passengers wearing seat belts or protected by safety air-bags may experience a 5 g deceleration before sustaining fatal injuries.

Physics:

Physics requires that in the collision of two objects that momentum be conserved. A simplified look at momentum can be made by assuming the mass of both vehicles is equal, the initial velocity of vehicle 2, V_{b1}, is 0, and no momentum is lost through friction.

$$m_1 V_{a1} + m_1 V_{b1} = m_1 V_{a2} + m_1 V_{b2}, \text{ or}$$

$$V_{a1} = V_{a2} + V_{b2}$$

For a perfect elastic collision, the speed of the moving vehicle transmits all its energy to the vehicle at rest. The vehicles therefore exchange velocities.

$$V_{a2} = 0 \ , \ V_{b2} = V_{a1}$$

For a perfect inelastic collision, the vehicles will stick together and have the same post collision velocity.

$$V_{a2} = V_{b3}$$

$$V_{a1} = V_{a2} + V_{b2} = 2\ V_{b2}$$

$$V_{a2} = V_{b2} = 1/2\ V_{a1}$$

From the above discussion it is seen that the instantaneous change in velocity of the moving vehicle is 100 percent for a perfect elastic collision or 50 percent for a perfect inelastic collision. Reality is somewhere in between, but for a worst case scenario we can assume 100 percent change in velocity over a distance equal to the crush space for both vehicles, i.e., the front end of the stationary vehicle does not move and the moving vehicle comes to a total stop in a short distance.

Assuming a constant deceleration rate of -5 g and a crush length of 1 m for each vehicle, we can substitute into the following acceleration, velocity, distance relationship:

$$V_{a2}^2 = V_{a1}^2 + 2ax$$

$$V_{a2} = 0 \ , \ a = -5g = -5 * 9.81\ m/s^2, \quad x = 2\ meters$$

$$0 = V_{a1}^2 + (2 * -5 * 9.81 * 2)$$

$$V_{a1}^2 = 196.2\ m^2/s^2$$

$$V_{a1} = 14\ m/sec = 50\ kph$$

The above analysis shows passengers could reasonably be expected to survive a 50 kph collision provided at least 1 m of crush space is provided at each end of the vehicle and the vehicle structure is carefully designed to absorb this energy in a controlled manner.

Collision of maglev vehicles suggests passengers could reasonably be expected to survive a 50 kph collision if the energy is absorbed at a constant rate and 2 m of crush space are provided.

The energy-absorbing capabilities of proposed vehicles structures and their masses are required before assuring this is a reasonable initial goal.

Small object impacts at full operating speed are not a safety consideration, as the maglev vehicles will have a baggage or equipment compartment between the vehicle front and passenger/crew compartment. Design for small object impact resistance will be based on economics.

Benefits/Risk Summary

The energy absorption concept is the lightest weight collision protection scheme available. It is also "friendly" to both vehicles involved in the collision. This concept has a very low risk associated with it, when combined with our baseline concept objective of collision avoidance.

Reference

1. Crashworthiness and Occupant Protection in Transportation Systems, ASME, AMD-Vol. 106, BED-Vol. 13

1.2.5 Impact of Push/Pull Recovery

Abstract

The basic Bechtel Team design is single vehicle that will require only a minimal ability to couple to a special maintenance vehicle for transport to a maintenance facility or, on extremely rare occasions, to be removed when disabled on the main line.

Key Requirements

The vehicle-to-vehicle attachment or coupler must be very light weight, inconspicuous, able to accommodate vehicle end effects in curves, automatic coupling, and have sufficient strength to accelerate or decelerate a disabled vehicle at speeds up to 4 m/s (15 kph) on air bearings only, and higher speeds when the superconducting magnets are operating properly.

Approach Used

The vehicle front end will have a pop-out plate behind which a catch for towing will be located. An ending coupler attached to a special rescue vehicle will engage the catch and tow the vehicle. The tow vehicle will provide air supply for the air bearings when required.

Description

Retaining a telescoping coupling mechanism in each end of the vehicle is unnecessary, will consume valuable space, and add unnecessary weight. Push recovery by another maglev vehicle is not a viable alternative. The only non-guideway malfunction to inactivate a vehicle on the guideway is loss of vehicle magnets. The disabled vehicle will then have to be moved on its air bearings at a maximum speed of 15 kph. Only a special recovery vehicle can provide the required air.

During a system-wide shutdown or guideway failure, special maintenance vehicles may remove the stranded vehicles at higher speed as the magnets will still provide levitation. The notch in the front of the vehicle will be structurally sound but must be carefully designed so as not to adversely affect crash worthiness of the vehicle. As such, detailed design is deferred until a detailed finite element analysis and energy management analysis are undertaken. This approach allows for the excess weight and complexity to be transferred to the recovery vehicle.

Benefits/Risks

The recovery system is simple and effective with complexity transferred to the recovery vehicle. There will be little or no weight or space impact upon the vehicle.

1.2.6 Center of Mass

Overview

The vehicle's center of mass is of concern for several reasons. First, the center of mass affects the overturning moments produced by the vehicle during banking maneuvers and factors into the vehicle's stability in high cross winds. Civil structural designers also factor the moments produced by the vehicle's center of mass into their calculations on the guideway structure to insure that adequate strength exists. It is desirable for the vehicle to have a center of mass along the length of the vehicle to distribute the weight evenly across all magnet bogies. Vertically, it is desirable to make the vehicle's center of mass as close to the top of the box beam as possible to minimize moments produced in turning/banking maneuvers and from crosswinds.

Analysis Used

Vertical center of mass of the vehicle was of most concern and therefore was analyzed thoroughly during the concept definition stage. Longitudinal center of mass will be studied in more depth during the detailed and final design stages.

To determine the vertical center of mass of the vehicle, a spreadsheet was created detailing each component, its mass, and its height above (positive) or below (negative) the box beam. Each component's effect was weighted by multiplying the mass by its corresponding lever distance. The total effect of all components was summed and divided by the vehicle's overall mass to determine the overall center of mass above the box beam. The center of mass information was also determined for the bogie and the carbody separately as this is useful for suspension/ride quality analysis. The results of the analysis are included in Table C1-3.

Cross Reference

The center of mass information is utilized in sections detailing guideway design and analysis, ride quality analysis, suspension dynamics and design, and guidance wheel/parking brake design.

1.2.7 Inner Tilting Body Design

Abstract

The vehicle's inner structure will tilt 15 degrees to either side of center as needed to maintain ride comfort and will contain all passengers, toilets, and galleys. It will be very light weight and will be isolated from the main outer coach for reduced interior noise and greatly reduced heating requirements.

Key Requirements

The Bechtel team has chosen an ultra-light tilting inner coach which must tilt 15 degrees with respect to the main vehicle, have side windows for passenger viewing, and a floor with sufficient strength to remain securely attached to the main vehicle, and will also allow passenger seats to remain securely attached in the event of a collision that produces a 5 g longitudinal load.

Approach Used

The team has based its design on an aluminum frame floor structure and a composite honeycomb material floor surface and shell.

Description

The Maglev Noise Assessments BAA 191 by Harris-Miller-Miller and Hanson showed severe environmental noise will result at high speed from any irregularities in the vehicle's surface. All externally tilting vehicles will produce noise well in excess of 102 dbA at 25 m as projected for the non-tilting TR07 at 500 kph. The Bechtel internal tilting vehicle will add no external noise. In

Table C1-3
Center of Gravity With Respect to Top of Guideway

Description	Cabin Mass	Cabin Distance	Cabin M*D	Bogie Mass	Bogie Distance	Bogie M*D
ASSEMBLED VEHICLE TOTAL						
PAINTING	23	1,860	42,273			
VEHICLE ASSEMBLY COMPLETE						
BASIC BODY	8,500	1,860	15,810,000			
AERODYNAMIC BRAKES	1,000	2,000	2,000,000			
HYDRAULICS SYSTEM	770	600	462,041			
AIR COMPRESSOR FOR AIR SUSPENSION	41	600	24,490			
AIR PIPING FOR AIR SUSPENSION	273	600	163,636			
CARGO DOORS, BOTH SIDES	200	2,300	460,000			
EMERGENCY COUPLER	500	600	300,000			
EMERGENCY PARACHUTE	40	3,300	132,000			
EMERGENCY EVACUATION SLIDES	400	800	320,000			
INSULATION--SPRAY ON	200	2,300	460,000			
WINDOWS	272	2,300	625,850			
FIRE EXTINGUISHER SYSTEM						
FIRE EXTINGUISHING AGENT SPHERES	37	600	22,155			
FIRE EXTINGUISHER PIPING	10	600	5,742			
SMOKE AND FIRE DETECTORS	2	3,335	6,050			
CO2 & HALON PORTABLE EXTINGUISHERS	54	2,300	125,170			
GUIDANCE CONTROL SURFACE	45	(300)	(13,605)			
LEVITATION CONTROL SURFACE	91	500	45,351			
ENVIRONMENTAL CONTROL SYSTEM	1,020	600	612,000			
INNER COACH	4,500	2,400	10,800,000			
SEATS--COACH CLASS	830	2,300	1,910,045			
SEATS--BUSINESS CLASS	340	2,300	781,164			
WINDOWS	91	2,300	208,617			
GALLEY	272	2,300	625,850			
GALLEY CART	60	2,300	138,000			
LAVATORY	272	2,300	625,850			
WATER SUPPLY TANK	200	600	120,000			
WASTE WATER STORAGE TANK	100	600	60,000			
PASSENGER COMMUNICATIONS & ENTERTAINMENT SYSTEM	106	3,300	349,800			
LIGHTING-Fixtures, controls, & wiring	200	3,300	661,576			
VEHICLE CONTROL SUBYSYSTEM						
COMMUNICATIONS SET	10	2,300	23,469			
COMPUTER SUITE & MANUAL CONTROL SUBSYSTEM	9	2,300	19,558			
CONTROL SENSORS	50	100	5,000			
INTERFACE CABLING	115	600	69,000			
SECONDARY SUSPENSION SUBSYSTEM						
LATERAL ACTUATORS & SENSORS	166	500	82,993	166	500	82,993
VERTICAL ACTUATORS, SENSORS & POWER SUPPLY	90	200	18,095	90	200	18,095
BOGIE LINKS	653	500	326,514	653	500	326,514
TILTING MECHANISM	1,000	600	600,000			
MAGNET BOGIE SUSPENSION SUBSYSTEM				7,230	(400)	(2,891,973)
AIR LEVITATION SYSTEM				457	100	45,714
SUPERCONDUCTING MAGNET SUBSYSTEM				11,544	(250)	(2,886,000)
MECHANICAL BRAKING SUBSYSTEM						
BRAKING ACTUATOR SUBSYSTEM				544	(100)	(54,422)
BRAKE PADS				109	(945)	(102,857)
WHEELS				522	(950)	(496,327)
CRYROGENIC REFRIGERATION SUBSYSTEM						
HELIUM & STORAGE DEWAR	2,333	2,000	4,666,667			
CRYOGENIC PUMP	1	600	600			
COOLANT DISTRIBUTION LINES	238	600	142,839			
FUSELAGE ELECTRICAL POWER SUBSYSTEM						
BATTERY	230	600	138,000			
UNINTERUPTABLE POWER SUPPLY	29	600	17,415			
POWER DISTRIBUTION & CONTROL EQUIPMENT	400	600	240,000			
FUEL CELL SYSTEM & 8 HOURS FUEL	1,487	621	923,427			
VARIABLE FACTORS						
PASSENGER LOAD	8,191	2,300	18,839,091			
PASSENGER SERVICE PERSONNEL LOAD	232	2,500	579,545			
WATER	114	2,300	262,200			
FOOD	48	2,300	110,818			
Misc. CONSUMABLES	10	2,300	23,000			
CARRY ON BAGGAGE	2,168	3,100	6,721,364			
BAGGAGE CONTAINERS	636	1,860	1,183,636			
CHECKED BAGGAGE	3,373	1,860	6,273,273			
	42,033		79,150,560	21,316		(5,958,262)
	Cg=	1,883 milimeters		Cg=	-280 milimeters	

Overall Mass= 63,349 kg
Overall Cg= 1,155 mm

addition, cabin interior noise will be greatly reduced as the vast majority of noise is aerodynamically induced into the outer skin and structurally borne to the vehicle interior. The tilt feature allows the passenger cabin to be isolated from the outer structure, breaking the structural path and reducing passenger cabin noise levels by a minimum of 5 dB.

By tilting passengers with an internal coach, the tilting mechanism can be separated from the secondary suspension, greatly reducing complexity of both.

The tilting coach will have ball bearing supports along the pivot centerline at each end of the coach. The bearings will be attached to the outer shell structure with a spiderweb support. Underneath the floor, the structure will be supported on rollers with rotation controlled by spur gears. Tilting force will be supplied through a series of hydraulic actuators on each side of the vehicle.

Benefits/Risk Summary

An internally tilting vehicle will result in higher reliability in both tilt and secondary mechanisms by reducing complexity. Reduced exterior and interior noise is a plus, as well as less power required for heating.

1.2.8 Minimum Bank Angle and Turn Radius

Overview

Banking refers to inclining the guideway beam and/or the maglev vehicle with respect to horizontal so that the maglev vehicle will be able to travel at high speed around a curve with less discomfort for the passengers. Banking essentially changes the direction at which the passenger is pushed from the lateral direction (toward the outside of the curve) to the vertical direction (downward into the seat). Passengers do not notice the downward motion nearly as much as the lateral motion. Careful consideration has been given to the amount of banking done to the guideway beam and vehicle.

Turn radius is a measure of the severity of a curve as the guideway winds its way along the route. Direction changes (according to points of the compass) are accomplished via horizontal curves, as opposed to vertical curves in which the guideway changes its slope to follow the up and down path through hills. The turn radius is measured in meters. The smaller the turn radius, the more severe the curve, and the more the maglev vehicle must slow down to prevent unacceptable accelerations. There is a penalty for making the turn radii too large as well, because a guideway that has

generously large turn radii will not follow interstate rights-of-way very well. A good compromise on minimum turn radius for a maglev system will balance these factors against one another.

Bank angle and curve radius are interdependent design parameters and therefore are discussed in the same section. This section discusses these various factors and sources of information which were used in making decisions about banking and turn radii.

Key Requirements

High passenger comfort level, minimum land use, and low guideway cost are the three primary requirements driving banking/turn radius decisions. Jostling of freight is a consideration as well, but is automatically included when passenger comfort requirements are met since the latter requirements are more stringent. The vehicle design is affected by minimum curve radius, because it is easier to design a vehicle that only travels on a nearly straight guideway than it is to design a vehicle that must travel on both straight guideways and guideways that have tight turns, and thus sort of bend around the curves.

Approach Used

Bank angle was determined primarily by the sideward forces on the guideway structure required in order to guide the vehicle's weight around the curves. The primary civil engineer on the Team made the decision to limit this sideward force to about 0.4 g, resulting in a maximum bank angle for the beam with respect to its supporting structure of 15 degrees.

Minimum curve radius can be determined from an equation relating curve radius to permissible vehicle speed; however, any firm decision about a minimum curve radius specification must be related to the actual proposed route and cannot be specified generically.

Discussion

The Bechtel Team balanced a number of competing factors before specifying bank angle and turn radius. Passenger comfort was given highest priority, since uncomfortable maglev trips would obviously doom the system to passenger rejection and subsequent failure of the system. The easiest and most important measures of comfort were the average steady passenger accelerations, both vertically, laterally, and longitudinally. These determine bank angle and minimum curve radius and also give direct and strong guidance to the designers. These accelerations are expressed universally in g's, with 1.0 g being equivalent to the pull of the earth's gravity at sea level.

We looked at TransRapid and JNR maglev practice first, and obtained data for various conditions of airliner operation, automobile operation, and high speed passenger train operation. It immediately became apparent that seated passengers could be subjected to greater g forces than passengers standing or walking in the aisle of the cabin, and therefore the team needed to specify g force limits for both seated passengers (assumed belted) and standing passengers. In addition, we felt that passengers would be accepting of greater g forces during emergency situations, depending of course on the severity of the emergency. We were sure that none of them would object to a very quick stop in order to avoid, for instance, a fallen guideway span due to an earthquake, so the Team also specified emergency braking g force limits that seemed practical to achieve.

The Team agreed on a set of g force limits in order to proceed with further aspects of the concept definition, and we were notified February 19, 1992, of ride comfort system requirements established for the SCD contractors. These new criteria, established by the NMI technical staff, did not differ greatly from the limits that the Team had already established for itself. Table C1-4 shows the limits originally set by the Bechtel Team as well as the new criteria which the team quickly agreed to abide by. Although the manner in which the two sets of data are specified is different, the most important specifications compare rather closely.

Banking: The RFP submitted by the Bechtel Team indicated that the banking would be accomplished by a combination of guideway beam tilt and vehicle tilt. We decided early to limit the total bank angle to 30 degrees, since more bank than that would make the required lateral guideway strength unreasonable. It was decided to have at least as much vehicle tilt as guideway tilt, since it would be necessary to right the passenger cabin if it should have to stop on a tilted beam. There are severe impacts of allocating higher tilt to the guideway beam, and that impact is that the beam's supporting structure in a fully banked curve must have additional strength (and hence cost) in order to resist the additional sideward forces on the structure. The more the beam is tilted, the greater is the required lateral strength (and cost) of the structure. Since it was expected that perhaps 40 percent of a maglev route would be curved and hence banked, and since the cost impact on the guideway was expected to be greater that the impact on the vehicle, the Team decided to allow 15 degrees maximum beam tilt and 15 degrees on the vehicle. This would also result in a zero cant deficiency when stopped on a curved beam.

Curve radius: It was determined early in the SCD that our vehicle would have distributed bogies that would be required to move laterally with respect to the vehicle cabin. This lateral motion capability would be provided in order to accomodate curves. The most severe curves were expected to be in maintenance yards where the vehicle would be moving very slowly, but

nevertheless increased lateral clearance would have to be provided by the bogie in order to allow the vehicle to negotiate such curves.

Table C1-4
Comparison of Bechtel and DOT Guidelines

Bechtel Team Early Specifications:

	Standing*	Seated	Emergency
Lateral force, g	.10	.10	--
Vertical force, g			
Upward	.05	.05	--
Downward	.20	.20	
Longitudinal force, g	.15	.25	0.80**
Total bank angle, degrees	.25		
Maximum pitch rate, deg/s	1	_	_
Maximum yaw rate, deg/s	1	_	_
Maximum roll rate, deg/s	2	_	_

* handgrabs on seatbacks to be installed for standing/walking passengers
**assuming airfoil braking to prevent overstressing the guideway

DOT Guidelines (issued Feburary 19, 1992):

	Design	Minimum Requirement	Seated and Belted
Lateral Curves			
Bank Angle, degrees	24	30	45
Roll Rate, deg/s	5		10
Lateral force, g	.10	.16	.20
Vertical Curves			
Upward force, g	.05	.10	.10
Downward force, g	.20	.30	.40
Longitudinal force, g	.16	.20	.60
Vector Combinations			
Lateral & Longitudinal force, g	.20	.30	.60
Lateral & Vertical force, g	.20	.30	.40
Total	.24	.36	.60

The specification for minimum curve radius on the main sections of any maglev route was driven by several competing factors. Given the g force limits agreed upon previously, smaller curve radii would have the following two predictable effects. It would result in longer trip time; the vehicle would have to slow down to lower speeds in the curve in order to stay within the g force limits. It

would also result in less land used outside a highway right-of-way; the smaller curve radii would be able to follow better along an existing highway (or railroad or power line) that was to be used for the maglev route.

Longer trip time is undesirable and less land use is desirable, so a tradeoff was required. In addition to the two effects listed above, passenger comfort could be a factor if the vehicle were to be accelerated and decelerated so often as to be a nuisance. On one early computer simulation of a maglev trip performed by the Bechtel Team, it was observed that with many curve radii less than 1,000 m (with one curve as low as 400 m) the vehicle was usually going up or down in speed at 0.25 g in between the curve sections. This amounted to more than 80 percent of the total trip time. An alternative that we considered was to speed up and slow down at only 0.05 g between curves on the main line, even at the cost of even longer trip times. In light of the effect on trip time, we reconsidered and agreed upon a 0.20 g normal acceleration/deceleration limit.

For a banked curve in which the guideway beam is already at its maximum tilt, the curve radius is a function of allowable lateral g force according to the following formula, which is derived in Appendix I.

$$R = \frac{0.0772v^2\cos(\theta)}{a + g\sin(\theta)}$$

where R=curve radius, meters
v=maximum vehicle speed required in the curve, km/hour
θ=total bank angle (beam + vehicle tilt), ($\theta = 25°$ used here)
a=lateral passenger acceleration allowed in m/s^2, ($a = 1.96\ m/s^2$ used here)
g=gravitational constant=$9.8\ m/s^2$

The two undefined quantities in the equation are curve radius and vehicle speed. Specifying either one determines the other. Table C1-5 shows how the vehicle must slow down as curve radius becomes smaller (i.e., the curve becomes more severe).

Table C1-5
Maximum Allowed Vehicle Speed Curve Radius
(using Bechtel Team's bank angle and g force limits)

Radius, meters	Vehicle speed, km/hour
2862	500
2000	418
1402	350
1000	295
800	264
600	229
400	187

It is apparent from the table that in order to prevent maglev vehicle slowdowns due to curves in the route, and to keep the average vehicle speed up in the 400 km/h range, it will be necessary to have curves with radii that are generally over 1,400 meters. This will not fit extremely well with existing rights-of-way. There are many curves with radio under 1,400 meters on a typical highway. Even though the maglev guideway might meander back and forth across a highway in order to mitigate the curve radius problem, some of the curves in the highway will result in a guideway that strays a significant distance from the highway right-of-way should the 1,400 m minimum radius specification be used.

A tradeoff must be made balancing trip time against land usage. This is not a technical tradeoff but instead is a judgment to be made on the basis of land acquisition costs and political reality, both of which depend so heavily upon the actual route between the cities to be serviced that an upfront specification of minimum curve radius cannot be made in this report. The important conclusion to remember is: following existing rights-of-way will require sharper turns and therefore will slow the maglev system down.

Benefits/Risk Summary

The benefit of using a small bank angle for the beam, in conjunction with a large bank angle for the vehicle with respect to the beam, is reduced guideway cost. This approach also results in a vehicle that can completely cancel beam tilt should it ever have to stop in a curve.

Faster trips result from using curves of large radius, but routes closely following a highway right-of-way result from using curves of small radius. No minimum curve radius has been specified.

Derivation of equation for curve radius vs speed

If the guideway and vehicle total tilt add up to θ degrees, then we have the following diagram.

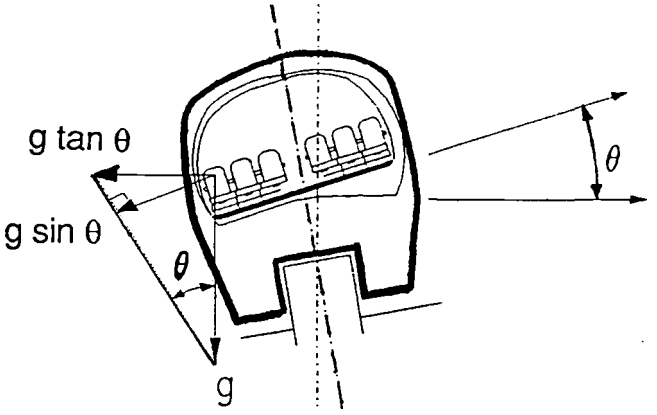

Also, during curving we will allow the passenger to feel some lateral acceleration of an amount "a" due to excess centrifugal forces as shown below.

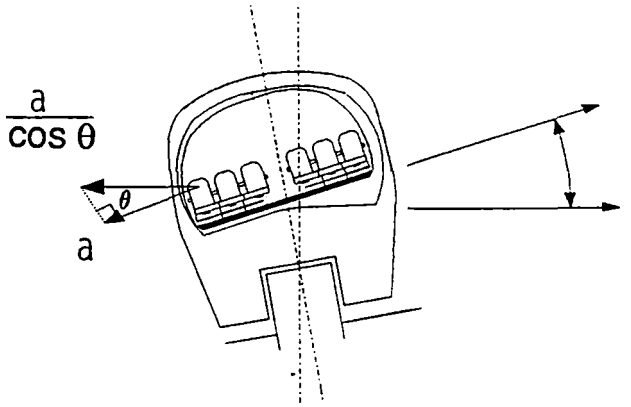

The total horizontal acceleration of the passenger due to curving is known to be v^2/R where v is the vehicle forward velocity (m/s) and R is the curve radius (meters). The total centrifugal force overcomes the tilt force and then some, by the amount $m_p a$ where m_p is the mass of the passenger and a is, as described before, the allowed lateral passenger acceleration. Equating the horizontal acceleration components only we get the following equation:

$$\frac{v^2}{R} = g \tan\theta + \frac{a}{\cos\theta}$$

which is equivalent to the diagram below.

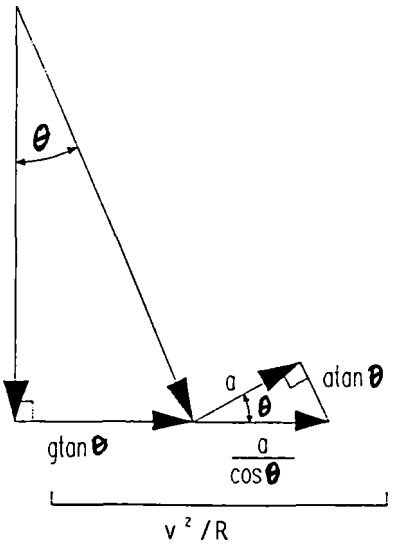

The diagram shows

$$Y = \frac{v^2}{R} = \text{centripetal acceleration}$$

$$= \text{total horizontal vector sum}$$

$$\frac{v^2}{R} = g \tan\theta + \frac{a}{\cos\theta}$$

$$\frac{v^2}{R} = \frac{g \tan\theta \cos\theta + a}{\cos\theta}$$

$$\frac{v^2}{R} = \frac{g \sin\theta + a}{\cos\theta}$$

$$v^2 = \cos\theta = R(a + g \sin\theta)$$

$$R = \frac{v^2 \cos(\theta)}{a + g \sin(\theta)}$$

These formulae apply if R is in meters, v is in meters per second, and a and g are in meters per second squared. When specifying v in kilometers per hour, we must multiply by the square of 138.88 m/s for each 500 km/hour, that is, 0.27776 squared or 0.0772 and finally we have

$$R = \frac{0.0772 v^2 \cos(\theta)}{a + g \sin(\theta)}$$

1.3 SECONDARY SUSPENSION ARRANGEMENT

1.3.1 Bogie Structures

Abstract

The bogie frame in the maglev vehicle design provides the structural connection between the magnetic propulsion and levitation systems and the vehicle carbody (structure). The bogie frame houses the magnet modules, supports the vehicle weight, and transmits forces between the guideway and vehicle. As such, the bogie frame is an important structural member of the maglev vehicle.

This section describes the physical aspects of the bogie structure, the functional requirements of the frame and its components, and results of preliminary stress analysis for the bogie.

Key Requirements

In response to the RFP, the baseline maglev vehicle is characterized by having a distributed magnet module design. These distributed modules are incorporated in six bogie frame assemblies, each four meters long. The bogie frame also provides the connection locations for the secondary suspension elements of the vehicle. The bogie structure is therefore designed for the expected static and dynamic loads encountered during vehicle operation.

Design Description

The baseline bogie structure is comprised of four structural air tanks attached to four sets of pedestal supports and a bottom sheet. A pivot box assembly interconnects the two middle air tanks while diagonal gussets connect the outer air tanks. Carbody link assemblies will provide the attachment to the vehicle structure. Figure C1-6 shows an isometric representation of the bogie structure. The bogie structure is made of high strength structural aluminum. Although the choice of an aluminum structure for the bogie is new to this application, it has been successfully proven in the aerospace industry as a high strength, low weight material.

The design of the bogie is very efficient and lightweight because the structural components are synergistic, i.e., they combine various functions. The physical features and functions of the bogie structure and its components are listed below.

- The superconducting magnet modules (SCM) are fastened to the pedestal supports with two pairs of 1-inch bolts. With this configuration, the cryostatic outer aluminum shell of the SCM not only provides the proper vacuum for the magnets but also resists longitudinal

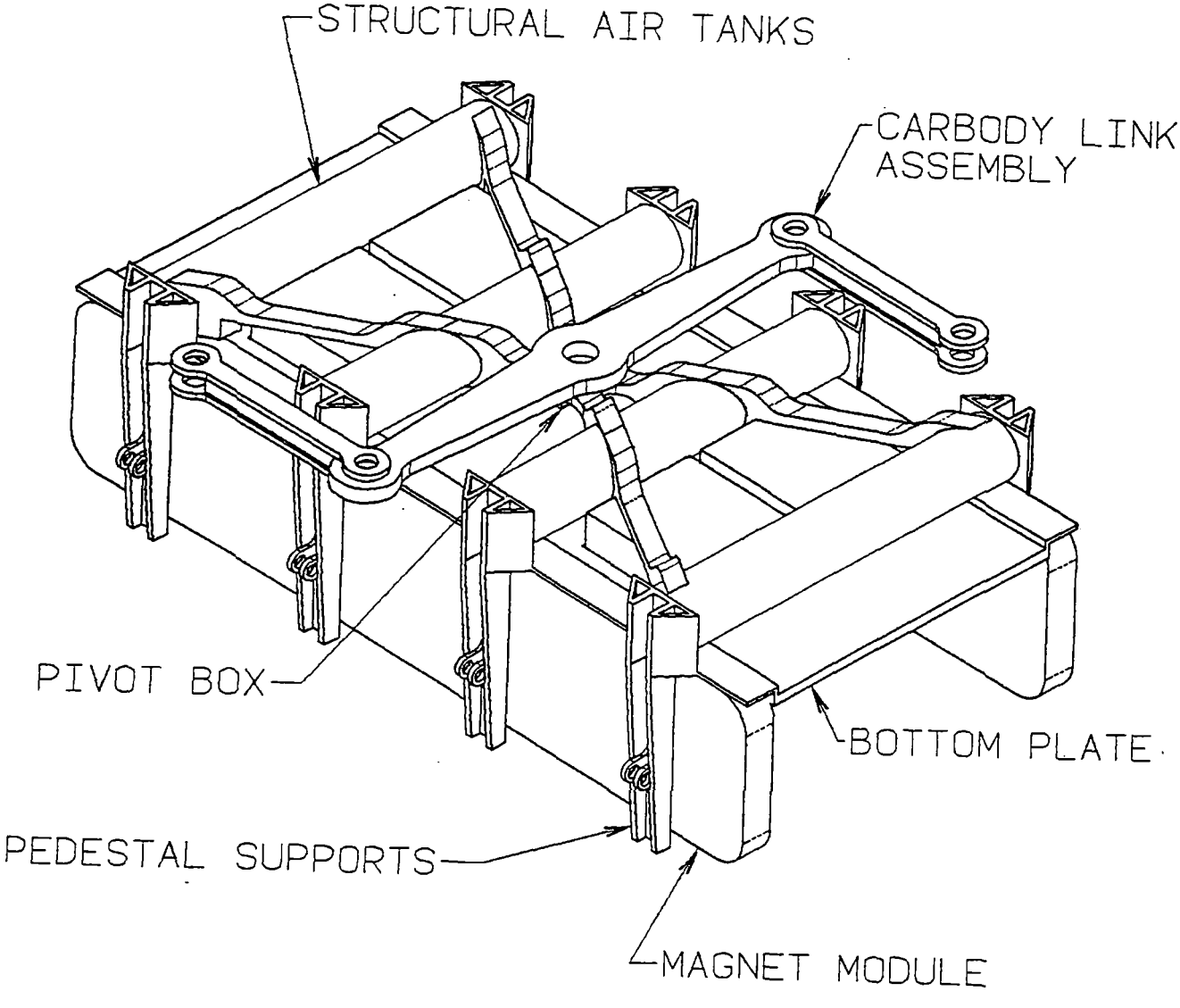

Figure C1-6 Bogie structure

deformations. Along with the pedestal supports, the SCM module provides the longitudinal stiffness for the propulsion and braking loads. The pedestal supports, with channel section thickness of 30 mm, provide the structure for the lateral loads from the guideway and the vertical loads from the suspension.

- The air tanks are mounted laterally and serve a dual purpose. They are pressurized at 100 psi in order to provide for the air bearings and are utilized as structural elements. They are elliptical in shape with the average of the major and minor diameters being about 280 mm, and an approximate wall thickness of 16 mm. The longitudinal carbody loads are transmitted via the carbody links, through the pivot box and distributed through the air tanks.
- Carbody link assemblies, arranged as a straight-line mechanism, has the center link pin connected to the pivot box assembly and the outer link arms are similarly attached to the carbody. The links, also made of high strength structural aluminum, transmit longitudinal forces between the bogie and carbody while also providing for the required lateral translation during curve negotiation.
- The bottom sheet of the bogie structure adds rigidity to the frame and provides a base of assembly for the pedestal supports, pivot box assembly, and the air tank structures. The air bearings are also housed in the bottom sheet section. This bottom sheet, approximately 50 mm in thickness, also provides a cover to the outside, allowing the air to flow over a smoother surface and improving the aerodynamics of the vehicle.

Previous versions of the bogie structure included a box-like structure but were considered overweight, structurally inefficient, and difficult for bogie component assembly.

Additional structure would be necessary to mount the air bearings and the pressurized air tanks, increasing weight and the overall height of the vehicle. With the current baseline concept, there is a 50 percent reduction in bogie structure weight and an overall reduction in vehicle height.

Analysis

In an effort to determine the feasibility of the bogie structure, stress calculations were done under various loading situations. These are preliminary stress calculations based on yield loading criteria. Fatigue loading and detailed stress analysis will be considered in the next stage of this project utilizing predicted bogie acceleration data obtained in the NUCARS modeling described in Section 1.3.3. The following loads were considered separately and in combination for structural design of the bogie.

- Vertical loads imposed on the pedestal supports due to carbody weight and suspension forces.
- Lateral loads imposed on the pivot box, air tanks, and pedestal supports during dynamic conditions such as guideway inputs, wind loads, and curve negotiation.

- Longitudinal loads at pedestal supports, pivot box, and air tanks resulting from propulsion and braking forces.

It should be reiterated that the loads analyzed here are not operational loads found in normal service but rather extreme occurrences where yielding criteria is examined. The application of the loads are shown schematically in Figure C1-7.

Results indicate that for almost all load combinations, the stresses were below 100 MPa in the bogie structure. The pedestal support area had some of the higher stresses due to vertical and lateral load combinations and mechanical brake application. Calculated stress levels were considered well below the yield strength of most high strength structural aluminum alloys. The following is a list of the maximum stresses calculated in various areas of the bogie structure.

- Pedestal supports – 250 MPa (bending stress due to vertical & lateral loading); 180 MPa (bending stress due to parking brake, curve, and wind load)
- Air Tank – 90 MPa (bending stress due to combination vertical & longitudinal loading)
- Pivot Box – 80 MPa (tension load due to combination vertical & longitudinal loading)

These preliminary results above are considered conservative and indicate that the bogie design concept is feasible.

Future Development

The next phase of concept development would entail a significant design effort in the structural refinement of the bogie. Design tools such as CAD solid modeling, finite element analysis, and NUCARS will aid in this development process. Future development for the bogie structure is planned for in the following areas:

- Utilization of NUCARS to determine bogie accelerations due to guideway inputs and steady-state curving. This activity will further define the design fatigue criteria for the bogie structure.
- FEA/FEM analysis will be used in conjunction with solids modeling to not only locate undesirable stress levels but also to optimize the bogie structure and components.
- Proceed with a design phase where bogie components are detailed and manufacturing processes (ie., castings, extrusions) are examined more thoroughly.

Layouts and detail prototype drawings of the bogie structure and its related components would be completed during this design phase. These drawings would then be the basis for prototype building and structural testing of a bogie model.

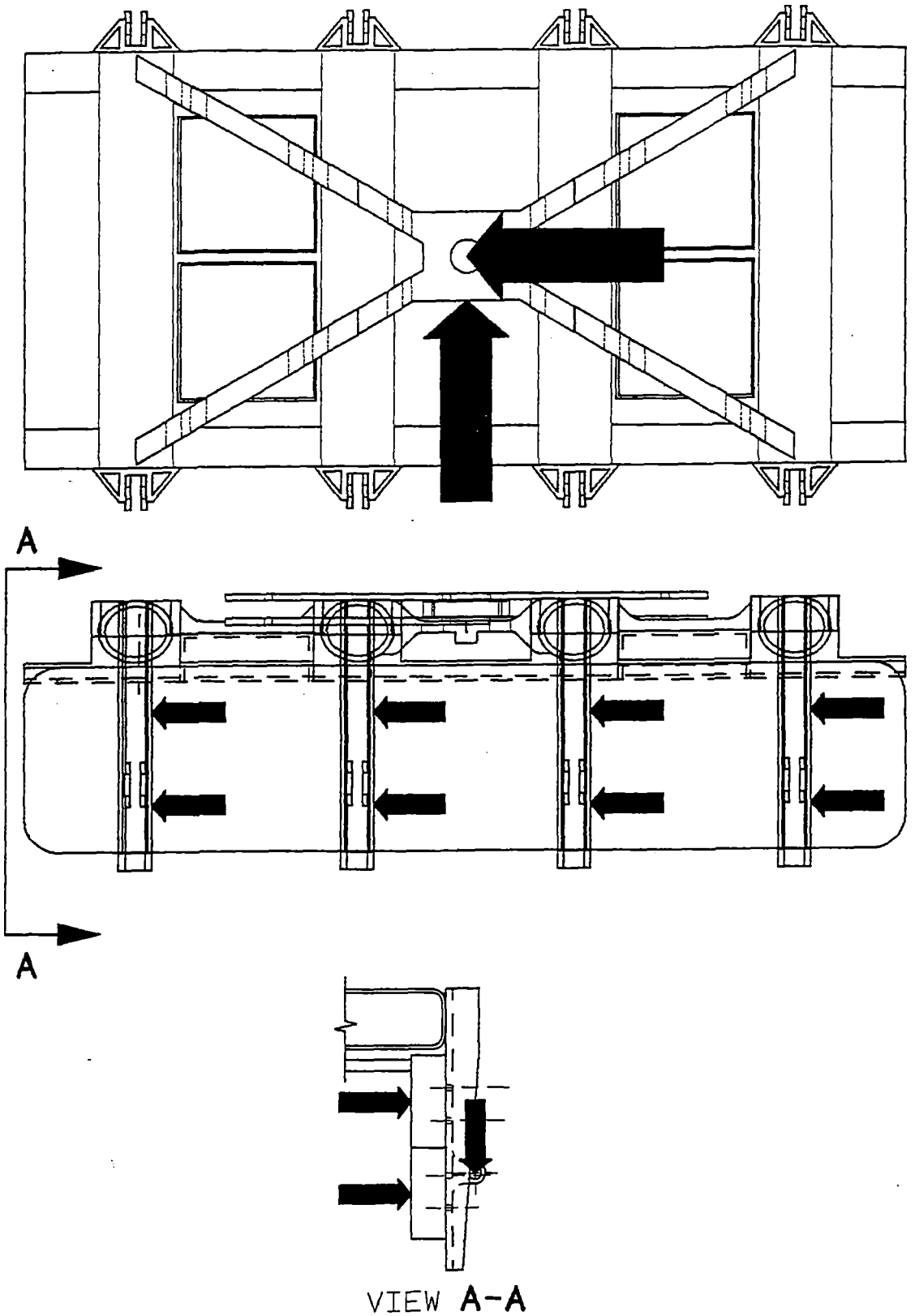

Figure C1-7 Bogie loading

1.3.2 Secondary Suspension Actuators

Abstract

A secondary suspension connects the bogie structure with the vehicle carbody and performs system interface functions between the magnet structure and the structure that houses the passenger compartment. As such, its main system requirements are the following:

- Isolate the carbody from random and harmonic inputs from the guideway during vehicle operation.
- Adequately perform the kinematic functions necessary to guide the vehicle through curves and switches in the guideway.

This section describes the manner in which these requirements have been incorporated into maglev vehicle design.

Key Requirements

In response to the RFP, the secondary suspension system is incorporated into the distributed bogie/magnet module design. The baseline vehicle suspension system, a major component in the control of vehicle dynamics, provides acceptable ride quality and stability for the vehicle. The secondary suspension is located between the bogie frame, which houses the magnet modules, and the carbody structure of the passenger compartment. An active suspension is combined with traditional stiffness elements ensure accurate dynamic control of the vehicle.

Design Overview

This section discusses the approach to defining the secondary suspension system for the maglev vehicle. As stated in the Key Requirements, an active suspension was selected as the baseline system for the vehicle. This decision is based on the following factors:

- The active suspension allows better isolation of dynamic inputs due to guideway/propulsion windings misalignment compared to traditional spring/damper systems. A greater allowable misalignment translates into lower structure costs for the guideway. The ride quality advantages of an active suspension are evaluated in Section C6.
- In case of a complete SCM failure, the active suspension is able to control the random bogie motions and instabilities, keeping the bogie from contacting the guideway during operation.

With only traditional stiffness and damping elements, the suspension system becomes idealized for a narrow range of frequencies and amplitudes, whereas in an active system, the suspension can adjust to a larger range of frequency inputs.

Once the type of suspension was selected, dynamic modeling analysis was done using NUCARS for the purposes of defining the suspension arrangement, quantifying secondary suspension forces, and determining the maglev vehicle response to various guideway inputs. NUCARS (New and Untried Car Analytic Regime Simulation) is a general purpose program, developed by the Association of American Railroads, for modeling rail vehicle transient and steady state response. It is, therefore, easily adapted to analyze a guided maglev vehicle. Detailed discussion of the NUCARS modeling is given in Section C1.3.3. Some of the analysis results are summarized in the following section.

Design Description

The maglev secondary suspension utilizes both coil springs and hydraulic actuators in parallel and is distributed equally on all bogies. Four vertical actuators and spring pairs are located at the corners of the bogie mounted with swivel brackets on the pedestal leg of the bogie frame and the carbody structure. Similarly, two lateral spring/actuator pairs are mounted between the bogie frame and the vehicle underframe.

The springs support the static vehicle loads and perform normal suspension functions. The hydraulic actuators provide the necessary damping and are able to make small force corrections in order to control the dynamic motions of the carbody relative to the bogie. A second important function of this system is that in the case of a bogie magnet failure (i.e., magnet quenching), the actuators are able to control the bogie positioning and stability, keeping it from contacting the guideway and causing an unsafe situation. Another feature of the secondary suspension is that the vehicle could continue operation at reduced speeds utilizing the coil springs if multiple failures of hydraulic actuators occur. The secondary suspension has also been designed to negotiate a minimum curve of 400 m.

The secondary suspension stiffnesses of the vehicle were determined based on a design goal of 0.5 Hz carbody lateral and 1.0 Hz carbody vertical natural frequency. These frequencies are typical for both mode separation and good ride quality. Baseline damping coefficients were set at 20 percent of critical values. Stiffness and damping values along with mass and inertia estimates are given in Table C1-6. The primary suspension parameters are solely based on the magnetic interaction between guideway and vehicle.

NUCARS was utilized to determine the connection forces in the suspension elements and the acceleration levels in the bogie and carbody due to a 1 mm lateral and vertical misalignment over a

25 m span of guideway. Results indicate acceptable bogie acceleration levels and carbody accelerations that are well below specified levels. Figures C1-8 through C1-13 show acceleration levels throughout the speed range up to 330 mph (10 percent exceedance of the 300 mph maximum cruising speed). These figures also indicate where resonances occur in the vehicle and bogie and that they are well controlled by the damping. The vertical and lateral connection forces between carbody and bogie were found to be very low, on the order of about 100 to 300 lbs, due to the relatively soft secondary suspension employed.

Table C1-6
Maglev Vehicle Characteristics

Masses/Inertias

Body Mass - 4.1E04 g
Body Roll Inertia - 8.6E04 g-m^2
Body Pitch Inertia - 4.2E06 g-m^2
Body Yaw Inertia - 4.2E06 g-m^2
Bogie Mass (per bogie) - 3.9E03 g
Bogie Roll Inertia - 6.1E03 g-m^2
Bogie Pitch Inertia - 1.2E04 g-m^2
Bogie Yaw Inertia - 1.7E04 g-m^2

Stiffnesses (entire vehicle, except as noted)

Primary Vertical - 5.0E07 N/m
Primary Lateral - 1.3E07 N/m
Secondary Vertical - 1.6E06 N/m
Secondary Lateral - 4.0E05 N/m
Bogie Yaw (per bogie) 9.0E3 N-m/rad

Damping (entire vehicle, except as noted)

Primary Vertical - 1.7E04 N-s/m
Primary Lateral - 8.4E03 N-s/m
Secondary Vertical - 1.0E05 N-s/m
Secondary Lateral - 5.0E04 N-s/m
Absolute Bogie Vertical - 4.4E05 N-s/m
Absolute Bogie Lateral - 2.2E05 N-s/m
Bogie Yaw (per bogie) - 5.6E02 N-m-s/rad

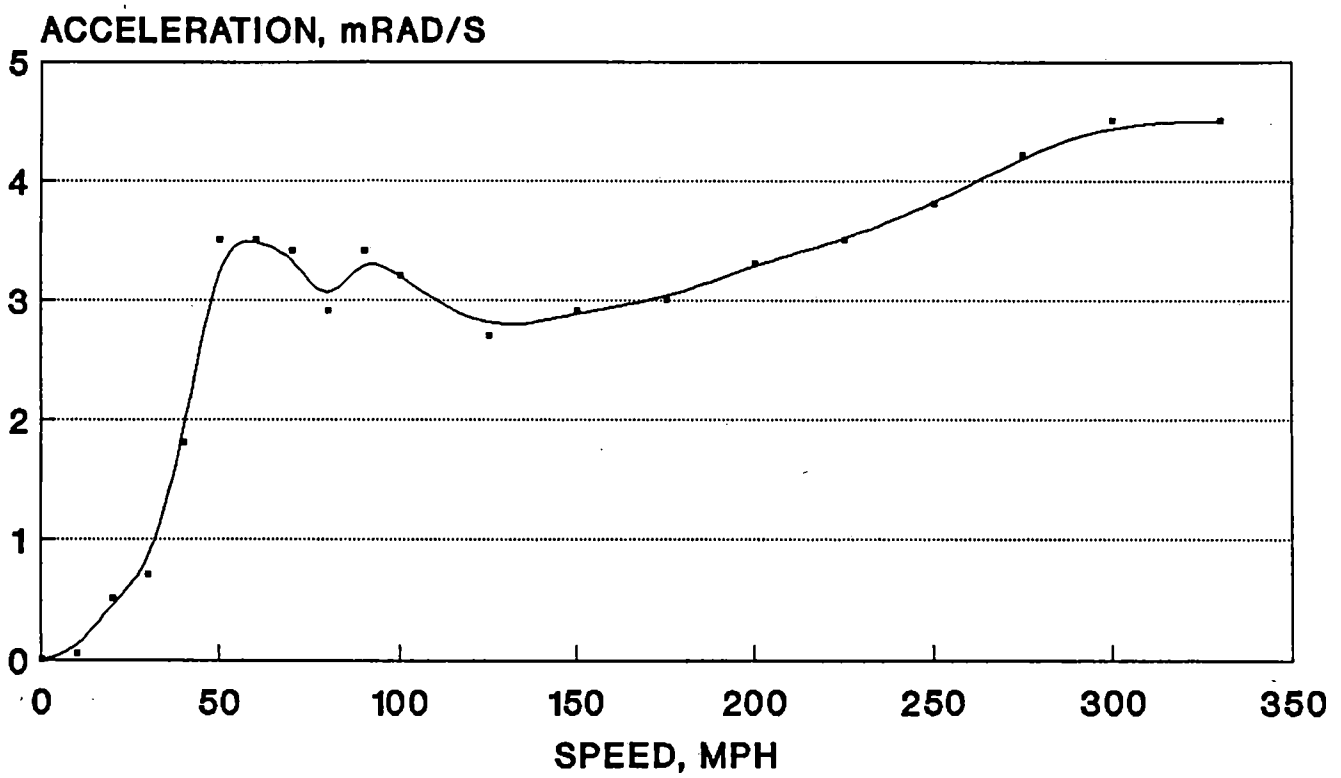

Figure C1-8 Bogie pitch acceleration vs speed

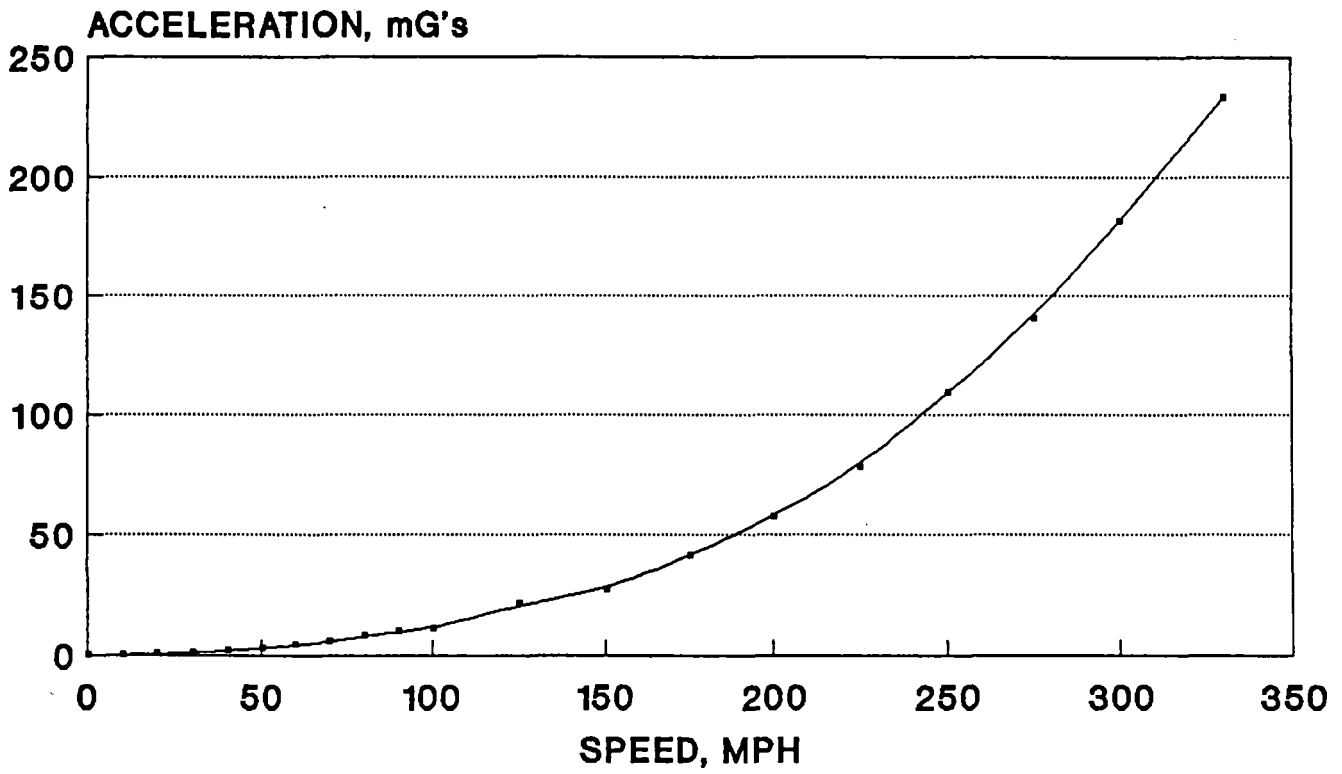

Figure C1-9 Bogie vertical acceleration vs speed

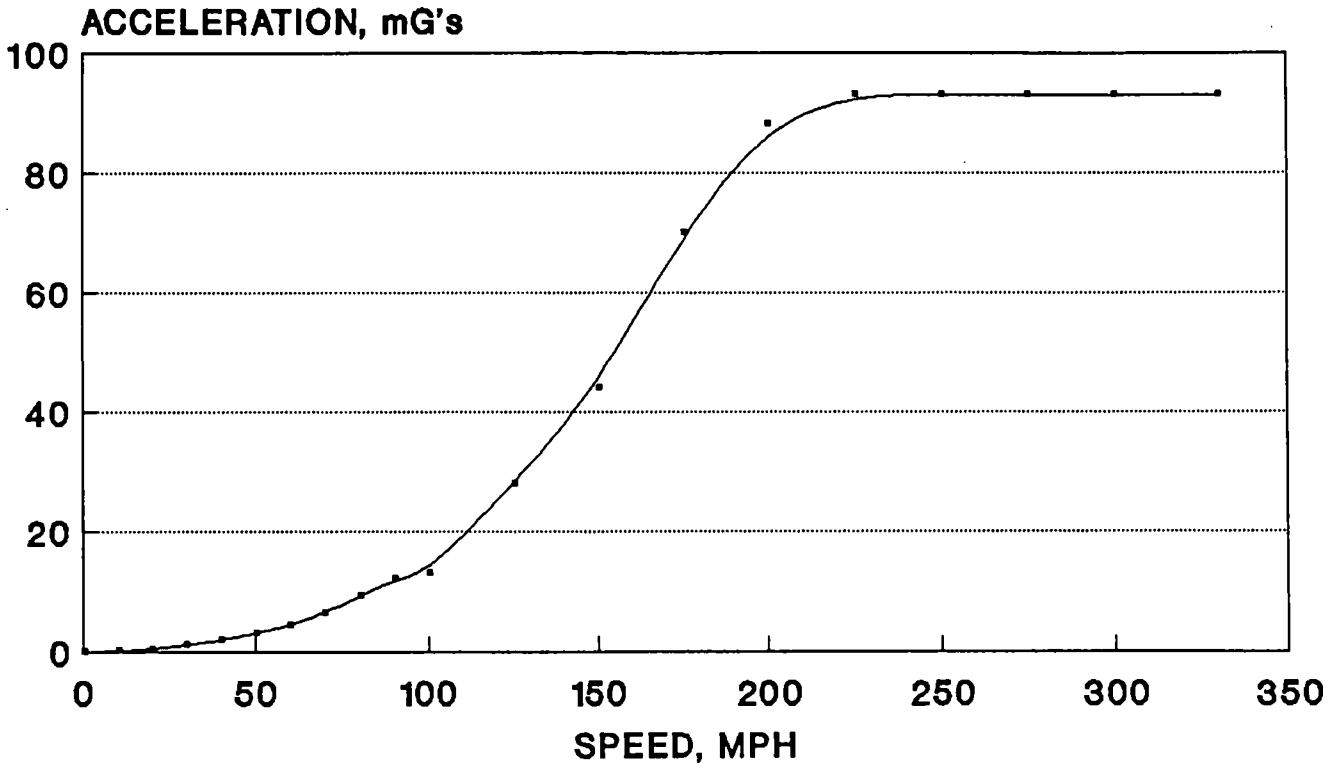

Figure C1-10 Bogie lateral acceleration vs speed

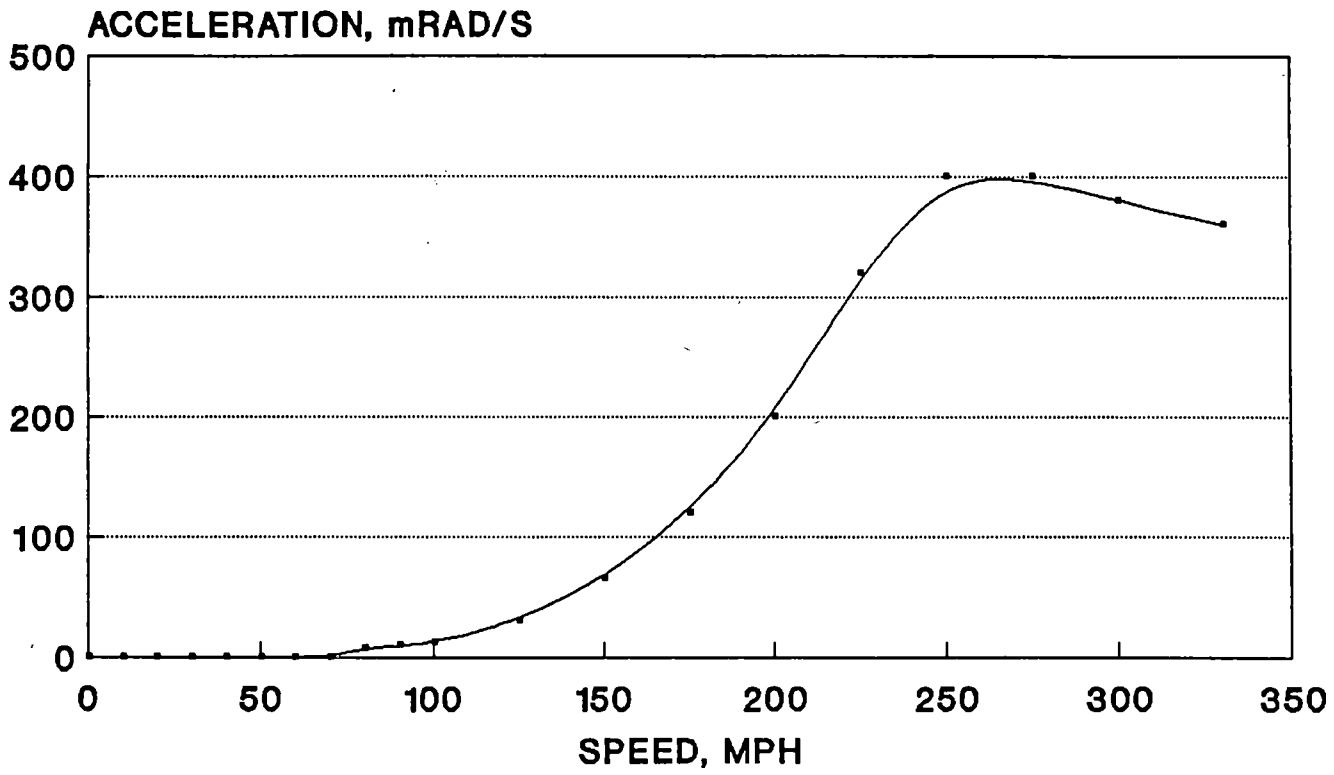

Figure C1-11 Bogie roll acceleration vs speed

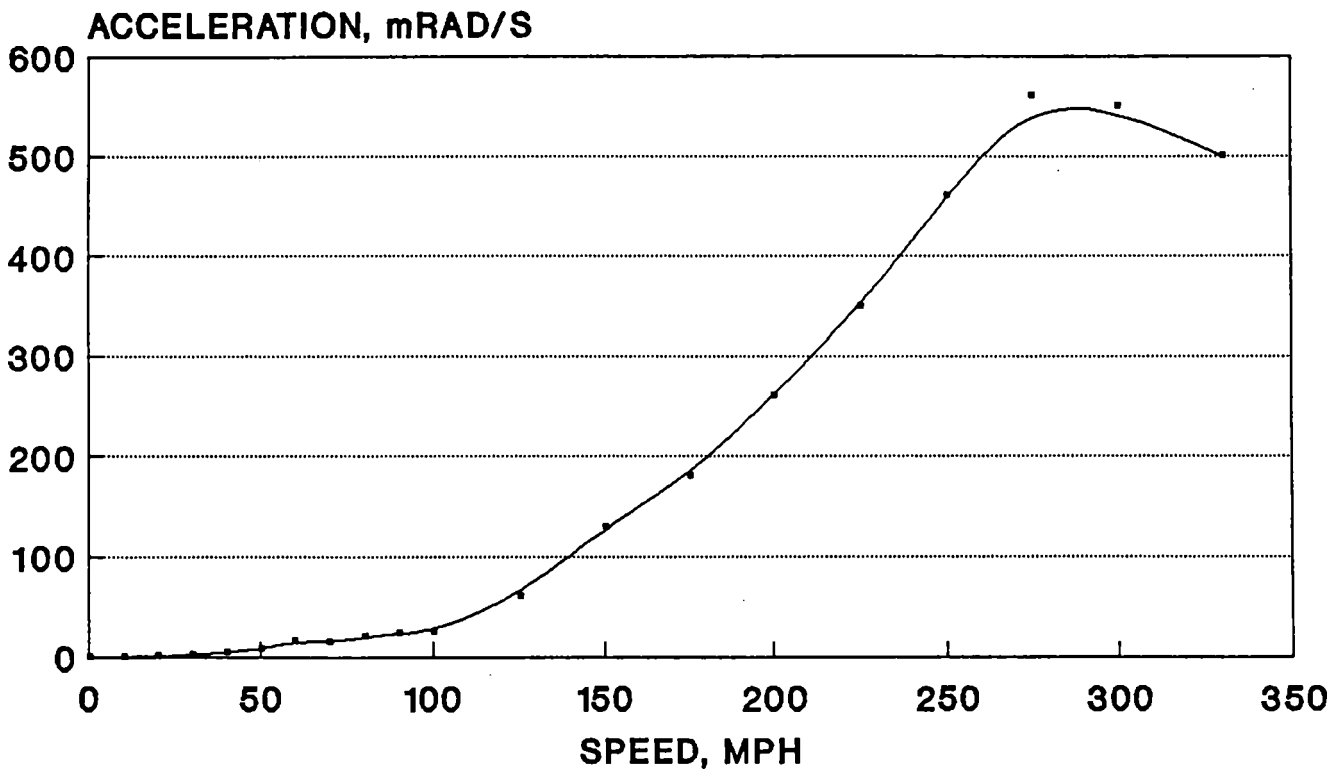

Figure C1-12 Bogie pitch acceleration vs speed

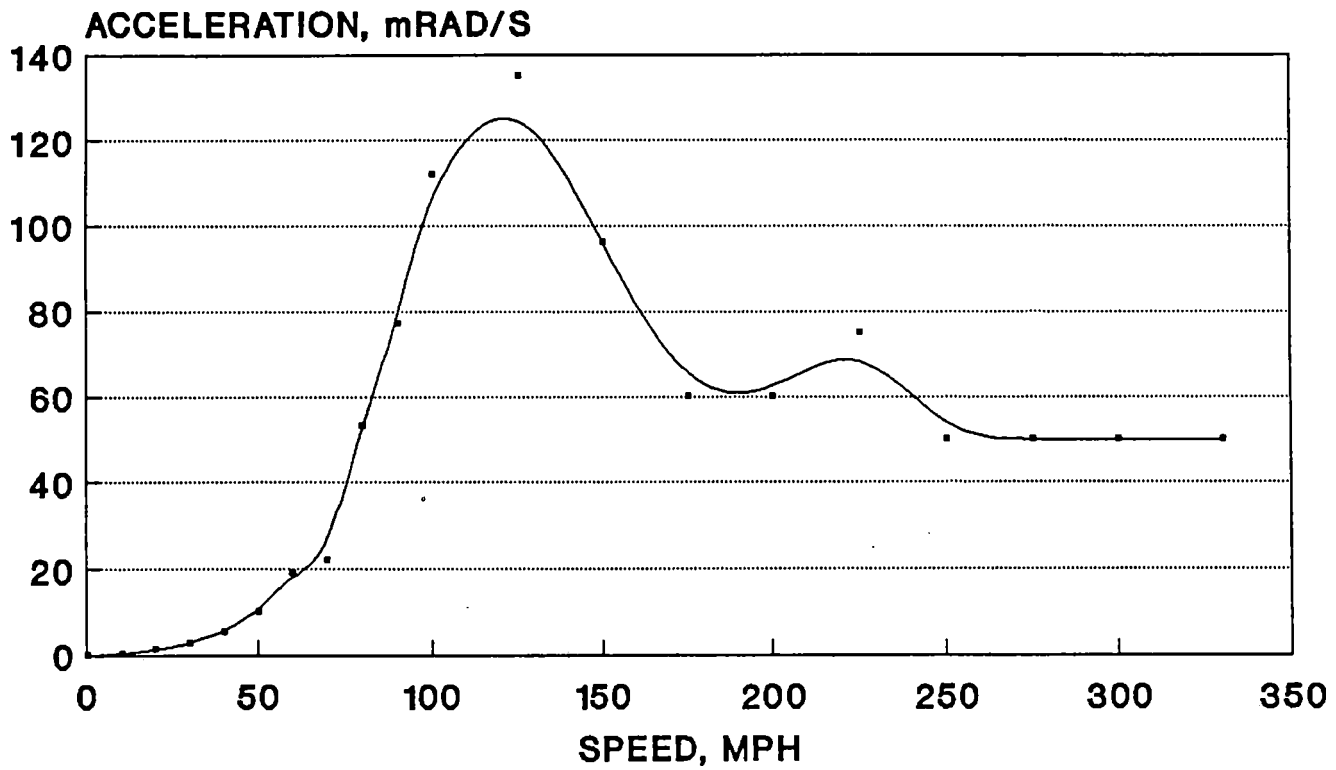

Figure C1-13 Bogie yaw acceleration vs speed

Future Development

The results of the NUCARS model, summarized above, will assist future development work of the secondary suspension, including dynamic analysis and bogie component design criteria. In a detail design stage of this project, the following activities would take place:

- A detailed description of suspension components will be done. Springs, actuators, and the corresponding hydraulic system, will be designed based on the predicted connection forces and secondary suspension displacements.
- The NUCARS analysis has provided adequate acceleration data that will help in defining design fatigue criteria for suspension components and attachment supports. An FEM analysis of components would also be part of the design process.
- Guideway alignment requirements would be examined further using the NUCARS model. Bogie and carbody accelerations may prove acceptable with larger misalignments, possibly further reducing guideway construction and maintenance costs.
- The active suspension systems will be refined during the detailed design stage. Transducer and signal requirements, as well as the feedback control systems, will be further developed.

Layouts and prototype component drawings would be completed during this design phase and provide a basis for a prototype bogie model.

1.3.3 Secondary Suspension Modeling

Abstract

A significant part in the process of developing a secondary suspension design for the maglev vehicle is predicting the dynamic response of the vehicle to various transient and steady state inputs. The purpose of this modeling effort was to determine acceleration levels of the bogie, identify which parameters have the greatest impact on acceleration levels. This in turn is used for structural design of the bogie.

NUCARS (New and Untried Car Analytic Regime Simulation) is a general purpose dynamics program that was used by Electro-Motive Division of General Motors to model the transient and steady state response of the maglev vehicle. This section describes the computer model, summarizes the results of the study, and discusses future utilization of NUCARS for maglev.

Key Requirements

To support the design effort of a bogie structure and a secondary suspension, a general dynamics computer model was utilized to determine the vehicle response to guideway inputs, quantify suspension forces, and assess bogie acceleration levels for structural design considerations.

This program provided the analysis for the secondary suspension configuration used in the baseline vehicle.

Model Description

NUCARS, a general purpose dynamics modeling program, was developed by the Association of American Railroads as a means of determining the performance of new or existing rail vehicles under various track conditions. In a broader scope, it can be used to predict the response of a number of interconnected bodies and suspension elements under a variety of inputs. Therefore, it is easily adapted to analyze a guided maglev vehicle. Most importantly, validation of NUCARS predicted output has been carried out by the AAR and rail vehicle manufacturers in track and vibration tests at the Transportation Test Center and elsewhere.

Listed below is a description of the various NUCARS model configurations of the maglev vehicle that were run, a description of the geometric inputs used to excite the system, and an index of the output files generated from the model.

NUCARS Maglev Vehicle Models

Description of Model Configuration

Baseline Vehicle (VB)

1. Magnetic stiffnesses for baseline magnet configuration; low magnetic damping coefficients (c = 8.0 laterally, 16.0 vertically, per bogie); distributed magnetic stiffness/damping: eight vertical and four lateral connections per bogie.
2. Secondary stiffnesses determined by desired lateral and vertical body natural frequency; design goal of 0.5 Hz lateral, and 1.0 Hz vertical; damping coefficients set at 20 percent of critical values; four vertical connections (at bogie frame corners) and two lateral connections (0.5 meter on both sides of the bogie pivot) per bogie.
3. "Skyhook" damping between a single stationary input body and the bogies; damping coefficient set at 20 percent of critical. This is an absolute reference damping which allows NUCARS to simulate an "active" type damping.

4. Four input bodies per bogie. Left and right side vertical magnetic stiffness pairs and 1 lateral magnetic stiffness element connected to the same single input body. These input bodies excite the system.

Modified Vehicle (VM)

1. Same as baseline, except body flexing modes are included.

   The modes are first vertical bending estimated at 6.5 Hz and first lateral bending estimated at 7.5 Hz. Body critical damping is set at 1 percent.

Special Vehicle (VS)

1. Same as baseline, except eight input bodies per bogie, to enable roll excitation of the maglev vehicle. This change will also require a small reconfiguration to the magnetic lateral stiffness and damping, and lateral skyhook damping connection arrangement.

NUCARS Geometric Inputs for Maglev Vehicle

Input File Description

Baseline (IB)

1. Lateral and vertical sine wave, in phase; 25 m wavelength, four cycles of input. Input amplitude was chosen to be 1 mm peak to peak based on current estimated suspension ladder tolerances. Identical lateral and vertical amplitudes.

Roll (IR)

1. Left and right side vertical sine wave input, 180 degrees out of phase; 25 m wavelength, four cycles of input, at the baseline input amplitude. This input will only be run in conjunction with the "Special" (VS) vehicle model.

Special (IS)

1. Same as (IB), except lateral and vertical inputs are 90 degrees out of phase. This input was used to excite roll motions.

Cusp (IC)

1. Four lateral and vertical cusps, 25 m wavelength, 0.5 mm amplitude. The cusp input represents a limiting input form.

Slow Curve (ISCR)

1. Steady state curve negotiation around minimum radius curve (400 m). Analysis of suspension connection forces in curving.

Fast Curve (IFCR)

1. Steady state curve negotiation at high speed around appropriate curve size. Analysis of connection forces in high speed curving.

The Baseline (IB) model was run over the entire vehicle speed range up to 300 mph. The speed sweep was done to identify any possible resonance conditions. The 10% overspeed was used as a safety factor.

NUCARS Data Outputs for Maglev Vehicle

Output File Description

Baseline (OB)

1. Body and #1 Bogie absolute accelerations - lateral, vertical, roll, yaw, and pitch. 10 outputs total. The body and bogie accelerations are of primary importance for structural loading considerations.

Special (OS)

1. All connection forces on the #1 bogie, both in the primary (magnetic) and secondary suspension - eight vertical and four lateral in primary; eight vertical and four lateral "skyhook" connections; and four vertical and two lateral secondary connections. Only used with baseline vehicle model, VB. This output is important is the design of the stiffness elements and actuator.

Body Flex (OBF)

1. Same as baseline, except absolute accelerations (lateral and vertical) measured along the carbody length, at the longitudinal centerline (both ends of the body seating area, and at the middle). Body bending modes are considered. Only used with modified vehicle, VM.

Roll (OR)

1. Same as (OS), except used only with special vehicle model, VS. Examines suspension connection forces in a roll environment.

The run combinations are summarized in Table C1-7 which lists each of the model codes, input codes, vehicle speed, and corresponding output code. An appendix includes copies of the model description, input geometry description, and also provides plots of the input geometries and a NUCARS representation of the maglev model for all run combinations that were examined.

The NUCARS vehicle parameters are listed in Table C1-8. The stiffness and damping values are dictated by the carbody and bogie mass. These values are the same as discussed earlier in Section C1.3.2 which summarize the secondary suspension arrangement.

Table C1-7
Summary of NUCARS Runs on Maglev Vehicle

Speed MPH	Model Code	Input Code	Output Code
10	VB	IB	OB
20	VB	IB	OB
30	VB	IB	OB
40	VB	IB	OB
50	VB	IB	OB
60	VB	IB	OB
70	VB	IB	OB
80	VB	IB	OB
90	VB	IB	OB
100	VB	IB	OB
125	VB	IB	OB
150	VB	IB	OB
175	VB	IB	OB
200	VB	IB	OB
225	VB	IB	OB
250	VB	IB	OB
275	VB	IB	OB
300	VB	IB	OB
330	VB	IB	OB
300	VB	IB	OS
300	VB	IS	OS
300	VB	IC	OS
300	VS	IR	OR
300	VM	IB	OBF
300	VM	IS	OBF
117	VB	ISCR	OS
300	VB	IFCR	OB

Table C1-8
NUCARS Maglev Vehicle Model Parameters

Masses/Inertia's

Body Mass - 4.1E04 g
Body Roll Inertia - 8.6E04 g-m^2
Body Pitch Inertia - 4.2E06 g-m^2
Body Yaw Inertia - 4.2E06 g-m^2
Bogie Mass (per bogie) - 3.9E03 g
Bogie Roll Inertia - 6.1E03 g-m^2
Bogie Pitch Inertia - 1.2E04 g-m^2
Bogie Yaw Inertia - 1.7E04 g-m^2

Stiffnesses (entire vehicle, except as noted)

Primary Vertical - 5.0E07 N/m
Primary Lateral - 1.3E07 N/m
Secondary Vertical - 1.6E06 N/m
Secondary Lateral - 4.0E05 N/m
Bogie Yaw (per bogie) 9.0E3 N-m/rad

Damping (entire vehicle, except as noted)

Primary Vertical - 1.7E04 N-s/m
Primary Lateral - 8.4E03 N-s/m
Secondary Vertical - 1.0E05 N-s/m
Secondary Lateral - 5.0E04 N-s/m
Absolute Bogie Vertical - 4.4E05 N-s/m
Absolute Bogie Lateral - 2.2E05 N-s/m
Bogie Yaw (per bogie) - 5.6E02 N-m-s/rad

Model Results

Over the past several months NUCARS has been used to quantify the dynamic response of the maglev vehicle to guideway geometric variations. These variations would most likely be due to suspension ladder alignment. Starting with the baseline vehicle model, variations have been made to identify which model parameters have the greatest impact on the acceleration level both within the vehicle body (ride quality) and at the bogies (structural loading quantification). In this section the primary interest in the NUCARS results has been the latter issue.

The initial modeling tasks with NUCARS examined the sensitivity of the maglev vehicle to various modeling parameters such as guideway alignment, mass, inertia, stiffness, and damping. This study concluded that guideway alignment had the greatest impact on controlling the vehicle

accelerations and suspension connection force levels. From the modeling results, it was determined that a ladder alignment limit of 1 mm over a 25 m wavelength, both vertical and lateral, was necessary to keep bogie accelerations within limits for structural loading concerns. At 330 mph (a 10% exceedance of the 300 mph maglev cruising speed), the following bogie acceleration levels were predicted:

Bogie vertical acceleration - 0.25 g's, peak to peak

Bogie lateral acceleration - 0.10 g's, peak to peak

Bogie roll acceleration - 0.40 rad/s^2, peak to peak

Bogie pitch acceleration - 0.55 rad/s^2, peak to peak

Bogie yaw acceleration - 0.14 rad/s^2, peak to peak

These acceleration levels are the basis of the bogie structural fatigue loading criteria.

In addition to guideway alignment, absolute reference damping of the bogies was found to have affect on the bogie acceleration levels. Figures C1-14 through C1-18 are summary plots of acceleration levels throughout the speed range for both vehicle and bogie. These plots indicate where certain resonances occur in the vehicle and bogie and that they are well controlled by the damping in the system.

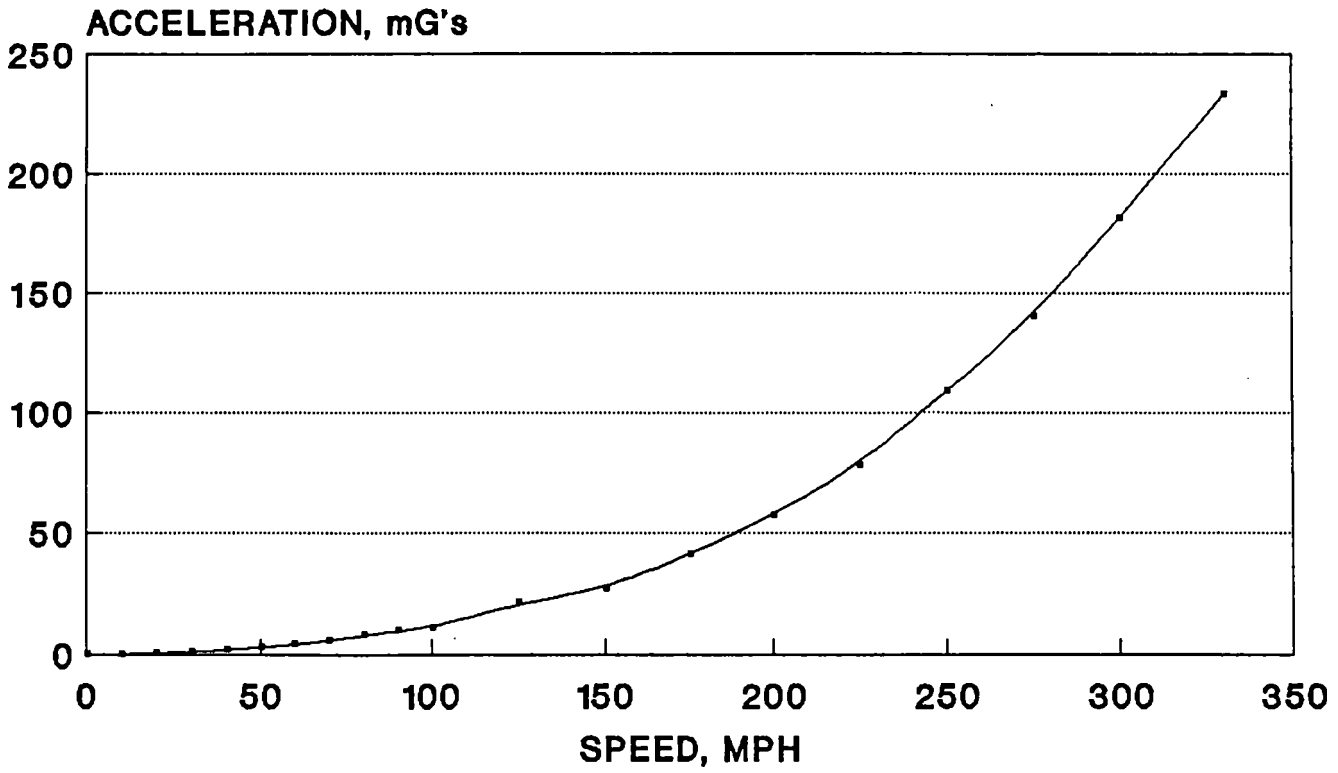

Figure C1-14 Bogie vertical acceleration vs speed

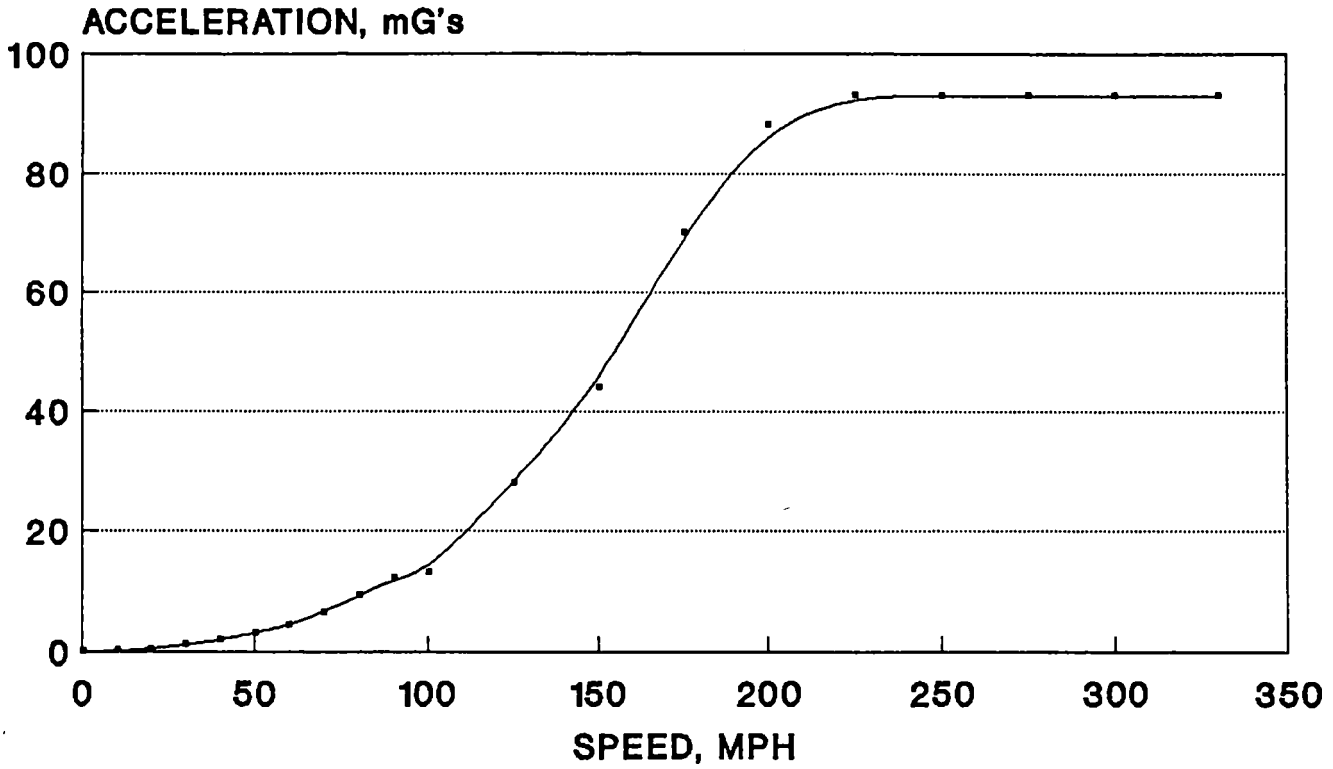

Figure C1-15 Bogie lateral acceleration vs speed

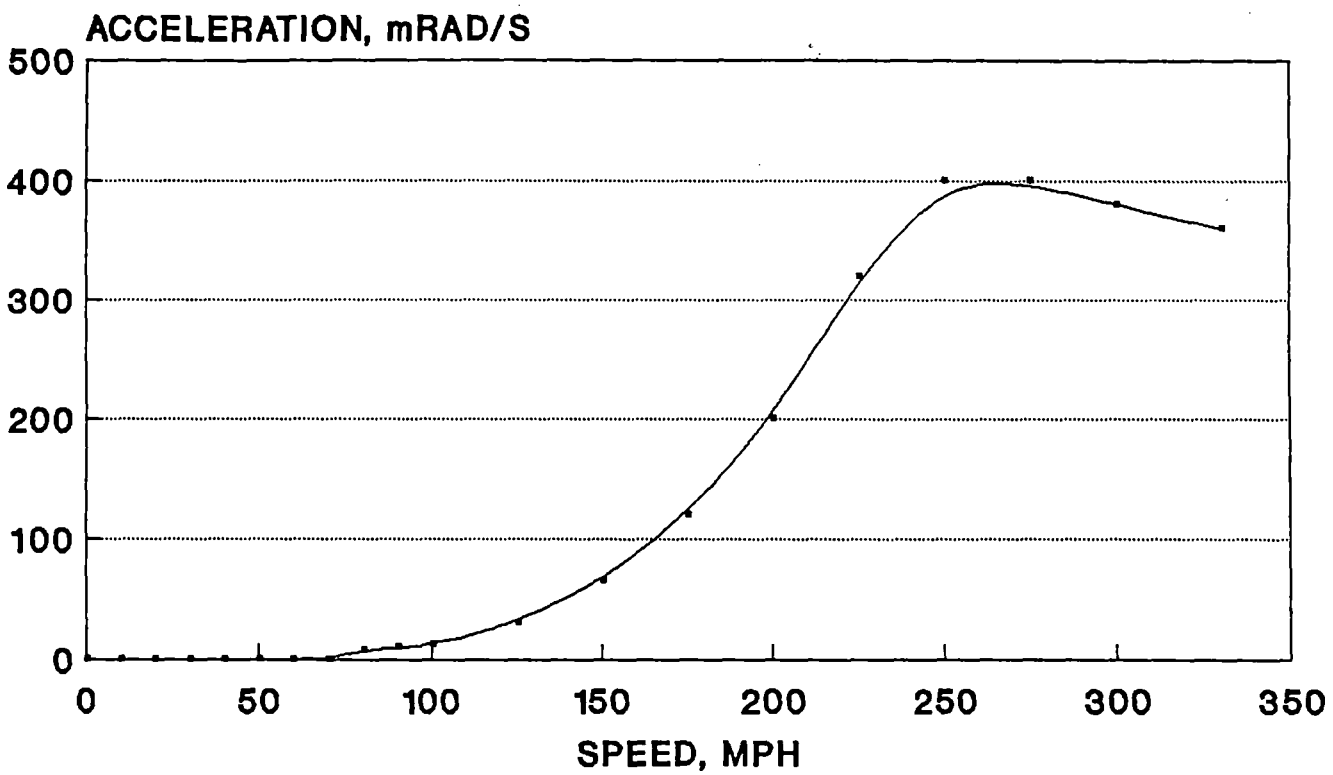

Figure C1-16 Bogie roll acceleration vs speed

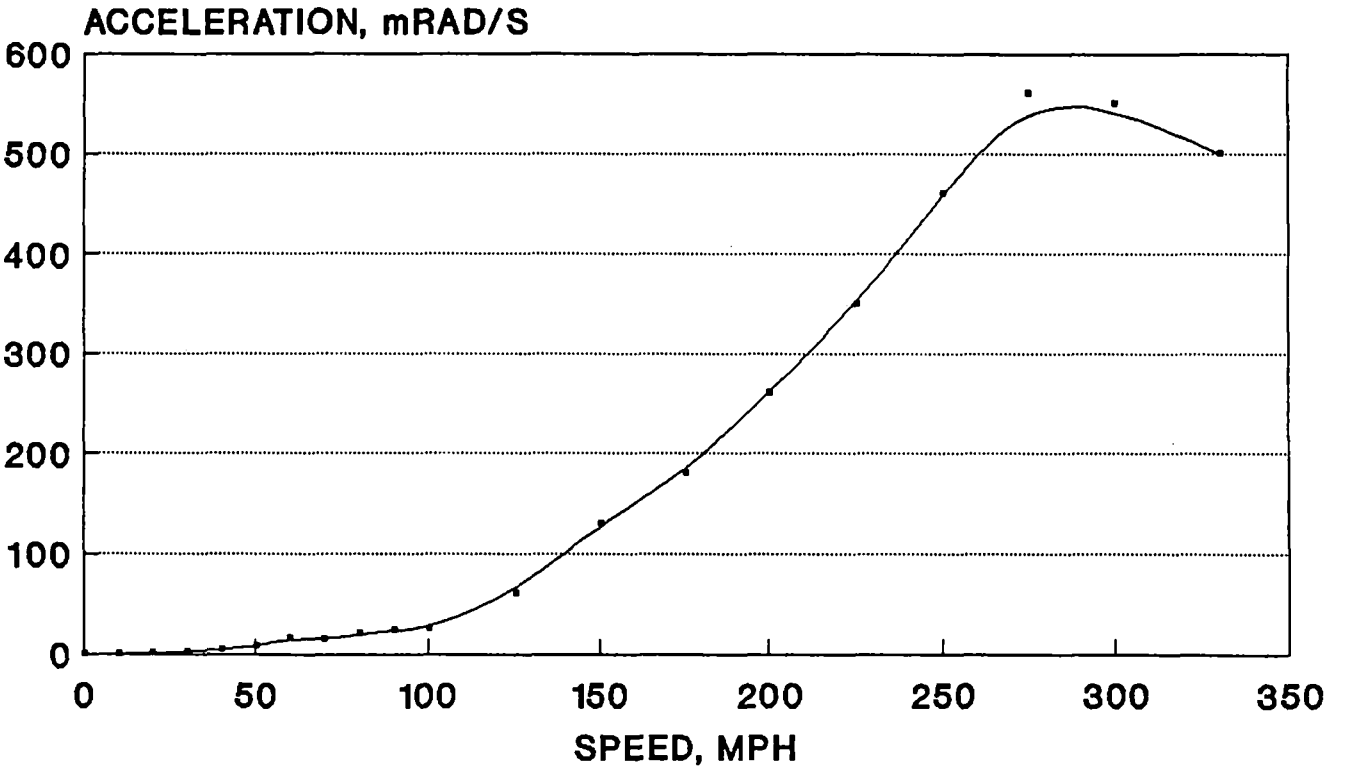

Figure C1-17 Bogie pitch acceleration vs speed

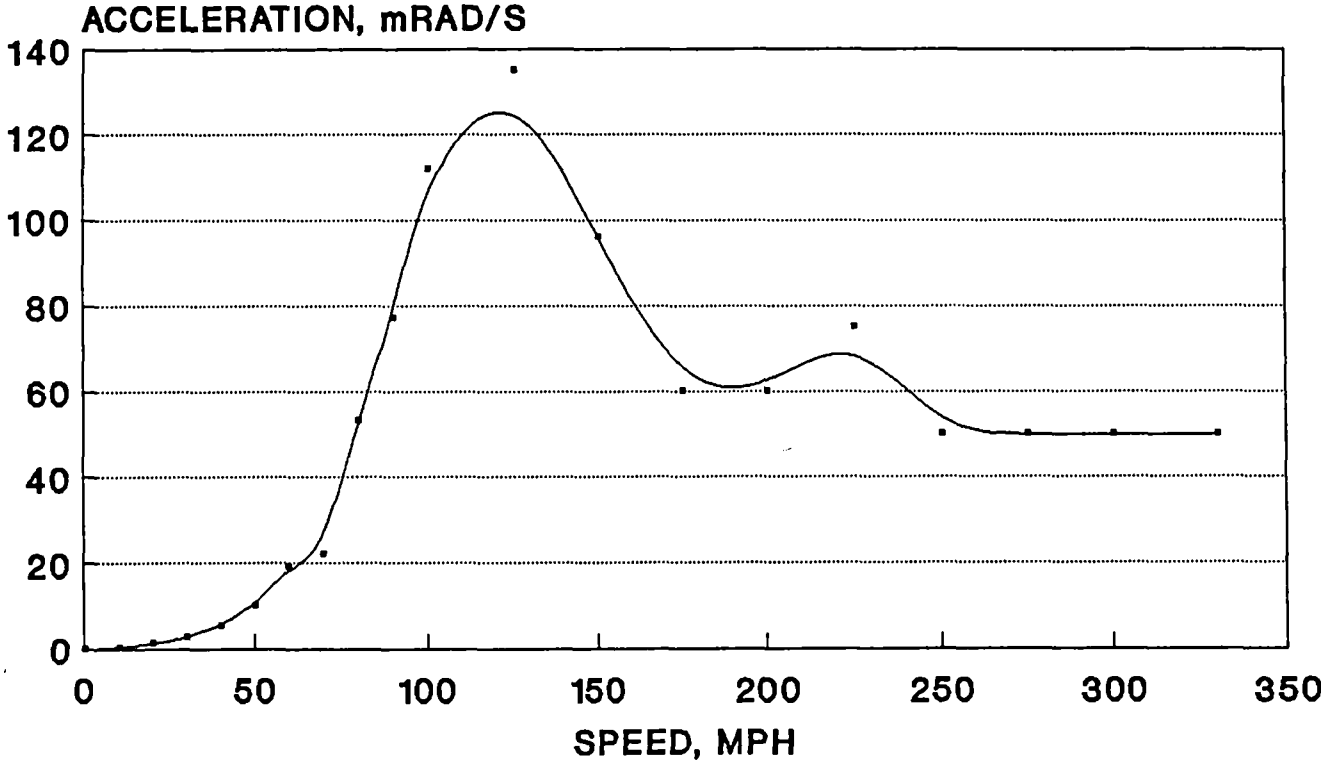

Figure C1-18 Bogie yaw acceleration vs speed

The connection forces between the body and bogie were found to be very low, on the order of 100 to 300 lbs, due to the soft suspension employed. It is expected, unlike on rail vehicles, that the largest amplitude suspension forces on a maglev vehicle will result from transient and steady state aerodynamic loading and curve negotiation.

The output of the NUCARS model including suspension responses and connection forces for the tabulated runs are located in the second appendix that relates to this section.

Future Modeling Development

The use of NUCARS has greatly assisted in the development and orientation of the secondary suspension and defining design fatigue criteria for the bogie structure and components. Future development utilizing NUCARS is planned for the following areas:

- Suspension ladder and guideway requirements would be further examined using NUCARS. With refinements in the model, bogie accelerations may prove acceptable with larger misalignments, possibly further reducing guideway construction and maintenance costs.
- In the next phase, NUCARS will be used to examine vehicle dynamics in curve negotiation. The program will help in determining forces and accelerations and possibly aid the design of the guide curve entry transitions.

As the detailed design of the maglev system proceeds, optimization of the bogie structure, suspension elements, and vehicle response are required. NUCARS will be part of this iterative process.

1.4 HYDRAULIC SYSTEM

1.4.1 Hydraulic System

Subsystems Requiring Hydraulic Actuation

Hydraulic devices on the maglev vehicle include the vertical and lateral bogie actuators, the guidance planes (fins), the parking brake/lateral wheel sets on each bogie, and the passenger compartment tilt actuators. All of these actuators derive their hydraulic power from lines supplied by two motor/pump sets located in the forward compartment above deck. These devices will be divided into two categories: bogies and carbody. Figure C1-19 is a schematic diagram of the hydraulic system.

Bogie hydraulics

The term bogie hydraulics is used here to include vertical and lateral actuators and the lateral wheel/parking brake actuators. Figure C1-20 indicates the locations of the hydraulic devices on each of the six bogies.

Vertical actuators: There are four vertical suspension actuators per bogie, to assist the vertical coil springs. Each actuator has a small enough outside diameter to fit within the coil spring that it assists. The actuators are basically hydraulic pistons with integral control valving that apply their forces in concert with and at the same effective locations as the coil springs. These forces are to be computer-controlled to accomplish the functions of damping, positioning, and/or locking. The assistance of a passive spring with an active device qualifies this arrangement to be termed semi-active vertical suspension.

The vertical suspension is not oriented perfectly vertically but has some slant to it in order to accommodate lateral bogie motion. There will be slight lateral force components exerted by the vertical suspension. Our analyses have included this effect, but the vertical actuators can be considered in an approximate sense to perform solely vertical suspension functions. These actuators will be operated at fairly high speed in order to counteract 7 Hz motions near the vehicle/guideway natural frequency, and are expected to put major hydraulic loads on the hydraulics supply system.

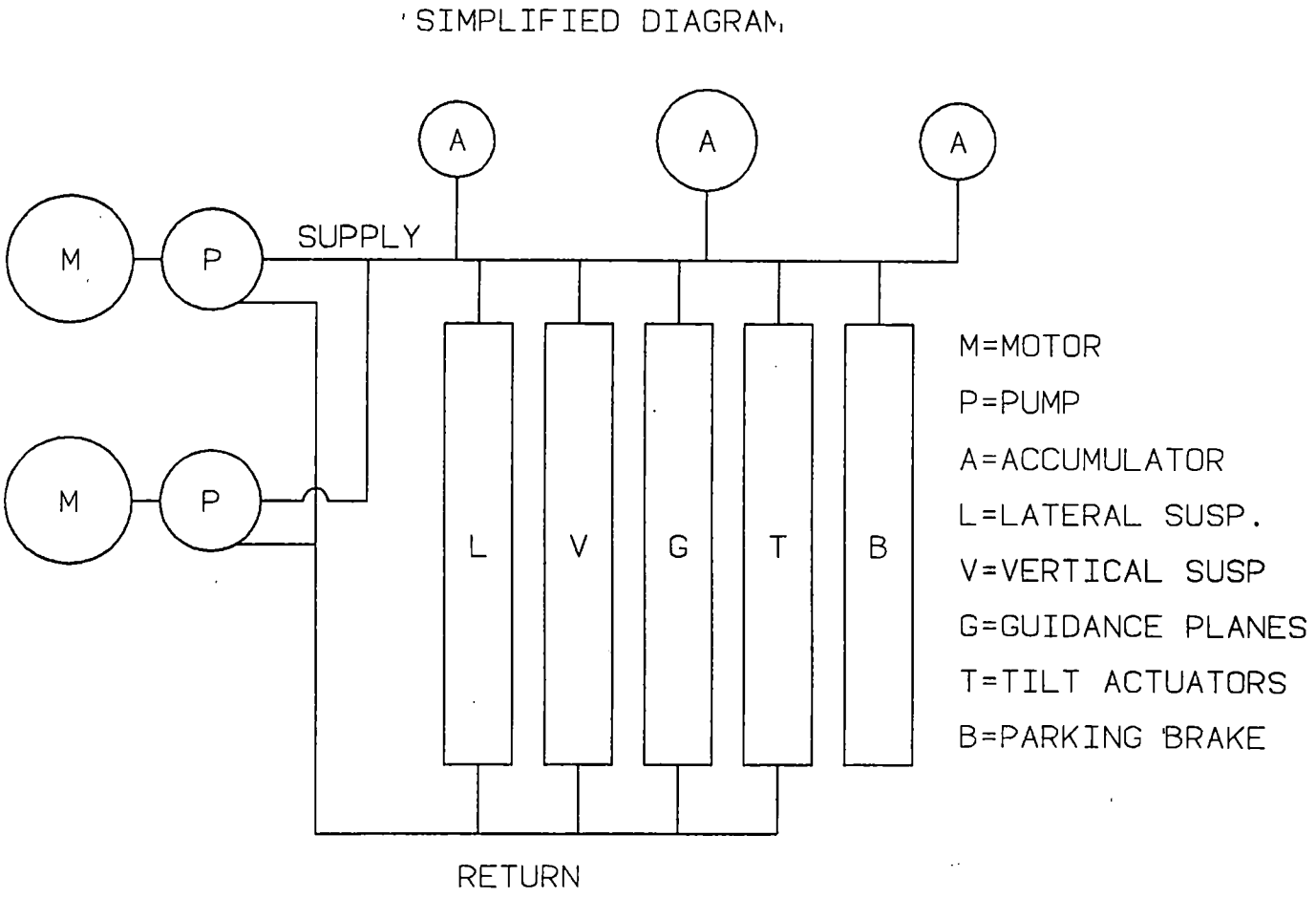

Figure C1-19 Hydraulic system components

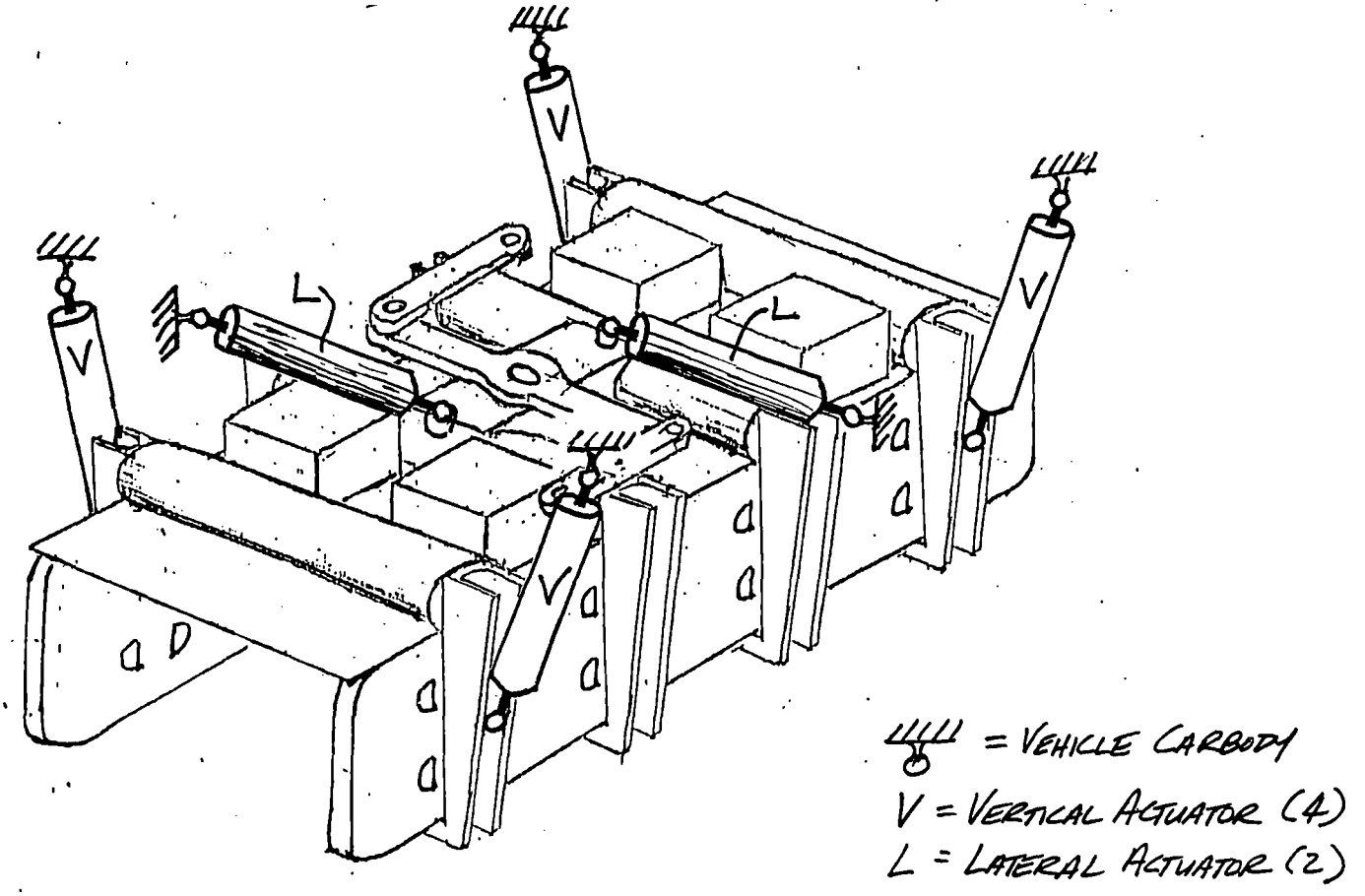

Figure C1-20 Locations of hydraulic actuators on each bogie

Lateral actuators: There are two lateral actuators per bogie to assist the two lateral springs which center the bogie links. As with the vertical suspension, the lateral actuators are located within the lateral coil springs and perform computer-controlled damping, positioning, and locking as part of a semi-active lateral suspension system. The lateral suspension elements are not oriented perfectly horizontally, but the vertical components of their associated forces are small. These actuators will be required to counteract large side wind forces and therefore will at times place large demands upon the hydraulics power supply.

Wheel/parking brake actuators: On each side of each bogie are located two sets of devices that perform a dual function: lateral guidance via very small wheels, and parking brake clamp/release. This device will be referred to as a wheel and brake assembly. It is intended for use only at very low vehicle speeds, namely 10 kph or below, including stopped. Each wheel and brake assembly is moved toward or away from the concrete guideway with a hydraulic actuator that we consider to be part of the wheel and brake assembly. The wheel, brake pads, actuator, hydraulic line attachment fittings, springs, shaft, and supporting framework are all part of a LRU intended to be quickly swapped out when service on the unit is required. The demand for hydraulic power by these devices will be minimal.

Carbody hydraulics

The term carbody hydraulics is used here to include the two tilt actuators and the locking brake located at each end of the passenger compartment module, and the guidance plane actuators.

Tilt actuators: The tilt actuators connect points on the vehicle carbody structural members to the bulkheads of the passenger compartment. There is a port actuator and a starboard actuator at each bulkhead. By extending one actuator hydraulically and retracting the other actuator hydraulically, the passenger compartment is made to rotate in its end bearings and thereby tilt in order to make the passengers more comfortable when the vehicle travels around a curve in the route. The entire compartment will be cradled in low-friction roller bearings, and the requirement for the actuators to overcome this bearing friction is expected to be negligible. There is little force for the tilt actuators to overcome except for the rotational inertia of the loaded passenger compartment. This inertia must be overcome only when starting to roll or stopping the roll of the passenger compartment, and not in the period of time when the roll rate is uniform. This means that it is the roll acceleration rather than the roll rate which determines the actuators' force requirements. The roll acceleration rate is expected to be low enough so that low capacity tilt actuators may be used. Each actuator will be sized to handle the entire tilt requirement alone in case of a failure of its companion actuator.

Guidance plane actuators: There are two fore and two aft guidance planes on the outside of the vehicle shell. They might be called stubby wings were it not for the fact that their purpose is solely to improve ride quality rather than to lift the vehicle (the term 'wing' might imply the function of providing lift). The aelerons at the trailing edges of the guidance planes are positioned by their hydraulic actuators, which are of the piston type connected to a bell crank linkage. The actuators tilt the planes about their transversely mounted shafts in order to push the carbody upward or downward using the resultant aerodynamic forces on the planes.

Hydraulic Supply System

Figure C1-19 is a schematic of the hydraulic supply system. Two motor/pump sets are provided for redundancy. Neither motor/pump set is sized to handle the full hydraulic requirements of the maglev vehicle. Should one motor/pump set fail, the hydraulic system would still be operational but at half capacity due to the presence of the second set. This would probably require operation at less than full vehicle speed in order to prevent an extremely rough ride.

For two major reasons, 3,000 psi was picked as the maximum operating pressure of the system. First, most hydraulic equipment in this country is applied at or below 3,000 psi and such equipment is therefore readily available. Secondly, higher pressure means lower weight, and weight is a continuing concern in our design approach. Any maximum pressure less than 3,000 psi would therefore be unacceptable from a weight standpoint. A more detailed hydraulic system concept study would undoubtedly lead to a higher system pressure selection, but the ease of obtaining information about components for a 3,000 psi system led to its selection for this SCD.

The electric motors driving the pumps would be high speed 4,000 rpm 400 Hz 12 pole 40 kW (each) 3 phase motors to reduce weight and volume. The pumps would be 3,000 psi 15 gpm (each) swash plate piston pumps; vane or gear type pumps at these pressures would require multistage pumps. The duty cycle on the pumps would be rather steady with the substantial accumulator sizes we have selected. The central accumulator has a capacity of 71 liters (19 gallons) and the fore and aft accumulators each have a capacity of 36 liters (9 gallons). The main trunk of the hydraulic supply lines will be large 5.6 cm inside diameter rigid lines due to the high frequency nature of this hydraulic system; branch circuits would have smaller lines but still relatively large lines. The connections to the bogie must be designed with bogie motions and actuator motions relative to the carbody in mind, requiring flexible lines.

Power Requirements

Section 1.4.2, Ride Control Hydraulic System Weight and Power, develops projected hydraulic pressure and flow for each of the major hydraulic devices. Pump mechanical efficiencies are already built into the calculations in that report section, whose bottom line power projections are as follows:

Actuator	Hp into pump	% of total
Fins	36.3	51.9
Lateral Bogie	18.5	26.5
Vertical Bogie	15.1	21.6
Total	69.9	100.0

A conservative estimate is obtained for system electrical power by dividing the pump input power (converted from horsepower to kW) by a motor and supply efficiency (0.8). This gives us a demand for 65 kW of electrical power at 440 volts ac for the vehicle hydraulics. This number was used in totalling the electrical loads in Section 1.5.1, On-board Power System. By providing two motor/pump sets for redundancy, each hydraulic set will require 33 kW.

Weight

Weight estimates for most of the hydraulic system components was obtained from Section 1.4.2, Ride Control Hydraulic System Weight and Power. Only the pumps and motors were not included in that section. In order to reduce weight and space requirements we expect to utilize high speed pumps and motors. There was no information available about the nonstandard 4,000 RPM pumps and motors, so those weights were obtained by ratioing the weight of commercially available 1,800 RPM equipment. The development program for the actual equipment for maglev vehicles would certainly include optimized custom designs with lightweight equipment. This, combined with the fact that rotating equipment weight is roughly inversely proportional to operating speed for a given power level, makes this approach reasonable. The following weight table is supported by the referenced report section:

Components	Weight, pounds	Mass, kg
Motor/Pump Sets (2)	472	214
Flaps & equipment	640	290
Lateral bogie & equip.	427	194
Vertical bogie & equip.	375	170
Accumulators	484	220
Total (2 systems)	2398	1088

1.4.2 Ride Control Hydraulic System Weight and Power

Introduction

As noted earlier, a maglev vehicle incorporates hydraulic actuation for several purposes: ride control via active suspension elements; ride control via aerodynamic surfaces; carbody tilt actuation; and wheel-set and parking brake actuation. The latter two functions involve relatively few actuators operating transiently and slowly, imposing relatively small power and weight requirements on a hydraulic actuation system. However, the former two ride control functions, via active suspension and via aerodynamic surfaces, involve a large number of actuators, operate continuously during vehicle operation, operate at high force levels and at a high bandwidth, and consequently impose large power and weight requirements on a hydraulic actuation system. In the following section we estimate power and weight requirements for a ride control hydraulic actuation system. Consideration of weight and power requirements for the other hydraulically actuated functions, carbody tilt, and wheel-set and parking-brake actuation, is omitted. Consideration of the hydraulic system power supply or pump(s) is omitted.

Ride Control Hydraulic System Configuration

Active ride control is achieved by a combination of: active hydraulic manipulation of each of four aerodynamic surfaces (flaps); and active hydraulic manipulation of the lateral, vertical, and orientational position of each of six support bogies. There are four flaps and four flap actuators. There are four vertical and two horizontal suspension actuators on each bogie. The ride control hydraulic system thus uses 40 flap actuators, two vertical actuators and four horizontal actuators on each of six bogies.

The ride control hydraulic system configuration is shown schematically in Figure C1-21. The components are shown arranged approximately according to the geometry of the maglev vehicle: the suspension actuators are associated with bogies, four vertical and six horizontal with each bogie, six bogies arranged from forward to aft; the flap actuators are associated with flaps, two forward, two aft. The actuators are assumed to be, and are shown as, conventional hydraulic cylinders; it is assumed that each piston rod is half the diameter of the actuator piston.

A major configurational assumption is that a conventional open-center four-way hydraulic servo valve is associated with each of 40 ride control actuators. The bases for the assumption are: independent servo control of each actuator is necessary, thus a valve is needed for each actuator; approximate symmetry of actuation of each cylinder is needed, thus each valve is assumed to be a four-way valve; and good servo control with smoothness through null and no discontinuities in gain is needed, thus each valve is assumed to be an open-center valve. The major system implication of this assumption is that none of the ride control actuators is ever "off." That is to say, there is always a substantial flow from supply pressure to reservoir pressure across any open-center four-way valve, whether its actuator is being stroked or not. Because of special circumstances associated with the ride-control actuators, namely that they are essentially always active and being stroked, the energy costs are not an issue. Also, these parasitic flows make approximate calculation of power usage a relatively easy task.

It is assumed that the hydraulic pumps are capable of a 3,000 psi hydraulic supply pressure, and that a minimum of 2,000 psi is always available under normal circumstances at the accumulators. The lower figure of 2,000 psi is used as the nominal supply pressure for sizing valves, actuators, accumulators, and all associated plumbing. The size of ports associated with valves and actuators is sized according to about a 50 psi drop across the ports at full flow rate. Plumbing diameters are assumed to be about 2.2 and 3.0 times the corresponding port diameters, for fin actuators and suspension actuators respectively.

A noted feature of the ride control hydraulic actuation system is its distribution along the length of the maglev vehicle, along the better part of 36 m (about 120 ft), as represented schematically in Figure C1-21. Another feature of the ride-control hydraulic system is the provision of three hydraulic accumulators spaced along the length of the vehicle. The issue addressed by this apparent redundancy is that the required unusually high response bandwidth, of the order of 7 Hz (7 cps), is comparable to the frequency response of the long hydraulic supply lines, and that supply from a single accumulator to all parts of the system would not provide sufficiently quick response.

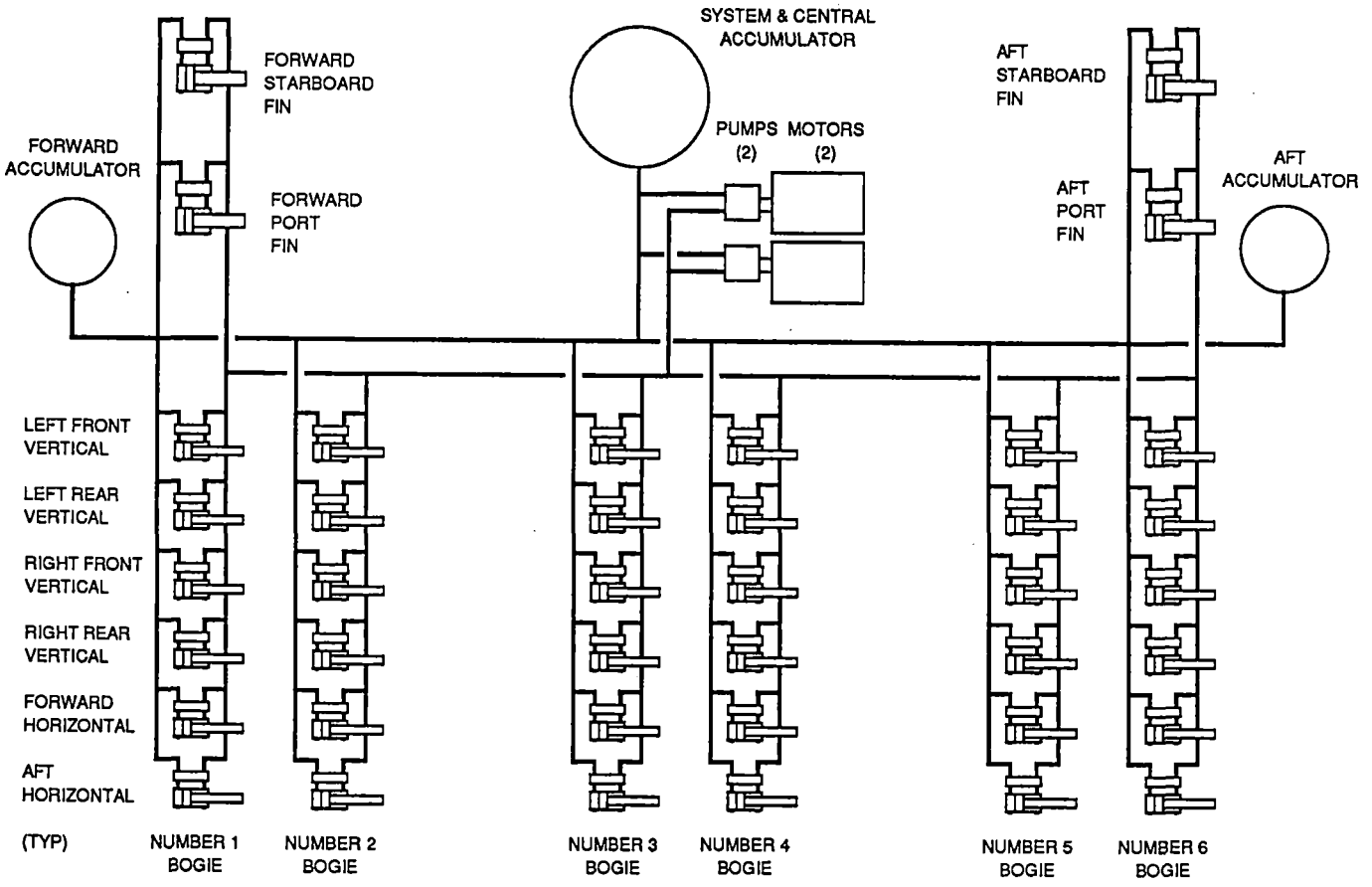

Figure C1-21 Hydraulic system configuration

It is for this reason that three accumulators are used. One may reasonably consider that one accumulator supplies the forward two bogies and the two forward flaps; one ditto aft; and that the center accumulator supplies the system and the two center bogies.

The aerodynamic control surface form is assumed to be an unswept fixed fin with a rotatable flap forming the after portion. The fixed fin occupies 70 percent of the planform chord; the rotatable flap, 30 percent. An early control surface form considered was a 100 percent flap; that is, the entire fin rotated about an athwartships axis to provide an angle of attack and lift. This early form proved to be mechanically awkward and was abandoned. A major issue was that the fin's moment of inertia was large such that inertial forces greatly dominated the aerodynamic forces associated with actuating the fin. Another issue was the inherent difficulty of supporting a fin in a cantilevered manner. One should note that a higher mode suspension resonance, at about 7 Hz, dominates the task of the ride-control system; that 7 Hz is a high bandwidth for a hydraulic actuation system of this size and power. That fact notwithstanding, there is no basic reason why such a system cannot be built; but that actuation bandwidth is the major system design determinant, having a great influence on system size, weight, and power.

Ride Control Hydraulic System Sizing Calculations

Preliminary calculation of weight and power of a ride control hydraulic actuation system has been done on a spreadsheet (in Microsoft Excel 3.0); so that any change in system parameters may be entered, and the quantitative consequences may immediately be considered. Two bases for sizing system components are used: a maximum loading basis and an root-mean-square (RMS) loading basis. RMS magnitudes are taken to be one-third of maximum magnitudes, according to estimates from earlier suspension operation calculations. Actuator parameters, stroke, diameter, flow areas, are based on maximum loadings and strokes; pump parameters, flows, power, are based on RMS loadings. This is a conventional approach in the sense that the actuators must always be prepared for maximum stroke and effort, but the pumps are almost always buffered from a maximum demand by the system accumulators. Of course, the assumption of open-center four-way valve use implies that not much pump size and capacity is saved by sizing the pumps to RMS-loaded flow and power.

A spreadsheet print, for nominal operating conditions, follows as Table C1-9. The sequential arrangement of the spreadsheet, top-to-bottom, is approximately as follows:

FIN AND FLAP CHARACTERISTICS
VEHICLE CHARACTERISTICS
FLAP KINEMATICS
FLAP FORCES
    Actuation (Mechanical) Power
    Hydraulic Power
FLAP ACTUATOR DESIGN
    Actuator Arm Length
    Actuator Weight
FLAP ACTUATOR VALVE DESIGN
    Valve Weight
FLAP ACTUATOR PLUMBING
FLAP ACTUATION SUBSYSTEM SUMMARY
    Weight
    Power
SECONDARY SUSPENSION ACTUATOR DYNAMICS
    Loads
    Rates
    Power
SECONDARY SUSPENSION ACTUATOR DESIGN
SECONDARY SUSPENSION VALVE DESIGN
SECONDARY SUSPENSION PLUMBING DESIGN
SYSTEM: ACCUMULATORS AND PLUMBING
OVERALL SUMMARY RIDE-CONTROL HYDRAULIC SYSTEM DATA
        Component-Weight Breakdown
        Sub-system Power Breakdown

Estimation of the ride-control hydraulic system weight and power is based on many details and assumptions. The following are among them:

Table C1-9
Ride control hydraulic activation system design

FIN & FLAP:			maximum	(max/3)=RMS
c	full chord, ft	4.59		
b	span, ft	3.67		
Aff	whole area, ft2	16.88		
Af	flap area, ft2	5.06		
CL (30% flap)	lift coefficient (w/o <)	1.51		
CD (30% flap)	drag coefficient (w/o <)	0.18		
δ	flap angle, radians		0.47	0.22
Wf	fin weight, lbs	27.34		
I	fin inertia, ft-lb-sec2	1.02		
VEHICLE:				
V(max)	maximum speed, ft/sec	492.13		
f	bandwidth, hz	7.00		
ω	bandwidth, sec-1	43.98		
Wc	car weight, lb	180400.00		
FLAP KINEMATICS:			amplitudes	amplitudes
δ	fin < amplitude, rad		0.47	0.22
ϕ	fin < rate, rad/sec		20.45	9.64
α	fin < accel'n, rad/sec2		899.51	424.04
FLAP FORCES:			amplitudes	amplitudes
L	lift, lb		3417.70	1611.12
D	drag, lb		190.03	42.23
sf	fin moment arm, ft	0.38		
Ma	aero moment, ft-lb		1201.89	605.44
Mi	inertia moment, ft-lb		913.76	430.75
Mt	total flap moment, ft-lb		2115.65	1036.19
Pfa	actuation power, ft-lb/sec		14422.93	3329.98
Pfa	actuation power, hp		26.22	6.05
Pfh	hydraulic power, hp		39.34	9.08
FLAP ACTUATORS:				
ps	working pressure, psi	2000.00		
d	actuator arm length, ft	0.40		
Ffa	flap ram force, lb		5289.13	
sfa	flap ram stroke, in		4.46	
vfa	flap ram speed, in/sec		98.17	
Afa	flap ram piston area, in2	2.64		
Dfa	flap ram piston diameter, in	2.45		
tfap	flap ram piston thickness, in	1.22		
Dfar	flap ram rod diameter, in	1.22		
Qfa	maximum flow rate, in3/sec		259.61	

Table C1-9 (Cont'd)

Afap	port area, in2 (p~50 psi)	0.48		
Dfap	port diameter, in (p~50 psi)	0.78		
tfaw	cylinder wall thickness, in	0.15		
tfaep	end plate thickness, in	1.39		
Wfa	flap actuator weight, lb	11.53		
FLAP ACTUATOR VALVES:				
hfav=wfav	height=width, in	4.28		
lfav	flap actuator valve length, in	6.85		
vfav	valve volume, in3	125.67		
Wfav	flap actuator valve weight, lb	37.70		
ACTUATOR PLUMBING:				
Dfat	tubing diameter, in	1.71		
(W/L)fat	tube weight/length, lb/in	0.46		
Wfat	plumbing weight (2x10 ft), lb	110.63		
FLAP ACTUATION SYSTEM:			peak	mean
Wfas	unit system weight, lb	159.86		
Wfas(t)	system weight, 4 flaps, lb	639.45		
Pfh	unit hydraulic power, hp		39.34	9.08
P4fh	hydraulic power, 4 flaps, hp			36.33
SECONDARY SUSPENSION:				
F1	lateral front force, lb	23015.95		
F2	lateral rear force, lb	7470.40		
F3	vertical front force, lb	4316.33		
F4	vertical rear force, lb	4219.67		
T5	front roll moment, ft-lb	27326.63		
T6	rear roll moment, ft-lb	31294.71		
S1	lateral front speed, ft/s	0.77		
S2	lateral rear speed, ft/s	0.35		
S3	vertical front speed, ft/s	1.71		
S4	vertical rear speed, ft/s	1.64		
R5	front roll rate, sec-1	0.05		
R6	rear roll rate, sec-1	0.03		
P1	lateral front power, ft-lb/sec	5892.41		
P2	lateral rear power, ft-lb/sec	883.96		
P3	vertical front power, ft-lb/sec	2453.19		
P4	vertical rear power, ft-lb/sec	2311.95		
P5	front roll power, ft-lb/sec	473.66		
P6	rear roll power, ft-lb/sec	305.65		
P1	lateral front power, hp	10.71		
P2	lateral rear power, hp	1.61		
P3	vertical front power, hp	4.46		

Table C1-9 (Cont'd)

P4	vertical rear power, hp	4.20		
P5	front roll power, hp	0.86		
P6	rear roll power, hp	0.56		
Pssa	suspension actuation power, hp	22.40		22.40
Pssh	suspension hydraulic power, hp	33.60		33.60
ACTUATORS:				
ps	working pressure, psi	2000.00		
Fh	horizontal ram max force, lbs	11507.97		
Sh	horizontal ram max stroke, in	6.00		
vh	horiz. ram max speed, ft/sec	0.77		
Ahsa	horiz. actuator ram area, in2	5.75		
Dhsa	horiz. actuator ram diam., in	3.61		
thsap	horiz. piston thickness, in	1.80		
Dhsar	horiz. actuator rod diam., in	1.80		
Qha	maximum flow rate, in3/sec	4.42		
Ahap	port area, in2 (p~50 psi)	0.02		
Dhap	port diameter, in (p~50 psi)	0.14		
thaw	cylinder wall thickness, in	0.23		
thaep	end plate thickness, in	1.05		
Wha	horizontal actuator weight, lb	20.30		
nWha (12 actuators)	12 horiz. actuators weight, lb	243.60	243.60	
Fv	vertical ram max force, lbs	3911.84		
Sn	vertical ram max stroke, in	6.00		
vv	vertical ram max speed, ft/sec	1.64		
Avsa	vert. actuator ram area, in2	1.96		
Dvsa	vert. actuator ram diam., in	2.10		
tvsap	vert. piston thickness, in	1.05		
Dvsar	vert. actuator rod diam., in	1.05		

Table C1-9 (Cont'd)

Qva	maximum flow rate, in3/sec	3.21		
Avap	port area, in2 (p~50 psi)	0.01		
Dvap	port diameter, in (p~50 psi)	0.12		
tvaw	cylinder wall thickness, in	0.13		
tvaep	end plate thickness, in	0.65		
Wva	vertical actuator weight, lb	5.55		
nWva (24 actuators)	24 vert. actuators weight, lb	133.29	133.29	
SUSPENSION VALVES:				
hhav=whav=hvav=wvav	height=width, in	2.16		
lhav=lvav	susp. actuator valve length, in	3.45		
vhav=vvav	valve volume, in3	16.01		
Whav=Wvav	susp. actuator valve weight, lb	4.80		
ACTUATOR PLUMBING:				
Dsat	tubing diameter, in	0.43		
(W/L)sat	tube weight/length, lb/in	0.03		
Wsat	plumbing weight (2x10 ft), lb	7.00		
Wsat+Wav	valve & plumbing unit wt., lbs	11.81		
36x(Wsat+Wav)	valve & plumbing total wt., lbs	425.09		
REMOTE ELEMENTS:				
Wtph	total wt, remote hydraulics, lbs			1441.42
Pth	total pwr, all hydraulics, hp			69.93
CENTRAL ELEMENTS:				
Vfa=Vaa	fwd, aft accumulator volume, in3	2165.29		
Rfa=Raa	fwd, aft accumulator radius, in	8.03		
tfa=taa	fwd, aft accum'r thickness, in	0.54		
Wfa=Waa	fwd, aft accumulator weight, lb	83.96		
Wfa+Waa	fwd & aft accum'r weight, lb	167.91		
Vca	central accumulator volume, in3	4330.58		
Rca	central accumulator radius, in	10.11		
tca	central accum'r thickness, in	0.67		
Wca	central accumulator weight, lb	133.01		
Wfa+Waa+Wca	3 accumulators weight, lb	300.92		300.92
Qml	main line flow, in3/sec	115.38		
Amlt	main line tubing section area, in2	3.81		
Dmlt	main line tubing diameter, in	2.20		
(W/L)mlt	main line tube wt/length, lb/in	0.76		
Wmlt	tubing weight (2x120 ft), lb	182.86		182.86
Pst	system total hydraulic power, hp			69.93
Wst	system total weight, lb			1925.20

Table C1-9 (Cont'd)

	BREAKDOWNS:			
FRACTION:	WEIGHTS:			
0.02	4 flap actuators, weight, lb	46.12		
0.08	4 flap valves, weight, lb	150.81		
0.23	flap system plumbing weight, lb	442.51		
0.33	flap actuation system weight, lb		639.45	
0.13	12 hor. susp. actuators, weight, lb	243.60		
0.03	12 hor. susp. valves, weight, lb	57.65		
0.07	24 ver. susp. actuators, weight, lb	133.29		
0.06	24 ver. susp. valves, weight, lb	115.31		
0.13	susp. system tubing weight, lb	252.13		
0.42	susp. actuation system weight, lb		801.98	
0.09	peripheral accumulator wt, lb	167.91		
0.09	central tubing wt, lb	182.86		
0.07	central accumulator wt, lb	133.01		
1.00	hydraulic system total weight, lb		**1925.20**	
	POWERS:			
0.52	flap actuation average power, hp	36.33		
0.48	suspension actuation power, hp	33.60		
1.00	hydraulic system total power, hp		**69.93**	

Flap weight estimate is based on a heavy aircraft-type aluminum structure with skin thickness about .063 inches and substantial framing.

For the calculation of fin and suspension kinematics and dynamics (speeds and forces), a narrow-band process at around 7 Hz is assumed to dominate the excitation and response spectrum. This characterizes the spectrum made available for this work.

Lift and drag coefficients for the aerodynamic ride control surfaces are calculated as averages of multi-term characterizations over the angle of attack range. Lift is taken to be proportional to angle of attack; drag proportional to the square of angle of attack.

Actuators are sized according to strength requirements but with a generous safety factor, making for relatively stiff and sturdy units. The flap actuators are proportioned to have a stroke that is about 1.8 times the cylinder bore. The freedom to proportion the cylinders in this way is provided by choice of the flap bell crank length. Shortening the bell crank calls for an actuator of greater diameter and reduced stroke, for example. Actuator end plate dimensions are based on strength needs, plus a need to accommodate substantial flow ports to handle displacement and bandwidth requirements. Valves are sized according to port-size and plumbing-diameter requirements. Here again, force and bandwidth requirements dominate the sizing of these components. The bases for sizing the plumbing, connecting the components across the length and breadth of the vehicle, are stated earlier. No independent consideration of rigidity of the actuators, or the other components, has been done.

Accumulators are sized to contain at least several seconds' supply of pressurized hydraulic fluid. Their weight is based on an assumption of steel construction.

Conventional hydraulics components make significant use of ferromagnetic materials; primarily cast iron, and cast and rolled steels ranging from high carbon steels to specialty tool steels. While it is understood that a material's ferromagnetism is an issue, consideration of component weight is based on an assumption of the use of steel. There are at least three materials issues in addition to that of a material's ferromagnetism: component strength, component stiffness, and valve spool-to-valve bore wear. Certain non-ferromagnetic stainless steels may successfully substitute for steel where material hardness or wear are no issue. Some components could perhaps be of titanium. Small ferromagnetic linings of valve body bores may be acceptable and useful.

This report is not to address detail design of hydraulic actuation components, but rather to estimate their weight and power. It is suggested that component weights will be approximately those of conventional ferromagnetic hydraulic components.

Effect of Actuation System Bandwidth on System Weight and Power

Increasing the frequency response of the ride-control hydraulic actuation system affects component weight and system power in at least two ways: increasing the effect of any inertial loading of actuators, inertial loading being proportional to the square of bandwidth; and increasing the physical size and weight of flow-handling components, to accommodate flows that increase in proportion to bandwidth. To emphasize and make clear these effects, the spreadsheet simulation has been interrogated to find how ride-control hydraulic actuation system weights and powers vary

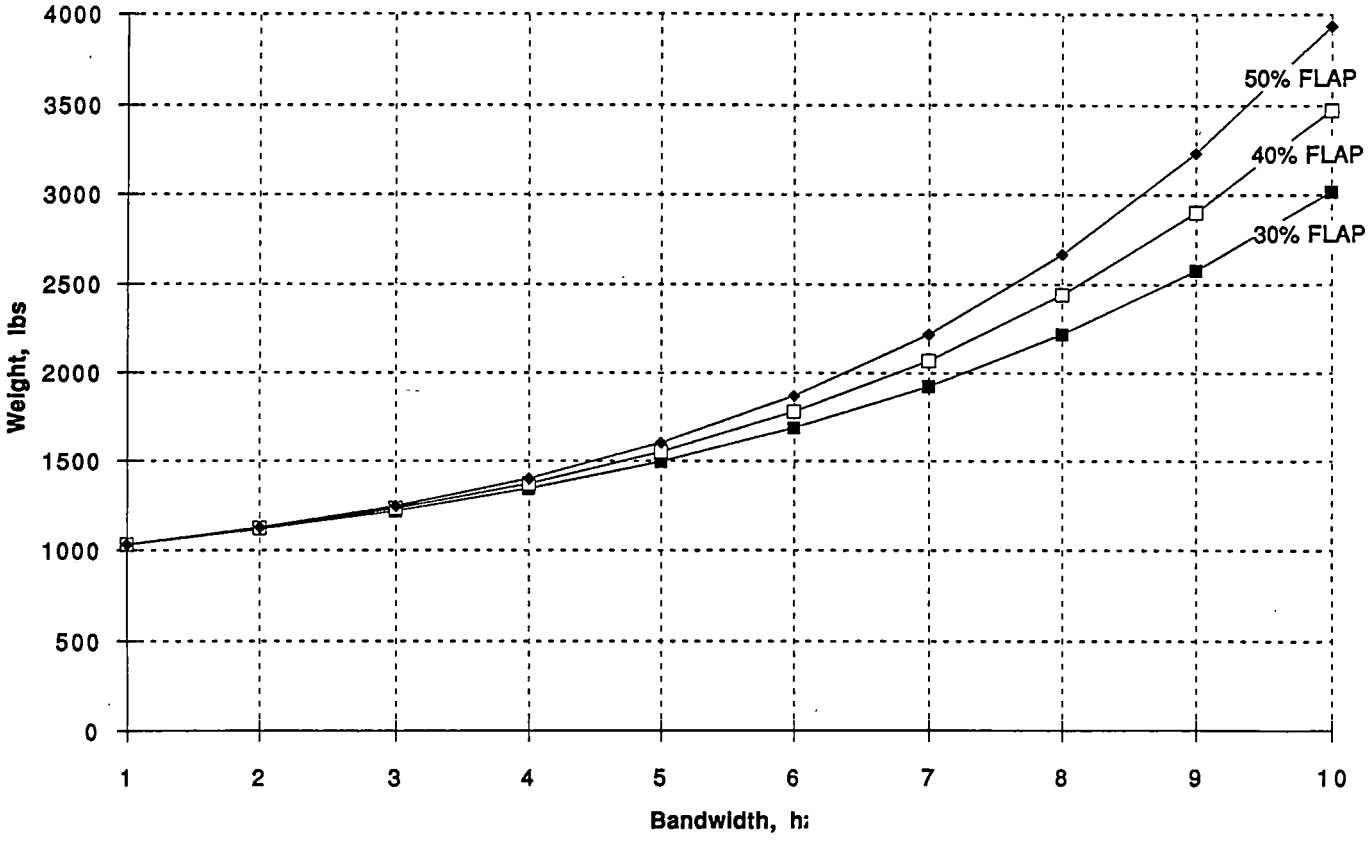

Figure C1-22 Hydraulic system weight as a function of bandwidth

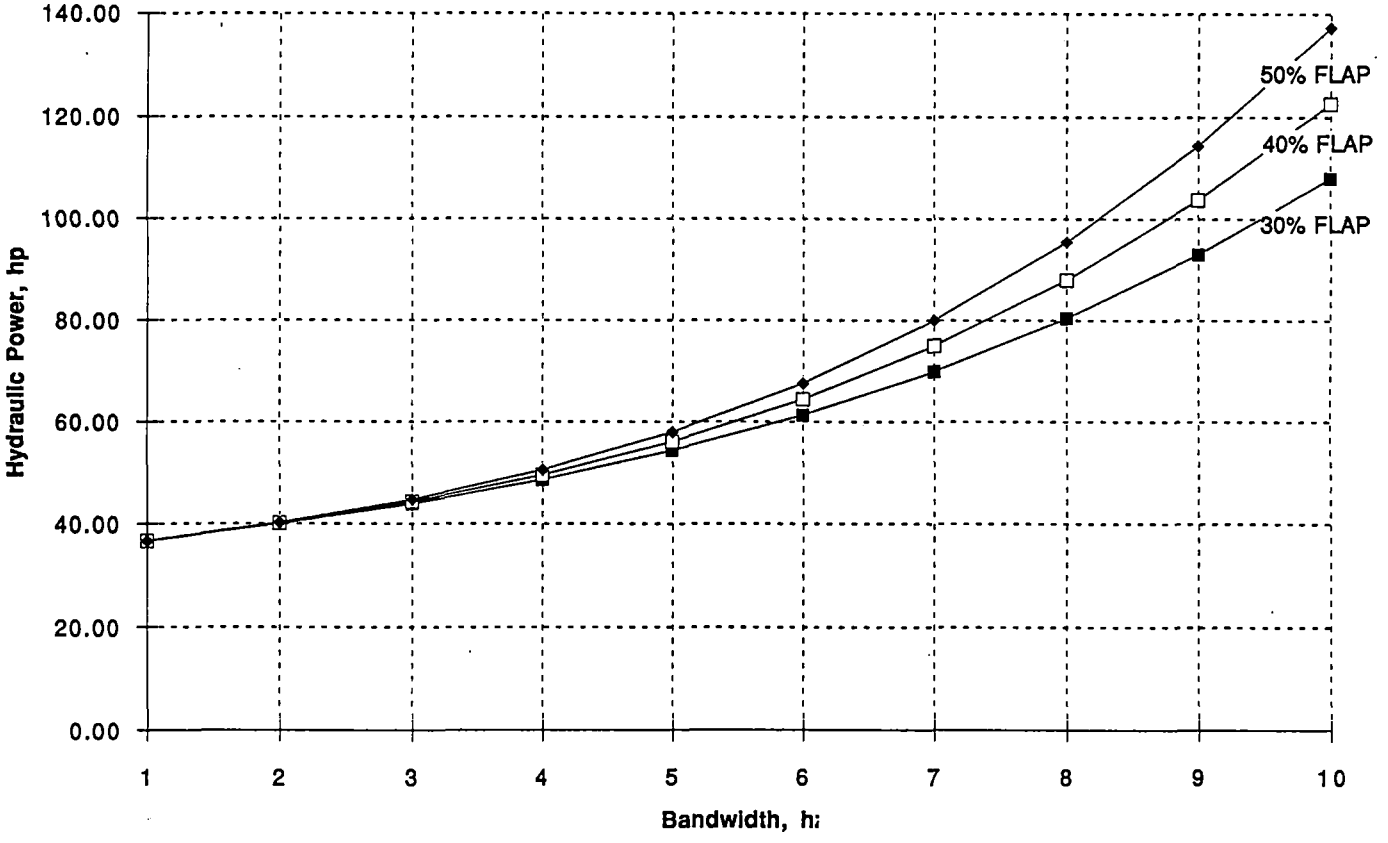

Figure C1-23 Power as a function of bandwidth

as a function of bandwidth, from 1.0 to 10 Hz, and as a function of flap fraction, from 30 percent to 50 percent. The results for system weight are presented in Figure C1-22; the results for system power in Figure C1-23. Examination of the graphs shows clearly the strong dependence of the ride-control hydraulic actuation system on system bandwidth.

System Weight and Power

The system weight and hydraulic power (pressure-flow rate product delivered to the hydraulic lines) of a ride-control hydraulic actuation system for nominal conditions, including a 7 Hz response bandwidth, are approximately:

	English:	Metric:
Weight:	1925 lbs	875 g-kg
Power:	70 hp	52 kW

1.5 ON-BOARD POWER

1.5.1 On-board power system

Overview

The on-board power system provides electrical power to the maglev vehicle's subsystems, namely lighting, control/communication electronics, hydraulics, HVAC (heating, ventilating, and air conditioning), air compressors, galleys, lavatories, and minor other electrical loads. The term "onboard" does not imply that the power source itself is onboard the vehicle, though that is the case in our vehicle concept. The term "onboard" pertains to the power distribution system that is onboard the vehicle and provides for vehicle onboard loads as opposed to propulsion power. Propulsion power dwarfs on-board power in comparison, and is provided from an electric utility company via inverters and linear synchronous motors along the guideway.

General Arrangement

Figure C1-24 shows the schematic diagram of the on-board power system. Since this is a concept definition study, circuit breakers and wire sizing and other essential power circuit design details have not been provided. We have divided the power circuit into two separate circuits (port and starboard) in order to increase redundancy and fault tolerance of the vehicle. Half the power system capacity and circuitry will still serve all of the essential electrical loads.

A crossover device will allow all loads to be served, at reduced capacity, if a failure in one of the two circuits is of a nature to allow such a crossover. If such a crossover is not possible due to the nature of the failure, half capacity operation of the subsystems is still possible because all of the subsystems are dual. There are two HVAC systems, two air compressors, two hydraulic pumps, two lighting circuits, two (two of everything), just so that an electrical failure in any one component is less likely to disable the vehicle.

Although failures in the electrical components might allow operation at only half capacity of a certain subsystem, the fuel cells each have a 30 percent continuous overload capacity. By running some subsystems at overload conditions for a period of time, or by running them at typical conditions (25 ° C, 350 kph) instead of extreme conditions, in many instances the vehicle will not be at all disabled by the failure of a component. This is a major benefit of having excess on-board power capacity.

Saving vehicle weight was a high priority design guideline from the beginning, so our first pass at specifying the electrical system started with the assumption of higher voltage and frequency than residential 220 volt ac 60 hertz power. Higher frequency machinery (higher speed machinery) means less weight. Three phase power means less weight than single phase. Higher voltage circuitry means less weight of cabling and connection equipment (up to a reasonable limit). We picked an alternating current system to avoid complex motor inverters and to save weight. We picked 400 Hertz because it has widespread use in aircraft where the weight factor is also crucial, yet 400 Hz is not so high a frequency that building motors to use it becomes troublesome. We picked three phases due to the widespread acceptance and engineering knowledge of three phase systems. We picked 440 volts because its insulation system is about as reliable as 220 or 208 volt systems, yet this well-known nominal voltage is not so high that unusual insulation and cabling requirements must be met.

Some of the minor vehicle loads are single phase loads which are better served by single phase instead of three phase, even if at 400 Hz. These include lighting, galleys, lavatories, running lights. Transformers are shown in Figure C1-24 that serve these minor loads.

There are two main circuit types serving the vehicle loads: the normal load bus and the emergency load bus. These are not to be confused with the port and starboard systems; each of those has a normal and an emergency bus.

Power Source

Many alternative power source approaches were evaluated before we made our decision to employ fuel cells. See the report section entitled "On-board Power Production" for a full description of our fuel cell power source and the many alternatives that we evaluated. A summary of some of the features of the fuel cells are:

- Dual 93 kW fuel cell units
- Surge batteries for load variations
- Methanol reforming PEM type
- Power density close to that of a spark ignition engine
- Noiseless, odorless, reduces regulated emissions by 90 percent, virtually no CO
- Operates at only 80° C

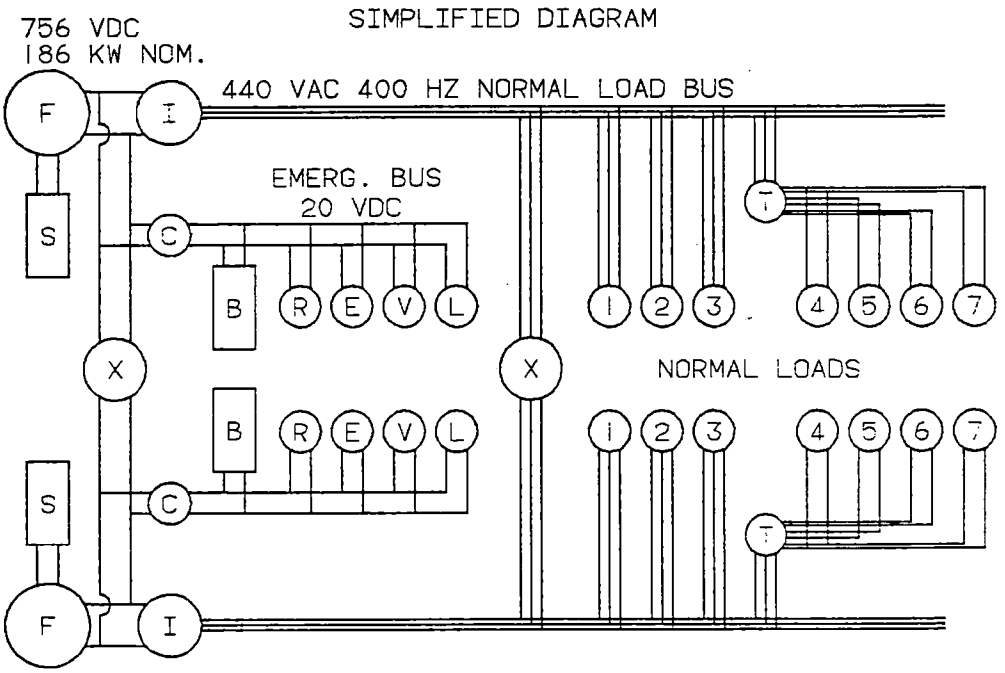

F=FUEL CELL SYSTEM
S=SURGE BATTERIES
I=INVERTER
C=CHARGER
B=BATTERIES
R=RADIO(S)
E=ELECTRONICS/COMPUTERS
L=EMERGENCY LIGHTS
V=DC VENTILATING FAN
X=CROSSOVER CIRCUIT
T=440/110VAC TRANSFORMER

1=HYDRAULIC PUMP MOTOR
2=HVAC MOTORS
3=AIR COMPRESSOR
4=CABIN LIGHTING
5=GALLEYS
6=LAVATORIES
7=RUNNING LIGHTS

Figure C1-24 Electrical system components

- High (50%) thermal efficiency
- Continuous 30% overload capacity
- Entails advanced proprietary technology from GM's electric vehicle programs

Normal Bus Loads

Loads that are required for normal vehicle operation are connected to the normal load bus. The loads are specified for full vehicle speed (requiring maximum hydraulics system power) and extreme weather conditions (50 ° C, 90 percent relative humidity), so that the average operating condition will be less than what the normal bus is sized for. The normal loads were sized individually. Derivation of the kilowatt demand of the larger individual loads in the following table can be found in the appropriate sections of this report. This table is for the **total vehicle**, and not just for each normal bus.

Normal loads

Hydraulics (500 kph)	65 kW
HVAC (50 C, 90% r.h.)	94
Galleys	10
Overhead lights	8
Running lights	3
Electronics	2
Lavatories	4
Total	186 kW

These normal bus loads are for extreme conditions. The typical load might have no running lights (daytime), about half the hydraulic power requirement (350 mph), and almost no HVAC requirement. Such loads should be used if studying annual fuel cell costs, for instance.

Typical loads

Hydraulics (350 kph)	33 kW
HVAC (25 C, 60% r.h.)	6
Galleys	3
Overhead lights	8
Running lights	0
Electronics	2
Lavatories	1
Total	53 kW

Emergency Bus Loads

Loads that are required in an emergency are on the small 20 v dc emergency bus. Some of these loads, such as control computers, electronics, and radios are loaded on the emergency buses all the time, but are placed on those buses because they are less likely to be out of service. Each emergency bus is so small we can still call the on-board power system a "440 Vac 3 phase" system. The following table defines the emergency loads **for either emergency bus.**

Emergency loads

Ventilating fans (dc motors on same shafts as 440 volt ac motors)	3 kW
Emergency lights	1
Electronics	1
Total	5 kW

Because there are two emergency buses and two sets of emergency equipment, it would take a total failure of both fuel cells or their distribution circuits, and total failures of both emergency battery sets or their distribution circuits, for the vehicle to be without emergency power. Even then, some of the emergency equipment would have its own built-in batteries or uninterruptible power supplies.

The emergency batteries are connected to the output of the battery chargers which actually feed the emergency bus during normal conditions. See the report section entitled "Emergency On-board Power" for more information .

Essential Loads

Here we define essential loads as the loads required to keep the vehicle and its passengers moving comfortably, even if at a somewhat reduced speed capacity. The vehicle must maintain power for control and communication electronics, hydraulics (to smooth out the ride), air compressors (if the air tanks are depleted, which should not happen), cabin lights, HVAC (ventilation fans only), and running lights (if at night). We concluded that galleys and lavatories were the only loads that should be shed completely. Instead of determining how much power was required for each of these loads, we took a pragmatic approach. We sized many of the essential loads at half the normal capacity to match the instances when one normal load bus or motor goes out of service, and to match our approach to providing "two of everything." The following table defines our essential loads.

Essential Loads

Hydraulics	33 kW
Ventilating fans (both)	6
Overhead lights	4
Running lights	1
Electronics/Radios	1
Total	45 kW

1.5.2 On-Board Power Production

Overview

The previous section, On-board Power System, defines the maglev vehicle's on-board electrical power requirements to be 186 kW mainly at 440 V, three phase. That section also explains the various circuitry and loads for the vehicle, with only minor discussion of the on-board power production source itself. This section describes several different ways of producing that electrical power. Please note that the baseline design uses fuel cells for this power production, and that the power being discussed is not intended to propel the vehicle but merely run its on-board loads such as lights, galleys, heating, air conditioning, hydraulics, and air compressors.

Arriving at the conclusion to use fuel cells required weighing several alternative methods and selecting the best alternative. Substantial information is presented about the alternatives, in order of least preferred to most preferred, so that the selection tradeoffs can be understood.

Some options for producing the on-board power include the following:

1. Energy storage
2. Power cable link
3. Sliding electrical contact
4. Linear generator
5. Linear transformer/inductive pickup
6. Wind turbine
7. Engine generator set
8. Fuel cells

These options, with their respective benefits and drawbacks, are discussed in this section. Again, please note that the fuel cell option has been selected for our baseline vehicle design, and all information about the alternative choices is presented in order to document our work and to put our choice of fuel cells in the proper perspective.

Alternative #1 – Energy Storage

A number of possible approaches which have been considered rely upon their initial energy content to provide continuous on-board power over a 3-hour period without energy transfer from

the guideway. The approaches include inductive energy storage (SMES), capacitive storage, battery storage, mechanical storage (springs, flywheels), thermal energy storage, compressed/liquefied air, and explosives. None of these technologies provides the required energy storage capacity within reasonable weight or volume limitations. The stored energy required to meet the needs of one maglev trip is formidable. The following calculation shows how the energy requirement for a 3-hour trip is established:

186,000 W/kW x 3 hours x 3600 s/hr = 2.008E+9 Joules or 2 Gigajoules

Fuel-based power sources are not included in this stored-energy category of on-board power sources even though stored chemical energy might be considered to fall into this category; fuel-based on-board power systems of several types are considered.

The following table shows the masses derived from Reference 1 for several of the stored energy systems that were considered. The numbers apply to energy storage and conversion systems for in-field military applications.

Description	Mass, kg	Volume, m^3
Flywheel in vacuum chamber	20,000	5
Magnetic/inductive (SMES type)	200,000	20
Capacitive	4,000,000	2,000,000,000
Batteries	20,000	N/A

Alternatives other than those listed in Reference 1 were considered as well. Rough calculations give the following results for three additional alternatives:

Description	Mass, kilograms	Volume, cubic meters
Compressed/liquefied air	45,000	485
Springs	506,000,000	64,516
Thermal energy (heated H_2O)	31,000	8

Fuel cell parameters in Reference 1 imply an on-board power system with a mass of 2,000 kg and a volume of 2 cubic meters. Advances in fuel cell technology since Reference 1 was written in 1989 have changed the picture for fuel cells. The fuel cell system that was eventually selected for the maglev vehicle has a mass of 1,210 kg and a volume of 1.74 cubic meters.

Alternative #2 – Power Cable Link

Another approach to generating on-board power would be to utilize magnetic fields from the high voltage +/-15 kVdc power cables that run from one inverter to another. The present plan is to bury these cables or run them beneath the guideway beam, but we considered running them on top of the guideway beam (protected) in order to create an on-board power source. Obviously, it is difficult to mount 15 kV equipment on the beam, but the cables forming this power cable link could be specialized, extra dc cables at very low voltage whose sole function is to create on-board power. Such a dedicated arrangement would effectively be a weak inductive pickup system.

The 15 kV dc lines present on the guideway are the power cables from substations to the inverters located along the guideway. These cables carry approximately 300 A at all times. The use of these cables for producing on-board power might be a significant cost-savings compared with installing specialized coils in the guideway. Investigation of the possible use of these cables requires looking at the following:

- Physical location of power cables and windings on vehicle
- Magnetic field produced by these cables
- Power generation requirements
- Physical limitations

Power cable link: configuration of equipment. To produce the maximum magnetic field close to the vehicle, the cables must be located as close to the vehicle along the guideway as possible. The cables cannot be located close to the ladder. If they were, the superconducting magnets would react against them and produce large, pulsating forces that would shake the vehicle. The only remaining location available to put the cables is along the top of the guideway. The cables would be located in the magnetically neutral plane in the center of guideway. The cables would crisscross every quarter meter (0.25 m) as illustrated below:

DC cables installed on top of guideway

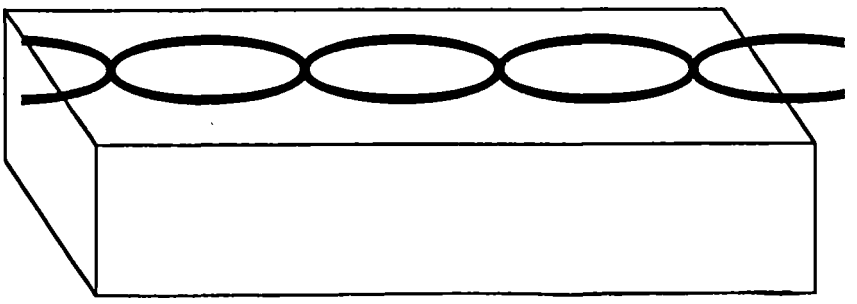

Since current flows from left to right in one of the cables, and from right to left in the other cable, current loops and associated north and south magnetic poles are formed. These magnetic poles can be used to generate electrical power in the vehicle.

The power link coils mounted on the vehicle would be attached to the underside of the vehicle located between bogies. There would be a total of five sets of coils mounted on the vehicle. The mean distance between the cables and the coils would be approximately 5 cm and the width of the cable loops would be approximately 30 cm. The polarity of the magnetic field is reversed in each loop because of the orientation of the wires. The changing flux linkage between this field and the coils on the vehicle is due to the motion of the vehicle. On-board power produced by this method would be proportional to vehicle speed and current in the 15 kV cables.

One might compare the power cable link approach to the inductive pickup approach where dc magnets on the guideway produce alternate north and south field regions. The two approaches are similar in many respects. We have not evaluated such a power transfer device because it would be similar in cost and size to the linear transformer approach, which will be discussed later in this same report section.

Power cable link: magnetic field produced by the cables. A cross section of the guideway and the cables and their magnetic field is shown below:

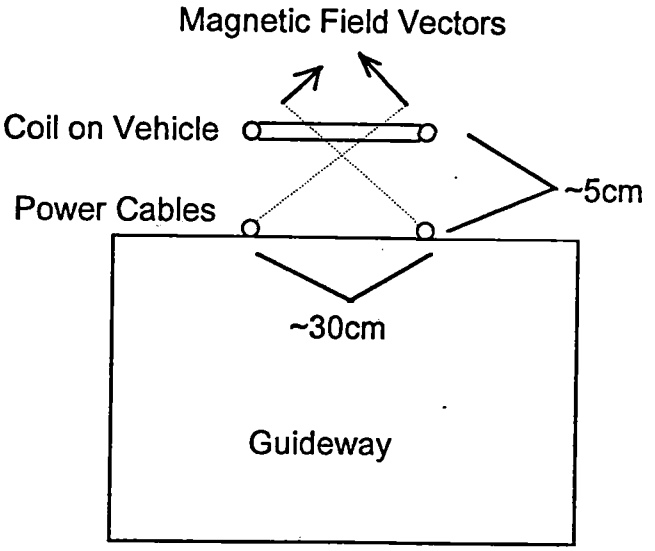

In computing the average magnetic field strength through the pickup coils on the vehicle, only the magnetic field components perpendicular to the coil's horizontal axis are important. The calculations for the power cable link that are found in the appendix are generous approximations and simplifications for calculating the field and induced voltage in the coils. Many refinements could be made; however, the computations give a good indication of the unfeasibility of this concept.

The calculated voltage per turn (84 mV) is a weak voltage level. As shown in the appendix, the mass of any type of pickup coil discussed in the report section is

$$M_w = \frac{445 L_t}{V_t} \qquad \text{(Eq. 1)}$$

where M_w = winding mass, kilograms

L_t = length of each winding turn, meters

V_t = volts generated per coil turn, volts

It may seem surprising that the turns, wire size, output voltage and current, and other parameters are not factors of this equation. Studying the derivation shows how these factors drop out of the equation by specifying 186 kW, output voltage, and current density allowed.

The length of each turn on the vehicle pickup coil is 3.14x0.25=0.785 meters, so the mass of the vehicle coils per equation 1 is 445x.785 / 0.012 = 29,110 kg. Not only is this too heavy, but the space required for this much copper wire simply is not available. And all this is at the vehicle speed of 150 m/s; lower speed operation gives proportional reductions in capacity. For these reasons we eliminated the power cable link approach to on-board power generation.

The pickup coils could be a little closer to the guideway which would result in a net decrease in the weight. This distance is primarily restricted by the vertical movement of the vehicle. It is not believed that the distance between the coils on the guideway and the pickup coils could be safely decreased to the point of making the power cable link units physically small enough or light enough to fit the vehicle.

Alternative #3 – Sliding Electrical Contacts

It would be possible to transfer auxiliary electrical power into the maglev vehicle via a third rail, catenary, or other frictional sliding arrangement. These approaches are commonly used for

transferring propulsion power to transit cars and electric passenger locomotives, so the 186 kW power requirement is not a limitation on such an approach. There are several other obvious factors that take precedence, as follows:

Transferring power at the full vehicle speed of 500 kph makes the approach different from its present applications. It would be expected that at such a high speed, the pickup equipment on the vehicle and the guideway would wear out quickly.

At 500 kph, maintaining contact between vehicle and guideway halves of the pickup would be difficult. If occasional bouncing of the pickup could be tolerated, then the associated wear problems are aggravated, and electromagnetic interference (EMI) problems become more severe.

Safety concerns of such an approach are heightened. One way to mitigate this is to choose as low a voltage as possible, placing more emphasis on the current collection design of the pickup equipment as opposed to the voltage design factors.

The cost of this approach is high because pickup equipment must be provided on virtually the entire guideway length.

Some of these concerns could be lessened if the vehicle were not required to pick up power at full speed, but only up to some fraction of full speed instead. For the sake of discussion, let us assume that the sliding contact approach is used up to 350 kph, and above that speed the pickup mechanism on the vehicle is lifted or otherwise physically disconnected from its guideway counterpart. Most likely batteries would be employed to run the on-board power system above 350 kph, which does have merit in the case of a system which closely follows an interstate highway and therefore goes up and down in speed often in order to go around the many associated curves. The resulting dependence upon batteries would increase vehicle weight and thereby further increase system cost. In addition, the amount of power transfer must necessarily increase, and the batteries must be able to take a very, very fast charge during the power transfer times. This approach cannot be entirely discounted without in-depth study of hybrid systems, but we regard this approach as unviable due to the many obvious technical headaches associated with it.

Alternative #4 – Linear Generator

The linear generator in the context of this report is a device which uses the currents induced in the levitation ladder rungs on the guideway for producing on-board power. In concept, the currents in

the stationary ladder rungs produce a varying magnetic field with respect to the moving vehicle, due both to the variations in the current with time and the changes in the rung-to-generator-coil proximity as the vehicle moves past the ladder. This magnetic field is linked by simple nonrotating coils of copper wire on the linear generator mounted on the maglev vehicle. As the magnetic field is varied by varying currents in the ladder rungs and by varying distance of the coils from the rungs, voltage is induced in the coils of the linear generator. This voltage would be fed into a rectifier/inverter for use on the vehicle.

No additional equipment would be required on the guideway or on the ground; the present ladder arrangement would provide the on-board power, almost for free. There is no such thing as "free power," though. The on-board power would be derived indirectly from the linear synchronous motor which would have to overcome the increased drag due to the linear generators; however, this would be an extremely economical way to pick up the on-board power because the LSM power only costs 8.5 cents per kilowatt hour in this SCD.

Important aspects of the linear generator design include the following:

- Linear generator location on the vehicle
- Magnetic field intensities and the magnitude of their variation in the location of the linear generator
- Power generation requirements
- Weight and size limitations

Linear Generator: location. To make the best use of the varying magnetic field produced by the currents in the ladder, the linear generator would have to be as close to the ladder as possible. The location decided upon for the linear generator was the one-meter space located between bogies along the sides of the guideway. One might observe that placing the linear generator coils directly between the superconducting magnets and the levitation ladder would result in the closest proximity to the highest ladder currents, but this is not feasible for two reasons:

- The superconducting magnets would have to be moved farther away from the levitation ladder in order to make space for the linear generator. This would degrade the performance of the levitation/guidance/propulsion apparatus.
- The ac currents in the linear generator would couple magnetically into the superconducting magnet coils and its cryostat and cause additional heating losses in them, degrading magnet performance.

It is envisioned that there will be one linear generator in each space between each side of each pair of bogies for a total of 10-units. Having 10-units would increase the redundancy and fault tolerance of the on-board power system. To minimize the parasitic ac currents induced into the superconducting coils, the coils of the linear generator would optimally be located midway between bogies. The surface of the linear generator closest to the ladder would be 5 cm away, the same distance as used for SCM to guideway clearance. The dimensions for each unit, containing many power pickup coils each, would be 90 cm high, 60 cm wide, and 9 cm thick. An individual pickup coil was sized at 30 cm high by 9 cm deep. These dimensions were chosen based upon the physical space available between the bogies, the size of the levitation ladder and the desire to have the linear generator as close as possible to the ladder. Magnetic field strength decreases in proportion to distance from the source so minimizing the distance from the ladder was crucial. The space allocated to the linear generator is illustrated below:

Side view of Linear Generator Location

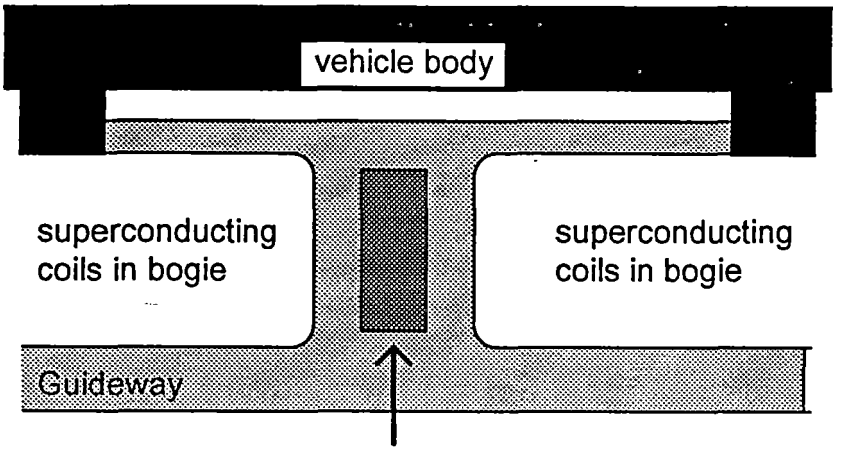

Linear Generator Coil Set Location

Linear Generator: magnetic field intensities and variation near the ladder. The varying currents in the ladder near the linear generators, in addition to the proximity and orientation of the pickup coils with respect to the ladder rungs, directly determine the varying magnetic field intensities. The change in flux linked by the linear generator pickup coils is directly proportional to the generator output voltage and power capacity.

The magnitude of the currents in the ladder was generated from results of an analysis by MIT. Dynamic circuit theory (Reference 2) was used to model the ladder behavior, along with a field analysis of four racetrack coils based on stick models (i.e., the Biot-Savart law). By superpositioning two sets of solutions, the currents in the interbogie space were derived from the MIT results. These currents are illustrated in Figures C1-25 through C1-29. In all of the graphs,

the rail and rung currents of interest are in the central part of the graphs, between rungs 16 to 22, since that is the interbogie space available for the linear generator coils.

These graphs illustrate the ladder currents when the superconducting coil centerlines are aligned with a rung of a ladder, or halfway between rungs (space centered). The power that can be extracted from these currents is proportional to the magnitude of change in them as the superconducting coils move from being rung centered to being space centered. The currents illustrated are currents induced in the ladder when the vehicle is moving at 150 m/s or 540 kph, since that case is what MIT provided. One can see that the rung currents vary more than the rail currents, so the rung currents were chosen as the power source.

The following diagram of the ladder illustrates the coordinate system used throughout this analysis:

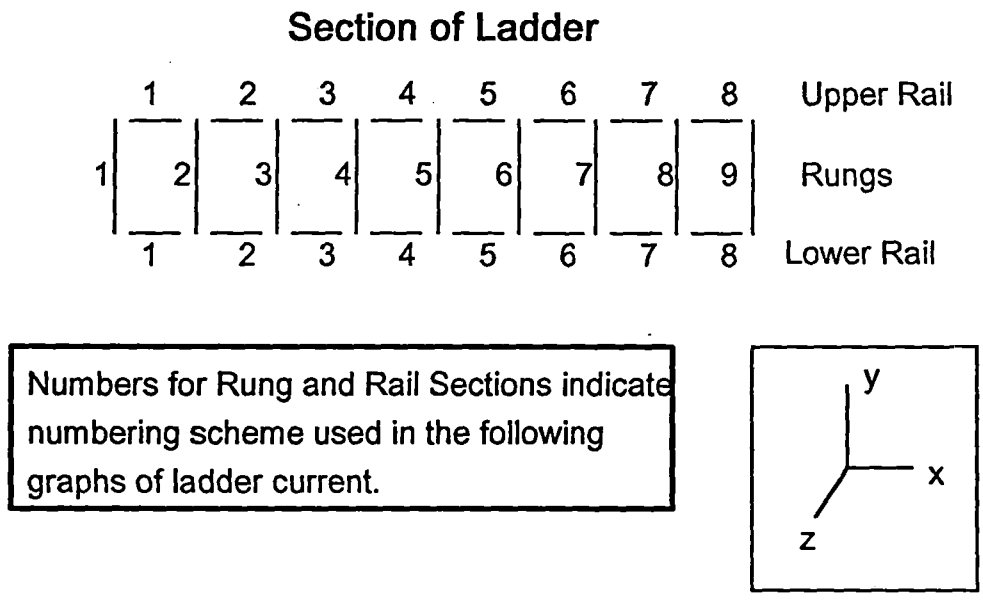

The currents in the rungs change significantly more than the currents in the rails in the ladder next to the linear generator. Thus, the maximum changing flux linkage can be obtained by coils in a vertical plane perpendicular to the ladder, i.e., in the yz plane. In the section of the ladder closest to the linear generator, the currents undergo a maximum change of approximately 1 kA when changing from rung-centered to space-centered. Figure C1-29 shows rung current versus time for rung 19, the middle rung. Although plus and minus 12 kA peaks are seen, those peaks never occur near the pickup coil but instead occur near the SCMs. As the strong currents arrive at each rung, the pickup coil has moved away.

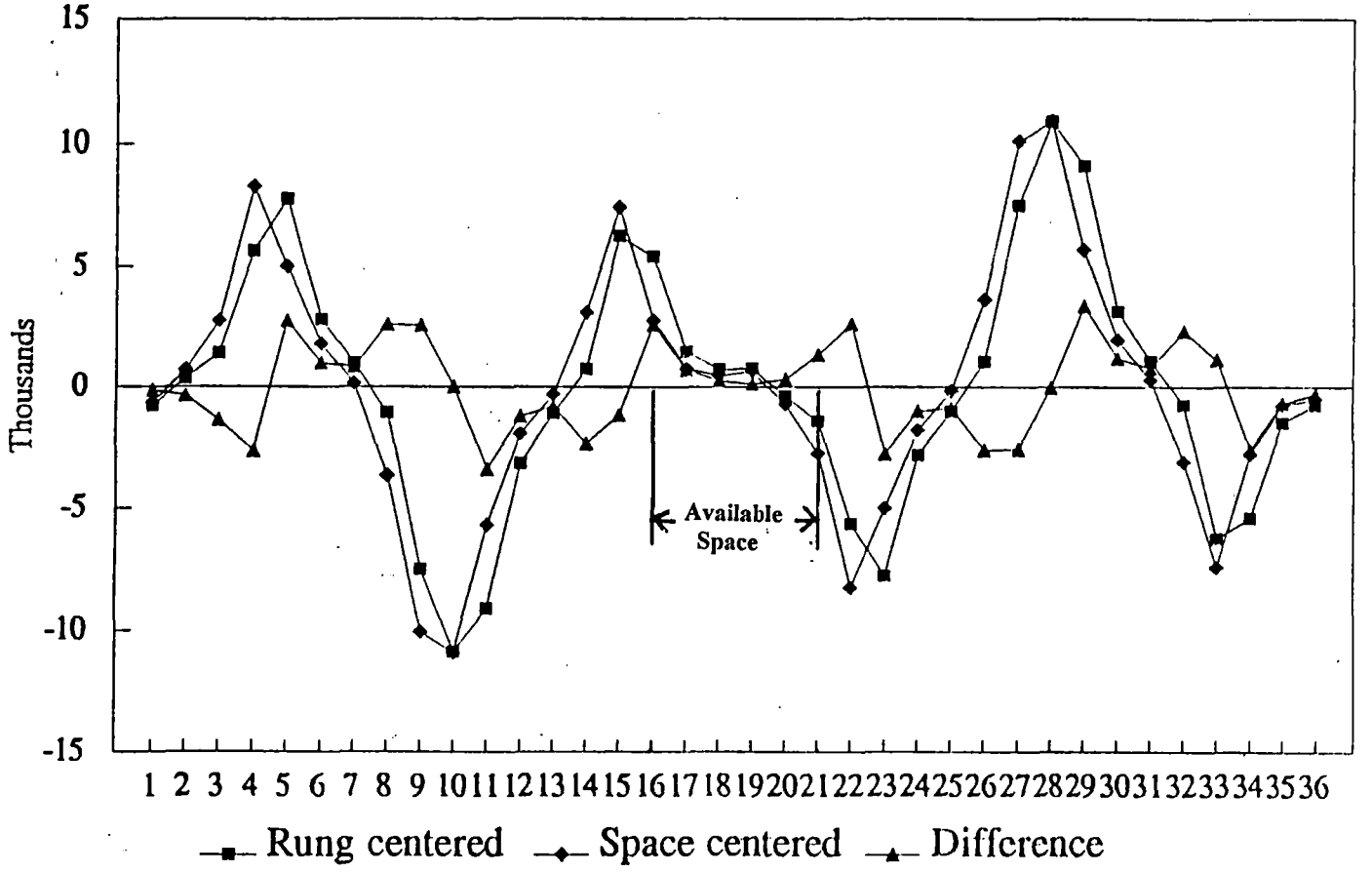

Figure C1-25 Rail currents

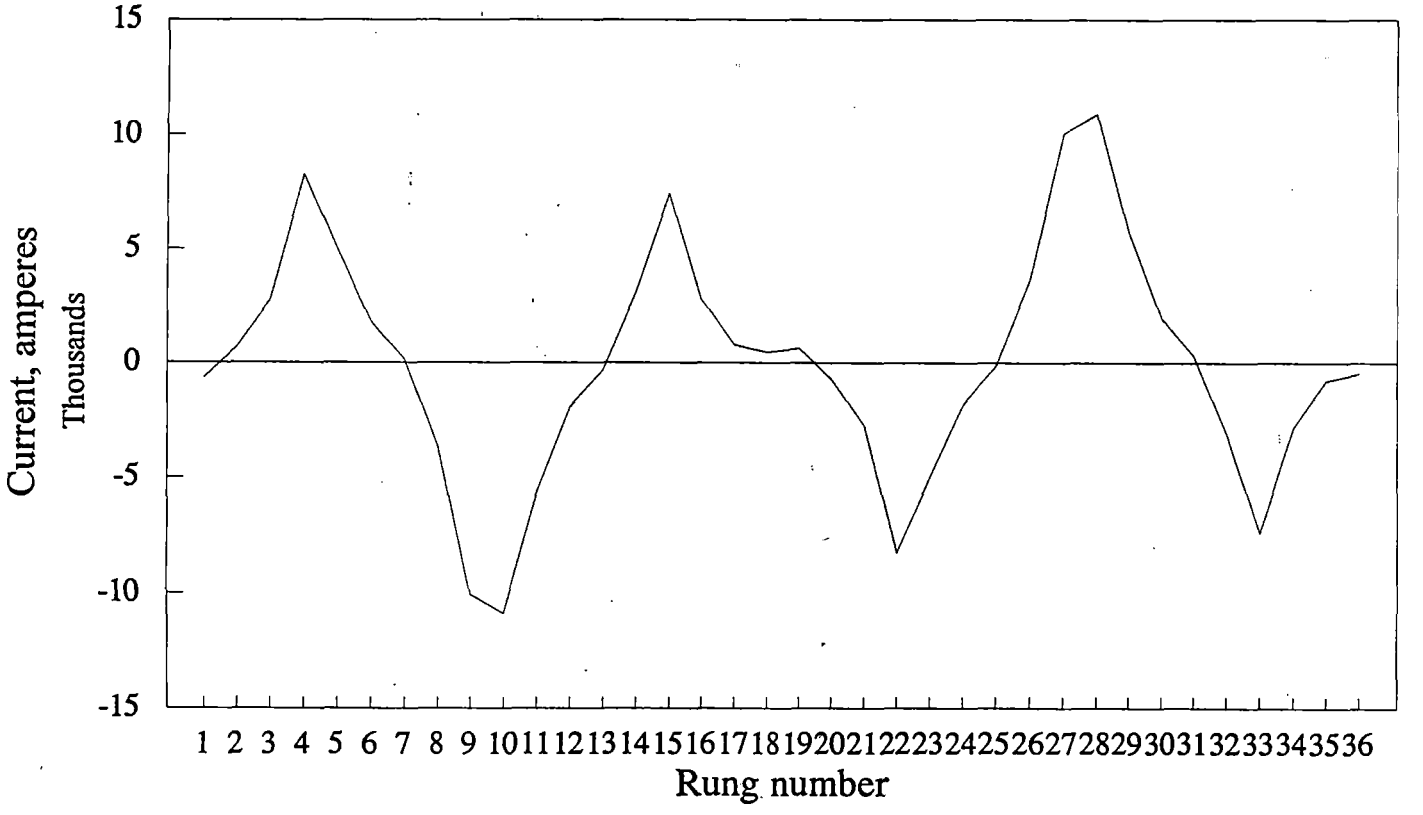

Figure C1-26 Rung currents – magnet centered on loop 19

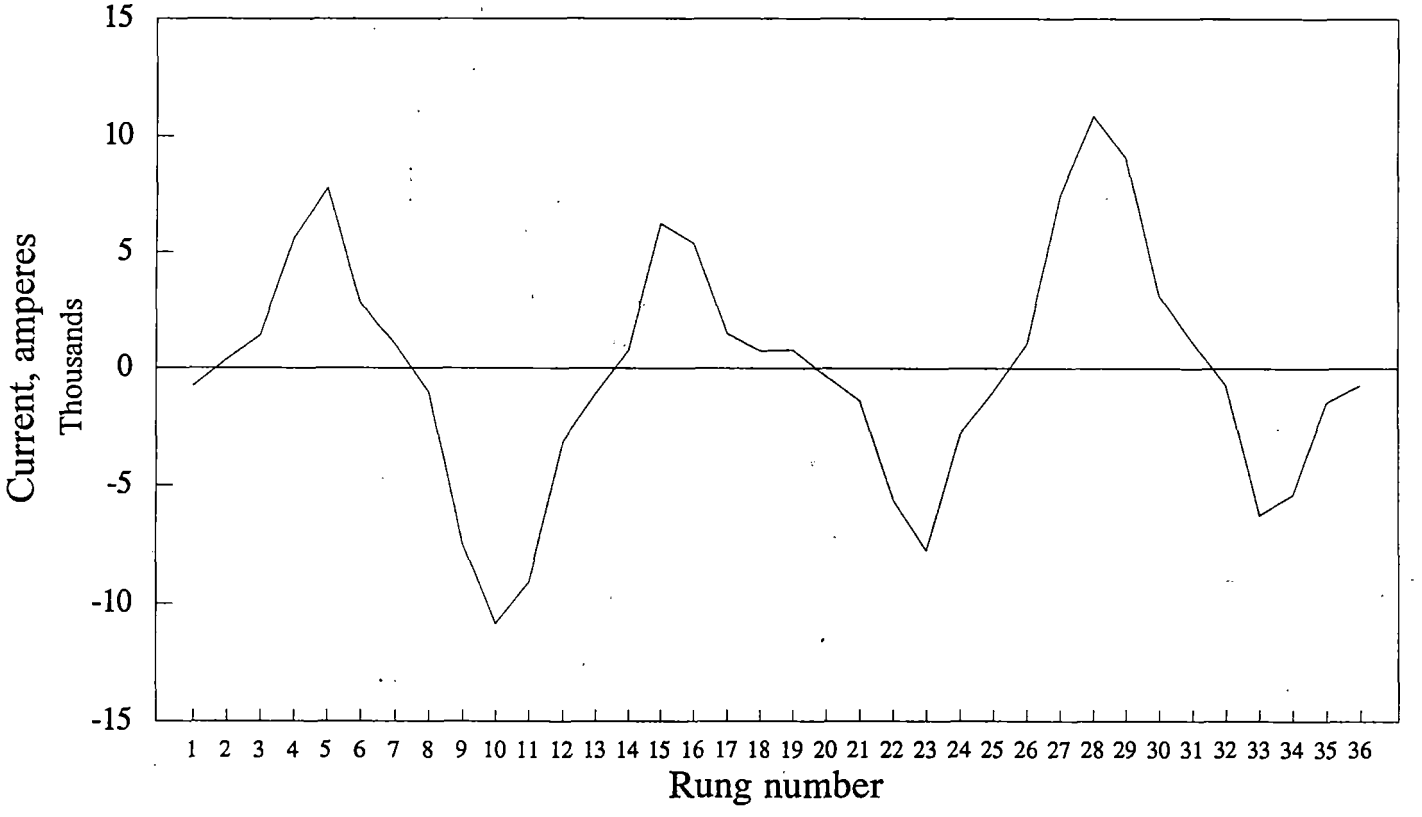

Figure C1-27 Rung currents – magnets centered on rung 19

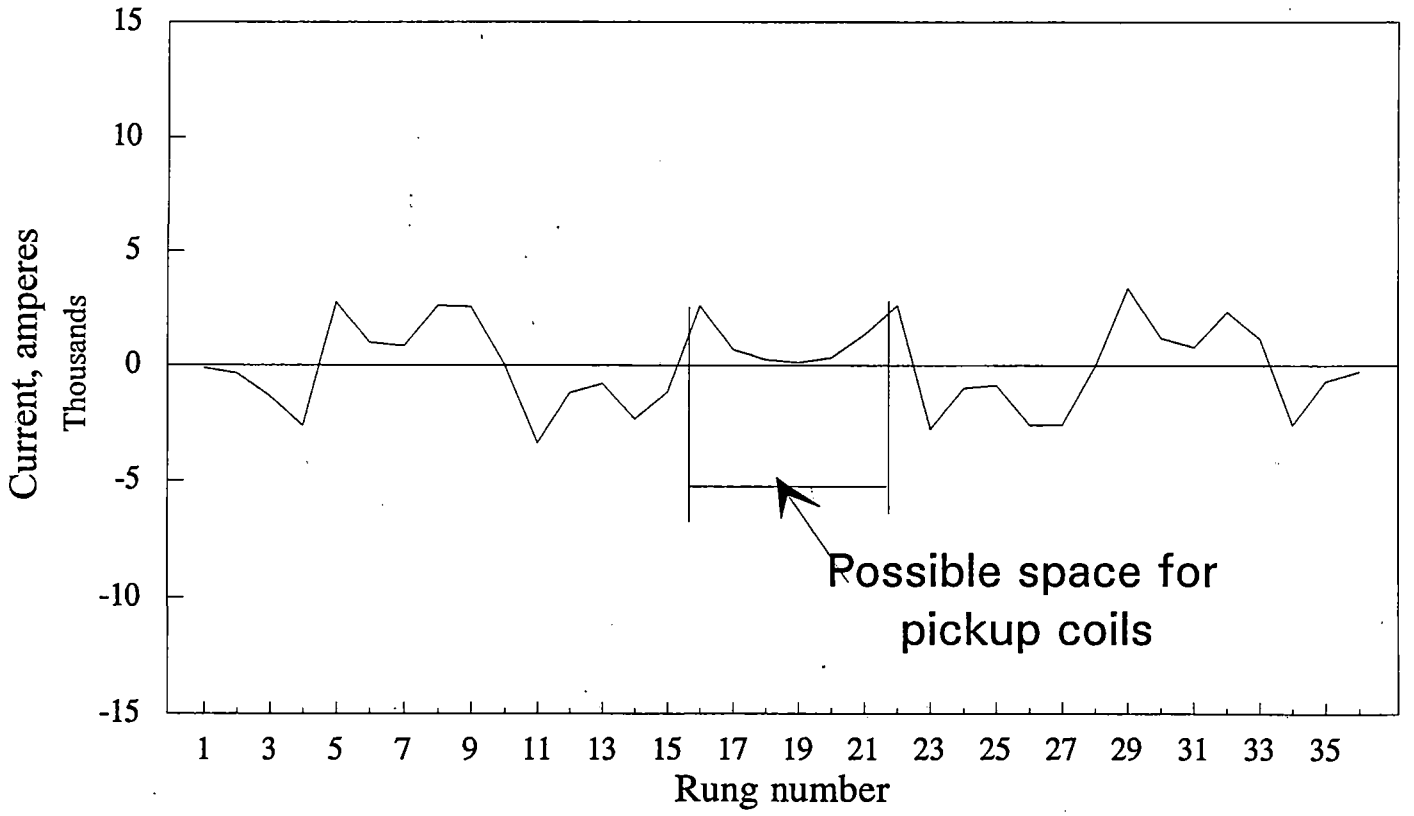

Figure C1-28 Rung currents – difference, rung vs loop centered

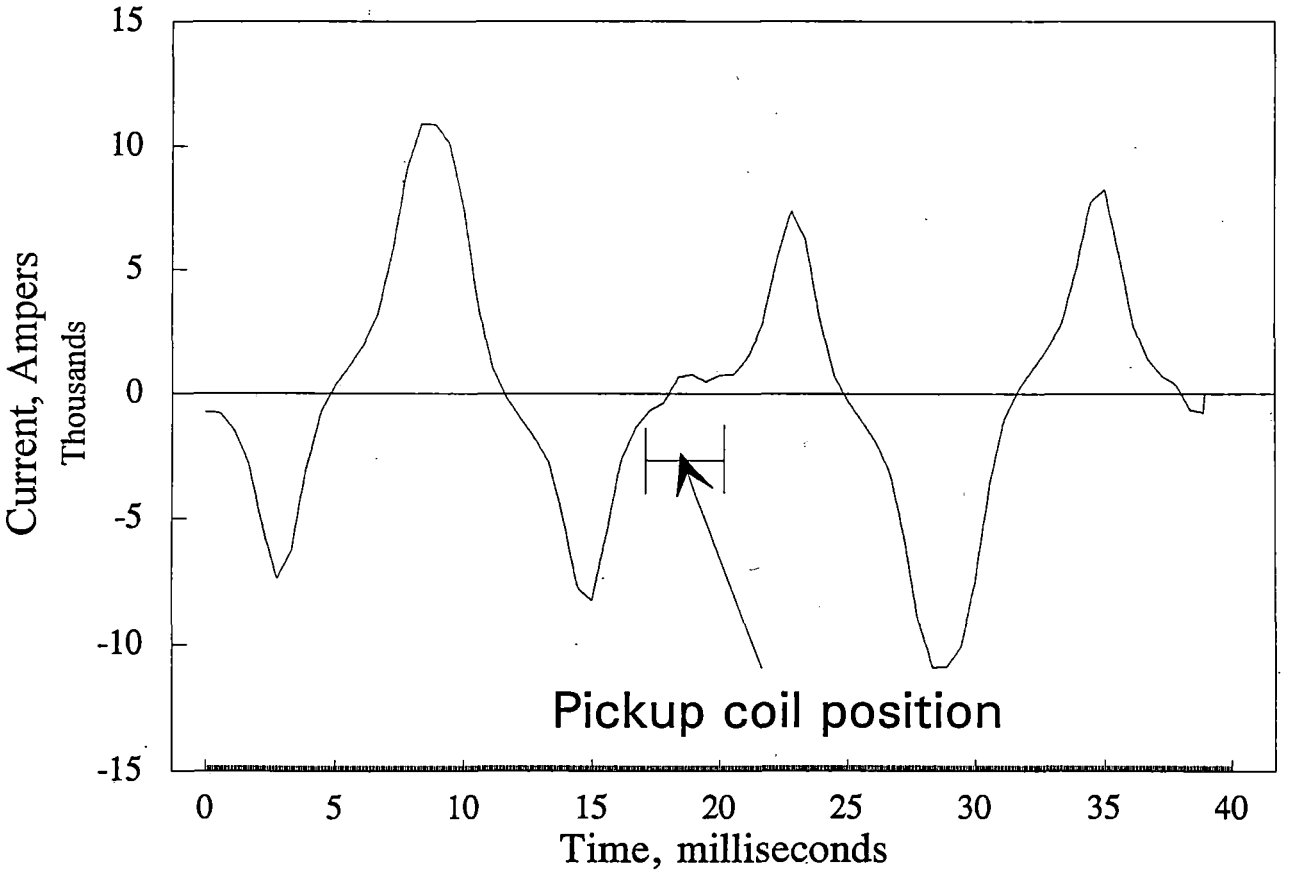

Figure C1-29 Rung current vs time at 150 m/s

Linear Generator: voltage calculations. The voltage induced in a pickup coil turn might be computed by Faraday's law as follows: The pickup coil is kept right next to a ladder rung and in the position of maximum flux linkages with that rung. Flux linkage changes with time are determined by computing the pickup coil flux linkage at maximum rung current, and at minimum rung current. The flux linkage difference, divided by the time it takes for the current to change from maximum to minimum, gives the pickup coil voltage per turn. This is an optimistic approach because in reality the pickup coil will move away from the rung on its path from the "rung-centered" case to the "space-centered" case and back to the next "rung-centered" case to complete a full cycle. Using this method, the computed induced voltage per turn of pickup coil is only 82 mV as shown in the appendix to this report section. Per equation 1 on C1-93, using a coil turn length of 0.78 meters, a mass of 4,233 kg is implied. This is heavy, yet not so heavy as to be excluded from consideration, so further analysis was required.

A more accurate analysis was performed by calculating the pickup coil flux linkages at many positions along the ladder. The rung currents were assumed to be varying from maximum to minimum sinusoidally as the coil position changed. This required a substantial amount of work in order to include the effects of both time variation of current and position variation of the pickup coil simultaneously. In addition, the pickup coil had to be given arbitrary starting positions at time zero since the phase of the ladder currents affects the pickup coil linkages. This was a very tedious analysis to get set up, but once the flux linkages in the pickup coil were calculated versus time, Faraday's law was invoked in the same way to compute the voltage per turn. Two of the many resulting voltage waveforms are shown in Figures C1-30 and C1-31 for two arbitrary starting positions of the pickup coil. Not surprisingly, the average pickup coil voltage is substantially less (about 1 mV per turn) than the simplified analysis in the preceding paragraphs, showing further that the extraction of power from the levitation ladder would be difficult at best. Using a 0.78 meter turn length, the mass implied by equation 1 is 347 metric tons! In this case, the previous calculations, implying 82 mV per turn, resulted in misleading conclusions.

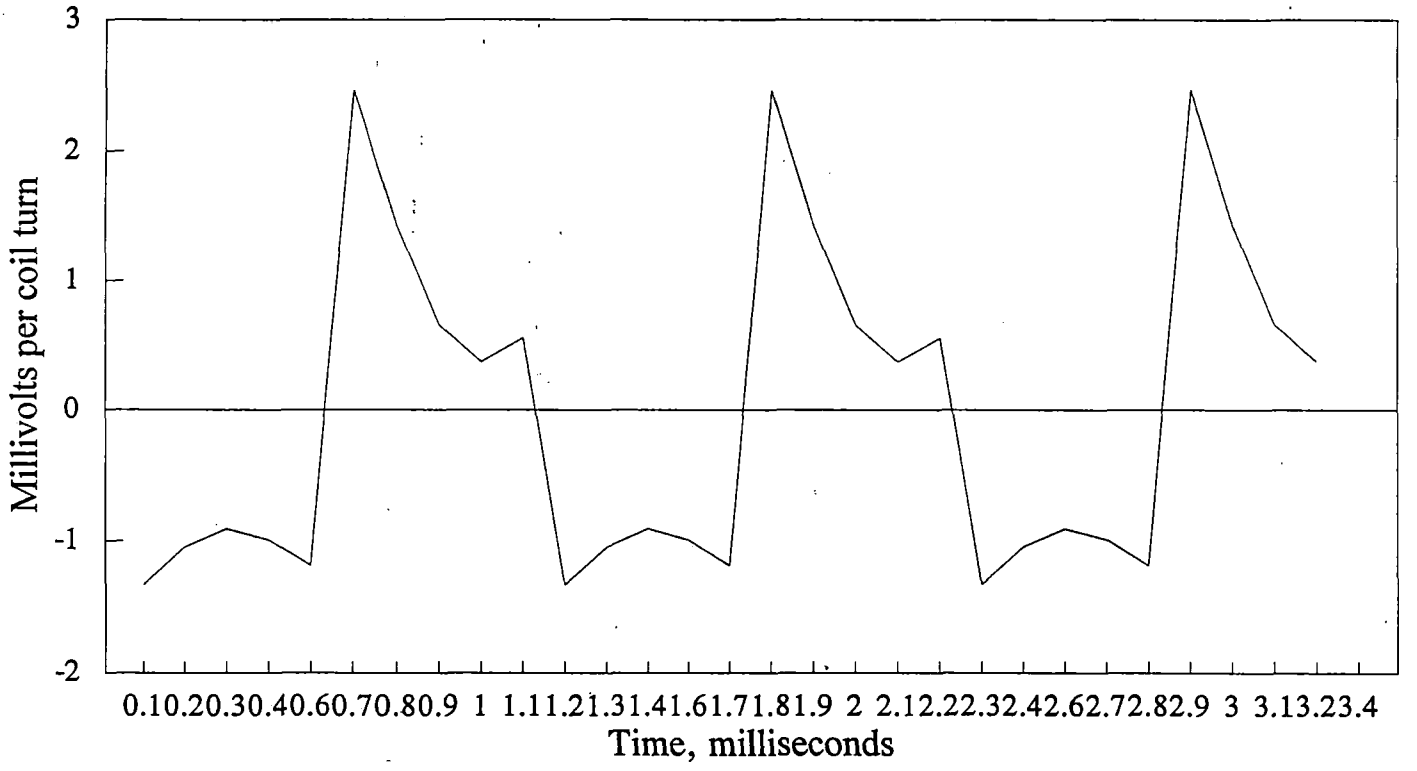

Figure C1-30 Pickup coil voltage – coil at x = 2.9167 at t = 0

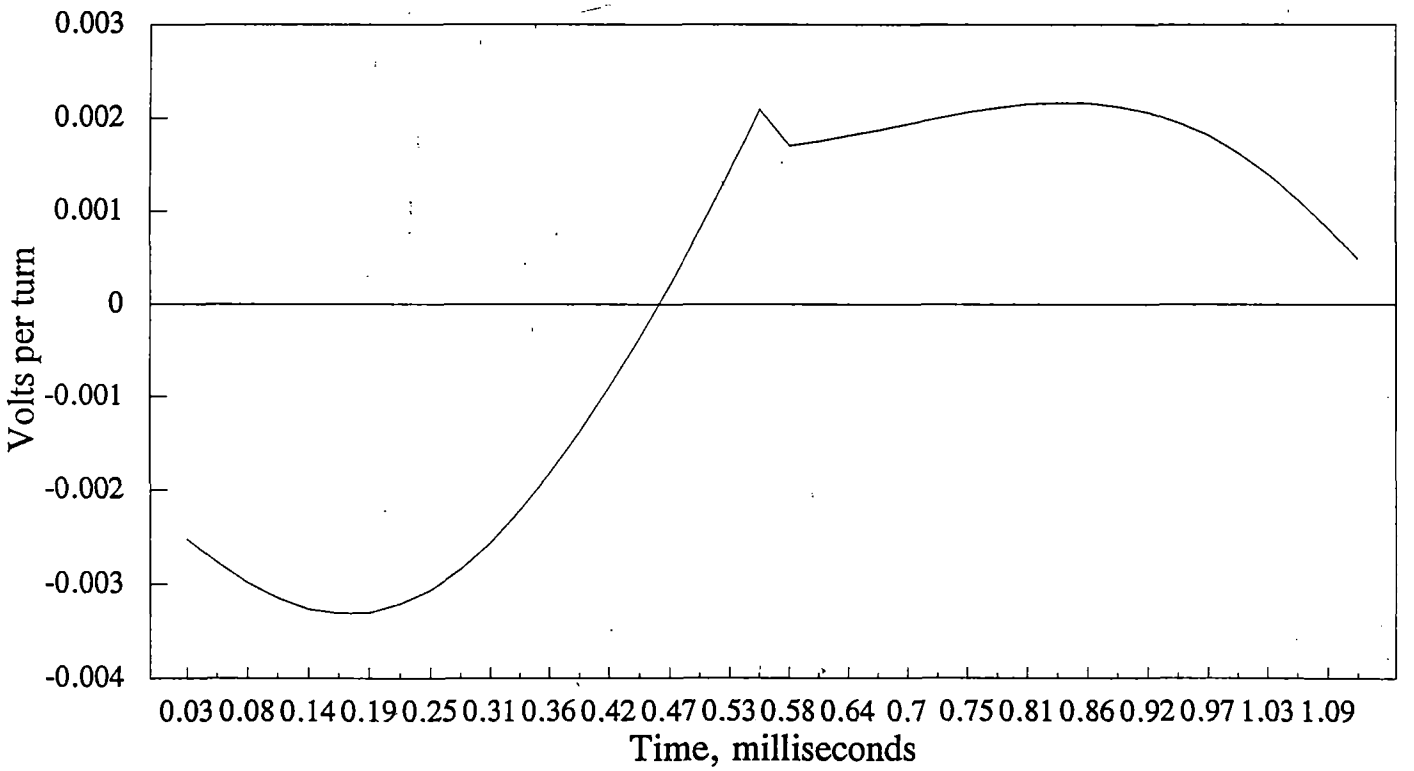

Figure C1-31 Pickup coil voltage – positioned over rung 17 at t = 0

The currents in the ladder rails have no significant impact upon the change in flux in the vertically oriented pickup coils. This is due to a combination of factors: the orientation of the coils, the magnitude of the changes in current in the rails versus the rungs, and most important: the distance between the current in the rungs and the coils changes as the vehicle moves, whereas the distance from the rails to **any** pickup coil would not change as the vehicle moves. The currents in rungs that are not near the pickup coil are also too distant to have a major impact.

In this analysis, the harmonic currents in the ladder were not considered; we analyzed them as pure sinusoids. While substantial harmonic currents may be present in the ladder, we did not have a model of them from MIT, and we do not expect that the magnitudes of these harmonics would make much difference to our analysis.

This linear generator clearly does not meet the weight limitations. If the linear generator coils were moved closer to the levitation ladder (an active position controller might be required), the voltage induced in the linear generator would increase due to the increased magnitude of flux linkage variation, but this power generation method would still be insufficient.

For our analysis, we have to consider the physical size of the linear generator coils in addition to their weight. It is not possible to physically fit the linear generator coils in the space allotted. The size of the coils would have to be reduced by several orders of magnitude before they could fit between the bogies near the guideway.

Alternative #5 – Linear Transformer/Inductive Pickup

A transformer in its commonest, stationary form transfers power from one side of an electrical circuit (the primary side) to another side of an electrical circuit (the secondary side), with an associated and desired change of voltage taking place as well. The linear transformer for maglev applications would be employed not so much because a transformer can change voltage levels, but because it transfers power from one place to another. The linear transformer for maglev would have its primary circuit laid out along the entire guideway, being fed power by wayside inverters specially built for the on-board power requirement alone. The secondary circuit would be mounted on the vehicle very close to the primary circuit on the guideway. Physical contact between the two transformer halves is not necessary or desirable; magnetic fields working at a small distance are responsible for the power transfer.

The linear transformer approach is different from an inductive pickup approach. The inductive pickup nomenclature implies, to this Team at least, a magnetic coupling of coils on the vehicle to dc magnets on the guideway. Relative motion of the vehicle's coils through the dc fields induces voltage in the vehicle that can provide for its on-board power. Although the operating principles are much different from those of the linear transformer, the type and amount of materials and labor to provide and inductive pickup system are probably quite similar. In the absence of the time required to do a conceptual design of an inductive pickup system, we defer to the design of the linear transformer and simply assume that the costs will be (in the light of hindsight) similarly unacceptable. It should be noted that an inductive pickup system has a low speed power capacity problem, as the voltage induced in the vehicle coils is proportional to the vehicle speed.

The linear transformer approach has the following pros and cons:

- Full on-board requirements are met at all vehicle speeds, including zero speed.
- If the linear transformer or its associated equipment fails in any particular section of the guideway, then vehicles cannot pick up power in that region and must rely upon on-board batteries to run essential on-board loads. This concern can be mitigated by the use of two half-power linear transformer systems for reliability's sake.
- The vehicle's secondary circuit would be separated into several pickups connected in parallel at different locations, so that a failure of one of the pickups would not totally shut down the vehicle's on-board power system but would merely reduce its capacity.
- Few concerns about safety are associated with the linear transformer approach.
- The primary half of the transformer could be mounted on top of the guideway beam, on its port side, its starboard side, or any combination of these three locations. Bottom mounting would be impossible due to the concrete support frames which would interfere with the vehicle pickup every 25 meters.
- The air gap between the primary and secondary halves is necessary in order to eliminate wear, but the air gap interferes with the power transfer. The design situation must include a tradeoff in order to arrive at an air gap size. On one hand, the smaller the air gap , the better the performance and capacity of the linear transformer. On the other hand, the smaller the air gap, the more difficult it becomes to prevent the vehicle's pickup from colliding with the primary half mounted on the guideway. Active position control of the pickup might become necessary if the gap is made small enough.

Linear Transformer: design approach. There are several ways to arrange coils and cores to effect a linear transformer capable of transferring 186 kW of power. Engineering judgment is invoked at this point to justify the following choices:

- A single phase system is selected to reduce complexity and therefore increase manufacturability and reliability.

- Purely sinusoidal voltage and current waveforms are to be used.
- One linear transformer primary would occupy space directly on top of and in the center of the guideway.
- One secondary half will be located in each space between bogies on the underside of the vehicle. Since this space is one meter long and there must be some allowance for clearances, we set the length of the pickup at 0.8 meters each.
- The operating frequency will be high enough that the use of Litz wire and ferrite materials will be required.
- The coil and core configuration will be the simplest one apparent to the person responsible on the Bechtel Team. If there is a simpler configuration available, the impact on the conclusions about the viability of the linear transformer approach is not expected to change, because there are limits on how hard one can work each kilogram of copper wire and each kilogram of ferrite core material.
- There will be one inverter feed for each guideway block (nominally 4 km long) in each direction of travel, since usually only one vehicle will be present there. Switching circuitry will be provided to energize only the primary sections of the linear transformer where the vehicle is located in order to cut down on the required supply voltage.

Linear Transformer: configuration. Figure C1-32 shows the configuration that was analyzed. The ferrite core is molded into a rather flat channel. The cutout in the channel provides space for turns on the winding. Each primary turn runs completely down the channel for 25 meters (one concrete beam length), then returns along one of the outside edges. This minimizes the depth of penetration of the core into the guideway beam. The width of the primary core is limited by the required nonmagnetic material zone near the edges of the beam, due to magnetic fields of the vehicle's superconducting magnets near the beam edges.

The width of the secondary core is closely allied to the width of the primary core, though its depth can be greater. Each secondary turn wraps around the 0.8 m long secondary core in a similar fashion to the primary winding. The secondary halves must be guided by a hydraulic or aerodynamic mechanism on the vehicle to maintain the small air gap between the primary and secondary halves.

Wherever the linear transformer is located, it will not be pretty. The appearance considerations are indirectly manifested in reliability issues in the sense that adding kilometer after kilometer of electrical equipment is more likely to have associated reliability and cost penalties, so one is well advised to keep the appearance issue in mind.

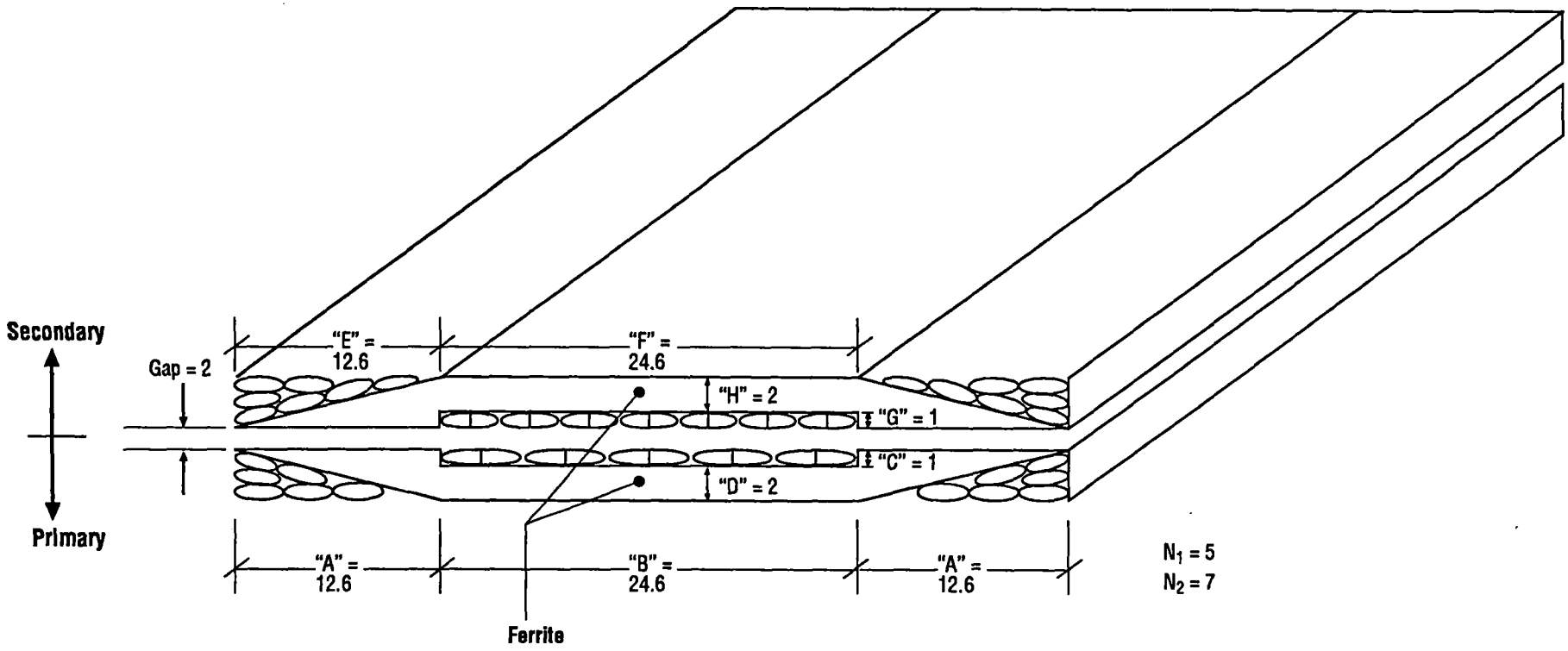

= Wire

All measurements are in centimeters

Figure C1-32 Linear transformer configuration

Linear Transformer: calculations. A computer program was written to optimize the transformer parameters and dimensions. The comments in that computer program, found in the appendix, explain how the program works on a line by line basis. The program was written in VAX FORTRAN. To simplify the program, the effects of winding and core heating were neglected, therefore transformer efficiency is assumed to be 100 percent, which is a reasonable simplification of the real problem.

The program was written to optimize a transformer of any power rating. The actual optimization was done at a power level of 250 kW instead of 186 kW because 250 kW was the projected power requirement at the time this work was done. The overall conclusions about the viability of the linear transformer approach are not influenced by that change, however.

The optimization was done in a manner that maximized the figure-of-merit function

$$f = \frac{\cos\theta}{\$x(V - V_o)}$$

where $\cos\theta$ = power factor at primary winding terminals

$\$$ = transformer cost per kilometer

V = supply voltage at primary winding terminals

V_o = desired value of V

The power factor should be maximized in order to lower operating costs and reduce transformer losses. Obviously, cost should be in the denominator so that the least cost design will be approached. Cost was computed by multiplying raw material costs by a factor of four. Material costs were \$3.31/kg for copper Litz wire for the windings and \$7.00/kg for ferrite core materials. The voltage at the primary gets high very easily, and to keep the voltage reasonable and avoid insulation and device rating problems, the factor V-Vo was placed in the denominator to loosely fasten the supply voltage to the desired voltage level.

Not all design parameters and dimensions were allowed to vary during the optimization process. For example, the length of the core halves were fixed at the space available. Also, the secondary voltage at rated load was fixed at 650 V per secondary winding because this gives 440 V after being inverted, with a 10 percent safety factor. The air gap was fixed at 2 cm after realizing that the design was hopeless at the nominal 5 cm clearance used at all other places between the vehicle and the guideway.

Design rules of thumb were:

- Core magnetic flux density 0.3 Tesla
- Coil fill factor needed 0.75
- Coil current density needed 1.9×10^6 A/m^2
- Desired primary voltage under load = 1,500 V

Voltages from 500 to 2,500 V were run; the cost per mile as computed by the program was insensitive to this parameter.

The fixed parameters, along with the design rules, left the following parameters to be varied in the optimization procedure:

- Frequency
- Number of primary turns
- Number of secondary turns
- Air gap flux density
- Core width (limited to 0.5 m)

When the final optimized design was computed, the number of turns on each winding was rounded off to the nearest integer, since fractional winding turns (except for halves) are not realizable.

Linear Transformer: resultant design. The final optimized design is shown in Figure C1-32, and the numerical listing of its performance parameters is as follows:

- Cost per km: $1.2 million
- Frequency: 5,862 Hz
- 5 primary turns: 7 secondary turns
- Primary voltage: 1,528 V
- Primary A: 681
- Primary power factor: 0.24
- Primary leakage reactance: 1.76 ohms
- Secondary leakage reactance: 0.056 ohms referred to primary

- Magnetizing reactance: 5.67 ohms
- Primary wire diameter (as solid): 2.14 cm
- Secondary wire diameter (as solid): 7.2 mm
- Core dimensions: see Figure C1-32

Its performance is poor due to the unavoidably large amount of leakage reactance. Leakage reactance is proportional to the length of the core, and the 25-meter length is so vast that little can be done to reduce the leakage reactance. Using a shallow, wide cutout in the channel helps. So would using shorter core lengths, but this is impractical since the secondaries always span a total length of 24 m and have to couple to active primary cores.

As it is, the vehicle would span two primary cores most of the time, so two primary sections always have to be energized. As the vehicle moves along, the proper primary cores would have to be switched in and out of the connection circuit to the inverters. This would severely and detrimentally impact the cost and reliability of the linear transformer system.

A most important result is the cost per km of the transformer itself. If we double the cost to include the inverter supplies and connection circuit costs, the result is $2.4 million per kilometer, or almost $4 million per mile. Clearly this is a cost prohibitive approach.

Alternative #6 – Wind Turbine

When the maglev vehicle is traveling at a high enough velocity, it is possible to guide air to one or more wind turbine generators to provide on-board power for the vehicle. Our concept for this alternative power source would be to provide two streamlined ducts in the nose of the vehicle to feed a pair of wind turbines located in the fore equipment compartment. The low velocity (spent) exhaust air would be ducted downward or sidewards to the exterior of the vehicle. Each turbine would have its own control subsystem to regulate its voltage and frequency (+/- 5 percent) via variable pitch blades. We would expect each generator driven by the turbines probably to be a lightweight synchronous generator, eliminating the need for an inverter to provide three phase 440 V power. This is a major advantage for the wind turbine approach. Again, two of these wind turbines would be used for reliability reasons, since two 93 kW turbine sets would weigh roughly the same as one larger set of 186 kW capacity.

One might think that an advantage of the wind turbine approach is that energy normally expended in overcoming aerodynamic drag is put to good use as a free source of energy for on-board power.

Again, as with the case of the linear generator, there is no free lunch. The aerodynamic drag of the vehicle is increased via the air turbine, eliminating the prospects of an enticing vehicle synergy. The power indirectly must be supplied through the linear synchronous motor on the guideway. As a matter of fact, the wind turbine efficiency would only be about 62 percent. When combined with the generator efficiency, the increase in linear synchronous motor power turns out to be 186/0.6/0.9=344 kW.

Estimates of turbine size and weight were provided by subcontractors at the University of Illinois via the Sunstrand Corporation, a commercial supplier of ram air turbines. Sunstrand has provided a graph (see Figure C1-33) of turbine size versus power and airspeed for two-bladed turbines. At 500 kph, a four-bladed turbine would be more desirable and would reduce this diameter by 23 percent. In any event, the curve shows that at 93 kW each, the turbines would be 0.94 meters in diameter. Regarding the mass of each turbine, additional information from Sunstrand gives the following rules:

Mass (kg) of turbine and strut=diameter in inches

Mass (kg) of generator =power (kW)

The projected combined turbine/generator mass becomes .94*39.4+93=130 kg per unit. Clearly this is the smallest projected power source mass of any of the alternatives so far (and upcoming as well) and is a distinct advantage for this alternative.

The disadvantage of wind turbine generators is obvious: they lack power capacity at low vehicle speeds because the low air speed will not drive the turbines at full capacity. This requires the on-board batteries to be larger, and requires that the vehicle not operate in a slowed mode due to struggling vehicles ahead, high-wind slow orders, etc. The projections above are for 500 kph operation. One way to alleviate this problem is to make the turbines bigger and heavier so they will have the required 186 kW capacity at a speed lower than 500 kph (e.g., 350 kph). Still, there will always be some slowed-mode situations where the turbines would be insufficient. A hybrid system where the small turbines assist some other source is possible, but combining approaches gives added complexity, and generally more weight and space is required. In an emergency power situation where a maglev vehicle is stopped, the wind turbines are totally useless and the other part of the hybrid system becomes the sole source of on-board power.

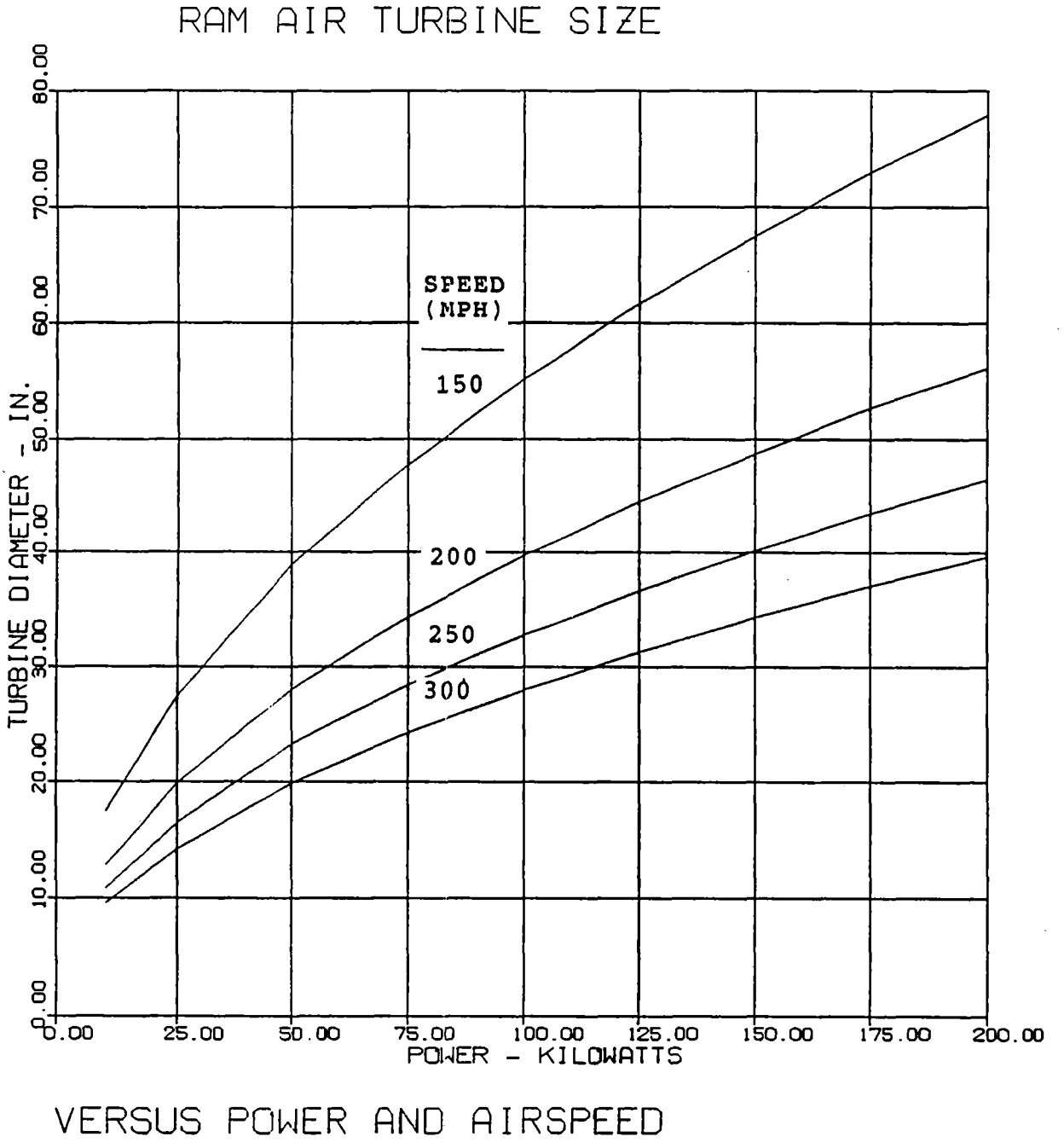

Figure C1-33 Turbine size vs power and air speed

Alternative #7 – Engine Generator Set

Obvious options for an engine in an engine/generator set include:

- Diesel internal combustion engine
- Gasoline internal combustion engine
- Jet-fueled aviation turbine
- Other less common fuels driving either engine type

Each would have a 400 Hz three phase generator mated to it. Most likely, as with so many other systems in this SCD, two half-sized systems would be provided in order to provide redundancy and fault tolerance. No inverter would be required in such an approach because the rotating generator would provide the required power type directly at its terminals.

The aircraft turbine would be the lightest of these options. All would require a fuel tank for operation, as well as significant ancillary equipment. Although muffled, all would be noisy and would emit undesirable exhaust gases. These are major drawbacks to using engine/generator sets for the on-board power source. The great advantages of this option are the simplicity, absence of inverters, low cost, and the availability of full power at any vehicle speed.

Baseline Choice: Fuel Cells

Recent technological developments have made fuel cells a very attractive and practical power source alternative. While fuel cells have long been considered too bulky and costly for many practical uses, recent research by General Motors into fuel cell application on hybrid electric automobiles has made tremendous advances. The type of fuel cells proposed for maglev on-board use has been developed and tested in a GM test facility and is a viable application of present day, or at least foreseeable future, technology.

Fuel cells operate by electrochemically bonding hydrogen and oxygen, which creates electricity with water as a byproduct. However, it is not necessary to use hydrogen directly. The proposed system begins with methanol as its fuel, uses steam to crack small volumes of it at any one time into hydrogen gas, and then combines the hydrogen with oxygen from the air to create electricity and water. This has the advantage of not having to carry hydrogen and/or oxygen tanks on-board. Instead, the much less volatile methanol can be used. Although hydrogen can also be used as a fuel directly, we feel that overcoming the ubiquitous though probably unjustified public perception of hydrogen as a dangerous fuel is a battle that we do not want to fight in this particular effort.

General Motors Corporation is working on a 10 kW fuel cell system for the Department of Energy, Electric and Hybrid Propulsion Division, Office of Transportation Technologies, under contract DE-AC02-90CH10435. The prime contractor is Allison Gas Turbine Division of GM ("AGT"), with participation by General Motors Research Laboratories, AC-Rochester Division of GM, Los Alamos National Laboratory, Dow Chemical Company, and Ballard Power Systems. Dr. Howard Creveling is the program manager at AGT, and the COTR (Contracting Officer's Technical Representative) at the DOT is Dr. Pandit G. Patil.

DOE

The subject fuel cell is actually a stack of individual cells. To achieve the 186 kW needed for the maglev vehicle's auxiliary power, a stack of 36 of these cells would be needed. A series connected arrangement of cells would give a 756 V, 250 A dc power source. By slightly chopping down the voltage and passing the power through a set of inverters, the fuel cells would supply the main 440 V vehicle ac lines. This can be done with readily available commercial equipment. Our implementation is actually to use two independent fuel cell systems, following our philosophy to use dual systems where weight is not increased much by doing so. Should one fuel cell system fail, the remaining fuel cell can run continuously at 30 percent overload (though at not-so-desirable fuel efficiency) to power all of the vehicle loads, though at slightly reduced capacity. This is a distinct advantage for this approach. A boost converter would be part of the inverter so that the 440 V bus can be powered from half the normal dc input voltage.

C?

The fuels cells operate at 80 °. This is a very manageable temperature, unlike the case of more primitive fuel cells which require temperatures of up to 1,000 ° C. The warm-up time for the fuel cells is only a few seconds, more than fast enough for use aboard the maglev vehicle. The only instance in which a fuel cell has a longer warm-up time is when it is starting cold. This added delay comes from heating the water into steam which is used to crack the methanol into hydrogen. The fuel cell design team is confident that they will be able to obtain a seven second delay from cold start to full output. However, on a maglev vehicle the only cold period will be when the vehicle is first starting out for a day's service, so a slightly longer delay will not cause a problem.

Fuel Cells: size/weight considerations. The projected system, which includes the fuel cell and the methanol processor, has a density of 556 kg/m^3. This is broken down as follows:

Volume: 0.003684 m^3/kW (271 kW/m^3)

Mass: 2.05 kg/kW

These numbers are optimistic for the present-day fuel cell. The fuel cell, which is the subject of the DOT contract mentioned above may miss the above design goals by about 33 percent, but with the development time available for a maglev system, the design goals would almost certainly be reached, according to the program manager at AGT.

It is appropriate to note at this point that the upcoming weight and volume calculations give slightly different results than shown on the vehicle weight spreadsheet in another section of this report. The numbers in the spreadsheet were entered at the time we were considering a 250 kW on-board power system, rather than the 186 kW system of the final baseline concept.

With the subject fuel cells, it is possible to obtain better efficiency by running the cells at less than their full load. A 70 percent load is very efficient for the proposed system. At 70 percent of the continuous load capacity the fuel cell runs at 51 percent thermal efficiency, much better that the 34 percent efficiency typical of state-of-the-art spark ignition engines. At fully rated load the fuel cell runs at 38 percent thermal efficiency, increasing the fuel cost per kWh by 34 percent. This, together with the fact that it is beneficial in some situations to have a 30 percent load capability cushion, caused us to decide to run the fuel cells at 70 percent of their load capacity at 186 kW on-board power demand. Running at this 70 percent load, to create 186 kW the system will have a mass of

$$186 \text{ kW} \times 2.05 \text{ kg/kW} \div 70\% = 545 \text{ kg}$$

and require

$$186 \text{ kW} \times 0.003684 \text{ m}^3\text{/kW} \div 70\% = 0.979 \text{ m}^3.$$

At a 70 percent load, the fuel cells consume 0.409 kg/kWh. The following chart shows the weight the fuel adds (+10% fuel tank weight) based on the recharge period. The density of methanol is 797 kg/m^3. If the fuel is only changed once a day, then the recharge amount would be equivalent to 16 operating hours out of each 24-hour day. However, all that is required to recharge the system is to refill the methanol tank. It may then prove economical to have a shorter recharge interval. Recharging would then be done at end stations after passengers disembark.

Recharge Period	Mass of Fuel+Tank
2 hours	168 kg
4 hours	336 kg
8 hours	672 kg
16 hours	1344 kg

The price of methanol is difficult to establish. We have obtained estimates ranging from 30 cents per gallon (in California, where the price is regulated) to $1.48 per gallon. If we assume a price of $1.00 per gallon ($0.33 per kilogram), the daily fuel cost works out to be 1344 x $0.33 = $443/day. The cost of providing the power via the linear synchronous motor, at 100 percent transfer/conversion efficiency, would be 186 kW times 16 hours/day times $0.085/kWh or $253 per day, or a difference of at most $190/day. We use the term "at most" to remind the reader that the 186 kW load is for extreme weather conditions and the highest speed, so the usual power system load will be only about 110 kW. The difference in operating cost then is approximately $112 per day.

The total mass for a fuel cell/fuel supply system with an eight-hour recharge period would be 1,217 kg. This is a low weight system for the power that is being created. In addition, if fuel cells are used, most of the emergency batteries that had been planned for can be removed to save even more on weight. Fuel cells would also be more useful in an emergency situation than the emergency batteries as they would allow full power to be maintained, whereas the emergency batteries would only have the power capacity to maintain 5 kW of selected emergency loads for just one hour. Clearly, this is a major advantage of the fuel cell approach and actually is a factor that provides a safer vehicle in non-threatening stopped emergency conditions. With batteries only supplying emergency power, passenger evacuation would be a likely event in many cases, and evacuation itself can lead to injuries. Keeping the passengers comfortable within the vehicle and not evacuating them is safer.

Fuel Cells: further safety considerations: The fly in the ointment regarding selection of a fuel cell system for on-board vehicle power is the fact that methanol fueling the fuel cell must be stored on board, increasing the possibility of a fire. This consideration is inescapable. Methanol is less likely to ignite than gasoline, diesel fuel, or jet fuel, but still it will burn if lit accidentally, even though it burns slower and cooler than the other fuels mentioned. Precautions would be taken to provide accident-resistant double or triple-walled storage tanks located sensibly and distributed in

multiple locations with check valves in the lines to reduce the amount of fuel provided to any fire. Of course, the lines themselves and their associated fittings are sources of fuel leaks, so a tradeoff study would involve this leak consideration as well.

If there were a simple way to change the methanol or impregnate it into some carrier to make it less flammable or even inflammable, then the electric vehicle program would have incorporated such technology, but this is not the case. The methanol tanks on our vehicle are located between the fuel cell proper and the spherical hydrogen dewar in the fore equipment compartment, providing protection from puncture in a collision. The nose of the vehicle will also be engineered to collapse in a vehicle collision and absorb crash energy, further reducing the probability of puncture of the tank. Of course, total commitment to crash avoidance via a properly engineered and operated control system would be the major line of defense against collision-induced fires, but total reliance upon crash avoidance would not be a wise engineering approach.

The fire hazard problem must be approached from several directions:

- Resistance of the storage tanks to puncture
- Location/distribution of the storage tanks to minimize the fire hazard
- Resistance of the lines and fitting to leaks
- Provision of check valves to avoid "gushing" spills to a fire
- Keep the leaks/spills away from the passenger compartment
- Provide moats and drains with sensors to detect leaks or spills
- Provide a water-flushing system to dilute spills and leaks
- Provide a video camera in the fore equipment compartment for visual inspection
- Provide an automated, tamper-resistant, spill-resistant filling system
- Provide fire extinguishing equipment of the proper type, reliability, number, and location
- Refill the methanol tanks at more frequent intervals in order to reduce the amount of fuel on board.
- Include methanol fire considerations in the vehicle evacuation plan

The Bechtel Team is not ignoring this safety issue, but feels that overall, when all considerations are taken into account, the safety hazard is small enough not to overshadow the previously discussed advantages of the fuel cell approach. By highlighting this issue in our own report section here, and openly discussing the fire hazard issue, we hope that our decision to put a

flammable liquid on-board our vehicle will be met with understanding. Automobiles, aircraft, diesel locomotives, power boats, and lawn mowers carry flammable liquids too, and the associated hazards have become accepted parts of everyday life. Our emphasis on crash avoidance via the control system will greatly reduce the safety impact of on-board fuel.

Comparison of Alternatives

The following table condenses some of the information from the foregoing text. The inclusion of a cost column in the table and the exclusion of a safety column does not imply anything about our emphasis, but instead merely shows that cost is more easily quantified than safety.

One of the advantages that has been somewhat of a "sleeper" is the emergency power capability. The ability of a power source to operate continuously in the event of total failure of the guideway electrical systems tempts one to speculate about driving the vehicle with one or more deployable dc motor-driven crawler devices if somehow the vehicle does not coast to a preferred stopping point. The crawlers would drive the vehicle from a stopped condition, upward in speed past the air bearing touchdown speed and past the speed necessary for magnetic levitation, yet stay below the peak of the drag curve. This would be about 20 kph, and the required electrical power to the crawler motors would be a total of only 10 kW due to our highly efficient suspension system. This device would be especially helpful to eliminate requirements for propulsion winding sectionalizing at such places as fuel and helium depots and storage sheds. Since we have not yet designed or drawn this crawler for our vehicle, we have not included it in our baseline design concept, but future design work would probably incorporate these crawlers.

Again, the choice we made for our baseline maglev concept is the fuel cell, based on the advantages and disadvantages of all of the alternatives described in the text of this section of this report. Although a fuel cell of the type proposed has not been developed at the 186 kW level, we expect the development of this technology over the next few years, in parallel with a maglev system development effort, to achieve the projected weight, volume, and performance levels quoted in this report. The present performance of this fuel cell is not far from those levels, and development of the technology is already under way at GM relative to electric automobiles. If the safety issues of this fuel cell turn out to be addressable relative to automobiles, then they should certainly be addressable relative to maglev vehicles as well.

Description	Advantages	Disadvantages	Capital Cost	Rating
Storage *Approaches	No transfer mechanism required	Impractical	Various	last
Power Cable Link	Uses cables to meet more than one need	Insufficient power at lower speeds, dependence upon cable current level	High	7
Sliding Contacts	High capacity at any speed	Wearout, EMI, safety, appearance	High	6
Linear Generator	Low capital cost, reliable	Insufficient power at lower speeds	Low	5
Inductive Pickup	High capacity	Low capacity at low speed, appearance, unknown reliability	Very high	4
Linear Transformer	High capacity	Unknown reliability, appearance	Very high	4
Wind Turbine	Very lightweight, no inverter required	Low speed capacity	Low	3
Engine/ Generator	Simple, reliable, no inverter required	Fuel onboard, high operating cost, noise, vibration, pollution, weight	Low	2
Methanol-Reforming PEM Fuel Cells	Lightweight, noiseless, nonpolluting, overload capacity	Fuel onboard, higher operating cost	Low	first

References:

1. Palmer, David N., "Downsized Superconducting Magnetic Energy Storage Systems," Proc. IECEC, Vol. 1, August 7-11, 1989, Table 6, page 456

2. J.L.He, D.M.Rote, and H.T.Coffey, "Computation of Magnetic Suspension of Maglev Systems Using Dynamic Circuit Theory," International Symposium on Magnetic Suspension Technology, NASA Langley Research Center, Hampton, VA, August 19-23, 1991

1.5.3 Emergency On-Board Power

Applicable Scenarios

An on-board emergency power supply is a crucial element to passenger safety and is essential in the design of the maglev vehicle. In the event of a power failure of both fuel cells or their electrical connections, these batteries must be able to supply the necessary power required for emergency lighting, communications, and emergency-only dc motors driving the normal ventilation fans. They will also power external flashing lights to make the vehicle more visible on the guideway at night. Each set of these batteries would be rated for up to one hour of emergency use, as it is assumed that in the event an emergency lasted longer than one hour the passengers would be moved out.

Redundancy of Emergency Equipment

The emergency load bus is energized at all times and delivers power to the "emergency loads" during normal vehicle operation. A battery charger fed by the fuel cells is the source of energy during these normal times, and the batteries are kept fully charged because they are also on the output side of the chargers. The electrical system schematic in the On-board Power System shows this clearly. Two emergency buses and two sets of emergency batteries are always active. Should power from the fuel cells be cut off, either emergency bus will run the emergency loads. If one set of emergency batteries or one of the emergency buses fail, the redundant approach provides enough capacity in the single remaining set of emergency batteries to run an emergency load bus. Should this happen, only the essential emergency lights, radio, computer, and fans would be kept running.

Battery Selection

A fibered Nicad battery system was chosen for emergency power. This system offered a high power-to-weight ratio and is very reliable, making it ideal for on-board emergency use. Design information used in the battery sizing calculations was taken from the manufacturer's catalog. The relevant sections of the catalog are reproduced in the appendix.

At the time the battery selection process was begun, we did not know the tradeoffs among power requirement, time, battery weight, space, voltage, and current factors. In addition, the catalog contained dozens of tables of ratings not only for battery classes (superfast, fast, medium, and slow discharge types), but each size and type rating information at different loadings. We scanned the relevant information into our personal computer, and wrote a BASIC program to sift through

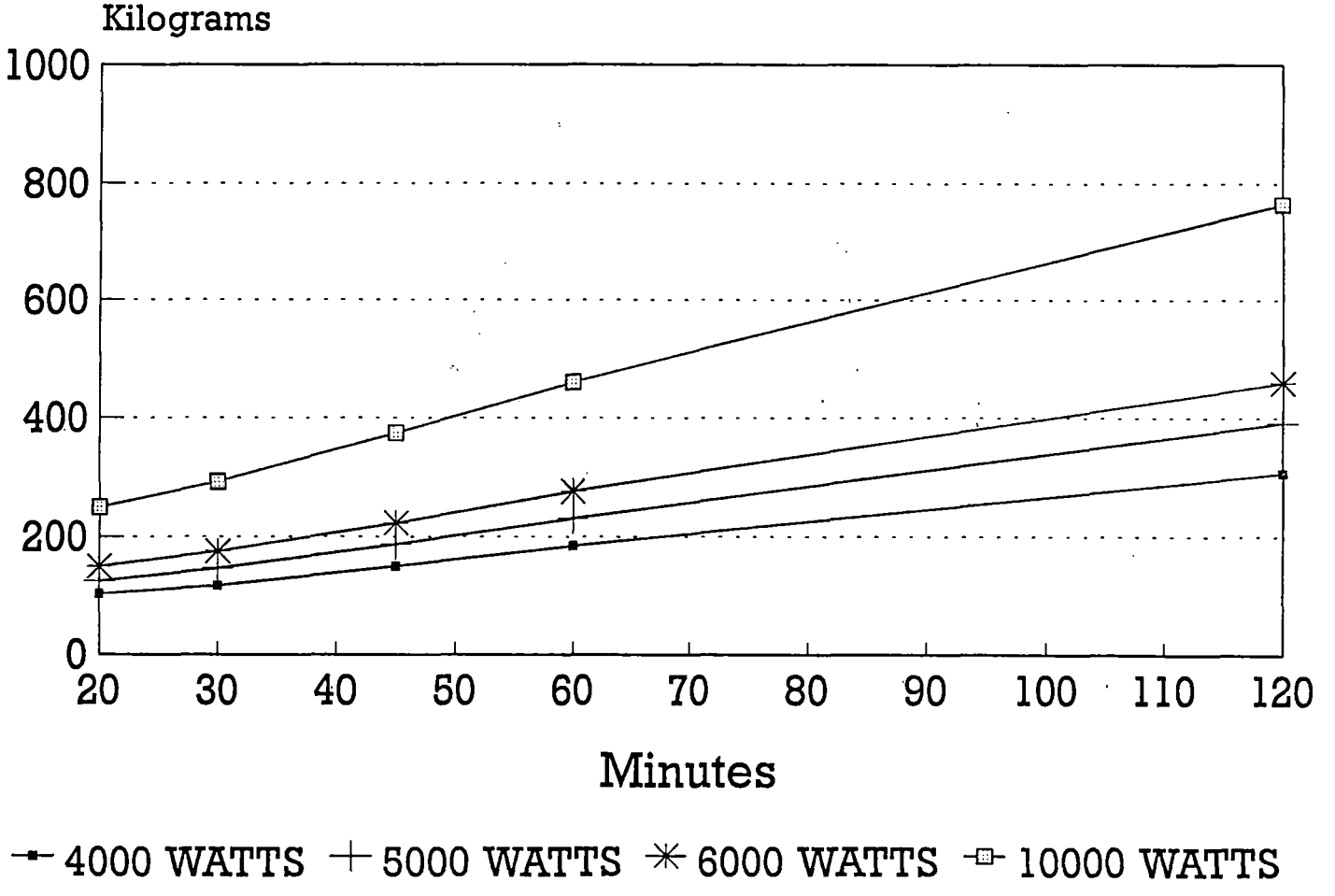

Figure C1-34 Battery weight requirements, emergency power system

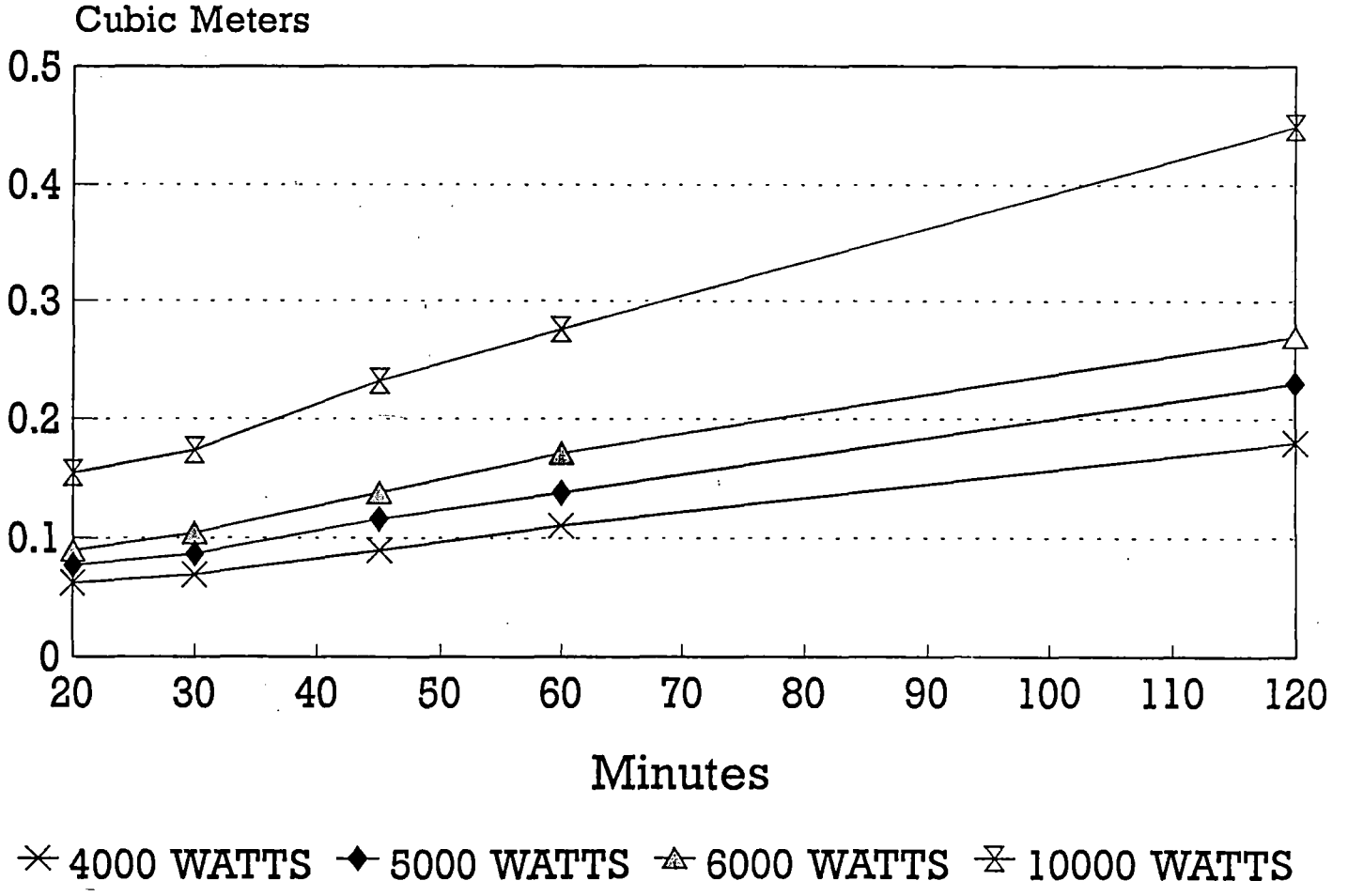

Figure C1-35 Battery space requirements, emergency power system

all the tabular information on the battery types and discharge rates at various kilowatt outputs in order to find the batteries with the minimum weight for any power and time demand. Figures C1-34 and C1-35 are the result, showing weight and volume versus time for any desired power demand. Looking at our expected 5 kW for 1 hour point, we see that doubling the time demand does not quite double the weight and volume; doubling the power demand does exactly double the battery weight and volume required. This is useful information for quickly determining the impact on battery weight and volume as the emergency loads become better defined, or to evaluate suggested load additions.

We allocated the true emergency loads generously as follows:

Ventilation Fans	3 kW
Lighting	1 kW
Radios/Computers	1 kW

During a critical emergency, one in which the car has to be evacuated for passenger safety, it is assumed that the emergency exits signs will be powered by their own internal power supplies. However, in the event of a night-time emergency, the on-board batteries could be used to power external floodlights for passenger safety and visibility in evacuating the vehicle. We determined that one hour seemed sufficient time for such a disabled vehicle to be reached for assistance; this then set our weight and size via Figures 1 and 2, and the computer program spit out the optimum battery set: 20 of Hoppecke type FNC 309M in series, loaded at exactly 1.0 V per cell. The amperage capacity is 252 A. The appendix shows more detail on this particular battery.

Battery Weight and Cost

The one hour, 5 kW Nicad system would weigh approximately 230 kg and would cost about $8,000.

No conversion equipment will be required; the emergency loads will run directly of the 20 V dc emergency bus.

1.6 AIR BEARING SYSTEM

1.6.1 Overview

The Bechtel Team's maglev concept includes devices to allow the vehicle to keep itself lifted off the guideway while stopped at any point in the route. Due to the fact the friction of a vehicle sitting directly upon its guideway is huge, the vehicle cannot be started into motion without elimination of that friction, hence the need for low speed levitation. Another section of this report describes electromagnetic lifting devices that can keep our vehicle suspended at zero speed in stations and perhaps at preferred stopping points (PSPs), but that equipment is not provided all along the guideway. What is needed is a mechanism to suspend the vehicle at zero or low speed at **any** point along the guideway. We have provided air bearings on the underside of our vehicle to accomplish that end. Air bearings are commonly used for moving heavy loads easily on concrete factory floors and in many other applications, and can be adapted to our maglev application as well. Our baseline design provides for four deployable/retractable air bearings mounted to the underside of each of the six bogies.

The ability to start and stop anywhere along the guideway is an advantage of our conceptual design, since it makes our concept flexible. This could be critical in an operational emergency, and possibly useful in maintenance yards, refilling depots, and the like.

1.6.2 Need for Zero Speed Lift

Magnetic lift and guidance of an EDS maglev system disappear when there is little or no relative speed between the vehicle and the guideway. This happens because it is the relative motion of a magnet past an aluminum sheet or coils or ladder that causes induced voltage, induced current, and induced forces on the aluminum sheet or ladder. The Bechtel Team's vehicle has a very efficient aluminum suspension ladder arrangement that will provide full levitation at very low speeds.

If the vehicle were to have no levitation assistance or no wheels at this low speed range, it would sit down on top of the guideway and slide to a stop whenever necessary. A skid arrangement would be provided for the contact areas between bogies and guideway. The skids would wear as the vehicle stopped or started up. We do provide pads on the bottom of our bogies that are actually attached to the air bearing backing plates, but these pads are only for resting the vehicle at a standstill and are not intended to be used for sliding conditions.

The skid wear of an intended-skid design would not be the biggest problem. Our main concern is that static friction of the skids against the concrete guideway would require excessively high tractive forces to be developed from the propulsion coils on the guideway in order to start moving the vehicle forward. If we assume the static coefficient of friction to be 0.25 and the vehicle to weigh 64 metric tons, then the extra propulsion force (in newtons) necessary to overcome the static friction would be

$$F = \mu Mg = 0.25x6400x9.8 = 156{,}800$$

newtons. This is more than our propulsion winding can exert even if beefed up for stations or steep grades. Surely, to provide for this starting force all along the guideway would drive the system cost up excessively. Providing low speed levitation so that static friction is eliminated is a necessary part of our vehicle concept.

1.6.3 Air Bearings vs Other Approaches

Landing Wheels

The air bearings have distinct advantages over landing wheels because the air bearings weigh much less than wheels and their associated retraction mechanism. We estimated the mass of a wheel and landing gear by equating it to a single Boeing 737-200 landing gear (1,979 kg) , although this is not a completely satisfying comparison. Admittedly these wheels are for high speed landing purposes, but then we omitted the structural weight penalty for the wheels. Also, wheels can be used for braking. We considered the low speed "crawler motor" possibilities of tying an electric motor to the wheels, but soon realized that maglev vehicles have a lot of magnetic drag that makes those motors very large. If we had done a totally integrated vehicle design with wheels in addition to our design with air bearings, then we would have derived a firm number for the weight penalty associated with wheels. We did not; we decided upon air bearings early in the SCD. Our weight spreadsheet shows a total air levitation system mass of 1,092 kg including the structural function of the air tanks. It is hardly likely that a system of wheels would have less mass.

The small amount of vehicle space required by the air bearings is also a big advantage over wheels. Very little if any structural weight and space is required for air bearings in our design, since the air bearing forces are transmitted along many of the structural members in place for supporting SCM levitation forces anyway. This would not be the case if we had incorporated landing wheels into our design.

Electromagnetic Lifters

We had decided at one point in this SCD to use the air bearings only in operational emergencies rather than at preferred stopping points, so they would be used only occasionally, perhaps once per year per vehicle. Our preferred provision for eliminating vehicle-to-beam friction is to use electromagnetic lifters, special versions of the inverters and linear synchronous motor and other lifting coils which can provide over 1 g of lift at any low speed (forward, stopped, or reverse).

Dual Approach

We have elected to design the vehicle's compressed air system in such a manner that the air bearings **could** be used for all routine stops and starts, so that the air bearings could be used if the electromagnetic lifters were out of service or perhaps even still in the development stages. This penalizes our vehicle design due to the additional compressor and electrical system weight, but it improves our vehicle design in terms of redundancy and fault tolerance. By having both low speed levitation methods (LSM lifters and air bearings) available, greater reliability will result.

1.6.4 Air Bearing Functional Requirements

The air bearing devices must provide nearly frictionless levitation. They must provide full levitation at zero speed and reduced levitation as the vehicle speeds up and becomes levitated via the SCMs and levitation ladders. They must be arranged in a fault tolerant manner to achieve maximum system reliability, and they must have a substantial service life to prevent excessive maintenance procedures. They must not create excessive aerodynamic drag forces when not in use, and they must be immune from surface roughness including debris, ice, and snow. They must not be excessively noisy, and they must work properly at extremes in environmental temperature. Guidance devices must be provided to prevent the vehicle sliding sidewards when stopping or starting on a tilted guideway beam in a curve.

1.6.5 Description of an Air Bearing

Figure C1-36 shows an air bearing general arrangement, although the proportions and seal arrangement could change for our application. This drawing was taken from the catalog of the American Solving Company. Figure C1-37 explaining how it works was also taken directly from that same brochure. The key to its operation is that the pressurized air in the center of the "rubber doughnut" leaks between the doughnut and the guideway, forming a nearly frictionless, extremely thin air film. The maglev could be said to be riding on a film of air rather than a cushion of air. Although air bearings as shown in the brochures are not normally used at 10 kph, the

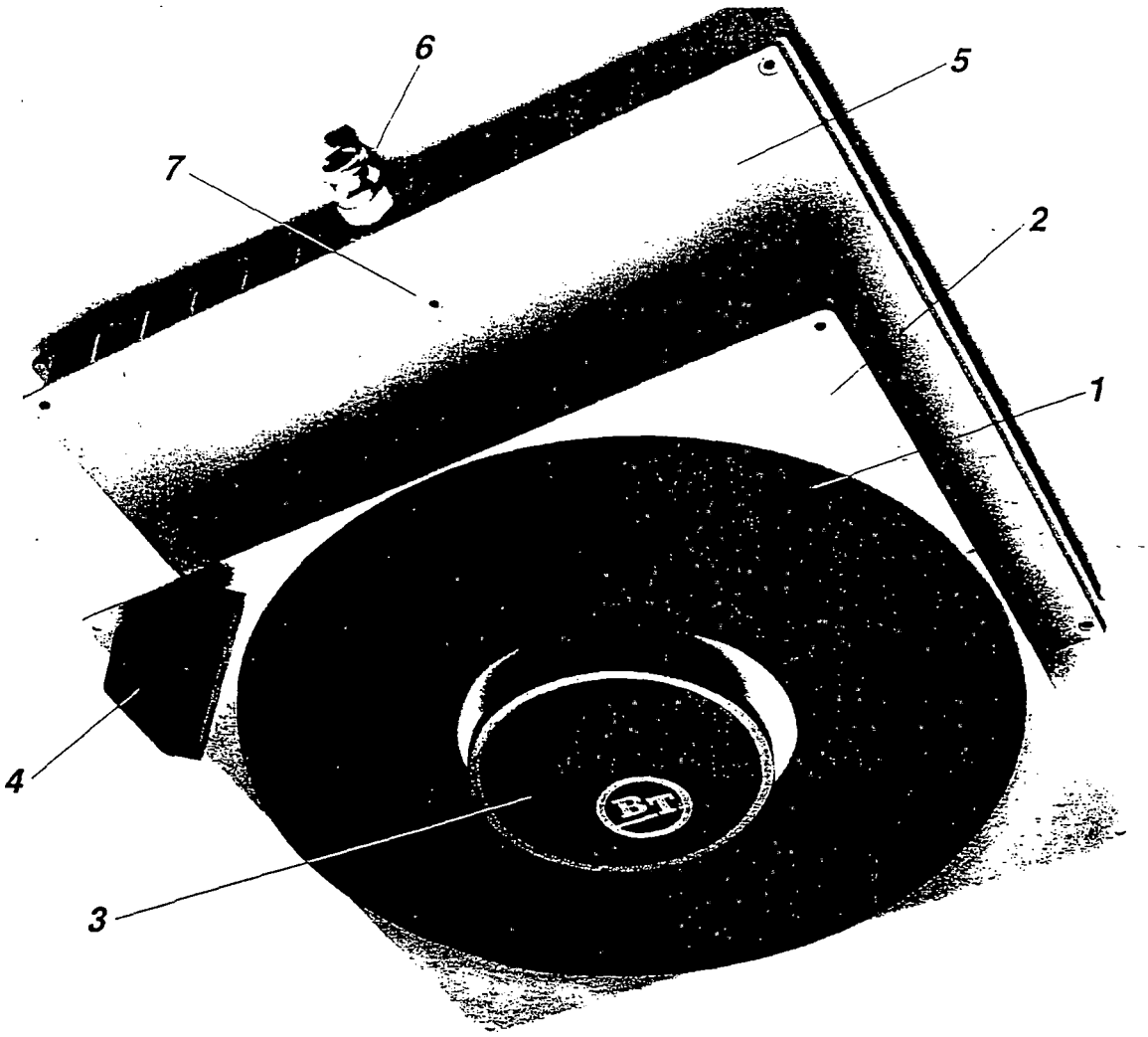

The illustration shows the components which make up a BT Air Bearing module.

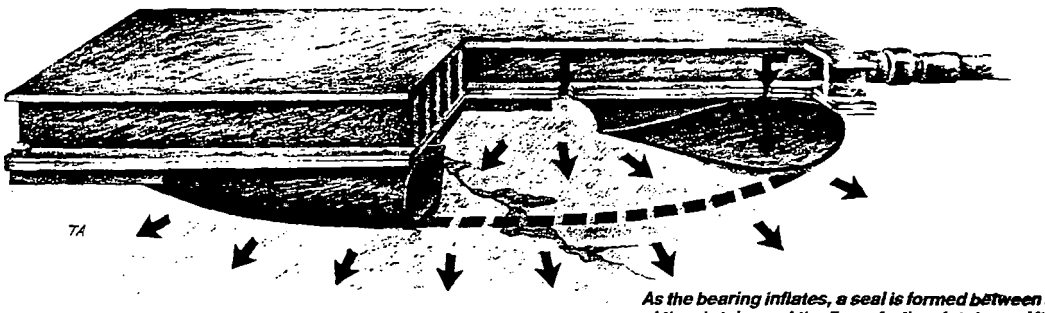

As the bearing inflates, a seal is formed between the surface of the air tube and the floor. As the air tube and its captive internal pressure increases, the module will raise until the entire encircled area is supporting the load. When maximum lift is achieved, pressure will continue to build up in the center of the bearing until air begins to escape between the air tube and the floor. This escaping air creates an air film under the whole bearing which enables the entire load to be moved around virtually friction-free.

Figure C1-36 Air bearing - general arrangement

How it works.

Modules can be fitted to a special load platform or individually positioned directly under the load.

An air bearing made of reinforced rubber (1) is vulcanized to an anodized aluminum plate (2). When the bearing is deflated, the load rests on the landing pad at the center of the module (3). Large capacity air bearings also have landing pads at the corners (4). The aluminum plate is fitted to a rigid load platform (5), which is also made of aluminum and forms a load module with a very high strenght-to-weight ratio. The supply of compressed air enters via a fixed connection in the end of the module (6) and then through a vent into the air bearing (7).

In order to achieve stability, at least three, but most often four, modules should be placed under the load. These are connected through the control unit to the compressed air supply.

The modules should be positioned as far apart as possible in order to optimise both the distribution of weight and load stability. Once they have been positioned, the valves can be opened one by one by means of the control unit. The pressure in the air bearings can be increased slowly until they lift the load and start to float. The load can now be moved with great precision in any direction and therefore be positioned exactly as required.

BT

Air Bearings – the transport and handling system of the future

Figure C1-37 Air bearing - how it works

manufacturer feels that tweaking the bearing design will result in a workable arrangement with satisfactory operating life.

Air bearings will not work well on extremely rough surfaces, although they conform well to gentle overall irregularities. The top of our guideway will be machined-trowelled concrete, which is a very acceptable surface for air bearing use. The rougher the surface, the larger the air pressure leak; capacity is not affected unless the air supply is insufficient. Snow and ice are no problem either; they might make the bearings work even better. Jagged, packed ice and hardened snow would be difficult for air bearings to work against, but this condition is hardly imaginable for a well run maglev system.

The weight of the vehicle is supported by the air pressure acting on the large doughnut hole area. The nominal pressure required will be 22 psig, and will be regulated by the vehicle's control computer as needed to keep the bogies square with respect to the box beam. Spreading out the weight over such a large an area on such a large a number of bearings keeps the structural requirements of this levitation method to a minimum.

1.6.6 Air Bearing Operating Sequence - Landing

As it starts to slow down to a stop the vehicle weight is fully supported by the magnetic suspension system, but the vehicle drops lower and lower toward the guideway the slower it goes. At some speed as the vehicle slows down, the bottom plates of the bogie would start scraping the top of the guideway were it not for the air bearings. The bearings are deployed in anticipation of the stop well before needed. They are locked in the "up" position behind cover plates when not needed, but when they need to be deployed the cover plates are moved out of the way, and an air bladder is inflated to push the air bearings to the locked "down" position. In this position they extend through the bottom plate by about 5 cm, waiting to meet the guideway as the vehicle settles toward it. As the vehicle gradually transfers its weight from its magnets to the air bearings, the air bearing doughnuts compress and become stiff until virtually the entire vehicle weight is being supported by the air bearings, and little or no lift is provided by the magnets. The air bearing touch-down speed can be made any speed desired by offsetting the SCM attachment points vertically, in effect raising or lowering the air bearings' locked positions. We expect that speed to be about 10 kph.

Since the air bearings are utilized to reduce friction and their effective coefficient of friction is a mere 0.001, the longitudinal and lateral forces on the air bearing system are almost negligible.

Note that when the vehicle has settled to rest on its resting pads that are attached to the air bearing face plates, the air bearings can be deflated and the force on the doughnuts is zero. The air supplies to the air bearings will be turned off and the vehicle will sit down with its full weight on top of the guideway beam when the air bearing levitation is not needed, such as immediately after the vehicle has stopped and immediately before it is to be started again. This approach would conserve compressed air and the electrical power required to compress it.

1.6.7 Air Bearing Operating Sequence - Taking Off

When it is time for the vehicle to start moving again the doughnuts are again filled with compressed air. The doughnuts inflate and the vehicle lifts slightly. The friction-eliminating air film is then in place and the vehicle can be propelled. As the vehicle speed increases, the vehicle weight is gradually transferred from the air bearing structure to the SCM structural support pedestals. The vehicle has completed its takeoff when the doughnuts separate from the guideway. They can then be unlocked, and a spring retracts them into their compartment. They are then locked into the "up" position and the aerodynamic cover plate closes the openings in the bottom plate of the bogie.

1.6.8 Lateral Guidance Wheels

Air bearings are extremely slippery. The effective coefficient of friction that results is only 0.001. This means that a 2,000 pound load on air bearings can be moved by a force as little as only two pounds. Such slippery bearings will cause the vehicle to slide itself sideways if it is ever on a tilted beam while landing or taking off. To provide for such a situation, lateral guidance wheels are provided to stabilize the vehicle during those times. These wheels will be required to carry their maximum load on a beam that is tilted by fifteen degrees. Multiplying the weight of the vehicle times 1 g times the sine of fifteen degrees, we get a static load requirement of 162 kN to be distributed among all of the 12 wheels on either side of the vehicle. This amounts to 13.5 kN per wheel. The rating of the guidance wheels will have to be greater than this in order to counteract side wind forces.

1.6.9 Reliability Measures

The consequences of having a vehicle stranded on the guideway if all of the air bearings fail include rescue of the vehicle via a dedicated special-purpose vehicle. Since maglev vehicles cannot go around one another, this would completely stop the maglev system in one direction in many cases. For this reason the air bearing system must be designed to be fault tolerant and to have redundancy in its components. By providing four air bearings per bogie on six separate bogies,

we have addressed the redundancy issue. Should all one bogie's air bearings be disabled, that bogie can be "picked up" by the vertical hydraulic actuators normally dedicated to ride quality duty until the vehicle takes off.

Should both compressed air systems fail, airstart cartridges can be used to provide the required air pressure and flow to the air bearing system. These devices are provided for backup duty only and are described elsewhere in this report.

1.7 HEATING, VENTILATING, AND AIR CONDITIONING (HVAC) SYSTEM

1.7.1 Overview

This report section describes the design and calculations done to provide HVAC service for the passenger version of our vehicle. The design provides for the cabin HVAC as well as the fore equipment and aft baggage compartments. We would expect to reroute ducting for a freight or train concept, but the HVAC equipment would most likely remain as is in the fore equipment compartment on those vehicle.

Although this report section is relatively brief, the amount of documentation of the design information and calculations is extensive. Most of this information has been moved from the main report body to the two appendices corresponding to this text section.

1.7.2 HVAC Fundamentals

Heating

Heating in the winter will be accomplished by passing air over electrical heating coils in the air ducts in the fore equipment compartment. The routing of the air is accomplished by ductwork and ventilating fans in the ducts which blow the air and force it to circulate. The heated air flows out of hidden ductwork in the passenger cabin ceiling, forward to return registers in the fore cabin bulkhead, through the heating coils, ventilating fan, and back up to the ceiling of the fore equipment compartment, through a sliding seal to accommodate cabin tilting, and into the overhead PC ducts to start another cycle. The heated air loses heat to the PC walls, floor, and bulkheads and needs to be reheated after circulation; however, this is not the main "heat load" to be overcome: heating the fresh air from outside the vehicle that must be mixed with the circulating air is the main heat load. This fresh air taken in for passenger comfort is known as infiltration.

Fresh air must be mixed into the circulating air to keep the passengers from feeling stuffy. Sometimes water droplets must also be added to the air if the outside air is too dry. The maglev HVAC system will be well sealed, so for every cubic foot per minute (cfm) of fresh air that is added to the circulating air, another cfm must be taken out of the circulating air and vented from the air stream. In our HVAC design we have a pressurization fan that takes in outside air and, in the process of adding the air into the circulating airstream, raises the cabin pressure by 1/2 inch of water. The exhaust air to be removed from the circulating air is vented partially into the aft baggage compartment and the rest into the fore equipment compartment, to heat those areas that are not served by the pressurized air system.

Cooling

Cooling in the summer will be accomplished by passing the circulating air over cold evaporator coils in the air ducts of the fore equipment compartment. As with most other air conditioning systems, freon is expanded from liquid to gas into the evaporator; the very cold gas inside the evaporator makes the evaporator cold and accomplishes two objectives. First it cools the circulating air, and second it causes much of the humidity in the circulating air to condense and be drained away, thereby drying out the air. All this requires an electric motor driving a freon compressor in order to make the freon circulate within its own closed plumbing system, as well as a freon condensing heat exchanger to cool the hot compressed freon via flow of outside air over the condenser.

As before when we consider the heat loads we find that most of the work that the air conditioning system does is to cool the fresh air and remove humidity from it. The conduction of heat from the hot vehicle outer surfaces to the cool PC causes the cabin air to rise in temperature and have its heat removed at the evaporator, but this heat load is small compared to the fresh air heat load.

1.7.3 General HVAC Equipment Arrangement

The total HVAC system has been separated into two half-capacity systems (one starboard and one port) to provide functionality in case of equipment failure in one system. The only common equipment to the two systems is the cabin thermostat. The drawing of the vehicle shown in another report section shows locations of the major elements of the HVAC systems. Each HVAC system consists of the following:

Item	Description	Location	Mass, kg	Power , kw
1	Ventilating Fan	EC-floor	20	3
2	Heating Coil	EC-bonnet	20	25
3	Freon Compressor	EC-floor	60	15
4	Condenser	EC-ducted to outside	10	0
5	Evaporator	EC-bonnet	10	0
6	Pressurization fan	EC-duct from outside	2	1
7	Air supply duct	PC-ceiling	10	0
8	Air return duct	PC-fore bulkhead	1	0
9	Air exhaust duct	aft PC bulkhead	2	0
10	Air filters, valves, recuperator, control hardware, plumbing, seals, registers, dampers, etc.	Distributed	--	--

Notes: EC=Equipment Compartment (fore)
PC=Passenger Cabin (amidships)
CC=Cargo Compartment (aft)
Item 1: Blower wheel driven by 440 volt 3 phase 400 Hz electric motor
Item 2: Electrical resistance heating
Item 3: Hermetically sealed 440 volt 3 phase 400 Hz unit
Item 4: Intake and exit ducts from outside vehicle are provided
Item 5: Bonnet located in duct of fore compartment. Includes thermal expansion valve
Item 6: Provides fresh air required. Can be turned off by attendants or computer if vehicle is in smoky or smelly surroundings
Item 7: Mutual but divided duct forms one duct for each system
Item 8: Grilled opening to return duct at bulkhead.
Item 9: With automatic damper control. Provides HVAC required for CC
Item 10: Details not set for concept definition

1.7.4 Equipment Type Selection

Although there are several alternative types of equipment to provide either heating or cooling, the choices were simplified by observing two design drivers. First, flammable fuels on board are frowned upon, making the electrical resistance heaters a straightforward selection over burners. Secondly, weight minimization is very important, making the vapor compression method a must for the air conditioning requirement, since any other approach would be much heavier, and also would push us toward burning fuel to provide heat. A complex tradeoff of these drivers is that electrical heating enlarges the on-board electrical system and makes it weigh more. Fortunately, the decision is made easier when we realize that burners and associated heat exchangers can be rather bulky and heavy; together with our aversion to the use of flammable liquids, these factors made us decide to use electrical heating coils. Our power source weight is projected to be 2.05 kg/kw x 79.1 kW = 162.1 kg heavier due to the heating load.

A hermetically sealed motor and compressor unit is well known to be the lightest and most reliable type and was automatically selected without considering separate motors and compressors. 400 Hz 440 V 3-phase units are not currently available but certainly could be designed and manufactured specifically for the maglev vehicle in order to reduce weight compared to 60 Hz units.

Some details of the ducting, heat exchangers, and other hardware can be found in the appendices. Currently available equipment was selected based on manufacturers' catalog data. Improvements in the performance and weight of this equipment would be improved via custom redesign for the maglev vehicle.

1.7.5 HVAC Capacity Calculations

Per NMI specifications, the maglev vehicle's operating environment includes full capacity operation from -40 to +50 ° C. Sufficient heating and cooling capacity has been provided to maintain the passenger cabin at 20 ° C under this range of temperature at either of these extremes, with either a full passenger load or an empty vehicle. The on-board power system has been sized to provide the corresponding electrical power requirements for the HVAC system.

Determining the ratings and therefore the size of the HVAC equipment is required in order to estimate the size, weight, cost, and electrical system impact. The calculation of these parameters via HVAC design procedures is a rather lengthy process consumes too many pages to be appropriate for inclusion in this report section, so the calculations are found in the appendix.

The following tables summarize the calculations found in the appendix:

HVAC Maximum Heat Load Analysis at Extreme Conditions

All loads are in kilowatts of heat transfer, not kw of electrical load

Summer cooling loads

Ambient conditions: -50 C, 90 percent relative humidity

Cabin conditions: +25 C, 60 percent relative humidity

PASSENGER BODY HEAT	12.3
ELECTRICAL EQUIPMENT IN CABIN	9.5
CONDUCTION THROUGH CURVED WALLS	1.8
WINDOW CONDUCTION	0.9
FLOOR & END WALLS	5.6
FRESH AIR COOLING -- GAS COMPONENT	35.9
FRESH AIR COOLING -- HUMIDITY COMPONENT	158.8
TOTAL	224.8

Winter heating loads

Ambient conditions: -40 C, 60 percent relative humidity

Cabin conditions: +25 C, 40 percent relative humidity

CONDUCTION THROUGH CURVED WALLS	2.8
WINDOW CONDUCTION	1.5
FLOOR & END WALLS	8.8
FRESH AIR HEATING-GAS COMPONENT	56.4
FRESH AIR HEATING-HUMIDITY COMPONENT	9.6
TOTAL	79.1

When heating electrically as in our concept, every kilowatt of heat load must be derived directly from the on-board power electrical source on a kw per kw basis, so the electrical demand for heating is 79.1 kW. When cooling this is not the case. The energy efficiency ratio for a typical air conditioner shows that normally 1 kW of electrical power will handle 3 kW of heat load. This is a true power amplification. If the heat energy were recoverable then we could use air conditioners to get free power, but we cannot because the heat involved is at too low a temperature. In any event, due to the high condenser temperature of 50 ° C, the air conditioner requires about 0.4167 electrical kW per heat kW, so the electrical power requirement is 0.4167 x 224.8 = 93.7 kW, which is still larger than the maximum heating load of 79.1 kW even considering the energy efficiency ratio of the air conditioner. The primary reason for this is the incredible heat transfer demanded by condensing moisture out of hot, 90 percent humid air.

Pie charts showing the load percentages are shown in Figures C1-38 and C1-39. Due to the large fresh air requirement of 15 cfm per passenger, the infiltration requirement dominates the HVAC design. Should that requirement be reduced, our HVAC system would be smaller, lighter, and require less electrical power to run it. 15 cfm is an ASHRAE standard and may not apply. This issue should be reviewed and made an RFP specification in future design exercises.

Several GWBASIC computer programs are listed in the appendices. We will provide copies of them on IBM diskettes to interested parties. These programs make it extremely easy to evaluate the impact changes in our vehicle design upon its HVAC requirements. Program EMDHEATF calculates the various steady state heating loads. Program EMDCOOLF calculates the various steady state cooling loads. Program EMDSTR calculates the transient heating or cooling time.

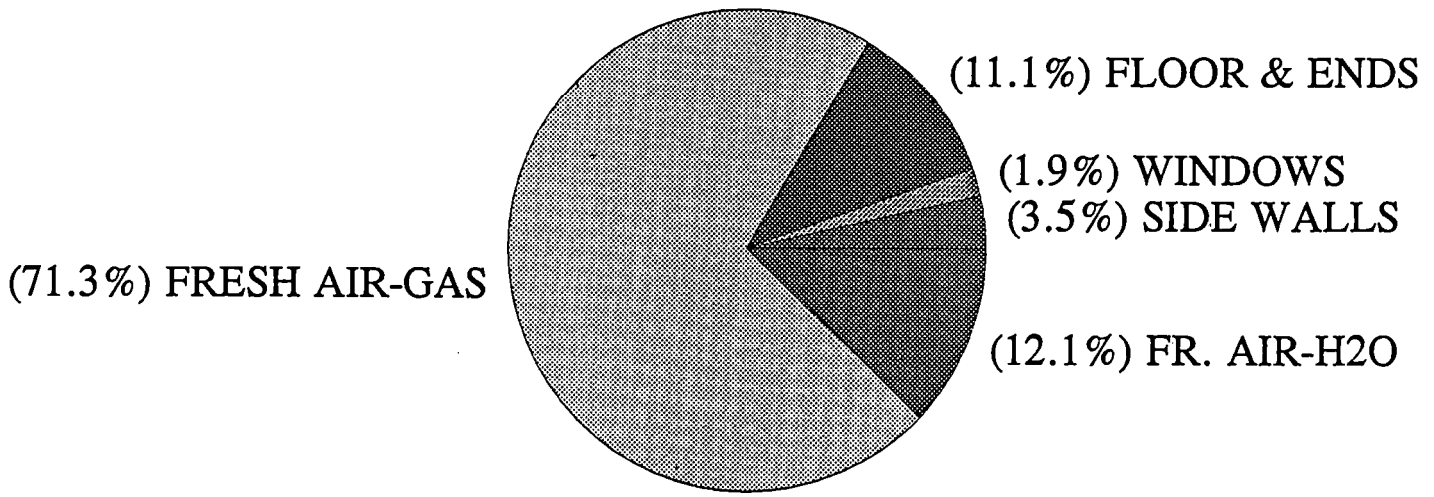

Figure C1-38 Winter heat loads at extreme conditions

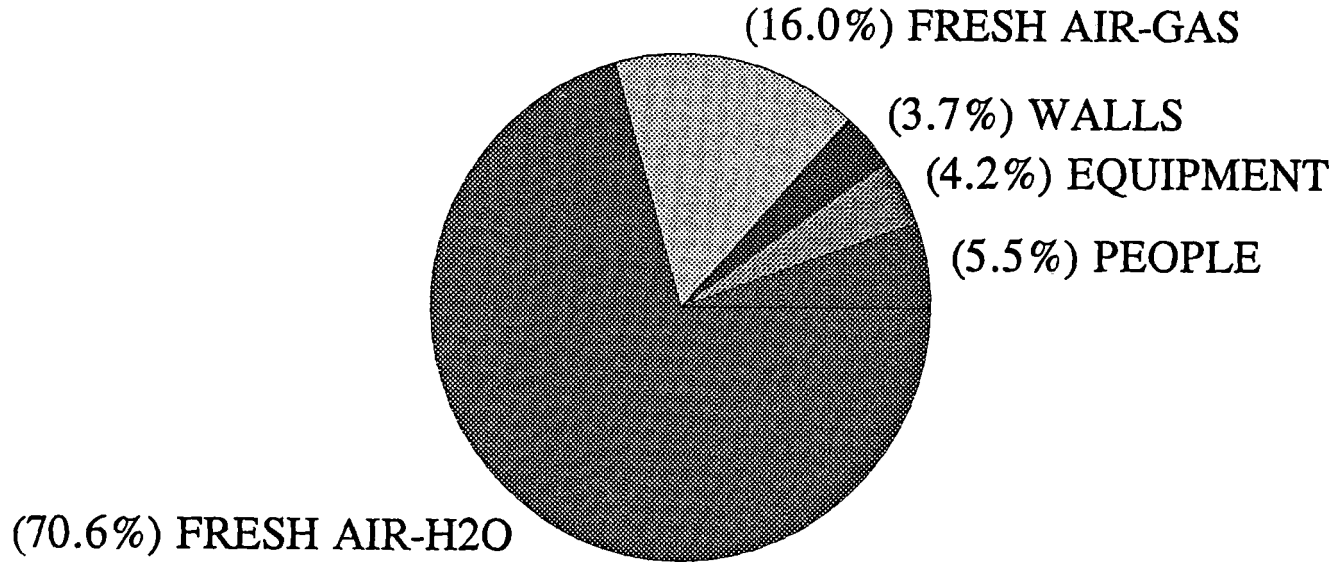

Figure C1-39 Summer cooling loads at extreme conditions

Some important aspects of the calculations found in the appendices are noted here:

- The combination of an inner passenger coach separated from a thickly insulated shell by an inch of still air reduces HVAC power requirements substantially and offsets vehicle weight and cost increases attributed to the tilting inner coach. We estimated this effect by setting the inner coach wall and dead air space thicknesses (L56 and L67) to zero and rerunning the computer programs listed in the appendices. The result was that electrical power requirement for heating increased by 25.5 kW and the for cooling by 6.8 kW.
- The largest component of the power required for either heating or air conditioning is the infiltration requirement. The humidity of the infiltrating air drastically effects the heat transfer demand for that fresh air. Figures C1-40 and C1-41 show how that demand is affected by humidity. Obviously our HVAC system would be smaller, lighter, and demand less electrical power if we did not assume that we must handle a 50 degree C, 90 percent humidity ambient air condition. This issue should be reviewed and made an RFP specification in future design exercises.
- A factor which affects the HVAC loads is the heating of the air at the vehicle exterior skin. At 500 kph vehicle speed, the air layer sliding over the skin generates frictional heat to 10 degrees Centigrade. Essentially, the skin temperature difference that the HVAC system works against is raised by 10 degrees.
- The transient performance computer program EMDSTR was run to estimate the heatup and cooldown time. This information pertains to vehicles that have been in a storage barn before starting a day's service. We would expect the HVAC systems to run at reduced capacity or to be turned off to save energy costs. The program runs shown in the appendices predict that it would take 40 minutes to cool the cabin from 50 to 25 degrees C; the time constant being 20 minutes. We regard this as more than satisfactory. The cooling time increases 22 percent when the material is density is varied from 50 to 300 kg/m^3. The cooling time increases 15 percent when the thermal conductivity of the walls varies from 0.01 to 0.06 (the baseline is 0.03).

1.7.6 Humidity control

Usually an air conditioner removes moisture from the air via condensation on the evaporator. When heating, the HVAC system will often add moisture to the air via a water spray nozzle. This is the same approach used in a building HVAC system in order to control humidity, which is an important ingredient in passenger comfort. Occasionally the HVAC system will be required to add moisture when air conditioning and the outside humidity is low, or to remove moisture when heating and the outside humidity is very high. In these cases both the air conditioning and heating systems are run simultaneously to achieve humidity control. In the former case the water spray nozzle is employed, causing no extra power requirement. In the latter case the air conditioner removes moisture but subcools the air, and the heaters must work extra hard to offset the subcooling. This does take additional on-board power, but fortunately it is not likely that this

would be simultaneously with outside air temperature at the extreme limits, and therefore the electrical system capacity is not affected.

1.7.7 Cabin Pressurization

The cabin will be pressurized via a pressurization fan and controlled exhaust air dampers. 125 Pa (0.5" H^2O, or 0.037" Hg) will be the pressure level, which is not noticeable by passengers and has no effect on them. When the vehicle doors are open, the pressurization system will be inoperative. Pressurization has the benefit that good HVAC control is made possible. Should the pressurization be lost, maintenance personnel would be alerted to the need to find the breach in the sealed cabin and repair it, restoring the HVAC system to its maximum capacity. Pressurization also prevents dirt, dust, smoke, and other unwanted contaminants from entering the cabin.

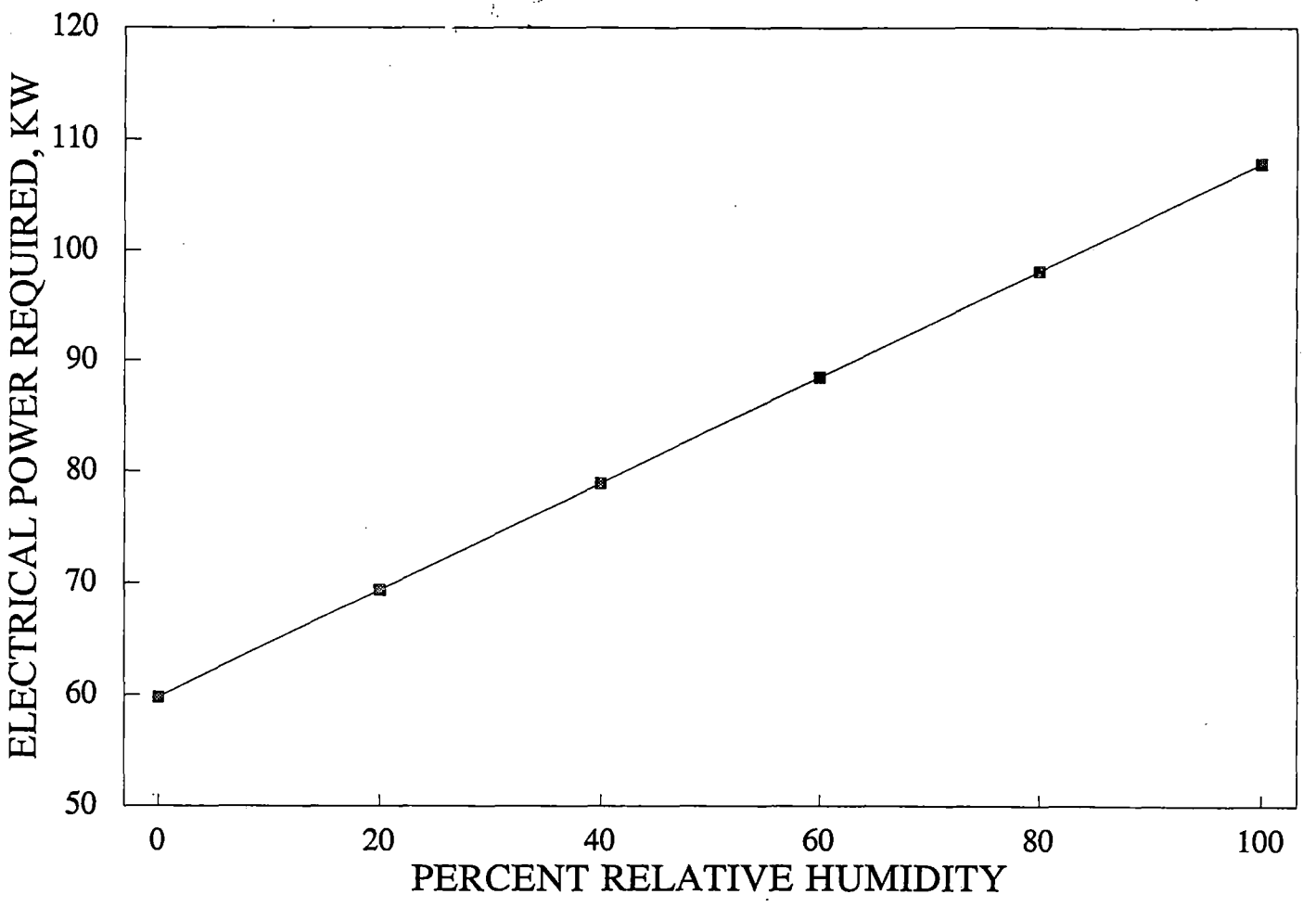

Figure C1-40 Effect of outside humidity on heating

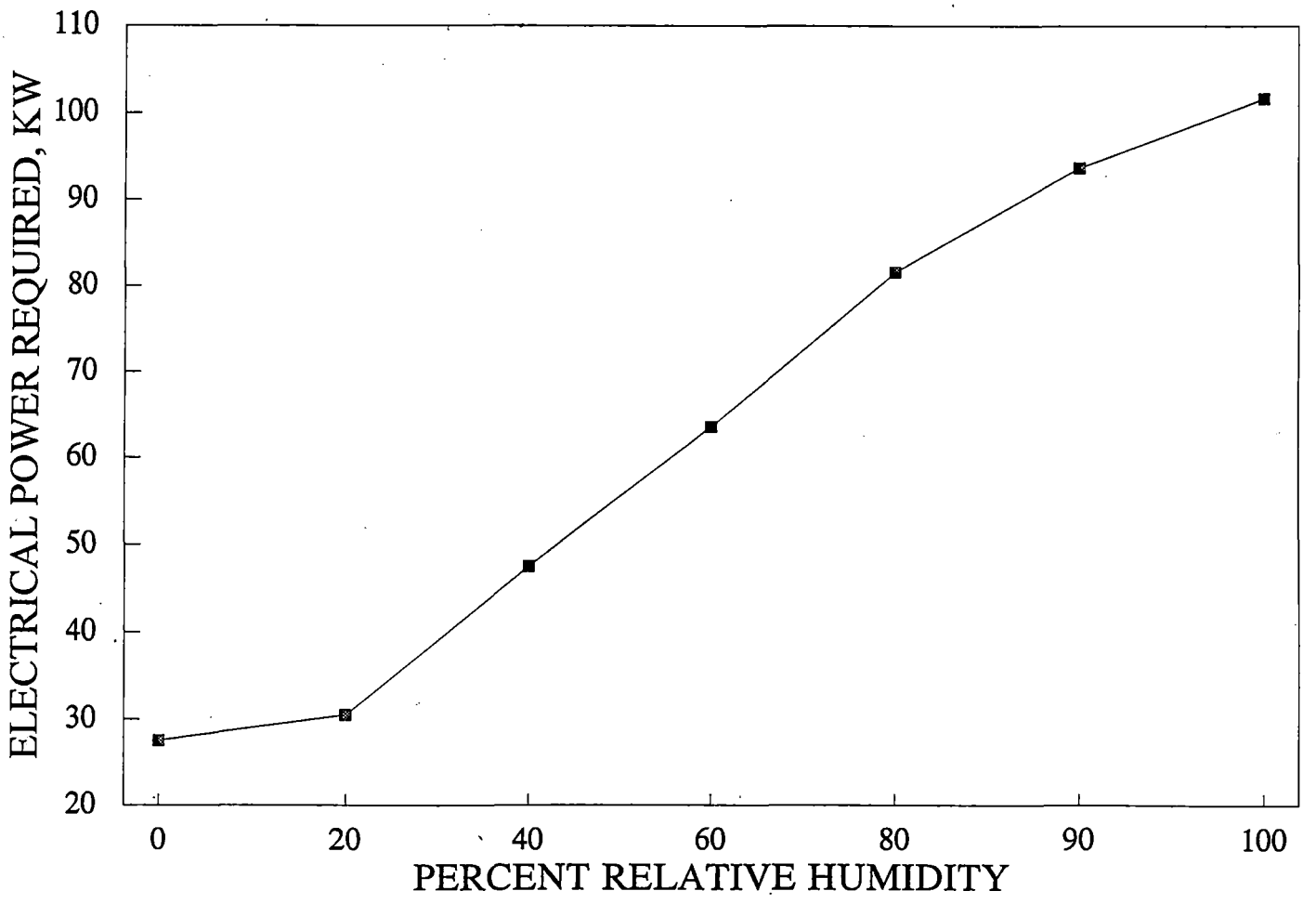

Figure C1-41 Effect of outside humidity on cooling

1.8 VEHICLE COMPRESSED AIR SYSTEM

1.8.1 Devices Requiring Compressed Air

The air bearings which provide low speed lift for the Bechtel Team's vehicle require a compressed air supply for their operation. They are described in detail elsewhere in this report. Toilets and galleys also may require small amounts of compressed air, but those requirements are intermittent and small, so they are not discussed further.

1.8.2 Air Flow Requirements

Figure C1-42 is a calculation sheet which shows how the required air flow and pressure for the air bearings has been determined. These calculations follow the recommended calculation method according to literature provided by the American Solving Company, a leading manufacturer of air bearings and associated equipment. The nominal air requirement at the air bearing air inlets is 95 scfm per bogie at 21 psi. This is four times the air flow, but the same pressure, for each of the four individual air bearings attached to each bogie. This air requirement is calculated assuming that all air bearings carry the same portion of vehicle weight, but in windy conditions there may be an imbalance between the port and starboard side bearings in order to counteract a wind moment. The compressed air supply will have to be sized for this windy condition.

Additional air supply considerations: Our air bearings have been designed to be deployable and retractable. Normally the air bearings will be inside the bogie behind a cover plate to reduce aerodynamic drag. This also protects the air bearing from damage due to flying debris. When the air bearing is needed, the protective cover plate is moved out of the way pneumatically. The air bearing is then lowered via an inflatable bladder that is filled with compressed air in order to push the air bearing downward to stops, at which point the air bearing is mechanically locked in position and the air bladder ceases to function. Figure C1-43 shows this arrangement, and Figure C1-44 shows the air requirement calculation for the air bladder and the cover plate mechanism. The information in Section C-1.6 should be consulted regarding compressed air volume calculations.

Operation time: The air bearings will need to support the vehicle only while coming to a stop between 10 kph and 0 kph, and when starting the vehicle from 0 to 10 kph. Each of these intervals will take, at 0.2 g deceleration/acceleration, roughly five seconds (we neglect jerk and jolt rate limitations for now). In between stopping and starting, the air bearings will be shut off and the vehicle will settle onto the guideway at zero-speed support pads on the air bearing face plates.

Area A = 24 bearings × $\pi D^2/4 = 24 \times \pi(21)^2/4 = 8308$ in^2

Operating pressure (nominal conditions)

$$W/A = 64{,}000 \text{ kg} \times 2.205 \text{ lb/kg} / 8308 \text{ in}^2 = 17 \text{ psig}$$

Seal drop = 4.9 psig ≅ 5 psig

Total pressure = 17 + 5 = 22 psig

Scfm (standard cfm: at 14.5 psi) per bearing = 12 to 71 depending upon surface condition

Machine trowelled concrete: 20 percent roughness factor.

Per American Solving's calculation procedure, the total air flow per bogie in scfm is

$$T = [(m_1 + m_2)p + m_2]n = [(71-12)(.2)+12]4 = 95.2 \text{ scfm/bogie}$$

Here, m's are upper and lower mass flow limits, p is the roughness factor, and n is the number of air bearings per bogie. Scfm numbers are always at 14.5 psi, not the actual pressure being used..

Figure C1-42 Air bearing flow requirements

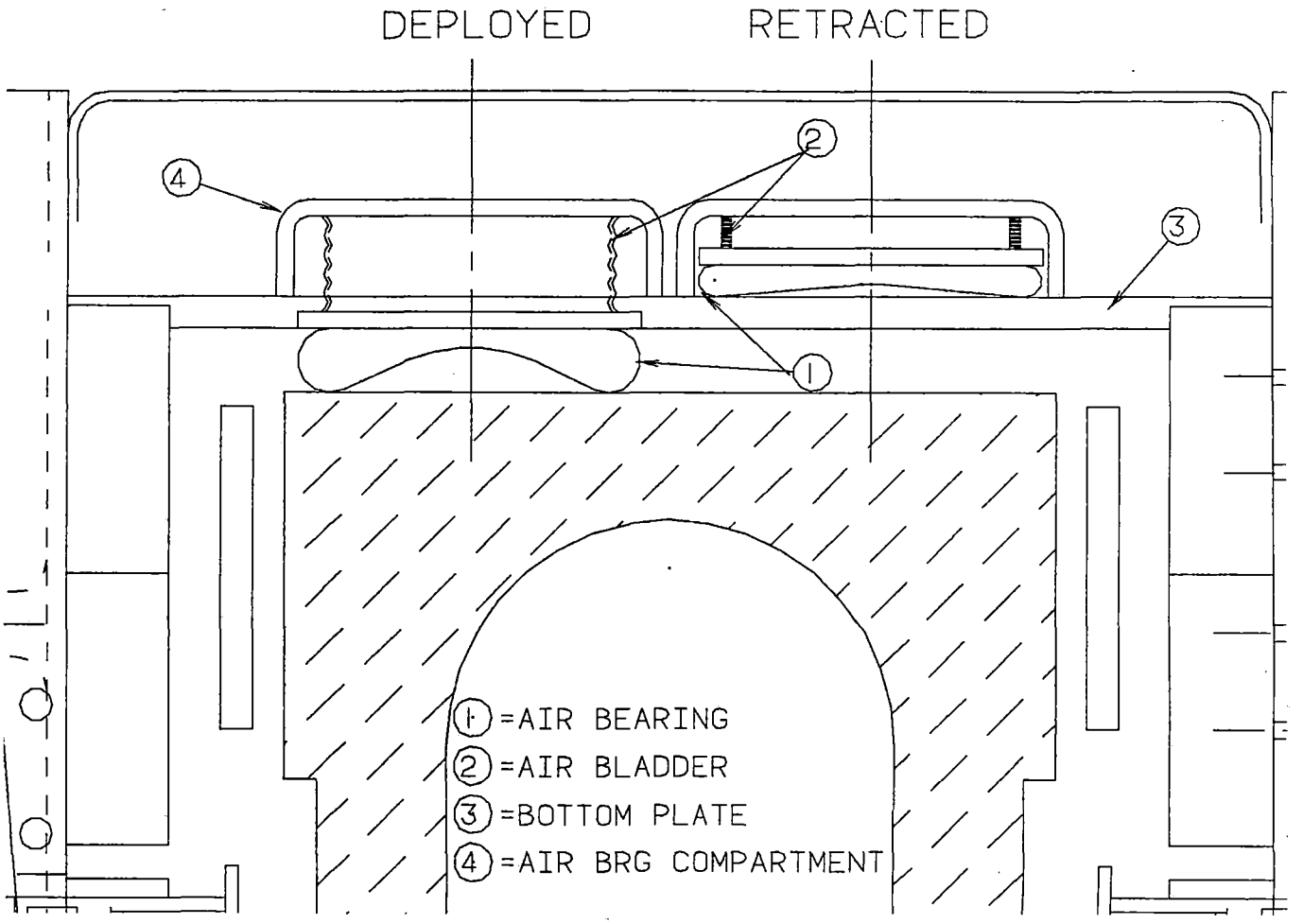

Figure C1-43 Air bearing arrangement

For air bladder:

Use same 22 psi regulated pressure from tank

Use same 21 inch diameter as bearing.

$F=PA=22\ psi \times \pi D^2/4 = 22\times\pi(21)^2/4=7620$ lbs/bladder, ×24 bladders=173,153 lbs

$V=AH=(\pi D^2/4)H = (\pi(21)^2/4)(5") = 1732\ in^3$, ÷ 1728 $in^3/ft^3 = 1.0\ ft^3$ per bladder

Scfm=1.0 ×22/14.5 = 1.52 scfm (@ 60 deg. F) per bladder/bearing

No leakage out of bladder once filled!

For cover plate actuator:

Assume 2" dia. pistion, 21" stroke

$V=AH=(\pi D^2/4)H = (\pi(2)^2/4)(21") = 66\ in^3$, ÷ 1728 $in^3/ft^3 = 0.038\ ft^3$

(Small enough to neglect)

Total Air Requirement per bogie:

- Bearings 95 scfm/bogie × 20 seconds/60 = 32 scfm
- Bladders 1 scfm × 4 bladders/bogie x 0 seconds = 0
- Cover plate actuators 0.038 × 4/bogie × 0 seconds = 0

Total 32 scfm per bogie

Figure C1-44 Total air flow requirements per bogie

In addition to the above 5-second operational intervals, we must consider inflation and actuation times for the air bearing, air bladder, and cover plate. Assuming that it takes another five seconds for the air bearing/bladder combination to inflate, and assuming the time for the cover plate to operate is negligible, then the total operational time required increases to 10 seconds per stop and 10 seconds to start, for a total of 20 seconds of air flow per incident. This results in a total scfm requirement of 32 scfm per air bearing, times 24=768 scfm per incident for the entire vehicle. If we allow the air compressors to recharge the air tanks between stopping and starting, this requirement is cut in half, at the expense of requiring a short waiting time after every stop. We did not elect to add this requirement to our concept, so the compressed air system has been sized for no delay between stopping and restarting the vehicle. We also decided to use a 100 psi working pressure in the tanks. We have a 768 scfm requirement, and 16 cu ft/tank x 24 tanks is 384 cu ft, so we only need (768/384)x14.5 =29 psig. By selecting 100 psig storage pressure there will be enough (ignoring throttling losses) for 100/29=3.4 stopping incidents.

1.8.3 Selection of Air Supply Method

There are several alternative approaches to providing the required air supply. Those that we considered are listed chronologically (as considered) in Table C-10.

Table C-10
Compressed Air Alternatives

Air/Gas Source	Storage Tanks	Redundancy	Weight	Comments
2 MDAC's in fore compartment	none	medium	high	High power demand
2 MDAC's, one fore, one aft	none	med-high	high	High power demand
6 MDAC's, one on each bogie	none	high	high	High power demand, too much unsprung mass
Expanded liquid nitrogen	none	medium if two LN2 tanks	medium	Current SCD has no LN2
2 small MDAC's, one fore, 1 aft	part of bogie	medium	low	Selected for baseline SCD
Expanded liquid helium	none	medium if two dewars	low	May not be feasible. Emergency only. Asphyxiation, icing.
Airstart cartridges	part of bogie	high-two at each air tank	low	For backup purposes only due to expense

Note: MDAC=Motor Driven Air Compressor

Our end result was a system of two-motor driven air compressors, one at each end of the vehicle, delivering air slowly to air tanks built integrally into each bogie. The advantages of this approach over the other approaches are:

- Storing air results in less vehicle weight than providing the required air flow continuously.
- Storing air requires less motor electrical power input and therefore reduces the on-board power electrical system requirements. (This advantage actually is a disguised weight advantage).
- Combining the functions of air storage and SCM force transmission into the top of the bogie weighs less and uses less space than separate air storage tanks and bogie structure.
- The bogie top structure, with four integral air cylinders, can provide about 16 cf of air storage space. Since the requirement is 32 scfm, the required air at nominal conditions can be stored at only 2 atmospheres of pressure elevation. Storing air at even higher pressure will allow the air bearings to be operated in windy conditions and still provide a safety margin. Since 100 psi is not difficult for compressors or air tanks, we set our air system pressure at 100 psi.

One of the more interesting proposals in Table C1-10 is the use of airstart cartridges. These cartridges screw onto a fitting somewhat like automotive oil filters are mounted. There is an electrical connection in the fitting that sets off the cartridge when compressed air (or more accurately, nitrogen) is needed. Such devices are used to start WW II vintage bomber engines when that aircraft's normal compressed air supply has been dissipated. The cartridges cost in the range of $100 each nowadays, so their use at every routine vehicle stopping point would be expensive. We include a pair of them on each air tank for further redundancy and fault tolerance in case of a compressed air system failure. When the LSM lifter concept has been developed into a reliable system, the need for sizable air compressors will disappear and the airstart cartridges may be employed as the sole air source for the air bearings.

1.8.4 Description of Equipment

High speed air compressors: Vehicle weight reduction is one of the major efforts in our study. In order to reduce air compressor and motor weight, we expect to use high speed compressors (4,000 RPM driven by 12 pole 400 Hz motors). Currently they are shown in the front compartment of the vehicle. Mounting one compressor on each bogie might be considered in order to reduce the high-pitched acoustical noise in the passenger compartment.

Air bearings: See separate report section on zero speed lift devices for a full description and discussion about the air bearings.

Air bladders: The air bladders which lower the air bearings onto the top of the guideway are expected to be similar in diameter to the air bearings themselves and to operate at the same inlet pressure as the air bearings. Locking mechanisms will have to be provided to keep the bladders and bearings in place when not in use. Mechanical stops will have to be provided to keep the air bladders from extending farther than intended when operational.

Air tanks: When combining the functions of air tank and bogie structure, it seems inviting to design the tank as a rectangular cross section rather than the normal circular cross section of a typical pressure vessel. This would seem to make the load-carrying function of the bogie easier (literally 'straight' forward). Pressure vessels have circular cross sections to reduce wall stresses, but rectangular pressure vessels can be used if the pressure is low and the resultant stress also low. The easiest way to keep the stress low, of course, is to keep the air pressure in the tank low. Since each bogie's tanks will supply four air bearings, it also seems natural to provide four air compartments in each tank (four tanks in one, if you will). This prevents loss of air to all four bearings in the event of a severe air tank leak (air levitation on three bearings is feasible). The air line from the air compressor to the bogie would probably feed a manifold to distribute air through check valves to each compartment. The aluminum air tank would be compartmentalized via internal flat walls welded longitudinally and cross braced laterally in order to withstand the air pressure from within. Suspension loads on the tank structure would be in addition to the air pressure loads.

Another approach is to provide cylindrical air tanks but use them as structural elements of the bogie. This approach has the advantage that the air tank mass can be concentrated where needed in order to carry the forces from the four pairs of superconducting magnets, and also that the pressure vessels will be roundish as is conventional. This is the approach that was taken and has been incorporated into our bogie design, as described in another section of this report. The tanks are actually elliptical with a 30.5 cm horizontal major diameter and a 25.4 cm vertical minor diameter, in order to make the tanks just a bit squatty and save a centimeter on vehicle height.

Air supply lines: We envision two main air supply systems as shown in the schematic diagram of Figure C1-45. Compressor system number 1 (MDAC 1) in the fore equipment compartment would supply air through a 1 inch stainless steel line on the port side of the vehicle, and MDAC 2 in the same area would supply air through a line on the starboard side. These lines would be connected via a crossover line with a control valve in it, between the two center bogies. The connection to the bogies would be made downward near the number 2 and number 5 bogie centers to minimize the amount of flexing required (these bogies have the smallest displacements relative

to the vehicle body). Interconnections of the air supply from one bogie to another would be made longitudinally using additional flexible lines.

There might be a provision made for filling air tank from an adjacent bogie's air tank instead of directly from the compressor. This might be useful in case of an air supply line rupture or a failure of one of the two air compressor systems. The second air compressor system would end up doing all the work, but computer-controlled crossover valves between all adjacent bogies might make the supply system more fault tolerant, assuming that the reliability of the crossover system were sufficiently high.

The air lines from the storage tanks to the bladders, bearings, and cover plates would be very short because the tanks are adjacent to these devices. Height-sensitive pressure regulators would control the flow to the bearings, while standard regulators would feed air to the bladders and cover plate actuators. Sensors would allow the air to be supplied only when the bogie is close enough to the guideway and the vehicle is moving slow enough, in order that the air not gush out of the tanks and through any huge gap between the bearing and the guideway surface.

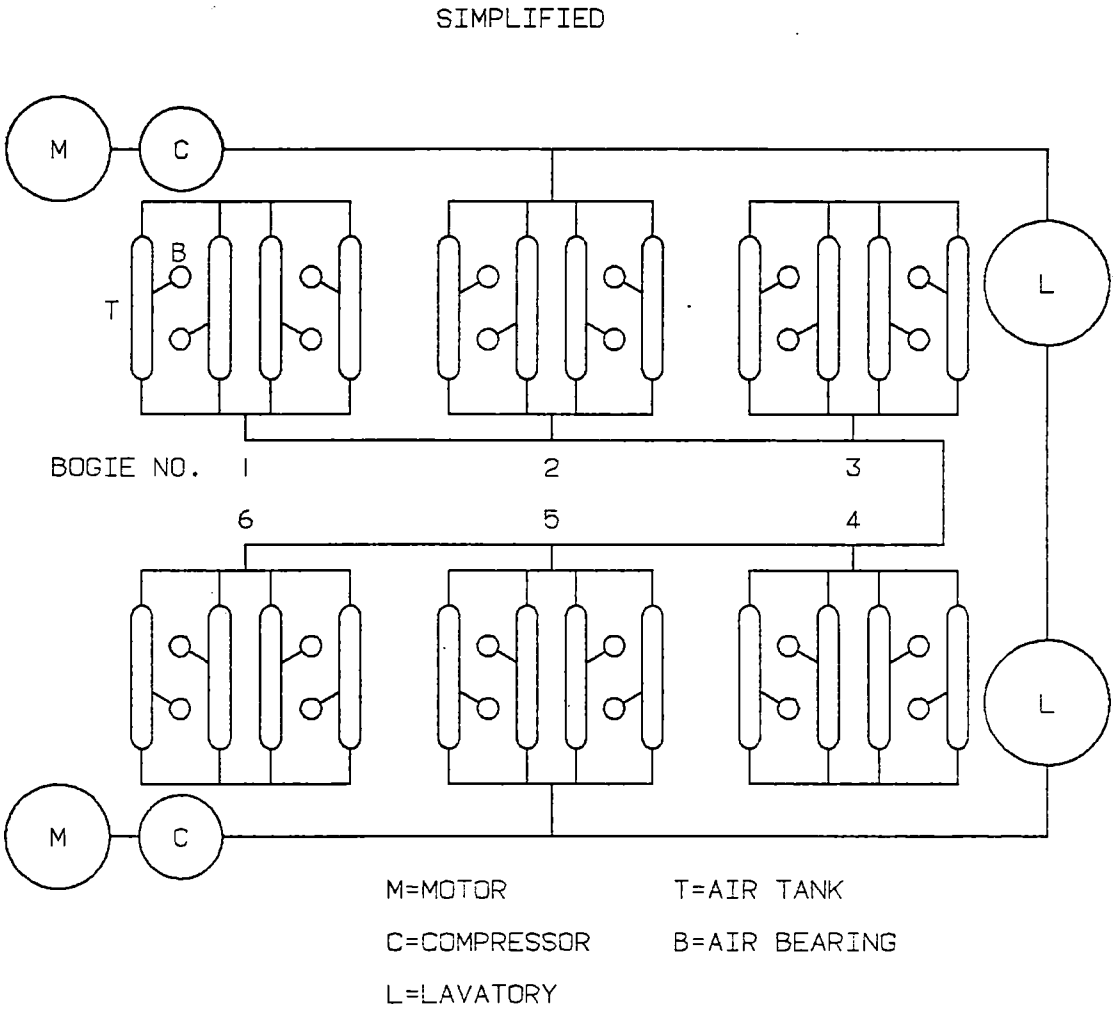

Figure C1-45 Compressed air system

1.9 PARKING BRAKE/GUIDANCE WHEEL ASSEMBLY

1.9.1 Purpose

The maglev vehicle operates in a severe environment in which there are naturally occurring forces. One of these forces that the maglev vehicle must be designed to handle is the side wind force which can have a magnitude of over 200 kN. When the vehicle is moving with respect to the beam, magnetic forces are produced to levitate and guide the vehicle along the beam. These same magnetic forces would counteract any external side wind forces and have been accounted for in the design of the levitation and guidance system, therefore it is not necessary for the vehicle to be designed to have a special mechanism to handle high side wind forces when the vehicle is levitating by magnetic forces. It is necessary, though, to provide a parking brake mechanism for the vehicle when it is stationary so that the side wind forces do not cause any unwanted motion of the maglev vehicle, specifically rocking. Our vehicle, with its totally exposed shell, mounted on to a rather narrow beam, is more vulnerable to overturning wind forces than more sheltered designs. We have always realized that we must provide our vehicle/guideway design with the ability to handle such wind conditions. It is also necessary to have lateral guidance wheels to reduce the friction and guide the bogies so that the vehicle can start moving again until the ladders and guidance coils start performing their functions.

1.9.2 Requirements

Verbal government communications stated that the maglev vehicle must be able to withstand side winds with velocities of up to 53.6 m/s (120 mph). It has also been calculated by Draper Laboratories that the vehicle would have to cease operation if wind speed of 26.8 m/s (60 mph) or higher exist. At a wind speed of 17.8 m/s (40 mph) the maglev vehicle can operate at normal conditions. The speed that the vehicle can safely operate at between wind speeds of 17.8 m/s and 26.8 m/s is a linear relationship. Therefore, as wind speeds increase from 17.8 m/s to 26.8 m/s the operating speed of the vehicle have to decrease linearly from 500 kph to 0 kph.

1.9.3 Description of Parking Brake and Guidance Wheel Assembly

The purpose of a parking brake for the maglev vehicle is to hold the vehicle in a stationary position on the beam. This concept is similar to the parking brake usually found on automobiles. The parking brake must hold the vehicle on a steep grade as well as in a strong side wind. A stopped 64,000 kg maglev vehicle on a grade with a resting pad friction constant of only 0.1 will not slide in the direction parallel to the beam unless the grade is over ten percent. The only purpose of the parking brake is to keep the vehicle stable when a side wind is acting on the vehicle.

The maglev vehicle does not have any appreciable guidance forces below a vehicle speed of about 4.5 m/s. At this low speed the vehicle uses air bearings to achieve a low friction surface between the top surface of the beam and the vehicle. The air bearings do not give any guidance forces. Due to the small flat surface area available on the vertical side of the beam, air bearings could not be used as used on top of the beam to help guide the vehicle. Small wheels in the parking brake assemblies will be used to provide the required guidance force.

Both the parking brake and guidance wheel will be required to be clamped onto the beam. Since both the parking brake and guidance wheel will be required to be applied in a clamping fashion, it is then practical to incorporate both mechanisms into one assembly. For simplicity, the term parking brake assembly will be used to denote the joint assembly of the parking brake and guidance wheel.

Figures C1-46, C1-47, C1-48, and C1-49 show the parking brake assembly designed for our maglev vehicle. The guidance wheel and parking brake are two different devices combined into one. The guidance wheel is able to slide horizontally along a track which is part of the parking brake mechanism. The guidance wheel center axle is guided by a track which is part of the parking brake structure. Part of the guidance wheel structure is a cylinder which fits though a hole in the parking brake structure. This allows the guidance wheel structure to move laterally with respect to the parking brake structure. The reason for this is that the guidance wheel requires a smaller amount of clamp force than the parking brake. The amount of clamp force for the guidance can be controlled by the specific design of the spring and the hydraulics. The parking brake clamp force can be applied directly by hydraulics that would move the attached lever arm as shown in Figure C1-48. To apply the guidance wheel to the beam, the hydraulics would move the lever arm to push the parking brake assembly laterally into the beam side. To apply the parking brake, an increased force from the hydraulics will be supplied that is great enough to collapse the spring which would cause the parking brake pad to move in toward the beam and engage it. The essence of the whole assembly is based on the design of the spring to not collapse at a certain load. Figure C1-49 shows the parking brake in contact with the beam.

1.9.4 Analysis: General Approach

Analysis of the effect of side wind forces upon vehicle/guideway reaction forces was accomplished using the free body diagram shown in Figure C1-50. Although the diagram is two dimensional, the side wind forces for a stopped vehicle are assumed to be at right angles to the longitudinal axis of the vehicle and evenly distributed over its length, therefore the simpler two

dimensional approach is valid. The equations of static equilibrium corresponding to figure 5 were written and solved in closed form and the resulting closed form solutions were checked using *Mathematica* software. Table C1-11 lists the parameters shown in Figure C1-50 along with the respective meanings and any known numerical values of the parameters of the analysis.

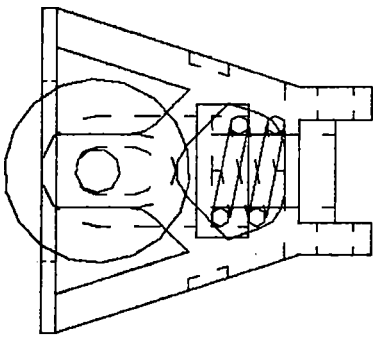

TOP VIEW

PARKING BRAKE ASSEMBLY
WITHOUT LEVER ARM

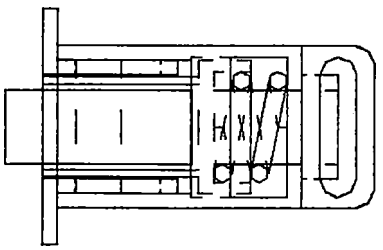

FRONT VIEW

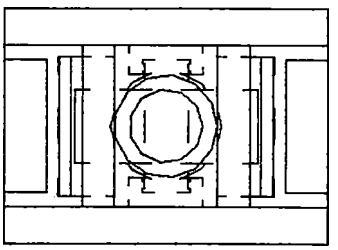

RIGHT VIEW

Figure C1-46 Parking brake configuration

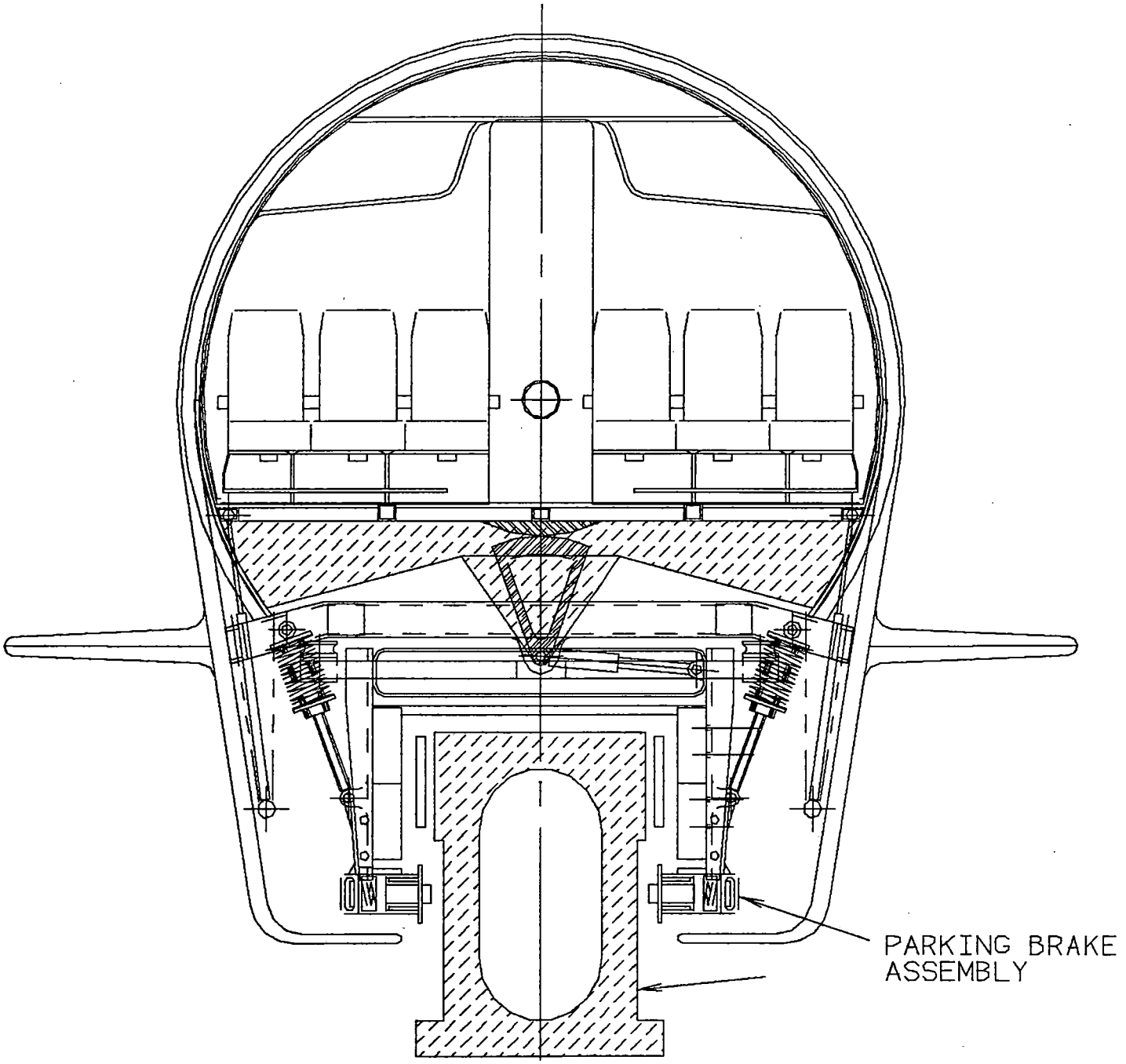

Figure C1-47 Parking brake configuration

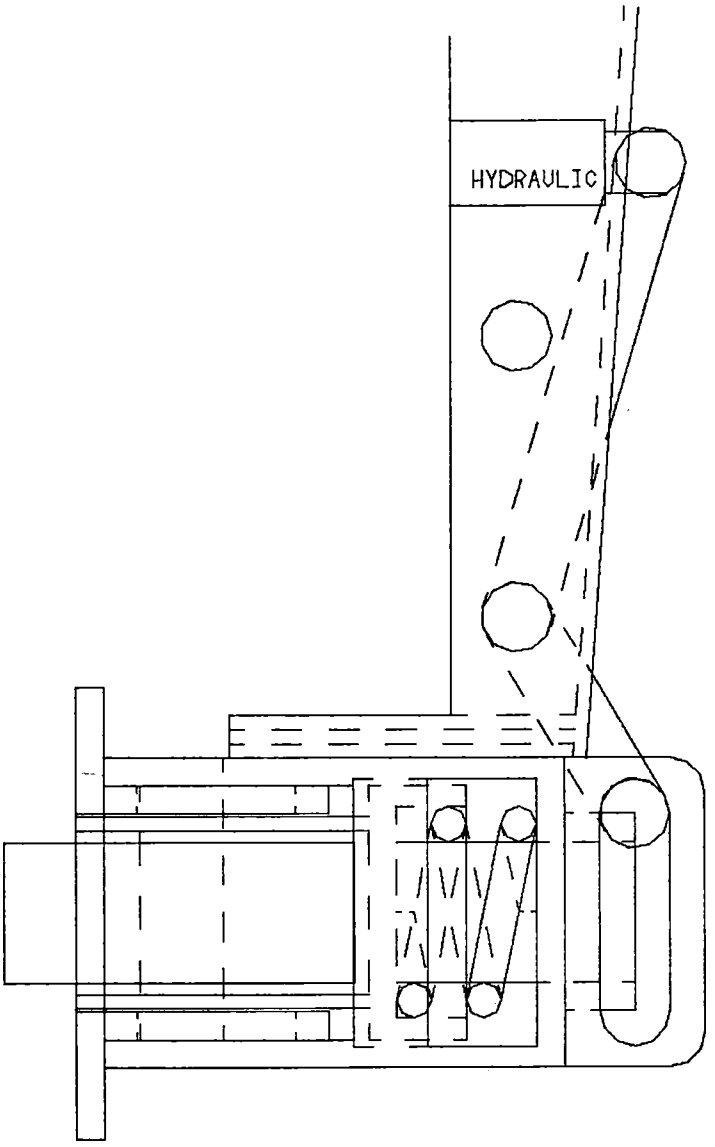

Figure C1-48 Parking brake configuration

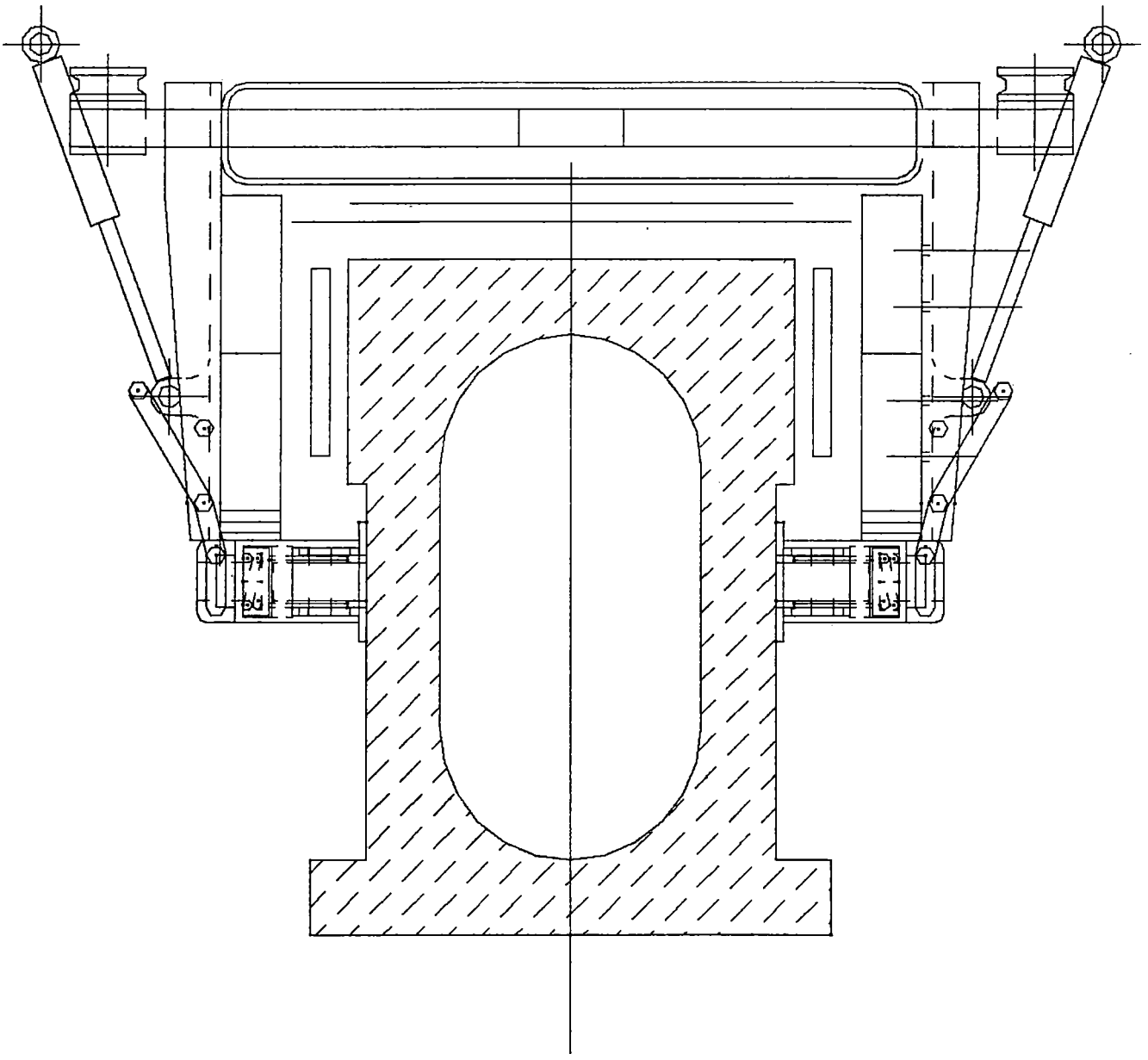

Figure C1-49 Parking brake configuration

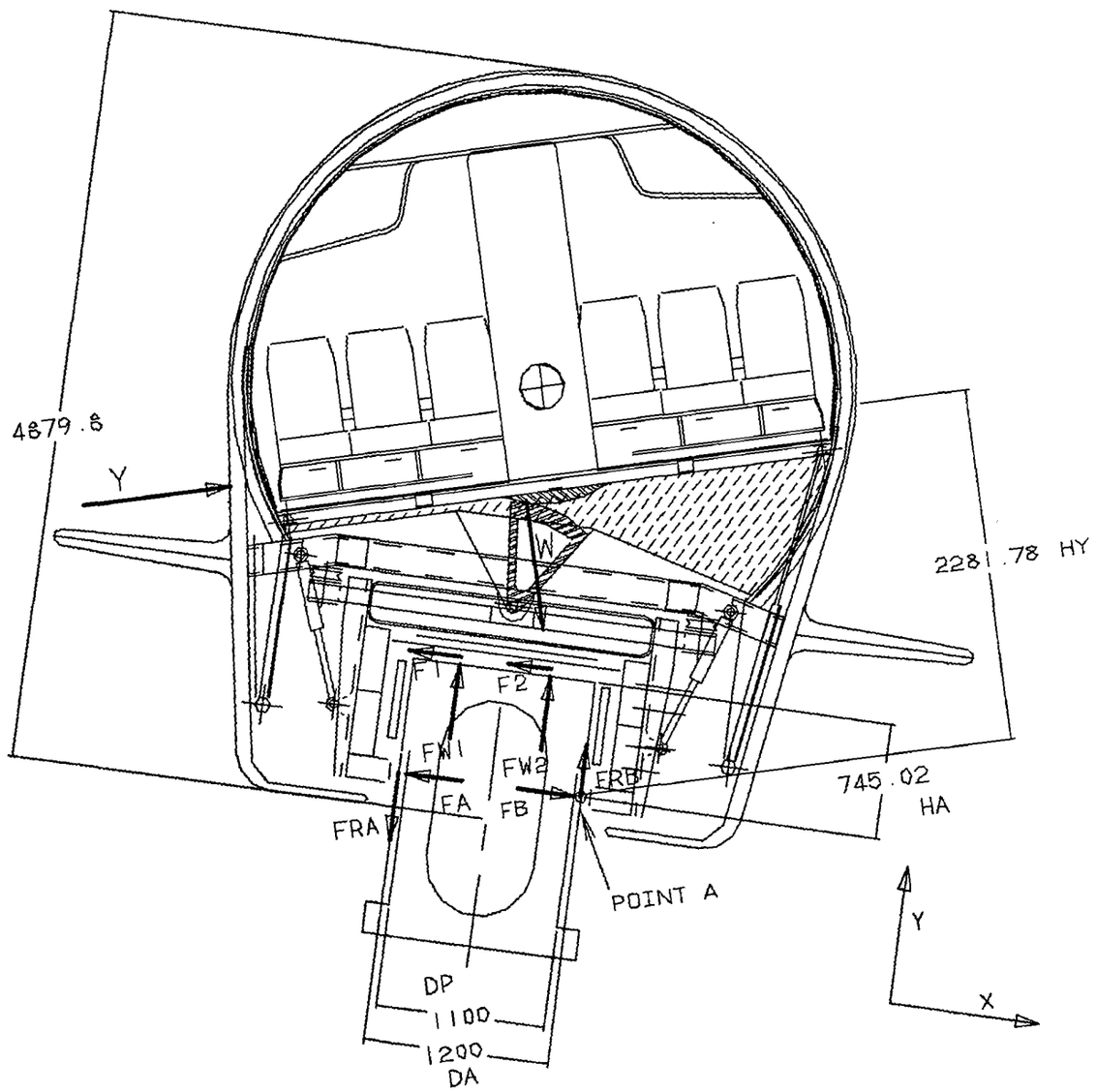

Figure C1-50 Vehicle lift due to side wind

Table C1-11
Parameters of Vehicle Lift Due to Side Winds

Symbol	Definition	Value
Y	side wind force	
W	weight of vehicle (64,000 kg mass)	627.2 KN
F_{w1}	reaction force from top surface of beam at center of starboard air bearing	
F_{w2}	reaction force from top surface of beam at center of port air bearing	
F_a	reaction force from starboard side of beam at center of parking brake	
F_b	reaction force from port side of beam at center of parking brake	
F_{r1}	friction force produced from F_{w1} on the beam	
F_{r2}	friction force produced from F_{w2} on the beam	
F_{ra}	friction force produced from F_a on the beam	
F_{rb}	friction force produced from F_b on the beam	
cg	vertical distance of vehicle's center of gravity from top of beam	1.1 m
h_c	normal distance from point A to center of pressure on side wall of vehicle	2.44 m
h_a	vertical distance from point A to top surface of beam	.745 m
d_p	width of top of beam	1.2 m
d_a	width of top of beam minus indentations	1.1 m
d_i	width of the indentation in one side of the beam	.05 m
μ_p	friction constant of parking brake pad against beam	0.6
μ_a	friction constant of air bearing or its resting pads against beam	0.6
θ	degree of beam tilt	15°
δ	normal distance from point A to weight vector	

Point A has no special significance; it is simply a convenient point from which to measure and therefore sum moments about. From geometry, the normal distance from point A to the line of action of the vehicle's weight is

$$\delta = \left(\frac{d_p}{2} - (h_a + cg)\tan\theta\right)\cos\theta$$

This wind force equation is derived in the aerodynamic section of this report. The force at 193 kph (120 mph) is 222.3 kN.

$$Y = \frac{C_d \rho v^2 HL}{2}$$

where

$C_d = .7$	: cross flow drag coefficient
$\rho = 1.225$ kg/m^3	: air density
v = 53.6 m/s (@120 mph)	: velocity of the side wind
H = 5.0 m	: vehicle height
L = 36.1 m	: vehicle length

The following three equations of static equilibrium are written from figure 5. The reaction forces F_{w1} and F_{w2} are located one fourth the width of the beam measured from the center of the beam.

$$\sum F_x = 0 \qquad Y\cos\theta + F_b - F_a - \mu_a F_{w2} - \mu_a F_{w1} + W\sin\theta = 0$$

$$\sum F_y = 0 \qquad W\cos\theta + \mu_p F_a - F_{w2} - F_{w1} - \mu_p F_b - Y\sin\theta = 0$$

$$\sum M_a = 0 \qquad h_c Y + \left(\frac{1}{4} d_a - d_i\right) F_{w2} + \left(\frac{3}{4} d_a - d_i\right) F_{w1} - \delta W - h_a \mu_a F_{w2} - h_a \mu_a F_{w1} - d_p \mu_p F_a = 0$$

Because these equations are general purpose equations, they were used for several analyses in addition to the ones described in this report.

1.9.5 Rocking Analysis: Beam Width and Tilt versus Wind Force

The worst case for our vehicle stability analysis is a rocking phenomenon, with the vehicle being supported by air bearings, with guidance wheels rolling against the windward side of the guideway, with the vehicle landing or taking off in a stiff side wind, and guideway beam tilted away from the wind. We would expect the side wind to start lifting the vehicle up off its starboard air bearings (according to Figure C1-50) because the windward guidance wheel cannot produce substantial vertical forces while it is rolling. This condition of impending motion was simulated by setting the left air bearing forces F_{w1}, the right guidance wheel forces F_b, the air bearing friction coefficient *a*, and the wheel friction coefficient *p* to zero. The three static equilibrium equations then contain three unknowns: the guidance wheels' force F_a, the air bearings' force F_{w1}, and the side wind force Y. The solution for Y is

$$Y = \frac{W(\delta - d_n \cos\theta)}{h_c + d_n \sin\theta}$$

where $d_n = \frac{1}{4} d_a - d_i$

Table C1-11 shows the resulting wind force and the associated wind speed to rock our maglev vehicle. Figure C1-51 shows the same results graphically. With our 1.2 meter wide beam on a 15 degree curve, our vehicle will tend to rock when landing on its air bearings even without a side wind. This result is obvious when the free body diagram is redrawn without F_{w1}, $\mu_a F_{w1}$, F_{ra}, F_1, F_2, and F_b, because with W pointing virtually right through the center of the port air bearing, the vehicle is on the verge of instability. This is not good.

This deficiency must be addressed by one or more of several methods, though we have not done so in our baseline design. Efforts late in the time schedule to lighten our vehicle were so successful that our vehicle's center of gravity moved significantly higher. Although we accomplished our goal of designing a 64 tonne vehicle, we aggravated the side wind stability problem. Obvious solutions would be to widen the beam, decrease the maximum beam tilt angle, separate the air bearing centers farther by using smaller bearings, lower the center of gravity, raise the lateral wheel to be closer to the top of the beam, or provide vertically oriented wheels that would roll on the bottom of a 15 cm structural protrusion out of the beam side wall on all severely tilted beams. A combination of several approaches seems likely. This design issue is one of the few issues insufficiently addressed in our SCD, but we are highly aware of the need provide an acceptable solution.

The structural protrusion/vertical wheel approach is attractive from two standpoints. First, taking the wheel forces directly along the length of the pedestals seems structurally efficient. Second, there would be no clamping on the beam and this would be more structurally efficient for the beam.

Table C1-11
Wind Force and Associated Wind Speed

Vehicle Rocking Analysis	H	5
Landing	L	36.1
No guidance hydraulics applied	ha	0.745
	cg	1.1
	W	627264
	dn	0.25
	hc	2.44

Beam width Da meters	Tilt angle thetad degrees	Tilt angle theta radians	weight arm delta meters	Wind force Y newtons	Wind speed v m/s	Wind speed kph	Per Wheel force fa newtons	Per Air brg force Fw1 newtons
1.2	0	0.0000	0.6000	89976	34.1	122.8	7498	52272
1.2	1	0.0175	0.5677	81686	32.5	117.0	7718	52145
1.2	2	0.0349	0.5352	73370	30.8	110.8	7935	52027
1.2	3	0.0524	0.5026	65032	29.0	104.4	8147	51917
1.2	4	0.0698	0.4698	56674	27.1	97.4	8357	51815
1.2	5	0.0873	0.4369	48299	25.0	89.9	8565	51722
1.2	6	0.1047	0.4039	39909	22.7	81.8	8771	51638
1.2	7	0.1222	0.3707	31507	20.2	72.6	8976	51562
1.2	8	0.1396	0.3374	23095	17.3	62.2	9180	51496
1.2	9	0.1571	0.3040	14677	13.8	49.6	9385	51437
1.2	10	0.1745	0.2705	6254	9.0	32.4	9589	51387
1.2	11	0.1920	0.2370	-2171	-5.3	-19.1	9796	51346
1.2	12	0.2094	0.2033	-10596	-11.7	-42.1	10003	51313
1.2	13	0.2269	0.1696	-19017	-15.7	-56.4	10214	51289
1.2	14	0.2443	0.1359	-27432	-18.8	-67.8	10427	51273
1.2	15	0.2618	0.1021	-35839	-21.5	-77.5	10643	51264
1.2	16	0.2792	0.0682	-44235	-23.9	-86.1	10864	51263
1.2	17	0.2967	0.0344	-52618	-26.1	-93.9	11089	51270
1.2	18	0.3141	0.0005	-60984	-28.1	-101.1	11318	51284
1.2	19	0.3316	-0.0333	-69332	-29.9	-107.8	11554	51305
1.2	20	0.3490	-0.0672	-77659	-31.7	-114.0	11795	51333

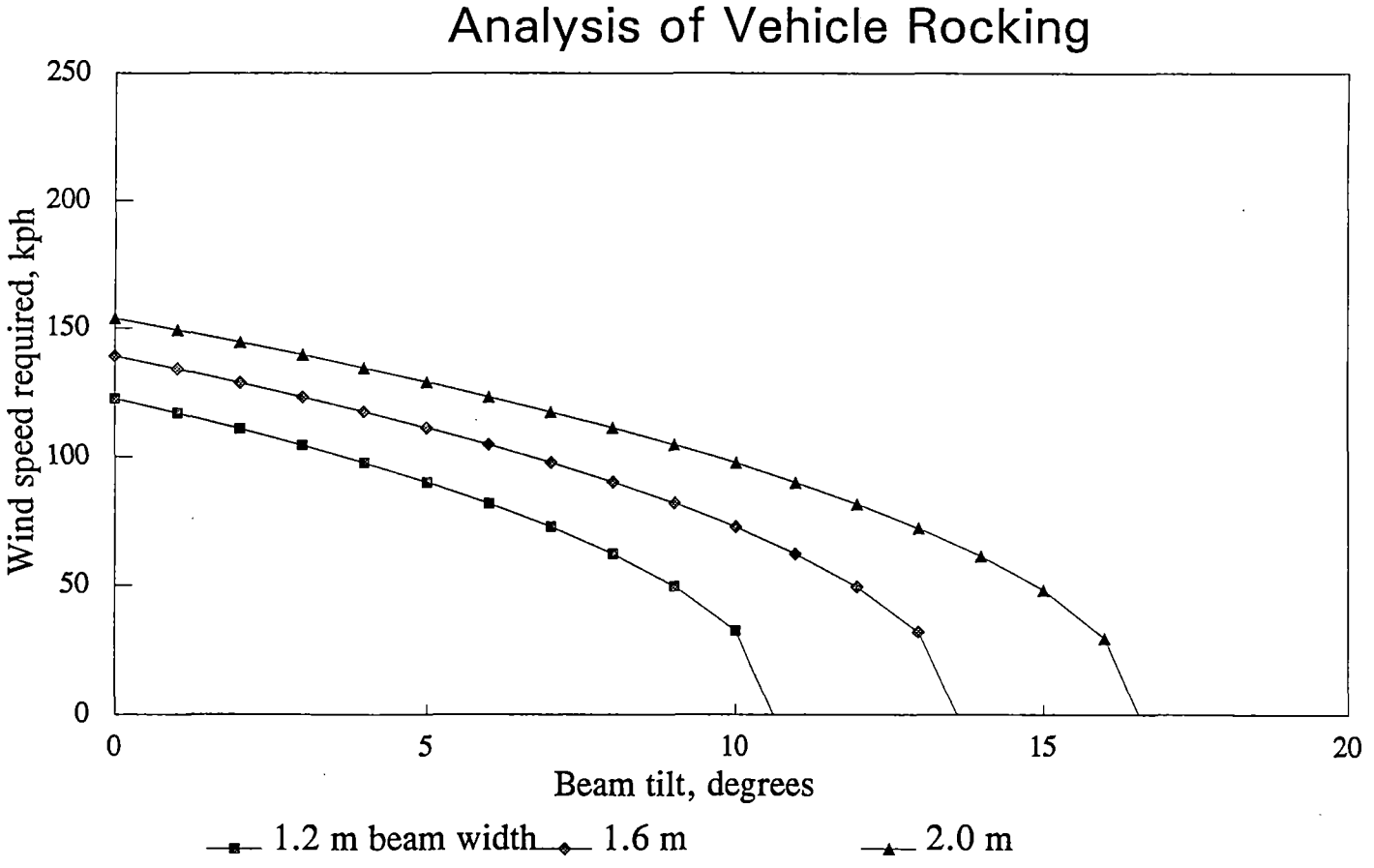

Figure C1-51 Wind force as a function of wind speed

Clamping the rolling lateral guidance wheels from both sides does not help. Although F_a and F_b are increased and changed, they both act through point A and therefore contribute no counter-moment to the wind moment. There is a small ledge at the top of the beam indentation for the lateral wheel to engage that counteracts the wind moment, but that ledge has been reduced to about 1 cm since this analysis was done (even though the table shows 5 cm) and would not reliably prevent the guidance wheels from climbing over it while rolling.

1.9.6 Analysis: Guidance Wheel and Air Bearing Forces

The force on all of the starboard guidance wheels was also determined from the previous analysis. The solutions for F_a and F_{w1} are

$$F_a = Y\cos\theta + W\sin\theta$$
$$F_{w1} = W\cos\theta - Y\sin\theta$$

For a 96.5 kph (60 mph) side wind and 15 degree tilt away from the wind, the F_a formula shows that the guidance wheel must be designed for a load F_a of 27.8 kN per wheel, and the F_{w1} formula shows the air bearing must be designed for a load of 49.4 kN. This is 31 percent over the normal air bearing capacity and would have to be accounted for by increasing the air pressure during these rare conditions.

1.9.7 Sizing of the Guidance Wheels

Table C1-12, below, lists several available wheels that would meet the 27.8 kN capacity. Using preliminary estimates, the guidance wheels that have been chosen for our drawings had a diameter of 250 mm, 100 mm width, and 30 mm diameter axle.

Table C1-12
Options for Guidance Wheels

Type	Diameter (mm)	Width (mm)	Axle Diameter (mm)	Capacity (kN)
Cast Iron	280	152	50	44.5
Forged Steel	200	100	50	44.5
V-Grooved Forged Steel	200	100	50	89.0

1.9.8 Sizing of the Spring

The spring design focuses on the required load to compress it fully. The equation below describes the proportional relationship between F, the force exerted on the spring, and L, the natural length of the spring, X, the length of the loaded spring, and k, the spring constant.

$$F = k\,(L - X)$$

For our purposes, the values L=125 mm, k=2000 N/mm, F=27.8 kN, and X=50 mm work nicely. A spring so defined can be obtained commercially. For example, a quote from one spring manufacturer company stated that a stainless steel spring of 50 mm inside diameter and a coil diameter of 18 mm can be produced with these parameters.

1.9.9 Analysis: Parking Brake Forces

The parking brake is designed to hold the vehicle on the beam with side winds of up to 193 kph (120 mph) which is equivalent to a 222 kN side force centered at 0.24 m below the horizontal centerline of the vehicle. Unlike the guidance wheels, the air bearings and parking brake will never be used at the same time. The previously discussed equations of static equilibrium are solved for F_a and F_b with Y=222000, a=0.6 (the vehicle is on its resting pads), μ_p=0.6, θ =15°. F_a and F_b are found to be 42.7 and 40.9 kN per brake pad, respectively. The average is 41.8 kN. The box beam has been designed to withstand these forces.

1.9.10 Hydraulic Piston Sizing

Figure C1-48 shows a side view of the lever arm and its related assembly. The distance from the center pin of this arm to the hydraulics is twice as long as from the same center pin to the parking brake assembly. From previous discussion, a maximum force of 41.8 kN must be supplied to each parking brake assembly. Due to the lever arm, the force to be supplied by the hydraulics, F_h, is only half this amount, or 20.9 kN.

Typical pressure available on our vehicle will be 13.8 MPa (2000 psi). The equation below describes the relationship between force, pressure, area and piston radius, ignoring the piston rod diameter and certain kinematic issues:

$$A = \pi r^2 = \frac{F_h}{P} \quad \therefore \; r = \sqrt{\frac{F_h}{\pi P}} = \sqrt{\frac{20900}{\pi(13.8E6)}} = 2.2\ cm$$

where

r = the radius of the hydraulic piston.

The stroke of the hydraulics must be the total distance that parking brake pads must move to contact the beam which is a total of 9 cm.

1.10 PROTECTION SYSTEMS

1.10.1 Fire Protection

Key Requirements

The concept maglev vehicle from the Bechtel Team is similar to most passenger aircraft; therefore, the fire protection system described below is modeled after those on passenger aircraft.

Description

The basic fire protection system includes fixed and portable systems. Fixed systems are mainly used for fire protection in non-cabin areas such as baggage compartments or auxiliary units. Portable systems are used for cabin fires.

Fixed systems are electrically powered and consist of two parts: a detection unit and a fire extinguishing unit. Detection units can detect the presence of a fire, overheating, or smoke. Different types or combinations of detection units maybe used throughout the vehicle. For example, a smoke detection unit may be used in the baggage compartment versus an overheating detection unit which would be used to detect quenching of the superconductor magnets. The fire extinguishing agent is usually contained in a pressurized container and released by rupturing a diaphragm through an explosive cartridge, set off electrically. Typical passenger aircraft usually have two or more of these pressurized containers. These containers are near the area to be protected on some aircraft and other aircraft use pipes to distribute the extinguishing agent to the affected area. Common extinguishing agents are halon 1211, freon, methyl bromide, and bromochloridifluoromethane. Each agent has its advantages and disadvantages, and should be chosen based upon requirements.

Portable systems are used in cabin areas. Aircraft regulations require that a fire extinguisher be supplied for each separate cabin compartment. Furthermore, the FAA has ruled that two halon 1211 fire extinguishers must be carried on board large aircraft. It should be noted that extinguishing agents that produce toxic gases should be avoided for portable systems where possible since the cabin is an enclosed area. Most large aircraft usually carry a dozen or more carbon dioxide and two halon 1211 fire extinguishers distributed throughout the passenger cabin.

Indicator lights should be installed to signal that a fire, overheating, or smoke problem exists and where the problem is located in the vehicle. Some maglev vehicles may be supplied with oxygen masks or smoke hoods for additional protection for the passengers.

1.10.2 Lighting and Static Charge Protection System

Purpose

Lightning is an unpredictable occurrence which can strike at unpredictable places. Use of lightning rods does not guarantee the diversion of a lightning strike away from the vehicle or guideway, but it would certainly decrease the probability of strikes on either. Other measures must be taken to assure that the vehicle, its on-board passengers, and equipment are not damaged, especially since the vehicle is not normally in contact with the ground when traveling.

Static charge will build up on the vehicle if measures are not taken to prevent it. This charge arises due to the frictional air flow over the vehicle surface. Such a charge could electrically shock a passenger stepping off a charged vehicle onto a passenger platform. Static-reducing vehicle coatings can be used, as well as static dissipating equipment.

Lightning and static charges are closely related in that they can be guarded against and diverted via the same mechanism described here. The discussions that follow involving lightning apply equally to static charge protection.

Guideway Protection

For the maglev guideway, the easiest and most effective method to protect from a lightning strike is to provide lightning rods, which attract impending lightning strikes (though not causing them) and provide an electrical path from the top of the rod to the ground. Not every point on the guideway can be protected but there should be at least some degree of lightning rod protection.

Buildings usually have a lightning rod mounted on top of the roof. A cable is attached to the rod and grounded. Typical cable used in buildings is 30 mm diameter copper cable. This size cable is usually sufficient to carry the current associated with lightning. Other materials and sizes might be studied to find an optimum cable for the guideway. The use of a cable could be eliminated if there existed a structure that was part of the guideway that could be used as the path for the lightning to travel though, e.g., a support beam made of steel.

Since our vehicle is 36 meters long and each guideway support beam is 25 meters apart it is logical to place a lighting rod at every other support beam. By doing so the vehicle will never be further than 4.5 meters from a lightning rod, yet rather than providing a rod at every support frame, the number of rods would be cut in half. The height of the lightning rod be should taller than the vehicle by perhaps two meters so that the lightning has a small probability of striking a vehicle. Such rods would extend upward to be 5.7 meters above the top of the beam. The rods would be located on the outside of the guideway rather than between the beams. Alternating side locations would be used.

The propulsion coils and levitation ladder are both good conductors of electricity. Both the propulsion coils and ladder will not be grounded at other than one point per circuit per 4 km zone (if at all), though the ladder could be grounded more often if there were a reason to do so. Measures should be taken to divert lightning away from these propulsion system elements.

There are inverter stations roughly every 4 km of guideway. The inverter stations will have some type of surge protector as part of the system which would give some protection to the propulsion coils as well as the inverter circuitry Surge protectors for the propulsions coils could be placed between the inverter stations on their output lines. Surge protectors for high voltage equipment can be expensive.

With present technology, optical communication and control equipment are being used more heavily, mainly in the aircraft industry, to replace the equivalent of their electrical counterpart. The maglev system should follow the same example and use optical equipment whenever possible. As for the electrical equipment that can not be replaced by optical equipment, e.g radio equipment, surge protectors should be a built-in feature. The weight of most surge protectors compared with the weight of the equipment it protects is usually a small percentage of the equipment's total weight. The size of surge protectors is also a small percentage of the equipment's size but not as low as the percentage weight.

Vehicle Protection

The following items about aircraft lightning strikes apply equally well to our maglev vehicle:

- The monocoque structure of the maglev vehicle has a thin aluminum skin fastened to a structural aluminum framework.
- Lightning strikes do not damage or significantly heat up the aircraft framework
- The lightning current is diverted around the passenger compartment and through the metal framework, so the passengers will be in no danger of electrical shock.
- Electrical equipment and circuits can be protected by adding surge arrestors inside the electronic equipment and at proper locations in the electrical wiring.
- Punctures of the aluminum skin often occur due to lightning entry and exit points. On airplanes the nose and wing tips get punctured; we do not know what to expect on the maglev vehicle, but there is no especially vulnerable point on the skin that we need to worry about. Adding a lightning rod to the vehicle itself would increase vehicle lightning strikes; the plan is to divert the vast majority of strikes to the lightning rods above the guideway. A lightning rod on the vehicle would merely exacerbate the problem, as would vertical airfoils (rudders) meant for yaw stability.

Whenever lightning does strike the vehicle there will probably be puncture damage to the vehicle outer shell, since the low melting temperature of aluminum does not resist electrical arc burning well. Such damage would be repaired, and experience would allow improved resistance to punctures by improved skin materials, coatings, and distributions.

The closest structures to the vehicle are the propulsion coils, the levitation ladder and the nonmetallic cover over them. The cover must remain nonmetallic due to eddy current phenomena associated with the vehicle's SCMs. Once lightning strikes the outer vehicle shell the lightning will usually travel to the easiest path to ground. This would mean that the lightning will most likely arc over from the superconducting magnet module to the propulsion coils and/or levitation ladder. Considerable damage can occur if this is allowed to happen. To protect against such incidents the frame structure would be cabled to a flying beryllium wire hung from the center of the bottom surface of the bogie (see Figure C1-52). In addition, a cadmium-plated copper strip will be attached to the top of the guideway so that the flying wire would drag lightly on this strip, maintaining loose contact or at least a very small gap (5 mm). By making the wire long enough and aerodynamically shaping its supports, then at any speed the wire would drag along and be basically in contact with the metal grounding strip. The lightning arc would in all likelihood jump the small gap and avoid traveling through the SCM and guideway electrical equipment. Quite often the beryllium wire would be sacrificially burnt off in establishing the arc. Providing two wires per bogie would provide for subsequent lightning strikes. Lightning current detection

transducers in the wire's feed circuit would allow the vehicle to detect when strikes have occurred; maintenance personnel would subsequently be alerted to check the wires and the rest of the vehicle at the next convenient time.

A typical size for the metal grounding strip used in buildings for lightning protection is a copper strip of 25 mm width and 2 mm thickness. Since the vehicle is able to move horizontally 5 cm from both sides of the center line of the top of the guideway there should be three flying wires spaced 2 cm apart at each holder to assure contact as the vehicle strays from side to side on the guideway.

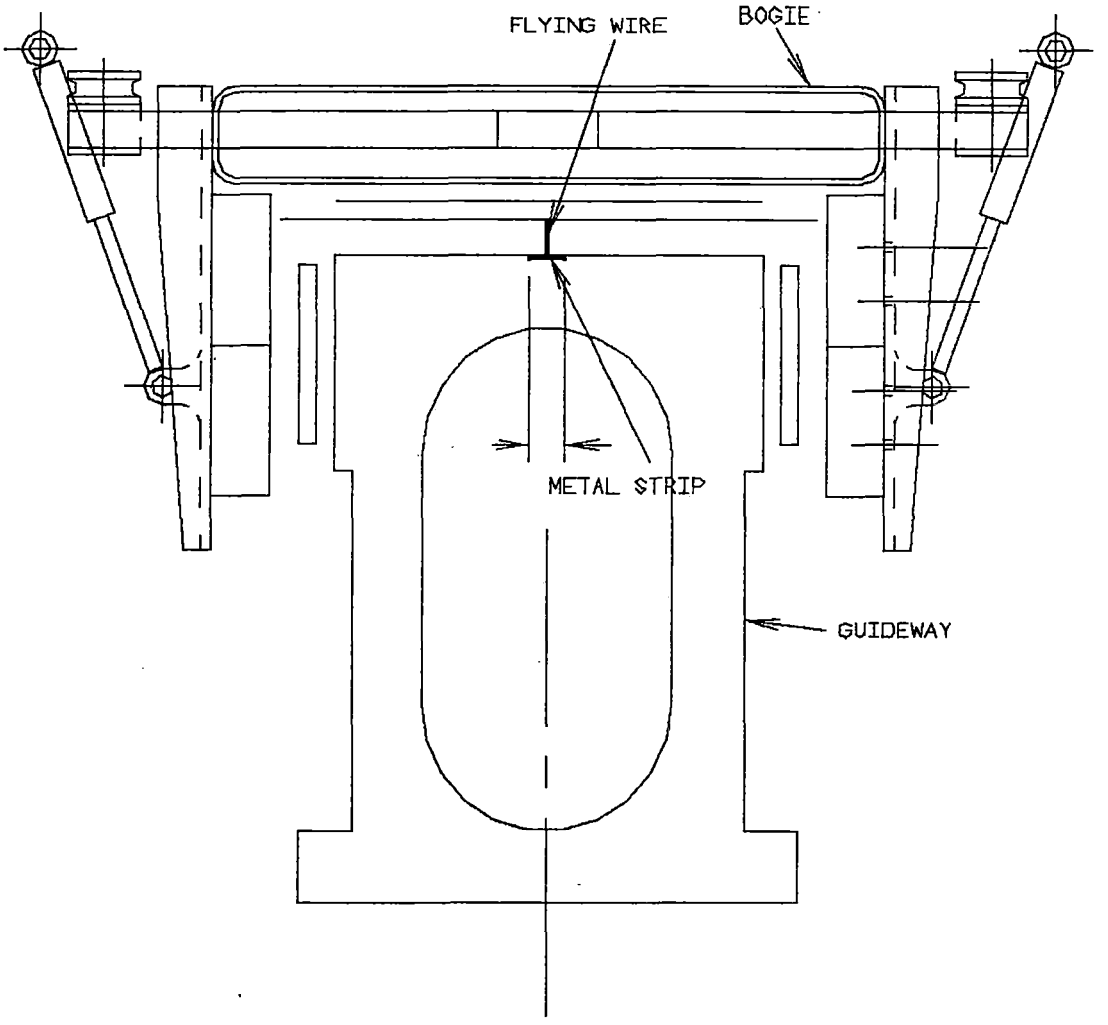

C1-52 Flying wire used for vehicle lightning protection

1.11 MAINTENANCE SCHEDULE

Abstract

Three levels of maintenance were identified at this stage for the vehicle: nightly running maintenance, quarterly inspections, and vehicle system overhauls. Vehicle subsystems are reviewed and maintenance items are identified and classified by type. No estimates were made for the duration of each inspection or maintenance cycle. Vehicle maintenance intervals were made as long as practical to minimize operating costs.

Key Requirements

Our contract requirements for a maintenance plan include projected facilities, automated systems (if any), personnel cost, and maintenance schedules for the entire maglev system and major components.

Approach Used

The maintenance schedule was developed for the vehicle, including identification of maintenance and inspections which are to be performed and at what interval. For detail of required maintenance for each subsystem see the section below.

Description

Each of the major vehicle subsections is listed below with an analysis and description of maintenance required and frequency of occurrence.

Superconducting Magnet and Cryogenic Subsystem

Daily Maintenance

- Inspection and fluid level check of helium, nitrogen, and cryocooler oil
- Quick inspection of all cryogenic distribution lines and SCMs for signs of wear
- Recharging of lost SCM current and reliquification of on-board helium (1 hour)

Quarterly Maintenance

- Replacement of helium and nitrogen filters
- Detailed inspection of all cryogenic distribution lines and SCMs for signs of wear

Overhaul Maintenance (3 years)

- Complete overhaul of cryogenic systems and magnets
- Functional requalification of systems after overhaul

Passenger Cabin Subsystem

Daily Maintenance

- Daily inspection repair of passenger comfort controls, lights, seat cushions, lavatories, galleys, and doors that may have been damaged

Quarterly Maintenance

- Functional requalification of all emergency systems and repair of damaged body panels or apparatus
- Inspection and qualification of HVAC system

Overhaul Maintenance (3 years)

- Possible reupholstering of seats and replacement of body panels that have been marred
- Complete cleaning of water systems and testing of electrical systems
- Detailed overhaul of HVAC system

Tilt Mechanism Subsystem

Daily Maintenance

- Quick visual inspection and functional qualification of tilt system components

Quarterly Maintenance

- Relubrication of moving parts of tilt mechanism and inspection of all actuators for possible signs of wear.

Overhaul Maintenance (3 years)

- Repacking of all tilt mechanism bearings and detailed inspection of all moving parts
- Replacement of worn parts

Vehicle Carbody Subsystem

Daily Maintenance

- Quick visual inspection of carbody and baggage compartments to look for signs of stress and cracking requiring attention

Quarterly Maintenance

- Detailed visual inspection of carbody and baggage compartments to identify signs of possible wear and cracking requiring replacement or repair

Overhaul Maintenance (3 years)

- Potential repainting of carbody due to nick damage from small flying objects

Magnet Bogie and Suspension Subsystem

Daily Maintenance

- Quick visual inspection of bogies, suspension elements, and emergency skids to identify signs of possible wear or cracking requiring correction

Quarterly Maintenance

- Detailed review inspection of each bogie and suspension elements to identify and replace worn or cracked elements
- Lubrication of pivot points
- Visual inspection of active suspension actuator lines for signs of wear
- Inspection and replacement of emergency wear skids if necessary

Overhaul Maintenance (3 years)

- Careful inspection of bearings at pivot points for signs of excessive wear and replacement if required
- Functional qualification of active suspension actuators, if required

On-Board Power Systems

Daily Maintenance

- Refill of fuel cell fuels (every 8 hours) and inspection to identify damaged components or leaks

Quarterly Maintenance

- Detailed review inspection of on-board power systems and replacement of filters

Overhaul Maintenance (3 years)

- Cleaning and detailed inspection of components to determine required replacement

Aerodynamic Control Surfaces

Daily Maintenance

- Quick visual inspection of control surfaces to identify signs of possible wear or cracking requiring correction

Quarterly Maintenance

- Detailed review inspection of each control surface to identify and replace worn or cracked elements
- Lubrication of pivot points. Visual inspection of all actuator lines for signs of wear

Overhaul Maintenance (3 years)

- Careful inspection of bearings at pivot points for signs of excessive wear and replacement if required
- Functional qualification of control surface actuators, if required

Benefits/Risk

Careful consideration has been given to minimize the frequency of required inspections and maintenance. Additional ideas are being develop to further lengthen maintenance cycles to reduce vehicle operational cost. Key to minimizing the impact of required maintenance is modular design which the Bechtel Team has followed during the design process.

1.12 BRAKING

1.12.1 Baseline Vehicle Braking Characteristics

To ensure the highest capacity for a single vehicle system, small headways are required. To provide small headways safely on a maglev system it is necessary to provide significant braking capacity. For the baseline vehicle system, five braking systems exist. The first two are inherent drag on the vehicle: aerodynamic and electromagnetic. In addition there are three system-controllable braking methods: propulsive, aerodynamic speed brakes, and an emergency drag chute. Each of these five braking systems is discussed in detail in other sections of this report.

Using the available braking systems and the equations detailed in the various report sections, four graphs have been created to detail maximum vehicle deceleration available in non-emergency conditions; maximum vehicle deceleration available in emergency conditions; stopping distance; and stopping time required under emergency and non-emergency conditions. These figures are

C1-53, C1-54, C1-55 and C1-56 respectively. Values used to generate the associated graphs are shown in Tables C1-12, C1-13, and C1-14.

The reader is also directed to the appendices of this report which relate to the topics of speed brakes, parachute braking systems, and drag chutes. Data in those appendices elaborate and supplement this text discussion.

From the results of the analysis and using the fact that control zones are approximately 4+ kilometers in length, it becomes apparent that vehicle collisions are unlikely since a trailing vehicle can stop within its current zone if required to do so.

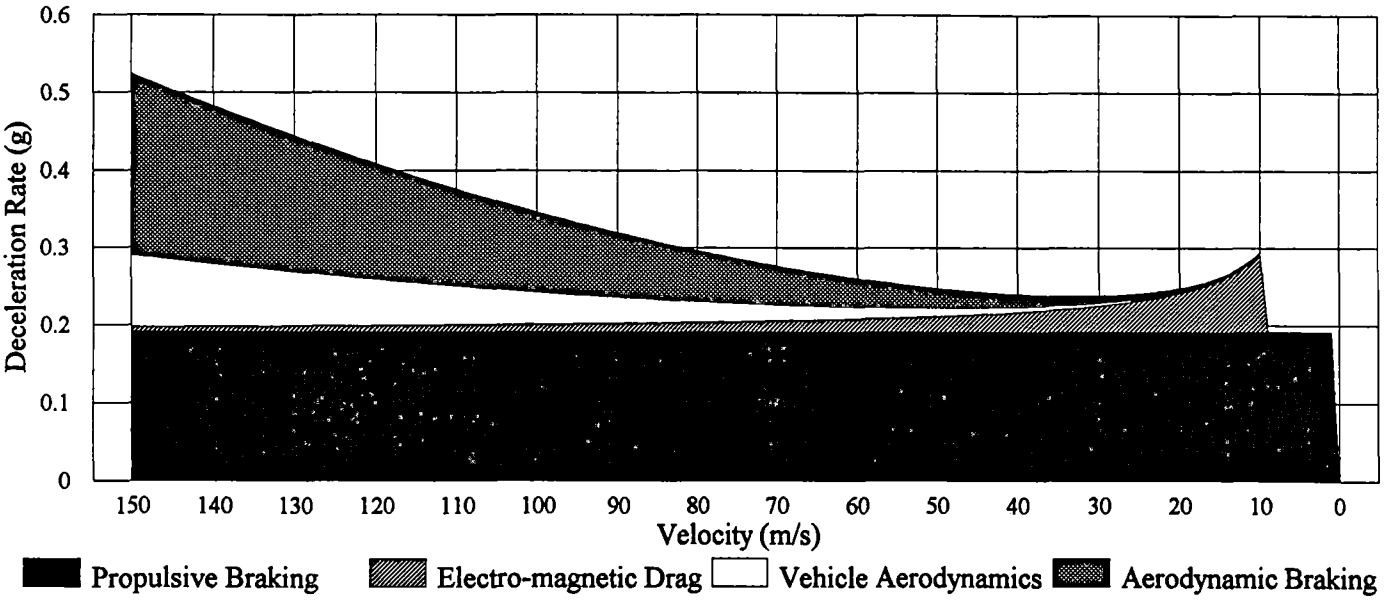

Figure C1-53 Maximum vehicle deceleration available in non-emergency conditions

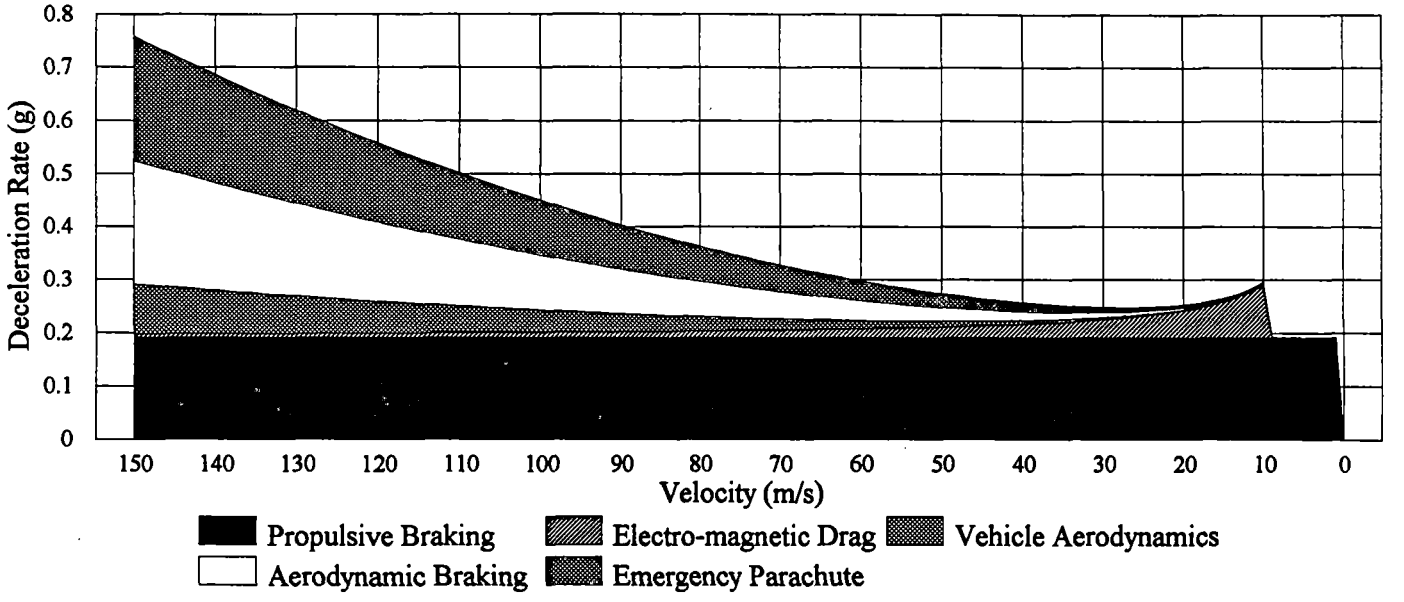

Figure C1-54 Maximum vehicle deceleration available in emergency conditions

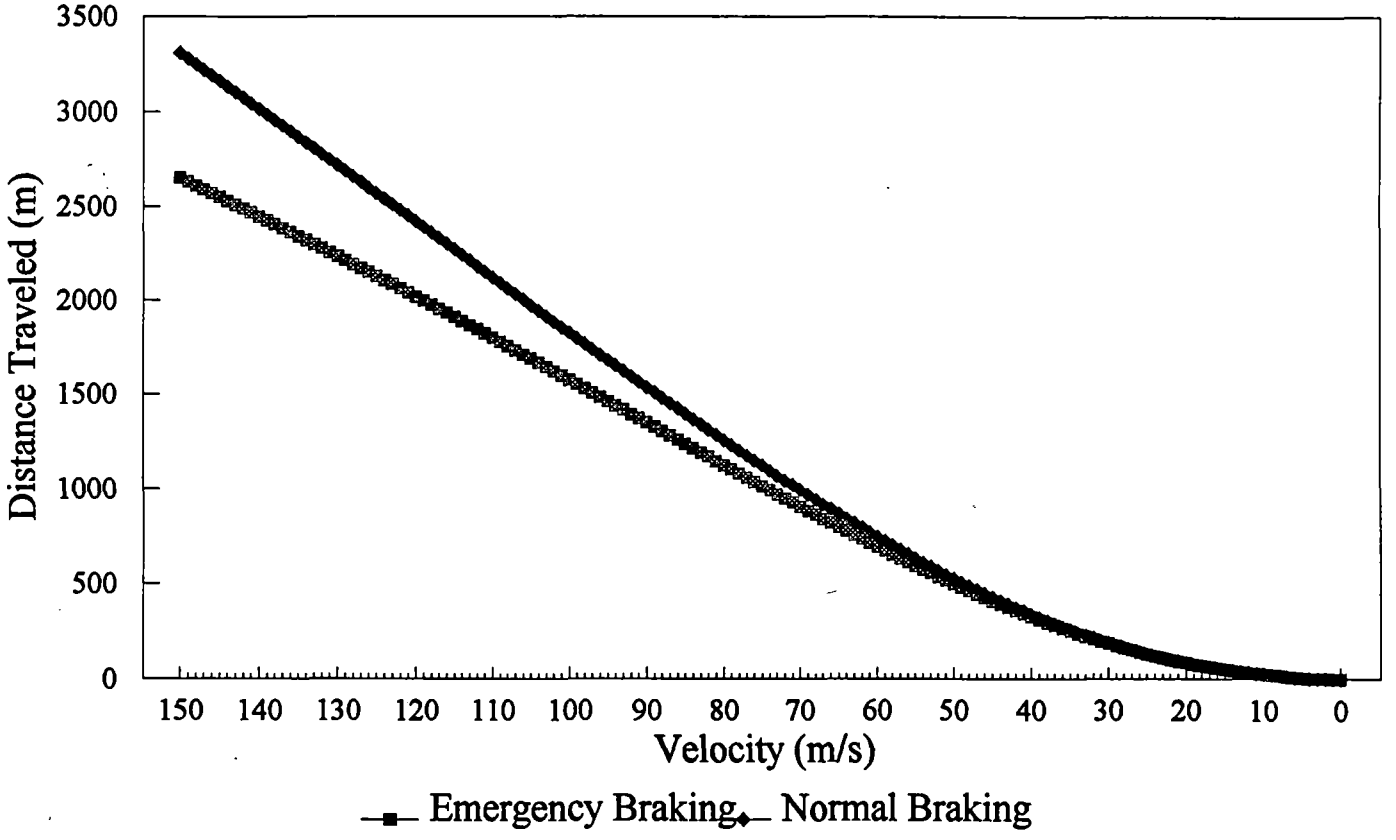

Figure C1-55 Stopping distance required under maximum braking conditions (normal and emergency braking)

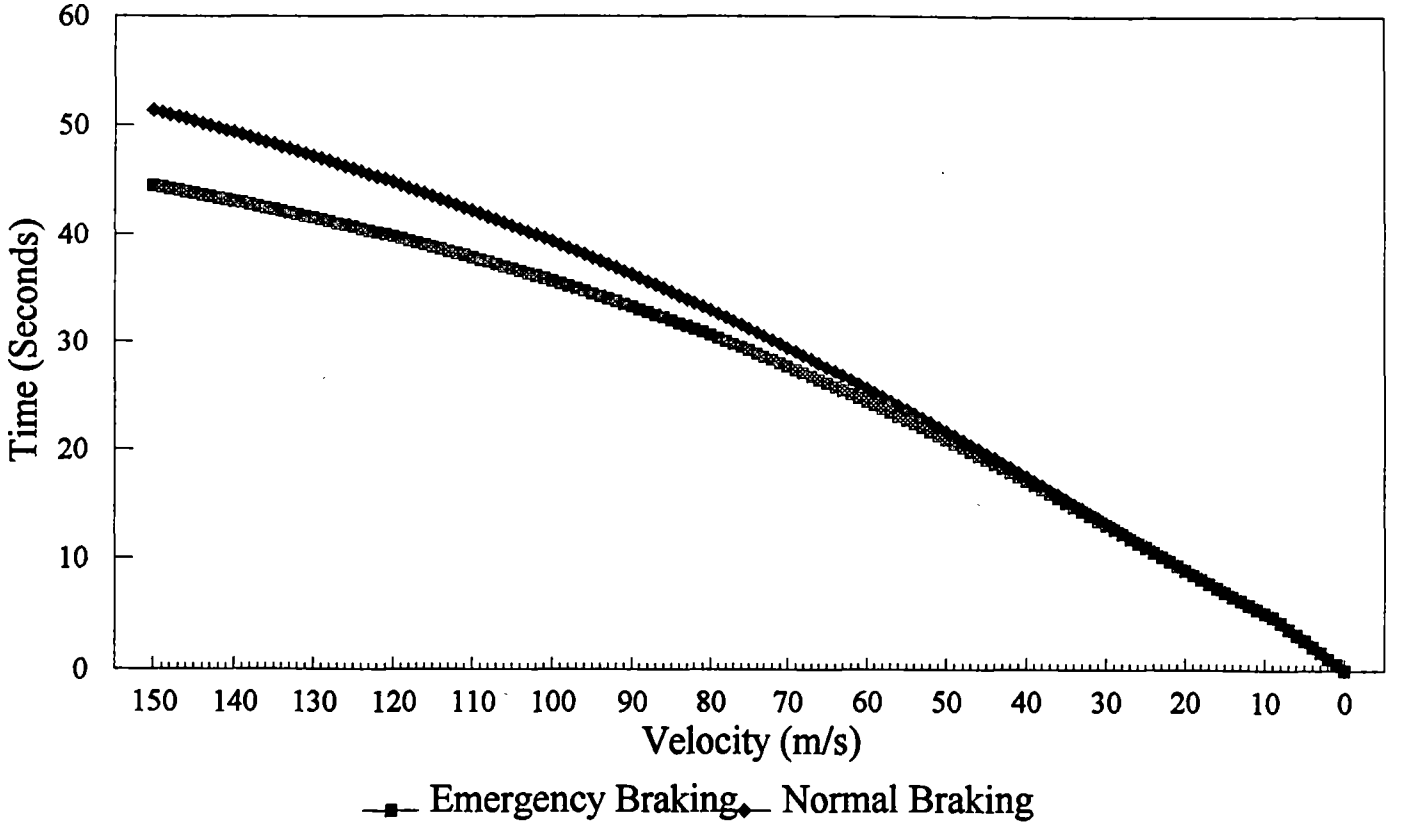

Figure C1-56 Stopping time required under maximum braking conditions (normal and emergency braking)

Table C1-12
Braking Study Parameters

Single Vehicle Concept

Vehicle Frontal Area (Entered)	15.7 sq. Meters	
Vehicle Skin Area/Car (Entered)	660 sq. Meters	
Frontal Drag Coefficient (Entered)	0.1	
Skin Drag Coefficient (Entered)	0.004	
Total Propulsive Force (LSM)	120 kN	
Normal Electro-Magnetic Braking Rate	1.875 m/s/s	0.2 g Thrust
Emergency Electro-Magnetic Braking Rate	1.875 m/s/s	0.2 g Thrust
Aerodynamic Brake Coefficient of Drag	1	
Aerodynamic Brake Deceleration Desired @ 500kph	0.2 g	
Minimum Aerodynamic Brake Size Required	11 sq. Meters	
Emergency Chute Coefficeint of Drag	0.8	
Emergency Chute Deceleration Desired @ 500kph	0.2 g	
Emergency Parachute Size	13 sq. Meters	
Emergency Parachute Diameter	4.11 Meters	
Vehicle Weight (Design Goal)	64,000 kg	

Table C1-13
Base Parameters
Non-Emergency Deceleration Data

Maximum Normal

Speed (m/s)	Propulsive E-M (g)	Levitation & Guidance E-M (g)	Aerodynamic Drag Vehicle (g)	Aerodynamic Brake Drag (g)	Chute (g)	Total Stopping Force (g)	Time Delta (s)	Distance Traveled (m)	Cumulative Distance	Cumulative Time
150	0.191	0.007	0.093	0.234	NA	0.524	0.2	29	3,309	51
149	0.191	0.007	0.092	0.230	NA	0.520	0.2	29	3,280	51
148	0.191	0.007	0.090	0.227	NA	0.516	0.2	29	3,250	51
147	0.191	0.007	0.089	0.224	NA	0.512	0.2	29	3,221	51
146	0.191	0.007	0.088	0.221	NA	0.507	0.2	29	3,192	51
145	0.191	0.007	0.087	0.218	NA	0.503	0.2	29	3,163	50
144	0.191	0.007	0.086	0.215	NA	0.499	0.2	29	3,134	50
143	0.191	0.007	0.084	0.212	NA	0.495	0.2	29	3,104	50
142	0.191	0.007	0.083	0.209	NA	0.491	0.2	29	3,075	50
141	0.191	0.007	0.082	0.206	NA	0.487	0.2	29	3,046	50
140	0.191	0.007	0.081	0.203	NA	0.483	0.2	29	3,016	49
139	0.191	0.007	0.080	0.201	NA	0.479	0.2	29	2,987	49
138	0.191	0.007	0.079	0.198	NA	0.475	0.2	30	2,957	49
137	0.191	0.007	0.077	0.195	NA	0.471	0.2	30	2,928	49
136	0.191	0.007	0.076	0.192	NA	0.467	0.2	30	2,898	49
135	0.191	0.008	0.075	0.189	NA	0.463	0.2	30	2,869	48
134	0.191	0.008	0.074	0.186	NA	0.459	0.2	30	2,839	48
133	0.191	0.008	0.073	0.184	NA	0.455	0.2	30	2,809	48
132	0.191	0.008	0.072	0.181	NA	0.452	0.2	30	2,780	48
131	0.191	0.008	0.071	0.178	NA	0.448	0.2	30	2,750	47
130	0.191	0.008	0.070	0.175	NA	0.444	0.2	30	2,720	47
129	0.191	0.008	0.069	0.173	NA	0.440	0.2	30	2,690	47
128	0.191	0.008	0.068	0.170	NA	0.437	0.2	30	2,661	47
127	0.191	0.008	0.067	0.167	NA	0.433	0.2	30	2,631	46
126	0.191	0.008	0.065	0.165	NA	0.430	0.2	30	2,601	46
125	0.191	0.008	0.064	0.162	NA	0.426	0.2	30	2,571	46
124	0.191	0.008	0.063	0.160	NA	0.422	0.2	30	2,542	46
123	0.191	0.008	0.062	0.157	NA	0.419	0.2	30	2,512	46
122	0.191	0.008	0.061	0.155	NA	0.415	0.2	30	2,482	45
121	0.191	0.008	0.060	0.152	NA	0.412	0.2	30	2,452	45
120	0.191	0.008	0.059	0.149	NA	0.409	0.2	30	2,422	45
119	0.191	0.009	0.058	0.147	NA	0.405	0.3	30	2,393	45
118	0.191	0.009	0.057	0.145	NA	0.402	0.3	30	2,363	44
117	0.191	0.009	0.056	0.142	NA	0.398	0.3	30	2,333	44
116	0.191	0.009	0.055	0.140	NA	0.395	0.3	30	2,303	44
115	0.191	0.009	0.055	0.137	NA	0.392	0.3	30	2,273	44
114	0.191	0.009	0.054	0.135	NA	0.389	0.3	30	2,244	43
113	0.191	0.009	0.053	0.133	NA	0.385	0.3	30	2,214	43
112	0.191	0.009	0.052	0.130	NA	0.382	0.3	30	2,184	43
111	0.191	0.009	0.051	0.128	NA	0.379	0.3	30	2,154	42
110	0.191	0.009	0.050	0.126	NA	0.376	0.3	30	2,125	42
109	0.191	0.009	0.049	0.123	NA	0.373	0.3	30	2,095	42
108	0.191	0.009	0.048	0.121	NA	0.370	0.3	30	2,065	42
107	0.191	0.010	0.047	0.119	NA	0.367	0.3	30	2,036	41
106	0.191	0.010	0.046	0.117	NA	0.364	0.3	30	2,006	41
105	0.191	0.010	0.045	0.114	NA	0.361	0.3	30	1,976	41
104	0.191	0.010	0.045	0.112	NA	0.358	0.3	29	1,947	41
103	0.191	0.010	0.044	0.110	NA	0.355	0.3	29	1,917	40
102	0.191	0.010	0.043	0.108	NA	0.352	0.3	29	1,888	40
101	0.191	0.010	0.042	0.106	NA	0.349	0.3	29	1,859	40
100	0.191	0.010	0.041	0.104	NA	0.346	0.3	29	1,829	39
99	0.191	0.010	0.040	0.102	NA	0.344	0.3	29	1,800	39
98	0.191	0.010	0.040	0.100	NA	0.341	0.3	29	1,771	39
97	0.191	0.011	0.039	0.098	NA	0.338	0.3	29	1,742	39
96	0.191	0.011	0.038	0.096	NA	0.335	0.3	29	1,712	38
95	0.191	0.011	0.037	0.094	NA	0.333	0.3	29	1,683	38
94	0.191	0.011	0.036	0.092	NA	0.330	0.3	29	1,654	38

Table C1-13
(cont'd)

Maximum Normal

Speed (m/s)	Propulsive E-M (g)	Levitation & Guidance E-M (g)	Aerodynamic Drag Vehicle (g)	Aerodynamic Brake Drag (g)	Chute (g)	Total Stopping Force (g)	Time Delta (s)	Distance Traveled (m)	Cumulative Distance	Cumulative Time
93	0.191	0.011	0.036	0.090	NA	0.328	0.3	29	1,626	37
92	0.191	0.011	0.035	0.088	NA	0.325	0.3	29	1,597	37
91	0.191	0.011	0.034	0.086	NA	0.322	0.3	29	1,568	37
90	0.191	0.011	0.033	0.084	NA	0.320	0.3	29	1,539	36
89	0.191	0.011	0.033	0.082	NA	0.317	0.3	28	1,511	36
88	0.191	0.012	0.032	0.080	NA	0.315	0.3	28	1,483	36
87	0.191	0.012	0.031	0.079	NA	0.313	0.3	28	1,454	35
86	0.191	0.012	0.031	0.077	NA	0.310	0.3	28	1,426	35
85	0.191	0.012	0.030	0.075	NA	0.308	0.3	28	1,398	35
84	0.191	0.012	0.029	0.073	NA	0.306	0.3	28	1,370	34
83	0.191	0.012	0.028	0.072	NA	0.303	0.3	28	1,342	34
82	0.191	0.012	0.028	0.070	NA	0.301	0.3	28	1,314	34
81	0.191	0.013	0.027	0.068	NA	0.299	0.3	27	1,287	33
80	0.191	0.013	0.026	0.066	NA	0.297	0.3	27	1,259	33
79	0.191	0.013	0.026	0.065	NA	0.295	0.3	27	1,232	33
78	0.191	0.013	0.025	0.063	NA	0.292	0.3	27	1,205	32
77	0.191	0.013	0.024	0.062	NA	0.290	0.4	27	1,178	32
76	0.191	0.013	0.024	0.060	NA	0.288	0.4	27	1,151	32
75	0.191	0.014	0.023	0.058	NA	0.286	0.4	27	1,124	31
74	0.191	0.014	0.023	0.057	NA	0.284	0.4	26	1,098	31
73	0.191	0.014	0.022	0.055	NA	0.282	0.4	26	1,071	31
72	0.191	0.014	0.021	0.054	NA	0.280	0.4	26	1,045	30
71	0.191	0.014	0.021	0.052	NA	0.279	0.4	26	1,019	30
70	0.191	0.015	0.020	0.051	NA	0.277	0.4	26	993	30
69	0.191	0.015	0.020	0.049	NA	0.275	0.4	25	968	29
68	0.191	0.015	0.019	0.048	NA	0.273	0.4	25	943	29
67	0.191	0.015	0.019	0.047	NA	0.271	0.4	25	917	28
66	0.191	0.015	0.018	0.045	NA	0.270	0.4	25	892	28
65	0.191	0.016	0.017	0.044	NA	0.268	0.4	25	868	28
64	0.191	0.016	0.017	0.043	NA	0.266	0.4	24	843	27
63	0.191	0.016	0.016	0.041	NA	0.265	0.4	24	819	27
62	0.191	0.016	0.016	0.040	NA	0.263	0.4	24	795	26
61	0.191	0.017	0.015	0.039	NA	0.262	0.4	24	771	26
60	0.191	0.017	0.015	0.037	NA	0.260	0.4	23	747	26
59	0.191	0.017	0.014	0.036	NA	0.259	0.4	23	724	25
58	0.191	0.018	0.014	0.035	NA	0.258	0.4	23	701	25
57	0.191	0.018	0.013	0.034	NA	0.256	0.4	22	678	25
56	0.191	0.018	0.013	0.033	NA	0.255	0.4	22	656	24
55	0.191	0.019	0.012	0.031	NA	0.254	0.4	22	634	24
54	0.191	0.019	0.012	0.030	NA	0.252	0.4	22	612	23
53	0.191	0.019	0.012	0.029	NA	0.251	0.4	21	590	23
52	0.191	0.020	0.011	0.028	NA	0.250	0.4	21	569	23
51	0.191	0.020	0.011	0.027	NA	0.249	0.4	21	548	22
50	0.191	0.020	0.010	0.026	NA	0.248	0.4	20	527	22
49	0.191	0.021	0.010	0.025	NA	0.247	0.4	20	507	21
48	0.191	0.021	0.010	0.024	NA	0.246	0.4	20	487	21
47	0.191	0.022	0.009	0.023	NA	0.245	0.4	19	467	20
46	0.191	0.022	0.009	0.022	NA	0.244	0.4	19	448	20
45	0.191	0.023	0.008	0.021	NA	0.243	0.4	19	429	20
44	0.191	0.023	0.008	0.020	NA	0.242	0.4	18	410	19
43	0.191	0.024	0.008	0.019	NA	0.242	0.4	18	392	19
42	0.191	0.024	0.007	0.018	NA	0.241	0.4	18	374	18
41	0.191	0.025	0.007	0.017	NA	0.240	0.4	17	356	18
40	0.191	0.025	0.007	0.017	NA	0.240	0.4	17	339	18
39	0.191	0.026	0.006	0.016	NA	0.239	0.4	16	322	17
38	0.191	0.027	0.006	0.015	NA	0.239	0.4	16	306	17
37	0.191	0.028	0.006	0.014	NA	0.239	0.4	16	290	16

Table C1-13
(cont'd)

Maximum Normal

Speed (m/s)	Propulsive E-M (g)	Levitation & Guidance E-M (g)	Aerodynamic Drag Vehicle (g)	Aerodynamic Brake Drag (g)	Chute (g)	Total Stopping Force (g)	Time Delta (s)	Distance Traveled (m)	Cumulative Distance	Cumulative Time
36	0.191	0.028	0.005	0.013	NA	0.238	0.4	15	274	16
35	0.191	0.029	0.005	0.013	NA	0.238	0.4	15	259	15
34	0.191	0.030	0.005	0.012	NA	0.238	0.4	14	244	15
33	0.191	0.031	0.004	0.011	NA	0.238	0.4	14	230	15
32	0.191	0.032	0.004	0.011	NA	0.238	0.4	14	216	14
31	0.191	0.033	0.004	0.010	NA	0.238	0.4	13	202	14
30	0.191	0.034	0.004	0.009	NA	0.238	0.4	13	189	13
29	0.191	0.035	0.003	0.009	NA	0.238	0.4	12	177	13
28	0.191	0.036	0.003	0.008	NA	0.239	0.4	12	165	12
27	0.191	0.038	0.003	0.008	NA	0.239	0.4	11	153	12
26	0.191	0.039	0.003	0.007	NA	0.240	0.4	11	142	12
25	0.191	0.041	0.003	0.006	NA	0.241	0.4	10	131	11
24	0.191	0.042	0.002	0.006	NA	0.242	0.4	10	120	11
23	0.191	0.044	0.002	0.005	NA	0.243	0.4	9	110	10
22	0.191	0.046	0.002	0.005	NA	0.244	0.4	9	101	10
21	0.191	0.049	0.002	0.005	NA	0.246	0.4	8	92	9
20	0.191	0.051	0.002	0.004	NA	0.248	0.4	8	84	9
19	0.191	0.054	0.001	0.004	NA	0.250	0.4	8	76	9
18	0.191	0.057	0.001	0.003	NA	0.252	0.4	7	68	8
17	0.191	0.060	0.001	0.003	NA	0.255	0.4	7	61	8
16	0.191	0.064	0.001	0.003	NA	0.259	0.4	6	54	7
15	0.191	0.068	0.001	0.002	NA	0.262	0.4	6	48	7
14	0.191	0.073	0.001	0.002	NA	0.267	0.4	5	43	7
13	0.191	0.078	0.001	0.002	NA	0.272	0.4	5	37	6
12	0.191	0.085	0.001	0.001	NA	0.278	0.4	4	33	6
11	0.191	0.093	0.000	0.001	NA	0.286	0.4	4	29	5
10	0.191	0.102	0.000	0.001	NA	0.295	0.3	3	25	5
9	0.191	0.000	0.000	0.001	NA	0.192	0.5	5	22	5
8	0.191	0.000	0.000	0.001	NA	0.192	0.5	4	17	4
7	0.191	0.000	0.000	0.001	NA	0.192	0.5	3	13	4
6	0.191	0.000	0.000	0.000	NA	0.192	0.5	3	10	3
5	0.191	0.000	0.000	0.000	NA	0.191	0.5	2	7	3
4	0.191	0.000	0.000	0.000	NA	0.191	0.5	2	4	2
3	0.191	0.000	0.000	0.000	NA	0.191	0.5	1	2	2
2	0.191	0.000	0.000	0.000	NA	0.191	0.5	1	1	1
1	0.191	0.000	0.000	0.000	NA	0.191	0.5	0	0	1
0								0	0	0

Table C1-14
Base Parameters
Emergency Deceleration Data

Emergency

Speed (m/s)	Propulsive E-M (g)	Levitation & Guidance E-M (g)	Aerodynamic Drag Vehicle (g)	Aerodynamic Brake Drag (g)	Chute (g)	Total Stopping Force (g)	Time Delta (s)	Distance Traveled (m)	Cumulative Distance	Cumulative Time
150	0.191	0.007	0.093	0.234	0.234	0.758	0.1	20	2,651	44
149	0.191	0.007	0.092	0.230	0.230	0.750	0.1	20	2,631	44
148	0.191	0.007	0.090	0.227	0.227	0.743	0.1	20	2,611	44
147	0.191	0.007	0.089	0.224	0.224	0.736	0.1	20	2,591	44
146	0.191	0.007	0.088	0.221	0.221	0.729	0.1	20	2,571	44
145	0.191	0.007	0.087	0.218	0.218	0.721	0.1	20	2,550	44
144	0.191	0.007	0.086	0.215	0.215	0.714	0.1	20	2,530	44
143	0.191	0.007	0.084	0.212	0.212	0.707	0.1	21	2,509	44
142	0.191	0.007	0.083	0.209	0.209	0.700	0.1	21	2,489	43
141	0.191	0.007	0.082	0.206	0.206	0.693	0.1	21	2,468	43
140	0.191	0.007	0.081	0.203	0.203	0.686	0.1	21	2,448	43
139	0.191	0.007	0.080	0.201	0.201	0.679	0.2	21	2,427	43
138	0.191	0.007	0.079	0.198	0.198	0.672	0.2	21	2,406	43
137	0.191	0.007	0.077	0.195	0.195	0.666	0.2	21	2,385	43
136	0.191	0.007	0.076	0.192	0.192	0.659	0.2	21	2,364	42
135	0.191	0.008	0.075	0.189	0.189	0.652	0.2	21	2,343	42
134	0.191	0.008	0.074	0.186	0.186	0.646	0.2	21	2,322	42
133	0.191	0.008	0.073	0.184	0.184	0.639	0.2	21	2,301	42
132	0.191	0.008	0.072	0.181	0.181	0.632	0.2	21	2,280	42
131	0.191	0.008	0.071	0.178	0.178	0.626	0.2	21	2,259	42
130	0.191	0.008	0.070	0.175	0.175	0.620	0.2	21	2,238	42
129	0.191	0.008	0.069	0.173	0.173	0.613	0.2	21	2,216	41
128	0.191	0.008	0.068	0.170	0.170	0.607	0.2	21	2,195	41
127	0.191	0.008	0.067	0.167	0.167	0.601	0.2	21	2,174	41
126	0.191	0.008	0.065	0.165	0.165	0.594	0.2	22	2,152	41
125	0.191	0.008	0.064	0.162	0.162	0.588	0.2	22	2,131	41
124	0.191	0.008	0.063	0.160	0.160	0.582	0.2	22	2,109	41
123	0.191	0.008	0.062	0.157	0.157	0.576	0.2	22	2,087	40
122	0.191	0.008	0.061	0.155	0.155	0.570	0.2	22	2,066	40
121	0.191	0.008	0.060	0.152	0.152	0.564	0.2	22	2,044	40
120	0.191	0.008	0.059	0.149	0.149	0.558	0.2	22	2,022	40
119	0.191	0.009	0.058	0.147	0.147	0.552	0.2	22	2,000	40
118	0.191	0.009	0.057	0.145	0.145	0.546	0.2	22	1,979	39
117	0.191	0.009	0.056	0.142	0.142	0.541	0.2	22	1,957	39
116	0.191	0.009	0.055	0.140	0.140	0.535	0.2	22	1,935	39
115	0.191	0.009	0.055	0.137	0.137	0.529	0.2	22	1,913	39
114	0.191	0.009	0.054	0.135	0.135	0.523	0.2	22	1,891	39
113	0.191	0.009	0.053	0.133	0.133	0.518	0.2	22	1,868	38
112	0.191	0.009	0.052	0.130	0.130	0.512	0.2	22	1,846	38
111	0.191	0.009	0.051	0.128	0.128	0.507	0.2	22	1,824	38
110	0.191	0.009	0.050	0.126	0.126	0.502	0.2	22	1,802	38
109	0.191	0.009	0.049	0.123	0.123	0.496	0.2	22	1,780	38
108	0.191	0.009	0.048	0.121	0.121	0.491	0.2	22	1,757	37
107	0.191	0.010	0.047	0.119	0.119	0.486	0.2	22	1,735	37
106	0.191	0.010	0.046	0.117	0.117	0.480	0.2	22	1,713	37
105	0.191	0.010	0.045	0.114	0.114	0.475	0.2	22	1,690	37
104	0.191	0.010	0.045	0.112	0.112	0.470	0.2	22	1,668	37
103	0.191	0.010	0.044	0.110	0.110	0.465	0.2	22	1,645	36
102	0.191	0.010	0.043	0.108	0.108	0.460	0.2	22	1,623	36
101	0.191	0.010	0.042	0.106	0.106	0.455	0.2	23	1,600	36
100	0.191	0.010	0.041	0.104	0.104	0.450	0.2	23	1,578	36
99	0.191	0.010	0.040	0.102	0.102	0.445	0.2	23	1,555	36
98	0.191	0.010	0.040	0.100	0.100	0.441	0.2	23	1,533	35
97	0.191	0.011	0.039	0.098	0.098	0.436	0.2	23	1,510	35
96	0.191	0.011	0.038	0.096	0.096	0.431	0.2	23	1,488	35
95	0.191	0.011	0.037	0.094	0.094	0.426	0.2	23	1,465	35
94	0.191	0.011	0.036	0.092	0.092	0.422	0.2	23	1,443	34

Table C1-14
(Cont'd)

Emergency

Speed (m/s)	Propulsive E-M (g)	Levitation & Guidance E-M (g)	Aerodynamic Drag Vehicle (g)	Aerodynamic Brake Drag (g)	Chute (g)	Total Stopping Force (g)	Time Delta (s)	Distance Traveled (m)	Cumulative Distance	Cumulative Time
93	0.191	0.011	0.036	0.090	0.090	0.417	0.2	23	1,420	34
92	0.191	0.011	0.035	0.088	0.088	0.413	0.2	23	1,397	34
91	0.191	0.011	0.034	0.086	0.086	0.408	0.2	23	1,375	34
90	0.191	0.011	0.033	0.084	0.084	0.404	0.3	23	1,352	33
89	0.191	0.011	0.033	0.082	0.082	0.400	0.3	23	1,330	33
88	0.191	0.012	0.032	0.080	0.080	0.395	0.3	23	1,307	33
87	0.191	0.012	0.031	0.079	0.079	0.391	0.3	23	1,284	33
86	0.191	0.012	0.031	0.077	0.077	0.387	0.3	23	1,262	32
85	0.191	0.012	0.030	0.075	0.075	0.383	0.3	22	1,239	32
84	0.191	0.012	0.029	0.073	0.073	0.379	0.3	22	1,217	32
83	0.191	0.012	0.028	0.072	0.072	0.375	0.3	22	1,194	32
82	0.191	0.012	0.028	0.070	0.070	0.371	0.3	22	1,172	31
81	0.191	0.013	0.027	0.068	0.068	0.367	0.3	22	1,150	31
80	0.191	0.013	0.026	0.066	0.066	0.363	0.3	22	1,127	31
79	0.191	0.013	0.026	0.065	0.065	0.359	0.3	22	1,105	30
78	0.191	0.013	0.025	0.063	0.063	0.356	0.3	22	1,083	30
77	0.191	0.013	0.024	0.062	0.062	0.352	0.3	22	1,060	30
76	0.191	0.013	0.024	0.060	0.060	0.348	0.3	22	1,038	30
75	0.191	0.014	0.023	0.058	0.058	0.345	0.3	22	1,016	29
74	0.191	0.014	0.023	0.057	0.057	0.341	0.3	22	994	29
73	0.191	0.014	0.022	0.055	0.055	0.338	0.3	22	972	29
72	0.191	0.014	0.021	0.054	0.054	0.334	0.3	22	950	28
71	0.191	0.014	0.021	0.052	0.052	0.331	0.3	22	929	28
70	0.191	0.015	0.020	0.051	0.051	0.328	0.3	22	907	28
69	0.191	0.015	0.020	0.049	0.049	0.324	0.3	22	885	27
68	0.191	0.015	0.019	0.048	0.048	0.321	0.3	21	864	27
67	0.191	0.015	0.019	0.047	0.047	0.318	0.3	21	842	27
66	0.191	0.015	0.018	0.045	0.045	0.315	0.3	21	821	27
65	0.191	0.016	0.017	0.044	0.044	0.312	0.3	21	800	26
64	0.191	0.016	0.017	0.043	0.043	0.309	0.3	21	779	26
63	0.191	0.016	0.016	0.041	0.041	0.306	0.3	21	758	26
62	0.191	0.016	0.016	0.040	0.040	0.303	0.3	21	737	25
61	0.191	0.017	0.015	0.039	0.039	0.300	0.3	21	716	25
60	0.191	0.017	0.015	0.037	0.037	0.298	0.3	20	696	25
59	0.191	0.017	0.014	0.036	0.036	0.295	0.3	20	675	24
58	0.191	0.018	0.014	0.035	0.035	0.292	0.3	20	655	24
57	0.191	0.018	0.013	0.034	0.034	0.290	0.4	20	635	24
56	0.191	0.018	0.013	0.033	0.033	0.287	0.4	20	615	23
55	0.191	0.019	0.012	0.031	0.031	0.285	0.4	19	596	23
54	0.191	0.019	0.012	0.030	0.030	0.283	0.4	19	576	22
53	0.191	0.019	0.012	0.029	0.029	0.280	0.4	19	557	22
52	0.191	0.020	0.011	0.028	0.028	0.278	0.4	19	538	22
51	0.191	0.020	0.011	0.027	0.027	0.276	0.4	19	519	21
50	0.191	0.020	0.010	0.026	0.026	0.274	0.4	18	500	21
49	0.191	0.021	0.010	0.025	0.025	0.272	0.4	18	482	21
48	0.191	0.021	0.010	0.024	0.024	0.270	0.4	18	463	20
47	0.191	0.022	0.009	0.023	0.023	0.268	0.4	18	446	20
46	0.191	0.022	0.009	0.022	0.022	0.266	0.4	17	428	19
45	0.191	0.023	0.008	0.021	0.021	0.264	0.4	17	410	19
44	0.191	0.023	0.008	0.020	0.020	0.262	0.4	17	393	19
43	0.191	0.024	0.008	0.019	0.019	0.261	0.4	17	376	18
42	0.191	0.024	0.007	0.018	0.018	0.259	0.4	16	360	18
41	0.191	0.025	0.007	0.017	0.017	0.258	0.4	16	343	18
40	0.191	0.025	0.007	0.017	0.017	0.256	0.4	16	327	17
39	0.191	0.026	0.006	0.016	0.016	0.255	0.4	15	312	17
38	0.191	0.027	0.006	0.015	0.015	0.254	0.4	15	296	16
37	0.191	0.028	0.006	0.014	0.014	0.253	0.4	15	281	16

Table C1-14
(Cont'd)

Emergency

Speed (m/s)	Propulsive E-M (g)	Levitation & Guidance E-M (g)	Aerodynamic Drag Vehicle (g)	Aerodynamic Brake Drag (g)	Chute (g)	Total Stopping Force (g)	Time Delta (s)	Distance Traveled (m)	Cumulative Distance	Cumulative Time
36	0.191	0.028	0.005	0.013	0.013	0.252	0.4	14	267	16
35	0.191	0.029	0.005	0.013	0.013	0.251	0.4	14	252	15
34	0.191	0.030	0.005	0.012	0.012	0.250	0.4	14	238	15
33	0.191	0.031	0.004	0.011	0.011	0.249	0.4	13	224	14
32	0.191	0.032	0.004	0.011	0.011	0.248	0.4	13	211	14
31	0.191	0.033	0.004	0.010	0.010	0.248	0.4	13	198	13
30	0.191	0.034	0.004	0.009	0.009	0.248	0.4	12	186	13
29	0.191	0.035	0.003	0.009	0.009	0.247	0.4	12	174	13
28	0.191	0.036	0.003	0.008	0.008	0.247	0.4	11	162	12
27	0.191	0.038	0.003	0.008	0.008	0.247	0.4	11	150	12
26	0.191	0.039	0.003	0.007	0.007	0.247	0.4	11	139	11
25	0.191	0.041	0.003	0.006	0.006	0.247	0.4	10	129	11
24	0.191	0.042	0.002	0.006	0.006	0.248	0.4	10	119	11
23	0.191	0.044	0.002	0.005	0.005	0.249	0.4	9	109	10
22	0.191	0.046	0.002	0.005	0.005	0.250	0.4	9	100	10
21	0.191	0.049	0.002	0.005	0.005	0.251	0.4	8	91	9
20	0.191	0.051	0.002	0.004	0.004	0.252	0.4	8	83	9
19	0.191	0.054	0.001	0.004	0.004	0.254	0.4	7	75	9
18	0.191	0.057	0.001	0.003	0.003	0.256	0.4	7	68	8
17	0.191	0.060	0.001	0.003	0.003	0.258	0.4	7	61	8
16	0.191	0.064	0.001	0.003	0.003	0.261	0.4	6	54	7
15	0.191	0.068	0.001	0.002	0.002	0.265	0.4	6	48	7
14	0.191	0.073	0.001	0.002	0.002	0.269	0.4	5	42	7
13	0.191	0.078	0.001	0.002	0.002	0.274	0.4	5	37	6
12	0.191	0.085	0.001	0.001	0.001	0.280	0.4	4	33	6
11	0.191	0.093	0.000	0.001	0.001	0.287	0.4	4	28	5
10	0.191	0.102	0.000	0.001	0.001	0.296	0.3	3	25	5
9	0.191	0.000	0.000	0.001	0.001	0.193	0.5	4	21	5
8	0.191	0.000	0.000	0.001	0.001	0.193	0.5	4	17	4
7	0.191	0.000	0.000	0.001	0.001	0.192	0.5	3	13	4
6	0.191	0.000	0.000	0.000	0.000	0.192	0.5	3	10	3
5	0.191	0.000	0.000	0.000	0.000	0.192	0.5	2	7	3
4	0.191	0.000	0.000	0.000	0.000	0.192	0.5	2	4	2
3	0.191	0.000	0.000	0.000	0.000	0.191	0.5	1	2	2
2	0.191	0.000	0.000	0.000	0.000	0.191	0.5	1	1	1
1	0.191	0.000	0.000	0.000	0.000	0.191	0.5	0	0	1
0									0	0

1.12.2 Dynamic Braking Energy Recovery

Overview

During the process of dynamic braking of trains, mill motors, cranes, and other equipment, energy is converted from the kinetic energy and potential energy of the vehicle through an electric motor (used as a generator) into electrical energy, which is most often dissipated as heat in a resistive grid. This differs from regenerative braking wherein the generated power is fed back to the electric utilility company.

In dynamic braking, the loss of kinetic energy slows the vehicle, and the guideway's linear synchronous motor (LSM) is the electric motor being employed. The LSM is used as a linear synchronous generator (LSG) to generate power. Our maglev vehicle, through the LSG's and bidirectional converters, could return this energy to the dc power distribution lines for use in propelling other vehicles. The resulting energy savings would significantly reduce the amount of power required from an outside utility company.

Analysis Techniques

To aid in collecting the data used in this report, a simulated computer run of the NMI's hypothetical route was performed using Electro-Motive's train simulation program ER574ZE. This simulation contained all of the relevant details such as speed limits on turns, grade information, air resistance, magnetic drag, and braking effort characteristics of the vehicle needed to make this analysis. The SST was used as a basis for projected yearly energy consumption costs as well as determining the recoverable braking energy amounts.

Proposed Energy Recovery System Design

The resistive grid normally connected to the output of the LSGs would be replaced by a converter which would convert the ac output at the LSG terminals to dc. The converters at the inverting station must be designed to allow the bi-directional flow of electricity, or else additional separater conversion equipment such as a stepup transformer and a phase-controlled rectifier. This increases cost, the energy cost savings would more than pay for the added equipment or equipment capabilities.

The converters would place the recaptured power back onto dc power distribution lines for use by nearby vehicles. If there are no vehicles nearby, the energy would travel along line until line losses

consumed the power or until it reached a vehicle. This additional power source would also assist in maintaining voltage levels.

Recoverable Energy and Efficiency

A simulated run of the hypothetical route showed that 34 percent of the input energy is dissipated as heat in the dynamic brakes. If 80 percent of this braking energy could be recovered and put back onto the 15 kV lines, it would represent an annual energy savings of 20 percent. (Note: 30 kV lines may be used in actual design for higher efficiency; 15 kV is used here for illustration.) The 60 percent efficiency number is arrived at by estimating 90 percent efficiency for the LSG and 97 percent efficiency for the stepup transformer and the rectifier and the dc distribution lines. Multiplying 0.9 x 0.97 x 0.97 x 0.97 gives 0.82.

The hypothetical route represents a mixture of sloping, curving terrain and smooth, straight terrain. Energy recovery would be much more prevalent where the brakes must be applied often, as is the case in curving or downward sloping terrain, and less of a factor in smooth, straight terrain.

Economic Feasibility

In order to judge the economic feasibility of the energy recovery system, an estimate must first be made of the annual energy consumption of a typical maglev route, simplistic as the estimate might be. The power required to counteract air resistance by a maglev vehicle traveling at 500 kph is 6.5×10^6 watts. However, due to curves and changing grades, assume that the average speed of the vehicle across the entire length of the route is 333 kph. Since air resistance is proportional to the square of the speed,

$$\text{Power per vehicle} = 6.5 \times 10^6 \text{ watts} \times (333 \text{ kph}/500 \text{ mph})^2 = 2.88 \times 10^6 \text{ watts.}$$

If we assume for illustration puposes the assumptions of 4,000 passengers per hour, 24 hours per day, 365 days per year, on the hypothetical route, 2 ways, 2.4 hours per trip direction, 2,880 kilowatts delivered power per vehicle, 0.82 efficiency, 8.5 cents per kwh, in propulsion 50 percent of the time, and 106 passengers per vehicle, then the yearly propulsion energy cost at the electrical meters will be

4000x24x365x2x2.4x2880x$0.085x0.50/106/.82=$486,000,000 or $ 486 Million/year

If we could save 20 percent of this energy by recovering the dynamic brake energy, we could reduce the annual energy bill by $97 million, a significant savings, and an amount of money that would easily pay for the extra equipent required.

1.12.3 Aerodynamic Speed Brakes

Abstract

Additional vehicle braking capabilities are needed for emergency situations. Aerodynamic speed brakes can add up to .2 g deceleration to normal braking at maximum operating speed where braking is most critical.

Key Requirements

Emergency braking should be most effective at high speeds and work in all weather conditions. Emergency braking must be deployable with on-board vehicle power, must not damage the guideway, must be inconspicuous when not in use, must be lightweight, occupy small volume, and be redeployable.

Approach Used

The Bechtel Team has chosen plug-type flat plate speed brakes which will be stored entirely inside the vehicle. Eight plates, four front and four aft will provide .2 g deceleration at 500 kph when fully deployed.

Description

Numerous aerodynamic speed brake designs were considered, including plug-type plates (flat surface plates opening fore and aft), curved vane plates, Kevlar window shade brakes, separating tail cones, and tail cone fans. Of these, the plug-type plates had the least effect on vehicle structure, their aerodynamics are well understood, and very little energy is required to deploy them. Figure C1-57 illustrates the deployment of flat surface plates.

The 11.6 m^2 plate area required will be divided into 8 plates 1.35 meters wide by 1.07 meters high with four plates placed forward of the cabin and four plates placed aft of the cabin. Using a built-up aluminum construction, the plates will be 35 mm thick and lightweight.

With the plug brakes stored in the vehicle there will be no aerodynamic drag or noise penalty during normal operation. Use of wormgear motors will insure rapid but controlled deployment to reduce shock effects on passengers.

Benefits/Risk

Benefits of the aerodynamic speed brake system increases as the system passenger capacity increases and vehicle spacing decreases. Speed brakes are forecast as being definitely required for 12,000 passengers per hour but will be more of a psychological benefit at 4,000 passengers per hour.

The brakes, their support structure, and drive motors will add about 1,000 kg and occupy 1 m^3 of vehicle space.

References

1. Maglev Speed Brake Design, 14 May 1992, by Jim Guglielmo (see appendix)
2. Speed Brake Options, 03 July 1992, by Tom Zych (see appendix)
3. Speed Brakes, 12 August 1992, by Tom Zych (see appendix)

1.12.4 Drag Chute Emergency Braking

Abstract

In an extreme emergency, it is necessary to have reserve braking power, particularly at cruising speed where a kilometer is traversed every 7 seconds. A ribbon-type drag chute with a cross-sectional area of 14.5 square meters or diameter of 2.2 meters can provide .2g deceleration. Combined with normal braking and aerodynamic braking, the addition of a drag chute can bring total vehicle braking to over .6 g.

Key Requirements

The drag chute should provide at least .2 g vehicle braking, should be deployable through a .25 m boundary layer, and opening shock force should exceed steady state braking force by only 50 percent.

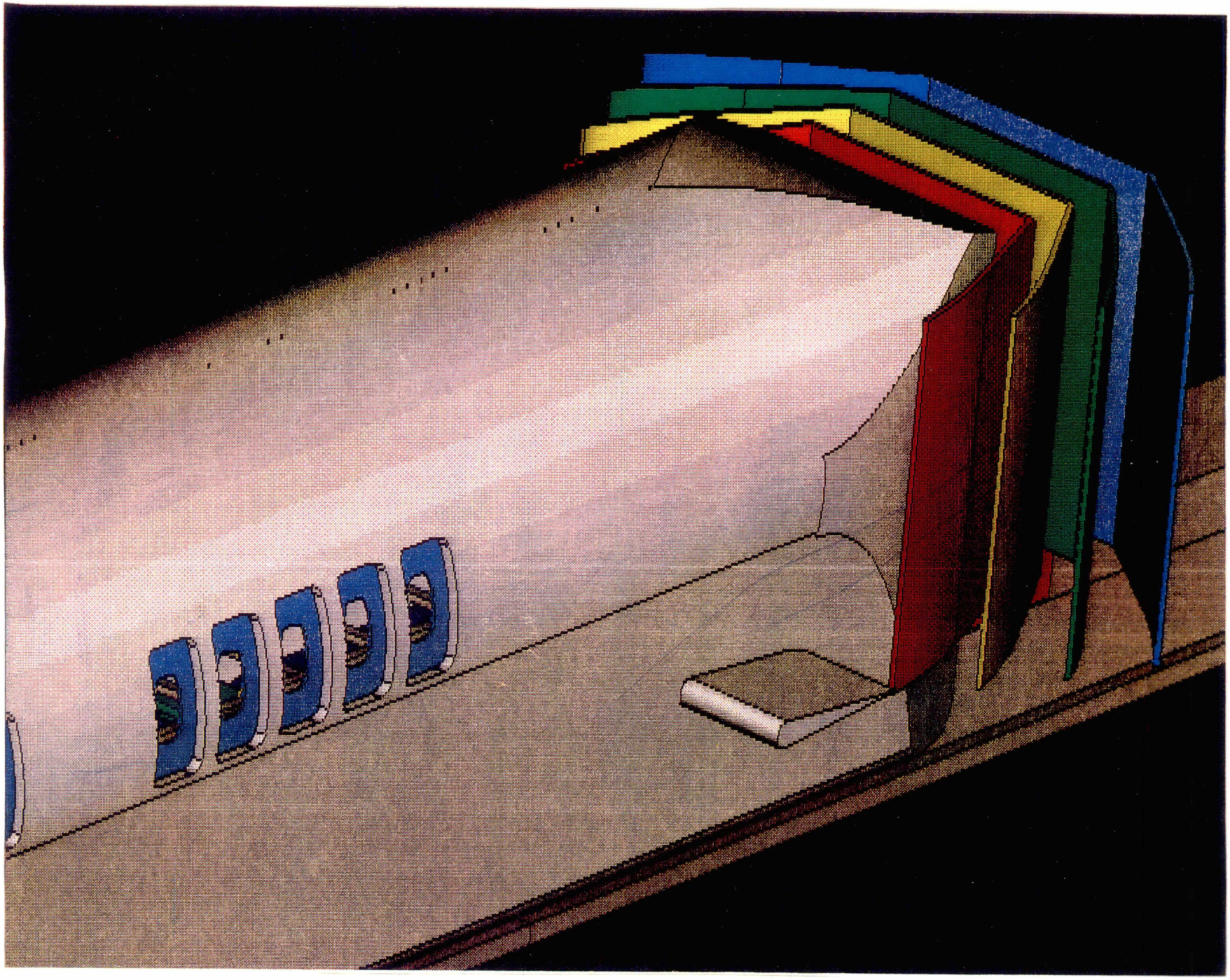

Figure C1-57 Deployment of flat surface plates

Approach

A ribbon-type drag chute with a mortar launch was chosen for the Bechtel vehicle. Kevlar was chosen for materials in the chute to minimize weight. The 40 kg chute/launch system is stored in a .5 m diameter canister 1 meter long at the rear of the vehicle.

Description

A number of chute types and materials were considered for this design. Being non-redeployable and seldom if ever used, it was decided weight and space were more important than cost. Therefore, Kevlar was chosen over nylon and steel for the chute and guide lines. Ribbon-type chutes, commonly used for aircraft and vehicle deceleration, were chosen for their low opening shock force of 1.1 to 1.5 times the steady state drag force. Commercially available mortar chute deployment systems would only need to be down-sized for the maglev vehicle.

1.12.5 Abnormal Vehicle Speeds

Overview

The Bechtel Team concept vehicle is designed for a maximum propelled speed of at least 500 kph. This section discusses what conditions may lead to abnormal vehicle speeds and how they have been mitigated.

Analysis

Analysis of abnormal vehicle speeds possible centered mostly around the aerodynamic equations since aerodynamic is the regarding force that must be overcome at high speeds to achieve an abnormal condition.

The governing aerodynamic equation is

$$D = 0.5\ p\ (c_f a_f + c_s a_s) v^2$$

where

$$p = 1.23\ kg/m^2$$

and for the Bechtel concept:

$$c_f = 0.1$$

a_f=17.7 m^2

c_s=0.004

a_s=660 m^2

Results of Analysis

Since maglev vehicles are normally propelled on a magnetic hump which in effect pushes the vehicle down the guideway, abnormal speeds are normally not possible because the vehicle must remain synchronized with this pulse. The only condition whereby an abnormal speed is possible is when this magnetic pulse is not existent, i.e., when synchronization is lost. If this occurs the vehicle can be "caught" again by another magnetic pulse since the propulsion system is capable of sensing where the vehicle is along the guideway.

The scenario most likely to leading to an abnormal speed is:

1) vehicle is traveling at or very near full velocity when magnetic drag is small and aerodynamic drag is large,

and 2) synchronization with the linear synchronous motor (LSM) is lost,

and 3) none of the vehicles' auxiliary braking systems (aerodynamic brakes and emergency parachutes) are deployed,

and 4) the vehicle is traversing a down grade.

Under these conditions, it is possible that the vehicle's mass can result in a force greater than the current aerodynamic drag resulting in the vehicle accelerating to a new equilibrium speed. All vehicles on grades have a force equal to 20 lbs/U.S. ton of vehicle weight/degree of grade). The Bechtel Team vehicle design goal mass is 64,000 kg (141,120 lbs); therefore, the down grade force on a 10 percent grade (maximum designed for) is 62.8 kN (14,112 lbs). Using the aerodynamic drag equation, we can solve for equilibrium speed.

$$62.8 = \_ (1.23)(0.1x15.7 + 0.004x660)V^2$$

Considering magnetic drag, the highest abnormal speed is less than 150 m/s, the maximum anticipated vehicle speed. It is worth noting that under normal conditions, the vehicle's normal

auxiliary braking system, the aerodynamic brakes, would be sufficient to ensure that the vehicle does not obtain a speed higher than the rated speed. It is possible to design the aerodynamic brakes to be deployed automatically when the vehicle speed exceeds a preset limit for a certain area of guideway.

1.12.6 Maximum Possible Unexpected Decelerations

Overview

Due to the nature of a maglev systems propulsion system, uncontrolled deceleration is highly unlikely. This section discusses possible scenarios resulting in rapid or unexpected decelerations.

Discussion

As discussed in the propulsion sections of this report, the maglev vehicle is propelled by an electromagnetic wave produced by the linear synchronous motor (LSM). As the name implies, for propulsion and braking to occur, the vehicle must remain synchronized with the wave. If a vehicle should slip off of the wave, it would simply coast, with only the aerodynamic, magnetic, and uphill grade drags retarding the motion. Since the aerodynamic drag at full speed is approximately 46 kN, if propulsion is lost an immediate deceleration of 0.09 g would be felt by the passenger in the maglev vehicle. This acceleration may actually be higher if the vehicle is just starting to traverse a steep uphill grade and the vehicle has yet to slow significantly.

As a safety precaution, all blocks within the propulsion system that do not contain vehicles are short circuited to ensure that if a vehicle enters an unauthorized block it will immediately start to slow down. The short circuit has the effect of applying a 0.2 g deceleration to a vehicle at full speed.

The previous two unexpected decelerations would not normally be considered emergency conditions provided that the control system realizes quickly what has happened and takes immediate appropriate action. All other uncontrolled decelerations possible would have to result from other failure mechanisms. Two such mechanisms are described below.

The vehicle's aerodynamic brakes are an auxiliary braking method, allowing the vehicle to slow quickly if desired. If these brakes should deploy suddenly, their full decelerative force of 0.2 g would be immediately felt. If this sudden deceleration is deemed unacceptable in later phases of the design, the aerodynamic brakes can be designed with interlocks and other devices to make this event extremely unprobable.

The most unexpected deceleration which may also result in overall system delays would be if a vehicle's emergency parachute deployed unexpectedly. This parachute would provide a 0.2 g deceleration force at full speed and would also require that the vehicle come to a complete stop until maintenance can be performed to detach the parachute. The emergency parachute system will have to be designed to ensure that the probability of this happening is very small.

1.13 PASSENGER CONSIDERATIONS

1.13.1 Temperature and Humidity

Overview

The cabin environment of the maglev vehicle must be kept constant at reasonable values in order for the passenger to feel comfortable. This section describes the temperature and humidity ranges within which the cabin should be kept to achieve a comfortable environment for the passengers.

Specifications

In the Ride Quality Guidelines, the DOT specifies that a cabin temperature of 18°C to 23°C must be maintained when passengers are inside the vehicle. No humidity requirements were specified by the DOT. For the maglev vehicle, a temperature of 18°C to 23°C and a humidity of 40 to 45 percent in the winter and 40 to 60 percent in the summer will be maintained when passengers are on board the vehicle. The temperatures specified by DOT are reasonable and other sources also describe temperatures similar to those required by DOT.

Description

Considering the worst case, in which the maglev vehicle is traveling at 134 m/s with an ambient temperature of -40°C, there is considerable heat loss from the vehicle in the winter. In summer, cooling is the problem. An average person gives off 120 watts of heat energy. In a vehicle loaded with 106 people on a warm day, this load on the cabin temperature must be removed, as well as heat from the electronics and galleys that are also in the passenger compartment. The HVAC system that controls the cabin environment must be designed to be able to keep the cabin air within the temperature range specified by the DOT while operating at extreme summer and winter conditions.

The humidity of the cabin air is also an important factor in passenger comfort. Low humidity, below 30 percent, can cause the passengers to feel considerable discomfort in the eyes, nose, and throat. Since the maglev vehicle does not have a wide range of elevation changes as aircraft do, changes in humidity will not be as drastic as in aircraft. However, the maglev vehicle is subject to

ambient environmental changes and therefore changes in humidity. The relative humidity of the environment can range from as much as 90 percent humidity and to as low as 20 percent humidity, depending on the season and on the region that the maglev vehicle is traveling in. This atmospheric humidity is a considerable factor in designing the HVAC system. Humidity can have large effects on the power requirement of the HVAC system. The HVAC system should be designed to compensate for these changes in the cabin and atmospheric humidity.

1.13.2 Lighting

Key Requirements

Proper lighting is an important factor in the design of a maglev vehicle. Good interior lighting must be supplied so that the passenger can see properly in normal and emergency conditions. Exterior lighting must also be supplied to identify the vehicle. The concept maglev vehicle from the Bechtel Team is similar to most large passenger aircraft and therefore the lighting system described below is modeled after those on large passenger aircraft and will follow some regulations on lighting set by the FAA.

Description

The maglev vehicle lighting can be grouped into three categories: interior, exterior, and emergency lighting.

Most large passenger aircraft use indirect lighting as the main passenger compartment lighting. This type of lighting gives even and concealed light. Studies have shown that for tasks such as reading, a level of 300 lux is sufficient. When the cabin is darkened to enable the passengers to sleep, a level of 50 lux is required for safe movement. On typical passenger aircraft, the passenger compartment lighting is controlled by a variable light intensity circuit. Individual reading lights should also be available. Other compartments such as the galleys or lavatories would require separate lighting. These compartments would be better off with direct lighting because the compartments are enclosed small areas where shadows are less likely to occur. These cabin compartments should be lighted at 300 lux or higher since there is more activity in these areas. Illuminated information signs are also needed for the passengers. Studies have shown that people can identify an illuminated sign better and more quickly than a large printed sign.

Passenger aircraft have an international standard for the kind of exterior lighting required. Exterior lighting supplied for the maglev vehicle depends on regulations and requirements that are not determined at this time. It is anticipated that the vehicle would require head lights, rear lights, and

marking lights. Head and rear lights would probably be used to identify the vehicle from ahead and behind and also to illuminate the guideway. Typical power rating for the head lights on large passenger aircraft such as the Boeing 747 is 600 watts per light bulb. Additional marking lights might be added to identify the vehicle easily from greater distances, i.e., red anticollision lights located on top of the vehicle.

Emergency lighting is an important issue when designing the lighting system. Proper care must be taken to provide adequate lighting for safe operations and passenger movement under emergency conditions. The FAA requires that on a passenger aircraft, a passenger must be able to identify the escape path and exits from markings and visual features that are positioned not more than four feet from the cabin floor, in case smoke or toxic gas obscures visibility in the upper area of the cabin. In addition to these requirements, passenger aircraft also have head high lights and illuminated information signs. Proper exterior emergency lighting must also be provided in case passengers have to exit the vehicle at night. Lighting should provide visibility adequate for safe evacuation of the vehicle.

1.13.3 Interior Vehicle Noise

Key Requirements

Due to aerodynamic noise alone, maglev systems will generate considerable carbody noise external to the vehicle. To provide adequate passenger comfort, interior cabin noise levels must be maintained at a low level and therefore consideration must be given in the vehicle design to minimize interior noise. The goal for cabin noise levels is 70 dBA or less.

Approach

Wall interior and floor insulation will be provided both to insulate the vehicle from the temperature variations and to provide a sound reduction layer for the passenger cabin.

Description

Aerodynamic flow over the vehicle's structure and its effects are the major source of noise which may permeate the carbody structure. Vibrations of the vehicle during operation is another source of cabin noise. Both of these noise sources can be minimized by good design. It is key to realize that noise reduction must be designed in rather than dealt with as an afterthought.

Panels and attachments are specified to be thick enough to avoid vibration. In addition, adequate wall and floor panel thickness has been identified to allow for the addition of insulation and sound reduction materials as needed. The weight of these materials has been tentatively accounted for in weight estimates given for the vehicle. It is important to note that the isolation provided by the inner tilting coach should result in an interior noise reduction of 5 dBA or more over a non-isolated cabin design.

Benefits/Risk

A tradeoff analysis will be made regarding the weight of insulating materials versus their sound deadening attributes to ensure minimal cabin noise.

1.13.4 Carry-On and Checked Baggage

Abstract

Potential maglev systems will transport passengers over distances in the 167 to 1,000 kilometer range (100 to 600 miles). Passengers are expected to be mostly business travelers and people on short trips where the amount of baggage will be small. These passengers prefer to keep their baggage with them; therefore, significant consideration has been given to accommodations for carry-on baggage. Although passengers with small amounts of baggage typically carry on their baggage, mail and other items are often carried by these vehicles and provide significant income to the system. Also, oversize items (e.g., ski gear or golf equipment) must be accommodated and this is best done in the checked baggage area.

Key Requirements

No specific requirements were given in the RFP for carry-on or checked baggage capabilities. However, maglev systems are envisioned to provide aircraft-like service which would include the ability to carry checked and carry-on baggage. Furthermore, freight-carrying capacity is desirable in maglev systems and freight is usually stored in the checked baggage area.

Approach Used

Information needed to analyze this topic was obtained from several sources including the following aircraft design books:

- Edwards, Mary and Elwyn, *The Aircraft Cabin: Managing the Human Factors,* Gower Publishing Company, Brookfield, Vermont, 1990.

- Raymer, Daniel P., *Aircraft Design: A Conceptual Approach*, American Institute of Aeronautics and Astronautics, Washington, D.C., 1989.

Description

Airlines typically allow each passenger one carry-on item (excluding a coat or jacket). The item must be storable in either the overhead bins or under the seat in front of the passenger. The allowable carry-on bag total dimensions and weight are not to exceed 1,150 millimeters (45 inches) and 18 kg (40 pounds) respectively.

According to Edwards in *The Aircraft Cabin,* regulations are based partly on the assumed loaded weight of the aircraft, which factors into performance calculations, and on the effect of baggage on efficient evacuation. Since vehicle weight and efficient evacuation are as important in maglev systems as in aircraft, it is envisioned that the same baggage rules should apply.

Typical aircraft designs allow for 50,970,324 mm^3 to 62,297,062 mm^3 (1.8 ft^3 to 2.2 ft^3) of storage room per passenger in the overhead bins. In addition, for a few large items, several closets are provided for use by all passengers.

The Bechtel Team's vehicle has been designed with closets, overhead bins, and under-seat storage to provide adequate storage capacity for passenger carry-on baggage. There is also provision for checked baggage.

Most airlines allow each passenger one or two checked items. The allowable checked baggage total dimensions and weight are not to exceed 1,524 millimeters/32 kg (60 in./70 lb) for the first item and 1,397 millimeters/32 kg (55 in/70 lb) for the second item (if allowed).

According to Reamer in *Aircraft Design,* typical cargo volume per passenger ranges from 0.23 m^3 to 0.42 m^3 (8.6 ft^3 to 15.6 ft^3) per passenger. In passenger aircraft, baggage is usually hand loaded onto the aircraft, a long and tedious process. Newer aircraft handle more of the baggage in standard cargo containers which helps the loading process. For example, a 747 aircraft usually has 128 m^3 (4,740 ft^3) of containerized baggage and only 27 m^3 (1,000 ft^3) of bulk baggage.

For a 106- to 120-passenger vehicle (US1 baseline), and assuming that the vehicle is designed with 0.23 m^3 (8.6 ft^3) per passenger, total checked baggage requirements would be 25.8 m^3 to 29.2 m^3. Providing for this amount of baggage volume on a maglev vehicle would not be very significant. For example, our baseline vehicle is approximately 4 meters wide and 2 meters high

(cabin floor to ceiling). Thus a baggage compartment 4 meters wide x 2 meters high x 3.2 or 3.6 meters long would be required. This would add only about 10 percent to a 30-meter-long single vehicle without checked baggage capability. However, the mass of the passengers' baggage is of greater concern. For example, if each passenger is allowed two checked items of 32 kg each then the mass impact on the maglev vehicle (and system) is 6,784 kg (106 passengers) and 7,680 kg (200 passengers). Because vehicle mass impacts guideway strength it is desirable to have vehicles with minimal overall mass. Thus the baseline Bechtel Team vehicle allows for each passenger to have only one 1,524 mm/32kg (60 in./70 lb) checked bag in addition to carry-on baggage.

As a result of the checked baggage restriction, the required cargo impact on the maglev system is 9 m^3/3,392 kg (318 ft^3/7,420 lb) for the 106-passenger vehicle and 10.2 m^3/3,840 kg (360 ft^3/8,400 lb) for the 120-passenger vehicle. The actual US1 cargo containers allow for 16.1 m^3 of cargo capacity. These containers were overdesigned to allow for packing inefficiencies, incomplete packing to help lower the vehicle's center of mass, and to allow space for odd shaped items.

The maglev vehicle has been designed with two cargo containers. These containers provide adequate checked baggage space per passenger and allow for efficient loading and unloading of baggage to minimize station dwell time. It is envisioned that the containers will be open and available in the loading area for the vehicle; therefore, the passengers will be able to load their own baggage into the container before embarking. It is felt that this might convince passengers to check more of their baggage since they will be sure that it will be loaded onto the vehicle and will reach their destination. When the vehicle arrives at the destination, the containers will be unloaded and passengers can pick up their baggage in the disembarkation area.

Baggage Impact on Station Dwell Time

Carry-on baggage effects would be expected to be similar to those experienced on jet aircraft; however, since the accelerations on board maglev vehicles are small it may be possible to allow the vehicle to proceed from the station while passengers are still stowing luggage.

Checked baggage is containerized and therefore is completely loaded before the vehicle arrives at the station. It is expected that checked baggage loading and unloading will take less time than the loading and unloading of passengers.

Benefits/Risk

The Bechtel Team's system has space allocated for carry-on baggage in the same range as modern passenger aircraft. This should provide adequate room for the needs for carry-on baggage of typical maglev system users. Additional space has been allocated within the checked baggage area for carry-on baggage overflow should that occur.

The US1 system has significant space allocated for checked baggage. This should provide adequate room for the needs for checked baggage of typical maglev system users and therefore should make maglev systems an attractive transportation means. Finally, our concept of containerized checked baggage loaded by the individual passengers should make for a workable checked baggage system which passengers will want to use.

1.13.5 Exits

Exits have two main functions: to provide means of loading and unloading people and baggage, and rapid escape from the vehicle in emergency conditions. There are many regulations regarding aircraft exits that should be considered for use with maglev vehicles. Our recommendation is to use type A aircraft doors on both sides of the vehicle near the front and back of each passenger seating area.

There are five standard types of doors in aifcraft today, and any of these door types could be used in maglev applications. The largest is a type A door (usually used for normal entry and exit) while the smallest door is a type IV (usually used for over-the-wing exits). Typical configurations are shown in Figure C1-58. Regulations for aircraft state that "there shall be sufficient suitable exits to facilitate the rapid excape of all occupants in the event of an emergency alighting" (BCAR D4-3 4.2). The actual number required depends upon passenger capacity. Larger doors allow for quicker emergency evacuation, as Figure C2-59 shows.

In aircraft, exits must be available on both sides of the fuselage. This requirement makes sense for maglev vehicles if one considers the unlikely possibilities of external fire on one side of the vehicle or stopping in a banked curve.

Studies have been completed on aircraft regarding the time it requires to reach an emergency exit. The data has caused the FAA to propose that the maximum distance of any seat row to the nearest exit should be 9 m (30 ft). Some researchers state that a rule should be devised that accounts for the fact that more actual passengers in the coach section would share an exit than would in

business or first class sections. BCAR D4-3 4.2.5 states that "easy means of access to the exits shall be provided to facilitate use at all times, including darkness." In addition, space is also required near the exit for an attendant to stand when assisting passengers out of the exit. Another factor to consider near an exit is proximity to baggage or galley items that may become dislodged, thus obstructing the exit.

BCAR D4-3 4.3.6 requires that "the means of operating emergency exits shall be rapid and obvious and shall not require exceptional effort." Just as important as the ability to open an exit is how easily it is to close in case it is necessary to do so (as in case of fire outside of the vehicle near the door). This is of particular concern if electric or spring activated doors are being considered. Most exits also include a means of ascertaining if fire is present before the door is opened. The exits must also be clearly marked with instructions on how to both open and close the door.

Aircraft regulations also require that all exits 2 m (6 ft) from the ground be provided with equipment to assist the passengers to descend. This must be carefully considered during the later design stages to ensure that safe egress is possible from the vehicle wherever the vehicle may stop in an emergency.

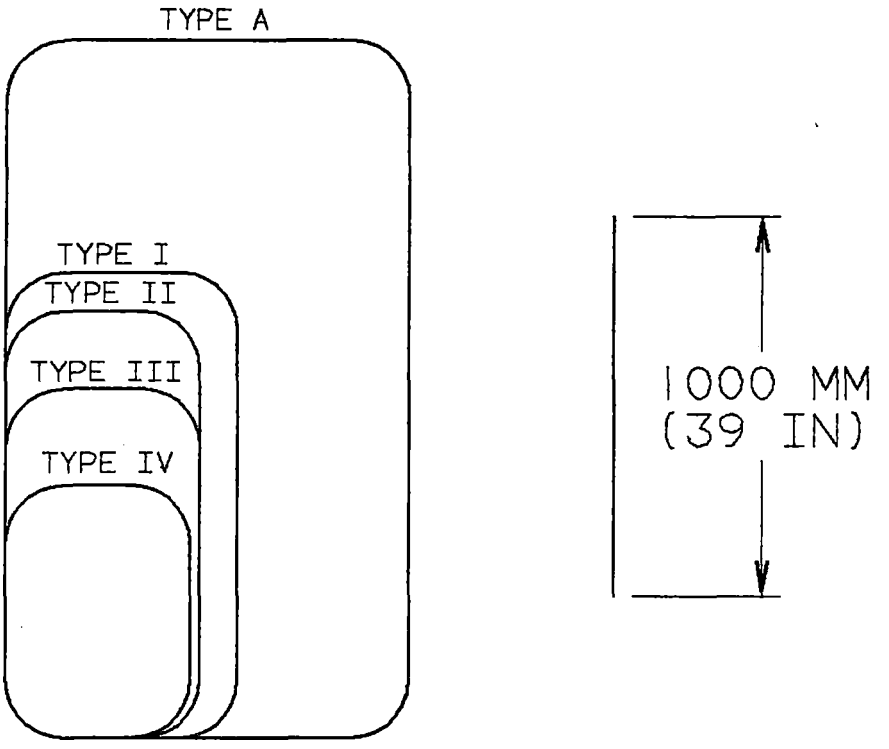

Figure C1-58 Typical door configuration used in commercial aircraft

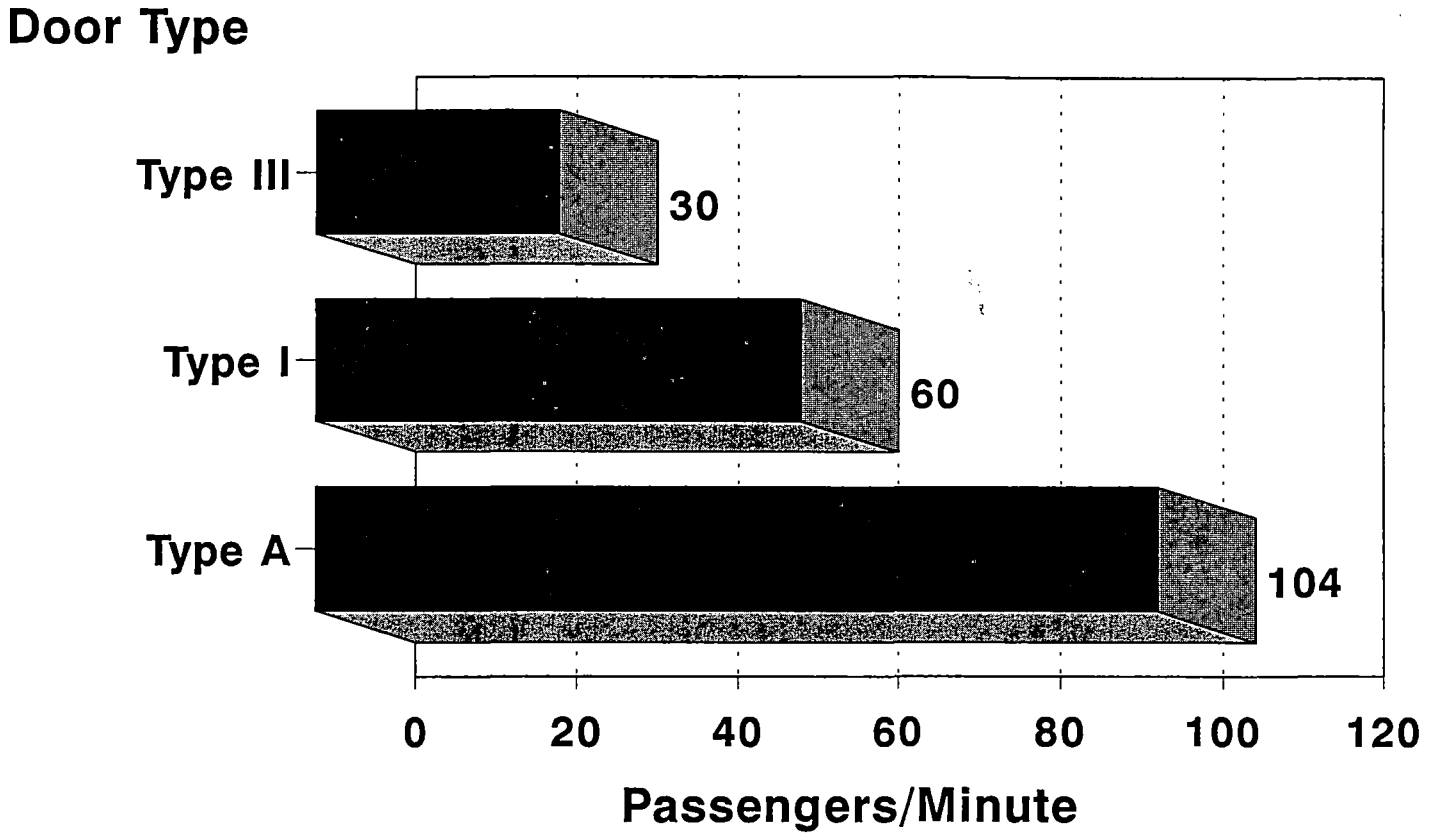

Figure C1-59 Number of passengers able to exit per minute through a single door

1.13.6 Cabin Attendants

Abstract

Cabin attendants' considerations involve tradeoffs both in terms of safety and service and in long-term operational costs of the maglev system. Cabin attendants are specifically not required by the RFP; however, a discussion of their function helps define our total Team concept in more detail.

Approach Used

The vehicle design allows for the provision of cabin attendants to assist in providing passenger comfort as well as emergency aid, if necessary. The number of cabin attendants is based upon final vehicle size. Current federal regulations for aircraft require one attendant for every 50 passengers.

Description

Some transportation systems, for example, rapid transit systems, operate without passenger attendants. Many systems have a pilot who can also act as an attendant if necessary, (e.g., busses and small turboprop aircraft). A few transit systems such as trains and aircraft have conductors or stewards acting as cabin attendants. Passengers typically prefer systems which have attendants, especially if the trip is of a long duration, and vehicle speed is high.

Attendants provide psychological benefits as well. Passengers know that there is help readily available if they have any questions, difficulties, or comfort concerns. Attendants also provide food and beverage service to make the trip more enjoyable.

Attendants provide leadership in emergency situations requiring knowledge of the vehicle and corrective actions. Attendants also assist in emergency evacuations if this action is necessary. The cabin attendants of aircraft have been often praised for their critical assistance in emergency situations.

For these reasons, especially those of safety, and the goal of providing aircraft-like service, three cabin attendants have been provided for in our baseline 106-passenger vehicle system.

1.13.7 Food and Beverage Service

Abstract

Typical aircraft accommodations include food and beverage service; therefore, maglev systems may be equipped with facilities to provide such a service. In addition, the typical maglev trip of 330 to 1,000 kilometers (200 to 600 miles) would take between one and three hours, providing ample time to serve light meals, beverages, and snacks.

Description

There are three methods of providing food and beverage service on maglev vehicles. Each of these methods will be briefly discussed including a discussion of which option was chosen and why.

The first method of providing food and beverage service uses galleys and cabin attendants in a fashion similar to commercial jet aircraft. Food and beverages are loaded into service carts before the vehicle leaves a major station and the carts are moved about the cabin during the trip to dispense food, beverages, and snacks. The disadvantages of providing service in this manner include blocking the aisle with the service carts during operation, providing an inconvenience to passengers as well as a safety hazard in an emergency or evacuation; cabin attendants are required to provide the service; and station stop time is increased to restock supplies.

A second method would be to issue all passengers a carry-on sack lunch bag at the station before embarking on the trip. The sack would contain all food, snacks, beverages, and utensils required by the passenger during the trip. Passenger would then be able to eat whenever it is convenient for them to do so. This method has been used in other countries successfully and theoretically does not require cabin attendants. The disadvantages of providing food service in this manner include: hot foods are difficult to supply; providing passengers with their choice of beverages and foods is potentially more difficult; the passengers do not feel that they are being served, so this method may not be as easily accepted as the galley and attendant method; and cabin cleanliness may be more difficult to maintain.

A third and extremely simple method of providing food and beverage service on the vehicle would be to provide on-board vending machines similar to those found in many cafeterias and lounges. With the addition of a microwave, hot foods could be provided. Also, this method allows passengers with special needs to bring their own foods on board and heat them if necessary. Theoretically, cabin attendants would not be required. The disadvantage of this method includes: passengers do not feel that they are being served; power consumption requirements and weight of

vending machines may be considerable; cabin cleanliness may be more difficult to maintain; and usage of machines may not be high, as is experienced in many buildings which have food provided in this manner.

The choice of providing food and beverage service based upon the use of galleys and attendants was made since the method is proven and the attendants are expected to be present on all vehicles for safety and security reasons.

Benefits/Risk

The benefits of providing food and beverage service to passengers of a maglev system should make the system more attractive to potential riders. The largest risk of providing such a service involves the additional weight impact on the vehicle, potentially making both the vehicle and guideway more costly. Less costly risks include the delay added into station stop times to restock the vehicle, as well as the potential safety impact of providing the service during vehicle operation.

1.13.8 Lavatories

Key Requirements

An adequate number of lavatories must be included in maglev vehicles. Lavatory size as well as supply needs should be considered in vehicle design and layout.

Approach Used

Information needed to analyze this topic was obtained from several sources including two aircraft design books and sales literature from Weber Aircraft, an aircraft lavatory designer. The two design books supplying material for the analysis of this topic were:

- Edwards, Mary and Elwyn, *The Aircraft Cabin: Managing the Human Factors*, Gower Publishing Company, Brookfield, Vermont, 1990.
- Raymer, Daniel P., *Aircraft Design: A Conceptual Approach*, American Institute of Aeronautics and Astronautics, Washington, D.C., 1989.

Description

Typical maglev passenger rides will range from 100 to 600 miles, providing for typical trip lengths from 30 minutes to three hours. Maglev systems are to provide aircraft-like service conditions to passengers. Passengers on aircraft are used to rushing to the aircraft knowing that they can always

use the lavatory on the airplane. It is expected that maglev passengers will act no differently; therefore, lavatories are required on the vehicles.

Typical short haul aircraft provide one lavatory for every 40 to 60 economy passengers and one lavatory for every 10 to 20 first-class passengers. Assuming that the Bechtel Team's typical vehicle carries 100 passengers (16 first class and 84 coach), approximately three lavatories are required.

A standard aircraft lavatory is approximately 1 meter wide by 1 meter deep, costs approximately $60-65,000 and weighs about 130 kg. The Edwardses, in *The Aircraft Cabin,* note that standard lavatories are space-constrained, and obese and disabled people are likely to have difficulties in using them. For some disabled passengers, use of standard aircraft lavatories may be impossible. Clearly, to make maglev systems more attractive, at least one easy-access lavatory must be provided for passengers with special needs.

Standard handicapped toilet stalls in commercial buildings are approximately 5 ft wide by 4 ft deep. They contain special features such as grab-handles and controls which are within easy reach. To provide a lavatory of this size, additional space must be left within the vehicle. In addition, the lavatory must be located near the passengers with special needs to provide for easy access. One lavatory of this type is included on each maglev vehicle in the front of the business class cabin since it is more space permissive.

1.13.9 ADA Provisions

The Americans with Disabilities Act (ADA) is the most comprehensive legislation of its kind ever passed in the United States. Its inherent rules and regulations impact the maglev vehicle's design from the start. This section discusses the impact.

Three areas of the vehicle are considered with regard to ADA impact: ingress and egress of passengers in wheelchairs; lavatory considerations for passengers in wheelchairs; and equal access to services provided to all passengers. The third requirement is inherent to the design, since the baseline system uses cabin attendants to provide passenger services. Thus, all passenger services are equally available.

The first consideration revolved around the mobility of wheelchair-bound passengers. On the baseline system the first class section of the vehicle would be utilized for wheelchair-bound

passengers since it provides more spacious accommodations and therefore easier access. Doors on the vehicle are one meter wide, well in excess of the 32 inches required. The first class section's aisle is also wide enough to allow full travel of a wheelchair through the first class section, thus providing access to the lavatories. Folding removable seats are provided in the first class cabin with appropriate wheelchair restraining methods to allow safe travel conditions for wheelchair-bound passengers. The last consideration was to the lavatories. The lavatory in the first class cabin was designed to meet accessibility regulations completely without special modifications to the vehicle.

The baseline concept is fully ADA compliant and will provide all passengers with equal access and equal service regardless of their physical or mental condition.

1.13.10 Vehicle Evacuation Methodology

Maglev vehicles are designed to be highly reliable with the highest possible probabilities of successful mission completion. However, at some point in a maglev systems operation an emergency evacuation of a vehicle will be necessary. A summary table of proposed evacuation methodologies in Table C1-15. Each method is discussed below.

Preferred Stopping Point

The Transrapid maglev system introduced the concept of a preferred stopping point. The basis of the concept is that a fast moving vehicle has significant coasting capability before it comes to a stop. Using the kinetic energy of the vehicle only, it is possible to control the vehicle's braking so that the vehicle stops at a particular section of the guideway. It is important to note here that the Bechtel Team concept has a vehicle evacuation plan that makes all locations on the guideway safe stopping points (SSP) and passengers can be evacuated safely from any location on the guideway. However, if it is possible the systems control system will attempt to have the vehicle stop at a more preferred location called a preferred stopping point (PSP). Preferred stopping points would be typically located at zone control stations which are normally spaced every 4 km along the guideways. Zone controller locations are preferred because they would already have access facilities to permit periodic inspection and maintenance of the power electronics.

To make the concept of a maglev vehicle coasting ability easier to understand two graphs are provided on succeeding pages to explain the concept. Figure C1-60 shows the actual vehicle deceleration rate in g's experienced by the maglev vehicle at various speeds which is dependent only upon vehicle body aerodynamic drag and electromagnetic drag produced from the levitation

Table C1-15
Proposed Evacuation Methodologies

	Method	Non-Height > 12m	Emergency Height < 12 m	Emergency Height > 12m	Height < 12 m	Works during loss of power	Comments
1	Preferred Stopping Point	Yes	Yes	Yes	Yes		Preferred method under all situations (located at each zone inverter station)
2	Ramp to Vehicle #2	Yes	Yes				Workable alternative with loss of power on one side of dual guideway only
3	Cherry Picker (Fire Dept.)	Maybe	Yes			Yes	Depends on terrain & availability of equipment. Backup of last resort.
4	Inflatable Slides on Vehicle		Not Preferred		Yes	Yes	Aircraft Style Evacuation
5	Walkway Parallel to Box Beam	Not Preferred	Not Preferred	Yes	Yes	Yes	$1,000,000 per mile cost addition
6	Push Recovery other Maglev Vehicle	No	No	No	No	Yes	Requires significant structural modifications to vehicle and is considered not feasible.
7	Push/Pull Recovery Special Vehicle w/Prime Mover	Yes	Yes			Yes	To be used only if power not restored in a timely manner

Note: Shaded boxes denote baseline evacuation methodologies for the Bechtel team concept. Choices were affected by assuming battery backup power is available at inverter or substation, especially regarding options 2 and 8. Many other options were considered but were disregarded for various reasons. Multiple vehicle stopping capability is being considered for preferred stopping points as it increases likelihood that all vehicles can reach a preferred stopping point

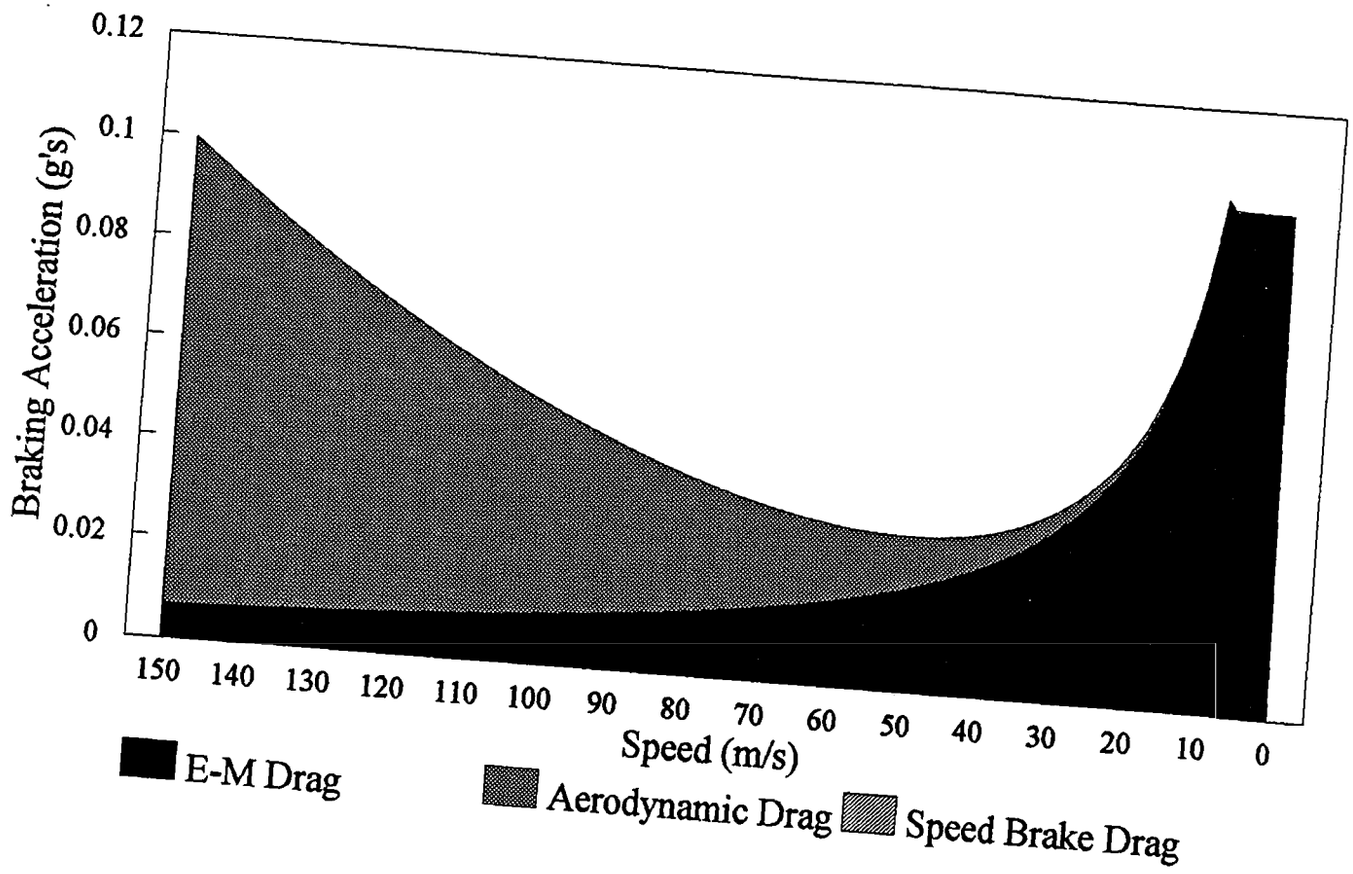

Figure C1-60 Stopping force available - non-propulsive

and guidance system. Due to the efficient nature of the electromagnetic system, electromagnetic drag is very small for high maglev speeds where aerodynamic drag is the greatest. As the vehicle slows down, aerodynamic drag drops and electromagnetic drag rises.

Figure C1-61 shows the actual effect of the varying drag profile by detailing the stopping distance required if the vehicle is only allowed to coast to a stop with only aerodynamic and electromagnetic drag retarding the motion. At a maximum normal system speed of 135 m/s (302 mph), the maglev vehicle would take approximately 22 kilometers to come to a complete stop on level track. In fact, for any velocity over 60 m/s (134 mph) a maglev vehicle would certainly be able to reach the next preferred stopping point (5.2 kilometer maximum coasting distance) provided the guideway is on level ground or a down hill grade. If the maglev guideway is currently traversing a steep vertical grade where concern exists whether or not the vehicle can reach a preferred stopping point for the expected operational speed, preferred stopping points may be placed closer together. This would result in a small increase in cost which would be determined and traded off during route alignment decision-making.

The preferred stopping point methodology is considered the baseline method of first choice for vehicle evacuation under emergency and non-emergency conditions.

Ramp to Vehicle #2

A possible evacuation method usable during non-emergency situations is to evacuate passengers from a disabled vehicle on one guideway to a vehicle traveling in the opposite direction on an adjacent guideway. This method requires that a special ramp be carried on each vehicle which would serve as the walkway between vehicles. This walkway is expected to be made of lightweight materials (less than 25 kg) so that it is easily set up by one person. One ramp would be stored next to each exit.

This evacuation method requires that: it is possible for a vehicle to approach on the adjacent track; that it is a non-emergency situation where time is not critical; that the tracks are adjacent and the standard separation is 7 m between centers of the vehicles; and that the vehicles are not stopped in a turn where the guideway is banked.

Because of the limitations, the ramp to vehicle #2 methodology was considered as a baseline secondary (rather than a primary) means of vehicle disembarkment under non-emergency conditions.

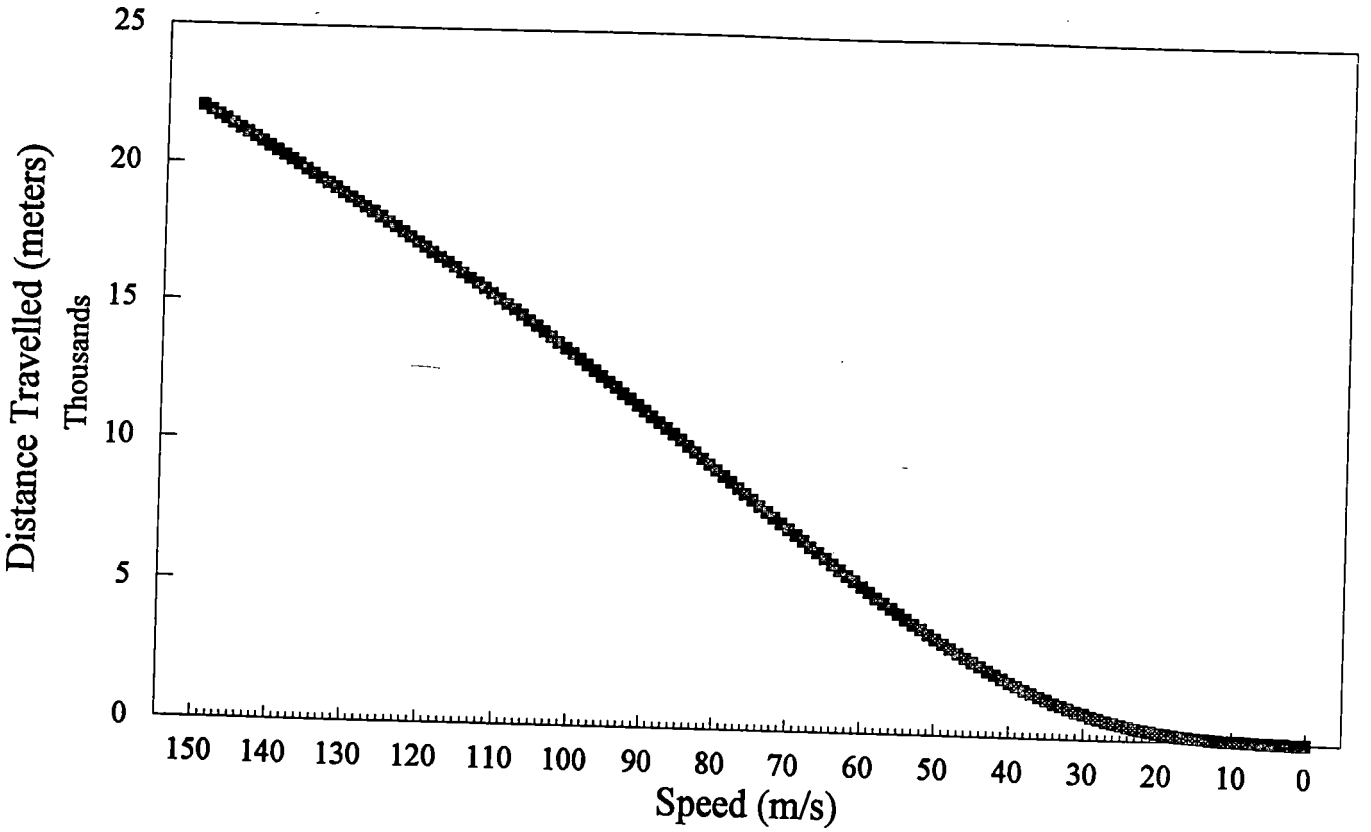

Figure C1-61 Vehicle coasting capability - straight and level guideway

Cherry Picker (Fire Department)

If a vehicle was stranded in a location accessible by normal fire equipment and the height of the vehicle is low, it is possible that standard fire equipment could be used to evacuate personnel from the vehicle. Due to the time it takes to obtain required fire equipment (especially in rural areas) this method was identified as a possible method for use in non-emergency conditions only when conditions permit and other methods are less desirable for one reason or another.

Inflatable Slides on Vehicle

This evacuation concept involves adding an evacuation slide at each exit door on the maglev vehicle. Since it would be easy for the braking systems to control the final stopping point to place one of the vehicles doors in such a way as to insure that it is not over a support column, this

method is feasible. Manufacturers of evacuation slides stated that it is possible to design evacuation slides for use on vehicle heights of up to 12 m. Slides typically open up-and-out; therefore, they would be usable for any vehicle height less than 12 meters although the slope of the slide would be less at lower guideway heights.

Emergency slides on the vehicle is a baseline vehicle evacuation method for heights of less than 12 meters.

Walkway Parallel to Box-Beam

When the guideway height is large (greater than 12 m) the most viable alternative is a walkway parallel to the box-beam for use in evacuation. The walkway would be suspended by the box beams and by the support columns. The actual number of ladder segments to the ground would be decided upon after consideration of the terrain. The cost of a walkway would be approximately $1,000,000 per mile. Since a guideway elevated more than 12 m would be built at additional cost the walkway cost was not considered significant compared to the remaining civil structure.

For guideway heights over 12 m, a walkway parallel to the box-beam is considered baseline. Figure C1-62 illustrates the positioning of the walkway and stairs to the ground.

Push Recovery of Maglev Vehicle

Push recovery of a maglev vehicle utilizing another maglev vehicle is listed only since it has been proposed before in other transportation systems. However, there are very few, if any, operational

scenarios which would allow for one vehicle to push another, making the prospect unlikely. In addition, since maglev vehicles are of lightweight monocoque design the structure is not designed to take an uncontrolled end loading. To design a methodology whereby one vehicle could push another would require considerable redesign of a maglev vehicle's structure. This would most likely add considerable weight and decrease its ability to manage energy in collisions. Therefore, the push recovery methodology was considered unfeasible.

Push/Pull Recovery of Maglev Vehicle Using Special Recovery Vehicle with Prime Mover

It is possible to design a special wheeled prime mover to allow a maglev vehicle to be push/pull recovered in non-emergency conditions. The vehicle would have to have sufficient traction to allow it to move and hopefully accelerate the maglev vehicle over the drag peak in an attempt to move the disabled vehicle to a safe location. If the maglev vehicle's superconducting magnets and supporting systems are operational then the recovery vehicle should be able to accelerate the vehicle to a speed whereby it is levitated. If the superconducting magnets are not functional then the prime mover must supply the required compressed air flow and pressure to allow the vehicle to be levitated and moved on its air bearings. The actual number of recovery vehicles needed per route would have to be determined on a route-by-route basis.

Push/pull recovery by a dedicated recovery vehicle equipped with a special prime mover is a baseline evacuation methodology which would be utilized in non-emergency conditions.

1.13.11 Rescue of Stranded Vehicles

Overview

If a vehicle cannot make it to a preferred stopping point on its own power, a rescue vehicle must be available to pull it to a maintenance facility. This rescue vehicle must be able to move on its own power so that it can operate in the event of a power outage, must be able to reach a disabled vehicle on any section of the track, and it must have the necessary equipment available to deal with any type of emergency. Note that this section deals only with the recovery of the maglev vehicle. It is assumed that the passengers, as the first priority, have already been evacuated and moved to safety if necessary.

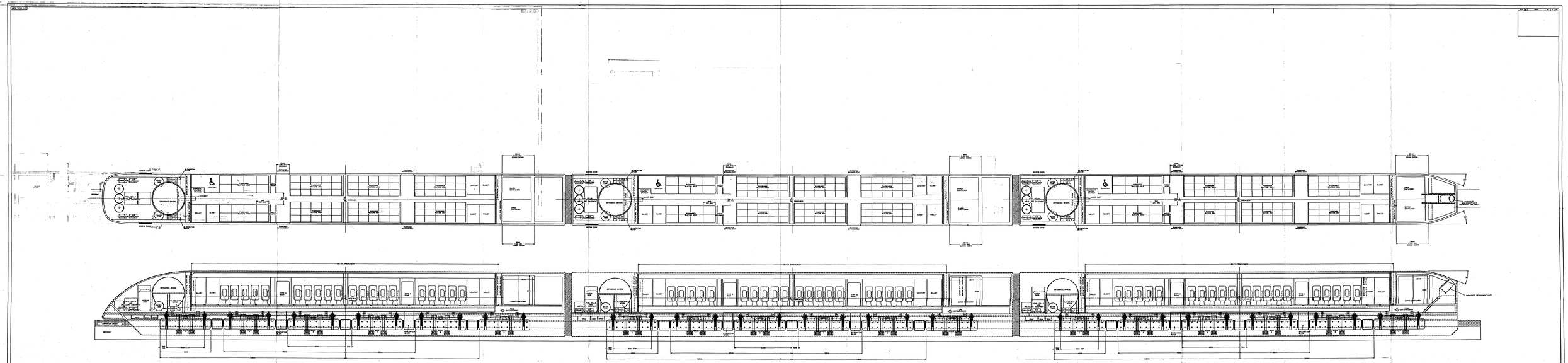

Figure C1-63 Multiple vehicle concept

Scenarios for use

For most emergencies involving the entire system, such as a widespread power loss, the vehicles will be able to reach a preferred stopping point by coasting on their magnetic lift. (See the section on emergency evacuation for details.) However, there exists the possibility of a single vehicle failure. If the vehicle lost its propulsion but retained its magnetic lift, another vehicle could link up with it and guide it to a maintenance facility. However, should the vehicle lose its magnetic lift, a rescue vehicle with special equipment would be required.

Rescue Vehicle Equipment

The rescue vehicle would be able to handle any kind of emergency. It would be able to supply electrical power, hydraulic fluid, and compressed air to the vehicle. It would also have the power to push a levitated or wheeled vehicle to a maintenance facility. It will run completely on its own power, and thus be usable during a power loss.

Rescuing a Non-Levitating Vehicle

Several steps will be required in the rescue of a non-levitating vehicle. The first step would be to get the vehicle up on its air bearings, using either the on-board air supply or the emergency vehicle's supply. Once this is done, support beams would be rolled underneath the vehicle and the air bearings retracted, allowing the vehicle to come to rest on the support beams. This would give enough room for wheeled carts to be inserted underneath the car. The wheels would then be locked into place on the carts and the air bearings deployed. This would give enough lift so that the support beams could be removed. The vehicle would then be lowered onto the carts and the wheels unlocked, permitting a rescue vehicle to push it to a maintenance facility.

Types of Rescue Vehicles

Two types of rescue vehicles readily come to mind. The first is a large rescue truck with an extending boom. This boom would have a U-shaped extension on the end, allowing it to grasp both sides of the vehicle from overhead. The advantage of having a truck for a rescue vehicle is that it will be relatively inexpensive. A disadvantage is that it cannot operate in some rare emergencies, such as when a vehicle is stranded on a bridge or in a tunnel. Also, in order for a rescue truck to be feasible, a maintenance road must be maintained along the track so that the truck can reach any area of track.

Another alternative is a helicopter/rescue vehicle combination. With this arrangement, a helicopter would fly a rescue vehicle out to the damaged car and set it down on the track nearby. A helicopter is needed because some way is needed to get the rescue vehicle past other vehicles in the guideway, for example those resting at preferred stopping points. The advantage of the system is that it will work under any conditions. In the case of a failure inside a tunnel, the helicopter would set the rescue vehicle down in front of the tunnel, allowing it to drive in and make the rescue. The same would hold for a vehicle trapped on a bridge. Disadvantages of this system are that it will be much more expensive than a truck-based system and that there may be difficulties in landing a rescue vehicle on the guideway. Perhaps the best alternative is a hybrid system, utilizing trucks for most of the track and only using helicopter rescue in areas of high inaccessibility.

Options for On-Board Vehicle Recovery Systems

Since the baseline vehicle has an on-board power system which is independent of the wayside power system, there exists the possibility of designing an emergency crawl capability into the vehicle. The crawl motors would probably involve a wheeled system to accelerate the vehicle and to maintain it at a levitated speed. The power required to maintain the vehicle at a speed of 58 kilometers per hour is 100 kilowatts. This system deserves additional design consideration in future design phases.

1.13.12 Multiple Vehicle Concept

Overview

The Bechtel Team concept is basically a single vehicle concept since required system capacities can be achieved by single vehicles of at least 120 passengers, provided braking systems are designed to allow for headways as small as 30 seconds. However, it may be desirable to have multiple vehicle consists for special purpose, non-standard, or international applications.

Discussion

Multiple vehicle concepts are designed significantly differently than single vehicle concepts. For example, high speed single vehicles such as aircraft usually provide restroom, galley, and baggage facilities on each vehicle. Multiple vehicle concepts such as high speed wheel on rail systems segregate parts of the consist to different functions such as the power car, passenger cars, dining cars, and baggage cars.

The Bechtel Team's vehicle is designed as a modular system. If a short multiple vehicle system is desired, several single vehicles are attached by removing the specially designed nose and tail sections of the single vehicles and replacing them with articulation mechanisms. This method

works for creating multiple vehicle consists of up to three vehicles in length. The length limitation is made based solely upon aerodynamic considerations since single vehicle systems are typically wider than multiple vehicle systems. This multiple vehicle concept retains all of the advantages of the Bechtel Team's single vehicle concept except that acceleration and deceleration rates would be limited since the propulsive force is fixed at 120 kN and the vehicle mass is now higher. Also, due to the single vehicle's design with the internal tilting coach mechanism and baggage compartments, movement between vehicle sections of the consist is not possible.

If a multiple vehicle concept was designed for export purposes, the major change would be in the carbody which would be designed narrower (seating four or five across) and the internal tilt mechanism would be removed to facilitate movement between vehicles via the articulation mechanism. The multiple vehicle consist would also have specially designed passenger, lounge, and baggage cars. In addition, the propulsion system would be designed to take into account the increased capacities required to account for the larger accelerations and decelerations of multiple vehicles.

The multiple vehicle concept is illustrated in Figure C1-63, and Tables C1-16 and C1-17.

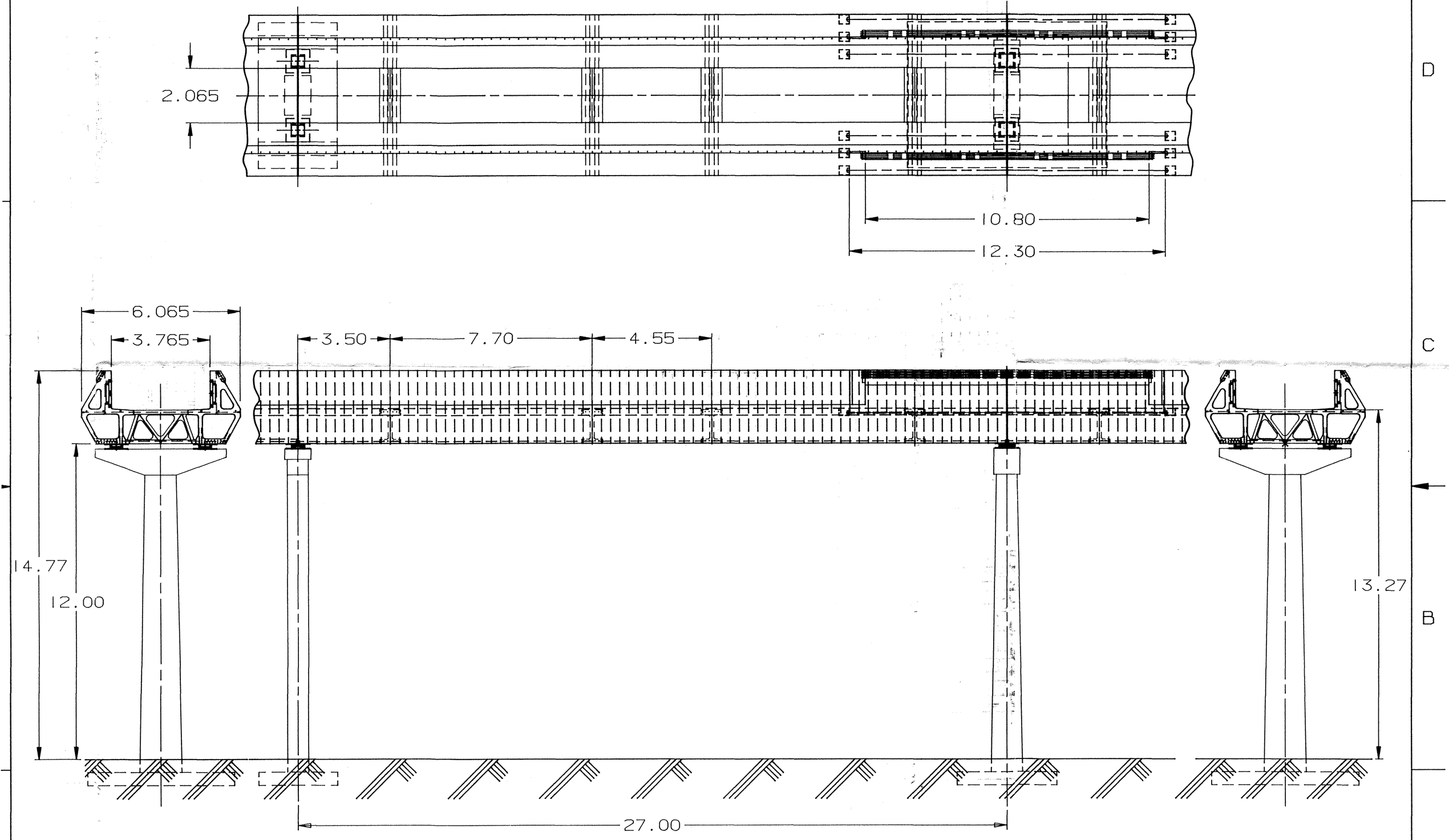

DIMENSIONS IN METERS

DESTROY ALL
OCT 1 2 1992
PREVIOUS PRINTS

UNLESS OTHERWISE SPECIFIED	DRAWN		
BREAK CORNERS .005-.015	CHECKED		
FRACT. ± .X ± .XX ± .XXX ±	APPROVED		
ANGLES ± MACH. SURF. ✓ MAX.	APPLICATION		
MATERIAL	NEXT ASSY		
HEAT TREATMENT	FINAL ASSY		
FINISH	MACHINE		
	PROJECT NO		

FOSTER-MILLER, INC.
350 SECOND AVENUE WALTHAM, MA 02254

ELEVATED GUIDEWAY LAYOUT

SIZE	FSCM		REV
C	30233	9399100	
SCALE 1/100	WEIGHT	SHEET 1 OF 1	

Table C1-16
Mass Breakdown for Possible Vehicle Configuration
Passenger Car

MULTIPLE VEHICLE PASSENGER CAR

DESCRIPTION	MASS kg (each)	QUANTITY	INDIVIDUAL MASS TOTAL	SPRUNG MASS TOTAL	UNSPRUNG MASS TOTAL	AGGREGATE MASS TOTAL
ASSEMBLED VEHICLE TOTAL						59,156
PAINTING	23	1	23	23		23
VEHICLE ASSEMBLY COMPLETE						59,133
BASIC BODY	8,500	1	8,500	8,500		
AERODYNAMIC BRAKES	125	8	1,000	1,000		
HYDRAULICS SYSTEM	770	1	770	770		
AIR SUPPLY SYSTEM FOR AIR BEARINGS	41	1	41	41		41
AIR PIPING FOR AIR BEARINGS	2	150	273	273		273
CARGO DOORS, BOTH SIDES	50	4	200	200		
EMERGENCY COUPLING AREA	500	1	500	500		
EMERGENCY PARACHUTE	40	1	40	40		
EMERGENCY EVACUATION SLIDES	100	4	400	400		
INSULATION–SPRAY ON	200	1	200	200		
WINDOWS	7	40	272	272		
FIRE EXTINGUISHER SYSTEM						
FIRE EXTINGUISHING AGENT SPHERES	6	6	37	37		
FIRE EXTINGUISHER PIPING	10	1	10	10		
SMOKE AND FIRE DETECTORS	0	4	2	2		
CO2 & HALON PORTABLE EXTINGUISHERS	5	12	54	54		
GUIDANCE CONTROL SURFACE	23	2	45	45		
LEVITATION CONTROL SURFACE	23	4	91	91		
ENVIRONMENTAL CONTROL SYSTEM	1,020	1	1,020	1,020		
INNER COACH	4,500	1	4,500	4,500		6,971
SEATS–COACH CLASS	28	30	830	830		
SEATS–BUSINESS CLASS	42	8	340	340		
WINDOWS	2	40	91	91		
GALLEY	136	2	272	272		
GALLEY CART	10	6	60	60		
LAVATORY	136	2	272	272		
WATER SUPPLY TANK	100	2	200	200		
WASTE WATER STORAGE TANK	100	1	100	100		
PASSENGER COMMUNICATIONS & ENTERTAINMENT SYSTEM	1	106	106	106		
LIGHTING	5	44	200	200		
VEHICLE CONTROL SUBYSYSTEM						0
COMMUNICATIONS SET	10	1				
COMPUTER SUITE & MANUAL CONTROL SUBSYSTEM	9	1				
CONTROL SENSORS	50	1				
INTERFACE CABLING	115	1				
SECONDARY SUSPENSION SUBSYSTEM						22,050
LATERAL ACTUATORS & SENSORS	55	6	332	166	166	
VERTICAL ACTUATORS, SENSORS & POWER SUPPLY	8	24	181	90	90	
BOGIE LINKS	218	6	1,306	653	653	
TILTING ACTUATORS & MECHANISM	1,000	1	1,000	1,000		
MAGNET BOGIE SUBSYSTEM	1,205	6	7,230		7,230	
AIR BEARINGS & AIR BLADDERS	76	6	457		457	
SUPERCONDUCTING MAGNET SUBSYSTEM	962	12	11,544		11,544	
MECHANICAL BRAKING SUBSYSTEM						1,176
BRAKING ACTUATOR SUBSYSTEM	23	24	544	544		
BRAKE PADS	5	24	109	109		
WHEELS	22	24	522	522		
CRYROGENIC REFRIGERATION SUBSYSTEM						2,572
HELIUM & STORAGE DEWAR	2,333	1	2,333	2,333		
CRYOGENIC PUMP	1	1	1	1		
COOLANT DISTRIBUTION LINES	7	32	238	238		
FUSELAGE ELECTRICAL POWER SUBSYSTEM				0		2,146
BATTERY	230	1	230	230		
UNINTERUPTABLE POWER SUPPLY	15	2	29	29		
POWER DISTRIBUTION & CONTROL EQUIPMENT	400	1	400	400		
FUEL CELL SYSTEM & 8 HOURS OF FUEL	1,487	1	1,487		1,487	
VARIABLE FACTORS						10,763
PASSENGER LOAD	77	106	8,191	8,191		
PASSENGER SERVICE PERSONNEL LOAD	77	3	232	232		
WATER	1	114	114	114		
FOOD	0.5	106	48	48		
Misc. CONSUMABLES	10	1	10	10		
CARRY ON BAGGAGE	20	106	2,168	2,168		
BAGGAGE CONTAINERS	159	4				
CHECKED BAGGAGE	32	106				
			TOTALS=>	37,528 SPRUNG MASS	21,628 UNSPRUNG MASS	59,156

Table C1-17
Mass Breakdown for Possible Multiple Vehicle Configuration
Baggage Car

DESCRIPTION	MASS kg (each)	QUANTITY	MULTIPLE VEHICLE BAGGAGE/CONTROL CAR INDIVIDUAL MASS TOTAL	SPRUNG MASS TOTAL	UNSPRUNG MASS TOTAL	AGGREGATE MASS TOTAL
ASSEMBLED VEHICLE TOTAL						38,695
PAINTING	23	1	23	23		23
VEHICLE ASSEMBLY COMPLETE						38,673
BASIC BODY	8,500	1	8,500	8,500		
AERODYNAMIC BRAKES	125	8	1,000	1,000		
HYDRAULICS SYSTEM	770	1	770	770		
AIR SUPPLY SYSTEM FOR AIR BEARINGS	41	1	41	41		41
AIR PIPING FOR AIR BEARINGS	2	150	273	273		273
CARGO DOORS, BOTH SIDES	50	4	200	200		
EMERGENCY COUPLING AREA	500	1	500	500		
EMERGENCY PARACHUTE	40	1	40	40		
EMERGENCY EVACUATION SLIDES	100	4				
INSULATION–SPRAY ON	200	1	200	200		
WINDOWS	7	40	272	272		
FIRE EXTINGUISHER SYSTEM						
FIRE EXTINGUISHING AGENT SPHERES	6	6	37	37		
FIRE EXTINGUISHER PIPING	10	1	10	10		
SMOKE AND FIRE DETECTORS	0	4	2	2		
CO2 & HALON PORTABLE EXTINGUISHERS	5	12	54	54		
GUIDANCE CONTROL SURFACE	23	2	45	45		
LEVITATION CONTROL SURFACE	23	4	91	91		
ENVIRONMENTAL CONTROL SYSTEM	1,020	1	1,020	1,020		
INNER COACH	4,500	1				0
SEATS–COACH CLASS	28	30				
SEATS–BUSINESS CLASS	42	8				
WINDOWS	2	40				
GALLEY	136	2				
GALLEY CART	10	6				
LAVATORY	136	2				
WATER SUPPLY TANK	100	2				
WASTE WATER STORAGE TANK	100	1				
PASSENGER COMMUNICATIONS & ENTERTAINMENT SYSTEM	1	106				
LIGHTING	5	44				
VEHICLE CONTROL SUBYSYSTEM						184
COMMUNICATIONS SET	10	1	10	10		
COMPUTER SUITE & MANUAL CONTROL SUBSYSTEM	9	1	9	9		
CONTROL SENSORS	50	1	50	50		
INTERFACE CABLING	115	1	115	115		
SECONDARY SUSPENSION SUBSYSTEM						21,050
LATERAL ACTUATORS & SENSORS	55	6	332	166	166	
VERTICAL ACTUATORS, SENSORS & POWER SUPPLY	8	24	181	90	90	
BOGIE LINKS	218	6	1,306	653	653	
TILTING ACTUATORS & MECHANISM	1,000	1				
MAGNET BOGIE SUBSYSTEM	1,205	6	7,230		7,230	
AIR BEARINGS & AIR BLADDERS	76	6	457		457	
SUPERCONDUCTING MAGNET SUBSYSTEM	962	12	11,544		11,544	
MECHANICAL BRAKING SUBSYSTEM						1,176
BRAKING ACTUATOR SUBSYSTEM	23	24	544	544		
BRAKE PADS	5	24	109	109		
WHEELS	22	24	522	522		
CRYROGENIC REFRIGERATION SUBSYSTEM						2,572
HELIUM & STORAGE DEWAR	2,333	1	2,333	2,333		
CRYOGENIC PUMP	1	1	1	1		
COOLANT DISTRIBUTION LINES	7	32	238	238		
FUSELAGE ELECTRICAL POWER SUBSYSTEM						0
BATTERY	230	1				
UNINTERUPTABLE POWER SUPPLY	15	2				
POWER DISTRIBUTION & CONTROL EQUIPMENT	400	1				
FUEL CELL SYSTEM & 8 HOURS OF FUEL	1,487	1				
VARIABLE FACTORS						636
PASSENGER LOAD	77	106				
PASSENGER SERVICE PERSONNEL LOAD	77	3				
WATER	1	114				
FOOD	0.5	106				
Misc. CONSUMABLES	10	1				
CARRY ON BAGGAGE	20	106				
BAGGAGE CONTAINERS	159	4	636	636		
CHECKED BAGGAGE	32	106	0	0		
			TOTALS=>	18,555 SPRUNG MASS TOTAL	20,141 UNSPRUNG MASS TOTAL	38,695

1.14 EMERGENCY PROPULSION POWER

Overview

In the event of the simultaneous occurrence of two events, namely a loss of propulsion power to the guideway and having a vehicle being in a slow curve far from a preferred stopping point when the power goes out, it is desirable to have some way of having all of the maglev vehicles reach a preferred stopping point. There are several approaches to reducing the probablity that this will happen or to providing the capability to reach the preferred stopping points:

- Place preferred stopping points in valleys along the route so that the vehicle can always coast downhill to them, in either forward or reverse direction. This would not work well on the plains of Kansas, but would be utilized where the terrain and other factors would permit.
- Dispatch a specialized rescue vehicle to push the stranded maglev vehicle to the preferred stopping point. See Section 1.13.11, Rescue of Stranded Vehicles, for discussion of this option. This would be a major inconvenience and source of concern for the passengers were they not evacuated before the rescue vehicle arrived.
- Provide crawler motors on the vehicle to allow its on-board power source to move it, though not at full speed, to the next preferred stopping point. See Section 1.5.1 On-board Power System, for discussion of this option.
- Place emergency batteries at the inverter stations. These batteries would be able to deliver power to the linear synchronous motor to propel a stopped vehicle to the next preferred stopping point. This option is described below.

Analysis

For the analysis performed in this paper, data was taken from a simulated computer run of the hypothetical route provided to us by the NMI. This computer simulation, run the Electro-Motive's in-house train simulator program number ER574ZE, included such factors as gradient, curvature (vertical and horizontal) magnetic drag, and air resistance, as well as any other pertinent details. A simulation of a maglev vehicle on the hypothetical route was performed, and it was from this data that the required information was derived.

The size of the emergency batteries would vary according to the gradient of the nearby route. It is desirable to propel the vehicle at about 20 kph for several reasons. First, this speed, with some leeway, will allow the vehicle to become fully levitated and will also deliver the vehicle to a preferred stopping point in a reasonably timely manner. Since the preferred stopping points would be, on the average, about 4 km apart, then at 20 kph the trip from midway between points forward or backward to the nearest PSP for 2 km would take 1/10 hour or 6 minutes. Second, to go any faster would increase the magnetic drag on the vehicle, consequently increasing the power required

to propel the vehicle. The power requirements to drag a vehicle at 20 kph, taken from a simulated run of the hypothetical route, are determined from the following formula:

where = total resistance to motion, newtons
= magnetic drag, newtons
= aerodynamic drag, newtons
= vehicle weight, newtons, = 64000 kg x 9.801 m/s^2
= gradient (rise/run) of guideway w.r.t. horizontal, in percent

The magnetic drag, in the speed range of interest, is basically a straight line function of speed. The aerodyamic drag in the speed range of interest small but still considered as proportional to speed squared, and the gradient can be positive (uphill) or negative (downhill) and therefore increase or decrease the total resistance. The total power required to overcome the vehicle resistance is then a strong function of gradient. The following results were derived from the train simulation program:

Grade, percent	kw needed
- 1.5 or less	0.0
- 1.0	10.2
- 0.5	27.6
0.0	45.3
+0.5	59.2
+1.0	80.7
+1.5	98.5

However, in an emergency situation, it does not matter whether the cars go forward to the PSP ahead, or return to the previous PSP. If a vehicle was traveling on an upward grade, instead of spending the power required to push a vehicle on an upward grade, it is more economical and technically feasible to simply stop the vehicle and pull it down the grade where gravity will assist rather than oppose the vehicle.

Note that if you are traveling down a 1.5 percent or greater grade, no batteries are needed. This is because once the air bearings are deployed, the vehicle will be accelerated by gravity to at least 20 kph. If the grade is less than 1.5 percent, the vehicle will still accelerate, but it won't reach 20 kph.

Battery Selection

On a first-pass analysis we used battery data selected as described in Section 1.5.3, Emergency On-board Power, i.e., NiCad batteries. We planned to obtain information about batteries that

might be more suited to the application, but the results with the NiCad data showed the general infeasibility of this approach. We would not expect the conclusions to change much with more relevant battery data. We did use the same computer program as before to select the battery type and number. We present the following results:

Rated Duration	Power	Price	Volume	Weight
20 min	15 kW	$ 13,200	.232 m^3	374 kg
20 min	30 kW	$ 26,000	.448 m^3	748 kg
20 min	50 kW	$ 43,600	.772 m^3	1246 kg

These prices represent only the cost of the batteries and do not reflect the added cost of storage facilities, smaller emergency inverters if required, or control circuits needed. However, all of these components are readily available and present no technical problems to overcome. The batteries have been sized and priced using present day quotes from the same battery vendor as before. These prices are also on a per-station basis. Pulling a vehicle at 20 kph, it would take 12 minutes to travel a full 4 km. Therefore, the batteries have been sized for a 20-minute duration.

We have not tried to project a cost per km for this equipment because it is so highly dependent upon the route. For that reason as well, the emergency battery substation is not part of our baseline system. The following section casts doubt on whether or not this battery system is even needed.

Necessity

A maglev vehicle weighing 64 metric tons and traveling at 500 mph has a huge amount of momentum built up. If its propulsion power from the guideway is lost, a vehicle traveling at top speed would be able to coast for several kilometers (the number depends upon the terrain) before wind resistance and magnetic drag finally slowed it down. Therefore, PSPs can be placed several kilometers apart on flat sections of the guideway where the vehicles will be at full speed and have maximum momentum. Near tight corners, the vehicles will have to reduce their speed and will have considerably less momentum. Consequently, PSP's will have to be placed near these low speed turns to adjust for the reduced distance the vehicles will be able to coast.

In the event of a power-outage, vehicles would simply coast on their own momentum to the next well-placed PSP. Using this philosophy, it is not likely that the control system would allow a majority of vehicles to travel slowly due to, for instance, a struggling vehicle many kilometers ahead. The control system would have the feature of the Musical Chairs game, either staying at or close to chairs (PSP's) when slow, or moving fast when not near a chair. Properly implemented,

these approaches would eliminate the need for the emergency propulsion batteries. The other approaches listed at the beginning of this section could be implemented and reduce the need for emergency propulsion batteries as well.

1.15 VEHICLE SYNERGIES

Overview

There are many subsystems aboard the vehicle which are designed by different engineering groups and are somewhat independent of each other, but our periodic meetings of the entire maglev team has emphasized that we should be looking for ways to make the vehicle lighter, smaller, and more efficient by tying together these seemingly separate systems, i.e., to look for opportunities to create vehicle synergies. We have recognized a number of synergies between systems, and they are described in this section of the report:

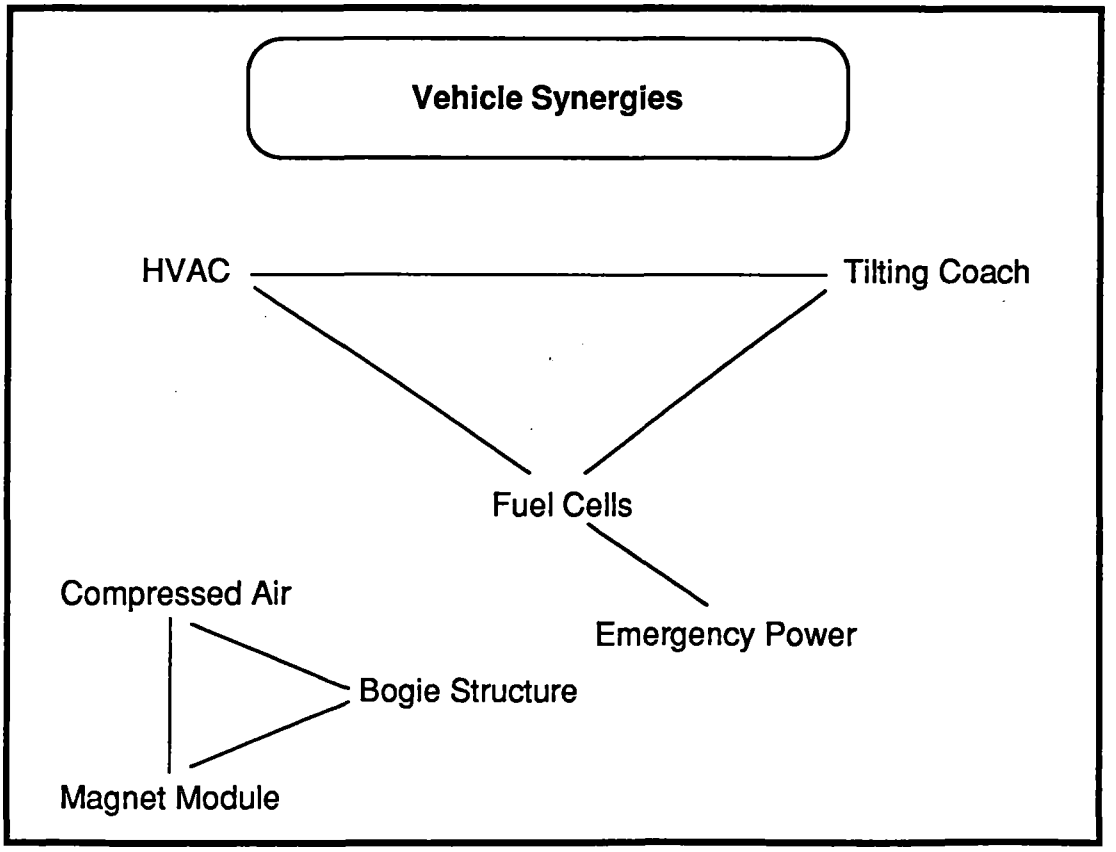

Fuel Cell - HVAC Synergies

- Fuel cell waste heat reduces heating load in winter.
- Fuel cell water byproduct will be used for humidification when needed.

- Methanol could be used as heating fuel but is NOT because fuel cell conversion of methanol to electrical energy is very fuel efficient.
- Air conditioned exhaust air from coach cools for equipment compartment (and fuel cells) and aft cargo compartment.

HVAC - Tilting Coach Synergies

- Double walls cut down heating/cooling load.
- Sealed coach allows good HVAC control.

Fuel Cells - Tilting Coach

- Fuel cell water byproduct is used in lavatories:
  - Toilets
  - Sink (safe to drink but tastes strange; do not use for drinking)

Fuel Cells - Emergency Power

- On-board source enables vehicle to run all vehicle systems at full capacity when guideway power is down.
- Batteries (part of fuel cell for surge power conditions) can be made available in case of failure of both fuel cells and both emergency battery sets to run computers, radios, emergency lights, ventilating fans.
- 250 kW power source makes it possible to use a deployable electrical tractor for complete vehicle mobility at low speed without the LSM, if air bearings are used.

Compressed Air: Bogie Structure /Magnet Module Synergies

- Air tanks are bogie structural members to save weight and space.
- Bottom plate of bogie reduces aerodynamic drag.
- Side walls of magnet stiffen bogie structure.

2. Baseline Guideway

2. BASELINE GUIDEWAY

The guideway baseline design is depicted in Figure C2-1. The elevated guideway consists of the guideway girder, the propulsion/levitation/guidance equipment, bearings, supporting frames or single columns, and foundations. Foundations can be either spread or pile foundations.

The design loads for these structures are based on a mass of 64,800 kg for the fully loaded vehicle. On curved track the girders are banked up to 15 degrees. A vehicle stopped on curved track sections would thus expose passengers to a substantial lateral load component and impair evacuation of wheel-chaired, elderly or handicapped passengers. The vehicle cabin is therefore equipped with a tilt mechanism capable of rotating the vehicle floor 15 degrees in either direction. This feature assures a coordinated turn capability up to a super-elevation angle of 30 degrees. Lateral load components on passengers will thus be avoided. The acceleration vectors for which guideway girders, supports, and foundations have been designed are shown in Figures C2-2 and C2-3. Note that in a stopped vehicle the lateral acceleration is 0.26 g and for full speed operation the normal acceleration is 1.12 g and the lateral is 0.3 g.

Girder

The rectangular hollow prestressed concrete girder has a structural depth of 1.8 m. The girder width at the upper section (0.65 m) is 1.20 m and at the base 1.10 m. The web thickness is 0.15 m. The girder end sections in the support area (1.00 m long) are closed to permit the use of standard prestressing anchors. The width at the base is 1.90 m to accommodate tie down anchors and bearing pads. The girder length is 25.0 m with a clear span of 24.20 m. Figures C2-4 and C2-5 show girder end and mid sections, respectively.

Magnetic fields in the vicinity of the cryogenic magnets on the vehicle require the use of FRP in lieu of regular steel reinforcement in the upper half of the girder section. The cross-sectional area of the FRP bars is 2.5 times larger than the area required for steel reinforcement. This replacement factor is based on the modulus of elasticity ratio of steel/FRP to assure that the elongation in the FRP does not exceed the elongation of steel reinforcement. Steel reinforcement is used at the base

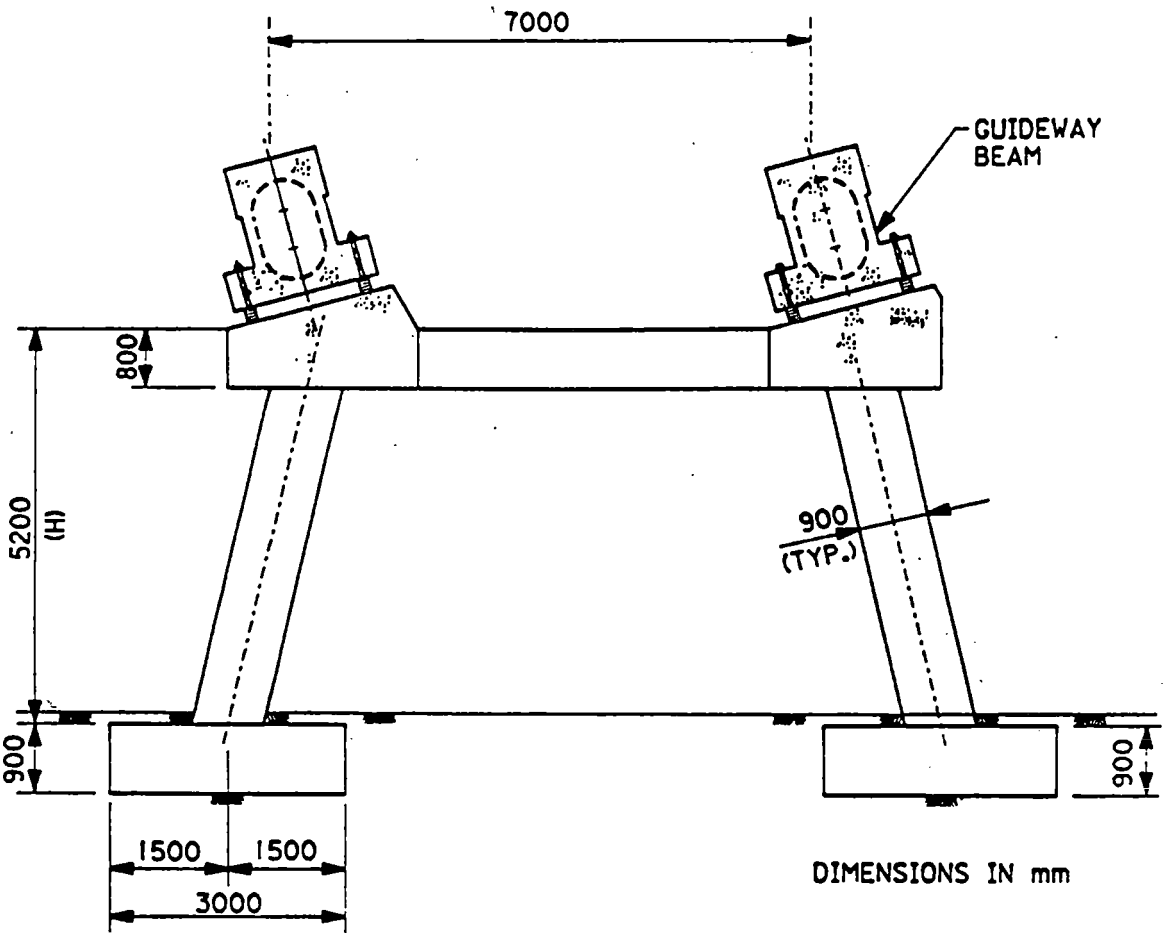

Figure C2-1 Frame elevation for dual curved track guideway with 25 m span

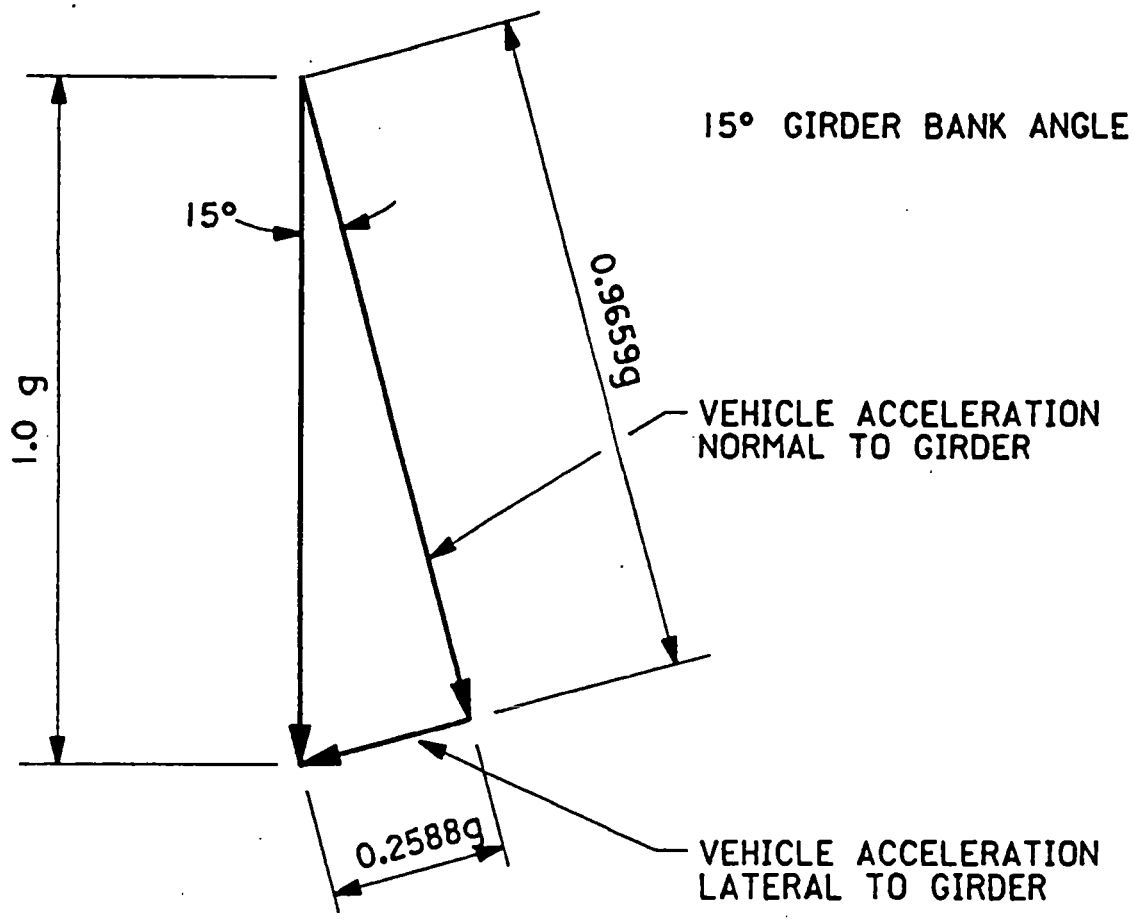

Figure C2-2 Acceleration vectors for stopped vehicle

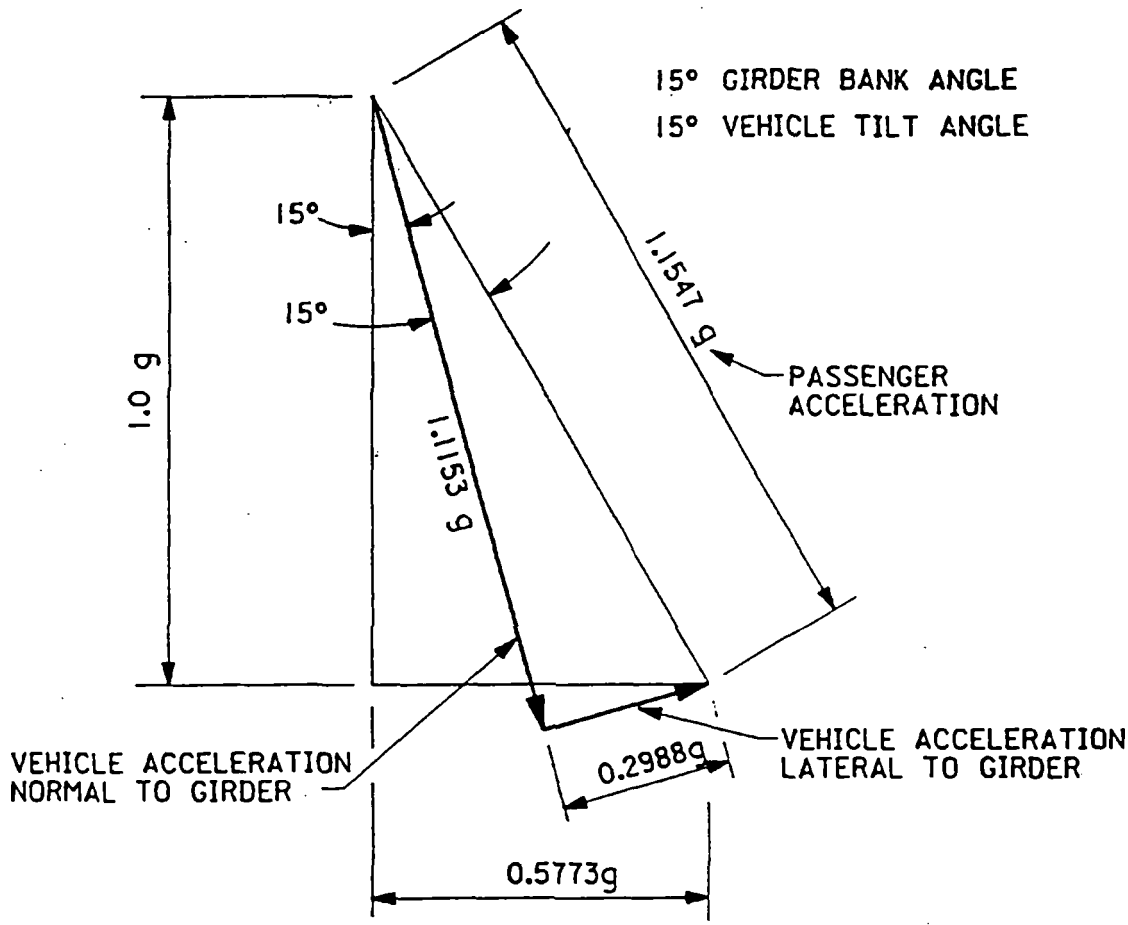

Figure C2-3 Acceleration vectors for full speed operation

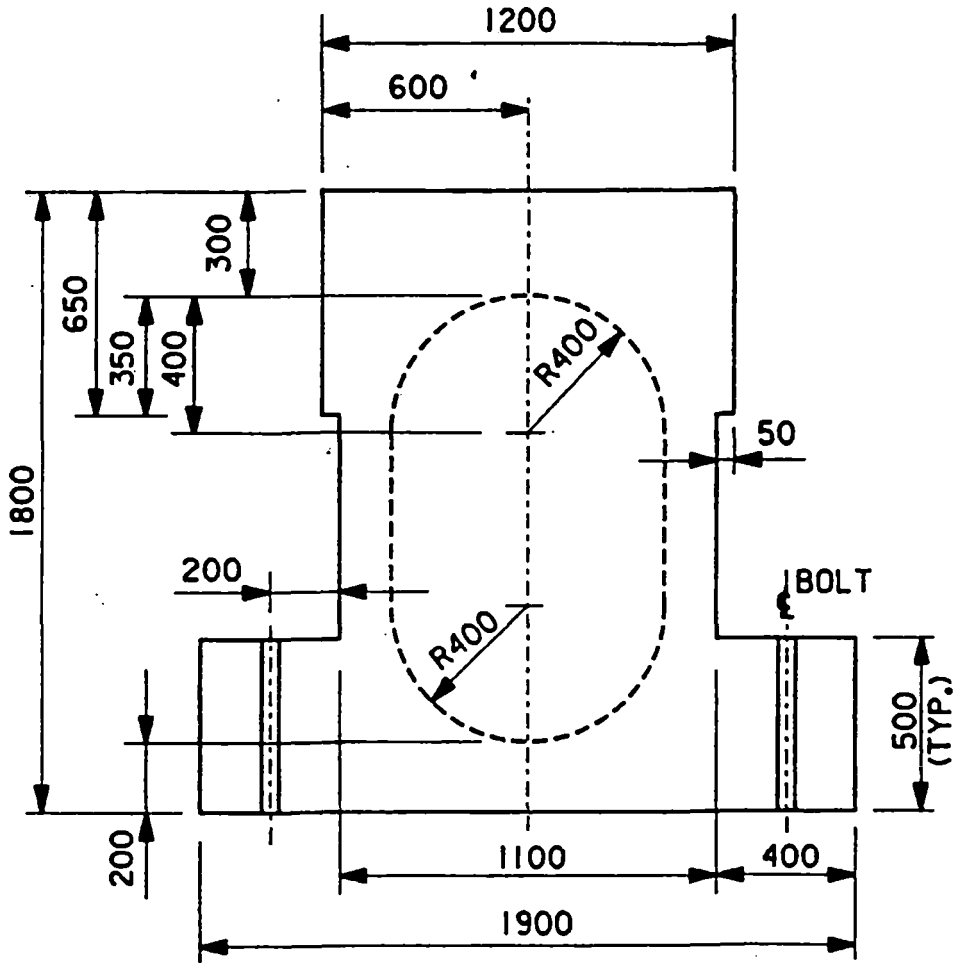

Figure C2-4 Girder end section for 25 m section

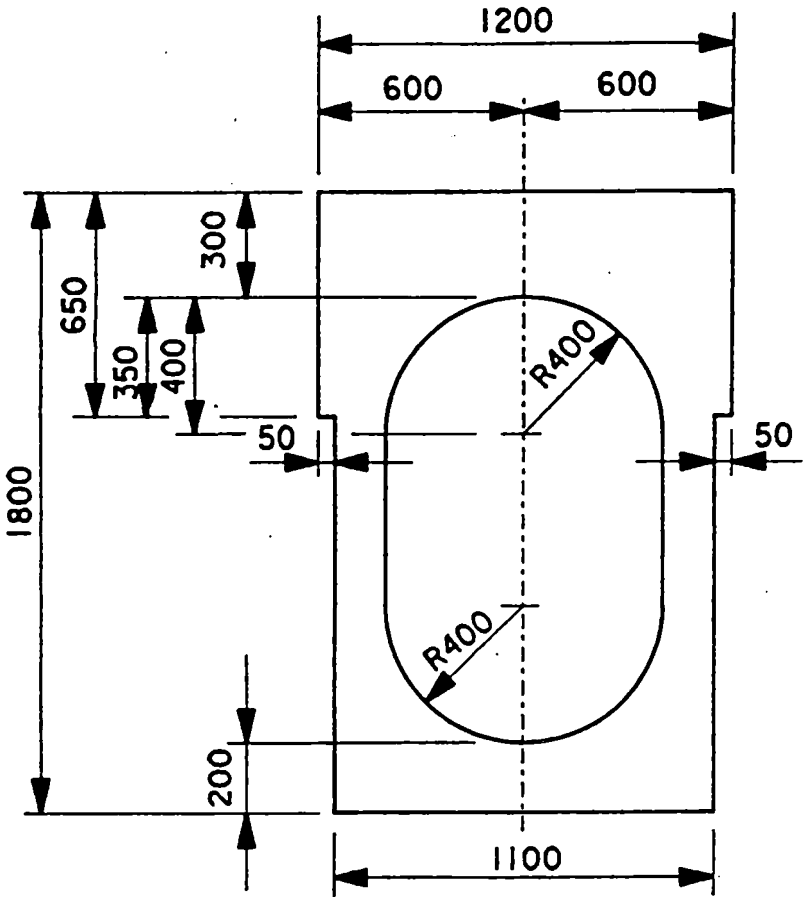

Figure C2-5 Girder mid section for 25 m span

of the end section and for longitudinal bars in the lower half of the girder. Prestressing steel and anchors are positioned below the area of magnetic fields. The negative moment developed by prestressing forces at the girder ends is covered by longitudinal FRP reinforcement at the top of the section. Straight track girders and their substructure are designed for a lateral acceleration of 0.07g to account for heeling of the vehicle.

Reinforcing details and prestressing forces are shown in Figures C2-6 to C2-9.

Dynamic amplification.

The dynamic amplification for the system has been determined based on BAA #62 prepared by D. Wormley.

The following parameters

$I = 0.4596\ m^4$
$V = 134\ m/s$
$E = 27 \times 10^9\ Pa$
$g = 2325\ kg/m^3$
$Ls = 24.2\ m$
$A = 1.141\ m^2$

produce a crossing frequency value Vc = 0.96. For higher strength concrete $E = 44.17 \times 10^9$ Pa and $g = 2500\ kg/m^3$, Vc is reduced to 0.78. Lower operating speeds produce lower crossing frequency and amplification values. As shown in Figure C2-10 the dynamic amplification is 1.25 for light low strength concrete and in the order of 1.08 for the 10,000 psi concrete selected for durability and stiffness. Since lateral sway of the substructure, vehicle roll on the girder, and specific suspension characteristics have not been considered in the above mentioned BAA report, we have elected to (conservatively) continue with our earlier dynamic amplification factor of 1.4.

Bearings

Girder bearings are the connecting elements between the girder base and the supporting structure. Two types of bearings are required, fixed bearings and expansion bearings. Expansion bearings allow the free end of the girder to expand or contract as a result of temperature changes. Lateral and longitudinal forces are transferred by a shear key at the fixed end of the girder. The key at the expansion end transfers lateral forces only. See Figures C2-11 and C2-12. Vertical forces are taken by anchor bolts and bearing pads.

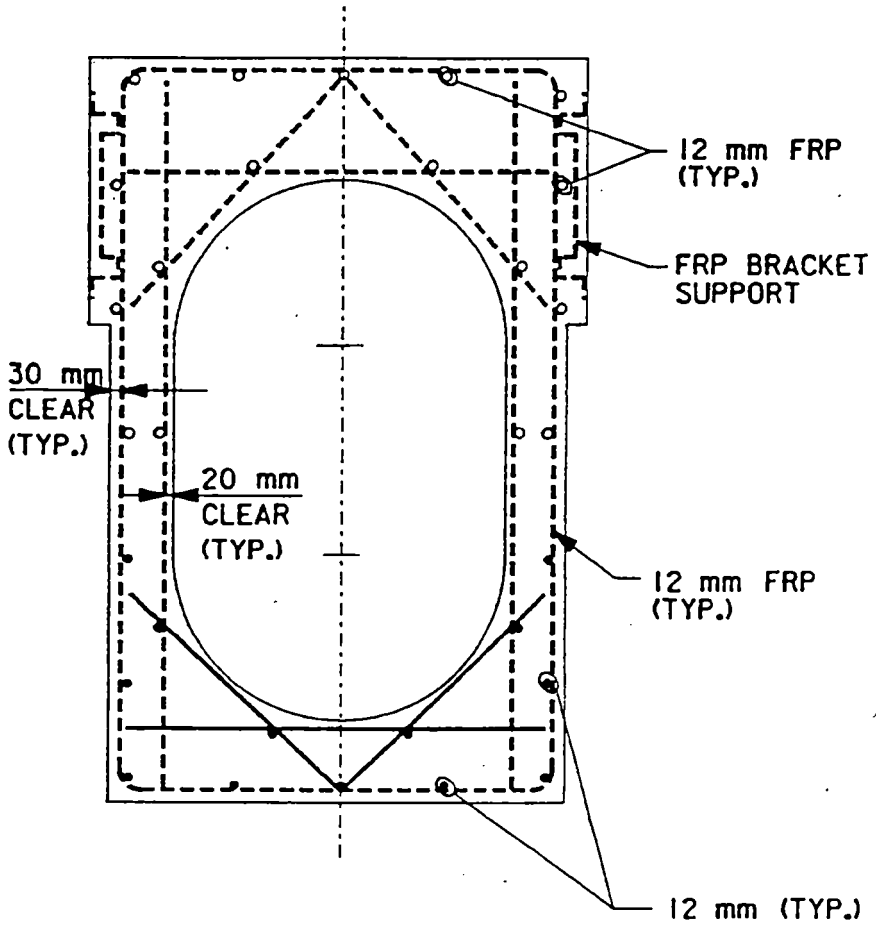

NOTE:

ALL LONGITUDINAL BARS OUTER FACE 12 mm ϕ 300 mm MAX. O.C.
INNER FACE AS SHOWN
STIRRUPS 12 mm ϕ. SPACING AS SHOWN IN ELEVATION

o --------- FRP REINFORCEMENT

• ——— STEEL REINFORCEMENT

Figure C2-6 Girder mid section reinforcement

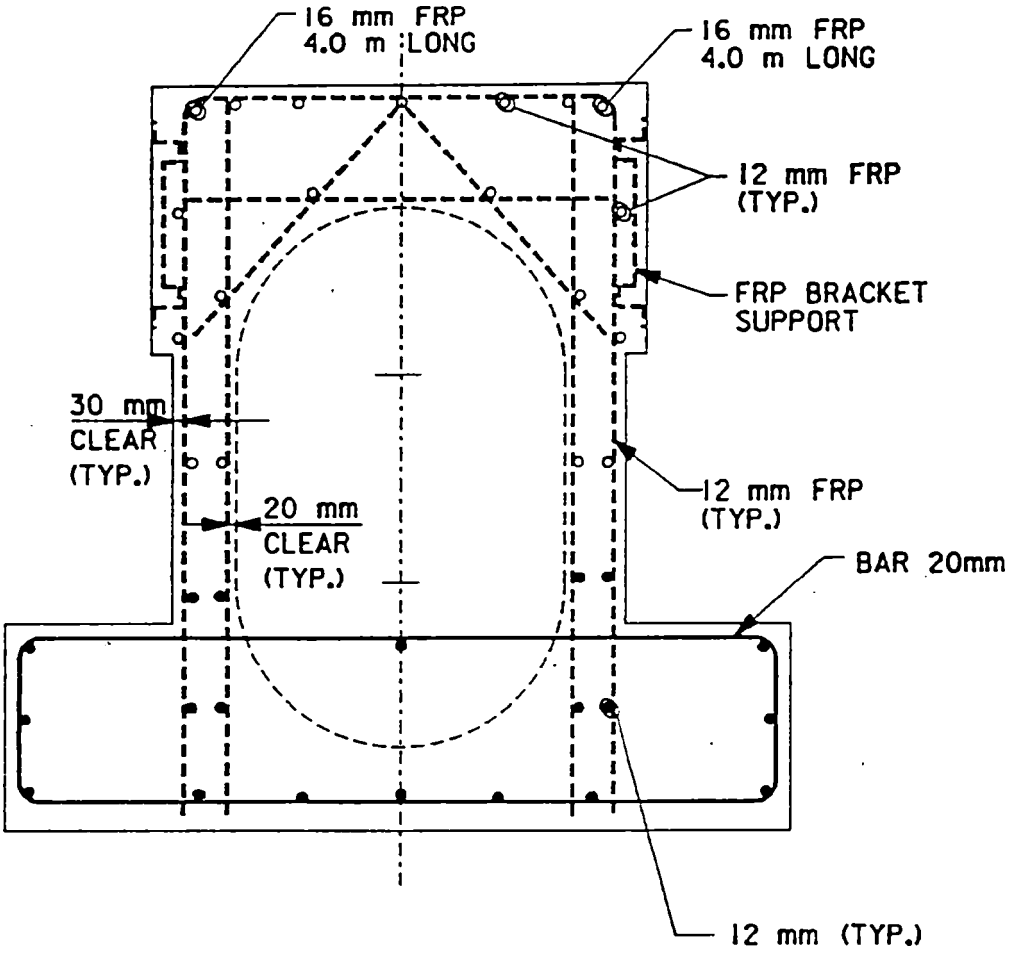

NOTE:

ALL LONGITUDINAL BARS OUTER FACE 12 mm ϕ 300 mm MAX. O.C.
INNER FACE AS SHOWN
STIRRUPS 12 mm ϕ. SPACING AS SHOWN IN ELEVATION

o -------- FRP REINFORCEMENT

• ———— STEEL REINFORCEMENT

Figure C2-7 Girder solid end section reinforcement

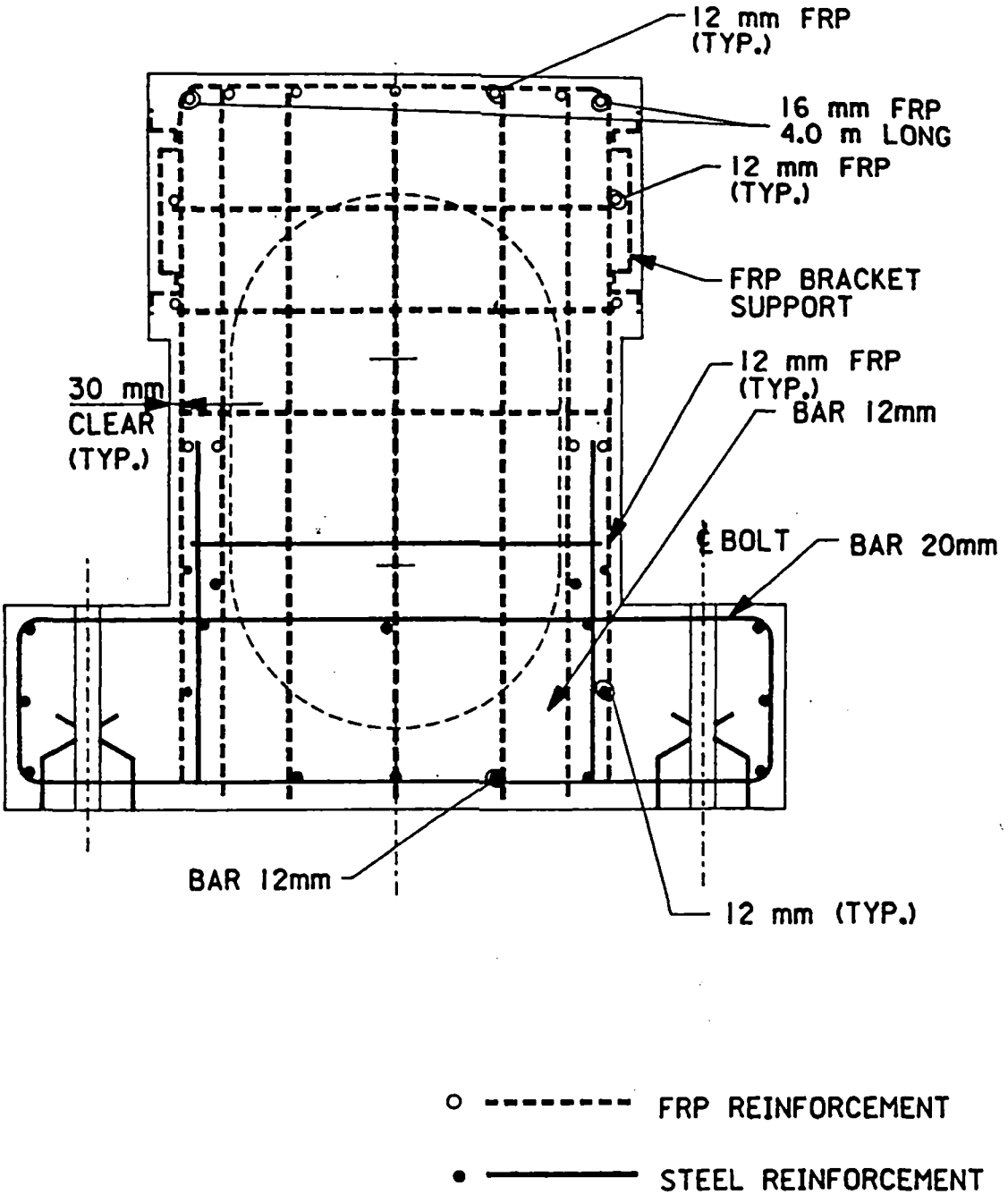

Figure C2-8 Girder end section face reinforcement

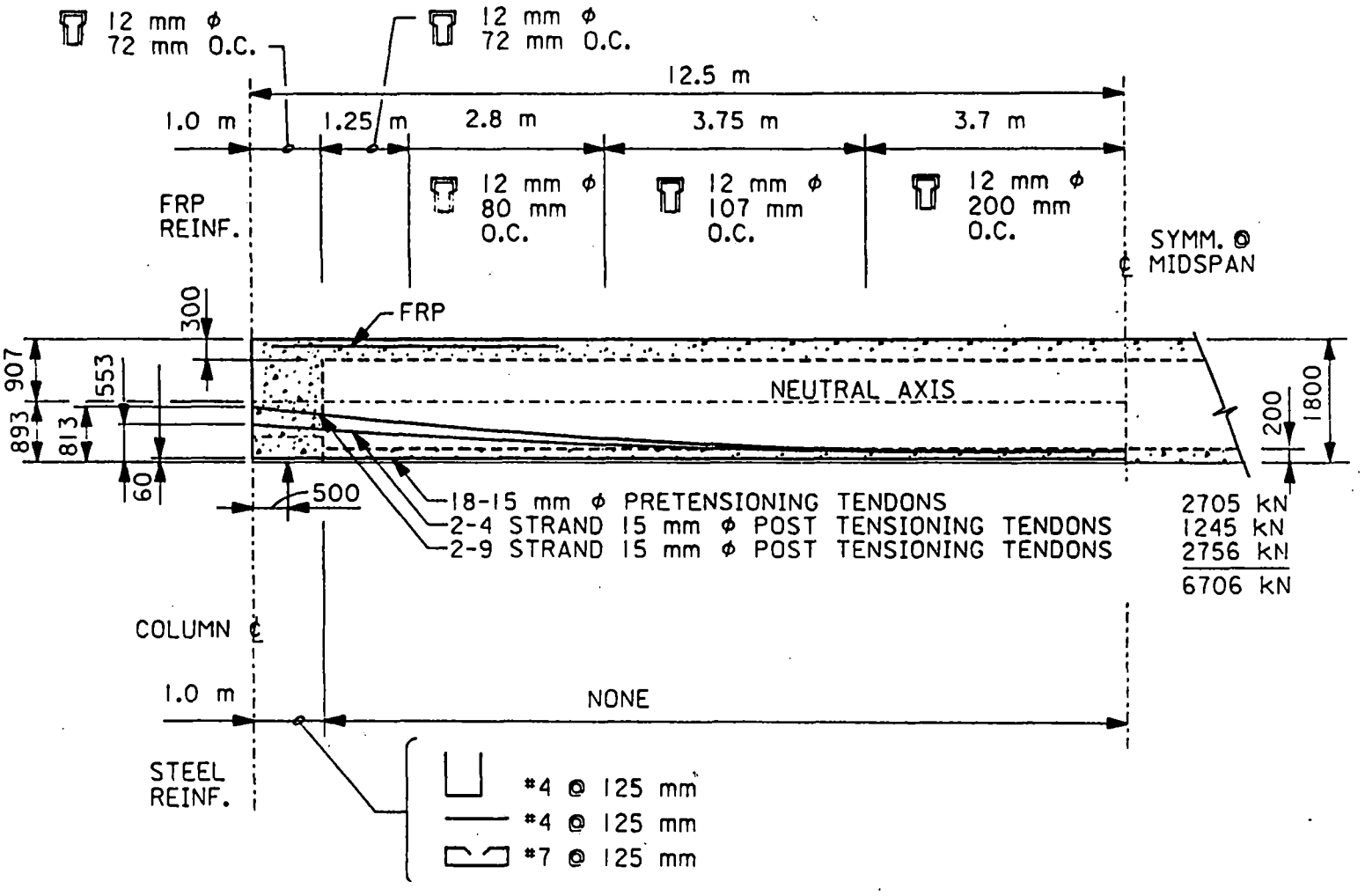

Figure C2-9 Girder elevation showing stirrups and tendons

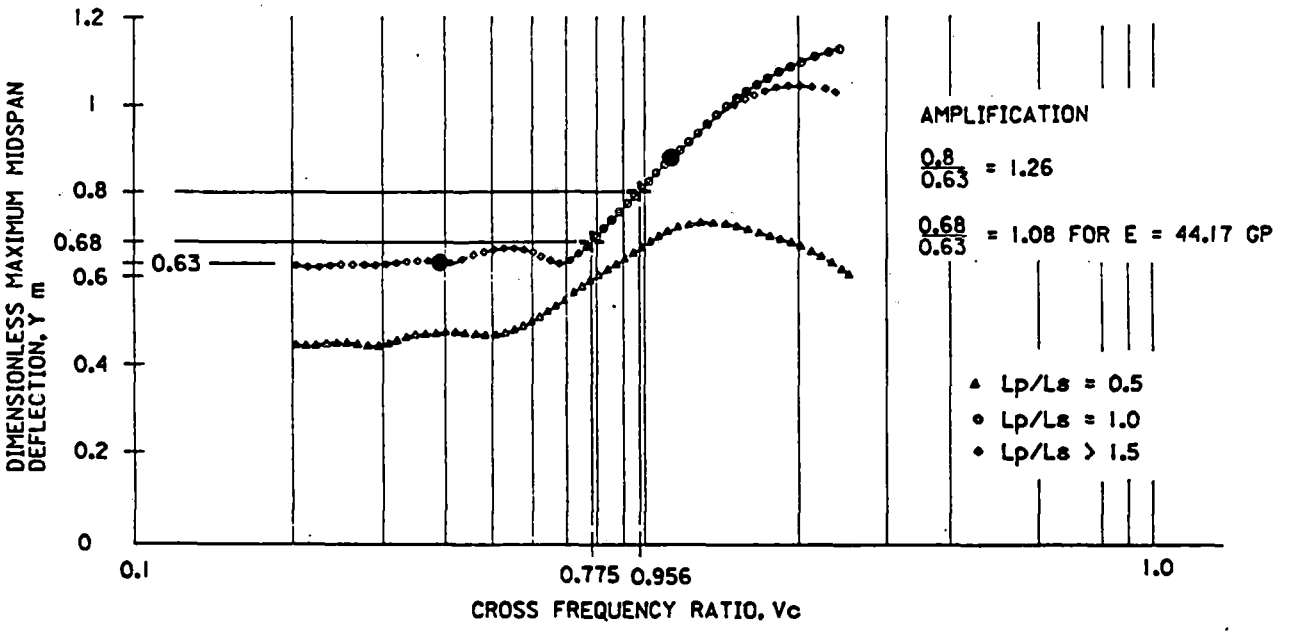

GRAPH IS FROM D. WORMLEY, BAA *62, VEHICLE/GUIDEWAY INTERACTIONS

DYNAMIC AMPLIFICATION = DYNAMIC DEFLECTION/STATIC (LIVE) DEFLECTION

● EARLIER GUIDEWAY CALCULATIONS FOR 134 m/s, 90 m/s, AND 45 m/s

+ BASELINE GIRDER PREDICTION: DYNAMIC AMPLIFICATION < 1.26. CONSERVATIVE FACTOR OF 1.4 CHOSEN

Figure C2-10 Maximum midspan deflection for single span guideway

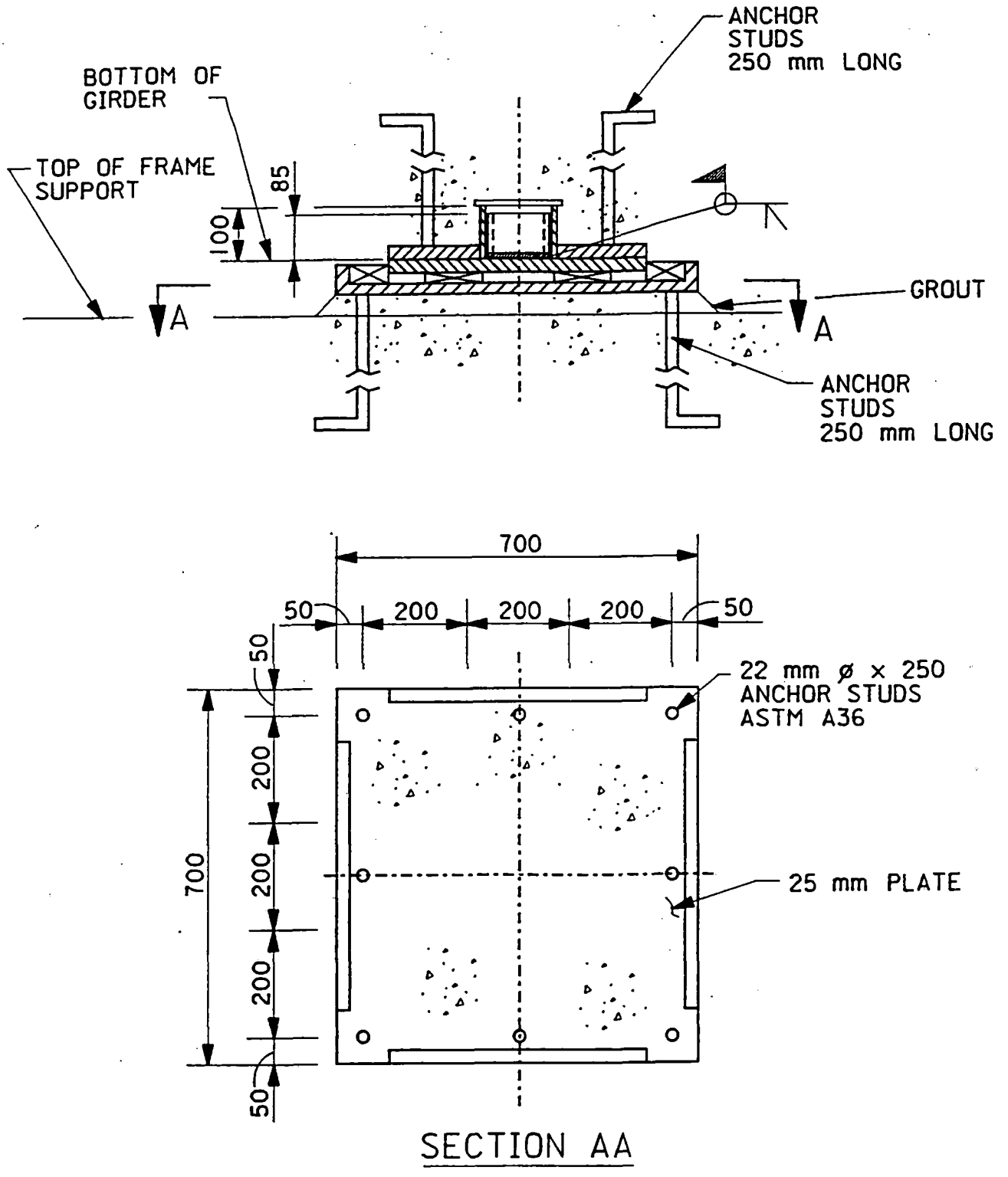

Figure C2-11 Shear key at girder fixed ends

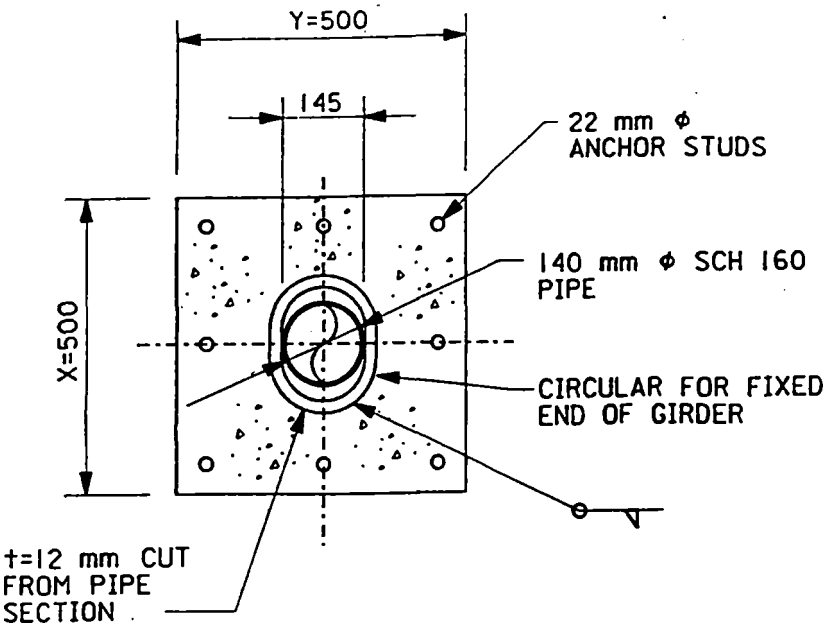

PLATE IN GIRDER
EXPANSION END

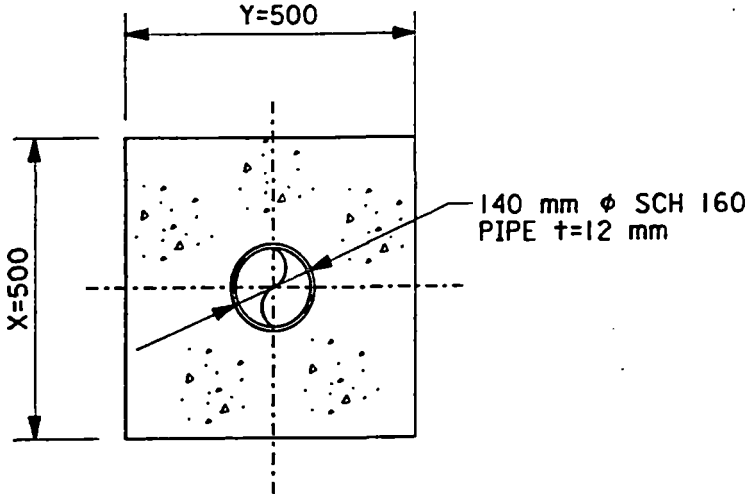

INTERMEDIATE PLATE

Figure C2-12 Shear key at girder expansion ends

Support Structures

Support frames for the curved dual track guideway and foundations are shown in Figures C2-13 to C2-18. The design for these structures is based on a concrete strength of 4,000 psi = 27.5 mPa cylinder strength. Single columns and foundations for curved track are shown in Figures C2-19 to C2-21. As standard baseline procedure, foundations, single columns and frames will be poured in place. As dictated by site conditions, or where high field labor rates may make it desirable, columns could be prefabricated and bolted to the foundations. Alternatively, columns could be inserted into formed recesses in the foundations and grouted into position. Figures C2-22 to C2-29 cover straight dual and single track elevated structures.

Propulsion/levitation/guidance system

This equipment transfers vertical, lateral, and horizontal forces from the vehicle to the girder. A major component is the high windload concentration near the front of the vehicle produces a yaw moment on the vehicle that has to be resisted by the guidance system.

Lateral forces from wind are based on recommendations by the Charles Stark Draper Laboratory. Our Team has designed for full speed operations (134 m/s) and lateral wind gusts up to 40 mph (17.86 m/s). For winds higher than 40 mph and up to 60 mph the operating speed will be reduced so that the lateral forces resulting from 40 mph crosswinds and full speed operation will not be exceeded.

The total lateral wind force is calculated as $y = Cy * q * A$

Cy = side force coefficient = 0.26
q = $\rho v^2/2$, ρ = air density = 0.002378 lbs/ft^3
q = 240 psf for 300 mph
A = $\pi Hv^2/2$; Hv = 14.6 ft
A = $3.14 \times 14.59^2/2 = 334.2$
y = $0.26 \times 240 \times 334.2 = 207850$ lbs = 9478 kg ≈ 93 kN

The larger fraction of this force is concentrated near the nose of the vehicle. For yaw moment calculations, 53% of y, 49.3 kN are applied at a point 3.75 m behind the front of the vehicle. The remaining wind force of 43.7 kN is uniformly distributed over the remaining vehicle length of 33.75 m. The concentrated wind load of 49.3 kN acts 15.0 m in front of the vehicle midpoint and the remaining wind force of 43.7 kN acts 1.875 m behind the vehicle midpoint. Thus the yaw moment is 49.3 x 15.0 - 43.7 x 1.875 = 657.6 kNm (see Figure C2-30).

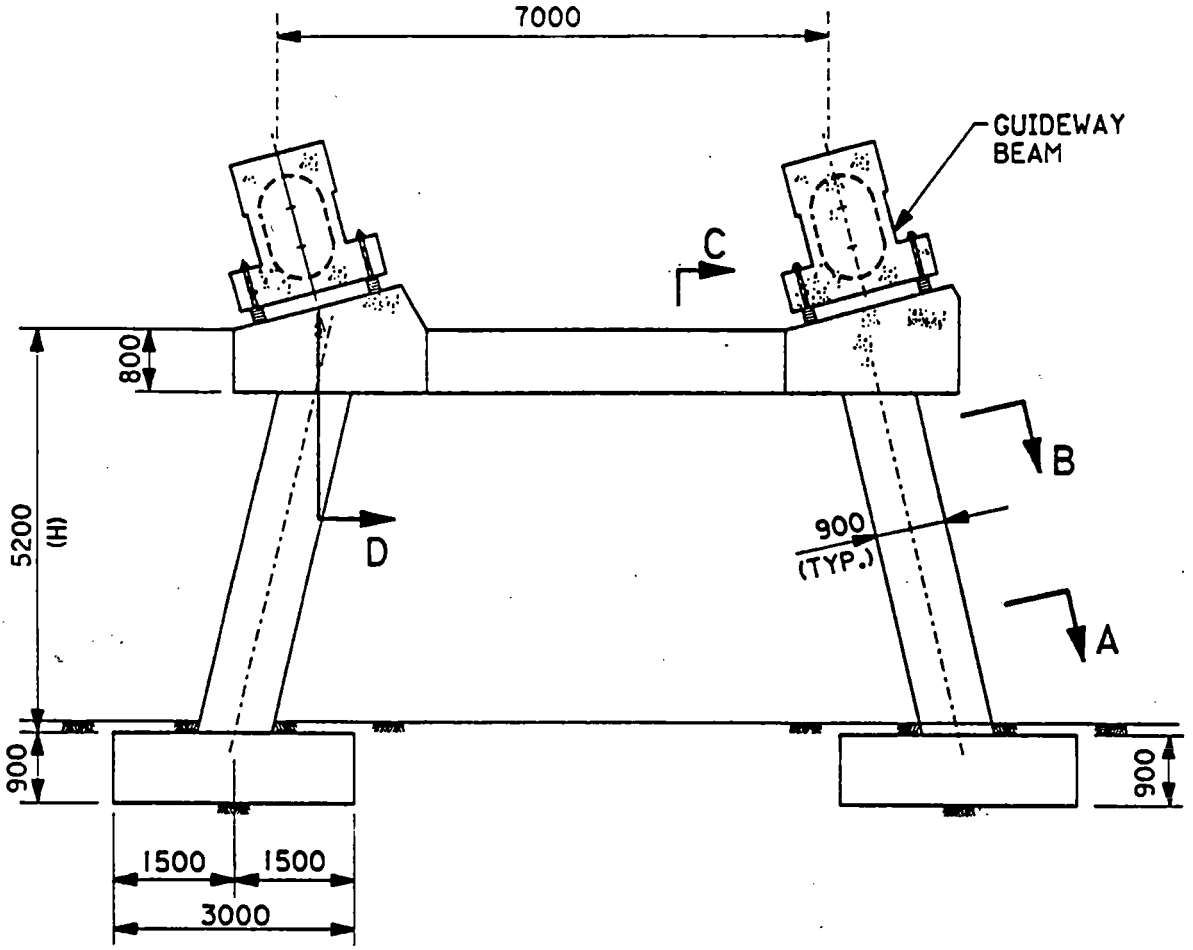

Figure C2-13 Frame elevation for dual curved track guideway with 25 m span with sections

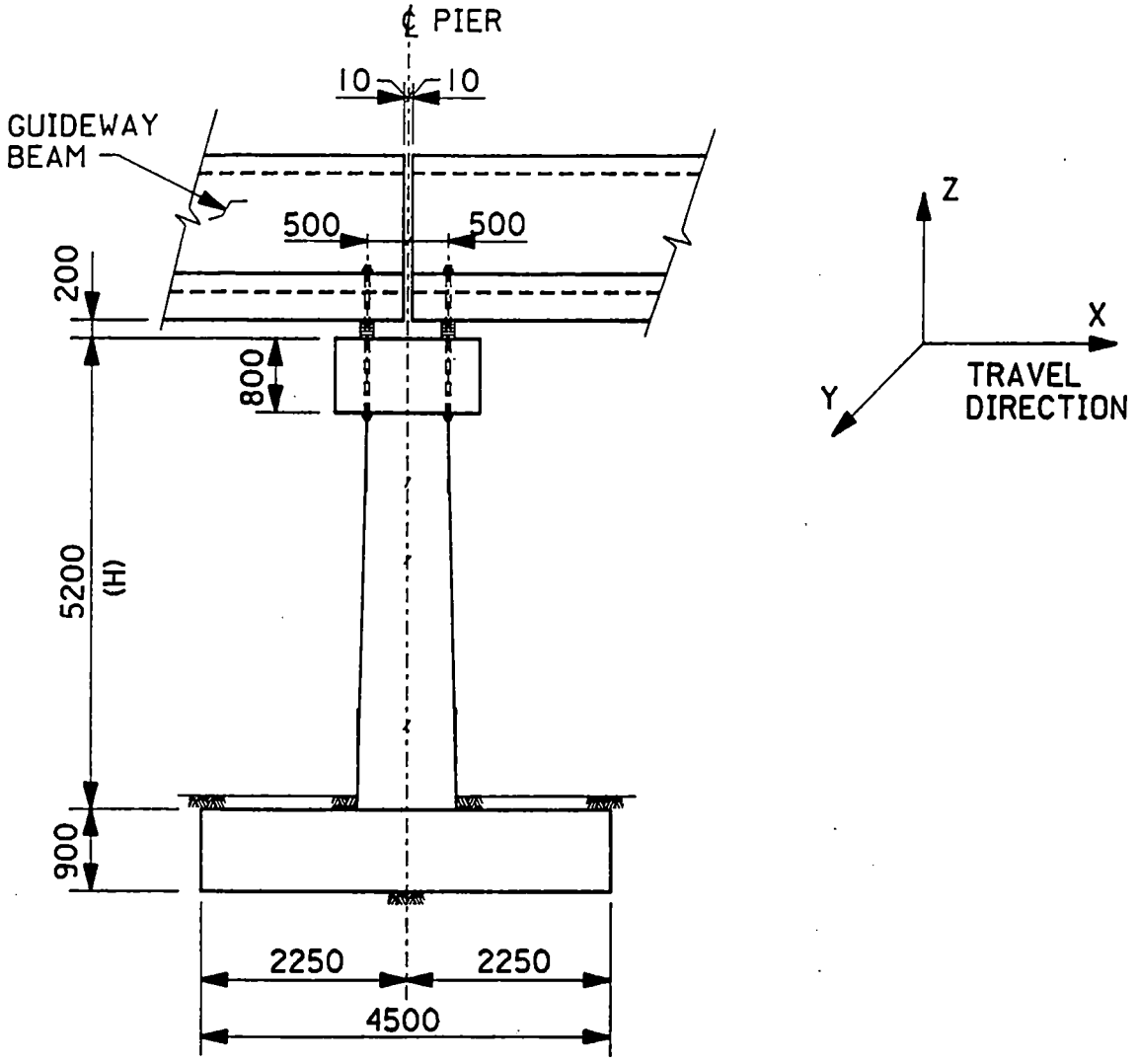

Figure C2-14 Frame side elevation for dual curved track guideway with 25 m span

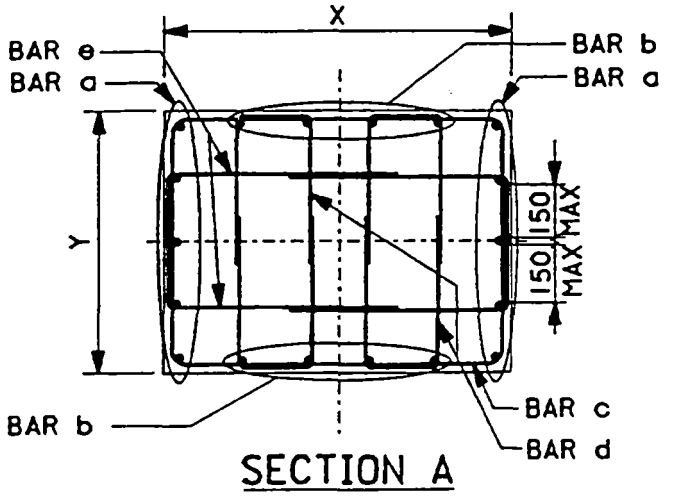

SECTION A

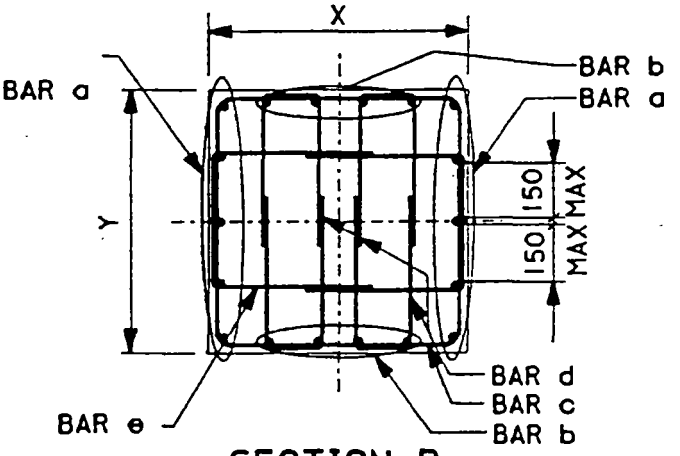

SECTION B

SECTION	DIMENSIONS (METERS)								
	COL. HEIGHT=5.20m			COL. HEIGHT=7.60m			COL. HEIGHT=9.20m		
	X	Y	Z	X	Y	Z	X	Y	Z
A	1.00	0.90	-	1.10	0.90	-	1.20	0.90	-
B	0.90	0.90	-	0.90	0.90	-	0.90	0.90	-
C	0.90	-	0.80	0.90	-	0.80	0.90	-	0.90
D	1.60	2.20	0.80	1.20	2.20	0.90	1.20	2.20	0.90

Figure C2-15 Support frame at column sections for dual curved track

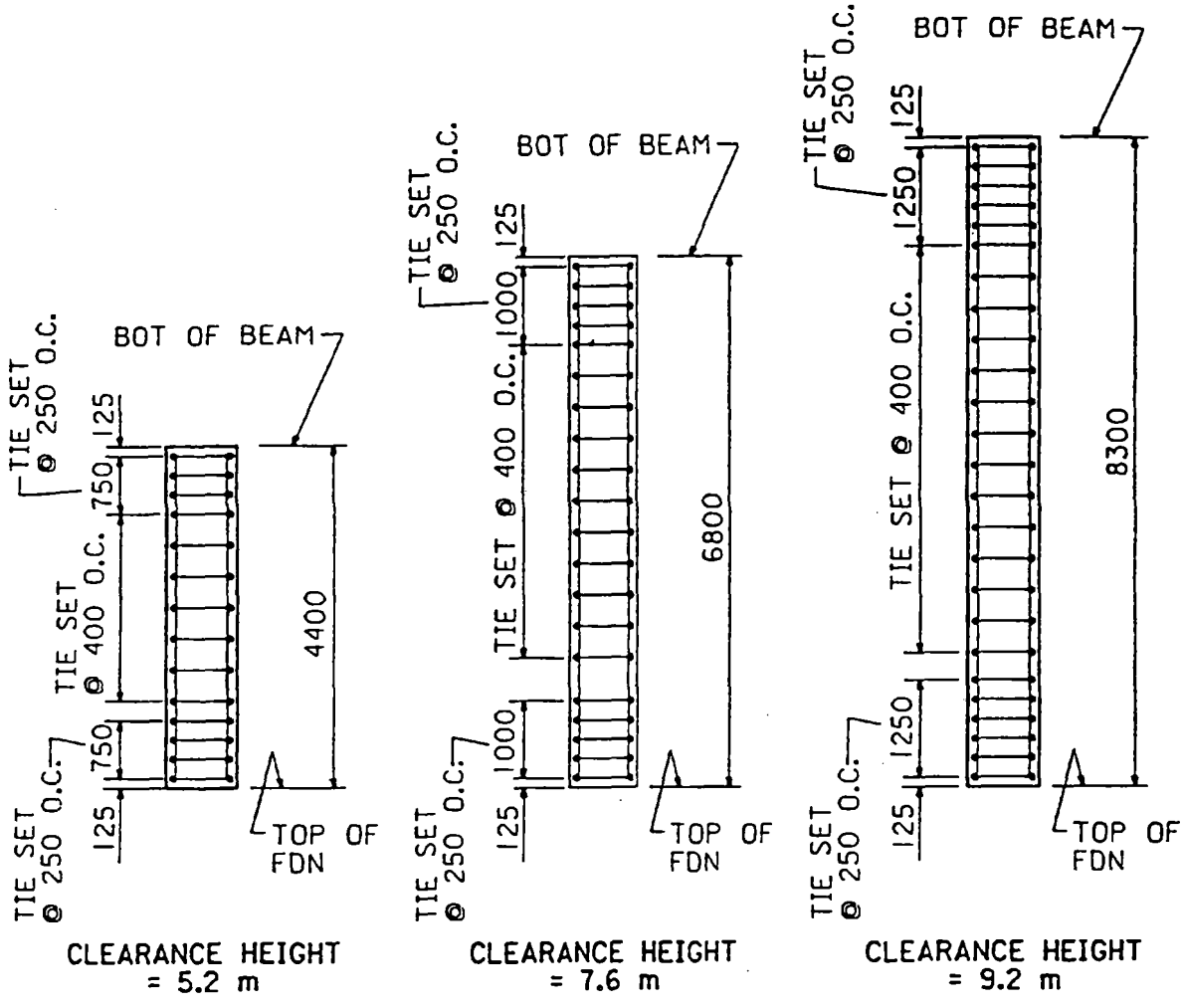

NOTE:

THE COLUMN TIES CORRESPOND TO THE DIFFERENT COLUMN HEIGHTS AS SHOWN FOR BOTH CURVED OR STRAIGHT TRACK SINGLE AND DUAL GUIDEWAY.

Figure C2-16 Column ties spacing schedule

SECTION	COLUMN HEIGHT m	REINFORCEMENT SCHEDULE				
		a	b	c	d	e
A	5.20	5- #11	3- #11	#4	#4	#4
B	5.20	5- #11	3- #11	#4	#4	#4
C	5.20	10- #11	4- #11	#4 @ 0.18	-	-
D	5.20	14- #11	2- #11	#4 @ 0.18	#6 @ 0.18	-
A	7.60	6- #11	3- #11	#4	#4	#4
B	7.60	6- #11	3- #11	#4	#4	#4
C	7.60	10- #11	4- #11	#4 @ 0.18	-	-
D	7.60	14- #11	2- #11	#4 @ 0.18	#6 @ 0.18	-
A	9.20	8- #11	3- #11	#4	#4	#4
B	9.20	6- #11	3- #11	#4	#4	#4
C	9.20	11- #11	4- #11	#4 @ 0.18	-	-
D	9.20	15- #11	2- #11	#4 @ 0.18	#6 @ 0.18	-

Figure C2-17 Reinforcing schedule for dual curved track

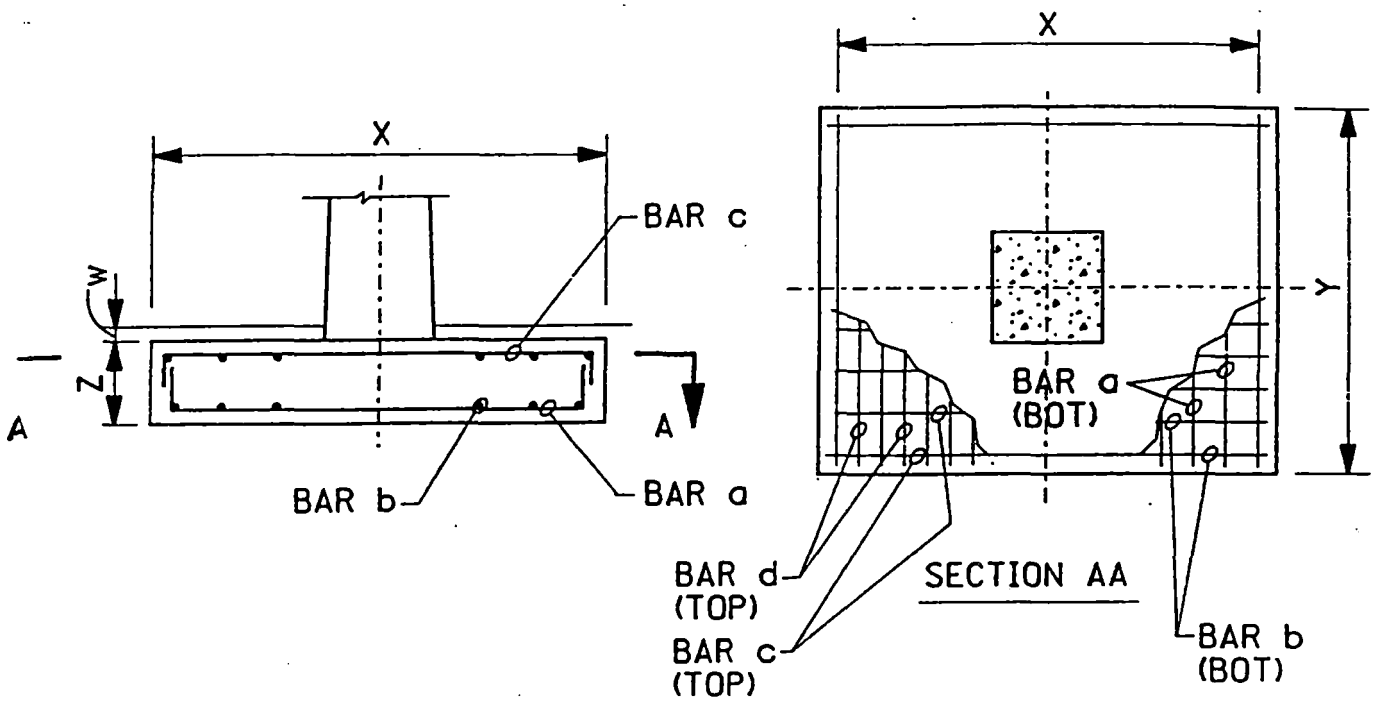

COLUMN HEIGHT	FOOTING F-2 SCHEDULE * CURVED-DUAL TRACK GUIDEWAY							
	X	Y	Z	W	BAR a	BAR b	BAR c	BAR d
5.20	4.50	3.0	0.9	0.1	#10 @ 0.2	#10 @ 0.2	#6 @ 0.3	#6 @ 0.3
7.60	5.0	3.8	0.9	0.1	#10 @ 0.2	#10 @ 0.2	#6 @ 0.3	#6 @ 0.3
9.20	5.30	4.0	1.0	0.1	#11 @ 0.2	#11 @ 0.2	#6 @ 0.3	#6 @ 0.3

* DIMENSIONS - METERS

Figure C2-18 Dual curved track foundations

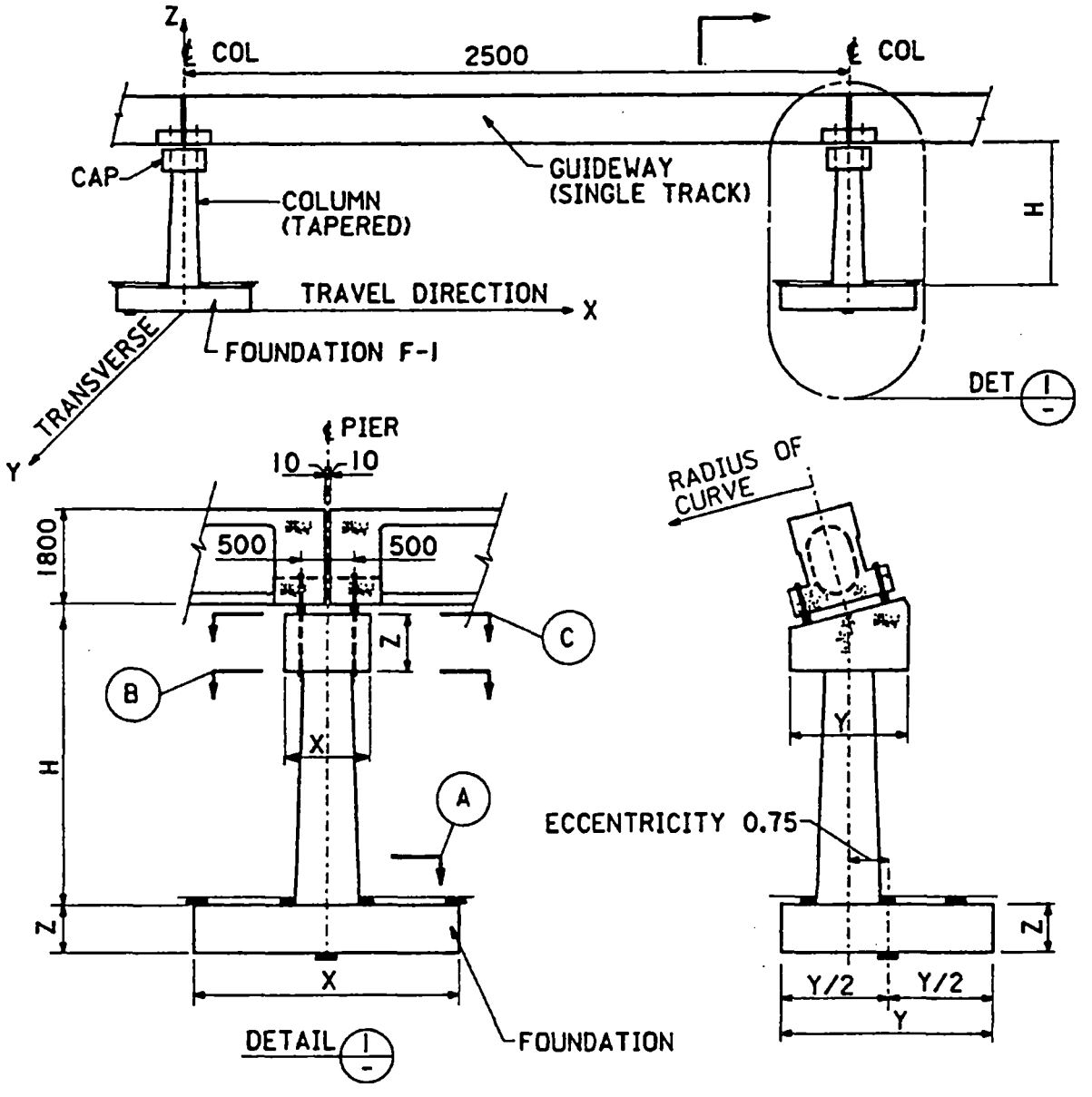

Figure C2-19 Elevation for single curved track

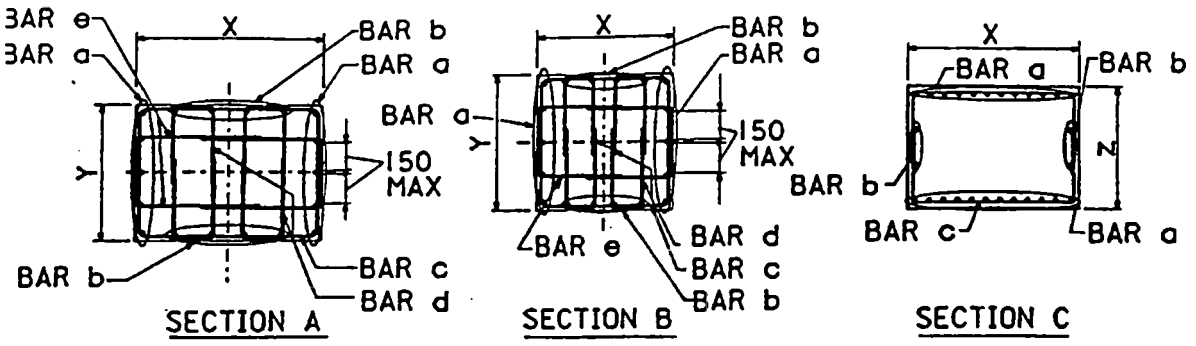

SECTION	COLUMN HEIGHT	DIMENSION (METERS)			REINFORCEMENT SCHEDULE				
		X	Y	Z	a	b	c	d	e
A	5.20	1.20	1.20	—	5- #10	3- #10	#4	#4	#4
B	5.20	0.90	0.90	—	5- #10	3- #10	#4	#4	#4
C	5.20	1.60	2.20	0.80	#6 ▭ @ 0.18	2- #6	#6	#6	#6
A	7.60	1.20	1.20	—	6- #10	3- #10	#4	#4	#4
B	7.60	0.90	0.90	—	6- #10	3- #10	#4	#4	#4
C	7.60	1.60	2.20	0.80	#6 ▭ @ 0.15	2- #10	#6	#6	#6
A	9.20	1.30	1.30	—	6- #11	3- #11	#4	#4	#4
B	9.20	0.90	0.90	—	6- #11	3- #11	#4	#4	#4
C	9.20	1.60	2.20	0.90	#6 ▭ @ 0.18	2- #11	#6	#6	#6

Figure C2-20 Column sections for curved single track

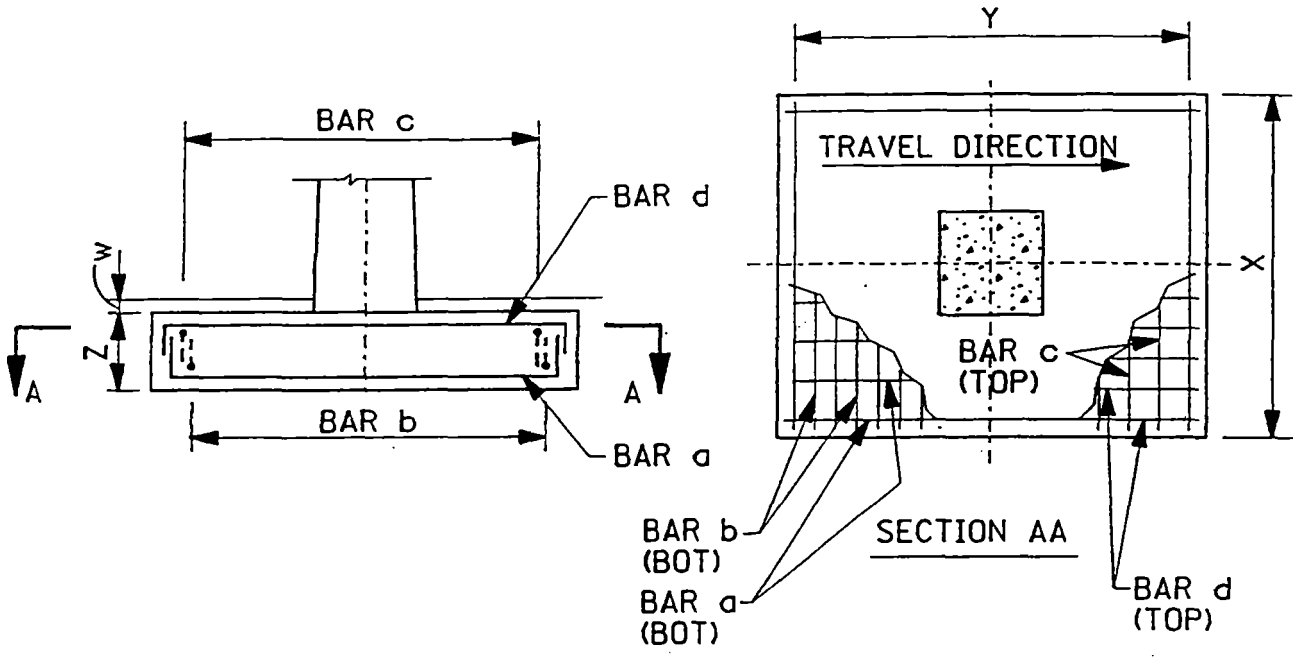

COLUMN HEIGHT	FOOTING F-1 SCHEDULE *							
	X	Y	Z	W	BAR a	BAR b	BAR c	BAR d
5.20	3.25	6.75	0.9	0.1	#10 @ 0.3	#10 @ 0.3	#6 @ 0.3	#6 @ 0.3
7.60	3.75	8.00	0.9	0.1	#10 @ 0.3	#10 @ 0.3	#6 @ 0.3	#6 @ 0.3
9.20	4.10	8.70	1.0	0.1	#11 @ 0.3	#11 @ 0.3	#6 @ 0.3	#6 @ 0.3

* DIMENSIONS - METER

Figure C2-21 Single curved track guideway foundation

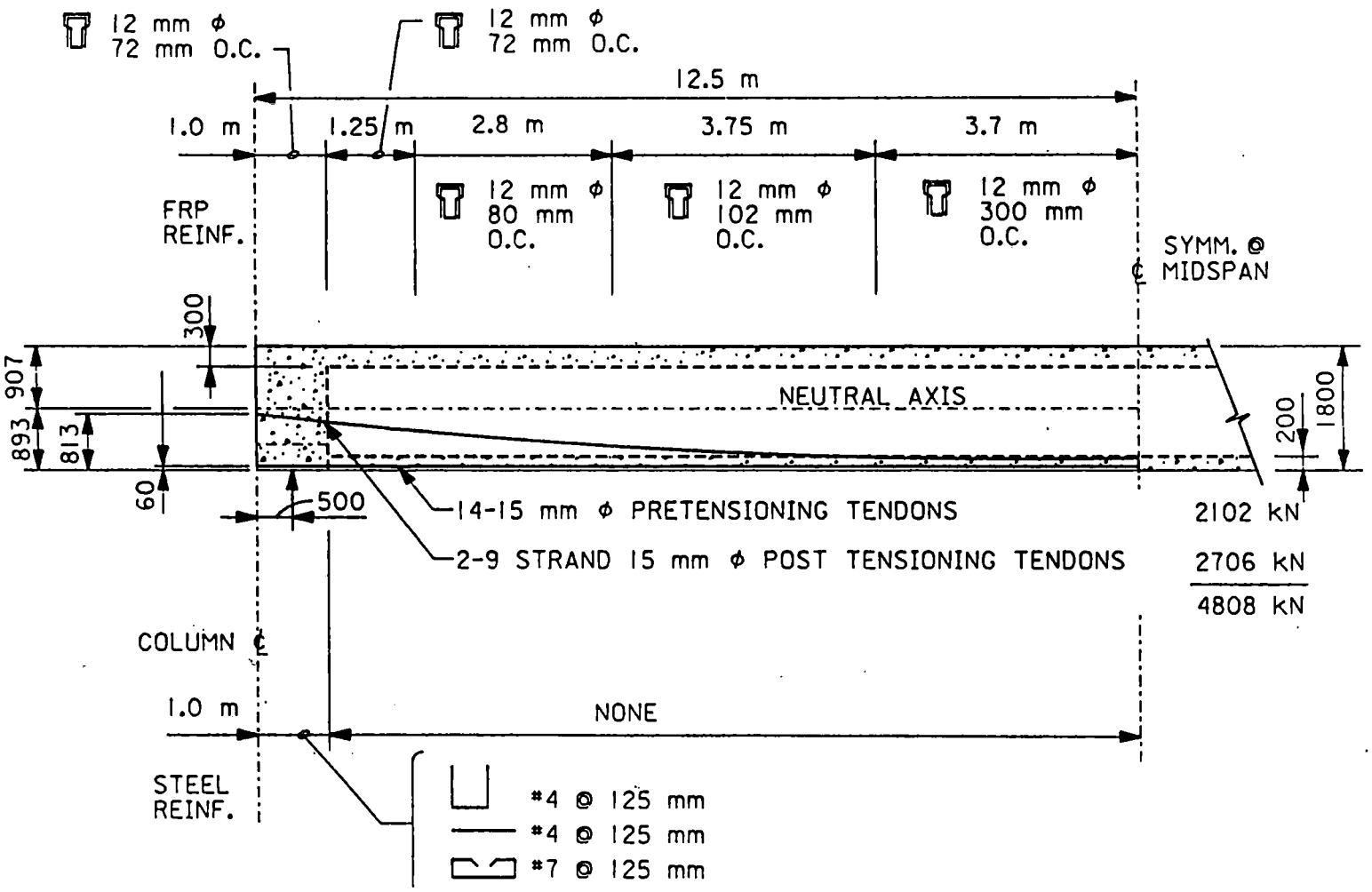

Figure C2-22 Straight double track girder elevation showing stirrups and tendons

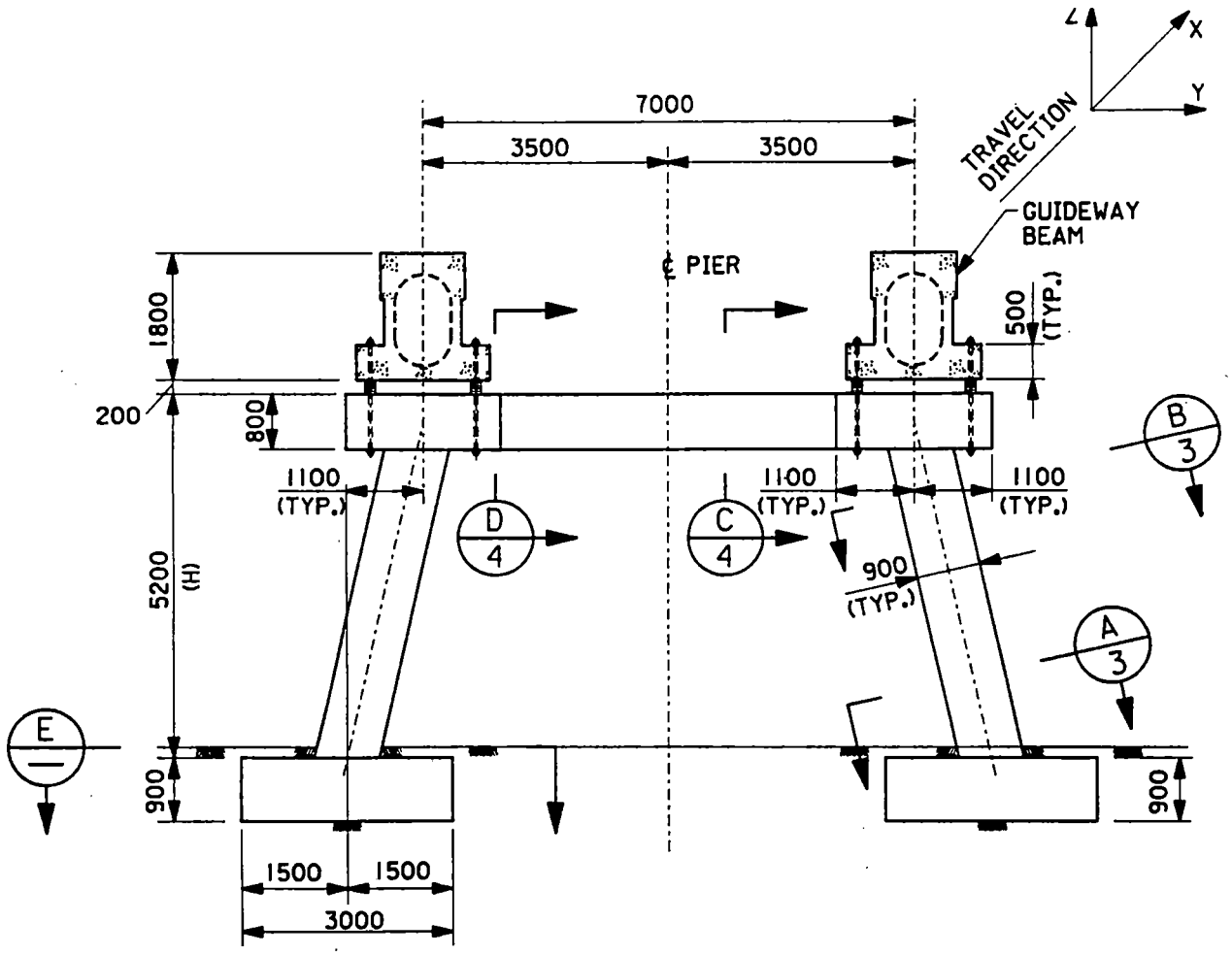

Figure C2-23 Frame elevation for dual straight track guideway with 25 m span

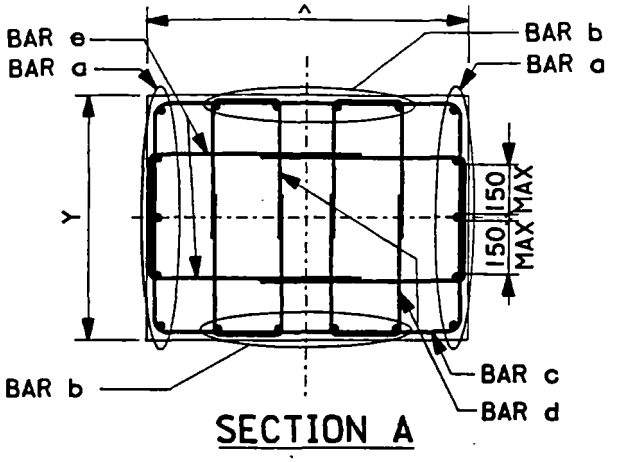

SECTION A

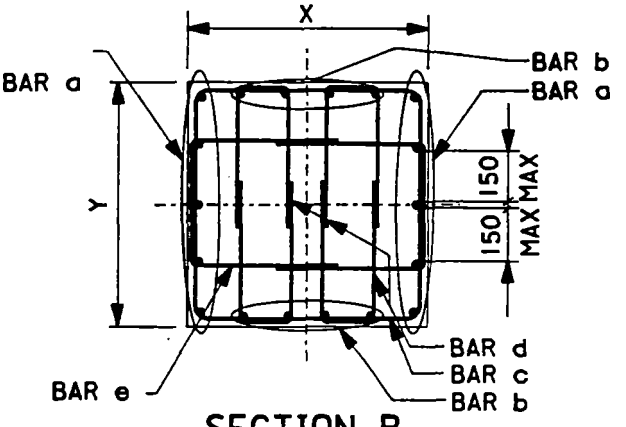

SECTION B

SECTION	DIMENSIONS (METERS)								
	COL. HEIGHT=5.20m			COL. HEIGHT=7.60m			COL. HEIGHT=9.20m		
	X	Y	Z	X	Y	Z	X	Y	Z
A	1.0	0.90	0.90	1.10	0.90	-	1.20	0.90	-
B	0.90	0.90	0.90	0.90	0.90	-	0.90	0.90	-
C	0.90	-	0.80	0.90	-	0.80	0.90	-	0.90
D	1.60	2.20	0.80	1.20	2.20	0.90	1.20	2.20	0.90

Figure C2-24 Support frame – column sections for dual straight track

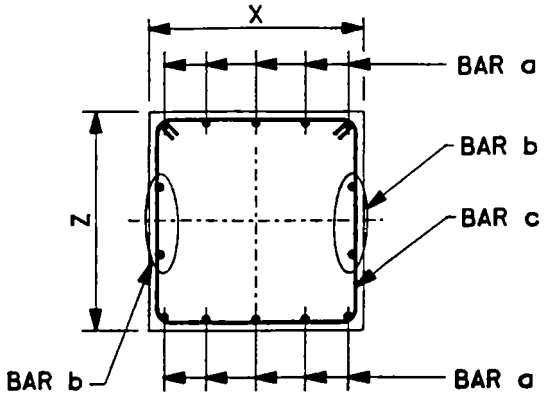

SECTION C

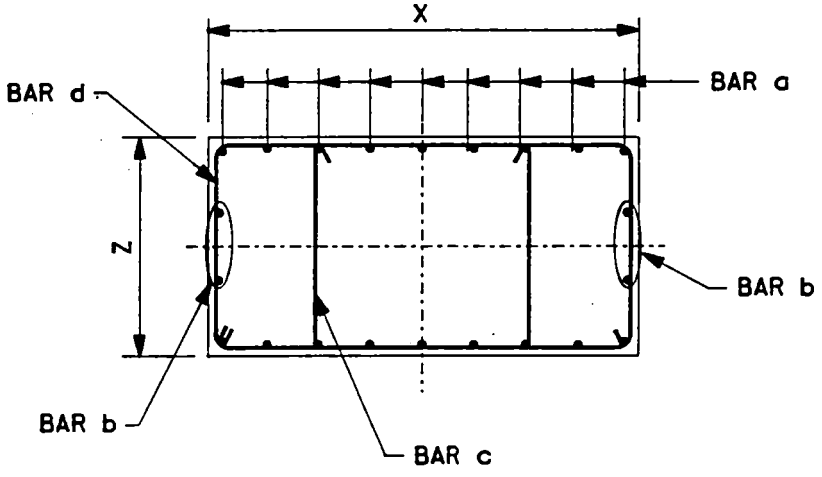

SECTION D

Figure C2-25 Support frame – beam section

SECTION	COLUMN HEIGHT m	REINFORCEMENT SCHEDULE				
		a	b	c	d	e
A	5.20	5- #10	3- #10	#4	#4	#4
B	5.20	5- #10	3- #10	#4	#4	#4
C	5.20	8 @ #11	4- #11	#4 @ 0.18	-	-
D	5.20	12 @ #11	2- #11	#4 @ 0.18	#6 @ 0.18	-
A	7.60	6- #10	3- #10	#4	#4	#4
B	7.60	6- #10	3- #10	#4	#4	#4
C	7.60	8- #11	4- #10	#4 @ 0.18	-	-
D	7.60	12- #11	2- #11	#4 @ 0.18	#6 @ 0.18	-
A	9.20	8- #11	3- #11	#4	#4	#4
B	9.20	8- #11	3- #11	#4	#4	#4
C	9.20	8- #11	4- #11	#4 @ 0.18	-	-
D	9.20	12- #11	2- #11	#4 @ 0.18	#6 @ 0.18	-

Figure C2-26 Reinforcing schedule for dual straight track frames

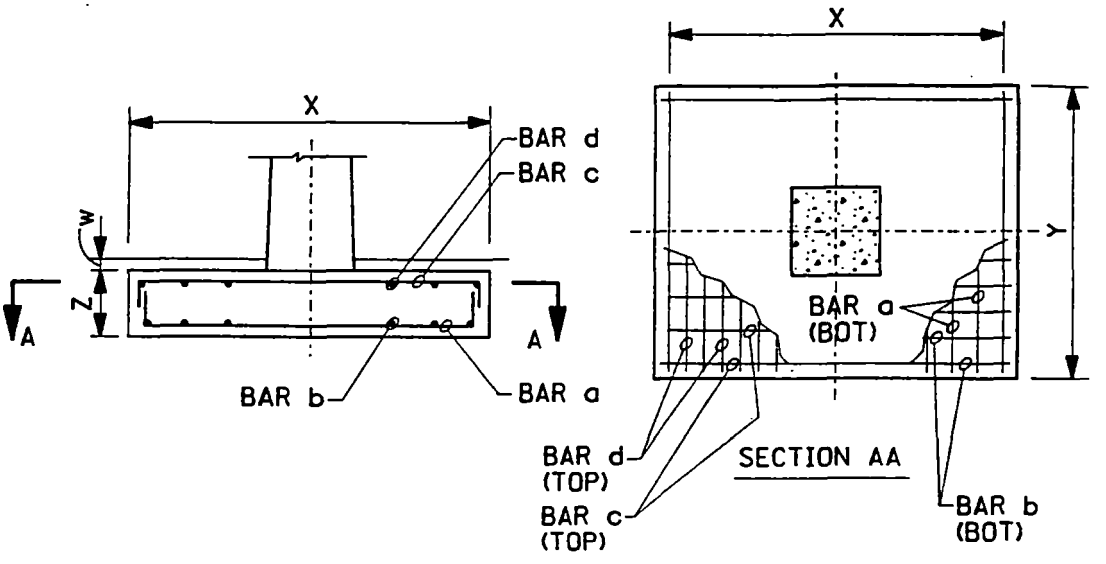

COLUMN HEIGHT m	FOOTING SCHEDULE							
	X	Y	Z	W	BAR a	BAR b	BAR c	BAR d
5.20	4.0	3.0	0.9	0.1	*10 @ 0.2	*10 @ 0.2	*6 @ 0.3	*6 @ 0.3
7.60	4.50	3.70	0.9	0.1	*10 @ 0.2	*10 @ 0.2	*6 @ 0.3	*6 @ 0.3
9.20	5.0	3.80	1.0	0.1	*11 @ 0.2	*11 @ 0.2	*6 @ 0.3	*6 @ 0.3

* DIMENSIONS - METER

Figure C2-27 Dual straight track foundations

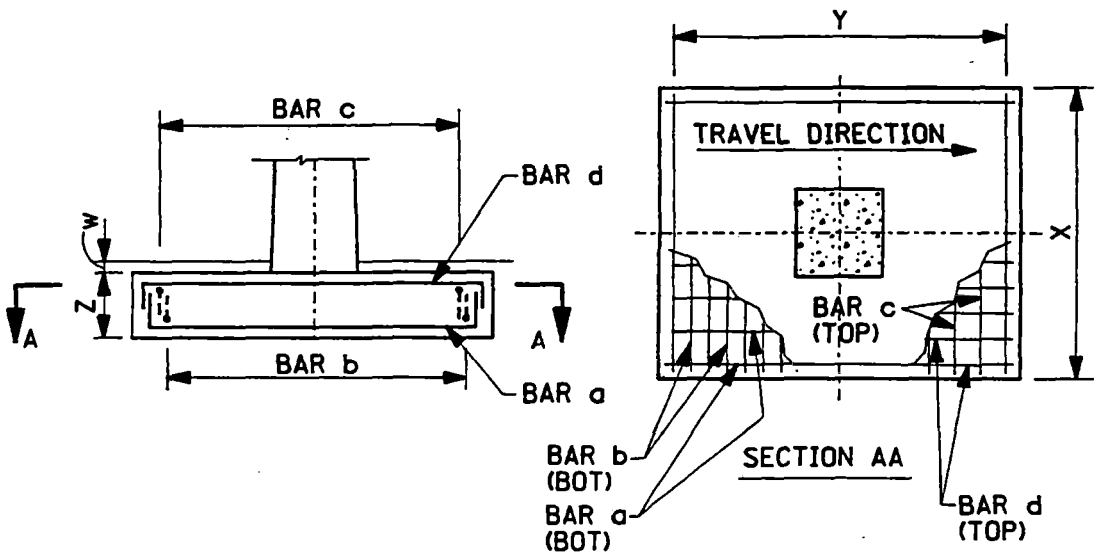

COLUMN HEIGHT m	FOOTING F-1 SCHEDULE *							
	X	Y	Z	W	BAR a	BAR b	BAR c	BAR d
5.20	3.25	6.75	0.9	0.1	#10 @ 0.3	#9 @ 0.3	#6 @ 0.3	#6 @ 0.3
7.60	3.75	8.0	0.9	0.1	#10 @ 0.3	#10 @ 0.3	#6 @ 0.3	#6 @ 0.3
9.20	4.10	8.70	1.0	0.1	#11 @ 0.3	#11 @ 0.3	#6 @ 0.3	#6 @ 0.3

* DIMENSIONS - METER

Figure C2-28 Single straight track foundations

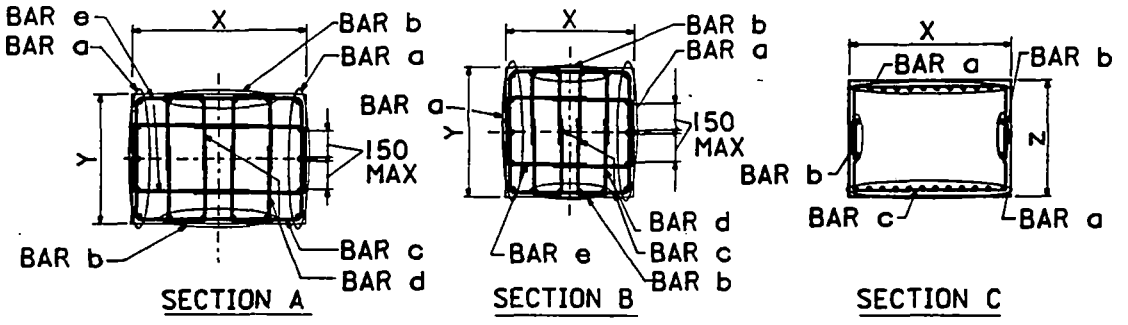

SECTION	COLUMN HEIGHT m	DIMENSIONS (METER)			REINFORCEMENT SCHEDULE				
		X	Y	Z	a	b	c	d	e
A	5.20	1.20	1.20	—	5- #11	3- #11	#4	#4	#4
B	5.20	0.90	0.90	—	5- #11	3- #11	#4	#4	#4
C	5.20	1.60	2.20	0.80	#6 ▭ @ 0.18	2- #6	#6	#6	#6
A	7.60	1.20	1.20	—	6- #11	3- #11	#4	#4	#4
B	7.60	0.90	0.90	—	6- #11	3- #11	#4	#4	#4
C	7.60	1.60	2.20	0.80	#6 ▭ @ 0.15	2- #10	#6	#6	#6
A	9.20	1.30	1.30	—	7- #11	3- #11	#4	#4	#4
B	9.20	0.90	0.90	—	7- #11	3- #11	#4	#4	#4
C	9.20	1.60	2.20	0.90	#6 ▭ @ 0.18	2- #11	#6	#6	#6

Figure C2-29 Reinforcing schedule single straight track columns

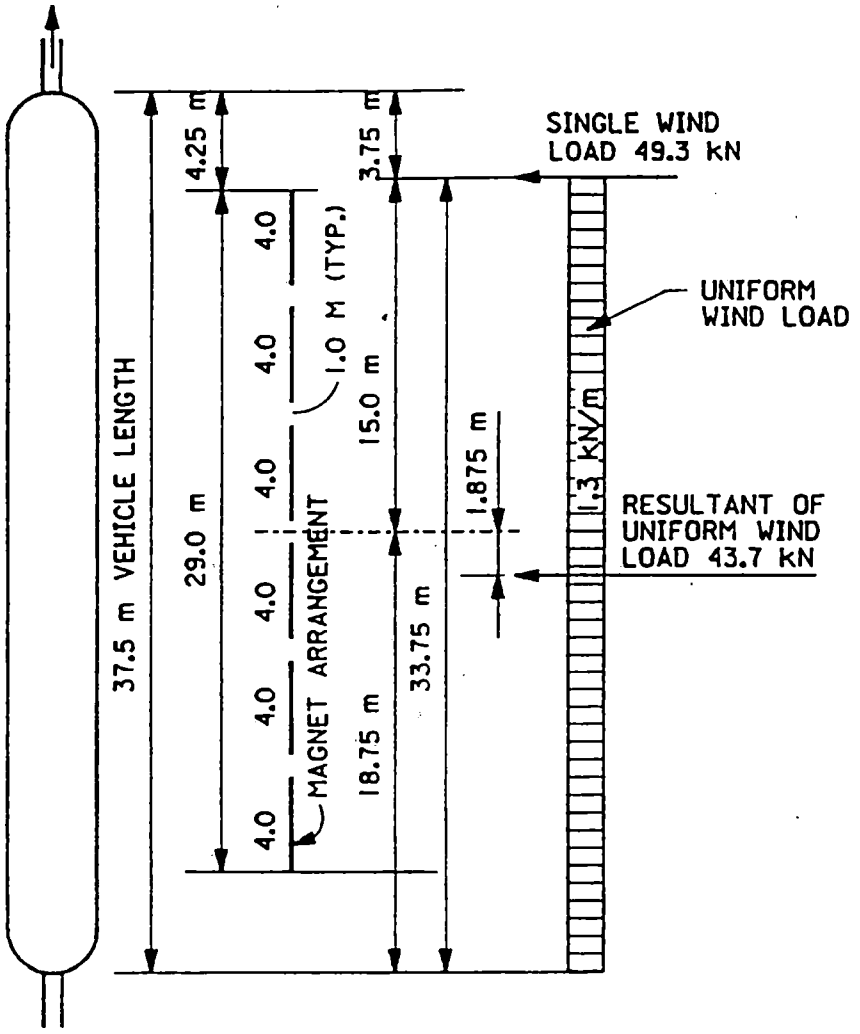

SIX 4.0 m LONG MAGNETS ARE ARRANGED ON EACH SIDE OF THE VEHICLE. THE SPACING BETWEEN MAGNETS IS 1.0 m. THUS THE MAGNETS COVER A TOTAL LENGTH OF 6 x 4 + 5 x 1 = 29.0 m

YAW MOMENT AT VEHICLE MIDLENGTH
49.3 x 15.0 - 43.7 x 1.875 = 657.6 kNm

Figure C2-30 Lateral forces distribution on magnets

Figure C2-31 shows the calculation for the maximum windload reaction on the front magnets of R1 = 32.26 kN. Each front magnet carries 32.26/2 = ± 16.13 kN or ± 4.03 kN/m.

Lateral acceleration forces on curved track sections with 15 degree girder bank angle and 15 degree vehicle tilt angle at full speed for a 64,800 kg vehicle including a dynamic amplification factor of 1.4 are 1.4 x 0.2988 x 64,800/102 x 24 = 11.07 kN/m or ± 5.54 kN/m on each side of the girder.

The maximum lateral force on magnets and guidance system is 4.03 + 5.54 = ± 9.97 kN/m.

Wind and centrifugal forces acting respectively 1.56 m and 1.15 m above the guidance system produce a roll moment of 2 x 4.03 x 1.56 + 2 x 5.54 x 1.15 = 25.28 kNm.

With a levitation ladder spacing of 1.31 m each ladder will carry a vertical force from roll moment = ±25.28/1.31 = ± 19.29 kN/m. The vehicle forces, including superelevation and dynamic amplification, (1.4 x 64,800 x 1.115) ÷ (24.0 x 2.0 x 1.02) = ± 20.66 kN/m. The maximum force is therefore ± 39.95 kN/m and the minimum is ± 1.37 kN/m. See Figure C2-32.

These forces represent a worst-case scenario and are based on the assumption that magnet displacements, suspension, and vehicle frame permit direct transfer of the concentrated wind load. A stiff vehicle frame and suspension will reduce these forces.

The propulsion/levitation/guidance system has been designed for the above forces. A section of this system is shown in Figure C2-33. The system consists of:

- Two 6-phase propulsion windings on either side of the girder
- Guidance system
- Levitation ladders
- Mounting bracket
- Shims, clamps and anchor bolts
- A cover plate

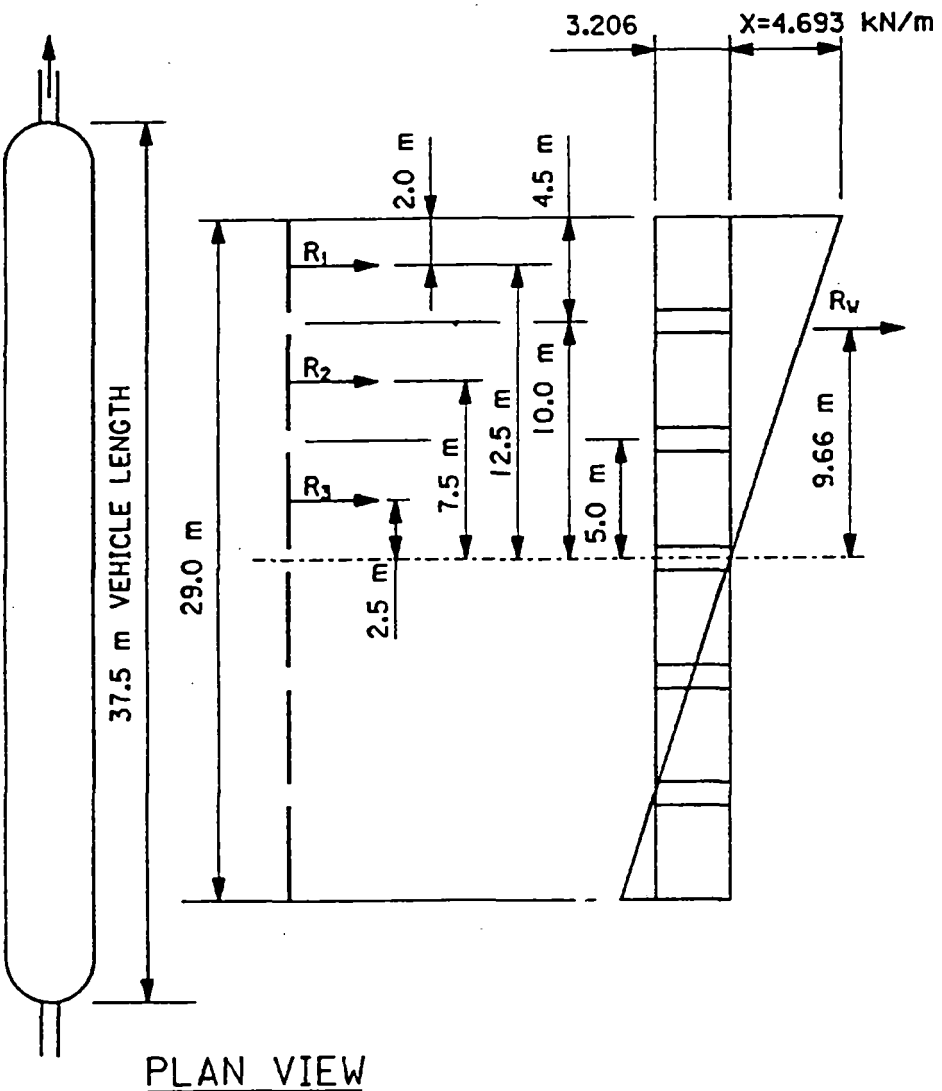

TOTAL WINDLOAD = 93 kN/29 = 3.206 kN/m
YAW MOMENT = 657.6 kNm
YAW MOMENT REACTION FROM
TRIANGULAR DISTRIBUTION AS SHOWN ABOVE

$$R_W = \frac{657.6}{2 \times 9.66} = 34.03 \text{ kN} ; \qquad X = \frac{2 \times 34.03}{14.5} = 4.693 \text{ kN/m}$$

$$R_1 = \left(\frac{4.693 + 4.693 \times 10/14.5}{2} + 3.206\right) \times 4.5 = 32.26 \text{ kN}$$

Figure C2-31 Lateral forces on front magnets

LATERAL FORCES ON FRONT MAGNET:

FROM WIND 32.26/2 = ± 16.13 kN ± 4.03 kN/m MAGNET

FROM LATERAL ACCELERATION

1.4 x 0.2988 x 64800/102 x 24 x 2 = ± 5.54 kN/m MAGNET

TOTAL ± 9.97 kN/m MAGNET

VERTICAL FORCES ON FRONT MAGNET:

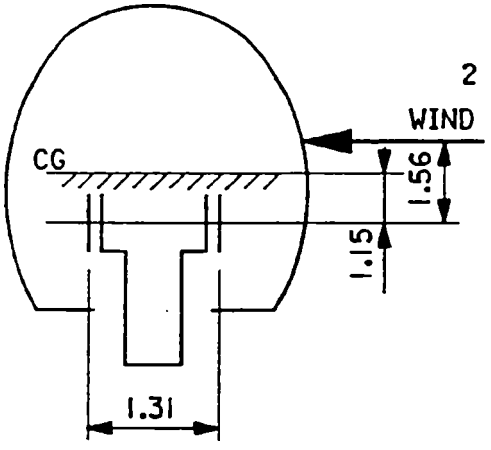

ROLL MOMENT

2 x 4.03 x 1.56 + 2 x 5.54 x 1.15 = 25.28 kNm

LEVITATION LADDER FORCES

FROM ROLL MOMENT 25.28/1.31 = ± 19.30 kN/m

FROM VEHICLE $\frac{1.4 \times 64800 \times 1.15}{24.0 \times 2.0 \times 102}$ = + 20.70 kN/m

MAX = + 40.00 kN/m

MIN = + 1.40 kN/m

Figure C2-32 Lateral and vertical forces on front magnets

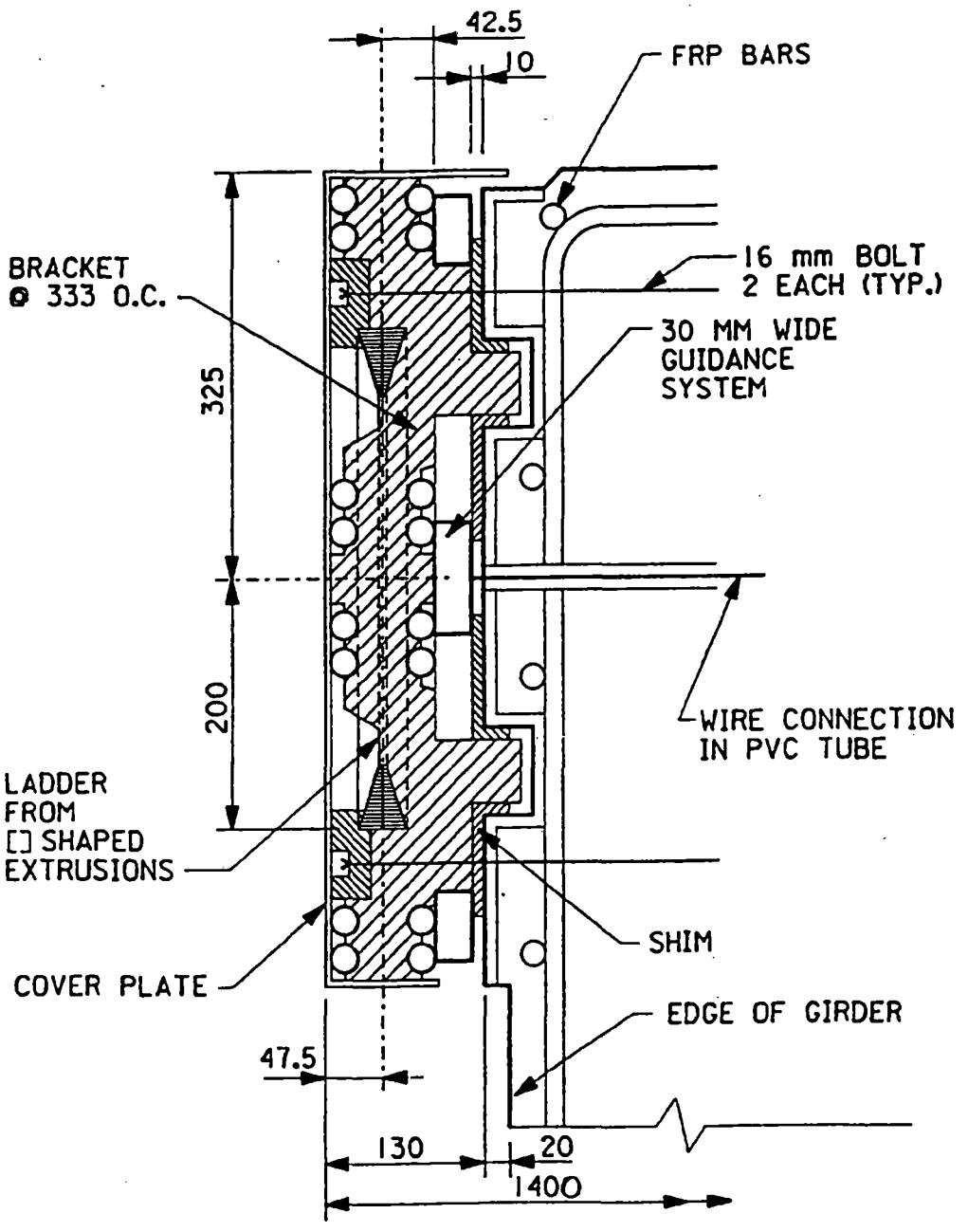

Figure C2-33 Propulsion/levitation/guidance mounting bracket

The 6-phase cable windings are two three-phase windings offset by 166 mm and are supported by the mounting bracket. The vertical sections of the 22.5 mm Ø propulsion coils are tied to the rungs of the levitation ladder. An elevation of a three-phase winding is shown in Fig. C2-34.

The guidance system consists of 525 mm^2 copper coils supported within FRP frames. These frames are 666 mm long and 610 mm high (see Figure C2-35). The perimeter sections of this frame are 30 x 55 mm and the centersection is 30 x 90 mm (1050 mm2 of copper). These frames are attached to the rear side of the mounting bracket and vertically and laterally supported. Lateral stresses in the FRP frames resulting from ~ 10kN/m lateral forces are in the order of 500 psi and ‹12000 psi permitted for FRP.

The levitation ladder is fabricated out of high strength aluminum alloy of good conductivity (as 6063-T6 or similar). Individual extrusions of variable dimensions are shown in Figure C2-36. These individual extrusions will have cut-outs to form 30 mm wide rung sections. The rung sections are spaced 166 mm on center to provide six rungs per meter. Each rung section is slitted to reduce electromagnetic drag leaving ten 1.0 mm x 3.0 mm sections (Figure C2-37). Seventeen ladder elements are bonded together to form one-half of the ladder. Two halves are bonded back to back (see Figure C2-37). The ladder has been structurally analyzed as a frame supported every 333 mm at the top and bottom railsection in vertical and horizontal direction. The forces are shown in Figure C2-38. This frame analysis shows maximum stresses in the rail of 7,000 psi and in the rung of 4,000 psi. Stresses for 6063-T6 with 500 x 106 load cycles and complete stress reversal are limited to 9,500 psi (ALCOA structural handbook). The rung sections are subject to a higher number of load cycles than the rail sections of the ladder but neither is exposed to full stress reversal. The rotating forces on the rungs will change 12 times for each passing vehicle (24 magnet sets). Assuming 50 years of operation, 24 hrs per day and 40 vehicles per hour we obtain only $12 \times 30 \times 24 \times 365 \times 50 = 210 \times 10^6$ cycles for a 50 year period. Preproduction testing will be required to optimize production methods and validate the assumptions made in this analysis.

The mounting bracket (Figure C2-33) transfers vertical and lateral forces acting between the vehicle magnets and the propulsion/levitation/guidance system by means of two shear keys to the guideway girder. Variable dimensions shims are used to provide vertical and lateral adjustment options of ± 10 mm in either direction. This permits precision alignment of the entire assembly. The shims engage in a 10 mm thick FRP faceplate attached to both upper sides of the girder. The

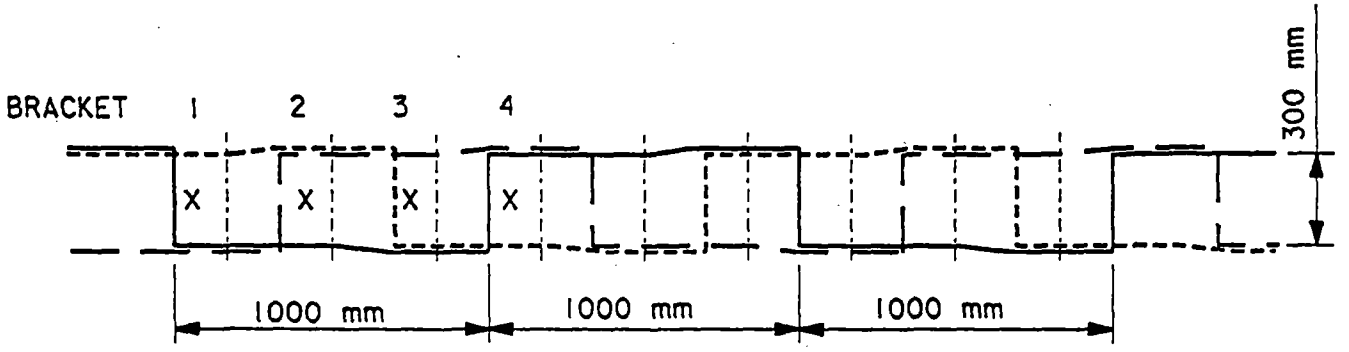

NOTE:

ONLY 1 UPPER 3-PHASE WINDING SHOWN.
VERTICAL CABLES LOCATED NEXT TO RUNG.
-------- VERTICAL OF 2nd 3-PHASE WINDING.
X — LOCATION OF MOUNTING BRACKET CENTERED BETWEEN RUNGS; 333 mm SPACING.

Figure C2-34 Propulsion coils elevation

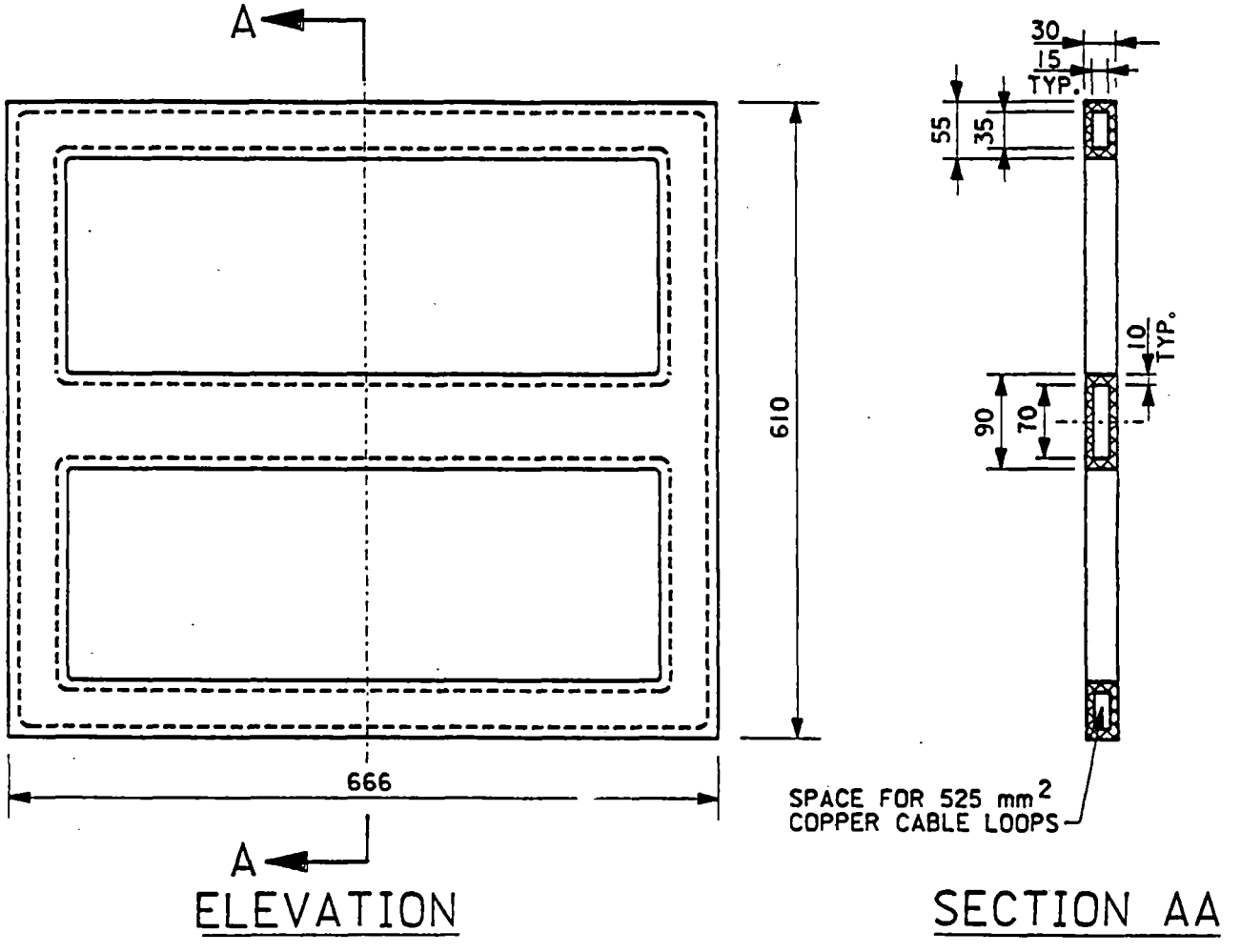

Figure C2-35 FRP support for guidance system

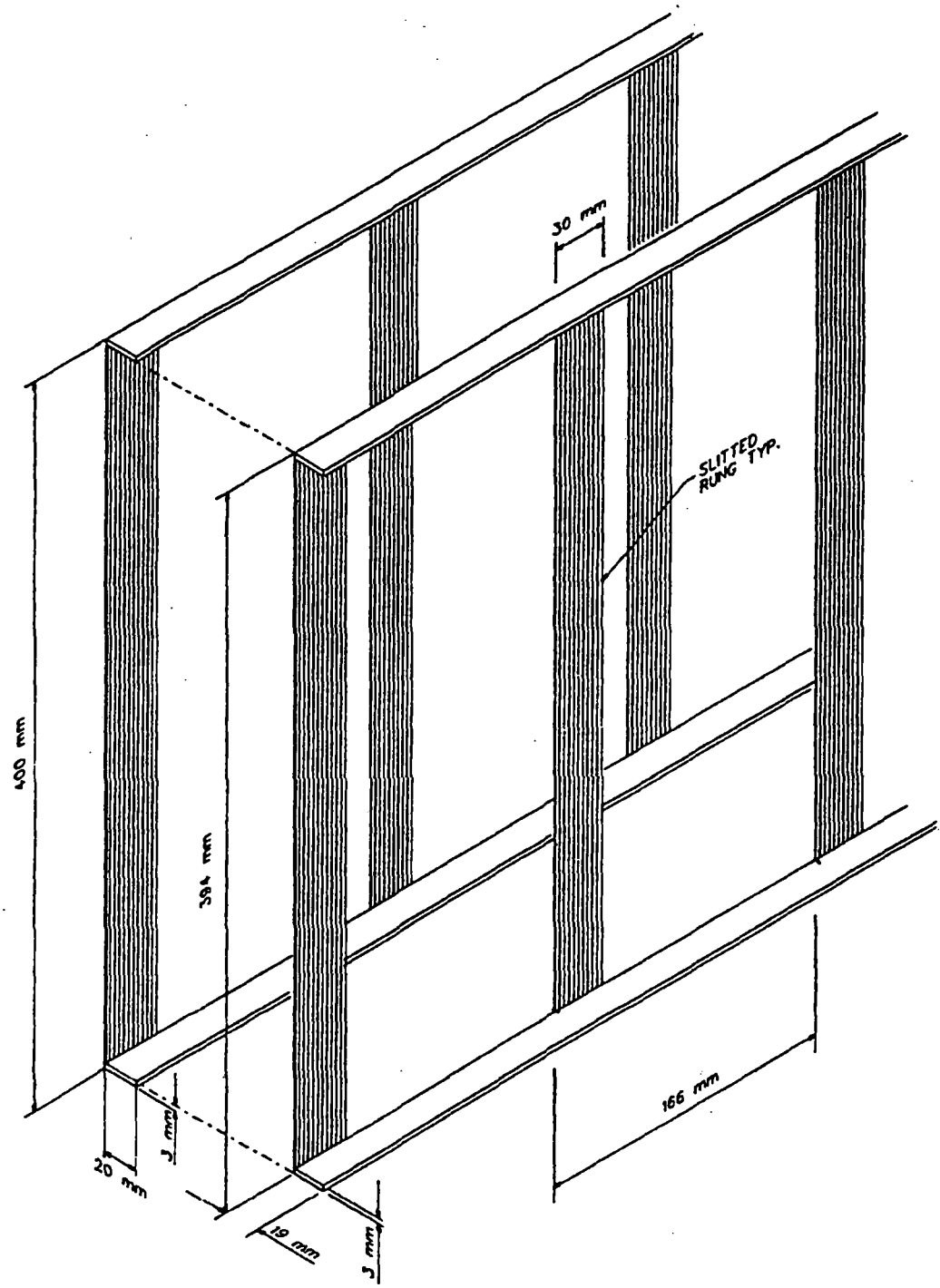

Figure C2-36 Levitation ladder elements

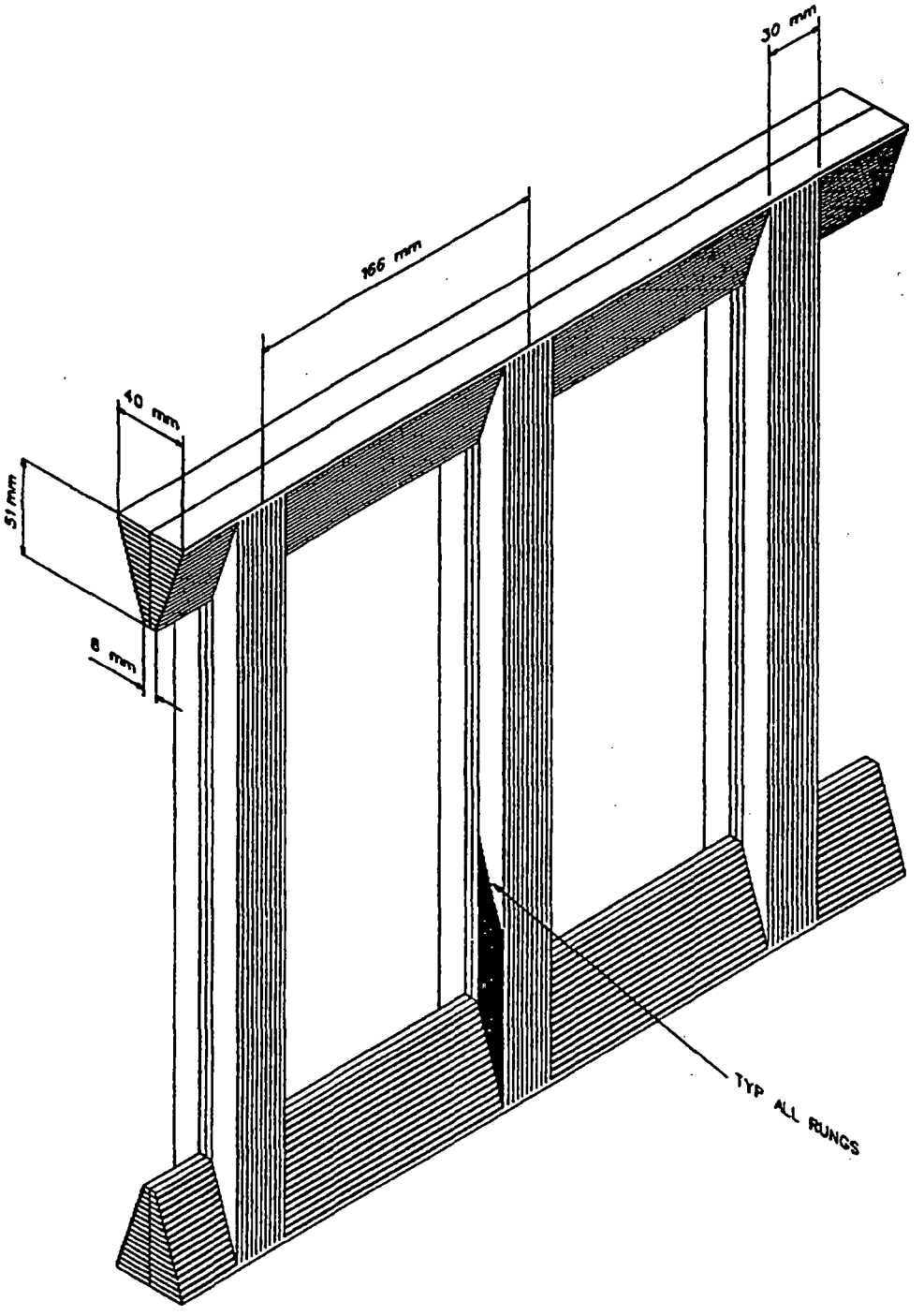

Figure C2-37 Levitation ladder

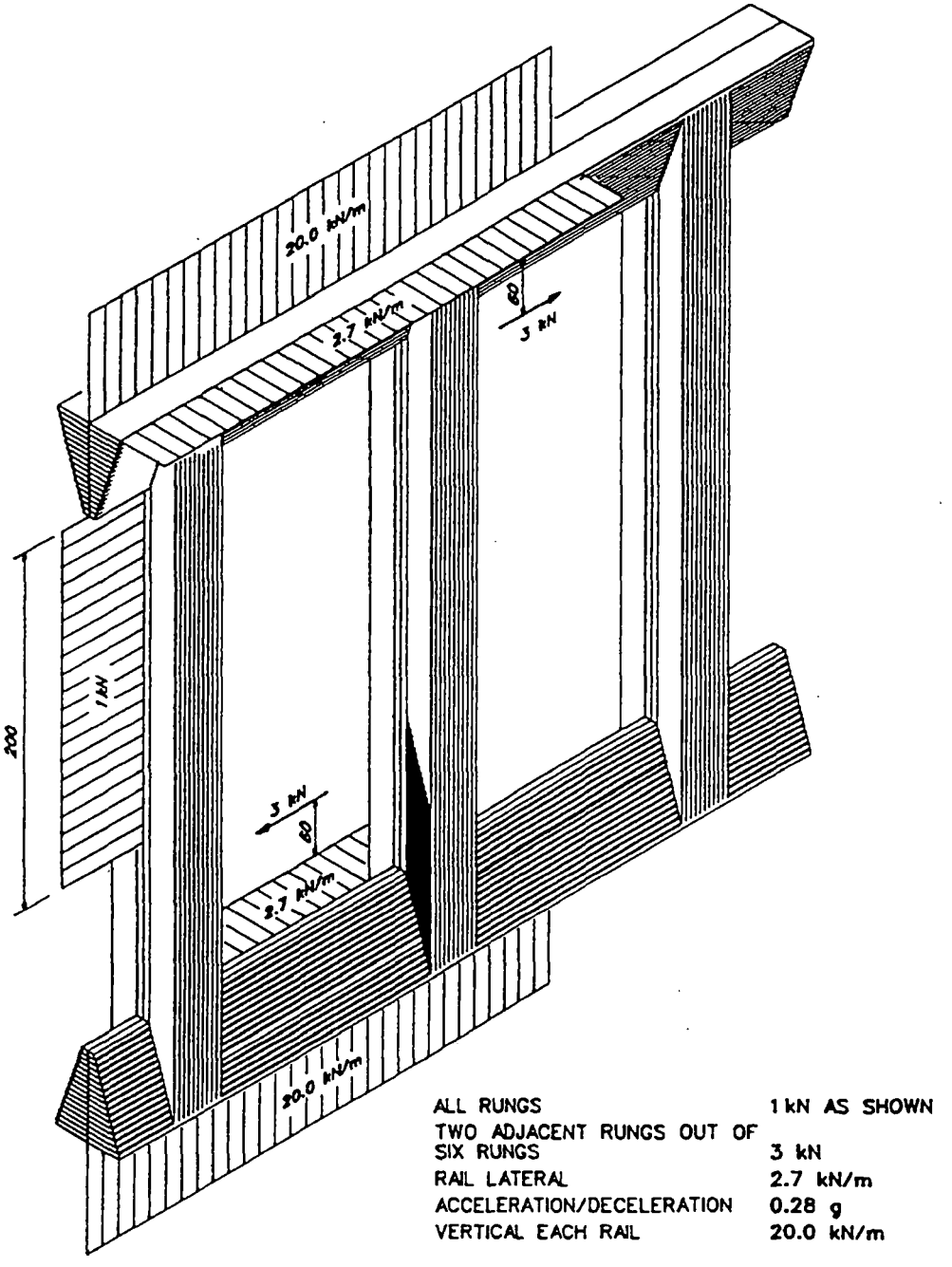

Figure C2-38 Ladder levitation forces

plate is bonded to the FRP stirrups. Four 16 mm Ø bolts fasten each mounting bracket to the girder. These anchors (DECO or similar) support a safe working force of 13.85 kN each. The maximum pullout force per meter guidance system is only ~10 kN.

The longitudinal force per meter magnet and girder side resulting from a 0.2 g acceleration/deceleration rate is 0.2 x 1.4 x 64850/24 x 2 = 378 Kg = 3.7 kN/m. The vertical propulsion cable sections (12 per meter and side) producing this force (3.7/12 = 0.308 kN per cable) are tied to the rungs of the levitation ladder.

On a 4-meter-long ladder section these longitudinal forces are 3.7 x 4 = 14.8 kN. Each 4-meter section is anchored at the center bracket by four anchor bolts with 26 mm Ø. These anchor bolts have a safe working load of 4 x 37.13 = 148.5 kN. Based on a friction factor of 0.2 the friction in this assembly is 29.7 kN thus providing a safety factor of 29.7/14.8 = 2.0.

The expansion joints of 4-meter-long ladder sections require for 55.5°C temperature changes an expansion space of $\Delta L = 0.0000213 \times 55.5 \times 400 = 0.5$ cm. An expansion joint detail is shown in Figure C2-39.

The propulsion/levitation/guidance system is protected by a 5 mm thick FRP cover plate to deflect debris and to reduce aerodynamic drag and noise.

The entire system will be assembled for each girder in a facility at the casting yard and mounted to the girder prior to transportation to its field location. After a period of about three months during which 60-70% of the creep deformations are expected to occur the propulsion/levitation/guidance system will be precision aligned utilizing variable dimension shims. This precision alignment will be done from a track mounted maintenance vehicle exceeding the girder length and equipped with surveying equipment capable of determining the present position of the levitation ladder. An on-board computer will compare existing X-Y-Z data to the offset dimensions of the ideal alignment. This comparison determines the size of the shims to be inserted at each bracket. Computer controlled robot arms will pull a ladder section 2.0 m in length away from the girder so that the shims can be inserted and anchor bolts fastened. The design of this maintenance vehicle and equipment will be similar to the TRI girder outfitting methodology but will require further study and development.

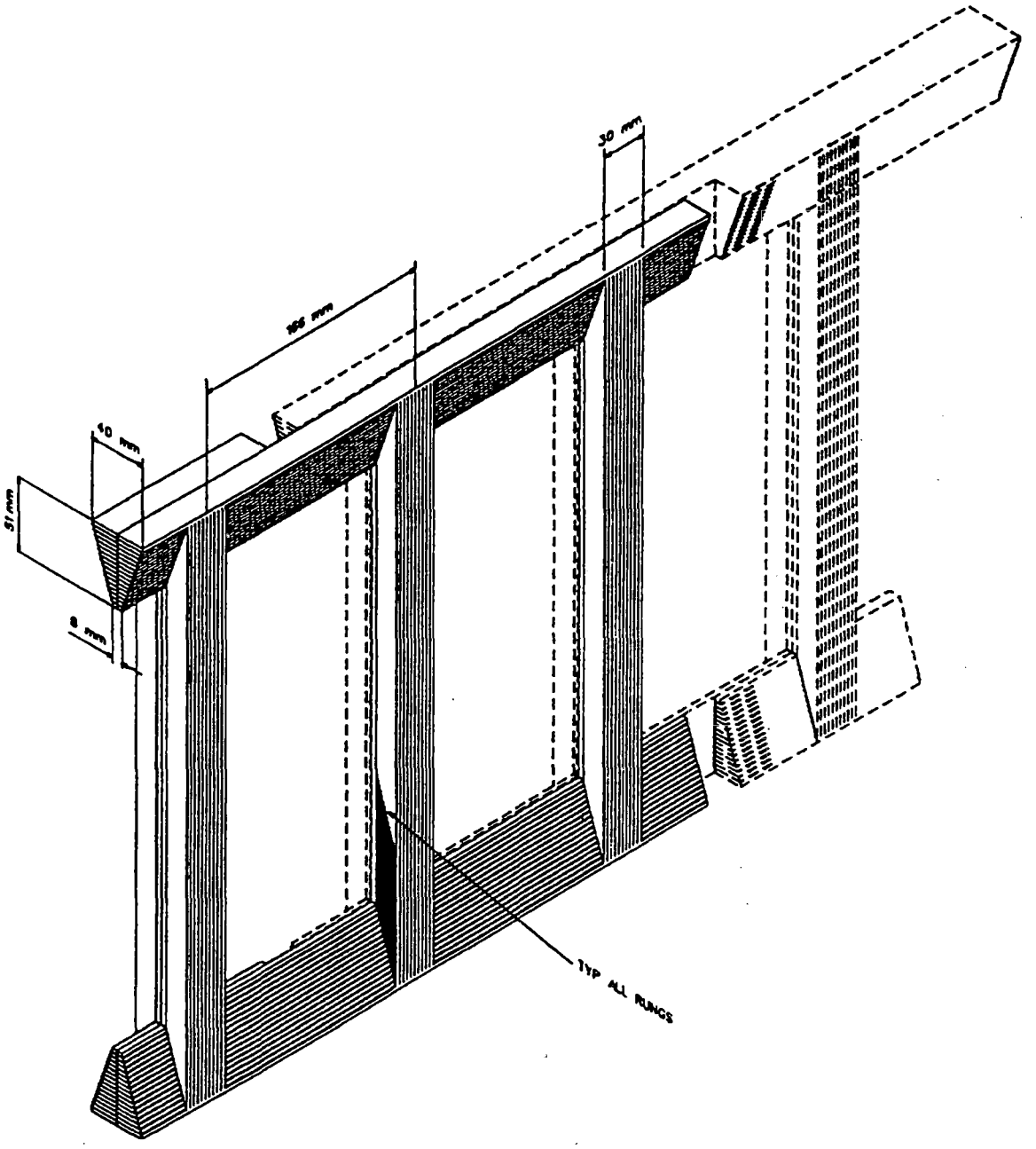

Figure C2-39 Levitation ladder joint

Entry/Exit Methods

The baseline switching concept is based on a flexible switch beam. This technology was developed in the late 1950s for overriding monorail systems. The flexible switch beam, with exterior dimensions equal to those of the girder sections, was constructed of high strength aluminum. Extensive testing proved the viability of this concept. These switches have been successfully deployed by many operative monorail systems in Japan and have proven their reliability and durability in many years of passenger operation. Transrapid uses steel in lieu of aluminum in its flexible switches at the Emsland test site.

The presence of strong magnetic fields in the upper area of the guideway girder precludes the use of ferromagnetic metal for our concept. The baseline switch has therefore been conceptualized based on FRP materials. The low modulus of elasticity ($E = 2.5 \times 10^6$ psi) assures that bending forces to move the switch beam from a straight to a curved track position are lower than for metal switches.

The bending principle in lateral direction is shown in Figure C2-40. The switch beam represents a simple span with cantilever arms of equal length on either side. The bending force P produces a triangular moment distribution on spans C-D and A-B since the reactive force at point A is equal to P. The triangular moment distribution between A-B and D-C flexes these sections to cubic parabolas which serve as transition curves. The constant moment at B-C produces a circular curve of radius R since $R = EI_y/M$. The lateral acceleration of a vehicle passing the switch and the jerk limit are $1.0 m/sec^2$ and $2.0 m/sec^3$ respectively. These limits and the design speed V determine the length of the transition curve c.

$c = 2v\ \Delta a/ä$ where

Δa = max lateral acceleration

ä = jerk limit

The offset between girder centerlines of the curved and straight track is determined by the width of the vehicle, safety clearance between vehicle and girder and one half the width of the adjacent girder (1.90+ 0.80+ 0.70 = 3.40 m).

This offset dimension equals $\emptyset \propto \times L$ where $L = 2c + a$ and $\emptyset \propto = Pc\ (c + a)/2EI$ (see Figure C2-40).

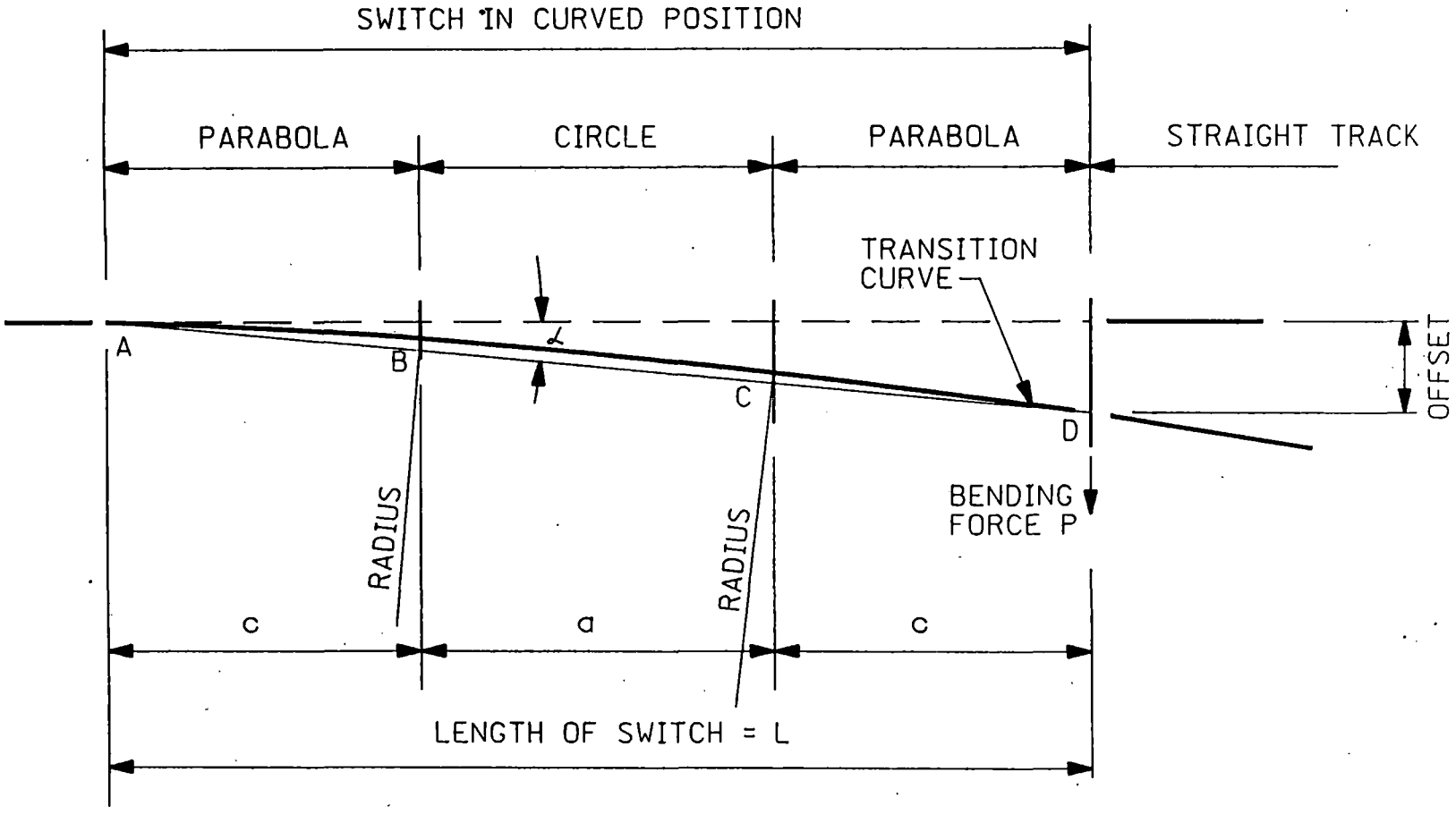

Figure C2-40 Baseline switch

The results of a design analysis for an operating speed of V = 32 m/s and a 3.4 m offset between girder center-lines are given in Table C2-1. The FRP cross-section is shown in Figure C2-41. The design of FRP switches is controlled by live load deflection limits.

The baseline flexible switch can be designed for higher speeds. For 200 km/hr = 55.5 m/s the critical dimensions are as follows.

Transition curve length c = 55.5m
Radius $R = v^2/\Delta a = 55.5^2/1.0 = 3080$ m
M max. from lateral bending = 207.0 kN m
Bending force P = 207.0/55.5 = 3.729 kN
Length L = 2c + a
Offset = 3.4 m = $\emptyset \propto$ x L
$\emptyset \propto$ = Pc (a + c)/2 EI
a = 41.7 m
L = 2 x 55.5 + 41.7 = 152.7 m

Intermediate supports are required to satisfy life load deflection limits.

Construction and Fabrication Techniques

Upon completion of site preparation activities and the completion of construction roads, required in certain areas, construction of foundations and support structures will commence. The production cycle of foundations and supports will precede girder production by at least one month. Contrary to the poured-in-place approach for foundations and supports, the guideway girders will be prefabricated in casting yards. The girders will be poured in reusable steel forms. A production cycle of 24 hours per girder and form can be achieved by steam curing the concrete. With 10 forms per casting yard producing 8 girders per day, 2.5 years (i.e., 500 working days) will be required for each 50 km section of guideway (i.e., 4000 girders). An area 410 m x 90 m will be required for storage of 135 to 160 girders. Girders will be partly pretensioned to reduce costs and to allow for handling. Post tensioning for live load conditions will be done after 28-day concrete strength has been obtained. The propulsion/levitation/guidance system will be assembled in a separate facility located within the casting yard. This equipment will be attached to the girders in the casting yard prior to transportation to their respective site location. See Figure C2-42.

Table C2-1 Baseline Switch Data

Design Speed	32 m/s
Six Spans	4 x 18 m; 2 x 14 m
Length	100 m
Fiberglass modulus	19 GPa
Ultimate stress	241 MPa
Allowable stress	96 MPa
Section	1.2 m x 1.8 m
Plates – top/bottom sides	4 cm 1.8 cm
Between girder cl	3.4 m
I_{yy}	0.0332 m^4
I_{xx}	0.0896 m^4
Lateral acceleration	1 m/s^2
Lateral jerk	2 m/s^2
Bending force	20 kN
Bending stress	11.4 MPa

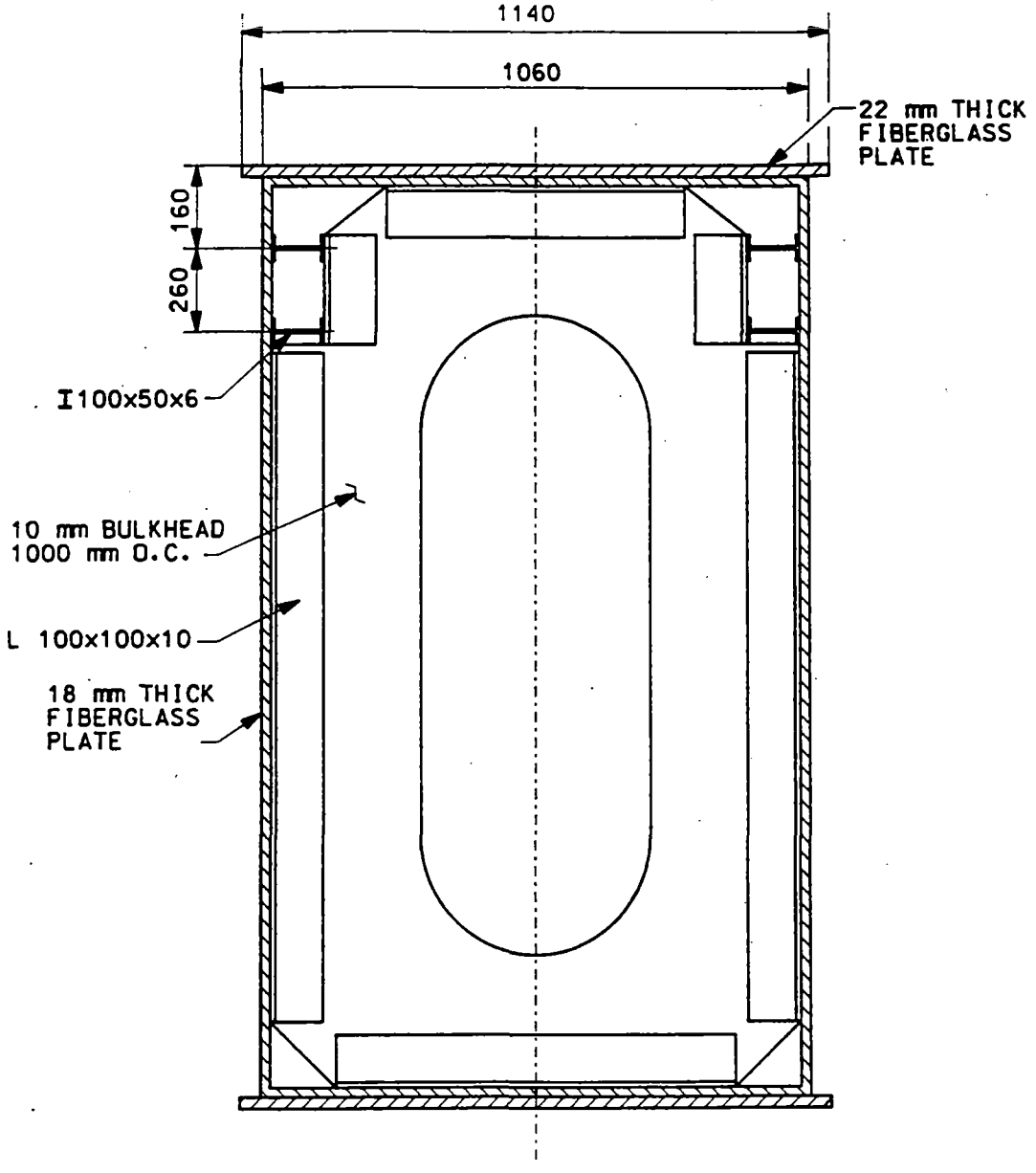

Figure C2-41 Baseline switch section

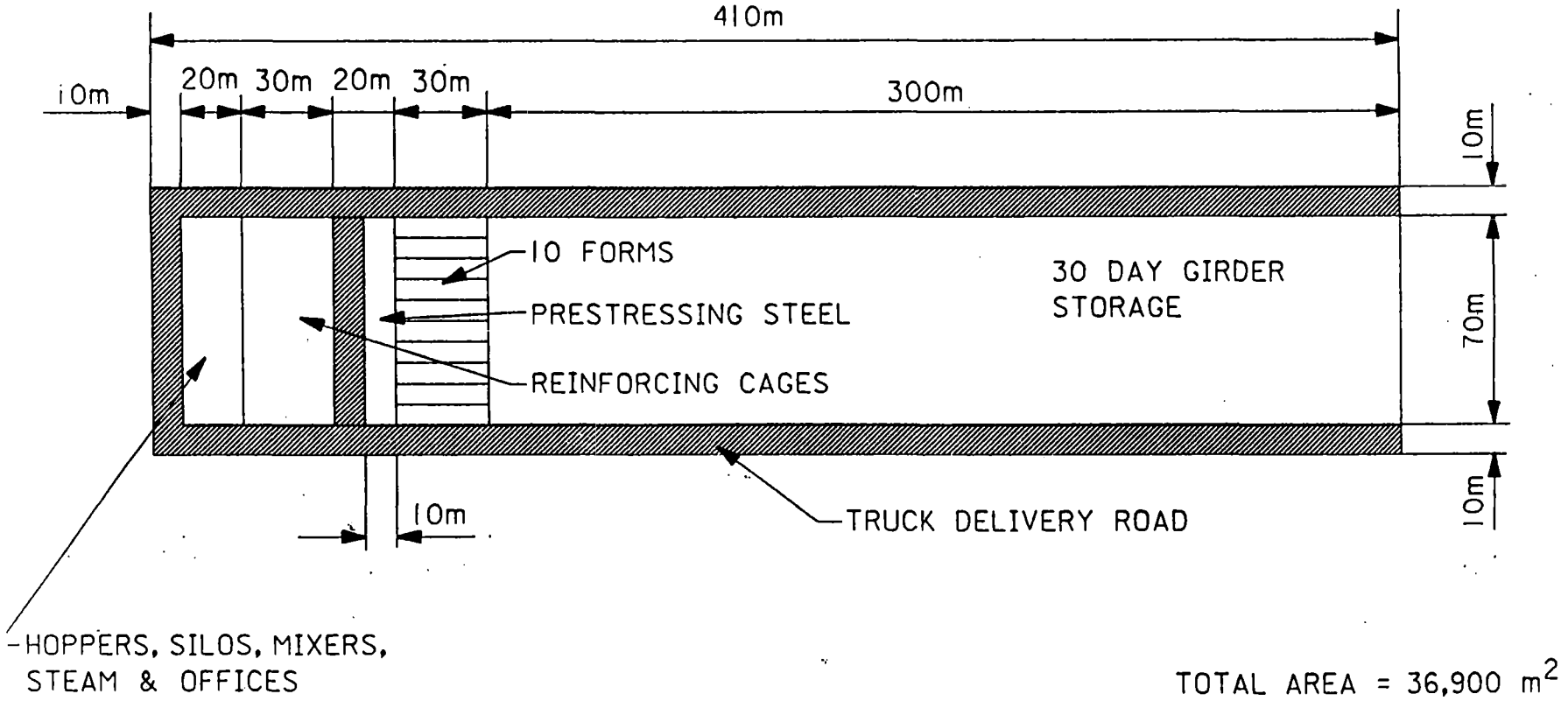

Figure C2-42 Casting yard for girder production

3. BASELINE MAGNET DESIGN

3.1 CONDUCTOR SELECTION

Analytical and experimental investigations in the fusion program have demonstrated the advantages of the cable-in-conduit conductor (CICC) approach from the operational stability standpoint. A preliminary study concerning the advantages of using this type of conductor in maglev applications has also been performed (R.J. Thome, et al, "Application of Cable-in-Conduit-Conductor to Maglev Magnet Systems," Final Report prepared for VNTSC under Contract No. DTFR53-91-C-00042, July 31, 1992, PFC\RR\92-12).

It can be shown that CICC conductors have an order of magnitude higher energy margin for stability against disturbances than epoxy-impregnated windings. Furthermore, Nb_3Sn has a much higher energy margin than NbTi at a given temperature. In view of these results we have selected the CICC approach as the baseline conductor configuration for this program.

Figure C3-1 shows a photograph of a CICC which has an outside dimension of about 5x5 mm (0.2x0.2 in). The characteristics of the conductor are summarized in Table C3-1.

The conductor described above was selected because we have had it manufactured at this size for another program, hence it represents a demonstrated capability. However, it was not intended for this application. We will assume that we can scale it up or down in size as we require and achieve the same overall current density. This is correct to first order since it is a cable of conductors and an adjustment to current capacity can be made by adding or subtracting strands in the cable or individual conductors. Minor variations in Nb_3Sn CICC capability from those assumed will have a minor impact on coil module weight or other general features.

The critical current density for this conductor is shown in Figure C3-2 as a function of the magnetic flux density experienced by the conductor and the operating temperature. This current density is based on the current carried, divided by the outer envelope area of the conduit enclosing the cable. The maximum flux density in the module conceptual design for this study is also indicated in Figure C3-2. The operating current density must be selected to be a fraction of the critical current density so as to allow for stability of the conductor to operational disturbances which could take the form of temperature excursions due to cryosystem fluctuations or losses generated by the conductor under transient conditions.

Table C3-1
Preliminary Characteristics of Maglev Conductor

Conductor Type	**Cable-in-Conduit**
Sheath Material	304 SS
Wall Thickness	0.38 mm (0.015")
Outer Dimensions (0.195x0.195")	4.95x4.95 mm
Inner Dimensions	4.2x4.2 mm (0.165x0.165")
Strand Material	Nb_3Sn with Cu
Number of Strands	27
Strand Diameter	0.71 mm (0.028")
Strand Area	10.69 mm2 (0.0166 in2)
Cable Space Area	17.64 mm2 (0.0272 in2)
Helium Area	6.95 mm2 (0.0106 in2)
Void Fraction	39%

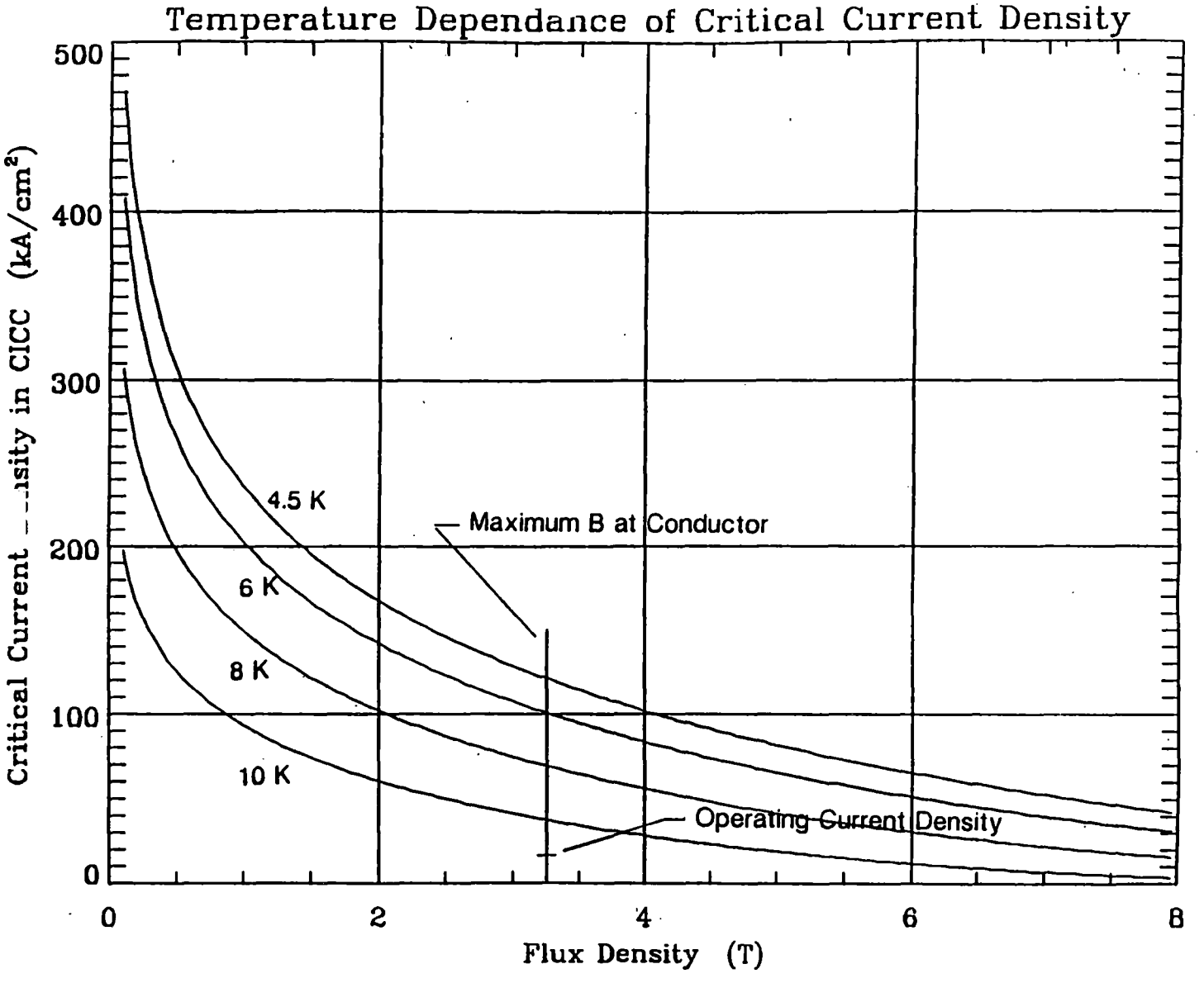

Figure C3-2 Design operating point for superconductor

The temperature and the magnetic flux density are not uniform throughout the winding in the coil system. In our case, the magnetic field experienced by the winding at full current will range from zero to 3.3 T and the temperature will be a maximum of 8 K. If the maximum field point and maximum temperature point in the winding coincide, then this would be the point of lowest margin relative to the critical surface for the conductor. Hence, in the winding for our case, the operating fraction of critical current density will be 24 percent or less. This should be ample margin to allow for operational uncertainties at this stage of the design process. The corresponding conductor current density for the design point is 1.62×10^8 A/m2.

The selection of an operating temperature must be done in light of the impact on conductor operating requirements as well as system level tradeoffs such as weight and auxiliary power required. If a refrigeration system is used, then there can be a substantial weight reduction and power input reduction if the operating temperature is raised. If liquid helium is carried on board, then the operating point selected may be somewhat lower than 8K, in which case we would have an increase in energy margin, or we could operate at a somewhat higher current density and reduce the weight of the winding.

The design operating current density has been selected as 1.62×10^8 A/m2 for this conductor. The number of amp-turns per coil required for this application depends on the total number of coils, the lift to be provided and the amp-turns required to provide sufficient thrust. For a preliminary design point, a reasonable lift and thrust can be achieved with a coil of this type if it provides 4.0×10^5 amp turns. This amp-turn requirement, together with the selected conductor current density and a conductor with the dimensions of the one in Table C3-1, leads to an operating current level of 4,200 A; a conductor with one-half the dimensions of the one in Table C3-1 would have an operating current of 1,050 A.

3.2 MODULE CONFIGURATION AND COMPONENT FUNCTIONS

This section describes features of the superconducting coil module designed as part of this study.

Figure C3-3 shows an external view of the module. The basic package is 4.0 m long, 0.90 m wide, and 0.16 m thick. The outer vessel is the ambient temperature portion of the cryostat and is constructed from aluminum plate nominally 9.5 mm (0.375 in) thick. The vehicle mounts (not shown) will be on the surface of the wide plate with suitable stiffeners to carry the main load to the location on the wall where the cold mass supports are anchored internally.

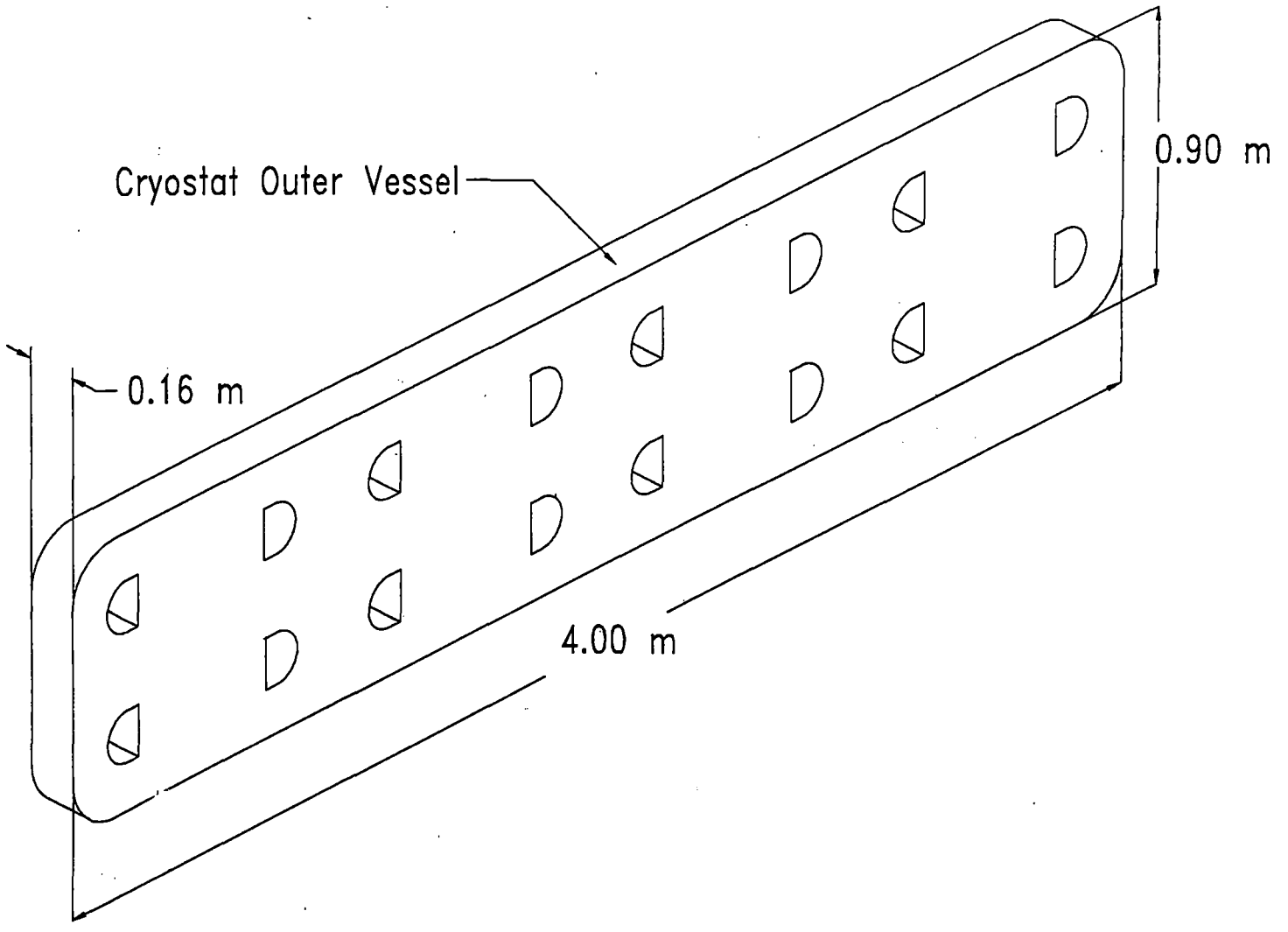

Figure C3-3 Coil levitation module

The 16 penetrations through the cryostat also pass through the center of the coils. The walls of the penetrations help to stiffen and support the wide flat plates of the cryostat outer vessel against the external atmospheric pressure and the vacuum within the vessel.

Figure C3-4 is a view of the module with the top cover plate and thermal radiation shield removed to show the internal components. The vehicle mounts will pass the loads to the cold mass supports, which, in turn, pass the loads to the coil support frame that is within the thermal radiation shield. The purpose of the latter is to intercept thermal radiation at a temperature intermediate between the ambient temperature of the cryostat and the cold coil system within and thus reduce the heat load on the cryogenic system. The radiation shield is also carried by the cold mass support, which will be described in more detail in a later figure.

Another view, with sections, is shown in Figure C3-5. Because of the high operating current density, the winding cross section is relatively small. This, coupled with an efficient structural and cold mass support system, allows the distance from the centerline of the coil winding to the outside of the cryostat to be relatively small. In this case we estimate that this can be 0.05m.

The cold mass supports and coil support structure are designed to minimize the distance from the coil center to the levitation and propulsion coils, hence the coil is not mounted in the center of the cryostat in this design. If both sides of the module surface were to be needed for electromagnetic interactions, for example, as in some of the conceptual switch designs, then a redesign would be in order and possible.

A better view of one of the cold mass supports is shown in Figure C3-6. It consists of a sequence of nested tubes to give a long thermal path from the connection to the vehicle mounts at room temperature to the coil at low temperature. The innermost tube is a stainless steel tube that spans the distance across the coil form/structure to attach to the coil at each end.

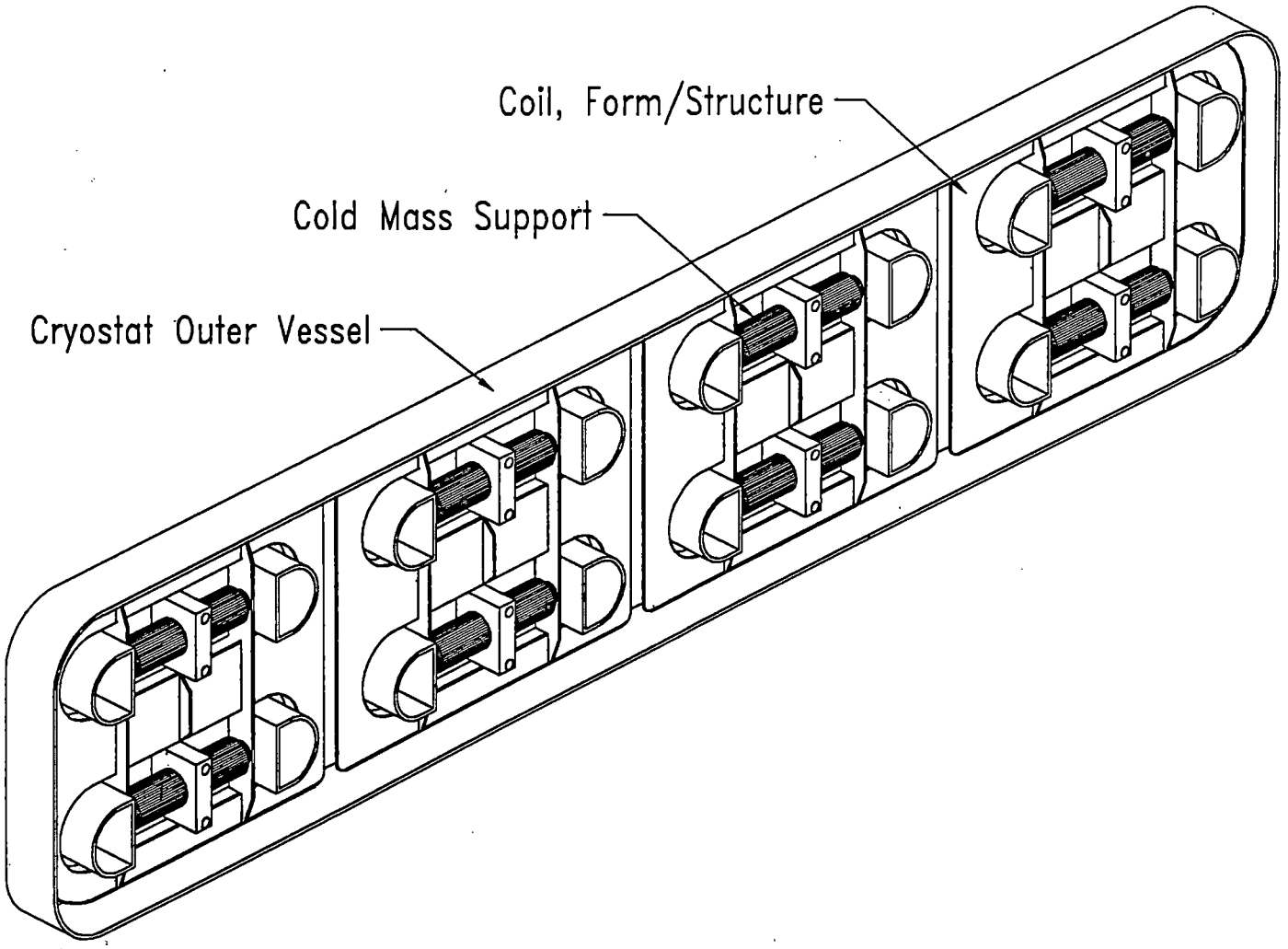

Figure C3-4 Major components of 8 coil module (cryostat cover and thermal radiation shield removed)

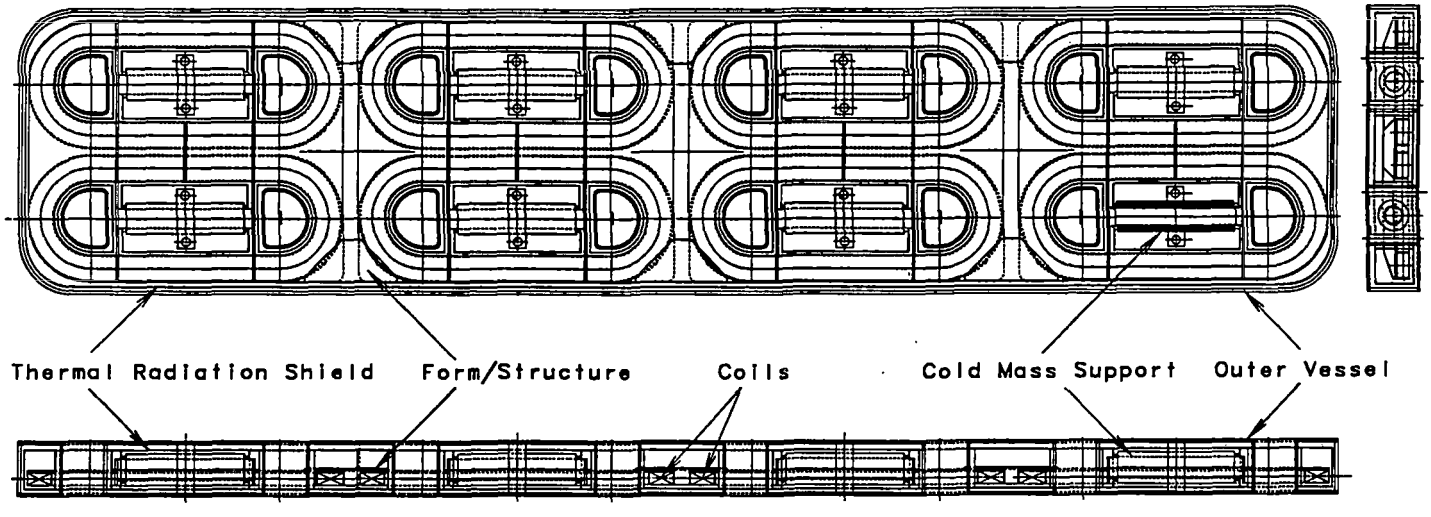

Figure C3-5 Major components of 8 coil levitation module

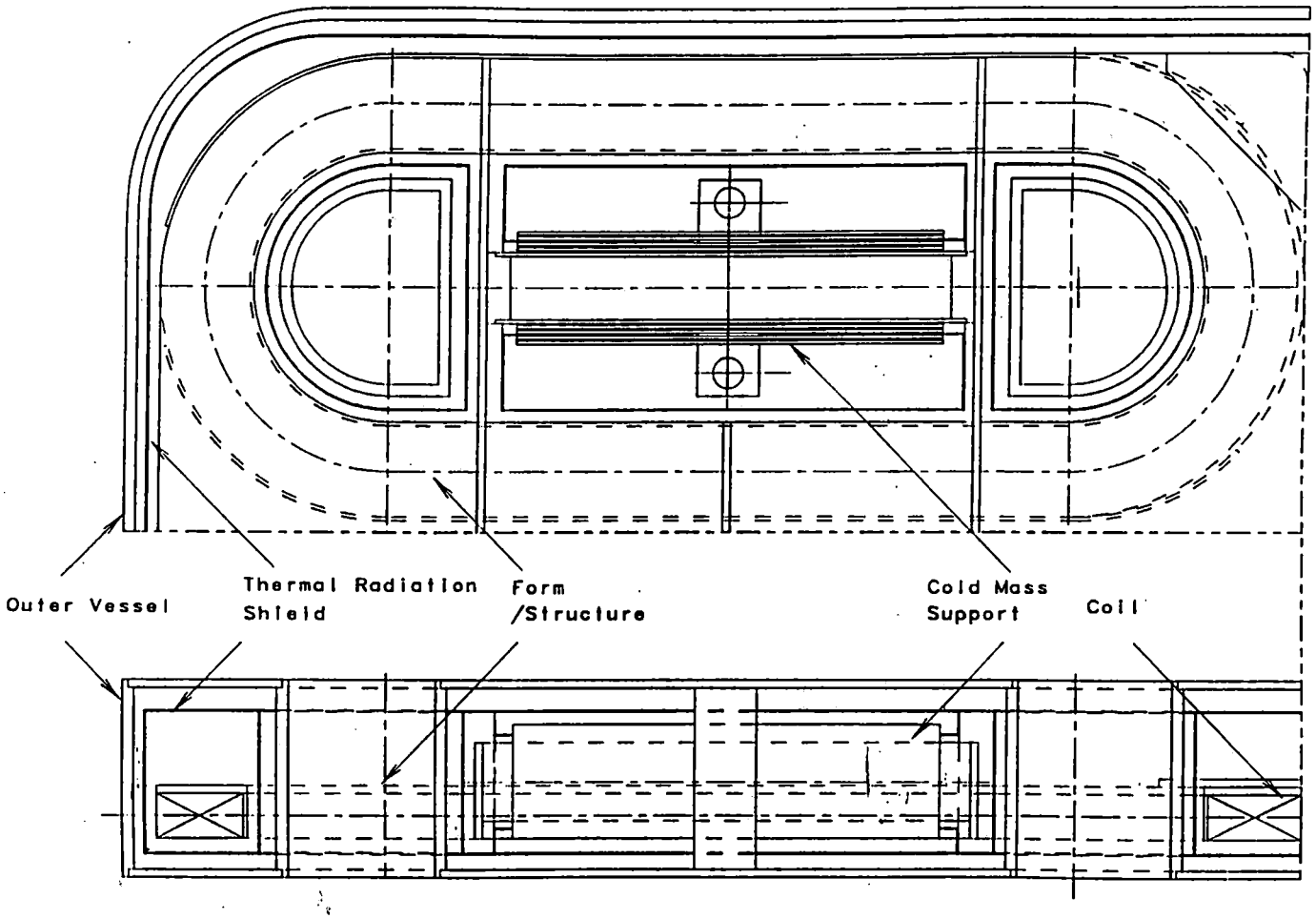

The above data is subject to the disclaimer printed on the inside cover.

Figure C3-6 Levitation module components

The coil form and structure are of stainless steel and support the winding which consists of the type of conductor shown in Figure C3-1. The conductor is insulated, wound on a form, removed, externally insulated with a ground wrap and mounted on the stainless steel form for assembly to the cryostat. The winding cross section is relatively small compared to the cryostat. This implies that variations from assumed requirements for levitation capability or variations in conductor properties from the values assumed could be compensated by increasing or decreasing the amp-turns without a major impact on module size or overall weight. The overall weights of module components have been estimated and are given in Table C3-2.

Table C3-2
Estimated Weights for Superconducting Coil Module Components
(400,000 AT per coil per module)

Component	Weight [Kg]
8 Coils	215
Coil Forms/Structure	258
Radiation Shield	82
Cold Mass Supports	54
Fittings & Mounts	20
Outer Vessel	272
Misc. @ 5%	45
Total Module Weight	946

The weight distribution indicates that the coils and the outer vessel are the major elements in the total weight. These may be reduced if we find that the design requires fewer amp-turns or if we reduce the conservatism in the relatively low current density assumed. The outer vessel is a prime area for R&D since we may be able to reduce the weight further by using titanium or fiber-reinforced composites in place of aluminum.

3.3 STRUCTURAL DESIGN

Figure C3-7 shows a coil and frame model as well as the local forces of electromagnetic origin at the nodes. These were used in a structural analysis of the coil form and structure. Analyses show that the loads on the coil are dominated by the coil self loading (i.e., zero speed loads) and that loads due to lift, drag, and guidance are relatively small.

3.4 COIL SYSTEM CHARGE AND DISCHARGE

Figure C3-8 is a schematic illustrating two relatively standard methods for charging a superconducting coil system and a third, innovative method that we propose as our baseline.

In method A, the superconducting coil is located within its cryogenic container or cryostat and connected to a power supply outside the cryostat via a pair of current leads passing through the cryostat boundary. These current leads are usually specially designed to reduce thermal conduction along the leads from ambient conditions into the cryostat because each watt of heat load into the cryostat represents a significant power requirement for the refrigeration or liquefaction system supplying the cryogen for the coil system. Alternately, in an "open" cryogenic system, a significant volume of liquid cryogen would have to be carried to support the heat load for this part of the total requirement for the length of the mission. For example, a well-designed pair of current leads will still produce a heat load of about 2 watts to the cryogen per thousand amps of current carrying capacity per lead pair. The power required by a refrigerator to support this part of the total heat load at low temperature is about 800-1000 w per watt of refrigeration required.

The persistent switch shown is optional in method A, in that one may choose to have none, charge the coil system with the power supply, and leave the power supply connected and "on" throughout operation. This is unlikely, however, because of the high heat load penalty. A more likely scenario would involve detachable leads and a persistent switch as in method B.

The persistent switch is typically a length of superconducting wire (possibly in coil form) connected across the terminals of the coil and located within the cryostat. It also has a heater which can be activated through relatively small current leads which pass through the cryostat boundary to a small power supply outside. To charge the main superconducting coil system, the switch on the main power supply is left open while the heater power supply on the persistent switch is activated

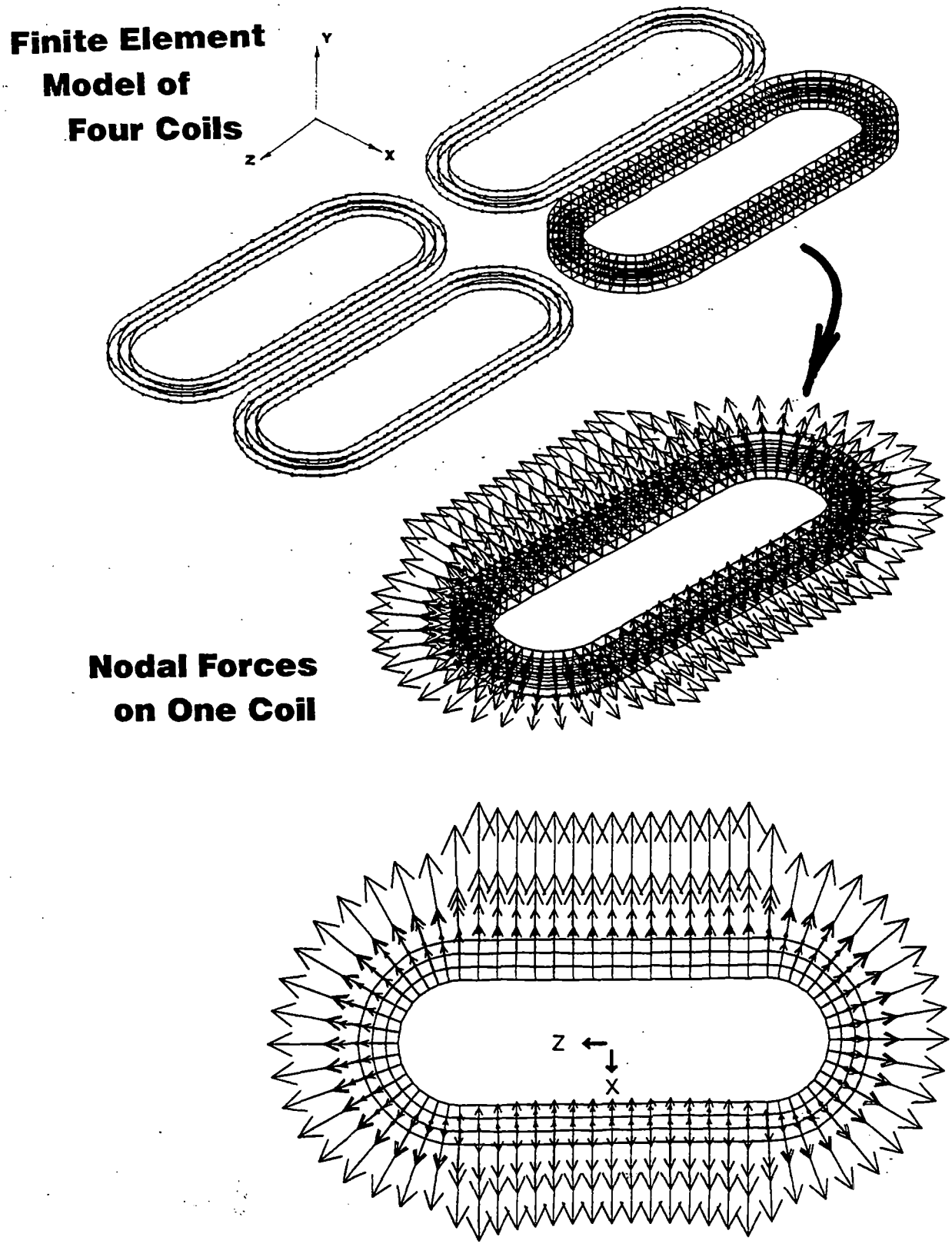

Figure C3-7 Load distribution for structural analysis

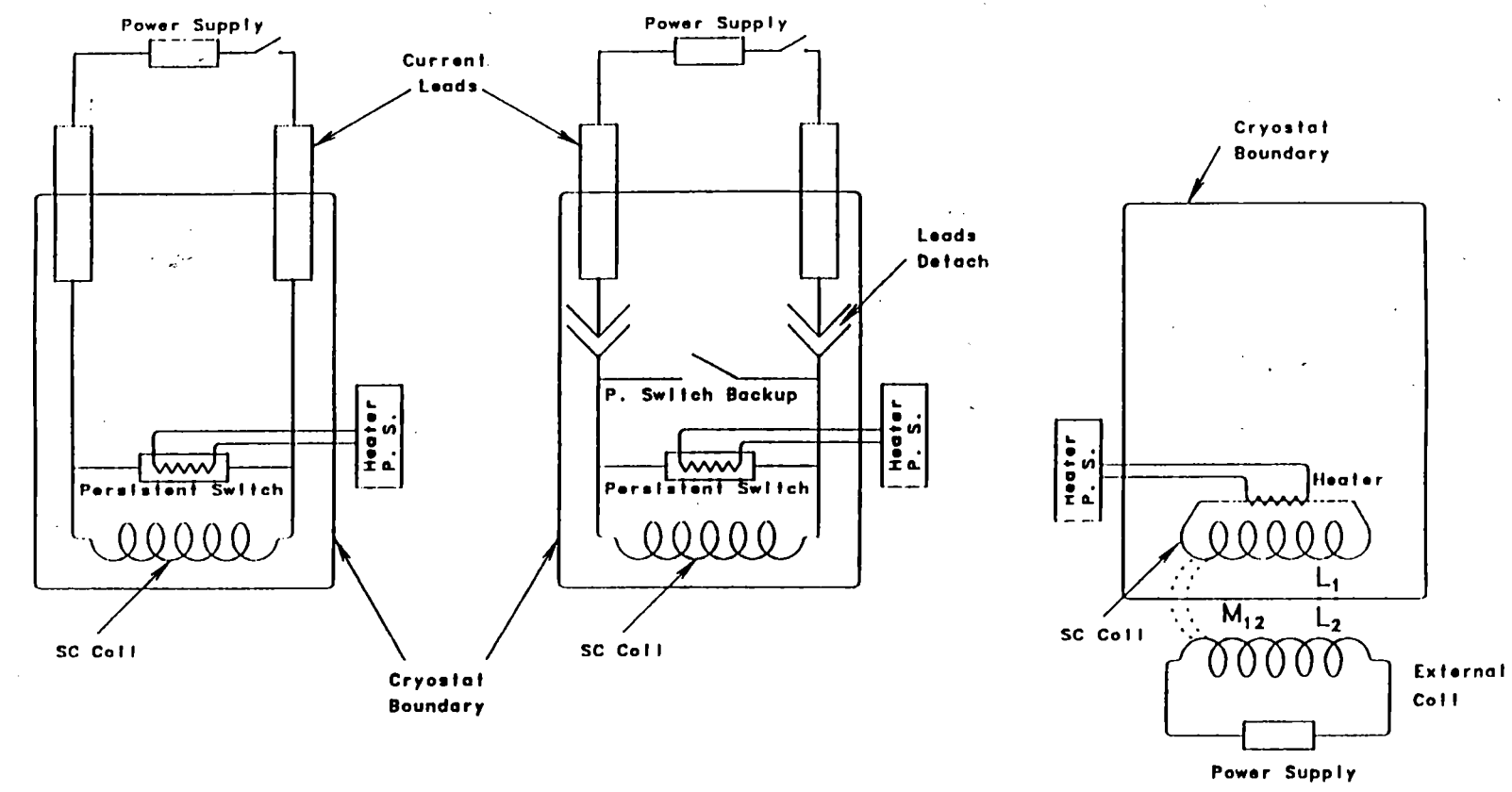

A) SC Coil System with Permanent Current Leads

B) SC Coil System with Detachable Current Leads

C) SC Coil System with no Current Leads + External "Flux" Supply

MIT-PFC

Figure C3-8 Schematic of three options for charging a superconducting coil for maglev applications

to a current level that raises the heater output until the persistent switch superconducting wire is above its critical temperature so that it is not superconducting. The level of resistance in the persistent switch at this point is selected when it is designed so as to be consistent with the desired charging vs time scenario. The main power supply switch is now closed and the main power supply current raised to the desired operating current level. The heater power supply is then turned off and the persistent switch is designed to allow the temperature of its wire to drop back below its critical temperature so that it is again superconducting. The current from the main coil power supply may now be turned down to zero without significant change to the current flowing through the superconducting coil because it is short circuited by the superconducting wire in the persistent switch. The current in the circuit will decay over time, depending on the inductance of the circuit and resistance (typically, only the resistance of the joints is significant and can be made quite small, i.e., of the order of 0.5e-9 ohms per joint, thus yielding a very long current decay time constant).

The approach schematically shown in method B is operationally identical to that in method A for charging the superconducting coil when the leads are connected to the coil. However, two additional features are shown in the schematic.

A back-up switch for the persistent switch is shown for reliability purposes. This may be another switch of the same type or a switch which is closed mechanically and has a high resistance so that it does not interfere with persistent switch operation, but provides protection for coil overvoltage in the event the persistent switch fails open while the coil is charged.

The other, more significant, feature in option B is that the current leads are made to be detached after coil charging, persistent switch closure (transition to superconducting state), and main power supply turn-off. This requires complex mechanical connections within the cryostat that can be detached from outside and that can allow complete removal of the leads or moving them far enough to significantly reduce the heat transfer down the leads into the cold cryostat. In this way, the heat load during coil operation can be reduced.

The approach in method C is the baseline approach for this system and has no current leads coming through the cryostat boundary from the main superconducting coil or circuit. The terminals of the superconducting coil are connected (short circuited) within the cryostat, but a length of the wire in the coil has a heater in close proximity to it. Outside the cryostat, another coil system, which may be conventional or superconducting, is brought near the superconducting coil. Both coils are assumed to be initially uncharged or in a zero current condition.

The current from the heater power supply is increased until the temperature of the main coil superconducting wire near the heater is above its critical temperature and, therefore, resistive. This becomes a resistance in series with the main coil. The current in the external coil is now raised to the necessary DC level by its power supply. During this time a small current will be induced in the main superconducting coil and will decay in time with a time constant dependent on circuit parameters. The heater power supply is now turned off and the main coil portion of wire is allowed to regain its superconducting condition. Note that operation at this point is somewhat different than a persistent switch because the wire is not required to carry any significant current while recovering its superconducting condition as it must in cases using a persistent switch. Finally, the external coil power supply or a switch is used to discharge the external coil. This induces a current in the main superconducting coil in the cryostat by transformer action.

The principles underlying this method are straightforward and have been demonstrated in other applications. For example, it is the method used to induce the plasma current in a Tokamak (at the MIT Plasma Fusion Center and elsewhere), where the plasma is analogous to the main superconducting coil in this method and the ohmic heating transformer (coil) is analogous to the external coil system in this method. As another example, an analogous process has been used at the MIT Plasma Fusion Center to induce a large current through a single turn superconducting coil to deduce the resistance of a joint.

3.5 HEAT LOADS AND CRYOSYSTEM

Figure C3-9 is a schematic that shows the six bogies per vehicle, with each bogie carrying two coil system modules (cryostats). Each module contains eight superconducting coils. Therefore, the total number of coils on one vehicle is 96.

The coils utilize a Nb_3Sn cable-in-conduit-conductor in which the conduit serves as the carrier for the supercritical helium, working fluid for the cold mass. The coils are not immersed in a bath of liquid helium. The working fluid terminal conditions for each coil are designated in the schematic as "i & o."

A single inlet and outlet for a cryostat is used, and the coils are connected to manifolds within each cryostat. Hence, each coil has essentially the same cryogenic inlet and outlet condition.

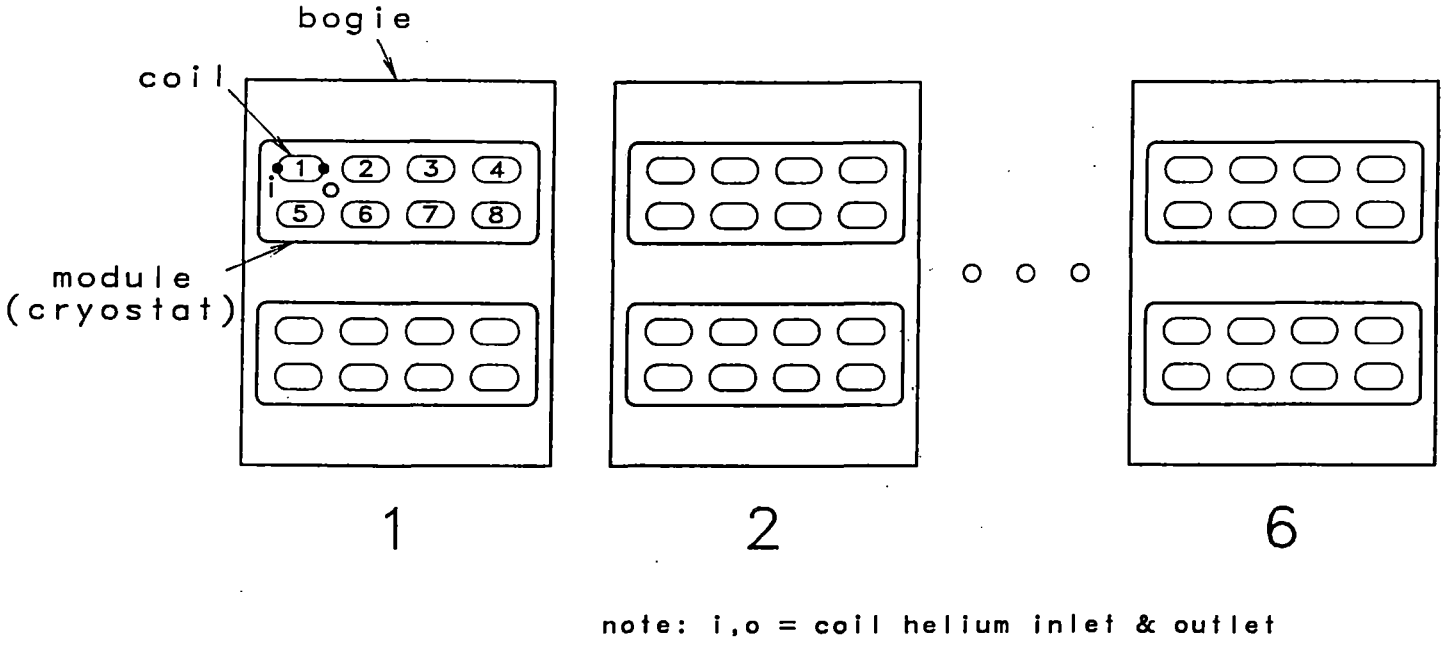

Figure C3-9 Schematic defining coil, module and bogie nomenclature

Table C3-3 lists allowable terminal conditions and flow rates for any given coil in the set. The table has three parts depending on Q, the total heat load to the single coil cold mass. The latter includes AC losses, thermal radiation and conduction. Values are given for Q = 0.25, 0.50, and 1.0 watt/coil. For each heat load, the table gives an assumed coil inlet temperature, T_i, and inlet pressure, P_i, where the former ranges from 4.5 to 5.5 K and the latter ranges from 4 to 5 atm. In most cases, the coil outlet temperature, T_o, has been restricted to 6.0 K because operating at this level would allow a small reduction in the present baseline coil weight at some point in the future, if that is found to be a favorable trade relative to cryosystem operation. In the last two rows, the coil outlet temperature is 8.0 K because this is allowable for the baseline coil design. Operating at this level would probably not allow a coil weight decrease in the future, but may be attractive from the cryogenic system standpoint. Each row also gives the required mass flow rate, m, and pressure drop, ΔP, for the single coil inlet and outlet conditions in that row. Note that the required flow rates per coil are of the order of 0.1 g/s and the pressure drop per coil (cryostat) is only a few psi. These are relatively modest requirements for the cryosystem.

Table C3-4 shows the breakdown of the estimated heat loads for the superconducting coil systems. They were computed and provided to cryogenic system specialists, together with the pressure drop and flow rate requirements in Table C3-3, to evaluate cryosystem alternatives and to recommend a baseline for conceptual design purposes. The alternatives that were considered, including the advanced cryosystem concepts that could be adopted in the future are summarized in Part D, Section 4.3.

Table C3-4 is based on a total of 12 modules with 8 coils per module, and a module (cryostat) size of approximately 4 m x 0.9 m x 0.17 m. The total heat load to the cold mass is 109 w. The greatest uncertainty is in the level of AC losses and losses in transfer lines.

One-half watt per coil has been assumed for AC losses in the table, but cryosystem options were evaluated for a range from 0.25 to 1.0 w per coil. The second largest uncertainty is in transfer line losses at this stage of the design, so we have allowed for it in Table C3-4 through a substantial assumption for contingency.

Table C3-3
Inlet Conditions, Mass Flow Rates, and Pressure Drops That Correspond to a Given Single Coil Heat Load and Outlet Temperature.

Q (w)	T_i (K)	P_i (atm.)	$\dot{m}$ (g/s)	T_o (K)	ΔP (psi)
0.25	4.5	4.0	0.02122	6.0	0.24
0.25	5.0	4.0	0.02641	6.0	0.37
0.25	5.5	4.0	0.03975	6.0	0.82
0.25	4.5	5.0	0.02854	6.0	0.37
0.25	5.0	5.0	0.03775	6.0	0.63
0.25	5.5	5.0	0.06330	6.0	1.68
0.50	4.5	4.0	0.04165	6.0	0.81
0.50	5.0	4.0	0.05100	6.0	1.22
0.50	5.5	4.0	0.07190	6.0	2.44
0.50	4.5	5.0	0.05655	6.0	1.28
0.50	5.0	5.0	0.07400	6.0	2.15
0.50	5.5	5.0	0.11580	6.0	5.04
1.00	4.5	4.0	0.07851	6.0	2.60
1.00	5.0	4.0	0.91950	6.0	3.65
1.00	5.5	4.0	0.11410	6.0	5.92
1.00	4.5	5.0	0.10930	6.0	4.23
1.00	5.0	5.0	0.13690	6.0	6.60
1.00	5.5	5.0	0.18150	6.0	11.76
1.00	4.5	4.0	0.02915	8.0	0.75
1.00	4.5	5.0	0.03232	8.0	0.74

Table C3-4
Heat Load Budget Estimate for Multiple Levitation Modules

No. Modules		12
No. of Coils per Module		8
No. Independent Circuits		12
Total Heat Loads to Cold Mass		
0.28 w.	Thermal Radiation/module	3.4
0.75 w.	Conduction (Cold Mass Spts)	9.0
0.5 w.	per Cryogenic Fitting	12.0
5E-10 ohms, joint resistance		0.2
4 w.	AC losses per module	48.0
50%	(Contingency + Trnsfr Lines)	36.3
	Total to Cold Mass, w.	108.8

Note: Joint resistive loss assumes 1050 A operation, 3 joints per coil and 1 persistent switch per circuit (2 joints per switch)

Total Head Loads to Liquid nitrogen or Intermediate Temp Shields

5.40 w.	Thermal Rad Shield/module	64.8
2.5 w.	Conduction (Cold Mass Spts)	30.0
50%	(Contingency + Trnsfr Lines)	47.4
	Total Intermediate Temperature Heat Load, w	142.2

The baseline cryosystem that was selected to satisfy the above requirements is described in R. Herring, G. Kinard, W. Miller, & D. Nahmias, "Closed Maglev Cooling System Without On-board Refrigerators," Air Products & Chemicals, August 20, 1992, a final report prepared under contract to MIT as part of this conceptual design study. The concept involves storage of an inventory of helium on board the vehicle to absorb the ambient heat load and heat load from magnet operations. The helium is not vented, but is stored on the vehicle, then periodically discharged to a ground-based system for reliquefaction. The estimated weight of the system ranges from 2330 to 3200 kg depending on magnet AC losses of 24 w or 72 w, respectively. The lower value is carried in the overall vehicle weight budget for conceptual design purposes, thus assuming

that an R&D activity on the superconductor can provide a conductor that operates at this level. The weight budget also includes 233 kg as an estimate for the vacuum jacketed transfer lines that will be required.

4. COMMUNICATIONS AND CONTROLS CONCEPT

In order to understand the design of the command and control system, it is first necessary to understand the requirements in response to which this design was developed. Therefore, this section is organized to present first the the requirements, then to describe our baseline design. The requirements are divided into performance requirements (Sections 4.1.1 through 4.1.4) and functional requirements (Section 4.2.1 through 4.2.3). Section 4.3 then covers the baseline designs of the vehicle, zone, and central control systems with special section on the baseline communications and guideway sensor subsystem.

4.1 GENERAL DESIGN REQUIREMENTS

The potential complexity for the communications, command, and control (C^3) portion of our concept to satisfy the multi-level system demands requires a well-defined and structured approach to an integrated system design. The system structure needs to operate in a fully automated, real-time environment and must contain specific requirements for performance, safety, reliability, and operational availability. Additional requirements for system modularity, expansibility, easy adaptation at the multiple sites, and cost have been examined as a part of the final report to the system concept definition of the maglev C^3 system.

4.1.1 Reliability, Maintainability, Availability, and Safety Requirements

Dependability is the trustworthiness of a computer system such that reliance can justifiably be placed on the service it delivers. Reliability, maintainability, availability, and safety are some of the properties that can be used to quantify the dependability of a system. Precise definitions exist for these metrics. These definitions are included below because subtle nuances sometimes interfere with their accurate usage in discussing various aspects of dependable systems. Although each metric is in theory quantifiable, arriving at a precise value is difficult. Nevertheless, an attempt is made here to formulate numerical values for each dependability metric for the control computer system related to our concept. Fault tolerant design is used wherever possible in the design of this system to achieve the dependability requirements set forward here.

Safety is the probability that a system will either perform its functions correctly or will fail in a way that does not disrupt other systems or jeopardize the safety of people associated with the system. The reliability is a function of time, defined as the conditional probability that a system will perform correctly throughout a given interval of time provided that the system was performing correctly at time zero. In other words, the reliability is the probability that a system

will operate correctly throughout a complete interval of time. Availability is a function of time, defined as the probability that a system is operating correctly at a given instant in time. Maintainability is the probability that a failed system will be restored to an operational state within a specified period of time. It is a measure of the ease with which a system can be repaired after it has failed [Johnson89].

The reliability requirement, stated as a probability of failure, for the maglev system control software, and presumably for the hardware upon which it executes, for commercial maglev transportation, is based on the commercial transport flight control requirements mandated by the U.S. Federal Aviation Administration (FAA)[1]. Those requirements pertain to a 10-hr commercial passenger flight. The reliability requirement for commercial transport, then, may be specified as follows:

"The maximum acceptable probability of failure of the (safety-critical) flight control system is 10^{-10} per flight hour per aircraft."

It should be noted that for aircraft, the terms reliability and safety are used interchangeably as far as the flight-critical controls are concerned. This is due to the fact that the failure of a flight-critical computer is always assumed to result in a catastrophic aircraft failure. In other words, for flight control computers, there is no fail-safe state. Hence, the reliability of the system, i.e. the probability that it will operate correctly over a given time interval, is equal to the safety of the system, which is the probability that it will operate correctly *or* fail in a safe manner. This is not the case for our system concept. If the control computer onboard the vehicle or in the wayside zone controller were to fail, it will not necessarily result in a catastrophic vehicle failure. For example, if the wayside zone computer enters a fail-stop mode, the vehicle will coast to a stop on the guideway. Since there are several alternatives available to bring our vehicle to a safe stop in the absence of a functioning onboard or wayside zone control computer which are not available to an aircraft in flight, the safety and the reliability requirements for the control computer system must be distinguished.

In particular, the reliability requirement stated above for a commercial transport aircraft becomes the safety requirement for maglev control computers, which then may be specified as follows:

---

[1] See Federal Aviation Regulation 25.1309, Amendment 25-23 and Advisory Circular 25.1309-1.

"The maximum acceptable probability of failure of the (safety-critical) control computers is 10^{-9} per computer per hour of operation."

This requirement applies to all parts of the control computer system which perform safety-critical functions.

The reliability requirement for maglev relates to the probability of successfully completing a trip and a reasonable value for not completing a trip due to computer system malfunction is 10^{-6} per computer per hour.

The overall reliability and safety requirements for our system concept definition exercise may be illustrated as follows: If one billion trips, each of 1 hour duration, were undertaken by a fleet of vehicles, then all except 1,000 trips should be completed successfully. Of the 1,000 trips in which the vehicles did not arrive at their destination without incident, only one would result in a catastrophic accident. If we assume that maglev trains have the same number of scheduled departures per day as planes, i.e. 14,000 per day, and that each trip averages one hour, these one billion trips will take approximately 195 years. Over that period of time, in our system, there would only be five incomplete trips per year. During the entire 195 year period there would be a total of one catastrophic accident attributable to the failure of the control computer system.

The availability of the maglev transportation system is going to play a very important part in the public's acceptance of this mode of transportation. For U.S. domestic commercial airlines, the availability of the airliners approaches or exceeds 99 per cent. Less than 1 per cent of the flights are delayed or canceled due to mechanical, electrical, hydraulic or other aircraft system related failures. As indicated above, there are more than 14,000 regularly scheduled commercial flights a day. It is obvious that the maglev transportation system will have to match or exceed this level of availability in order to be accepted by the public. A reasonable availability requirement for our concept may be specified as follows:

"The maximum acceptable probability of not being dispatch ready to leave a terminal on time for each maglev vehicle will be 10^{-2}."

This requirement applies to all the subsystems onboard each vehicle. The unavailability apportionment for the onboard control computer subsystem is assumed to be one-tenth of this, or 10^{-3} per vehicle per trip. That is, only one-tenth of the unavailable vehicles will be stuck due to onboard control computer system failures.

Since each wayside zone control computer is directly involved in the control of the vehicles traveling through their zone, a breakdown of one of these computers will disable the maglev transportation along an entire route. Furthermore, the system would be unable to operate safely for any extended period of time without a fully functional central control computer. Clearly, the availability of the wayside zone computers and the central control computer must be greater that of a single vehicle. An acceptable level of downtime for a wayside zone control computer on a given route for which no alternate route exists is one hour per year. Similarly, an acceptable level of downtime for a central control computer overseeing an entire region in the maglev network is also one hour of downtime per year. These requirements imply that the wayside zone computers and the central control computer have adequate redundancy to continue to operate in the presence of faults and that most faults be repairable while the system remains on-line and fully operational.

The maintainability of our concept must support the required availability discussed above. In other words, for on-board vehicle computers, unscheduled repairs can result in the disruption of no more than 0.1 percent of regularly scheduled departures. For the wayside and central computers, maintenance procedures can result in no more than one hour of downtime per year. Furthermore, for both the central and wayside computers, only on-line repairs are allowed. Thus, these computers are never taken off-line for repairs. Instead, they are designed to be able to continue operation with a subset of "unfailed" hardware while failed components are replaced. In addition, they must have backup options which allow the system to continue to operate even if a software fault occurs. For the on-board vehicle computers, off-line repair is also possible during the part of the day set aside for maintenance. For the on-board vehicle computers to achieve the required availability, 99.9 percent of all repairs should be performed during regularly scheduled maintenance.

Part J of this document describes the safety issues relevant to our maglev system concept.

4.1.2 Implementation Requirements

The development approach used by our team focuses on commonality of software and hardware architectural components, on the maximal use of commercial-off-the-shelf products, modularity, open architecture, and fault-tolerant and safety-conscious design to allow for flexibility in growth, both in terms of sheer capacity and potential functionality. In addition, the architecture will reflect the operational needs for responsiveness and availability in the careful partitioning of centralized, decentralized, and distributed data, processes, and control. When the requirements are defined by

the current concept definition phase, allocations to alternative command and control architectures will be made during the preliminary engineering phase.

For the initial point-to-point route, command and control is relatively straightforward, involving the scheduling and monitoring of vehicles starting at a terminus, stopping at or bypassing a number of stations and turning back at the other terminus. However, the command and control system must be designed with network control in mind, because of the need to interconnect some "N" number of city pairs and multiple stops within each city. A networked, rather than point-to-point system represents a significantly more complex set of challenges in collision avoidance (at merge points), conflict resolution and dynamic re-scheduling.

To manage the complexity and to provide increased cross validation, the command and control architecture uses a hierarchical approach (see Figure C4-1). That hierarchical command and control structure will be reflected in the developed architecture with three levels of software command and control: the highest or executive level will provide the centralized supervisory

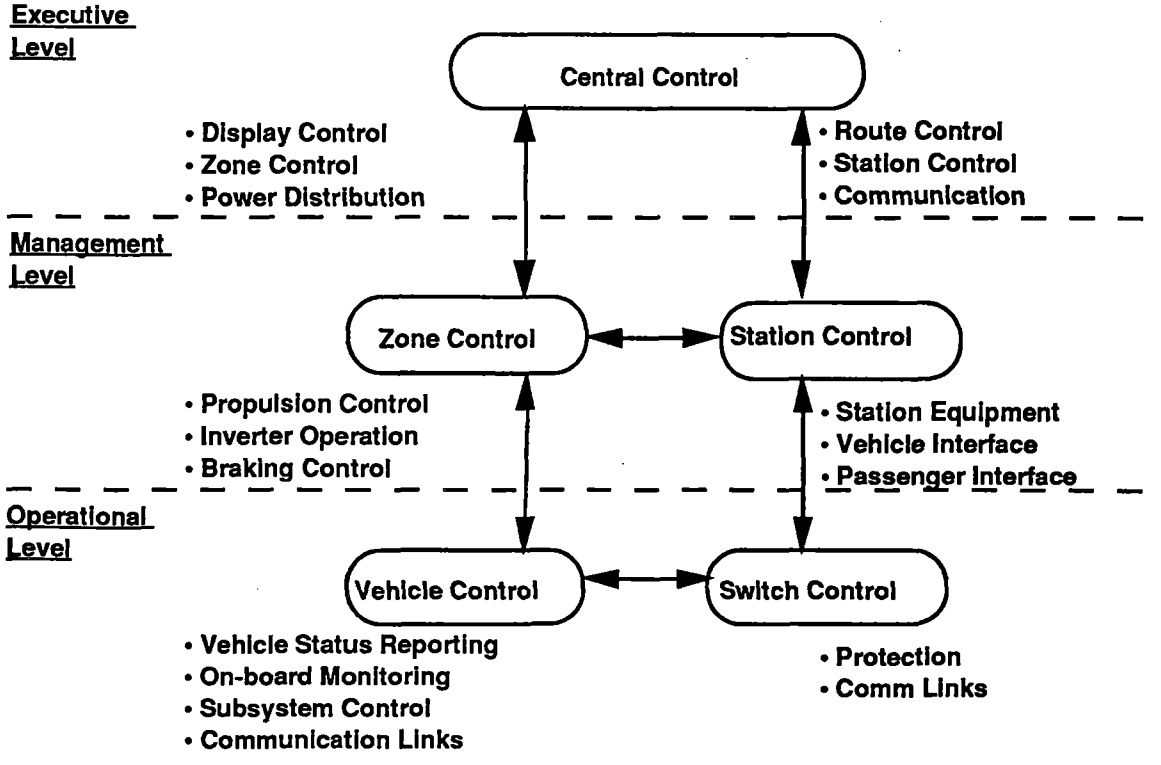

Figure C4-1 Hierarchical command and control structure

knowledge for the management of the flow of vehicles at the Central Command Facility (e.g., at switch points and stations and the handling of anomalies, diversions, delays, and emergencies); the second tier or management level at the zone controllers will do the route and speed control of the vehicles and make some dynamic adjustments, say, for wind events; and the lowest level of control at the vehicle will control the ride dynamics and all onboard systems. This hierarchical approach puts the responsibility at the nearest point of need and at the point of clear visibility for the necessary scope. An infrastructure of multiple communications modes will enable fail-safe operational knowledge of all vehicle locations at all times and provide the necessary human communications as well.

Utilization of a hierarchy of control matches the safety hierarchy approach which allows for the independent calculation of system parameters for cross-checking. For example, it is possible for the smart vehicle to calculate a desired speed for it to achieve a scheduled arrival time. The vehicle is then focused on achieving the mission of timeliness, within its knowledge of its health and status. The zone controller has a pre-planned route speed for the vehicle within its control zone, but is aware of environmental status and may dynamically calculate a new "safe" speed. The Central Control Facility (CCF) is monitoring all vehicle locations and status and has full visibility of the approaching vehicles at potential points of collision (e.g., at switch points), and may calculate a "safe speed" to enable a smooth flow of vehicles through the routes (e.g., through the switches). These three speed limits may be compared and an algorithm might take the lowest of the three speed limits as the "accepted safe speed limit." This scenario has many implications. For example, the use of this "lowest speed" algorithm at the wayside control points must be considered by the central control computer when planning its collision avoidance and routing strategies. Thus scenarios such as these must be generated, studied, and simulated to determine the best combination of criteria for command and control. One thing is clear, however, the hierarchy allows for greater flexibility in the C3 structure.

While site-specific command and control software (vehicles, power substations, zone controllers, switch controllers, central command facilities, maintenance facilities, etc.) in a fully implemented ultimate networked system will have much in common, there may be parameter differences at each location (e.g., with respect to specific route data or environmental data, etc.). Furthermore, each site may be configured slightly differently (e.g., a zone controller at a passenger station or terminal may have increased power ratings to handle the initial movement of maglev vehicles). Because of the differences, the command and control implementation approach utilizes a configuration and automated site shredding approach that uses parameterization and a table driven or adaptation data approach to make maximal use of common software while tailoring the specific

data required at each site. This is an approach used on many of the current command and control systems for air defense, air traffic control, and command, control, and information, and train control systems. It makes for efficient development of requirements for similar, but different sites.

In addition to the adaptation and site configuration techniques above, software modularity is stressed. This forms one of the underlying concepts allowing the commonality and flexibility above. In the modular approach, software is built in well-interfaced, clearly separated modules to allow for adaptability. For example, normal zone controller logic may be augmented with separate switch control logic modules at those zones that correspond to the switch control area. In general, because of the need for safety and redundancy, a number of the zones immediately adjacent to the switch will be enabled with that logic. As another example, the zone controllers that also span a station may entail more logic associated with the station functions related to vehicles. That logic is also modular and may be allocated to the zone controller. If sufficiently complex logic is required at the stations, the top-down requirements will be compared with the bottoms-up component capabilities and an appropriate design tradeoff achieved during preliminary engineering design. Figure C4-2 below shows some of the fundamental concepts and illustrates some of the modularity ideas. Note that the switch controller logic could be assigned to a number of the zone controllers.

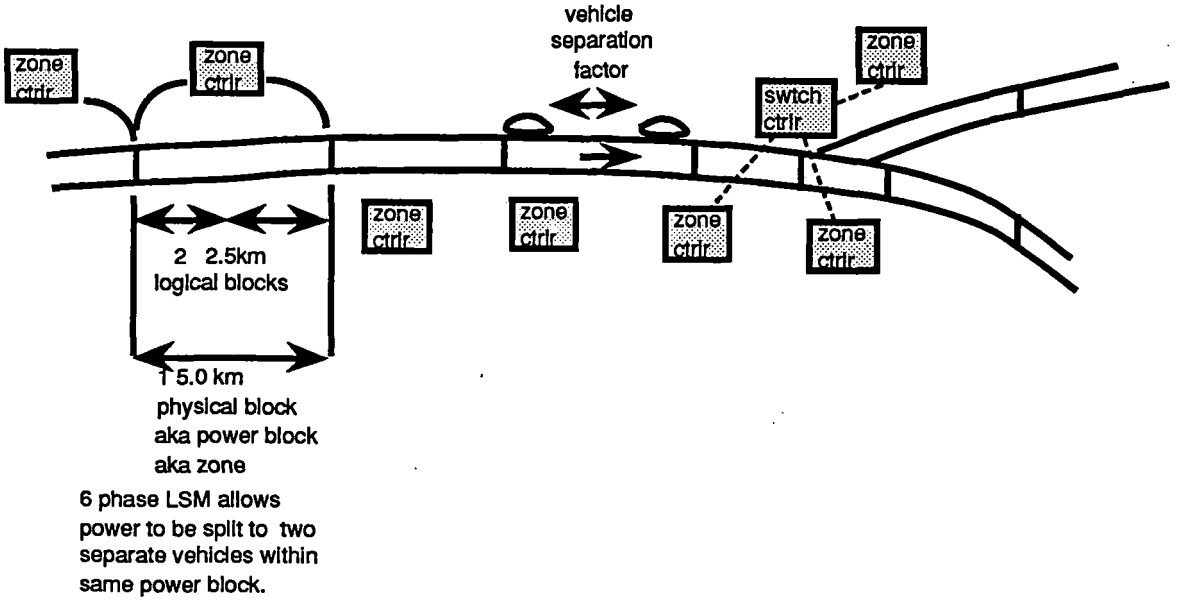

Figure C4-2 Switch controller and zone controller interdependence

To keep development life cycle costs down, standard, commercially available products, both hardware and software are emphasized to avoid unnecessary customization. For example, the use of commercial database management systems is maximized for data storage and retrieval, wherever response time permits. Further trade-off analysis must be done during preliminary design, because this particular aspect of command and control has proven to be a difficult trade-off in related systems, because of the need to respond quickly during route management. The use of commercially available products must not take precedence over the safety-critical response time needs. Workstation choices will similarly be traded off for sufficient display power at the Central Command Facility and cost effectiveness.

The software architecture is modular and designed to be a scaleable and expandable system to accommodate the expansion of capacity from 4,000 pphpd (passengers per hour per direction) to 8,000 pphpd to 12,000 pphpd. For example, the master database of route information and the database structure definitions reside in the global route database at the CCF. The data specific to particular route and to a geographical region are initialized at each zone controller in a local database for its route. This data is expected to be relatively stable and updated only as needed. Means to update to infrequently changing data online need to be investigated for possible overnight updates. As the routes expand, the master database is updated and the appropriate additional zone controllers are added without affecting data on existing zone controllers. The parameters needed at the zone controller are pre-planned so that as expansions occur, data modifications (such as guideway status) may be updated, but the functional logic remains largely unchanged.

The software architectural approach will utilize standards and open architectural philosophies to enhance inter-operability (ability to interface to other systems, e.g., external reservations systems, and emergency systems under the control of other agencies) and integration of commercial and other systems.

4.1.3 Operational Concepts and Requirements

Operational Modes

There are two major modes of operation:

- Normal service mode
- Degraded service mode

In the normal service mode, the fully automated, software controlled vehicles operate with a headway strategy based on the optimum system capacity on a dual-track guideway, with off-line stations, at a maximum speed of 500 kph. Vehicles operate in either an express mode, where some stations are bypassed, or a local mode in which every station is serviced. The normal service mode employs a variable block approach with fault tolerant microprocessor zone controllers to manage anti-bunching and de-bunching to assure the vehicles are properly spaced throughout the system. With the capability to engage a high-speed switch and with a network of alternate routes, the system will have the flexibility to meet unexpected demands. The system is also designed to manage vehicle turn around at the terminals without a remotely located yard. Terminal points have a small radius turn back loop to reverse the unidirectional vehicles.

The degraded service mode consists of three different operational profiles: the short turn back profile, the shuttle profile, and the single track profile. The short turn back profile is established if a section of the dual track guideway is completely out of service. In this profile, appropriately spaced turn loops or wyes are used to turn the vehicles short of the closed guideway section, thereby providing limited service on each section of the guideway. The shuttle profile utilizes the reduced speed reverse direction capability of the vehicles to provide service to points where no turn around facilities exist. The single track profile is used if only one side of a dual track guideway is inoperable. Using crossovers, vehicles traveling in both directions utilize the same short portion of the guideway.

Operational Headway Control

The principle for any headway control during normal operations is to enforce a pre-determined vehicle separation strategy providing the highest level of safety along with the maximum throughput to meet the system requirements. The Engineering Operational Headway is the headway between vehicles at which the system is able to operate continuously and still maintain schedules without vehicle bunching as a result of normal disturbances and passenger induced delays. For our system concept, the preliminary analysis, based on the normal vehicle braking and acceleration capability and the projected ridership/demand, shows that the system capacity requirements can be met with a headway of 72 seconds for peak transit periods on a regular route in the initial stage. Real guideway alignments may impose certain conditions which require the minimum headway to be greater.

The three most commonly used headway control strategies are: constant time headway control, constant distance headway control, and constant safety factor headway control.

(i) A constant time headway control uses an algorithm which maintains a constant time slot (e.g., 40 seconds) between vehicles at the command speed. The command speed is a functional speed dictated by the system supervision and controlled by the inverter substation. The master speed will be the command speed of the leading vehicle and the slave speed is derived for the following vehicle by adjusting the slave speed for a constant time slot after the leading vehicle but varying in distance. A real time sensor for vehicle speed is critical in this approach. System capacity (pphpd) for this approach at any speed is dependent on the allowed time slot and the locations of the control stations.

(ii) A constant distance headway control uses an algorithm which maintains a constant distance between vehicles at the command speed. The same system command speed profile is applied here as the constant time headway control strategy. The master and the slave speed are also calculated. The strategy is to maintain a constant distance between vehicles but varying the time slot. A real-time sensor for measuring the distance between vehicles accurately is critical to this strategy. Capacity at any speed is dependent on the allowed separation distance and the length of the control blocks.

(iii) The constant safety factor control provides a very conventional approach for maintaining the separation of the vehicles. It is based on an engineered system braking capability to ensure the time or the distance is maintained for a safe stopping before any problems projected along the guideway. The safety distance or constant time separation will be observed in which the most critical measure will determine the control strategy. The strategy will follow the same command speed profile from other strategies. Then the approach is to assess both the master and the slave speed and use the most critical measure as control criteria for the separation of vehicles. A set of real-time sensors for measuring the distance and projected impact time between vehicles is critical to this strategy. It is more complex in determining the measures, but it provides a redundancy for the safety of the vehicles. Capacity at any speed is dependent on the allowed separation criteria and the length of the control blocks.

The system's optimum control point lies within the area bounded by these three different headway control strategies. The choice for any headway control strategy depends upon the speed of the vehicles at a certain moment and the position of the vehicle related to the location of the control block.

Another critical factor to the final implementation of the headway control strategy is the capability of the substation (or the length of a typical inverter control block) to propel the vehicle. Since one of the characteristics of LSM is to produce a synchronization of motoring between stator (the guideway) and rotor (the vehicle) with a unique propulsion frequency based on the particular requirement at the block, it allows only one vehicle for each block (motor section) at a time. Thus the design of the block in the long-stator propulsion system will create a natural separation (or headway) between the vehicles and limit the total number of vehicles in the system. In general, this proves the concept like the shorter the block the closer the headway is more evident in this case than the conventional system. It generally means that the shorter block system can accept more

vehicles in the system for increasing overall capacity typically measured in pphpd (passenger per hour per direction). But it could also drive up the capital cost with more of inverter substations along the guideway. The zone location (or the block length) of the inverter substations is application dependent and should be based on the final system requirements and the actual alignment. For Bechtel's system concept, based on the SST system baseline requirement, the average zone length of the inverter station is set at 4,000 meters with 6-phase inverter application divided into two blocks control section (2,000 meters per block). Hence, the running headway could be as short as 2,000 meters with reduced speed is almost 8-10 times shorter than the TR-07 system.

At the system concept level, the analysis of the final requirements for an optimum headway control strategy is mostly application dependent such as the projected ridership, the location of the propulsion unit, the horizontal or the vertical grades of the alignment, the command speed profile, and the braking and acceleration capability. The final applications in the real time system could be a strategy mixed with all three different approaches.

Following is a parametric table to illustrate the headway control strategies for various system capacity requirements based on following performance factors:

Route distance: 800 km
Normal braking rate : 3.0m/sec/sec
Consist: 1
Vehicle Capacity: 120 passengers

Case I: Safety/brickwall stop

Avg trip time	8.0	4.0	2.6	2.0	1.6
Avg Speed(kmph)	100	200	300	400	500
Avg Speed(m/s)	28	56	83	111	139
Time to stop(sec)	9	19	28	37	46
Dist. to stop(m)	236	650	1321	2249	3434
Block(m)*1	2000	2000	2000	4000	4000
Eq.H/W(sec)*2	72	36	24	36	29
# Vehicles/hr	50	100	150	100	125
Pphpd*3	6000	12000	18000	12000	15000

Note:

1. Reduced speed performance with 3-phase power block of 2,000 meters.
2. Average time to cross the block with defined average speed.
3. Peak performance system capacity.

Case II: Constant distance>= 4000 meters

Avg trip time	8.0	4.0	2.6	2.0	1.6
Avg Speed(kmph)	100	200	300	400	500
Avg Speed(m/s)	28	56	83	111	139
Time to stop(sec)	9	19	28	37	46
Dist. to stop(m)	236	650	1321	2249	3434
Block(m)	4000	4000	4000	4000	4000
Eq.H/W(sec)	144	72	48	36	29
# Vehicles/hr	25	50	75	100	125
Pphpd	3000	6000	9000	12000	15000

Case III: Constant time >= 40 sec

Avg trip time	8.0	4.0	2.6	2.0	1.6
Avg Speed(kmph)	100	200	300	400	500
Avg Speed(m/s)	28	56	83	111	139
Time to stop(sec)	9	19	28	37	46
Dist. to stop(m)	236	650	1321	2249	3434
Block(m)	2000	2000	4000	4000	4000
Eq.H/W(sec)	72	40	48	40	40
# Vehicles/hr	50	90	75	90	90
Pphpd	6000	10800	9000	10800	10800

Remarks:

1. It is evident that all three headway control strategies are capable of meeting the full system requirement of 4,000 pphpd at the initial stage as well as the full system capacity requirements of 12,000 pphpd stated in the RFP.
2. All three headway control strategies will be part of the final headway control options depending on actual alignment and route applications.
3. The system concept in this analysis is based on off-line station operations or on an express mode.

4. The average speed for the SST simulation analysis is 243 mph or 388 kmph on 800 km alignment. That result illustrates the Bechtel's system capacity is achievable to the 12,000 pphpd as peak performance.
5. Based on the system performance requirement, the current operating capacity could be increased again without any major effort through the utilization of the multi-vehicles concept.
6. The constant distance strategy provides the least system capacity at the reduced speed operations.

Line Capacity, Fleet Size, Vehicle Length and Spare Vehicles

Line capacity is measured by the passengers per hour per direction (pphpd) that can be carried past a given point by nominally loaded vehicles. The initial system capacity requirement is 4,000 pphpd and it is projected to grow to 12,000 pphpd in the next 30 years. The headway control and the capacity requirements are the factors which establish the size of the vehicle and the number of vehicles required. Based on our current concept for an ultimate system, the 36-second operational headway means that 100 vehicles can be dispatched per hour with 120 passengers carried on each vehicle to meet the 12,000 pphpd requirement. If it takes 2.0 hours to complete the route, then one-way operation will require a minimum of 200 vehicles. For two way traffic, the system will need a minimum of 400 vehicles not including stand-by vehicles. The current system requirements based on the previous analysis for the line capacity, fleet size and the spare vehicle requirements for dual direction of transportation (assumed at the 10 percent level of support) can be summarized as follows:

- Line capacity for peak performance is 12,000 pphpd.
- Fleet size at 120 passengers capacity is 400 vehicles.
- Spare vehicles at 10 percent level is 40 vehicles.

4.1.4 Performance Requirements

The initial requirements for point-to-point connections will serve as information, but not be the driver for the command and control requirements. It is already recognized that if the maglev technology is to grow it must be treated as part of a national transportation concept. As such, command and control must anticipate a complex network control problem. The performance requirements as such are significantly more complex. If a network concept is assumed from the beginning, growth and capacity planning become more viable. The command and control philosophy is to decentralize functionality by allocation to a distributed local control and

processing structures as possible. However, global asset management and flow management concerns will necessitate some centralized knowledge and capability.

In the beginning, one Central Control Facility is envisioned as powerful enough to handle the initial network. As incremental growth occurs, it may be necessary to add other Central Control Facilities in regions of significant size. Then inter-CCF coordination will be required. If continental oversight is required, a national level of command and control may be needed. The maglev transportation system may be able to pre-plan that need in the preliminary engineering design phase and can look to the existing air traffic control efforts worldwide to leapfrog those concepts and to augment and improve the concepts.

Performance requirements will be refined during preliminary engineering design by taking the concepts from the current phase and applying scenarios of workloads for hypothetical routes (real intended usage) as distinguished from the severe segment test which exercises and stresses each design concept without purporting to address real route design. This is necessary to produce performance requirements for the top-down analysis/design refinements of the current concepts. Then the refined design concepts can be assessed for bottoms up capability assessments and the alternative command and control functional allocations traded off for cost effectiveness, predicated on safety, availability, and capacity.

When the architecture is developed, scaleability and excess capacity for growth will be considered to enable the 3-fold growth over time.

4.2 FUNCTIONAL REQUIREMENTS

Each of the three principal functions which must be performed by the system, i.e. vehicle control, protection, and supervision, can be decomposed into several well-defined sub-functions. This purely functional analysis of the control system may be used as the basis for the design of a control architecture. By partitioning the sub-functions among the various control elements which make up the system, an optimal design for safety and reliability can be achieved. The results of the functional decomposition of our concept's control system are presented in Table C4-1.

Table C4-1
Functional Decomposition of the Maglev Control System

CONTROL	PROTECTION	SUPERVISION
Vehicle State	Safe Vehicle Separation	Route Planning
Velocity Control	Vehicle Position Control	Route Scheduling
Cryogenic Control	Route Integrity	Dispatching
Propulsion Control	Emergency Stopping	Maintenance Scheduling
Secondary Suspension Control	Emergency Speed Control	Operator Interface
Switch Control	Emergency Position Control	Status Displays
Vehicle Systems Monitor and Control	Emergency Response	Passenger Supervision
Environment Monitoring	Failure Management	Station Supervision
Station Operation		

4.2.1 Control Functions

This set of functions is performed by various components of the computer control system to safely operate the vehicle within the system as well as to operate all automated onboard systems.

Vehicle State Monitor (Safety Critical)

The vehicle state operational function sets and monitors the vehicle positions, travel direction, acceleration/deceleration and speed. The vehicle position is important both in absolute terms along the guideway, as well as in relative terms with respect to the switches, safe stopping places, and station locations. This function provides the feedback information required in real time by other control and protection functions to determine the actuation necessary to achieve the position, acceleration and speed called for by existing conditions and the mandated speed profile of the vehicle.

Velocity Control (Safety Critical)

The vehicle operation control function causes the speed and direction of travel of each vehicle to match the speed mandated by its speed profile in accordance with the existing conditions on the guideway which include radius of curvature, degree of incline, bank angle, and weather conditions.

The vehicle operation control must coordinate the activities of the individual propulsion power units in the guideway, whose position will vary somewhat with terrain but on average are spaced at approximately 4 to 5 km intervals. The vehicle operation control communicates directly with the lower level propulsion control to maintain the operational velocity and scheduling. Inputs to this function include information about the condition of the guideway in the next zone, the distance to the vehicle ahead, the speed and expected time of arrival to next zone, conditions of the switches to be navigated as indicated by the travel profile, the speed mandated by the travel profile for this zone, and zone-wide operation guidelines. Service and emergency braking is controlled by this function. This function also coordinates its actions with the control function of systems which perform takeoff and landing operations, i.e., velocity control during low and zero speed operation.

Levitation Control (Safety Critical)

Although the electrodynamic suspension system does not require active control to maintain or achieve levitation, a takeoff and landing mechanism is required for low speed and zero speed operation. This function is performed by air bearings mounted on the vehicle bogies. Control of the air bearings during low speed operation is performed by this function.

Cryogenic Control (Safety Critical)

The temperature of the superconducting on-board electromagnets needs to be carefully monitored. The temperature must be maintained at approximately 5° K or below. If the temperature rises above this operating temperature, a phenomenon known as quenching will occur, which ultimately causes the magnets to fail. Thus, the onboard cryogenic system must maintain the temperature of the superconducting magnets within their operating range. The operation of the onboard cryogenic function has to be designed as a fully automated, self-contained unit and situated away from the passenger compartment. It has a redundant operational control processor that meets the safety and hazard control requirements defined by either the industry wide practices or the government procedures.

Propulsion Control (Safety Critical)

Bechtel's maglev vehicles are propelled by a linear synchronous motor (LSM) also known as a long stator propulsion system. The primary power source in the LSM concept comes from the electrically excited windings on the guideway which creates a traveling magnetic wave which acts upon the super conducting magnets onboard the vehicle to propel the vehicle in synchronism with the motion of the field. The propulsion control function here also includes the coordinated activities for the levitation and guidance control functions. It is an integrated operation. The next

level of control as part of the propulsion control function is provided by the motor control function which controls the power switching devices in the inverter. The motor control function accepts commands from the zone controller which houses the element of the inverter. The inverter is the power module that converts dc power distributed along the guideway to ac power that excites the motor windings. It maintains precise synchronization between the phase of the ac power and the position of the vehicle, as is required for synchronous propulsion. The synchronization is based on the phase angle position sensing feedback loop. Since loss of this signal would make precise control of the vehicle difficult, there are redundant sensor systems to ensure its reliable and uninterrupted input.

Each inverter provides power to the motor along a section of guideway called a zone. The motor controller provides the appropriate thrust to make the vehicle follow a prescribed speed profile. The speed profile it follows is one of several possible profiles that have been predetermined to satisfy all operational and safety conditions. The scope of control of a motor controller extends only over its own zone. The motor controller follows the speed profile specified by the zone controller.

Secondary Suspension Control (Safety Critical)

The secondary suspension control includes two major control mechanisms: the active damping subsystems underneath the passengers compartment and the external aerodynamic flaps. The purpose of the secondary suspension system is to provide a satisfactory level of ride comfort to passengers in the vehicle. Bechtel's concept vehicle employs a fairly stiff primary suspension. The active damping element of the secondary suspension provides a level of isolation between the coach body and the guideway. When the speed of the vehicle is sufficiently high, aerodynamic control is critical to provide a better ride quality. This is accomplished by controlling a flap at either the trailing edge of a vehicle or several flaps positioned around the vehicle body to provide secondary suspension. The control algorithm for this application is similar to control algorithms for lift in an aircraft. For both slow and high speeds, the active secondary suspension is provided by digitally controlling hydraulic dampers which stabilize the roll motion and the vertical / lateral motion of the vehicle with respect to the magnetically levitated bogie. In order to maintain high speed around curves with relatively short radii, both the the vehicle and the guideway are banked. These coordinated curves are accomplished with the use of actively controlled tilting hydraulics as part of the secondary suspension subsystems. The control algorithm used to coordinate the bank angle requires as inputs the speed of the vehicle, its acceleration, the radius of curvature of the guideway and the vertical curves.

Switch Control (Safety Critical)

The switch monitoring function provides the vehicle the current status on one of two possible paths at switching points in the guideway. The route profile on the vehicle indicates the correct path to take at every switch. Vehicles may either remain on the main guideway or exit at the switch point to stop at a station. Eventually, switches may be added to connect branch lines to the main route. In the baseline design, the direction of travel is determined by the switch which positions a moveable section of the guideway to direct the vehicle along the correct branch path. The correct position of the switch must be ensured before the arrival of the vehicle such that in the event of a failure of the switch to engage properly, the approaching vehicle will have adequate time to stop. Vehicles which traverse a switch in the main direction of travel do not have to reduce their speed. However, vehicles which are existing from the guideway, must slow down such that their speed conforms to the safe exit speed required by a switch. Alternate designs employ passive switching mechanisms. In any case, automated control of the switching operation is provided by this function.

Vehicle Systems Monitor and Control (Mission Critical)

During operation, the on-board vehicle systems are monitored and regulated periodically. This includes controlling on-board power generation and measurement of the charge level of the on-board batteries. Other on-board systems such as on-board lighting, temperature, air pressure, air flow, i.e. all HVAC functions, and door position control are monitored and regulated for comfort and safety. Smoke and fire detection equipment are present and able to signal an alarm in the event of a fire. The electromagnetic field at various positions within the coach is monitored. Since high electromagnetic field strengths may pose a health risk to passengers, a running average is maintained and readings above a certain threshold are logged. Finally, the position of the "panic button" is monitored. The on-board technician can press this button to indicate some extraordinary condition requiring an immediate stop. If the button is down, emergency measures are activated.

Environmental Monitoring (Mission Critical)

Wind speed and direction and external temperature are measured periodically. Local and regional weather conditions are monitored continuously because of the significant impact that high winds can have on the system. Seismological measurements are also taken in areas where earthquakes pose a threat to safe operation. Finally, vibration and acoustic information is collected to monitor the changing condition of the guideway and its associated structures.

Station Operations

Station operations includes the execution of the programmed starts and stops, control of the station dwell time for arriving vehicles, coordination of the station door operations with the door operations of the vehicle, station departure procedures, and the coordination of the on-line merging operations of the vehicles going from off-line stops to the on-line traffic. Station operations also manages the berths and time slots at the station. A programmed station stop is executed by the associated zone controller through control of vehicle speed and final application of brakes under pre-determined jerk and deceleration limits, to enable a precision station stop that aligns with the station doors. The station zone controller applies special procedures to ensure the safety of the passengers and vehicle through low speed collision avoidance algorithms, sensors, and devices. The station also exercises control of the zero speed levitation devices in stations having this special equipment.

The normal stopping positions at each station platform are sized for ridership requirements and provide berthing or queuing operations with reasonable loading and unloading delays for passengers. For vehicle control, the station monitors the actions of the local zones to coordinate station operations functions with the movement of vehicles. Station operations controls the dispatch of spare vehicles or maintenance vehicles strategically located along the guideway for any unexpected emergency operation. These are in addition to any separate major maintenance facilities for the routine care of vehicles. For these operations, there is a link to the station supervision, which has oversight and planning and high level procedural responsibilities.

Station operations also includes any necessary interfaces or added functions for the handling of passenger ticketing, baggage, mail, or freight. As concepts evolve further, there may be a mix of some limited freight and mail aboard maglev vehicles, but a separate freight and mail type station is also being considered.

4.2.2 Protection Functions

These functions provide a fail-safe mode of operation. Therefore, they can override the actions of the system providing normal mode automatic operation and take control of a vehicle which has exceeded some safety threshold.

Safe Vehicle Separation Control (Safety Critical)

For normal operation, a minimum spacing of one control zone length must be maintained between any two consecutive vehicles on the guideway at all times. Prior to entering a new zone, the

distance to the vehicle ahead is calculated. The speed of that vehicle is also determined. If this distance is less than the required minimum, emergency stopping procedures are activated. For example, a vehicle traveling at the maximum speed of 500 kph can be decelerated to zero kph in a distance of approximately 4 km if a deceleration of 0.25 g is used.

Vehicle Position Control (Safety Critical)

This function uses the actual vehicle position and the desired vehicle position to determine the error, if any, between these two values. If the vehicle is not within safe tolerances of its expected position as required by its travel profile, then the vehicle poses a safety hazard to itself and other vehicles which may be exiting or entering the guideway. Therefore, corrective action is taken, typically by increasing or decreasing its speed, with appropriate cautions for existing conditions, to cause it to conform with the expected position called for by the travel profile.

Route Integrity Control

This function includes guideway sensors which monitor, record, and transmit data concerning the integrity of the guideway and the propulsion and levitation coils. The guideway must remain properly aligned and free from debris, e.g., ice or litter, which could obstruct the route. Sensor data is pre-processed and condensed before transmission. The function also interprets this sensor data to detect anomalous situations and initiates the proper response, such as, alerting a CCF operator or embargoing sections of the guideway until inspection and repair can occur. Because of the high speeds and short headway of our system, it is essential that the route integrity be automated using sensors to detect any compromise of route integrity.

Route Integrity Requirements

This section details the requirements for physical sensing in order to maintain route integrity. Sensors should determine physical guideway integrity, foreign obstacles, intruder detection, guideway magnet coil integrity, propulsion subsystem integrity, environmental conditions, collision avoidance, route switching integrity, and motive power availability. Each of these are described below.

Physical Guideway Integrity

The sensor subsystem is able to detect any misalignments of the guideway itself. Mechanical interface of guideway sections is monitored for slippage. Switching sections are monitored, since

these sections will be subject to wear and tear. Sensors are employed that detect catastrophic damage.

Foreign Objects

The guideway is kept free and clear of any objects larger than a predetermined size. The clearances necessary are of the order of 10 cm, and thus anything larger than this in effective diameter requires removal.

Intruder Detection

Security sensors are used to ensure that the route is clear of personnel.

Guideway Magnet Coil Integrity

Sensors are used to detect problems with the magnet coils mounted on the guideway.

Motive Power Availability

Sensors monitor the operation and health of the propulsion subsystem.

Environment and Weather

Operation in high speed wind conditions, rain, snow, hail, ice, fog, or earthquakes are degraded dependent upon the severity of the conditions. To make a proper determination of these conditions, sensors relay the appropriate data both to the zone controller, and the vehicle.

For each condition, a look-ahead distance needs is determined. For weather related conditions, this requires looking ahead from 30 to 100 miles. The distance to look-ahead for earthquakes depends upon the magnitude of the quake, and is about the same distance range as for weather.

Measurement of wind speeds allows our vehicle to operate in high wind conditions at a slower safe speed. Normal meteorological instrumentation at intervals along the route in conjunction with data provided from key weather stations give reliable determination of wind conditions for general routing.

Gusts are a problem in that they are localized to a relatively small area. Winds aloft and gust warnings issued for aircraft by services such as Flight Service Stations (FSSs) are used in a

limited way. To reliably sense local gusts surrounding the vehicle, either very closely spaced wind sensors on the guideway, or wind sensors on the vehicle are used.

Area determinations of rain, snow, hail, ice, and fog are gathered by weather monitoring equipment to estimate the severity of the condition. Actual environmental conditions of the route use need additional sensors to determine such things as snow depth, ice formation, and visibility in fog. Existing object detection sensors are used for detection of snow, hail, and maybe even fog.

Earthquakes are a distributed rather than a local event, so information is collected from existing earthquake detection centers, such as Cal Tech in Pasadena.

For areas not located within an earthquake detection center region, special earthquake detectors that give an indication of the magnitude of the quake are installed along the guideway route to provide detection and a rough order of magnitude of the severity of the earthquake. The sensors are used in conjunction with guideway integrity sensors to give the best picture of the route environment.

Collision Avoidance

The avoidance of collisions is part of route integrity. Some collision avoidance sensors are dedicated to this task; other functions may provide information to the collision avoidance function. For instance, sensors used for determining block occupancy by a vehicle are used for collision avoidance, making sure that an appropriate number of empty (no vehicle present) blocks are kept between vehicles.

Due to the curving of the track in many situations, and subsequent blockage of line of sight, use of sensor apparatus such as radars and/or laser range-finders are limited to only secondary vehicle sensing systems.

The primary system for sensing another vehicle is independent of line of sight constraints. For example, a sensor subsystem that determines if a guideway block is in use would be line of sight independent, and provides a way of avoiding collisions by requiring the next block to be unoccupied before allowing the following vehicle to traverse the block.

The "block in use" sensor subsystem detects and reports when a vehicle enters and leaves a specific block. These sensors are spaced every other block and maintain a one-block resolution, since the entering and leaving sensors need not be placed on adjacent blocks.

Route Switching Integrity

Switching sensors provide proper operation of the switching function and provide fail-safe operation. The sensors primary task is to verify the guideway switch position and the operational status of the switching mechanism.

Sensor Types

This section is an overview of sensor types which have been considered for application. Route integrity sensors are categorized based upon the technology used for detection and measurement. These include: visible light video sensors, infrared video sensors, optical sensors, fiber optical sensors, microwave-radar sensors, inductive sensors, capacitive sensors, and, acoustic sensors.

These sensors are based on the function and frequency of the measurement. For example, acoustical sensors are classified by their function of sound measurement and are further classified as sonic if frequencies are from 20 Hz to 20,000 Hz, subsonic if below 20 Hz, and ultrasonic for frequencies above 20,000 Hz.

Visible Light Video Sensors

Visible light video sensors detect the electromagnetic spectrum generally considered to be within the range of the human eye and consists of an array of energy detectors in two dimensions. With the advent of capacitance coupled devices (CCDs) and vidicons, visible light video sensors have had a dramatic increase in capability and a drastic reduction in cost. Image processing can be used in conjunction with the visible light video sensors to interpret the scenario automatically, communicate the results, and/or take appropriate action.

Some disadvantages of using visible light video include: obscuration due to dust, precipitation, and humidity; necessity for sophisticated interpretation of image by human or image processing; and high data bandwidth on communication of visible light video signals to signal processors.

Infrared Video Sensors

Infrared video sensors (IRV) are exactly analogous to visible light video sensors mentioned above with the following exceptions. Infrared tends to be diffused less by precipitation or fog because of the lower frequencies involved. Infrared sensors can also be made active by illumination of the desired object with a laser or diode or laser diode. Passive and active infrared can "see" in the

dark, so to speak, since the sensor is detecting the heat given off by the object, and not just the reflected light. All bodies not at absolute zero give off heat (blackbody radiation - Planck's Law).

Additional disadvantages tend to be higher costs, required cooling of IR detectors, and less resolution than visible light video.

Optical Sensors

The difference between optical sensors and video sensors in this report is that optical sensors are better modeled as taking measurements point by point, whereas the video sensors are two-dimensional measurement images.

For example, an optical beam across the route that is broken by the passage of a vehicle can do little more than detect continuity or discontinuity of the beam. It can tell us nothing about what the vehicle looks like, except perhaps its length.

Optical devices (sensors) can use both visible light and IR waves. The advantages of optical sensors would be low cost and system simplicity. The disadvantages would be the limited amount of information upon which to make operational decisions.

Fiber Optical Sensors

Fiber optical sensors can be of the attenuation or interferometric type. The idea is to embed or attach a length of pre-stressed fiber optic cable along a run of guideway and pump light through it. For the attenuation fiber optic sensor subsystem, any changes in the guideway length due to stresses, strains, or catastrophes are detected as a change in the amplitude of the transmitted light beam. With the interferometric sensor subsystem, interference fringes are generated. By counting the changes in the interference fringes, a determination can be made of the amount of movement (expansion or compression) that the guideway has undergone. Temperature effects are compensated for. Catastrophic lost of the guideway (destruction or major break) would immediately show up as a loss of light signal. Small fractures in the guideway would be indicated by a large change in the fringes. Time domain reflection interferometry could then be used to locate the fracture.

Microwave Sensors/Radars

Microwave sensors detect electromagnetic radiation usually from 1 to 30 GHz. More recently, millimeter wave sensors have been used in the 30 to 300 GHz range. A gigahertz (GHz) is a thousand million cycles per second.

Microwave sensors can be active or passive. Active sensors are called radars. Passive sensors are called radiometers. Only radars are considered here.

Microwave radar energy can be emitted which can penetrate all weather environments. This is an advantage over higher frequency visible and IR energies, however, the price is paid in terms of reduced resolution. Synthetic aperture radar can increase this resolution by using multiple sensors that are phased appropriately, or by passing the sensor over a path and using the path length as the effective aperture of the radar. Synthetic radars, however are costly.

A disadvantage of microwave (compared with video or optical sensors) is the relatively large antennas that must be used for concentrating the beam width at longer wavelengths.

For shorter wavelengths, the antenna diameter reduces proportionately for a given beam width, however, the microwave energy is attenuated greater by weather conditions when the wavelength is less than 10 cm.

Inductive Sensors

Inductive sensors sense the change in environmental inductance. This change in inductance indicates that an object is in proximity. Usually some sort of loop of wire is placed appropriately a the desired location. A current flows in the loop. The presence of any ferrous metal in the vicinity will change the net inductance, effecting a change in the current and/or voltage in the loop.

For maglev, special consideration should be given to the use of inductive sensors, since maglev uses magnets for levitation and propulsion, and the sensors must be immune to the effects of the fields produced by these magnets.

Capacitive Sensors

Capacitive sensors are analogous to inductive sensors in that a change in current or voltage is effected by the proximity of another body.

The advantage of capacitive sensors over inductive is that the object doesn't have to be made of a ferrous material, but can be a dielectric. This type of sensor would be more resistant to spurious electromagnetic fields than would inductive loops, and generally can be packaged into a smaller area.

Acoustic Sensors

Sound waves can reveal a lot about the environment. It is possible to identify certain sounds by analyzing its associated spectrum. Sounds are classified according to their frequency band as subsonic (less than 20 Hz), sonic (20 Hz to 20,000 Hz), and ultrasonic (above 20,000 Hz). Subsonic sounds will not be considered here.

Sonic sounds are the sounds normally associated with the frequency range of human hearing. Sensors may be mounted along the route always in a listening mode. The sounds would be digitized and relayed to a computer for analysis and recommendation. It could also be communicated to the approaching vehicle for a human listener to determine if anything is amiss. For example, a sonic sensor could pick up a flock of geese that had landed on the guideway. The human operator could be trained to recognize these sounds, and possibly a computer program could be developed to determine that large birds had landed on the guideway. The response might then be to activate a warning horn on the guideway to frighten the geese into flying away before the vehicle passed.

Ultrasonic sounds are above the frequency range of hearing of humans. In addition, the sounds tend to be attenuated greater for a given distance. This is advantageous in that background noise is minimal and the ultrasound does not carry far.

Usually, ultrasound is used as a sort of radar, with short bursts of sound energy being reflected from an object. The time lapse between transmission of pulse and reception of pulse provides the distance to the object. Other types use continuous radiation of energy, and detect only radial velocity of an object. The amount of change of frequency of the reflected wave form indicates the radial velocity of the object with respect to the ultrasound radar. There is also an ultrasound radar that is exactly analogous to microwave pulse-doppler radars, where both mechanisms are combined giving both distance and velocity measurements.

Operational Braking Control

There are two types of braking, designated "soft stop" and "hard stop." The soft stop uses the LSM to provide dynamic or regenerative braking, and this allows controlled braking up to a maximum reverse thrust of 2 Newtons per kilogram of vehicle mass. The aerodynamic and magnetic drag create additional retarding forces so the total deceleration can be as high as 2.5 to 3 m/s^2, depending on speed. Aerodynamic drag is proportional to the square of the velocity and the magnetic drag is inversely proportional to the velocity of the vehicle. Thus, as the vehicle slows down, the overall deceleration rate remains roughly constant. An audible warning of an impending hard stop is issued to give passengers as much warning in advance of the application of the brakes as is possible.

The hard stop is only done when the undesirable consequences of more severe braking are judged to be preferable to the longer time required for a soft stop. The hard stop is accomplished with dynamic braking and can be done even in the event of a complete failure of either the inverter or the motor controller. Dynamic braking depends upon the existence of short circuits or suitable passive resistors connected across the LSM windings. This connection can be performed with standby power sources even if a total power outage occurs on all parts of the guideway.

If there is a zone malfunction so severe that all active control efforts are rendered inoperative, any vehicles in that zone will coast to a stop without collision, assuming only that the spacing between vehicles was correct prior to the malfunction. Unlike rail or rubber tires, or EMS vehicles, maglev vehicles with EDS have a magnetic drag which increases with decreasing speed. The combination of aerodynamic and magnetic drag means that a vehicle will coast to a stop in a reasonably short distance, even when traveling down a downgrade as steep as 4 percent. If the vehicle coasts out of a malfunctioning zone into one that is functioning correctly, the vehicle may proceed in a normal fashion.

Emergency Speed Control

The motor controller can be instructed to follow any one of several predetermined speed profiles. Included in the choice are profiles with deceleration up to the maximum possible with the available reverse thrust of the LSM.

In the event of the failure of the motor controller, the next functional element in the maglev control hierarchy, the zone controller, can exert limited control of the zone directly. It may either let the vehicle coast to a stop or to the next zone with no power applied, or can initiate dynamic braking.

These override actions can be done in spite of all efforts by the motor controller to control the velocity of the vehicle in some other manner.

Emergency Position Control

The zone controller continuously monitors the position of a vehicle in its zone. This monitoring in done with at least three independent position sensor systems. When two systems agree and the third disagrees, then a failure in the third sensor system may be indicated. If there is not at least two-way agreement, a serious malfunction has occurred requiring action by the central control authority.

For normal operation, the motor controller follows predetermined velocity profiles to move vehicles through its zone. In case of certain types of emergency, however, it may be desirable for the next level up in the control hierarchy, i.e. the zone controller, to direct position control in real-time. This mode is supported, but only when the vehicle is traveling at a reduced speed. For low speed operation the zone controller can issue commands to control velocity and acceleration much as an automobile driver controls velocity and acceleration. In this way it is possible to effect fine control of vehicle position as a function of time.

Emergency Response Management (Safety Critical)

Emergency response management handles the immediate safety critical logic and actions for crises. It is the first aid applied when degraded conditions occur and will include both automatic actions by the various control computer systems and operator-initiated actions by operators at the CCF. For minor delays and anomalies, failure management performs an adjustment. These adjustments are designed to avoid safety hazards and avert emergencies. If during dynamic re-scheduling severe conflicts or safety hazards occur, emergency response is invoked, but the algorithms are designed to avoid this scenario. Emergency responses occur at the various components of the system. Once safety is assured, failure management takes over.

Environmental concerns such as poor weather conditions may cause a slowdown or even a shutdown of services. Careful pre-planning of procedures is required in these events. For example, severe wind gusts necessitate travel at reduced speeds. This is part of the algorithm for dynamic re-scheduling of vehicles. If unexpected environmental events cause degradation, the zone controller pre-empts the pre-planned route and provides local emergency adjustment to enable the vehicle to proceed to the final destination at an adjusted schedule. The CCF then incorporates the changes and dynamically reassess the network impact to assure safety and mitigate the impact

to the network availability. In certain cases, such as global impacts as a result of this re-adjustment, then the zone controller can be overridden by the CCF.

For more serious events, such as a fire on board a vehicle, emergency agencies are notified and safety procedures followed. Tracking of the emergency situation is done at the CCF which serves as an emergency coordination/communication capability. On board the vehicle, the senior attendant follows emergency procedures, e.g., fire extinguishing procedures, emergency stop request, etc.

Should route integrity flaws occur, emergency response at minimum stops all vehicles not already past the safe stopping distance of the catastrophe (in severe events, such as earthquakes, etc.) within the affected routes. Brick wall procedures are still initiated on all vehicles. If route integrity determines non-hazardous changes, emergency responses are simply the transmittal of advisement messages from the CCF to the wayside or zone controllers to effect a reduction of the pre-determined speed limits within that zone.

Failure Management (Mission Critical)

When safety is assured, failure management functions respond to rapidly restore the system to maximum operational capability. Although some restorative activities may be automatic, most actions under this function will be initiated by operating personnel. The strategies include:

- Zone controller or central computer ability to detect and reset minor anomalies and provide the fail-safe or fail-op operation
- Adequate guideway switches, crossovers, sidings (or pocket tracks) or storage tracks along the main routes and beyond the terminal stations to facilitate the operation of reserved or management of the failed vehicles
- Procedures for recovery or removal of stalled vehicles with motorized removal by special-purpose, auxiliary, non-levitated vehicles
- Procedures for the evacuation of stranded passengers under crisis conditions
- Procedures for emergency system startup and shutdown of the magnets and cryogenics
- CCF operator capability to remotely initiate startup of vehicles onto routes
- Transition from the normal operating mode to a degraded mode of operation.

Transition between the normal operating mode and the degraded mode of operations may occur with automatic commands from either the wayside zone controller processors or the central control facility overriding the normal vehicle operations with calls for reduce speed profiles. Service mode transitions or delays to any vehicles en route of a non-stoppage nature are recovered as soon as possible in as automatic a fashion as possible. Dynamic recalculations of the vehicle trip progress with new estimated times of arrival/departure are made with the aim of recovery with minimal delays within safety constraints. New potential conflicts are determined and a revised flow management scenario developed. If passenger notification criteria are met, then delay notices and announcements are triggered for passenger benefit. In the event of severe conflicts, emergency responses are invoked.

Failure management calls for coordination procedures, functions, and inter-operations of the maintenance facility and the command center. For important scenarios of failure management, advanced software approaches such as artificial intelligence aids in planning, crisis management, and decision support need to be explored.

4.2.3 Supervision Functions

Route Planning

Route planning establishes the master network schedule of predetermined trips for some fixed period of time (seasonally adjusted, based on market information and resource availability). It establishes the route profiles for the trips including the initial/final terminal points, station stops, switch points, switch settings, speed profiles for each zone, and scheduled times of departure and arrival for the individual trips.

Route re-planning occurs in situations of temporary outage of guideway sections, in instances of guideway changes or integrity conditions, or in demand surge periods of passenger overload. The route profiles are routinely updated with information provided from the maintenance systems which indicate, for example, that sections of guideway can only support degraded speed profiles and the degraded rating. Under both route planning and re-planning, the CCF global database is updated and the appropriate zone controller local database updates are made with respect to any route integrity and condition changes. Periodicity and means of update at the zone controllers is to be determined during the preliminary engineering design phase.

Route assignment will associate individual vehicle identification codes with the individual trips and is made at some fixed time before each daily schedule. Thus, the specific vehicle assigned to a

particular trip allows for routine maintenance cycles and repair. The extent of route data and the periodicity and means of their update is to be determined in further command and control architecture refinements. Route dynamic scheduling adjusts the schedules on a demand basis depending on the actual load and constrained by the upper limits on capacity and safety requirements on each route.

Within the constraints of route planning and re-planning, vehicle flow management is engaged. Unlike air traffic control which evolved over many years to the notion of flow management, from their beginning maglev systems can utilize flow management techniques geared to the unique concerns of the new technology. Flow management in maglev systems is defined to be the capability to anticipate and recognize the overload of pre-defined maglev route management components and to respond with timely flow control through these components such that the system capacity and availability are preserved or minimally impacted. Maglev route management components are defined to be at least the switches to off-line stations, station berths, the off-line to on-line merge switches, the route switches, and the terminal points (see Figure C4-3)

In addition, the route segments will form part of that flow management. In the preliminary engineering design phase the granularity of needed control will be determined. It may be sufficient to manage the route segments between the above mentioned components (although the conjecture is that granularity may be too coarse); it may be necessary to manage the zones in a lower level hierarchy of control; or it may be necessary to manage each zone at the same level of flow management as the route management components mentioned above. These alternatives form part of the command and control hierarchical architecture design tradeoffs.

The availability of each of the significant route management components is to be managed on a time slot basis.

Dynamic vehicle flow management occurs during the actual trips made and is a part of dynamic route scheduling.

Dynamic Route Scheduling

Route traversal or trips are monitored at the CCF and displayed for the CCF operators. When a vehicle has been given a specific route assignment on a particular trip or flight, the position of the vehicle is tracked and compared to the data in the route profile database. Hand-offs of vehicles are

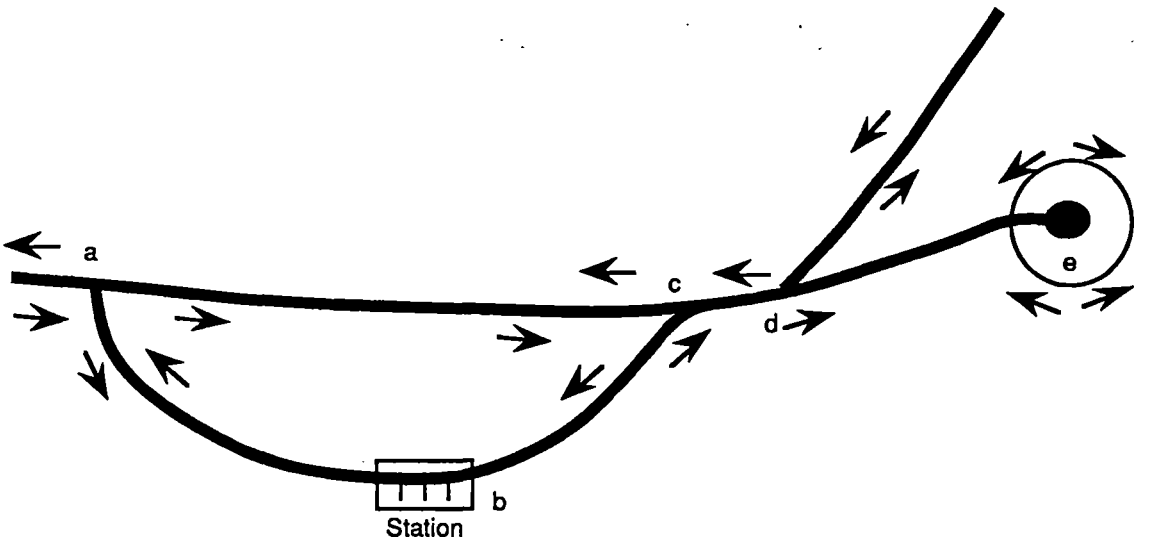

Flow Management (normal operation)

a: switch to offline station
b: station berth
c: offline to online merge switch
d: route switch
e: terminus

Figure C4-3 Maglev route flow management points

made at the zone controller level and monitored in progression at the CCF so that at all times, all vehicle locations and statuses are known. If the speed profile is not being followed for a particular vehicle, an extrapolation is made to assess the impact of the differential. Conditions such as overspeed protection violation are detected. Projected delays are mitigated or annulled by adjustment of the nominal or rated speed profile limit (safety, energy consumption, and ride comfort constrained) within the absolute safe speed limit for the zone (safety constrained). The effects of the changes are checked for impact in the vehicle flow management of the maglev route assets. The exact allocation of this function will be made when the architectural tradeoffs are made in more detail during the preliminary design phase.

Figure C4-4 shows in more detail the entire process covered in the Route Planning and Dynamic Route Scheduling functions. The entire process is divided into two phases: planning and execution. Planning covers the first three boxes.

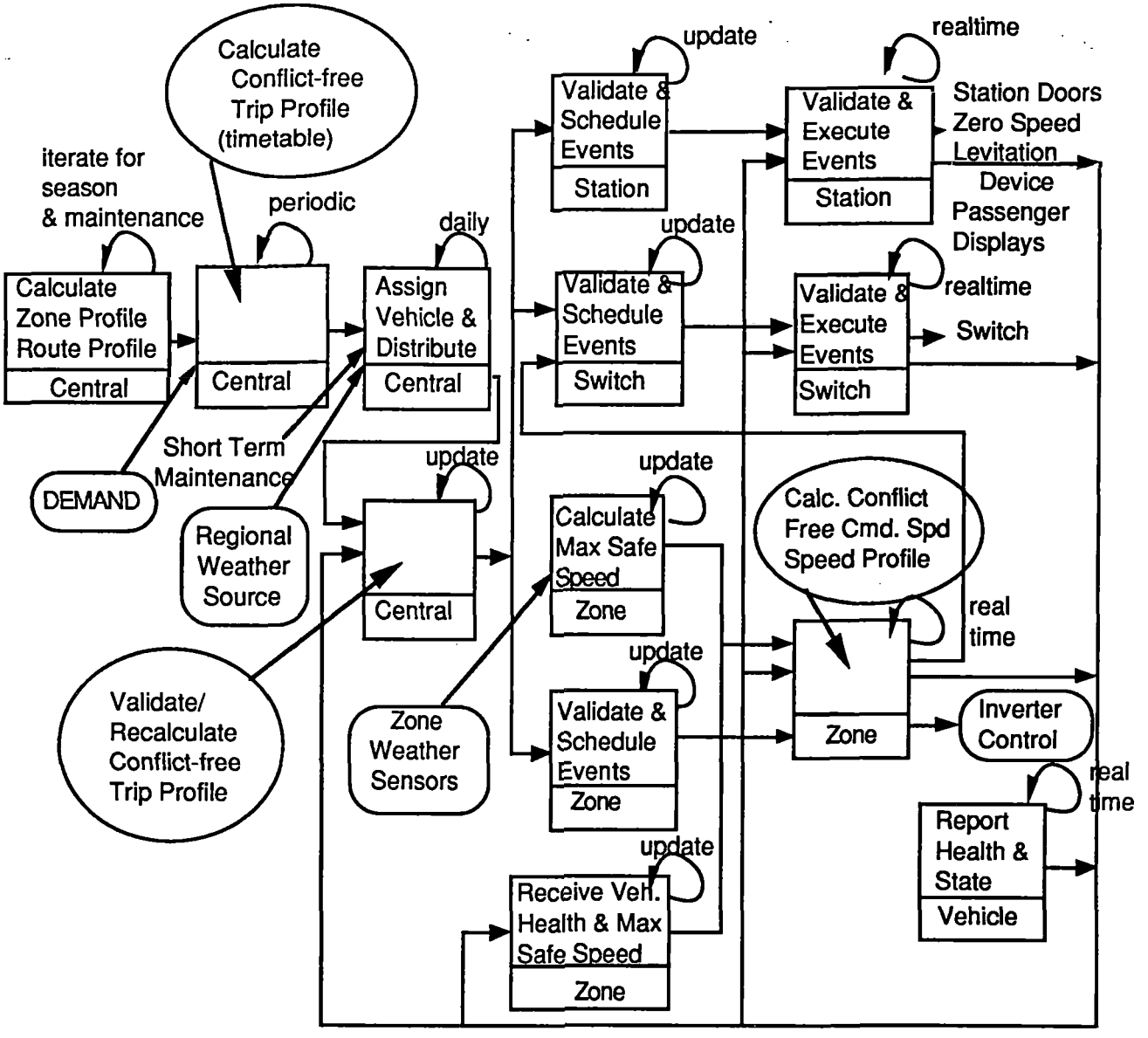

Figure C4-4 Overview of control thread for vehicle scheduling and movement

Calculate Zone Profile and Route Profile

Calculate maximum speed profiles for each zone based on topography of zone (curves, grades, switches, stations, etc.) and on the expected range of environmental conditions (wind, snow, etc.).

Calculate route profiles for all possible non-stop routes between all stations based on acceleration and de-acceleration rates and maximum speed profiles for each interior zone

Calculate Conflict-Free Trip Profiles (Timetables)

Based on demand as determined by marketing activities, calculate a set of conflict-free train movements (timetable) for normal operations and for any expected degraded operations (likely bad weather, etc.)

Assign Vehicles and Distribute

Shortly before the start of a day's operations, assign specific vehicles to each movement and distribute the day's timetable to all stations, switches, and zones.

Validate/Re-calculate Conflict-free Trip Profiles

Based on feedback from any of the executing elements (zones, switches, and stations) that vehicle movements are not occurring according to the planned timetable, and that the executing element cannot recover to the timetable without causing conflicts, calculate conflict-free revisions to the timetable until recovery to the original timetable can be accomplished.

Validate and Schedule Events (Station/Zone/Switch)

Each element will validate the integrity of the message and then will schedule all vehicle movements and associated actions such as powering up the inverters or throwing a switch. Each element will also validate the safety of each action, such as, detecting that two vehicle movements are scheduled without sufficient time in between to throw a switch.

Calculate Maximum Safe Speed

The zone will calculate the maximum safe speed based on local environmental conditions.

Receive Vehicle Health and Maximum Safe Speed

The zone will receive, from the vehicle, health information and any other indication from the vehicle that the vehicle can only safely operate at a speed which is less than the normal maximum safe speed.

Calculate Conflict-Free Command Speed Profile

The zone, based on the scheduled operations from the timetable, and of over-riding safety limits from zone and vehicle sensors, will calculate the maximum safe speed profile for a vehicle transiting the zone and provide this profile to the propulsion equipment.

Validate and Execute Events (Station/Switch)

The element will check all planned actions against the current situation and, if safe, will execute the event.

Report Health and State

The vehicle will monitor its own health and state and report that state and health to other system elements.

Dispatch and Docking Control (Safety Critical)

Dispatch is done on a special acceleration zone. The zone controller requires the vehicle to follow a specific velocity profile so as to merge onto the guideway at a specified time and place. Once a vehicle has merged with the main guideway, its further acceleration and velocity is controlled by the zone and motor controller for the zone it has entered.

Associated with the acceleration zone is a guideway switch which operates correctly to allow through vehicle traffic to continue but allow the merging vehicle to enter the guideway and continue to accelerate. The operation of the switch is a safety critical function and is closely coordinated with the dispatch function. The switch position operates in an interlocking fashion with reliable input from redundant sensors to determine the state of switching mechanisms so as to guarantee the fail-safe entry of a vehicle onto the main guideway and to prevent any possible collision with through vehicles. These operational requirements apply whether the switching mechanism is passive or active.

There is also an abort capability to allow the vehicle to stop and then back up if a problem is detected before the vehicle reaches the switch. The merging speed is only about 40 m/s (89 mph), and the acceleration zone is designed to abort departure if switching cannot be safely completed.

Docking is done in a special deceleration zone. The zone controller brings the vehicle to a safe stop at the correct place. This is also a safety-critical operation because the docking is performed in an area where there may be many people and other vehicles. Suitable warning and collision avoidance procedures are used to insure a safe docking. Note that the deceleration rate is no more than 1.5 m/s^2 so people may stand up and walk in preparation for leaving the vehicle. This reduces the time required for stopping and does not pose a safety problem.

Vehicle Operator Interface (Mission Critical)

Each vehicle has a human interface on board to display the status of all on-board systems as well as the relative position of the vehicle on its route, its velocity, weather conditions, safe stopping points, and stations. The on board passenger service personnel are responsible for ensuring that passengers board and disembark safely before closing the doors prior to allowing the automatic systems to take control of the vehicle. The vehicle cannot move if the doors are open. Although doors are opened automatically, they are closed under operator control. When the vehicle is moving or being towed on its air bearings for emergency operation, the vehicle is under manual control.

On-Board Passenger Supervision (Safety Critical)

This function directs the on board activities of passenger and crew regarding passenger safety and comfort. These functions allow the crew to deal with any emergency situation which may arise. This function notifies the passengers of any schedule changes.

Station Supervision

Station supervision encompasses vehicle, passenger, baggage, freight, and mail handling. Under passenger handling, the automated fare/ticket collection and reservation systems is considered. Passenger information and interface systems include the arrival and departure information, delay information and announcements, berth or gate information, and passenger paging capability. Security is also an integral part of the station supervision.

Vehicle handling includes the switching, merging, routing, and berthing of the vehicles; the interfaces between the station supervision and other system components such as the zone controllers managing the vehicle speed, the CCF monitoring the vehicle status and location, and switch controllers managing the arrival and departure of the vehicles at switch points, etc.; the communication links between the vehicle and station capabilities, and the vehicle reservation and dispatch system interfaces to add passenger vehicles for overload conditions, and so forth.

Associated with the vehicle handling requirements are special procedures such as the zero speed levitation and programmed start/stop operations with special power needs as well as the special collision avoidance applications that are applied in the station transits and in densely populated areas. For responsiveness to unexpected ridership requirements, demand scheduling provides slot creation and vehicle routing to handle added vehicles.

Passenger handling includes station graphics, audio announcements (Public Address or PA), video surveillance or recording, and alarm or change of message display capabilities for any unscheduled vehicle operation.

Central Operator Interface

The capabilities delegated to the CCF operators are a major part of the command, control, and communications system architecture and are essential for overall system operation integrity. The operator interface capabilities include all equipment, computer hardware and software, including data storage subsystems (which can be significant and sizable), and other devices that enable the operator to manage the overall system operations efficiently. The functions include: system operation, consisting of vehicle control and zone or wayside power distribution subsystems, passenger interaction, surveillance, audio/visual communication devices, and operations related to emergency situations.

The central supervision operation has the responsibility for monitoring and managing the overall operation of the command and control system. It includes the ability to expand the system operations to meet the ultimate ridership requirements of 12,000 pphpd without the redesign of the status display subsystem. It provides all the interfaces for both human and automated inter-operating systems and provides the coherent top-level view of the maglev capability. Through the Central Command Facility or CCF one should be able to assess the current overall health of the entire network. Stress points in the operations should become clear in the monitoring function and dynamic route scheduling invoked to alleviate overload, fix delays, or field emergencies and failures.

That overall fusion of data is provided through audio and visual displays and output. Central operators may then assess the conditions and status of all subsystems and take appropriate actions. The status display consists of a system schematic display including the conditions of the power subsystem, the guideway status, switch position and status, station condition, queues, and possible congestion, and the status of all communication links, whether for vital or non-vital functions. These displays use high resolution graphics capability to present the real-time data exchange about all aspects of the system, including the identification of all vehicles, travel direction, vehicle status relative to its scheduled position, the operating modes, wayside or zone controller equipment status such as the backup power status, and the connectivity status of communication subsystems.

The power subsystem display presents the conditions of the presence or absence of electrical power in each zone of the guideway, including the status of the circuit breakers, switches, and condition relative to its normal operating positions from the primary feeders.

The general system display serves the integrated system performance including the yard and maintenance operations. It provides the central operators the capability to assess and determine the emergency response requirements while interfacing with all other display subsystems. The general system display provides the interfaces to remotely manage crises and failures on a system-wide basis.

The CCF interface operations also include the reporting of alarms and malfunctions along the guideway/stations and coordinating the recovery actions for any unscheduled events with potential security or safety problems. For example, the data communications between the CCF and the vehicles and zone controllers is monitored for connectivity as part of a CCF operator's overall system safety assurance function (as well as at the other systems components for self awareness of interconnectivity status). With a fault tolerant computer, once the persistent failure of communication transmissions is detected, the CCF operator initiates pre-determined corrective actions to minimize the impact on the overall system performance for the route planning and scheduling activities.

4.3 PRELIMINARY COMMUNICATIONS AND CONTROL SYSTEM ARCHITECTURE

4.3.1 System Components

In the current preliminary design, there are at least six physical elements with command and communications capabilities. These are the vehicle, the zone, the switch, the station, the central control facility, and a maintenance facility. The command and communications functional requirements, as developed in the preceding paragraphs, must be allocated to one or more of these physical elements. After a short description of each physical element, the preliminary allocation of functions is then given in the following paragraph.

Vehicle

The vehicle is the movable device which will carry passengers, and perhaps freight, from point to point on the maglev network. It includes all hardware and software which is actually onboard the vehicle and does not include anything which is not onboard the vehicle. As such, it includes the passenger compartment and all onboard facilities to maintain passenger comfort, the onboard

suspension, levitation, and propulsion equipment and their onboard controls, onboard communications equipment, and onboard controls for manual emergency control of vehicle movement.

Zone

The zone is a section of the guideway (usually about 4 km. long) which is controlled and powered by a single wayside controller. It includes the guideway, its supporting structure, the wayside controller and power equipment, all sensors on the guideway, the communications equipment at the wayside controller, as well as communications links running along with the guideway. It does not include any onboard equipment on the vehicle. Figure C4-5 shows the zone control arrangment.

Switch

The switch is a movable section of guideway and includes the movable guideway and the control and power equipment to move the guideway. It also includes the communications equipment at the switch controller. Levitation and propulsion on the movable section of the guideway is part of and controlled by the zone equipment and not the switch equipment.

Station

The station is the equipment and structure which abuts against a section of the guideway (itself part of a zone) for the purposes of on-loading and off-loading passengers and freight. It interacts with one or more zones for moving vehicles through the station and with switches to direct vehicles to or around the station. It also includes all facilities for handling passengers and freight including doors for controlling access to the vehicles, passenger waiting areas, ticket counters or machines, public address and displays for announcing the arrival and departure of vehicles, passenger access to the station, freight loading docks and transfer equipment, and parking areas. It also includes station operator facilities and communications equipment at the station. The station control system is shown in Figure C4-6.

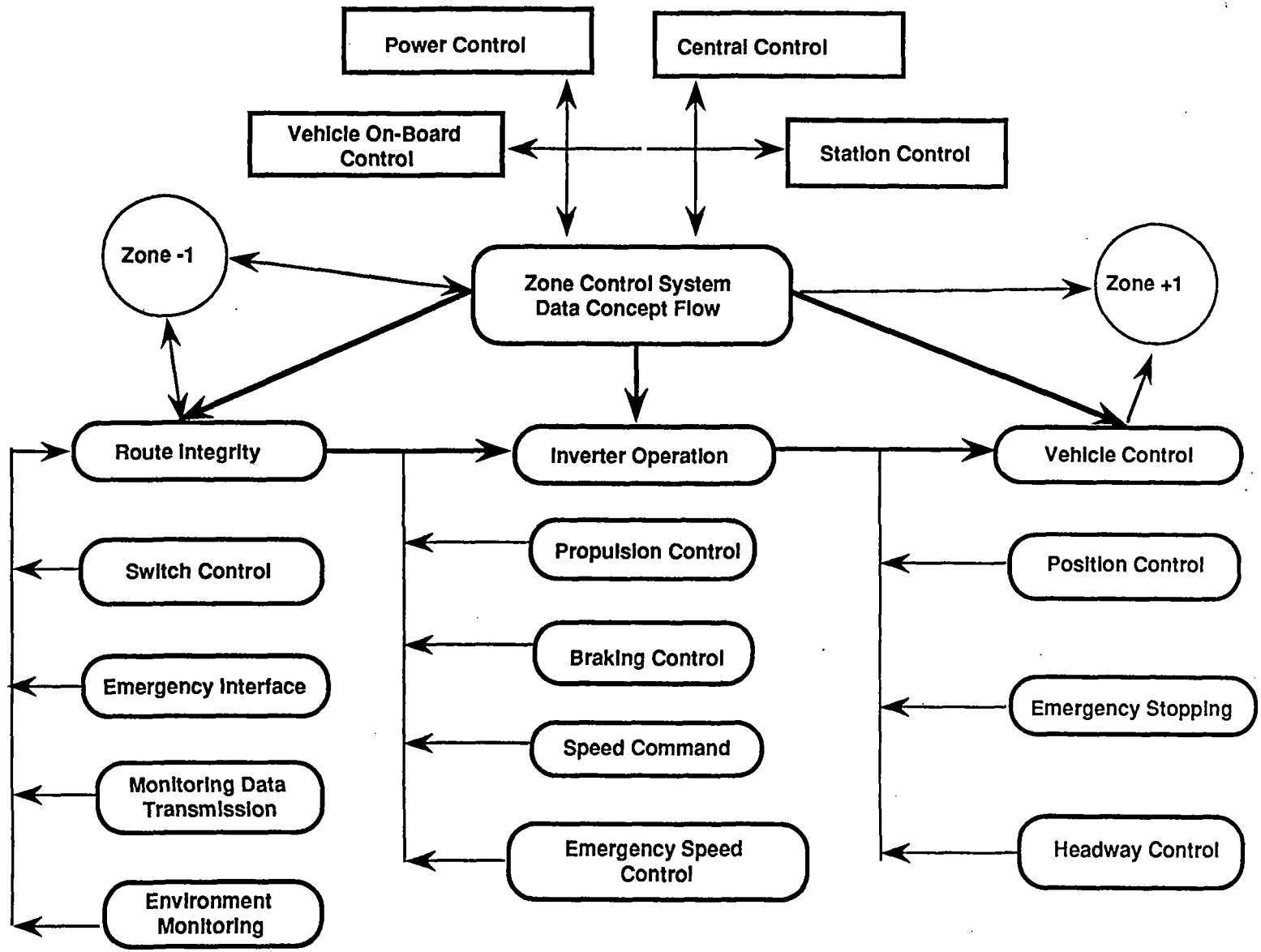

Figure C4-5 Zone control block diagram

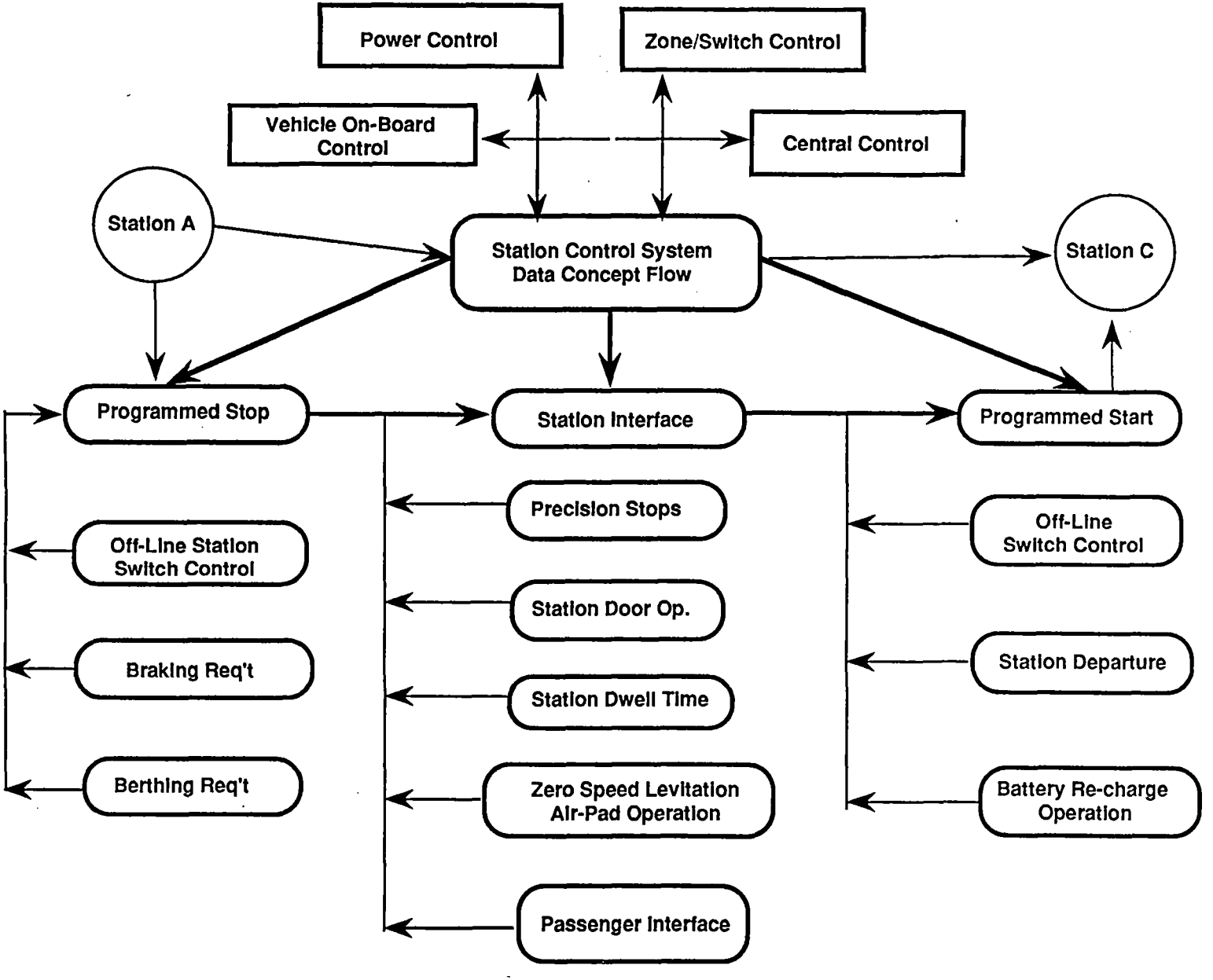

Figure C4-6 Station control block diagram

Central

The central facility is the top level control facility for all other elements of the maglev system. It is seen as a single site which would be manned 24 hours per day. It consists of data processing equipment, displays, and terminals for an operator interface, and communications equipment. It has both a long term planning role, for operations and maintenance, and a short term intervention role for all system anomalies which can not be handled automatically at the zone/station level. It also provides the operators with information to monitor normal operations and to alert them to abnormal situations. The Central Control system is shown in Figure C4-7.

Maintenance

The maintenance facility (seen as one site for system wide maintenance) is responsible for maintaining and repairing all parts of the system. This includes the hardware and software of the vehicles, zones, switches, stations, central, and the maintenance facility itself. It also has the responsibility for obtaining maintenance on equipment and software leased for use in the system. It does not include the zones and switches necessary to route vehicles into and around the maintenance facility but interfaces with these zones and switches. It does however, include an operator position to control and monitor the movement of vehicles within the facility. It is also be responsible for maintaining configuration control of the equipment and software of the system. It also includes a research and development area for analyzing system performance and investigating system improvements.

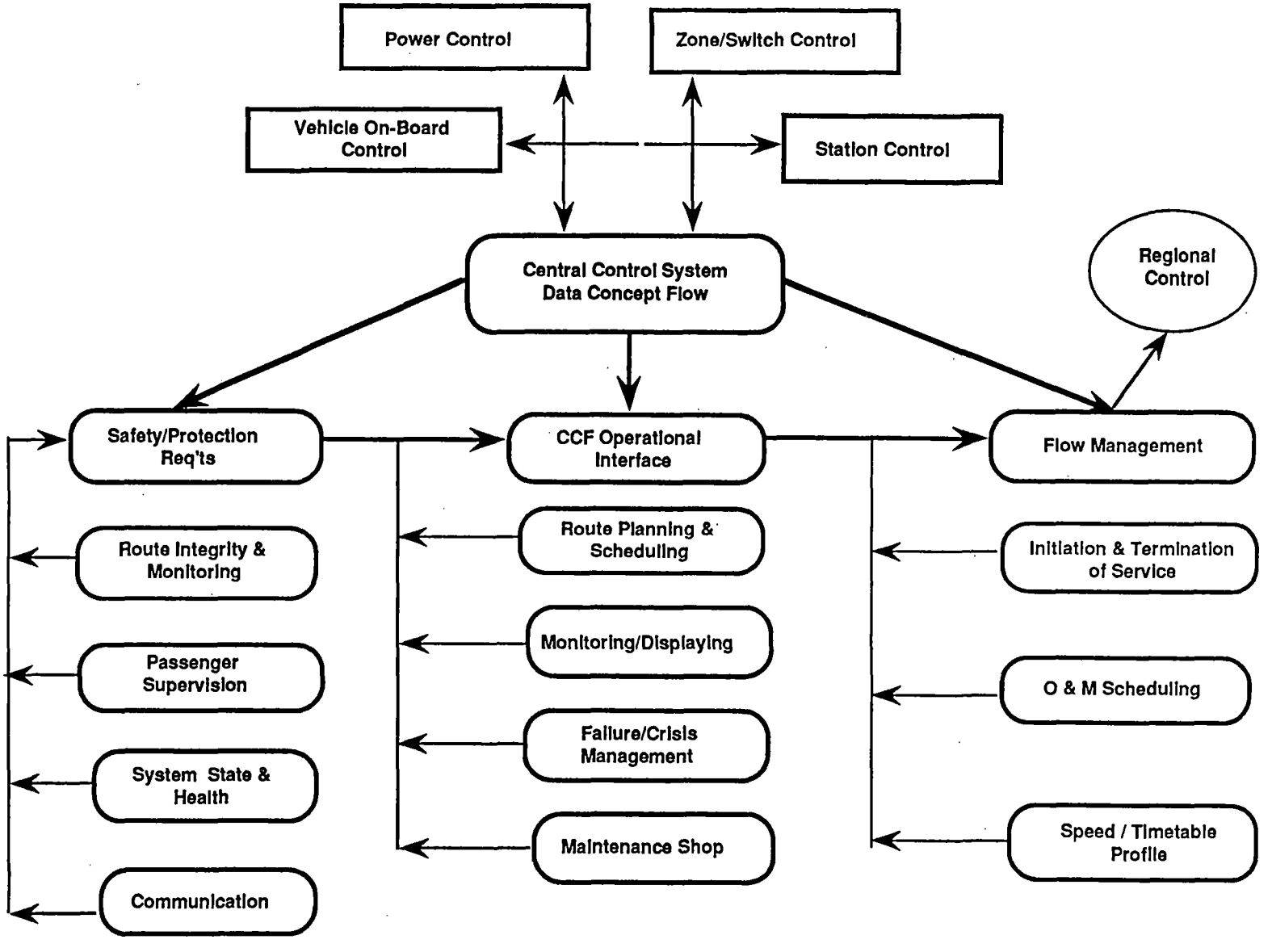

Figure C4-7 Central control block diagram

4.3.2 Preliminary Allocation of Functions

Following the definition of the functional requirements, and with a baseline architecture identified, the next step is to begin the allocation of those functions to those architectural elements. A variety of global goals, both traditional and system specific, need to be satisfied. Among the more important goals are:

- Fully automatic operation, that is, no real-time operator intervention, at the vehicle, zone, station, or central, is required for normal operations
- Minimum communications between facilities, especially where RF links are required
- Accommodate future expandability, both in the extent of the system and in ability to interface with adjacent maglev system, but alto to accept future enhancements in technology and functionality
- Allocating functions to the most local level at which they can safely and reasonably be performed to simplify the cognitive overhead needed to produce a given element, enhance its reliability, and reduce its scope of control so that malicious failure modes are constrained
- Provide redundancy and back-up modes to achieve extremely high levels of availability

Furthermore, after the minimum requirements are fully defined, understood, and met, the system is designed to be built at the minimum cost.

For our system concept definition, vehicle control is fully automated. The high speed of the vehicles and the short headway between them require the ability to respond to changing conditions which far exceeds the capabilities of a human, however vigilant and well trained. Thus, the three principal functions used to operate the maglev transportation system, i.e. control, protection and supervision, are, for normal operations, fully automated, tightly coupled, and have significant amounts of information flow between them. An earlier section presented the principal functions to be performed by the control system. The control system comprises three spatially distributed hierarchical levels: onboard vehicle computer system, wayside zone control computer system, and central control facility (CCF). Data is acquired, transmitted, and processed at all three levels. Figure C4-8 shows the three hierarchical components of the maglev control computer system.

Eventually, there may be a need for national control of the maglev system. This would probably require a hierarchical organization similar to that of the U.S. air traffic control system. This fact has been borne in mind during the design of the present architecture which governs operations for a regional system, thus facilitating the implementation of a national control system in the future.

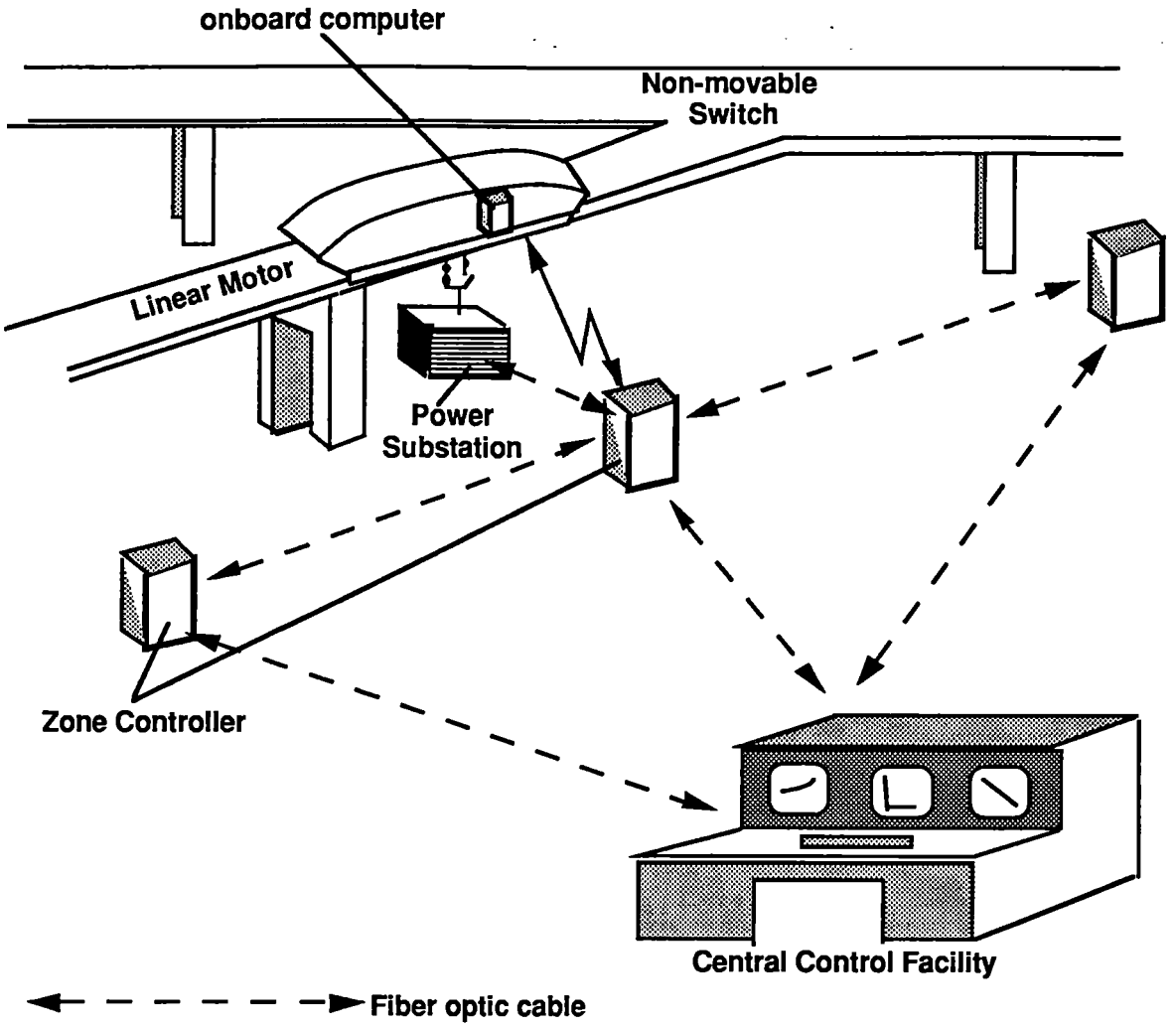

Figure C4-8 Maglev operational control system

The various functions have been mapped to specific computation sites within the overall control computer architecture. Table C4-1 presented the functions which are necessary to perform automatic train control. In order to facilitate future expandability, reduce the communication overhead, and simplify the cognitive overhead needed to produce a given module, thereby enhancing the software reliability, the design philosophy for this architecture will be to place functions at the most local level at which they can safely and reasonably be performed. This approach is consistent with an expandable system since only the highest level program will need to be modified to include interaction with a more global control mechanism.

In this architecture, the protection subsystem operates independently from the control functions and therefore provides a fail-safe mode of operation. In cases where the speed or position of a

vehicle exceed safety thresholds, these protection functions can override the actions of the control functions and assume control of the vehicle.

The supervision function is performed by the central facility computer system, which also includes major computing subsystems located in stations. However, the supervisory data which is needed by the primary control computer to adequately perform its function is transferred to that computer on at least a daily basis and may be updated more frequently. This information will be referred to as the route profile for a given vehicle. The format of this information will vary, depending on whether it is to be used by the on-board computer or the wayside computer. This method of anticipating future behavior of the vehicle and confirming its correct behavior in the present supports the method of train scheduling which views all normal train travel as planned in advance and all passengers riding in reserved seats. However, the design also could be adapted to a more dynamic method of operations, based, for example, on the airlines shuttle service. This service is demand driven, rather than schedule driven and requires more real-time planning capability. Planning algorithms typically require significant memory and throughput in their computing platforms. Hence, the capacity of the present architectures would need to provide adequate and easy means of expandability if this functionality is to be addressed in the future.

When a certain function can, for obvious reasons, best be performed in one site over another, it is assigned to that site. For example, the control of the cryogenic system, secondary suspension, and on-board systems like air conditioning and lighting all require the control of on-board actuators. Furthermore, the sensors needed to obtain feedback information for these systems are also on-board. Hence, the control of these functions should obviously be performed by an on-board computer. Another example of a set of functions which can most easily be performed by an on-board computer is that of emergency stopping, emergency speed control, and emergency position control in the event of a failure of the propulsion system itself. Control of these functions by the on-board system would need to be performed until the vehicle had either coasted to the next guideway zone or until it is safely stopped at a designated safe stopping point to await a manual operation takeover.

The trend in most automated train control systems is to control the speed of the vehicle speed from an onboard computer, the upper limit being set by the central control facility. In traction driven systems, this approach makes sense since the motor driving the train is typically on board. However, unlike conventional transportation systems in which the power for vehicle propulsion is on board, the maglev system is powered from the guideway. The propulsion control platform must be co-located with the power converters since the required iteration rate is so high as to

preclude an allowance for any communication overhead. But control of the electronic power conversion equipment is a very low level function which takes as inputs voltages and currents. These values are derived from a knowledge of the desired vehicle velocity. Determining the correct value of the vehicle speed is no trivial matter and is, in fact, one of the most crucial components of system safety. A simplified version of the algorithm which the wayside zone controller uses to determine the correct vehicle speed is as follows. Obtain from locally stored non-volatile memory the maximum allowed speed for this zone, a value based on such things as guideway curvature and angle of elevation. Obtain from the next vehicle about to enter this zone the maximum speed at which it can travel, a value based on local weather and wind conditions and any other factors which the vehicle can sense in its environment, as well as its current velocity and acceleration. Obtain a value of any system-wide velocity de-rating from the CCF, which is based on regional conditions which may be remote from this zone. Using the most recent copies of this data, choose the minimum value as the correct vehicle speed. Convert this to current and voltage values which can be passed as commands to the propulsion controller. Since a zone controller only controls one section of the guideway, a failure here cannot propagate beyond this zone. The communication between wayside systems can be carried out through very reliable media such as redundant fiber optic cables. By locating sensors in the guideway, the vehicle location and route integrity functions can also be performed by the wayside using sensors embedded in or alongside the guideway for these purposes. Again, collecting this information from stationary sensors can be accomplished through secure media. Route control, or the direction of the vehicle through a switch, can also be performed from a wayside computer. This function to subsystem mapping is detailed in Table C4-2 (following Figure C4-9). Figure C4-9 provides a simplified analysis of the data flow in the system. In this figure, **P** signifies the primary assignment, **B** signifies the backup assignment used for verification and consistency checking, and **O** represents an oversight function which can override the primary control function for safety reasons.

A Quantitative Analysis of Maglev Control Functions

The computational requirements of an application are embodied in the scheduled tasks which perform its functions. In order to specify the control computer architecture for the maglev system, each major function which the system must perform has been analyzed quantitatively. To perform this analysis, estimates have been made of each of the following operating parameters for each major function.

(1) Iteration rate (Hz)

(2) Throughput

(3) Memory requirements (Megabytes)

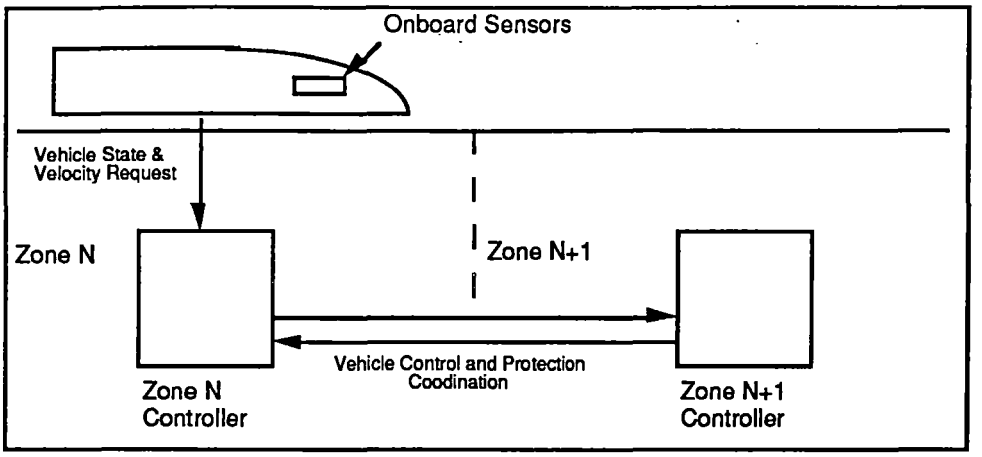

Figure C4-9 Simplified data flow diagram of the control computer architecture

(4) Input (kilobits per second)

(5) Output (kilobits per second)

The iteration rate, often referred to as the frame rate, is the frequency at which a control law must be applied to the system being controlled. During each iteration, new sensor readings are obtained, the control law algorithm is executed, and new actuator commands are generated. Some control laws applied to the control of vehicles, especially aircraft, have hard, i.e. inflexible, real-time constraints. These control algorithms are based on the assumption that they will execute in a periodic manner with exactly the same amount of time between the start of each iteration. Any deviation from this periodicity is called jitter. The degree of jitter which can be tolerated varies from application to application. Some control functions do not have demanding real-time requirements. This class of real time applications is able to tolerate jitter. It may be possible to accommodate both classes of control functions within the same computer by allowing low priority applications to execute when time is available and by allowing high priority functions to interrupt the execution of lower priority functions so that they can meet their hard real-time deadlines.

Scheduling various control applications so that demanding tasks run on time and complete within their time allotment is a challenging aspect of control system design and implementation. The validation of real-time scheduling algorithms is an especially difficult task. For the maglev control system a wide range of iteration rates and priorities are required. The throughput of a computer is the number of instructions which it can execute in a second, often measured in MIPS (millions of instructions per second). The throughput requirement of a task is calculated by using two different methods, with the larger result prevailing. In the first method, the iteration frequency in Hertz is multiplied by the maximum number of instructions which the task could execute during an

Table C4-2
Function Assignment for the Control Computer Architecture

	Onboard	Wayside	Central	Station
CONTROL				
Vehicle State Monitor	**P**	P		
Velocity Control		**P**	O	
Cryogenic Control	**P**			
Propulsion Control		**P**		
Secondary Suspension Control	**P**			
Switch Control		**P,B**	O	
Vehicle Systems Monitor and Control	**P**	O	O	O
Environmental Monitoring	**P**	**P**	**P**	**P**
Station Operation			O	**P**
PROTECTION				
Safe Vehicle Separation Control	O	**P,B**	O	
Vehicle Position Control	O	**P,B**	O	
Route Integrity Control	B	**P**		
Emergency Stopping Control		**P**	O	
Emergency Speed Control		**P**	O	
Emergency Position Control		**P**	O	
Emergency Response Management	B	B	**P**	B
Failure Management			**P**	B
SUPERVISION				
Route Planning			**P**	
Dynamic Route Scheduling			**P**	B
Dispatch and Docking Control				**P**
Maintenance Scheduling			**P**	
Vehicle Operator Interface	**P**			
Onboard Passenger Supervision	**P**			
Station Supervision				**P**
Central Operator Interface			**P**	

A graphical view of the functional allocation is shown in Figure C4-10.

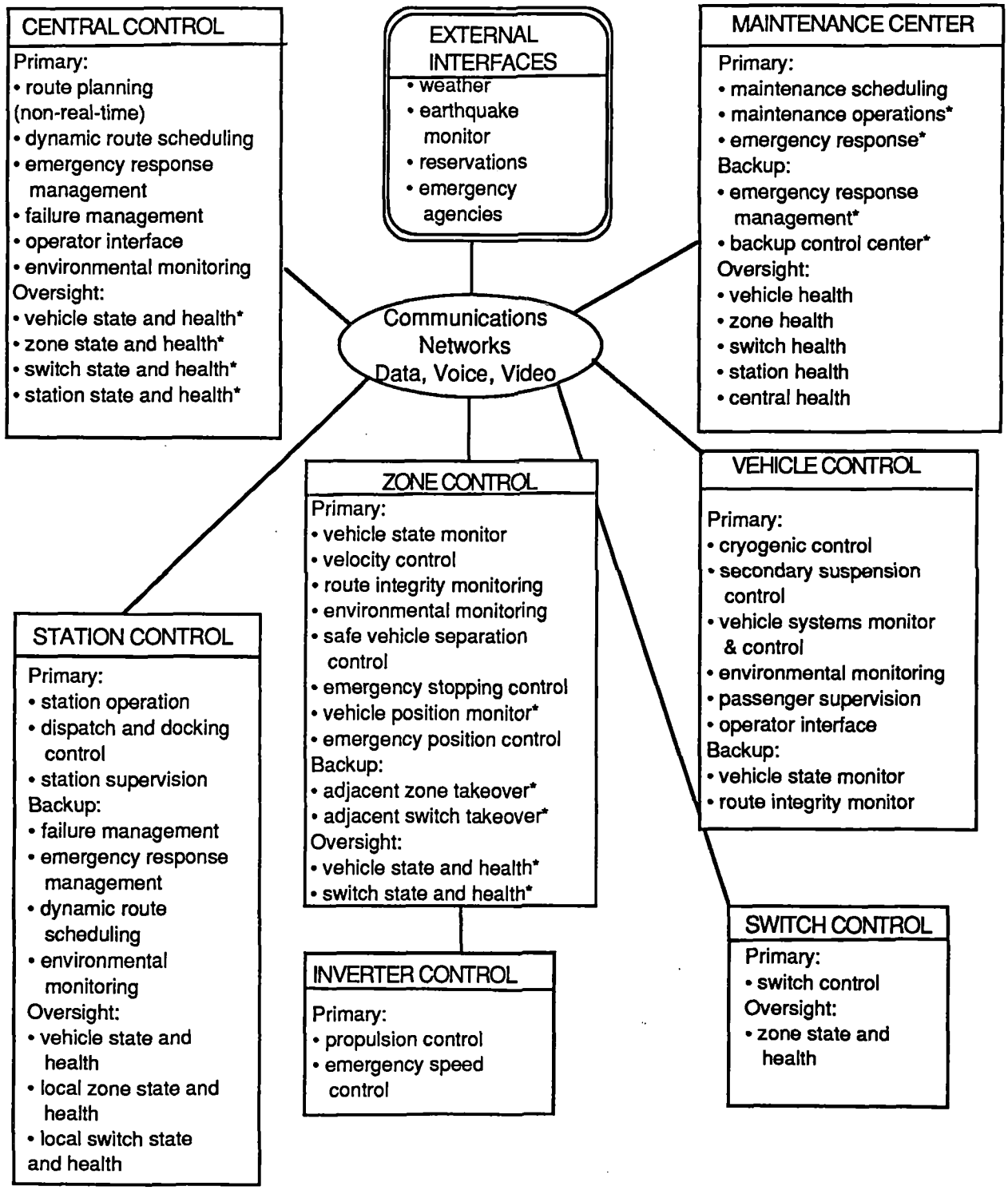

Figure C4-10 Functional allocation

iteration. In the second method, the maximum number of required instructions per iteration is divided by the maximum allowed processing lag. Processing lag, also called transport lag, is the time interval between the time a sensor, which provides a value to the control law, is read and the time an output value is delivered to an actuator. An application which only uses a few instructions per iteration most likely has a throughput requirement dominated by the size of its processing lag. On the other hand, the first method probably generates a more demanding throughput requirement for an application which requires many computations, i.e. instructions, per iteration.

Throughput, however, is a very course measurement to use when sizing a computing platform for a given application. In the first place, internal machine architectures play a significant role in the magnitude of these numbers. Reduced Instruction Set Computers (RISC) typically have very high values of MIPS compared to CISC machines (Complex Instruction Set Computers). However, a single CISC instruction may incorporate many RISC instructions. In the second place, on a given machine, different instructions take different amounts of time to execute. Hence, most manufacturers provide an instruction-mix throughput value which is probably favorable to their machine. Various instruction-mix benchmarks can be used to measure the throughput of a given machine, such as the Digital Avionics Instruction Set (DAIS), Whetstones, Dhrystones, VAX Units Per Second (VUPS), Specmarks, etc., however, these may not accurately reflect the mix in a given application. A more significant assessment of the actual processing lag can be obtained as a design proceeds by bench marking a given application using a specific programming language, compiler, operating system and processor. Furthermore, it is customary to require an additional margin of throughput from a computing platform to allow enhanced capabilities in a given function to be easily accommodated and also because it is often difficult to obtain accurate quantitative measurements about an application early in the development cycle. The values of required throughput for the various maglev functions presented in Table C4-3 represent generous estimates of various experts working on specific functional areas or from comparisons to equivalent avionics applications and may be used at this stage for preliminary gross system sizing.

The memory requirement of a given function is the amount of RAM needed to perform its calculation. Generally, much smaller amounts of ROM are needed. Applications such as signal processing, which handle large arrays of data, require significant amounts of memory. However, since reliable memory devices in the megabyte range are economically available, these requirements can easily be accommodated. Memory usage is difficult to estimate before a software module exists. At that time, measurements can be taken and more accurate requirements can be established. Furthermore, it is important to allow a generous margin of additional memory to allow for function growth and enhancement in a system. The maglev functions have a wide

Table C4-3
A Summary of the Quantitative Analysis of Primary Maglev Control Functions

	Iteration Rate (Hz)	Throughput	Memory (MBytes)	Input (kbits/sec)	Output (kbits/Sec)
CONTROL					
Vehicle Location	4-8	<< 1 MIPS	<< 1	~2	~2
Velocity Control	4-8	<< 1 MIPS	<< 1	~4	~4
Levitation Control (EDS)	1-2	<< 1 MIPS	<< 1	~1	~1
Propulsion Control	1000	a few instructions	<< 1	~1500	~1000
Secondary Suspension Control	200	1.2 Mflops	< 1	400	128
Route Control	1	<< 1 MIPS	<< 1	~4	~4
Vehicle Systems Monitoring	1	<< 1 MIPS	<< 1	~1	–
Vehicle Systems Control	1	<< 1 MIPS	<< 1	~1	~1
Environmental Monitoring	1	<< 1 MIPS	<< 1	~1	–
PROTECTION					
Safe Vehicle Separation	1 - 100	< 1 MIPS	< 1	1 - 10	<< 1
Vehicle Position	4 - 8	< 1 MIPS	1 - 2	< 1	<< 1
Route Integrity	1 - 1000	1 - 400 MIPS	1 - 2	1-10,000	1 - 2
Emergency Stopping	on demand	< 1 MIPS*	<< 1	~4	~4
Emergency Speed Control	on demand	< 1 MIPS*	<< 1	~4	~4
Emergency Position Control	on demand	< 1 MIPS*	<< 1	~4	~4
SUPERVISION					
Route Planning	not real time	10 - 20 MIPS	10-40	–	–
Route Scheduling	not real time	10 - 20 MIPS	10-40	–	–
Dispatching	1-10	1 - 5 MIPS	1 - 5	10 - 20	10 - 20
Maintenance Scheduling	not real time	10 - 20 MIPS	10 - 40	–	–
Operator Interface	6-10	< 1 MIPS	1 - 4	< 1	–
Status Displays	5-10	< 1 MIPS	4 - 8	1 - 1000	1 - 1000
Passenger Supervision	1	<< 1 MIPS	1 - 2	1 - 10	1 - 10
Emergency Response	on demand	2-4 MIPS*	1 - 4	1 - 1000	1 - 1000
Failure Management	on demand	< 1 MIPS*	1 - 4	1 - 1000	1 - 1000

* Throughput requirement during operation.

range of memory requirements. The entries in Table C4-3 are conservative, i.e. generous, estimates garnered from experts working on the various functions or from comparisons to equivalent avionics applications.

Input bandwidth is the number of bits transferred per second from an input device, such as a sensor, to a recipient task. Similarly, the output bandwidth is the number of bits per second transferred from a control function task to an output device, such as an actuator. Since neither transfer can take place instantaneously, each form of communication has an associated latency. Typically, the processor and its sensors and actuators communicate with each other over a network or a bus with a fixed protocol and communication bandwidth. The bandwidth of the communication system must, in general, be much larger than the bandwidth required for any given task because it must be able to service all of its subscribers, have extra capacity for the communication overhead needed to handle protocols and error detection schemes, plus have a margin for growth. The values of input and output bandwidth shown in Table C4-3 for our concept is a summation of values representing the total bandwidth between a given function and a set of possible I/O devices.

Typically, a processor interfaces with sensors and actuators by means of analog-to-digital (A/D) and digital-to-analog (D/A) converters, synchro-to-digital (S/D) and digital-to-synchro (D/S) converters, and I/O controllers, which are micro-programmed interface devices. To obtain greater accuracy, the sampling rate of a sensor may be significantly higher than the rate at which the processor reads the sensor value from the A/D converter. The input latency is the time interval between the sampling of a physical phenomenon by a sensor and the delivery of the data from that sensor reading to the control task which uses it. Output latency is the time interval between the generation of an actuator command by a control task and the delivery of that data to an output device. The execution latency is the time it takes the control task to compute the actuator command, once it has all of its sensor input. The sum of the input, execution and output latencies is equal to the transport lag.

It should be noted that in order to produce a detailed design for the maglev control system, more detailed information than that presented in Table C4-3 is necessary. For example, from the preceding discussion, it is clear that this table does not include values for transport lag, I/O latencies, and execution throughput and communication bandwidth margins. Furthermore, the table also omits bandwidth values for intertask communication, which require a more detailed software specification than is presented here. Finally, the table does not present information on specific scheduling priorities, precedence and dependency relationships between functions, or pre-

emption constraints, all of which are needed for a detailed hardware and software design. However, the data is quite sufficient for an initial system specification. This specification would be refined as detailed functional requirements became available.

4.3.3 Preliminary Data Processing Architecture

The process of matching the maglev requirements with computer capabilities is simplified by considering the performance related requirements and the reliability related requirements as two orthogonal sets, each of which can be mapped independently of the other as a first order approximation. The performance related maglev requirements such as throughput, memory, input/output bandwidth, etc. determine the virtual architecture of the system. The reliability related requirements such as safety and availability determine the physical architecture of the system. The virtual architecture definition includes the number of processing sites, the allocation of control functions among these sites, and the number and type of sensors and actuators and their interconnections to the processing sites. The physical architecture definition includes the redundancy level of each processing site, the redundancy level of sensors and actuators, and the redundancy level of communication interfaces and media.

For the Bechtel maglev system, there are four principal computing sites: on board the vehicle, along the guideway at inverter stations, at stations, and in a central control facility. Each of these have different performance and dependability requirements as explained in the analysis above. All of these requirements can however be addressed by the versatile architecture of the Fault Tolerant Parallel Processor (FTPP) whose major features are discussed below. Following this discussion, preliminary computing platforms will be specified for each of the four principal sites in Bechtel design.

4.3.3.1 Architectural Details of the Fault Tolerant Parallel Processor

The FTPP has several properties which make it suitable for a maglev control computer system. In addition to ultra-reliability and real-time performance, the FTPP is flexible, easily extensible, highly programmable and has excellent communication interface capabilities. Attributes which make it very desirable for use in complex, safety-critical systems which must be verified and validated to the satisfaction of a Government oversight agency include Byzantine resilient fault tolerance, adequate fault and error containment, a simplex programming model, on-line reconfigurability, rigorous separation of redundancy management software and application software, and reliable communication with external devices. Furthermore, these attributes are not dependent on any specific technology of implementation.

The same properties which make the FTPP ultra-reliable also make it highly available and readily maintainable. For example, the FTPP is able to continue to operate correctly in the presence of failed components until they are replaced during regularly scheduled maintenance. As part of its normal fault tolerant operation the FTPP maintains detailed fault logs and other diagnostic information. This information facilitates the identification of a faulty component and is readily available to operations and maintenance personnel.

The fundamental components of the FTPP are the Processing Elements (PE) and the Network Elements (NE). The multiple PEs provide both a parallel processing capability and the raw material for hardware redundancy. The NEs cooperate to perform interprocessor communications. From the viewpoint of the PEs, interprocessor communications are conducted using bus semantics. NEs also efficiently perform various operations which are required by a system which is designed in strict compliance with the rigorous theoretical requirements of Byzantine fault tolerance described below.

FTPP Virtual Architecture

The programming model of the FTPP used by the applications engineer is that of a standard uni- or multi-processing architecture, using familiar operating system calls and constructs. As seen by the applications programmer, the FTPP supports a virtual architecture of a number of computing tasks which may execute in parallel, subject to preemption, data, and control flow dependencies. The programmer's model is that of a number of communicating tasks, as shown in Figure C4-11. The tasks communicate using message passing.

The application programmer has no knowledge of the redundancy level of the host computer supporting a particular task; the exact same code will run on any site regardless of whether it is simplex, triplex, or quadruplex. Moreover, when redundant sites are used, the application programmer is able to develop parallel applications under the greatly simplifying assumption that all processing sites are reliable. Thus the application programmer need not consider the possible effects of faulty component behavior upon his or her algorithm, thus allowing the programmer to focus on the sufficiently difficult problem of developing and optimizing a parallel application.

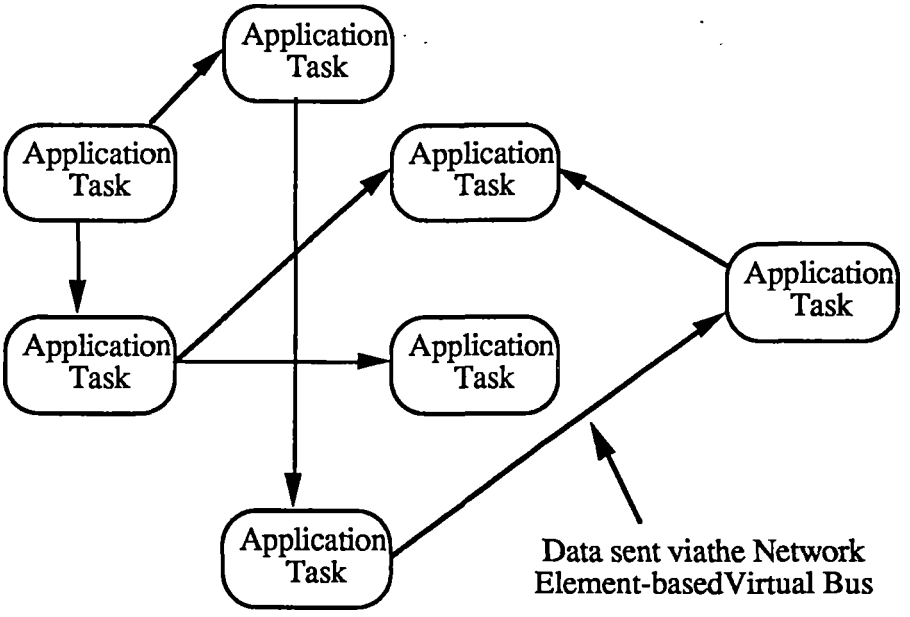

Figure C4-11 FTPP programming model

Byzantine Resilience Approach to Fault Tolerance

The reliability requirements of systems whose failures could result in the loss of human life are very demanding, with the probability of surviving such a failure approaching unity. Typically these are systems which cannot tolerate any errors in the computer system outputs, because such errors can result in irreversible behavior by the system being controlled. These computer systems are used to control modern aircraft, spacecraft, and weapons systems, to monitor nuclear power plants, and to direct various medical procedures. The control of maglev vehicles is another such life-critical application.

The traditional approach to the design of a reliable system is to perform a Failure Modes and Effects Analysis (FMEA). Using this approach, a supposedly exhaustive list of likely failure modes is compiled. An estimate of the extent and effects of each failure mode is predicted. For each failure considered to possess a reasonable chance of occurring, a fault tolerance technique is devised. This is clearly an impossible task for digital computers due to the extremely large number of possible component failures and combinations that must be analyzed.

For the maglev control computer system to achieve the required reliability level, fault tolerance approaches based on restrictive hypothetical models of anticipated failure behavior are completely inadequate. The possible failure modes of this complex system cannot be exhaustively enumerated. Therefore, to achieve correct outputs from the maglev computing platform with acceptably high probability, the platform must be designed to tolerate arbitrary failure behavior.

This form of fault tolerance is known as Byzantine Resilience. The term Byzantine Resilience has its origins in the seminal paper on the theory of fault tolerance by Lamport, Shostak, and Pease in which an analogy is drawn between communication among distributed computers and communication among generals in the Byzantine Army laying siege to an enemy city. Fortunately, simple theoretical architectural requirements exist which, if followed, ensure this important system attribute.

The requirements of Byzantine Resilience are stated succinctly in Table C4-4. Compliance with these requirements confers on a system of redundant processing elements the ability to reach agreement, i.e. come to the same conclusion, in the presence of faults. An f-Byzantine Resilient architecture is capable of functioning correctly in the presence of f arbitrary faults. These requirements are supported by rigorous mathematical proofs.

A system which meets these prerequisites is called f-Byzantine resilient. In a minimal 1-Byzantine resilient processing site, four participants, each of which is connected to the other participants by three disjoint communication paths, must execute a synchronous two-round protocol to obtain consensus in the presence of a Byzantine fault. The FTPP is designed in accordance with these architectural precepts.

Table C4-4
Requirements of an f-Byzantine Resilient Architecture

There must be at least 3f+1 participants in the communication algorithm, each within its own Fault Containment Region [20].
Each participant must be connected to at least 2f+1 other participants through disjoint communication paths [22].
The communication algorithm must utilize a minimum of f+1 rounds of communication among the participants [23].
The participants must be synchronized to within a known skew of each other [24].

It is important to note that all the requirements for Byzantine resilience to faults refer to the communication function of the system, which is provided by the NEs of the FTPP. By analogy to the original Byzantine Generals' problem, all of these operations can be carried out by the messengers. Although an ultrareliable communication network alone does not make a very interesting or useful system, when processors are connected to the network, a very powerful system emerges. The number of processors which can be attached to each fault containment region (FCR) depends on the bandwidth of the fault tolerant network, the bandwidth of the

processor interface to the network, and the reliability and throughput requirements of the application. The FTPP architecture provides a minimal region of high bandwidth interprocessor connectivity to be shared by a set of processors which time-division multiplex its services, resulting in minimal power, weight and volume overhead and minimal performance overhead for fault tolerant operation.

Systems like the FTPP which are designed according to this rigorous theory have the ability to mask errors in real-time by voting redundant copies of the outputs they produce, thereby providing uninterrupted delivery of the computational service in the presence of arbitrary, random hardware faults. They can recover from transient faults without loss of spare capacity and reconfigure themselves by using spare components or by gracefully entering a degraded operating mode when permanent faults occur. The validation of their fault tolerance capacities is facilitated because it is relatively easy to confirm the architecture's compliance with the theoretical requirements of Byzantine Resilience.

Physical Architecture

The basic unit of the FTPP comprises at least 4 FCRs, each with a Network Element and an associated Processing Element (PE). The addition of a fifth NE can provide greater reliability to the system. The design of the fault containment regions (FCR) satisfies requirements which prevent a fault in one FCR from propagating to another FCR, namely, electrical isolation, physical isolation, independent power and independent clocking.

The NE is a Draper-designed component, at least four of which are fully connected and which operate in tight synchrony to perform message exchanges according to the rules of Byzantine resilience. Each NE can host from one to N PEs, where N is a design parameter dependent on the application requirements. Each PE is a commercial off-the-shelf (COTS) processor with local memory. The prototype laboratory models have employed Motorola 680x0 processors; however, this selection is not a design criterion and, in fact, the FTPP is capable of supporting heterogeneous processors. This is facilitated by the use of an industry standard bus (in this case, the VMEbus) to interface the PEs to the NEs. All processors communicate using the FTPP's Byzantine resilient communication protocol regardless of the processor type. Figure C4-12 shows an FTPP with four NEs connecting sixteen PEs and four IOCs (Input/Output Controllers).

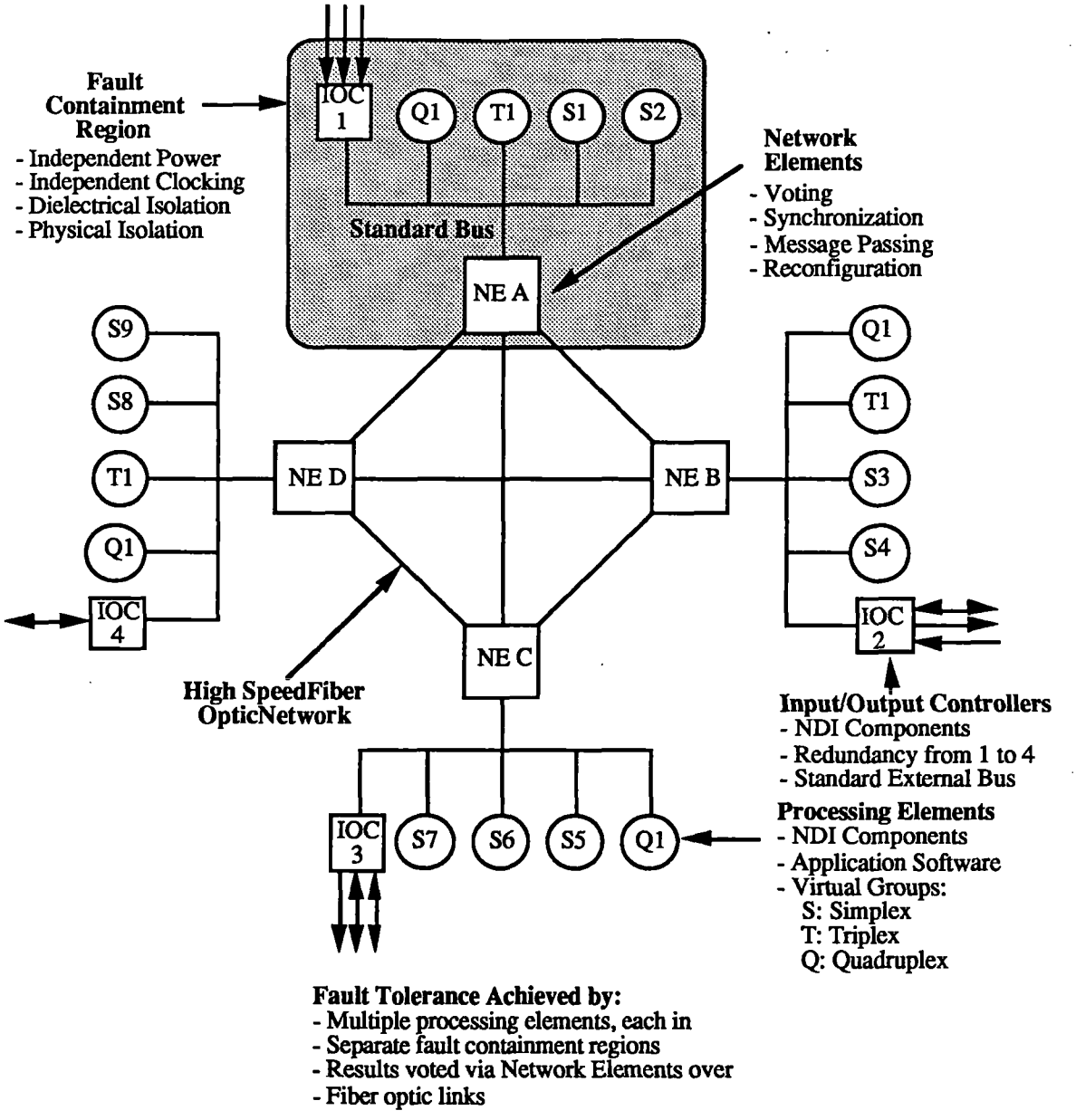

Figure C4-12 Sample FTPP architecture

When a set of PEs are assembled together to act in unison as members of a redundant group, the resulting computer can be view as a highly reliable, fault-masking Virtual Processor (VP^2). VPs are logical views of the computing resources capable of accepting work in a parallel processing environment. In order to satisfy the theoretical requirements of Byzantine resilience, each member of a VP must reside in a different fault containment region. For example, a quadruplex would comprise four PEs each resident on a different NE. Instantaneous fault tolerance on the FTPP is

---

[2] In other documents discussing the FTPP, the terminology Virtual Group(VG) is used interchangeably with VP.

achieved by fault masking within a VP. Hence, a VP is also referred to as a fault masking group (FMG). Fault manifestations in a fault masking group can occur without any degradation in system performance or correctness. Furthermore, these faults can be readily diagnosed.

VPs are composed of either 1, 3, or 4 Processing Elements; consequently, they may be simplex, triplex or quadruplex. Within a VP, each PE is referred to either as a channel or a member. When operating redundantly, each member of a VP executes a suite of tasks whose state is bitwise identical to the state of the corresponding tasks executing on other members of the VP. Simplex VPs are merely individual processors executing tasks with no redundancy which may be used for low-criticality processing functions. The notable exclusion of duplex VPs from the set of possible VP configurations illustrates an important concept in fault tolerance. Two processors can detect that they have values which disagree. What they cannot determine is which one of them is faulty. Many business-grade systems claim to be fault tolerant by using two processors and a simple comparing scheme to detect a fault. Only one processor is active at any given time. When an error is detected, a set of self-tests is run by both in the hopes of identifying the faulty module. However, self-tests are capable of identifying only a tiny subset of possible faults. Furthermore, regular processing must be suspended while the self-tests run. When the self-tests do not identify the faulty machine, the active system is generally brought off-line and the backup is switched in. Then a maintenance team is dispatched to deal with the problem. The flaws in this scheme are obvious. Most importantly, since it is impossible to determine which of the two systems produced the erroneous result, there is a one out of two chance that the faulty system, i.e. the backup, will be brought on-line! Clearly, such a strategy would not be satisfactory for life-critical systems. Since duplex configurations create more problems than they solve in that they require special logic to process detected faults, the FTPP does not allow this type of redundancy among its VPs.

As shown in Figure C4-12, the FTPP architecture also supports mixed levels of redundancy which in turn means that mixed levels of reliability are possible in this design. Since maglev applications consist of functions with varying requirements for reliability, this feature allows the computing platform to expend the minimal amounts of power, weight and volume needed by their application to achieve the required level of reliability. For example, control of the secondary suspension system is considered more critical than monitoring of the air conditioning system. On the FTPP, tilt control could execute on a quadruply redundant processor while an air conditioning monitor could execute on a simplex VP. Furthermore, a full complement of PEs is not necessary for system operation. Thus the system is not only efficient in the short run but expandable in the long run, should additional throughput be needed to support new applications at a later date.

System Designer's View of the FTPP

As discussed above, the FTPP's redundant nature is hidden from the view of the application programmer. However, the system designer who is configuring an FTPP as the computing platform for a given application is very much concerned with this view, especially as regards the required safety, reliability, and availability of the system at hand. The FTPP's virtual bus topology showing several example virtual processors is shown in Figure C4-13. From this perspective a system designer can use the quantitative performance and reliability requirements of the application to determine the number of required processing sites, the redundancy level of each site, and the number of any necessary spare simplex processors. Furthermore, the bandwidth of the Network Element Virtual Bus can be considered in assigning tasks to processors. This is the format which will be used to specify the computer architectures for each of the principle computing sites for the Bechtel maglev system.

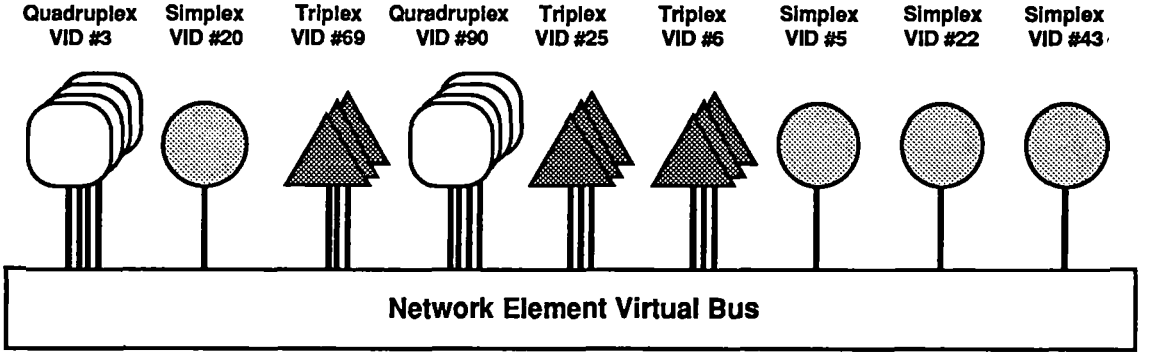

Figure C4-13 FTPP virtual configuration

Redundancy Management on the FTPP

The physical architecture of the FTPP supports a very powerful redundancy management scheme called parallel-hybrid redundancy, which is a combination of both static and dynamic redundancy techniques. Static redundancy provides the ability to mask faults instantaneously as they occur. For maglev, this means that a failed processor cannot provide incorrect commands to the propulsion system or to an aerodynamically controlled secondary suspension system, since the incorrect outputs of the faulty processor are masked by the correctly functioning majority members of its VP. Dynamic redundancy refers to the ability of the system to reconfigure itself automatically in response to failures by replacing failed components with existing spares. Without dynamic redundancy, the reliability of the system would degrade as faulty components accumulate. Dynamic redundancy allows the reliability of the FTPP to be restored following a

failure, greatly increasing the availability of the system provided that adequate spares are installed initially. For example, for the configuration shown in Figure C4-12, if Q1 lost the channel from NE A, S1 could be used as a replacement. This spare capacity increases the availability of the system, especially important for a transportation mode like maglev whose market depends on timely service not interrupted by unexpected failures, by allowing repairs to be deferred to the normally scheduled maintenance period.

Parallel-hybrid redundancy is a redundancy management scheme that is ideally suited to the maglev control computer system. Like fly-by-wire avionics applications, the maglev system performs many control functions which cannot tolerate an erroneous output command to an actuator. Hence, fault masking at the outputs in real-time, as provided by the FTPP, is absolutely essential. There is no performance penalty to be paid for this type of protection, since it is part of the normal behavior of the FTPP. However, reconfiguration does require some additional computing overhead. Therefore, during certain modes of operation requiring high throughput, it may not be desirable to reconfigure the system. However, a maglev vehicle frequently changes modes of operation as it moves from a station to a high-speed section of the guideway and on to another station. Similarly, the wayside zone controllers also have frequent operational mode changes as vehicles enter and leave their zones. During less critical operational modes, e.g. when a vehicle is stopped in a terminal or when a zone is idle, it is possible for the system to undergo a reconfiguration, by bringing in a spare PE or NE in place of one determined to be faulty. This reconfiguration is effected automatically, i.e. without the need for the intervention of a maintenance crew. Typically the reconfiguration process is accomplished in less than one second.

The reliability and availability of an FTPP implementation is clearly dependent on the fault recovery options used. An important aspect of a recovery method is the way it deals with transient errors. Since transient component failure rates usually predominate over permanent rates, and since the number of spares are finite, it is important to be able to differentiate between a permanent and a transient fault so as not to deplete the supply of spares unnecessarily. When an FTPP is reconfigured to exclude a faulty component, the component is not physically removed or disconnected from the system. Hence, during non-critical mission phases, such as a station stop, the system can perform extensive self-diagnosis and restore a component whose fault is deemed transient, thereby restoring the reliability and availability of the system and further enhancing its maintainability.

Maglev Control Computer Preliminary Design Specifications

The following preliminary design specifications for the maglev command and control computer system are based on the quantitative performance requirements presented in Table C4-3, the dependability requirements discussed in Section 4.1.1, the concept of operations, and the design requirements enumerated in Section 4.3.2.

For the onboard vehicle computer, a quadruplex FTPP architecture is used. This architecture meets both the throughput and RMAS requirements of the onboard computer system. The virtual onboard architecture is shown in Figure C4-14 Since both PEs and NEs are easily installed line replaceable units (LRU) and since the vehicle makes frequent stops in stations which can stock spare LRUs, this architecture provides both adequate reliability and availability for the onboard computer system. If either a PE or a NE fails during a safety-critical mission phase, no safety hazards are incurred. Even the failure of a second PE is not a safety risk. Once the vehicle is brought into a station and the fault is deemed permanent, a new LRU can be installed.

The many subsystems which the on-board computer must monitor and control are shown in block diagram form in Figure C4-14a. The sensor input and actuator output for the operation of these systems is carried over a fault tolerant data bus employing authentication protocols. Authentication protocols utilize a form of encryption to reduce the amount of hardware redundancy needed to support a theoretically correct Byzantine Resilient system. Figures C4-14b through C4-14h present block diagrams of the sensors and actuators connected to the fault tolerant data bus which are needed to control the following subsystems: tilt control, secondary suspension control, cryogenic control, smoke/fire detection and suppression, communications, cabin lighting, and vehicle door control. In all cases special attention has been paid to providing adequate redundancy of sensors and actuators to meet the availability requirements of the vehicle.

Figure C4-14c shows the secondary suspension cryogenic control system. Four accelerometers are positioned in the four corners of the vehicle body to provide sensor information to secondary suspension control algorithm. Information from the accelerometers placed on the bogies can also be used by secondary suspension control laws, but are intended as a source of information about the smoothness of the guideway. The accelerometers on the vehicle do not accurately reflect the state of the guideway since the vehicle motion has been damped by the action of the secondary suspension control.

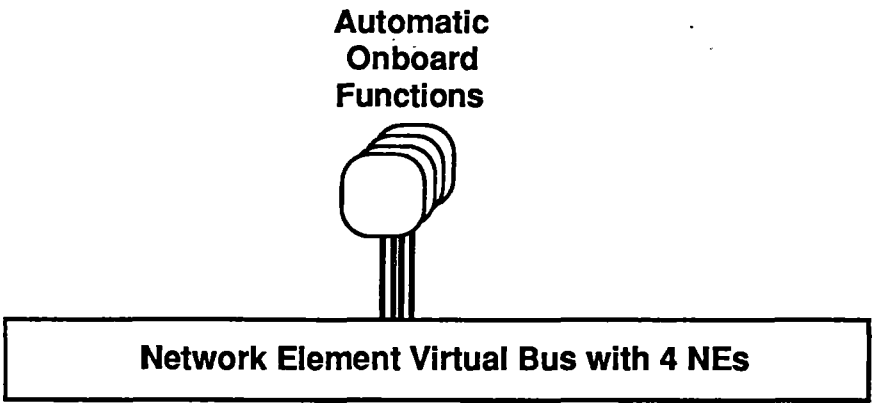

Figure C4-14 Virtual FTPP architecture for the on-board computer

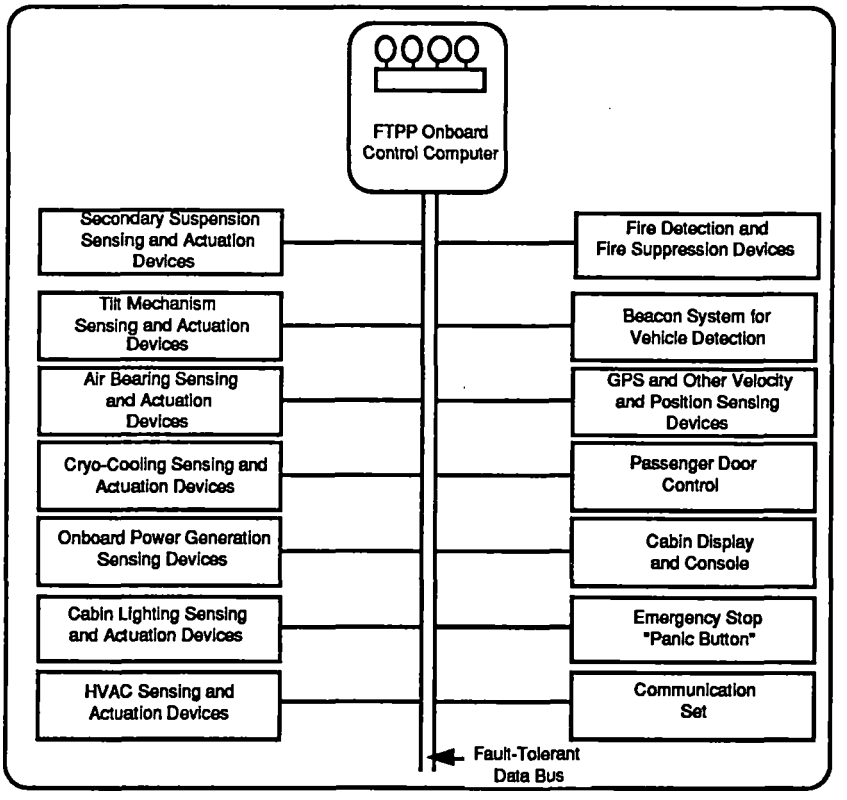

Figure C4-14a On-board control system block diagram

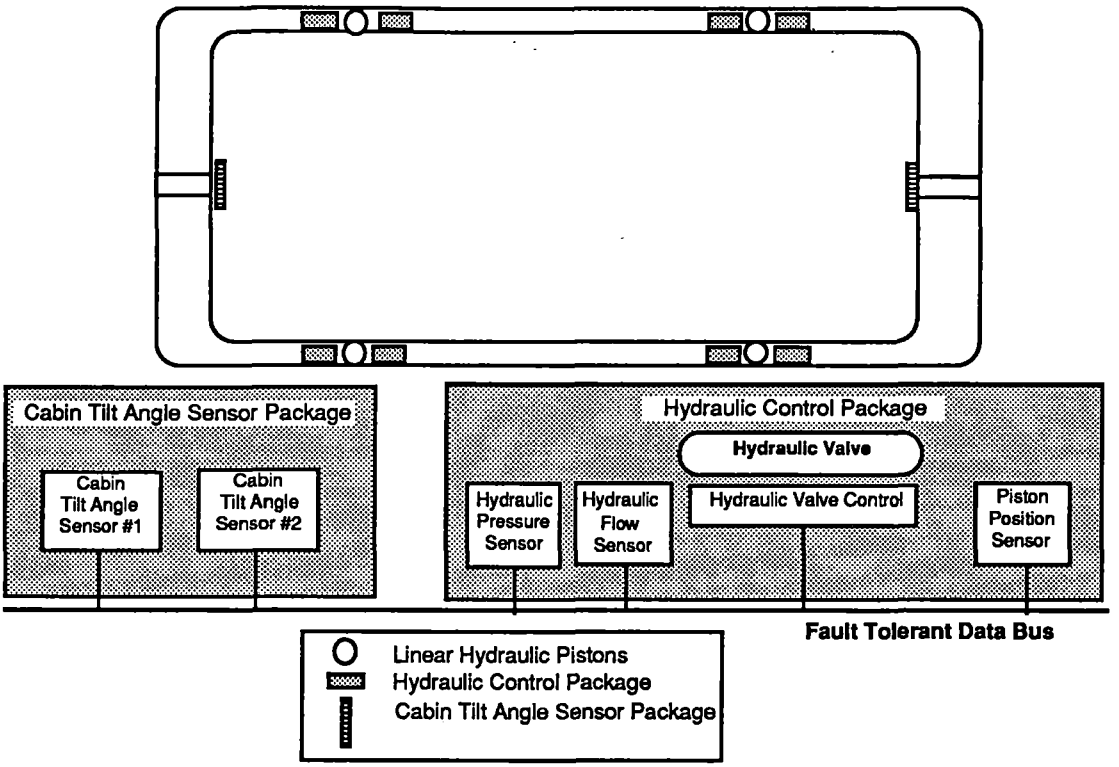

Figure C4-14b Tilt control

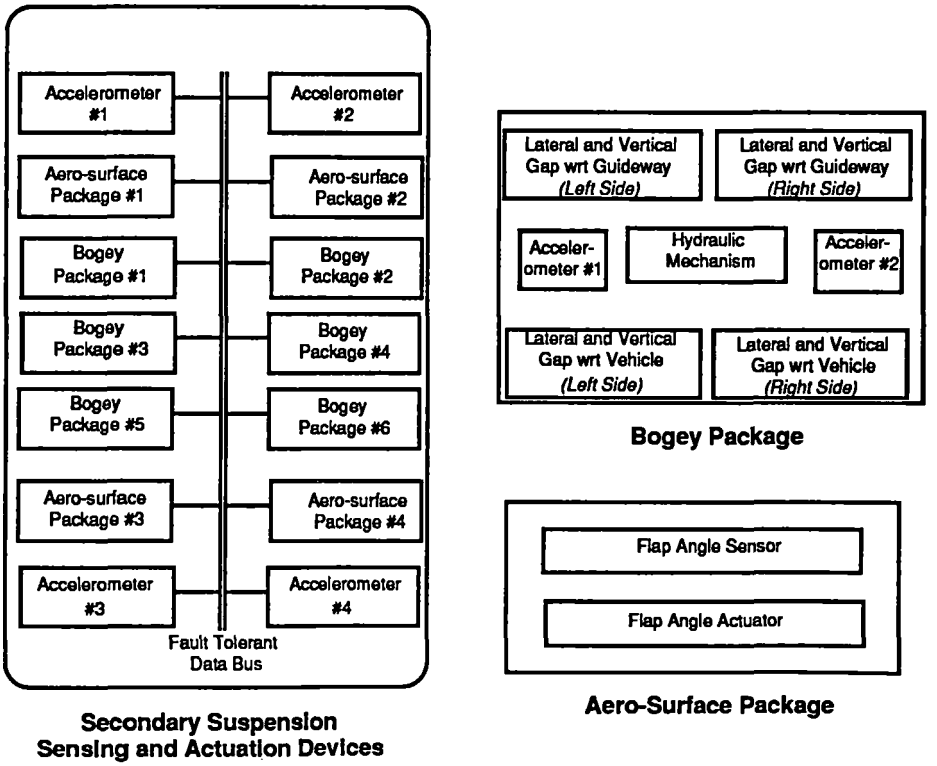

Secondary Suspension Sensing and Actuation Devices

Bogey Package

Aero-Surface Package

Figure C4-14c Secondary suspension control

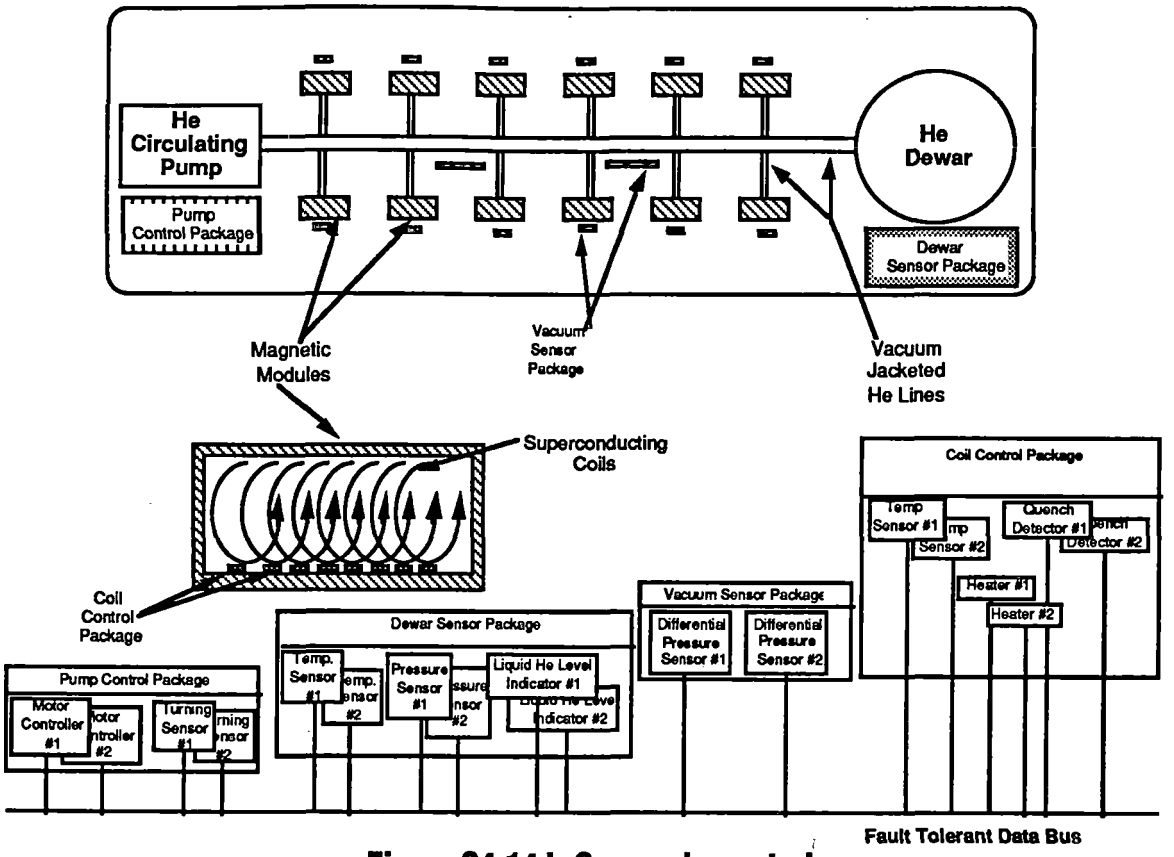

Figure C4-14d Cryogenic control

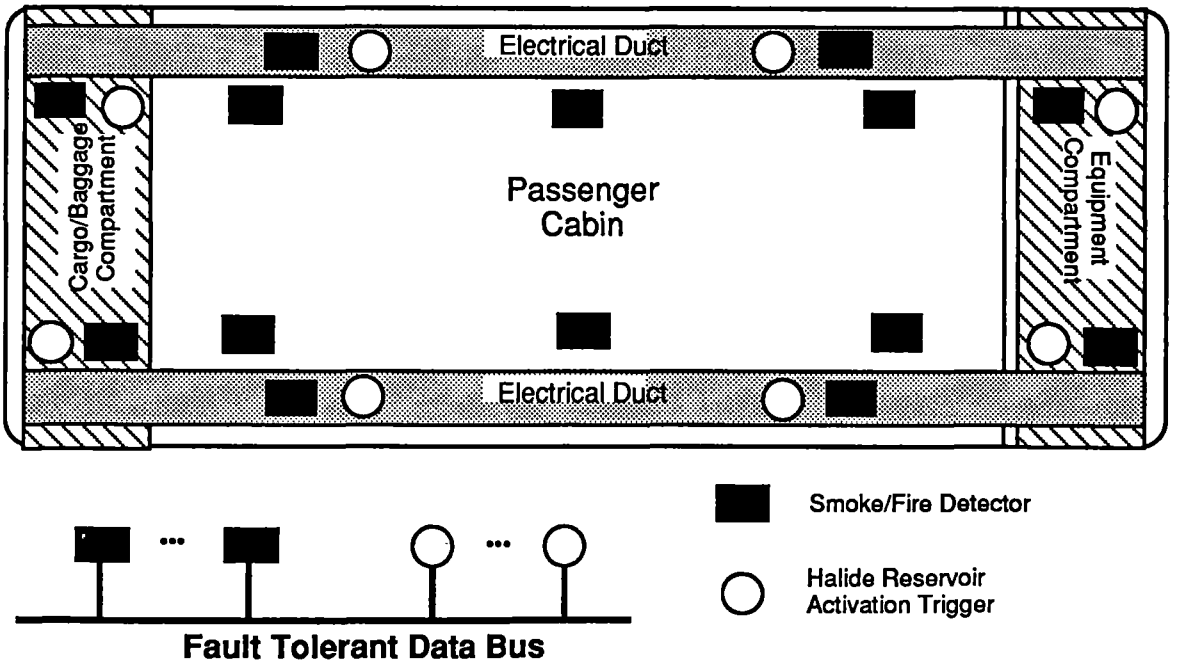

Figure C4-14e Smoke/fire detection and suppression

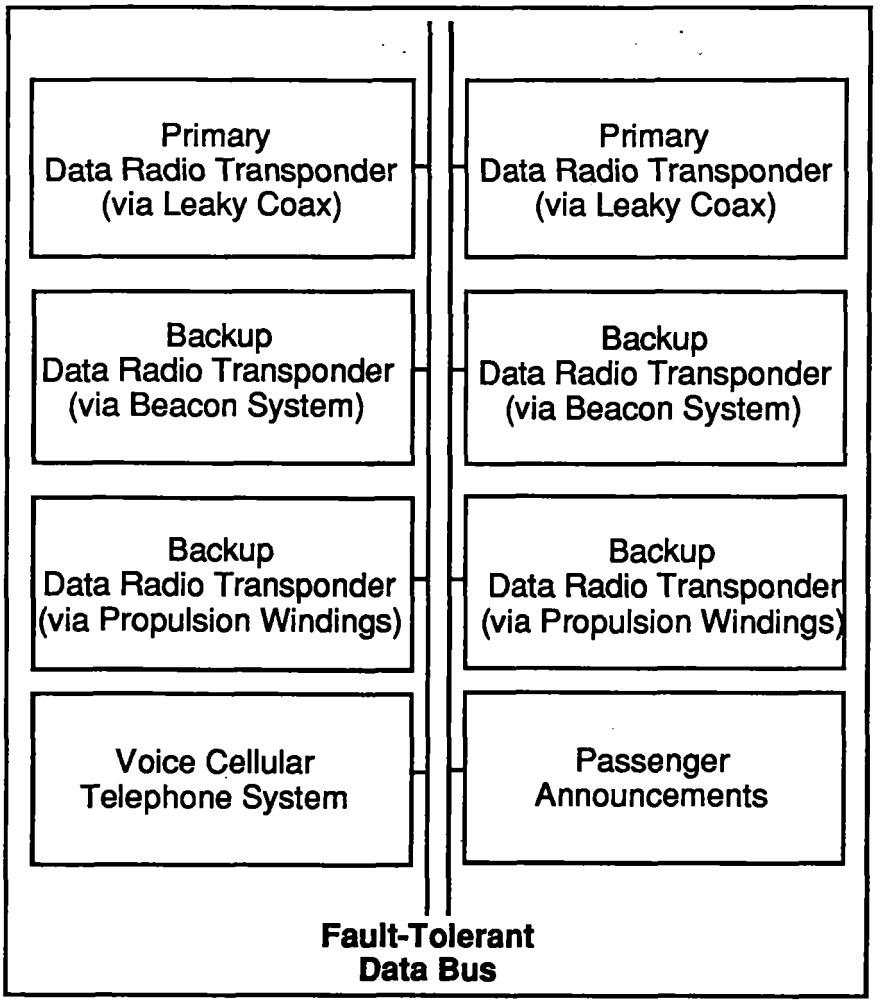

Figure C4-14f On-board communications

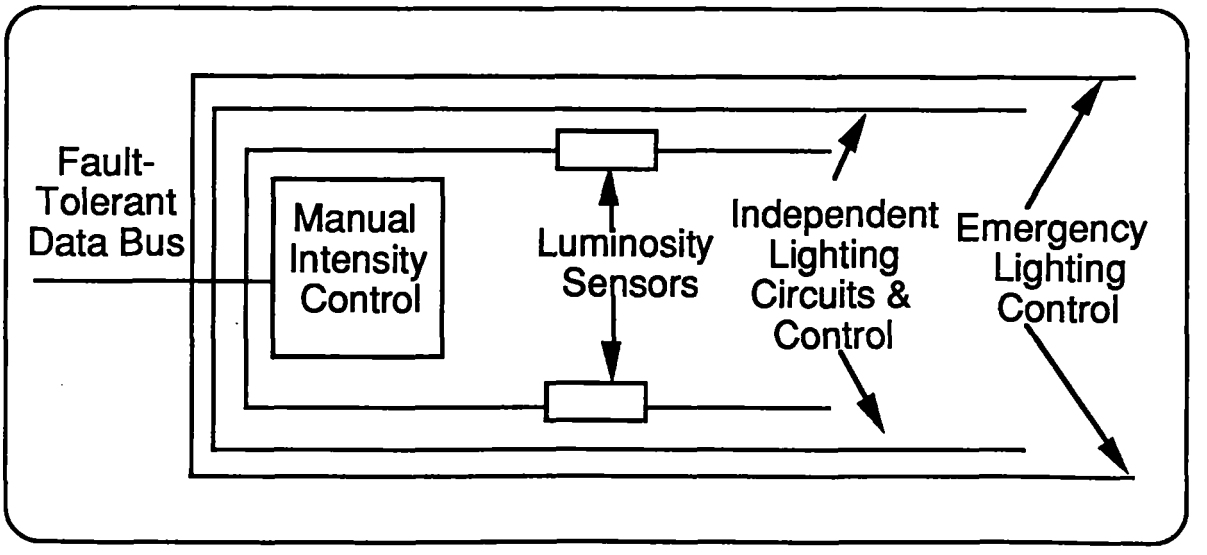

Figure C4-14g Cabin lighting control

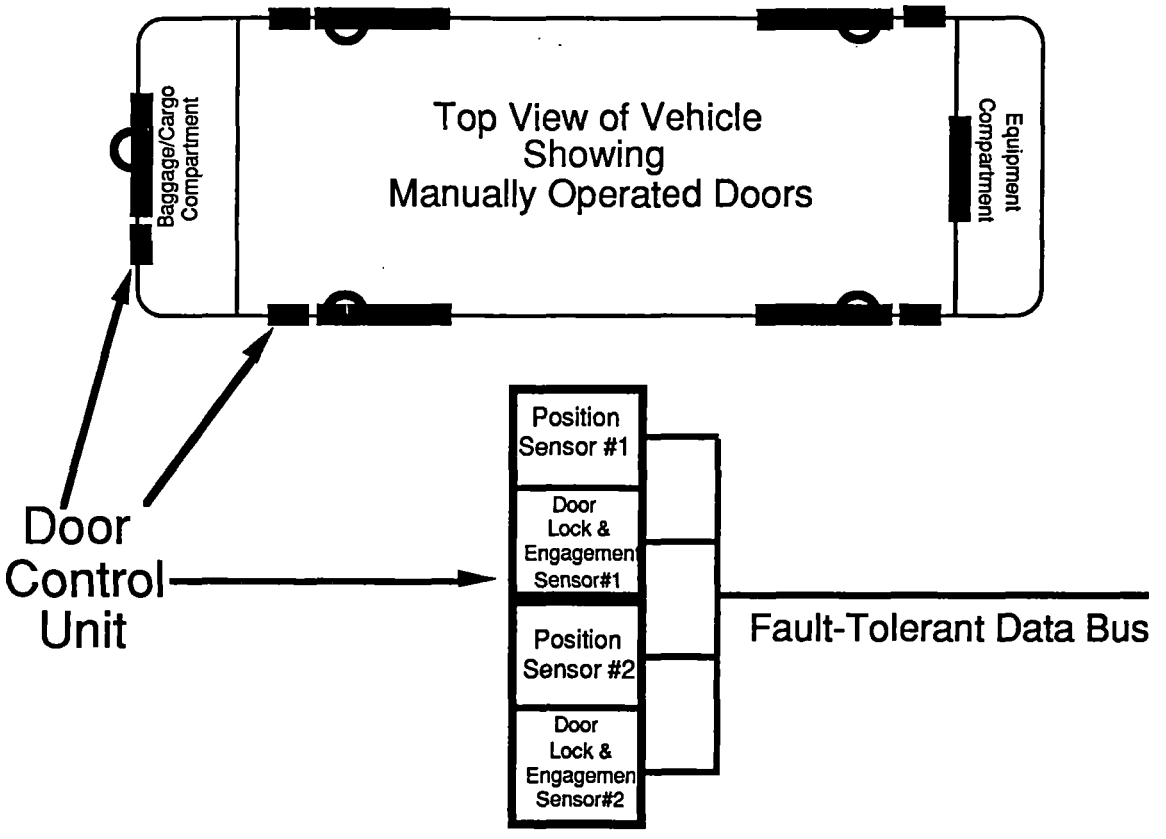

Figure C4-14h Vehicle door control

Figure C4-15 shows the virtual architecture of the FTPP which hosts the station control functions for a single station. It is estimated that 3 VPs would be sufficient to provide the throughput needed for station control. Hence an FTPP with 3 quadruplex VPs would be able to meet the throughput and RMAS requirements of these functions. To allow for greater availability and full fail-operational squared safety, a 5 NE architecture has been selected, with one simplex spare PE provided in each FCR. This design utilizes only 16 PEs. Since this FTPP can accommodate a full complement of 40 PEs there is still adequate capacity for future growth and expandability. The FTPP can be repaired on-line. Thus, when either an NE or PE fails, it can be replaced automatically without disrupting normal operations and while the system is still has sufficient redundancy to cover any arbitrary fault in real-time. Furthermore, since this system has enough spare capacity to allow reconfiguration in real-time, a transient fault does not reduce the supply of spares.

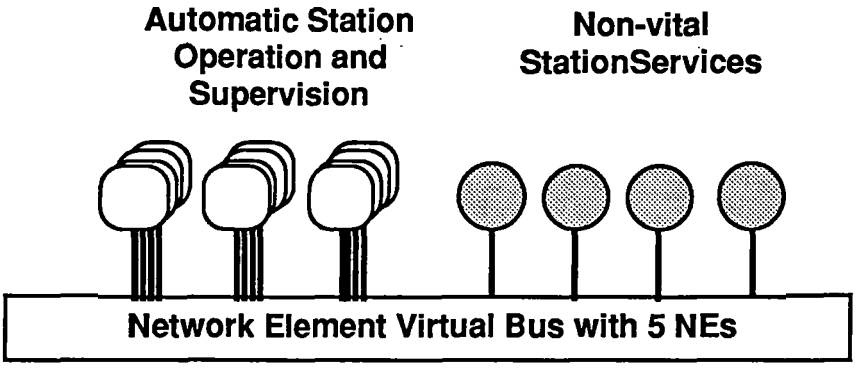

Figure C4-15 Virtual FTPP architecture for the station computer

The central computer system is also based on a 5 NE FTPP architecture. Initially, this system is populated with two quadruplex VPs and two triplex VPs. The quads are used for real-time functions and the triplexes are used for non-real-time computation. Two spare PEs provide on-line redundancy to cover faults and gain a maintenance and availability advantage. The virtual architecture for this system is shown in Figure C4-16.

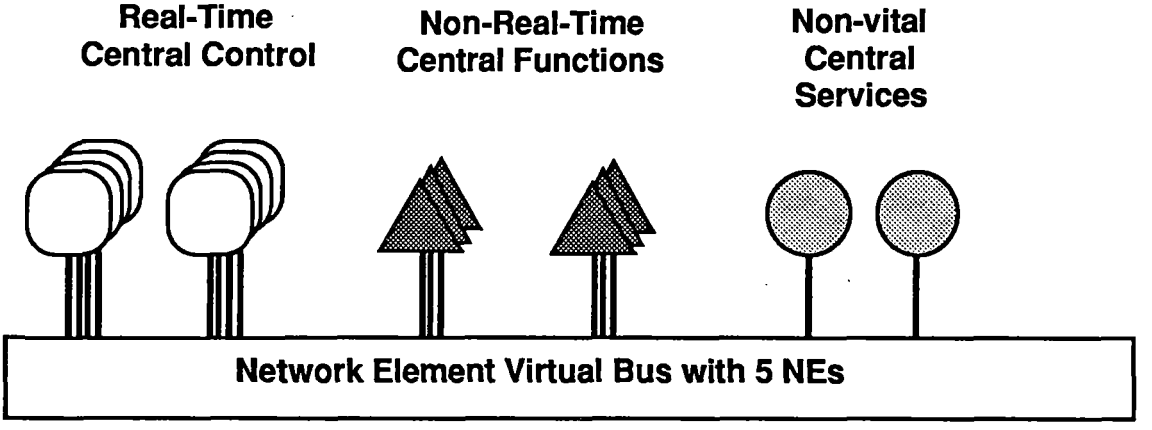

Figure C4-16 Virtual FTPP architecture for the maglev central facility computer

The zone controller will also be implemented with a fault tolerant computer architecture. Due to the large number of zone controllers, and their remote locations, local fault tolerance to protect against hardware failure is required. However, to protect against common mode faults, redundancy of the zone controller level is also provided by backing up each zone controller with its neighboring zone controller. When two or more zone controllers detect a failure in another zone controller, a pre-selected zone controller will assume control of the inverters of the failed zone controller. The spatial separation of the redundant zone controller lessens the likelihood that a common mode failure will cause two adjacent zone controllers to fail simultaneously. Each zone controller will be sized to perform the functions of its own zone and one adjacent zone.

4.3.4 Preliminary Communications Concepts

The communications subsystem provides a transparent and guaranteed transfer of information (voice and data) to and between all other subsystems in a fully automated and fail-safe manner with sufficient reliability to maintain the overall system availability and safety goals. An open architecture integrated area network based implementation is used to provide the necessary connectivity without undue location and addressing concerns.

The communications architecture and its components are divided into two major components. The first is the land line network that is used to connect all fixed sites. The second is the radio frequency connection to the moving vehicles. The major requirement which have been considered in selecting the communications components are bandwidth, throughput, security, and cost.

The design of the communication subsystem is based upon an understanding of the maglev command and control concepts of operations and the functions and communications requirements of each system element. Even though these concepts are undergoing revision and growth, the following paragraphs describe the communications requirements as presently understood.

Vehicle Communications Requirements

The vehicle, as the mobile element, has a unique set of communications requirements. In general, since RF bandwidth is limited, and lossy, it is desirable to keep the vehicle communications to a minimum. The design of the vehicle also helps, in that the vehicle has no control over movement. The vehicle can report its status, position, speed and acceleration. It can also request a speed reduction (or a stop) based on unacceptable ride comfort or an emergency situation. The vehicle receives route and schedule information such as station arrival time or a route deviation. In a station the vehicle uses communication to coordinate station and vehicle doors. In addition to these operational requirements, the vehicle communications system provides both voice and data communications services to the passengers. Finally, the vehicle has the capability to communicate with local emergency service providers such as local police and fire departments.

The operational requirements are on the order of a few kilobits per second which can easily be handled by several technologies, even with the large overhead required for error free transmission. The primary link from the vehicles is to the zones, and for redundancy, independently to several zones. A backup communications link to the central control facility, independent of the guideway infrastructure, is provided.

Zone Communications Requirements

The zone is the primary point of vehicle propulsion control as well as the primary collection point for vehicle status and location and for guideway condition, including environmental conditions along the guideway. As described above, it is in contact with the vehicle to receive status data. It is also in contact with adjacent zones for vehicle movement coordination and vehicle hand-off. It exchanges data with stations and switches on vehicle movement. Finally, it communicates with the Central Control Facility on vehicle movements and on guideway status. The zone also acts as the initial relay point for all vehicle communications with other system elements and with external elements (such as the local telephone network).

Zone to zone, zone to station and switches, and zone to central communications have much higher bandwidth requirements than zone to vehicle communications since these are the primary paths for vehicle control. Given the demanding requirements on vehicle headway, these paths must be very rapid and very secure. A large bandwidth fiber optic network, with highly reliable protocols for ensuring on-time message delivery, is used.

Station and Switch Communications Requirements

Stations and switches, although different elements, have the same type of requirement to communicate with the immediate and adjacent zones to ensure safe operation with respect to vehicle movements. Switches receive control signals from the zone or from central. Stations, in addition, communicate passenger related information to and from central and also provide information to external agencies such as inter-modal transportation services. Both stations and zones user the fiber optic network with back-up communications to central.

Central Control Facility Communications Requirements

The Central Control Facility, with its responsibilities for controlling region-wide vehicle flow, for monitoring and for emergency and failure response, and for passenger handling, requires wide bandwidth communications with all other elements of the system. In addition, emergency back-up communications links, with significantly less bandwidth, are provided to all other elements. The Central Control Facility is connected to the fiber optic networks providing baseline communications as well as being the central receiving point for any terrestrial or satellite RF links.

Candidate Communications Architectures

Figure C4-17 shows the baseline design for the infrastructure of the communications network.

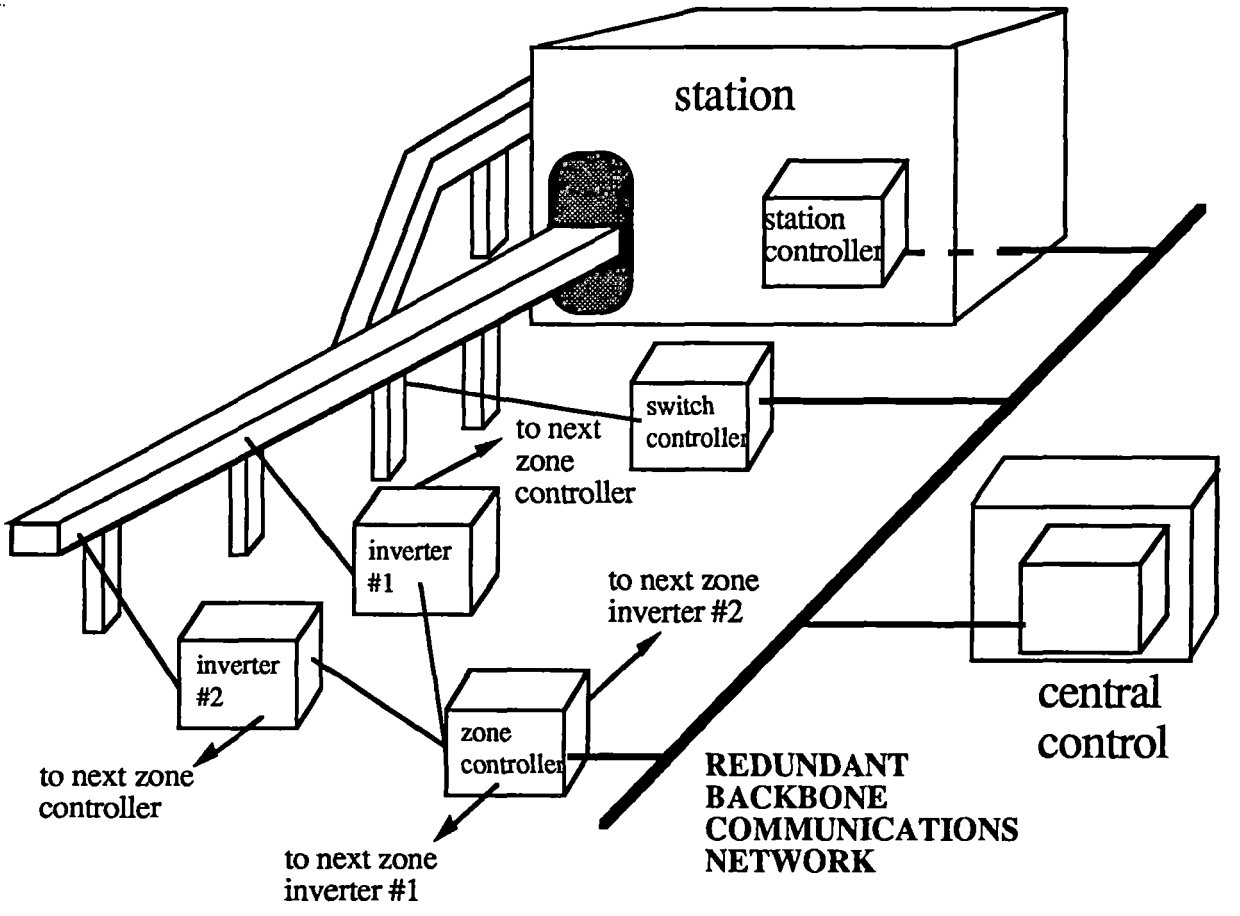

Figure C4-17 Baseline fixed site communications architecture

Backbone land line communications between the fixed site elements of our design are provided by a set of fiber optic cables forming a high speed digital network. Redundant paths are implemented with fiber optic cables so that single point failures will not interrupt communications. Figure C4-17 shows that the major elements of the Central Control Facility, the station controllers, the zone controllers, and the switch controllers will all be interconnected by the fiber optic network. This allows all system elements to communicate directly as needed. Connections to external communications networks (i.e., the public telephone network) are made at either the Central Control Facility or at the station. Between the zone controller and the propulsion inverters and between the switch controller and the switching mechanism, an independent land line paths are used.

In past transportation systems, the need for both data and voice communication have typically been met with two separate systems. However, advances in communication technology have provided

the capability to combine voice and data over a single digital link. ISDN is an example of this. Our design takes advantage of this advanced technology by including voice with other digital communications.

Networking Concepts

Various communications link topologies have been examined for use in our design. These are a point to point and a network topology. Point to point, as its name implies, is concerned only with communication between two distinct points or sites, whereas a network connects more than two communications points. Networks are classified as a bus, ring, star, tree, or mesh. For localized networks, one of these is usually agreed upon and implemented. For broad area networks, a combination of the different topologies usually results as a tradeoff between cost, performance, reliability, and realizability.

A representative point to point topology for six communicating sites is shown diagrammatically in Figure C4-18. Assuming that each area is connected to another by one link, we can calculate the number of links by the combination formula of six things taken two at a time, giving a total of 15 required links.

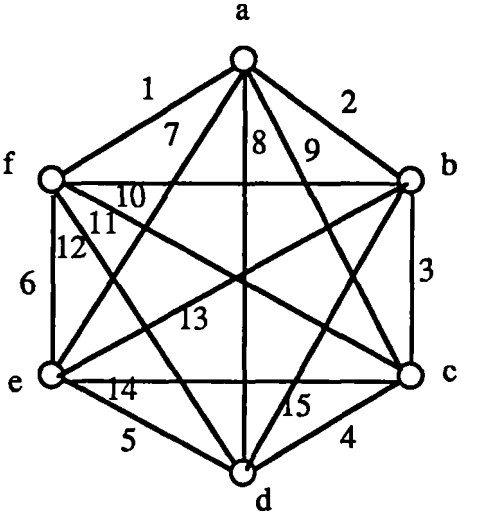

Figure C4-18 Point to point communications topography for six points

Such a topology, though redundant, is overly complex. A more reasonable topology would be that of a dual redundant bus, or a redundant tree structure.

For our baseline design, the Aeronautical Telecommunications Network (ATN) serves as a model of the maglev redundant backbone communications network. As the ATN interconnects avionics, air/ground and ground networks to appear as one global data network to the user, this concept generally adapts the Air Traffic Management (ATM) communications system concept by changing the platform definition from an aircraft to a maglev vehicle.

In the ATN-based concept, the ASC facilities are interconnected through a redundant communications network, using both satellite and land-based telecommunications service in multiple configurations. In this adaptation, the functionality is provided primarily by area network topologies where the network provides intrinsic message path management. A spanning tree architecture is used with a technique known as a directed acyclic graph (DAG). This is a standard network methodology whereby the network message integrity is inherently fault tolerant providing both self-healing and self-optimization for capacity requirements.

Although the ATN serves as an architectural model, it is not based on an Open System Interconnect (OSI) protocol. In our baseline design, the maglev network protocol implementation is OSI compatible (ref. ISO recommendation 7498). Many vendors are providing OSI compatibility in their products (e.g., Digital Equipment Corporation phase 5).

OSI is a seven-layer model for communications protocols allowing compatibility of communication at each layer. The lowest layer is the physical layer which consists of the hardware, medium, and electronic bits that are transferred. The second is the datalink layer which consists of the reliable transfer of data across the link through synchronization, flow and error control. The third is the network layer which insulates the upper layers from data transmission and switching responsibilities: it controls the routing of data. The fourth is the transport layer providing reliable transfer of data between end points and end-to-end recovery from errors as well as flow control end-to-end. The fifth is the session layer which establishes, manages, and terminates connections between cooperating applications. The sixth is the presentation layer which allows each application to have its own data representation (different syntax) by converting to a common one. The seventh and highest OSI protocol layer is the application layer which provides access to the OSI environment for users and applications and also provides distributed information services (Ref. *Data and Computer Communications*, William Stallings, 3rd ed.).

Vehicular Communications

Both vehicle and guideway are unique with respect to the communication technologies employed. The vehicle is moving and this mobility will require a communications subsystem that works well in a moving environment. Both the vehicle and the guideway are subject to intense electromagnetic disturbances due to the nature of the magnetically levitated and propelled transportation system. Like the requirements for communications between fixed sites, multiple paths must be provided for vehicle communications. In addition, consideration is given to actions to take if vehicle communications are lost, even temporarily. However, in our design the vehicle can safely be moved even without communications, so the normal action to take is to continue the trip to the next station where, if necessary, the vehicle can be taken out of service for repair. A diagram of our design is shown in Figure C4-19.

Figure C4-19 Baseline vehicle communications architecture

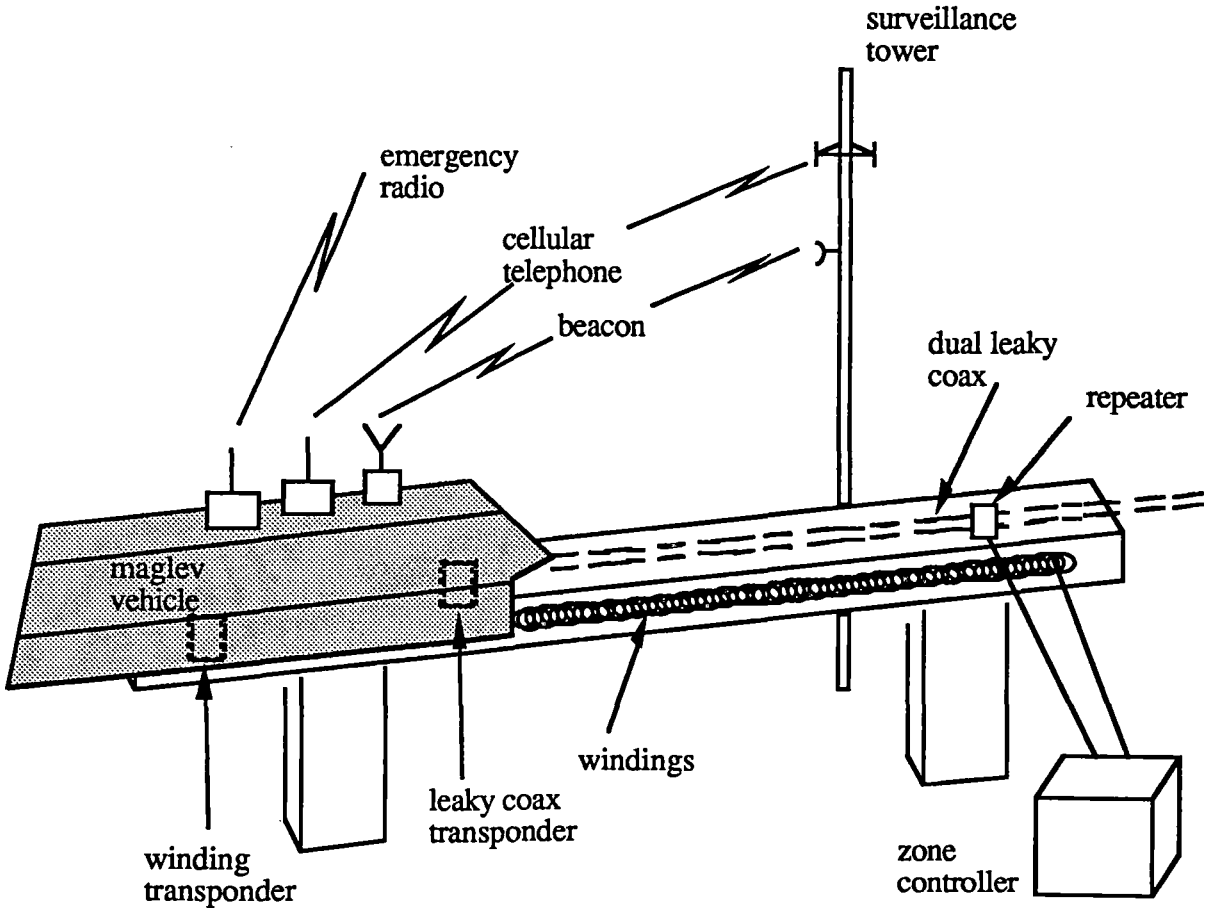

The primary technology selected for our design is that of a leaky coaxial cable. A leaky coax is essentially a method for providing an antenna which can be chosen to operate over a broad range of frequencies. The primary advantage of a leaky coax antenna is that it provides a continuous transmission path between the vehicles and the wayside transceivers that may extend for up to 20 km. Our design employs dual interleaved leaky coax cables so that the vehicle can communicate a minimum of 10 km. both in front of and behind its position at all times. A network-like protocol is specified so that the vehicle can communicate with other vehicles as well as the zone controllers. At a 4 km. zone spacing, the vehicle is able to communicate with at least two zone controllers in front of and two zone controllers behind the vehicle. The communications protocol is specified to provide both voice and data services.

For the primary method of providing voice communications services to the passengers, we have selected standard cellular telephones. Although cellular telephone services have been extended along many of the nations interstate routes, it may be necessary to provide new cellular telephone networks for some routes. These new networks provide a secondary source of revenue by providing cellular telephone services to motorists on adjacent highways.

The secondary method of providing vehicle communications is through a beacon system This system employs a beacon reader on the vehicle and beacon transponders located along the guideway. The spacing of the guideway beacons has not yet been selected but could be as close as a few hundred meters. In addition to providing location information (see the next section) the selected beacon technology incorporates communications protocols which allow the exchange of several kilobits of data with each beacon even though the vehicles are traveling at maglev speeds.

A third method of exchanging data between the vehicle and the zones is implemented though the windings of the propulsion system. Low frequency signals can be modulated onto the power windings and picked up by the vehicle. Data can also be sent via the same path from the vehicle to the zone controllers.

The final method of communications to be provided is UHF emergency radios which are to be used to talk to local emergency providers when the vehicle is stopped on the guideway.

4.3.5 Preliminary Guideway Sensor Concepts

Our design incorporates a more complete set of guideway sensors than has been implemented on any existing transportation system. The requirements are detailed in the section above titled Guideway Integrity. To repeat briefly, the sensor requirements are:

- Detect guideway movement and alignment
- Detect vehicle on guideway
- Detect and measure objects on guideway
- Detect other objects on guideway
- Detect and measure snow and ice accumulation
- Detect and measure wind velocity

The set of guideway sensors selected for our design in shown in Figure C4-20. The general philosophy for reaction to sensor warnings is to automatically stop any vehicles which could be in danger. Movement is only allowed to start again when a visual inspection has been made and the guideway declared safe.

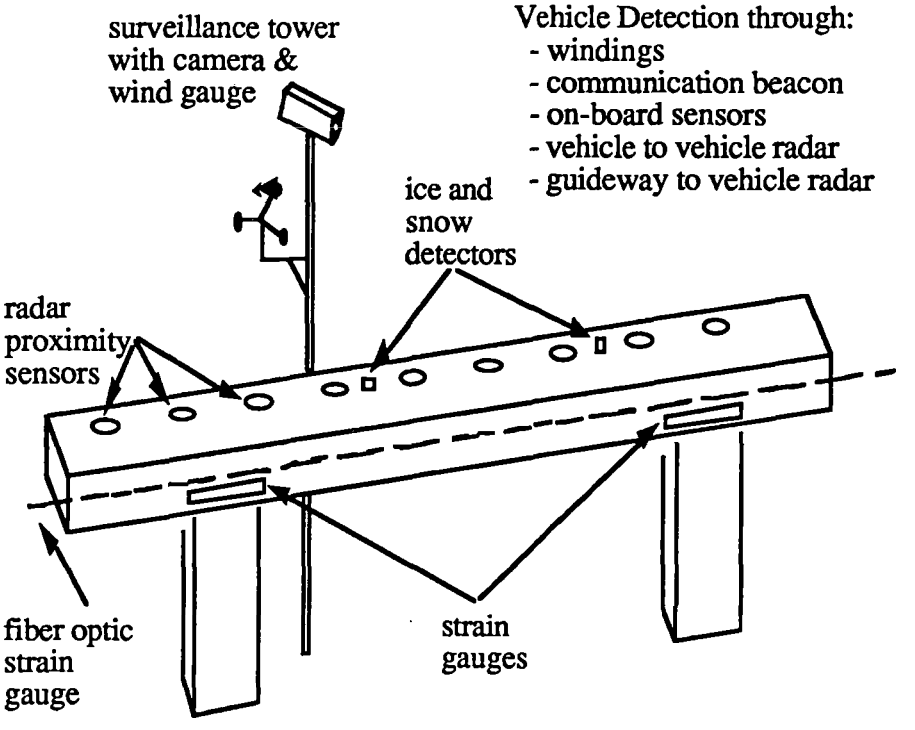

Figure C4-20 Baseline guideway sensor architecture

Detection of movement of the guideway, due to such events as an earthquake or if the guideway structure is struck during a traffic accident, is detected by one of two sensor systems. One uses a fiber optic strain gauge imbedded in one of the fiber glass reinforcement bars of the guideway beam. Light shown thorough the fiber optic path will be distorted when the reinforcement bar is stressed for its normal condition. The second means is with a standard strain gauge mounted across the junction of two guideway beams. Any movement of either beam will be detected by these strain gauges.

In order to detect any intrusion onto the guideway, we employ radar proximity detectors mounted along the guideway beam. These detectors take advantage of the fact that normally the volume surrounding the guideway is completely static, except for the passages of vehicles which, in turn, is quite predictable. Therefore, whenever the radar detects a disturbance of sufficient magnitude to indicate the intrusion of a hazardous object, vehicle movement along the guideway is halted until the guideway is inspected. This inspection is normally conducted by the CCF operators using a television surveillance system located alongside the guideway. The television surveillance cameras are located at intervals such that the entire guideway can be observed by panning and zooming the cameras. In addition, if necessary, snow and ice detectors of a design to be determined, are located along the guideway to detect and measure hazardous accumulations.

Finally, in order to detect the most dangerous objects on the guideway, namely other vehicles, five methods are used to cross-check each other. The primary means of location is for the guideway propulsion equipment to track the movement of each vehicle through the windings of the LSM. This method can detect the location of the vehicle to within a few centimeters and is needed for commutation of the motor. Sensors on-board the vehicle are also able to use the same method to calculate its own position. Periodic updates of vehicle position are provided, both to the guideway and to the vehicle, each time a communications beacon is passed. This method unambiguously determines the exact position of the vehicle. Finally, radar ranging sensors are used both by the vehicle, to detect other vehicles which are in sight, and by the guideway to detect the location of a vehicle as it approaches the station berthing sites.

5. Aerodynamics

5. AERODYNAMICS

5.1 VEHICLE AERODYNAMIC DRAG

5.1.1 VEHICLE AERODYNAMIC DRAG FOR OPEN GUIDEWAYS

An easy way to represent the flow around an object traveling near a ground plane is to imagine that there is a mirror image of the object below the ground plane, and both objects are traveling through unrestricted air. The resulting symmetry means that there is no flow across the ground plane, as required. In this situation, one can obtain good streamlining if the object plus its image form a shape which would be well-streamlined in the absence of the ground plane, i.e. begin with a conventional streamlined body like an airplane fuselage and cut it in half to form a good shape for operation near a ground plane. The resulting shape has a sharp corner at the leading edge, which should be rounded with a radius which is proportional to the ground clearance. The same reasoning can give us some guidance as to the proper shape for a vehicle on a box-beam guideway, i.e. the leading edge of the vehicle body should be close to the top of the box and the leading edges of the vehicle sides should be close to the sides of the box. It is worth noting that the nose of the Transrapid TR06 had a fairly high leading edge which led to both drag and noise. The TR07 has a lower leading edge which helps to avoid these problems.

The Bechtel Team vehicle uses the above approach at the front end. There are also established ways to reduce the base drag at the tail end. One of the simplest and most effective ways is to use "boat-tailing." The base is tapered to a certain extent and then cut off. This reduces the base drag in two ways: it increases the base pressure, and the base area is reduced. Practical boat-tail shapes for axisymmetric bodies have been given by Mair (Ref. 1). The aft end is rounded followed by a conical section with an angle of 22 degrees. The exact shape to give minimum drag for our maglev vehicle, which is not axisymmetric, would require a more detailed study.

The results of these ideas on the design of the Bechtel vehicle are illustrated in Figure C5-1.

J. L. Peters, aerodynamics project manager for Krauss-Maffei, states that "The drag of the complex magnet bogies...can easily amount to two-thirds of the total aerodynamic drag." (Ref. 2) Thus the drag coefficient which is chosen for a maglev vehicle at the present conceptual stage depends mainly on how optimistic one chooses to be about the drag due to the flow in the gap between the vehicle and the guideway. Drag due to the flow over the exterior of the vehicle can be calculated relatively accurately.

Vehicle on guideway showing boat-tail dimensions

Section Through Nose. The leading edge height as given by the parameter B is kept small.

A = Height of vehicle bottom above guideway
B = Height of tip of nose above guideway
B - A = 30 cm

Figure C5-1 Nose and tail shapes to minimize drag

One useful formula for estimating drag may be written

$$D = \frac{1}{2}\rho V^2(C_f A_w + C_{dp} A_C)$$

where

C_f = Surface friction coefficient

A_c = Cross sectional area

A_w = "Wetted area" = pL

C_{dp} = Partial drag coefficient due to frontal area

p = peripheral length around cross-section

L = Vehicle length

ρ = Density of air = 1.225 kg/m^3

V = Vehicle velocity (134 m/s)

The simple equation shown for wetted area is chosen for simplicity. The difference between this and the actual wetted area is very small.

The drag formula essentially states that the vehicle has a certain amount of drag due to the fact that it has a nose and a tail plus some additional drag due to flow along the length. One member of the Bechtel Team, Draper Laboratories, has a BAA contract with the Federal Railroad Administration to study aerodynamic drag. Drag data from Germany and Japan were compared. The following coefficients for a box-beam type vehicle are the result of this effort:

C_{dp} = 0.11

C_f = 0.004

The value given for C_f is more than double what one would expect from flow over a smooth surface. This additional drag is included to account for the complex flow between the vehicle and the guideway, which gives rise to large scale turbulence due to the magnets and the guideway ladder if they are not shielded. Both the German and the Japanese experience tells us that this is a major source of drag. Because of the lack of experimental data on our specific configuration, the value chosen is the same as that used by the Japanese to estimate drag for their commercial vehicle. The value given for C_{dp} assumes a proper nose and tail shape as described above.

For the baseline Bechtel concept, p = 18.1 m, L = 36.1 m, and A_c = 15.37 m^2. Inserting these numbers, we obtain

D = 47 kN

Drag of Multi-Car Consists

Although this is not part of the baseline concept, it is of interest to compute the drag of longer trainsets. This can be computed with the following formula:

D = 47 + 29 N (kN)

where N is the number of additional cars behind the lead car. Thus for a two-car trainset N = 1 and the drag is 76 kN.

References

1. Mair, W. A., Reduction of base drag by boat-tailed afterbodies in low-speed flow, Aero. Quart. Vol.20, pp 307-320, 1969.

2. Peters, J. L., Aerodynamics of very high speed trains and maglev vehicles, Int. J. of Vehicle Design, Special Publication SP3. Printed in U.K., 1983.

5.1.2 Vehicle Aerodynamic Drag/Pressure Transients in Tunnels

Transients experienced by maglev vehicles, as they enter, pass each other, and exit a tunnel, are of importance for the system concept definition study. It would be desirable for the vehicle to be able to enter a tunnel at normal cruising speed and to maintain this speed through the tunnel. It can also be assumed that only a short part of the total travel distance is spent within tunnels and thus the performance of the vehicle within a tunnel is not as important and performance compromises can be accepted. In this subsection passing transients are computed for an approximation of the baseline concept vehicle, tunnel cross-sectional areas, vehicle-speed, and surface-friction coefficients. For blockage ratios (vehicle area/tunnel area) under 0.2, pressure increase/decrease outside the vehicle is not significant. Also the drag force on a vehicle is increased three times while passing through a tunnel with a blockage ratio of 0.2 and is only increased 80 percent while passing through a tunnel with a blockage ratio of 0.1. Tunnel dimensions should be optimized by comparing tunneling costs with propulsion costs. Larger tunnel cross-sections lead to higher tunneling costs. Smaller tunnel cross-sections lead to larger drag and thus higher propulsion costs.

Vehicle Transients in a Tunnel

A vehicle passing through a tunnel has a major modification to its aerodynamic behavior. When a vehicle passes through a tunnel, the flow past the vehicle must take place through the annular space between the vehicle and the tunnel. A vehicle moving in a tunnel causes flow in the tunnel and disturbances created by the vehicle are transmitted down the tunnel. On entering the tunnel, the vehicle will experience a rapid drag increase followed by a slower decrease as it proceeds through the tunnel. This drag increase is a function of the blockage ratio defined as the ratio between the vehicle cross-section area to tunnel cross-section area. There might also be a substantial pressure increase on the front of the vehicle and a pressure decrease at the rear. During its travel through the tunnel, the vehicle will be subjected to several rapid changes in pressure caused by the pressure waves that are generated. Pressure fluctuations are important from both a structural and ride quality aspect. The environment created by the vehicle entering, in, and exiting a tunnel is also a cause for concern.

For our analysis, it will be assumed that the air is incompressible and that the far flow field can be treated as one-dimensional unsteady flow and the near flow field can be treated as a steady flow field in vehicle-fixed coordinates. For large L/d_t ratio vehicles, a quasi one-dimensional approach is adequate for the near flow field. In such an analysis only flow velocities in the direction of the tunnel are considered. The vehicle velocity through the tunnel, u_s, is assumed to be constant. The following procedure is followed for computations of transients during vehicles passing through tunnels. It is described in four steps with a discussion provided for each step completed.

Initial Drag Coefficient for Vehicle

The drag on a vehicle consists of two parts, the friction drag and the pressure drag. For the present, we will consider the vehicle to be a streamlined vehicle in which only friction losses occur. The drag coefficient for such a vehicle is given in Hammit (Ref. 2) as:

$$C_{Db} = \frac{4\, c_s\, L}{d}\left\{\frac{\sqrt{\beta} + \left[1 + (1-\beta)\frac{u_s}{V_1}\right]\left|1 + (1-\beta)\frac{u_s}{V_1}\right|\beta}{(1-\beta)^3}\right\} + \alpha\left(\frac{\beta}{1-\beta}\right)^2 \qquad (1)$$

Here, C_{Db} is the vehicle drag-coefficient based on tunnel area, c_s is the coefficient of skin-friction drag, L is the length of vehicle, d is the diameter of the tunnel, V_1 is the air velocity ahead of the vehicle relative to the vehicle, β is the blockage-ratio, and α (between 0 and 1) is a coefficient to describe how much of the exit loss should be considered, depending on exit conditions. This drag coefficient, based on the wetted area of the vehicle, is:

$$C_{Dw} = \frac{C_{Db}\, d}{4 L \sqrt{\beta}} \qquad (2)$$

To compute these drag coefficients we need to find c_s, the skin-friction drag coefficient. Hoerner (Ref. 1) has a good treatment on this subject. At high Reynolds numbers, the flow is turbulent. A simple formula approximating Schoenherr's equation within $\pm$ 2 percent is given as:

$$c_s = \frac{1}{(3.46 \log R_l - 5.6)^2} \qquad (3)$$

where R_l is the Reynolds number based on body length. If u_s is 150 m/s (492 ft/s), and L is 75 m (246 feet, assuming a three-car consist), then $R_l = 7.76 \times 10^8$. This gives $c_s = 0.0016$. In this present analysis for our team concept we will use $c_s = 0.004$. This larger value is chosen to allow for the drag of the magnet bogies and to be on the conservative side. Our baseline concept vehicle diameter for purposes of this calculation, d_t, is assumed to be 4m (13.12 feet). Actual width of the baseline vehicle is 4.1m and its height is 4.88m. Diameter of the tunnel, d, is $d_t/\sqrt{\beta}$. Plots of C_{Dw} and C_{Db} versus the blockage ratio are presented in Figures C5-2 and C5-3 respectively. C_{Db} for α =1 and β = 0.1 is 0.054 and for α = 1 and β = 0.2 is 0.182. These values will be used below.

Compute Induced Flow in the Tunnel

A vehicle passing through a tunnel will cause a flow within the tunnel. If fluid flows about the vehicle, a pressure difference must exist about the vehicle. If the fluid was at constant pressure before the vehicle started to move through the tunnel, then the passage of the vehicle through the tunnel will establish the pressure field in the tunnel. The pressure in front of the vehicle (p_1) must be high enough to cause the acceleration of the flow ahead of the vehicle and overcome the friction on the tunnel walls. Similarly, the pressure behind the vehicle (p_2) is reduced by the inertial and the friction forces plus the pressure change at the inlet of the tunnel. The pressure difference between p_1 and p_2 depends on the drag of the vehicle. The three equations for p_1, p_2, and vehicle-drag are given by (Ref. 2).

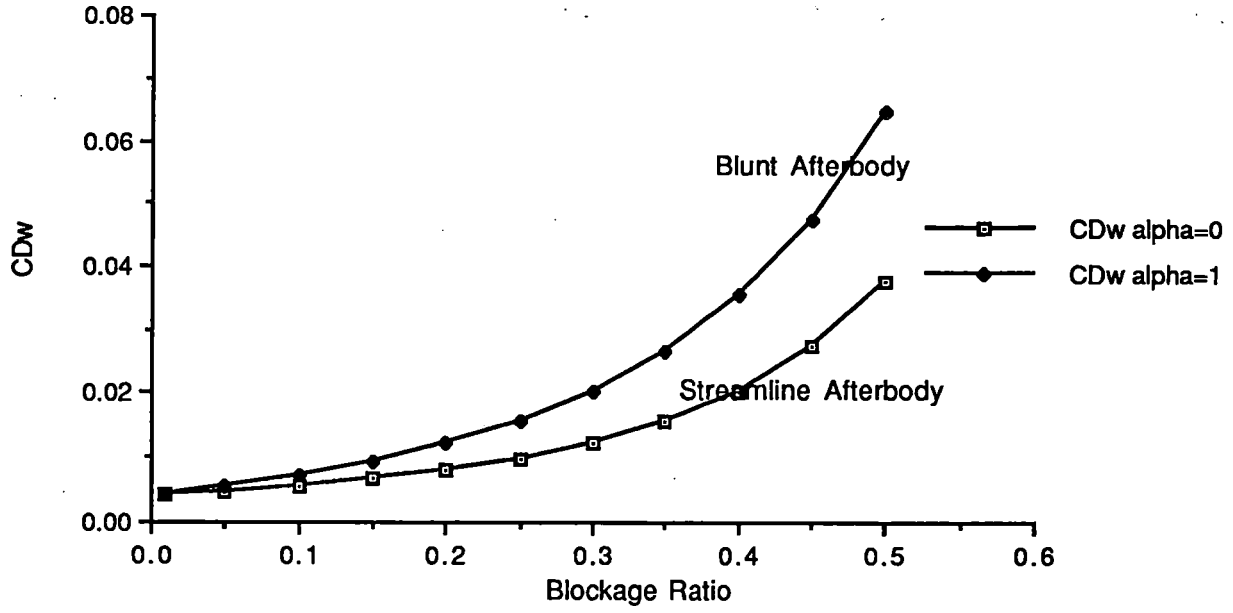

Figure C5-2 Vehicle drag coefficients (train wetted area) vs blockage ratio, no induced flow

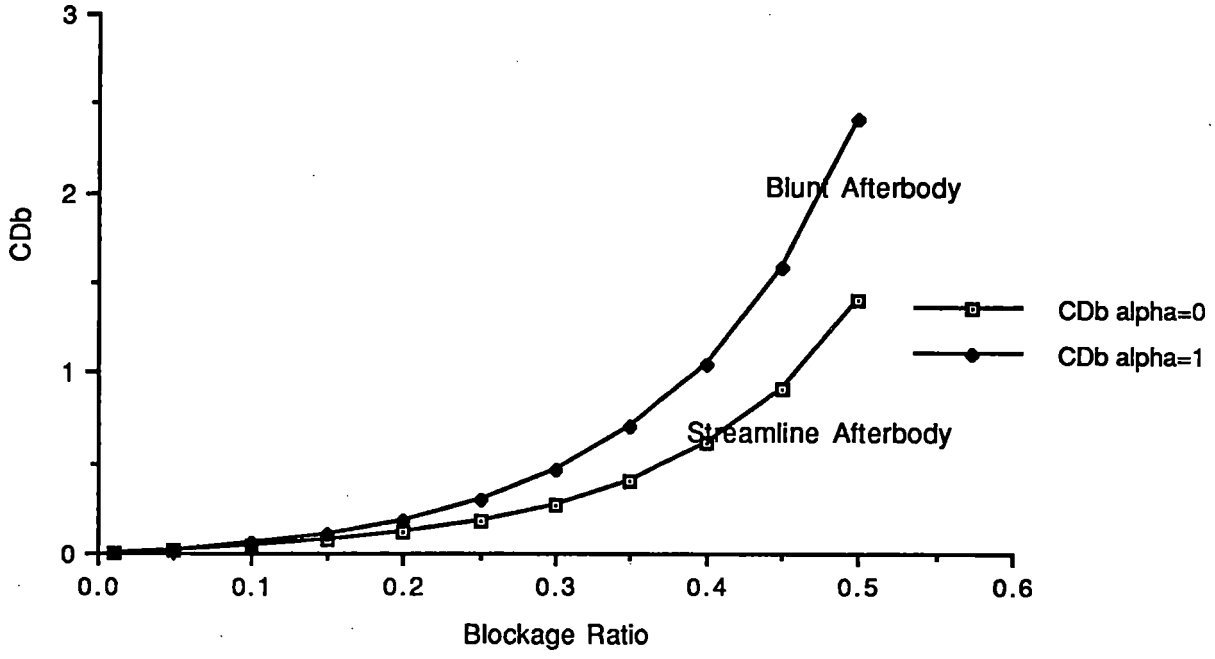

Figure C5-3 Vehicle drag coefficients (train wetted area) vs blockage ratio, no induced flow

$$\frac{p_1 - p_\infty}{\rho} = (1 - x)\frac{du_1}{dt} + \frac{2\,c_s\,(1 - x)}{d}u_1^2 \tag{4}$$

$$\frac{p_\infty - p_2}{\rho} = x\frac{du_1}{dt} + \frac{2\,c_s\,x}{d}u_1^2 + \frac{k}{2}u_1^2 \tag{5}$$

$$p_1 - p_2 = 1/2\,\rho\,(u_s - u_1)^2\,C_{Db} \tag{6}$$

Here, p^∞, is the far-field pressure, l is the tunnel length, x is the distance along the tunnel, and k is a coefficient equal to 1 for nicely rounded inlet and larger for a sharp-edged inlet. For a constant vehicle-speed, these three equations (4 through 6) can be combined to obtain the induced flow u_1 as given below.

$$\left(\frac{4\,c_s\,l}{d} + k\right)x/l = \sqrt{\frac{2}{B}}\left\{\ln\left[\frac{(B\text{-}2)\frac{u_1}{u_s} - B - \sqrt{2B}}{(B\text{-}2)\frac{u_1}{u_s} - B + \sqrt{2B}}\right] - \ln\left[\frac{B + \sqrt{2B}}{B - \sqrt{2B}}\right]\right\} \tag{7}$$

$$B = \frac{2\,C_{Db}}{\frac{4\,c_s\,l}{d} + k} \tag{8}$$

Solving for u_1, we obtain:

$$\frac{u_1}{u_s} = \frac{(B^2 - 2\,B)\left[1 - e^{\frac{A}{\sqrt{2/B}}\frac{x}{l}}\right]}{(B - 2)\left[(B - \sqrt{2B}) - (B + \sqrt{2B})\,e^{\frac{A}{\sqrt{2/B}}\frac{x}{l}}\right]} \tag{9}$$

where,

$$A = \frac{4\,c_s\,l}{d} + k \tag{10}$$

For our vehicle concept we assume l = 5000 m (16405 feet), k = 1, and $d = d_t/\sqrt{\beta}$. Here d_t is the vehicle-diameter. If d_t is 4m (13.12 feet) then d = 41.5 feet for $\beta = 0.1$ and 29.35 feet for $\beta = 0.2$.

The induced flow u_1 is plotted in the Figure C5-4 as a percent of vehicle-speed u_s versus x/l for $\beta = 0.1$. Here A = 7.3, and B = 0.015 and $C_{Db} = 0.054$. And the induced flow u_1 is plotted in the Figure C5-5 as a percent of vehicle-speed u_s versus x/l for $\beta = 0.2$. Here A = 9.94, and B = 0.037 and $C_{Db} = 0.182$.

Pressure distribution in the tunnel

Equations 4 through 6 can also be used to compute the pressure distribution in a tunnel. The pressures are:

$$\frac{p_1 - p_\infty}{p_\infty M_\infty^2} = \frac{\gamma}{2}\left[\left(1 - \frac{u_1}{u_s}\right)^2 C_{Db} - k\frac{u_1^2}{u_s^2}\right]\left(1 - \frac{x}{l}\right) \qquad (11)$$

and

$$\frac{p_2 - p_\infty}{p_\infty M_\infty^2} = -\frac{\gamma}{2}\left[\left(1 - \frac{u_1}{u_s}\right)^2 C_{Db}\frac{x}{l} + k\frac{u_1^2}{u_s^2}\left(1 - \frac{x}{l}\right)\right] \qquad (12)$$

The left-hand side of equation (11) divided by C_{Db} is plotted in Figure C5-6, versus x/l. The maximum of this plot occurs at the entrance of the tunnel and equals 0.7. This value for pressure difference is computed (for Mach no. of 150/340 = 0.44) to be 0.007 P_∞ for $\beta = 0.1$ and 0.025 P_∞ for $\beta = 0.2$. The left-hand side of equation (12) is plotted in Figure C5-7, versus x/l. The pressure behind the vehicle is reduced maximum at tunnel exit. This difference is computed (for Mach no. of 150/340 = 0.44) to be 0.007 P_∞ for $\beta = 0.1$ and 0.021 P_∞ for $\beta = 0.2$.

Final Drag Coefficients of Vehicle

Next, vehicle drag coefficients based on tunnel cross-section areas and vehicle-speed are computed for various induced flows. These are presented in Figure C5-8. To obtain drag-coefficients based on vehicle cross-section area, C_{dt}, we divide C_d of Figure C5-8 by the blockage ratios. The value for $\beta = 0.1$ is 0.536 and for $\beta = 0.2$, the value is 0.905. Free stream (blockage ratio of zero) C_{dt} can be computed to be 0.30. Hence at a blockage ratio of 0.2, the drag coefficient is increased by a

factor of 3 and for a blockage ratio of 0.1, the drag coefficient is increased by 80 percent. Based on drag numbers alone we are recommending a blockage ratio of 0.1.

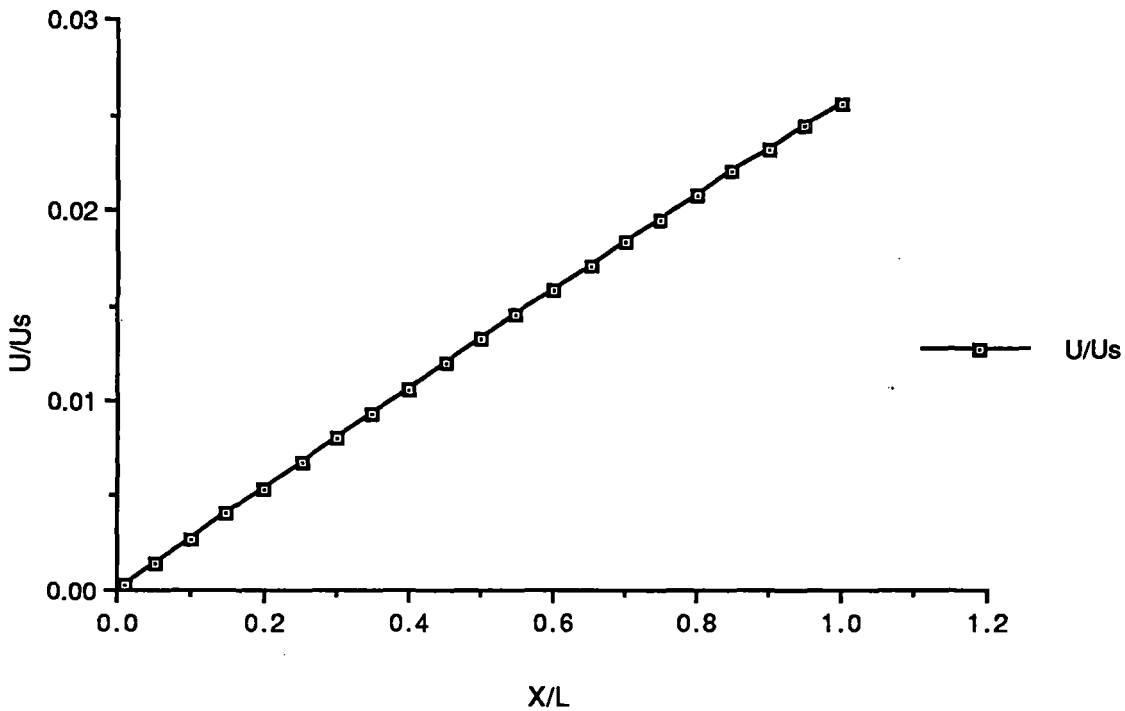

Figure C5-4 Velocities induced in a tunnel by passing vehicle

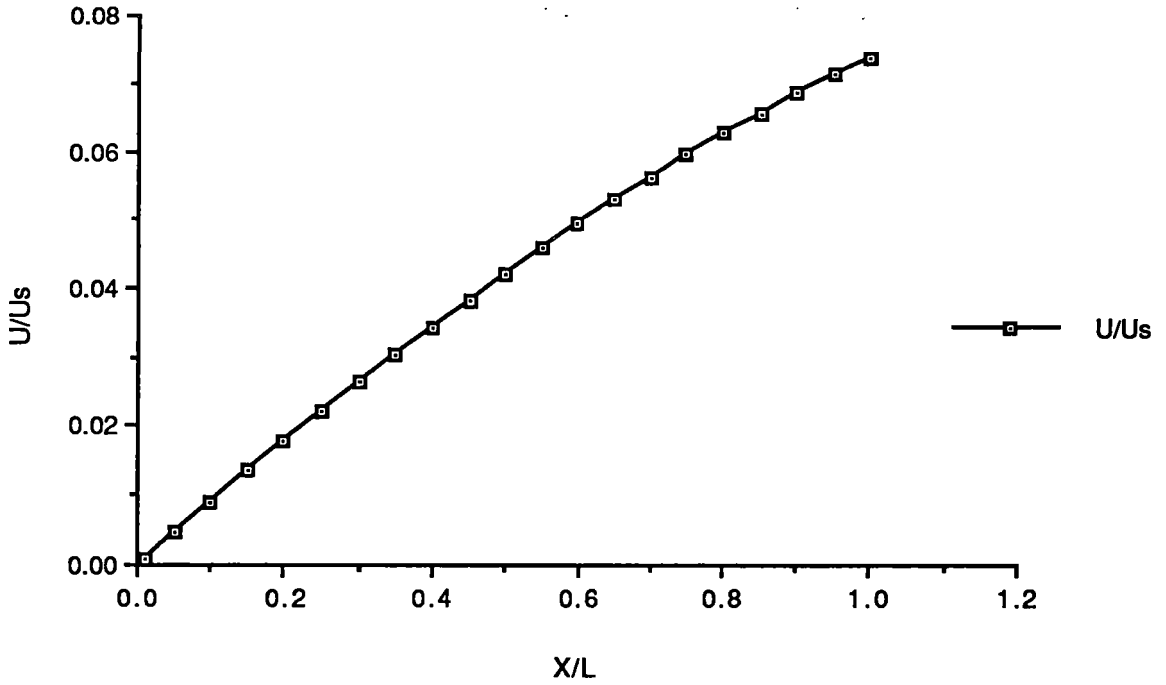

Figure C5-5 Velocities induced in a tunnel by passing vehicle

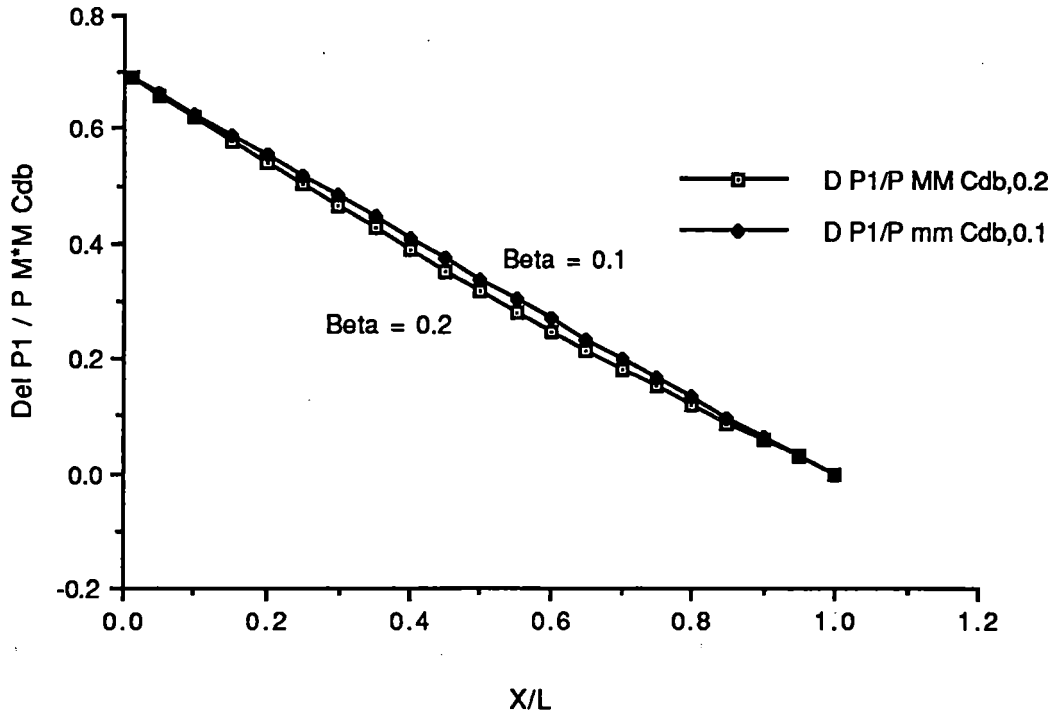

Figure C5-6 Pressure induced in front of the vehicle passing a tunnel

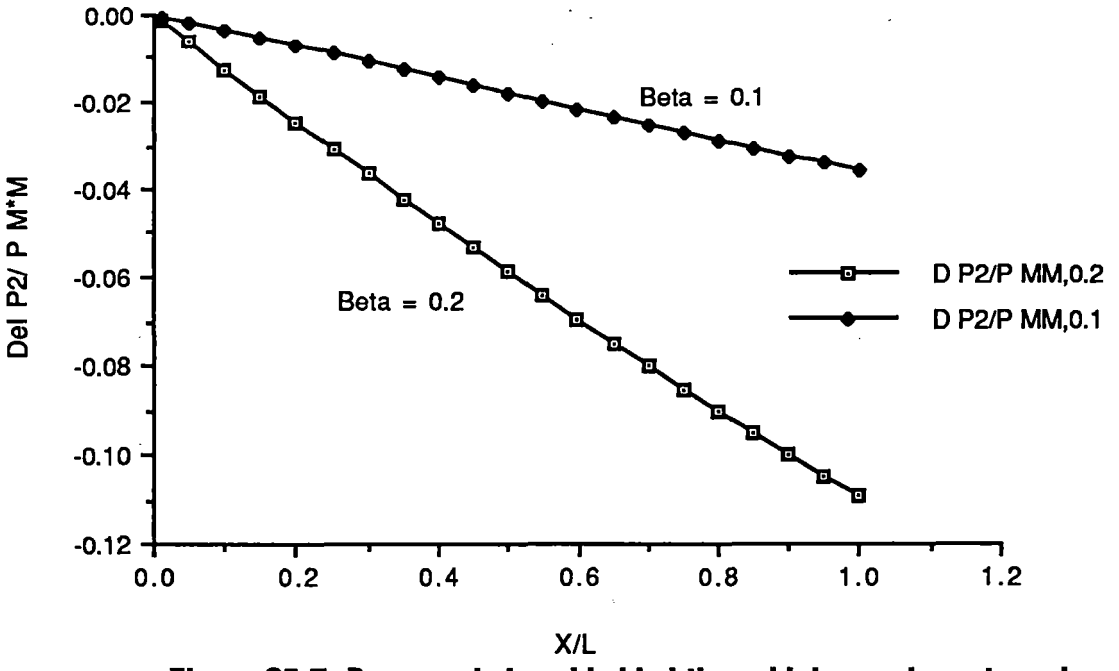

Figure C5-7 Pressure induced behind the vehicle passing a tunnel

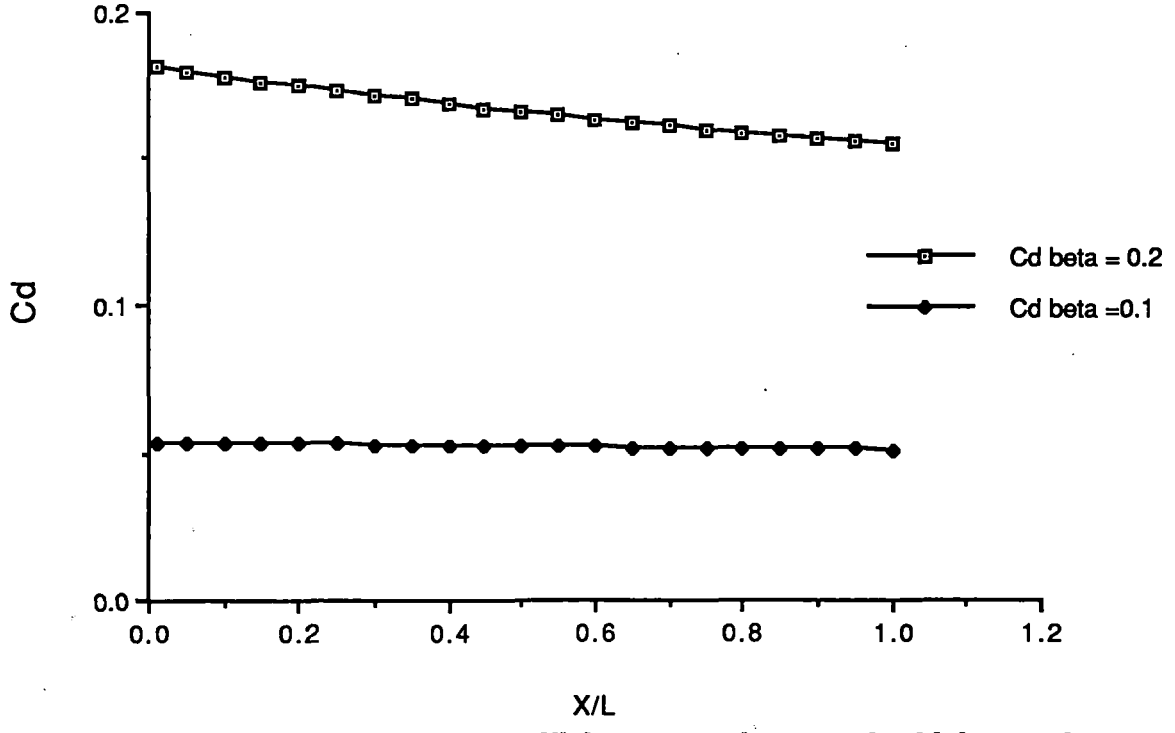

Figure C5-8 Vehicle drag coefficient - tunnel area and vehicle speed

References

1. Hoerner, S. F., Fluid-Dynamic Drag: theoretical, experimental and statistical information, 1965.

2. Hammit, A. G., Aerodynamics of High Speed Ground Transportation, Western Periodicals Co., North Hollywood, CA, 1973.

5.2 OTHER FORCES AND MOMENTS ON THE MAGLEV SYSTEM

The maglev system will be subjected to a variety of climatic effects. The first subsection below discusses the effects due to crosswinds. The second subsection discusses additional effects.

5.2.1 Crosswind Effects

The maglev vehicles and guideways will be subjected to forces and moments due to crosswinds. These climatic forces and moments are computed in this subsection. Specifically, side-forces, yaw-moments, and roll-moments on vehicles and guideways for the maglev system are computed. For side-forces and yaw-moments on vehicles the classical unsteady Wagner model, as given in Reference 1, is used as the basis for computations. Reference 2 develops these equations for the tracked air cushion vehicle (TACV) in trains of one or more cars. This analysis provides a method for estimating the transient, viscous airloads. The equations account for transient slender-body effects and the growth of vortices on the lee side. This method is believed to be conservative. Side-force and yaw-moment coefficients and the resulting forces and moments are computed for train speeds between 30 to 150 m/s and steady crosswinds varying between 6.7 m/s and 28.6 m/s. These computations are compared with available data in References 3 and 4. For a stopped vehicle, a crossflow drag coefficient of 0.7 is used to compute crosswind forces. Roll moments on vehicles are estimated from measurements presented in Reference 4. A suggestion for reduction of crosswind effects is also listed. For bare guideways, a crossflow drag coefficient of 2.05 (Ref. 5) is used to compute crosswind forces.

Side Forces and Yaw Moments on the Strawman Vehicle in a Steady Crosswind

In the analysis presented, it is assumed that the vehicle has an elliptical cross-section. This body is assumed to be a 2:1 ellipse, where $2H_V$ is the height of the vehicle (Figure C5-9). Let $\lambda_1 H_V$ be the length of the nose of the vehicle and the cross sections at any X on the nose are assumed similar to section A-A (Figure C5-10).

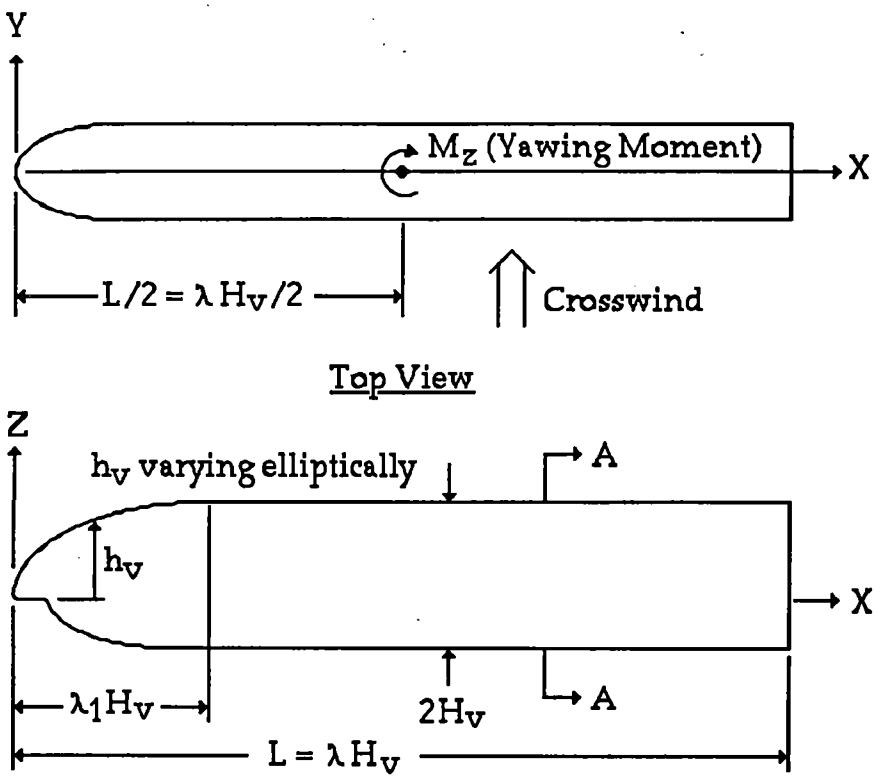

Figure C5-9 Vehicle dimensions for crosswind analysis

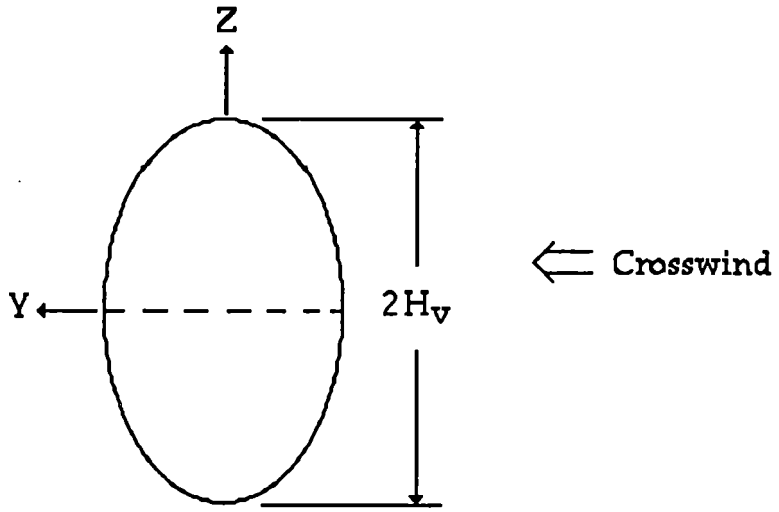

Figure C5-10 Vehicle cross section for crosswind analysis

The aerodynamic loading on this vehicle is assumed to be made up of two parts: non-viscous, slender-body part and viscous, cross-flow part. The two parts are computed separately and superimposed.

The side force and the yawing moment are defined as:

$$Y = C_y \, S \, q \tag{1}$$

$$M_z = C_n \, S \, L \, q \tag{2}$$

Where ;

$q \equiv$ Dynamic Pressure, $\frac{1}{2} \rho \, V_r^2$

$V_r \equiv$ Relative wind velocity magnitude, $\sqrt{V^2 + v_c^2}$

$V \equiv$ Vehicle speed

$v_c \equiv$ Crosswind velocity

$S \equiv$ Reference area, $\pi \, H_v^2$

$C_y \equiv$ Side force coefficient

$C_n \equiv$ Yaw moment coefficient

If subscript s denotes the part of loading from slender-body theory and subscript c denotes the additional loading due to viscous 'cross-flow,' then :

$$C_y = C_{ys} + C_{yc} \tag{3}$$

And

$$C_n = C_{ns} + C_{nc} \tag{4}$$

Steady-state coefficients are given by:

$$C_{ys} = 4\,\beta \int_0^{\lambda_1} \bar{h}_v(\xi)\,\bar{h}_v'(\xi)\,d\xi \qquad (5)$$

Where

$C_{ys} \equiv$ Slender-body part of C_y

$\beta \equiv$ Sideslip angle

$$\xi = \frac{X}{H_v}$$

$$\bar{h}_v(\xi) = \left[\frac{\xi}{\lambda_1}\left(2 - \frac{\xi}{\lambda_1}\right)\right]^{1/2} \qquad \xi \le \lambda_1$$

$$\bar{h}_v'(\xi) = \frac{1 - \xi/\lambda_1}{\lambda_1\,\bar{h}_v}$$

$$C_{ns} = \frac{1}{2}C_{ys} - \frac{4\,\beta}{\lambda}\int_0^{\lambda_1} \xi\,\bar{h}_v(\xi)\,\bar{h}_v'(\xi)\,d\xi \qquad (6)$$

$C_{ns} \equiv$ Slender-body part of C_n

$$C_{yc} = \frac{2}{\pi}k\,\beta \int_0^{\beta\lambda} g(\sigma)\,d\sigma \qquad (7)$$

$C_{yc} \equiv$ Viscous cross-flow part of C_y

$k \equiv$ Factor to incorporate the effects of body cross-sectional configuration

$g(s) =$ Modified-Bryson Function presented in Reference 2 and reproduced here in Figure C5-11. Turbulent boundary layer is assumed.

$$\sigma = \frac{X\beta}{H_v}$$

$$C_{nc} = \frac{1}{2} C_{yc} - \frac{2k}{\pi\lambda} \int_0^{\beta\lambda} \sigma\, g(\sigma)\, d\sigma \qquad (8)$$

$C_{nc} \equiv$ Viscous cross-flow part of C_n

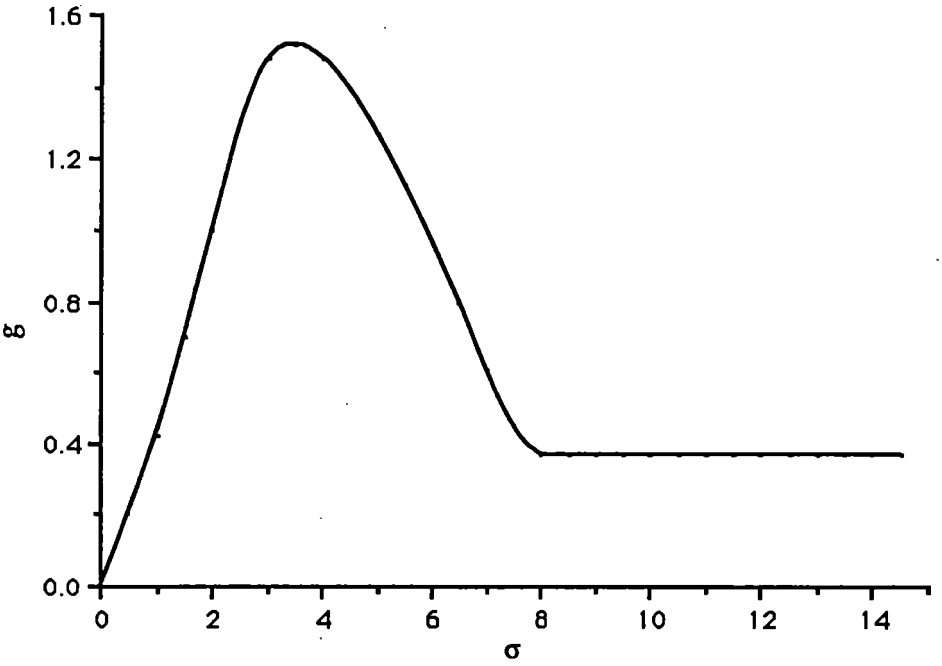

Figure C5-11 Plot of modified Bryson function

The steady-state values of the transient side force (C_y) and yawing-moment (C_n) coefficients were calculated using equations 3 through 8. These computations are presented in Figures C5-12 and C5-13. Here beta is the sideslip angle. The strawman vehicle used for these computations is 36.129 m long and 5.275 m high. H_V for this vehicle is 2.64 m and assumed nose-length of the vehicle is 7 m. Hence, λ is 13.70 and λ_1 is 2.65. Length to height ratio of the vehicle is 6.85. The baseline vehicle has a height of 4.88 m with the same length. Some of the results were recomputed for this height and were found to be only slightly different from the results presented here. Two values of the factor k, which incorporates the effects of body cross-sectional configuration, nose

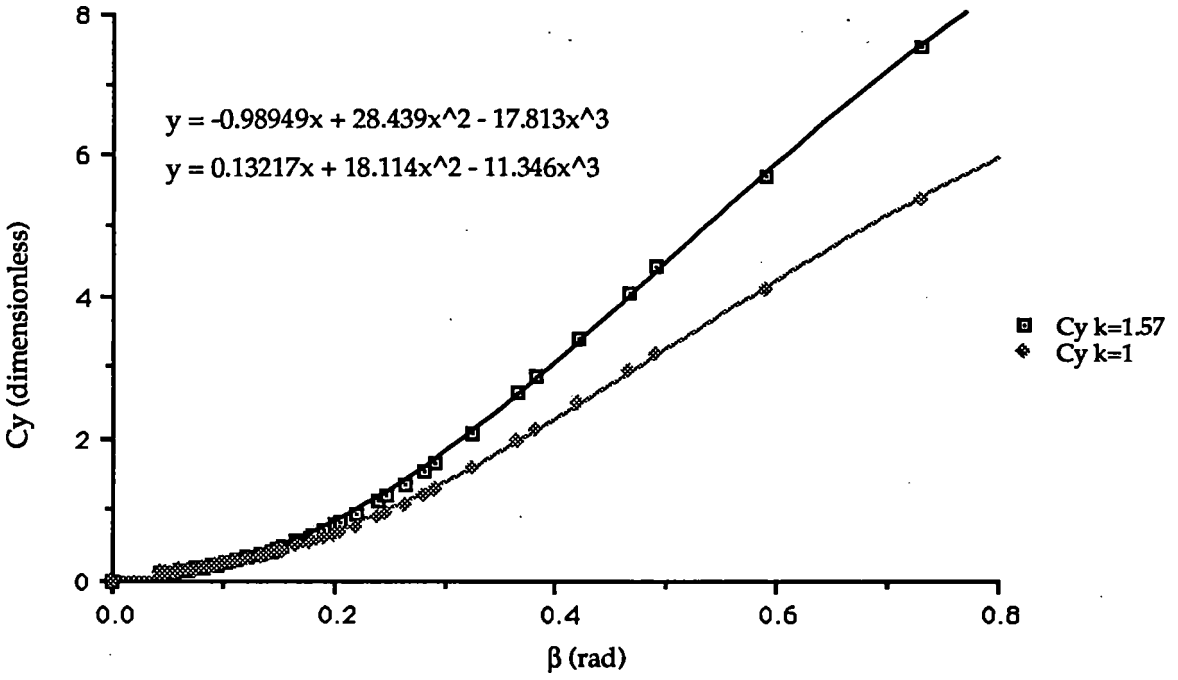

Figure C5-12 Steady state transient side force coefficients vs sideslip angle

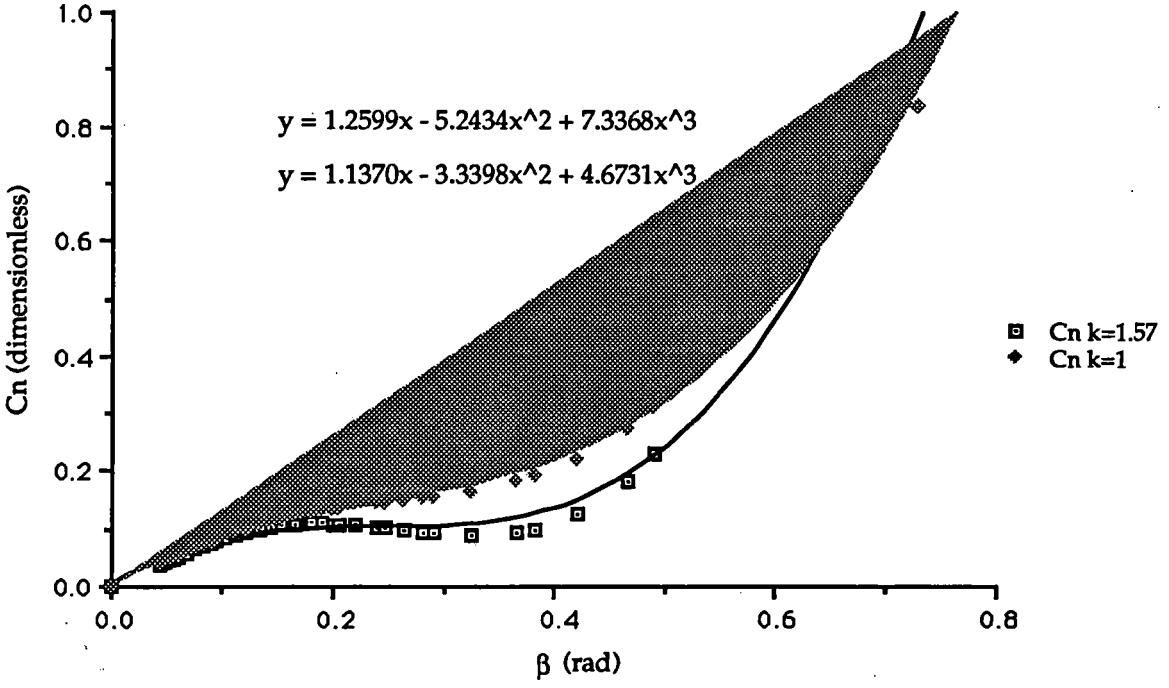

Figure C5-13 Steady state yawing moment coefficients vs sideslip angle

profile and other differences between measurements and theory, were chosen. k equal to 1 represents a circular cross-section and k equal to 1.57 was computed in Reference 2 for TACV vehicles. Various vehicle speeds (30m/s to 150m/s) and gusts (6.7m/s to 26.8m/s) were used to compute these results.

Third order polynomials were fitted to the computations presented in Figures C5-12 and C5-13. These fits are listed in the figures.

Comparison of Computed Results With Measurements

Measurements of C_y and C_n have been made by Grunwald (Ref. 3) and Tracked Hovercraft Limited (THL) (Ref. 4) for similar vehicle bodies. These data are overlaid on the computed plots for k = 1 in Figures C5-14 and C5-15. THL data is for a very similar vehicle whereas Grunwald data presented is for a circular-cross section configuration which is close to the ground.

Comparisons are very good and hence C_y and C_n equations for k = 1 are used for force and moment computations. These equations are:

$$C_y = 0.13\ \beta + 18.11\ \beta^2 - 11.35\ \beta^3 \qquad (9)$$

$$C_n = 1.14\ \beta - 3.34\ \beta^2 + 4.67\ \beta^3 \qquad (10)$$

Using equations 9 and 10 and a crosswind of 27 m/s, side force and yaw moments are computed for a train traveling at speeds ranging from 30 m/s to 150 m/s. These computations are presented in Figures C5-16 and C6-17. The yaw moment is about the center of the train .

Side Forces on a Stopped Vehicle in a Crosswind.

For this case, the classical square drag law is used. The vehicle has a projected area, A_P, of 190.6 m^2. If we assume a crossflow drag coefficient of 0.7 then for a q of 440.6 N/m^2 (27 m/s wind), side-force Y is 58.8 kN. There is no yaw moment as the force is uniformly distributed. When these points are added to Figures C5-16 and C5-17 we obtain Figures C5-18 and C5-19. Data for speeds of 30 and 40m/s are omitted because our theory for higher sideslip angles is suspect. For a 53.6 m/s (120 mph) wind, side force is four times greater, equal to 235kN.

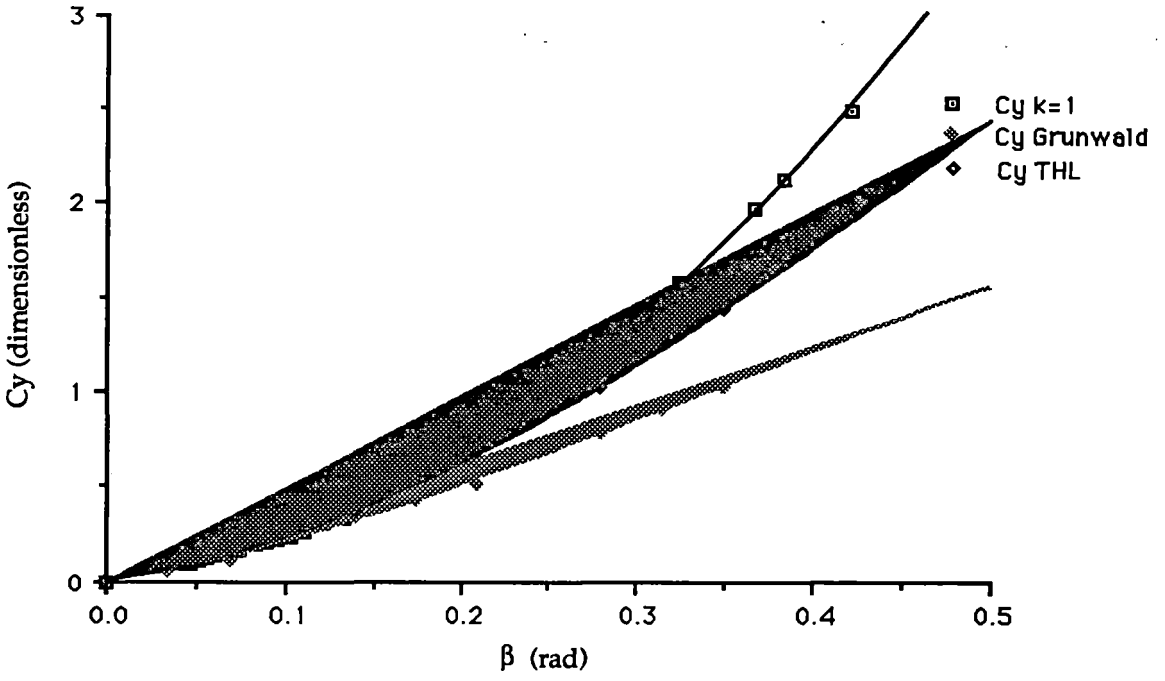

Figure C5-14 Comparison of calculated and measured transient side force coefficients

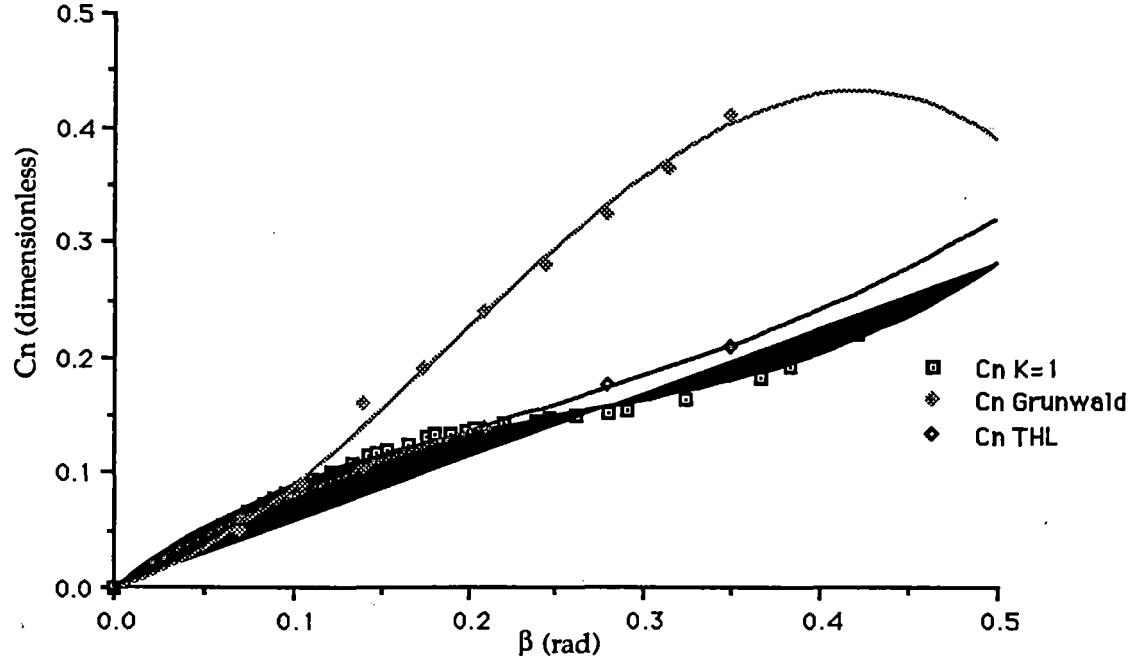

Figure C5-15 Comparison of calculated and measured yawing moment coefficients

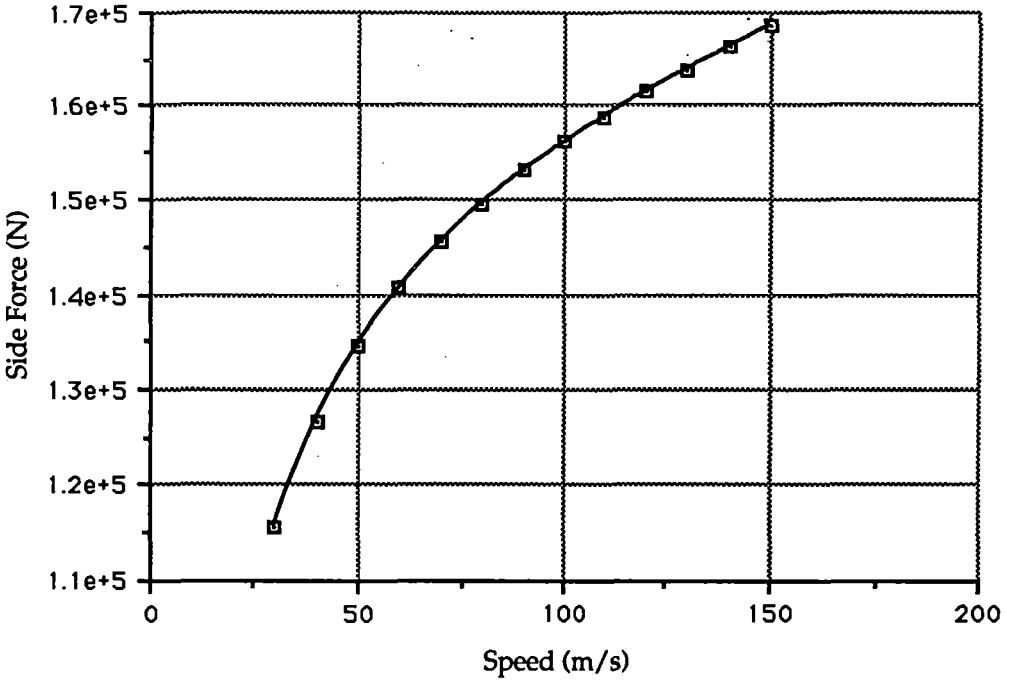

Figure C5-16 Side force vs speed

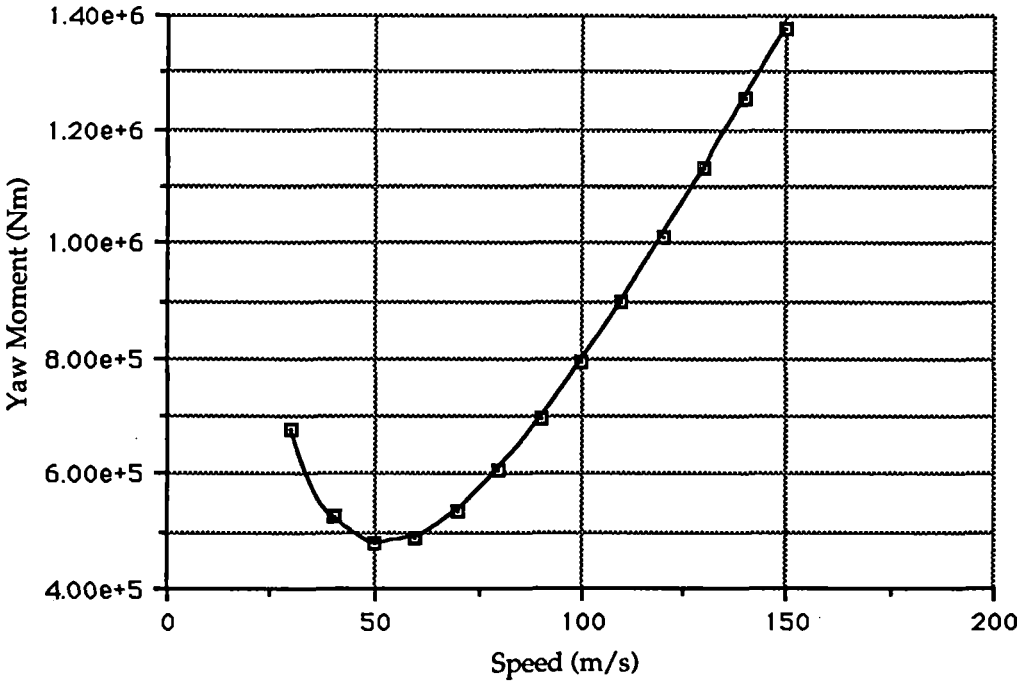

Figure C5-17 Yaw moment vs speed

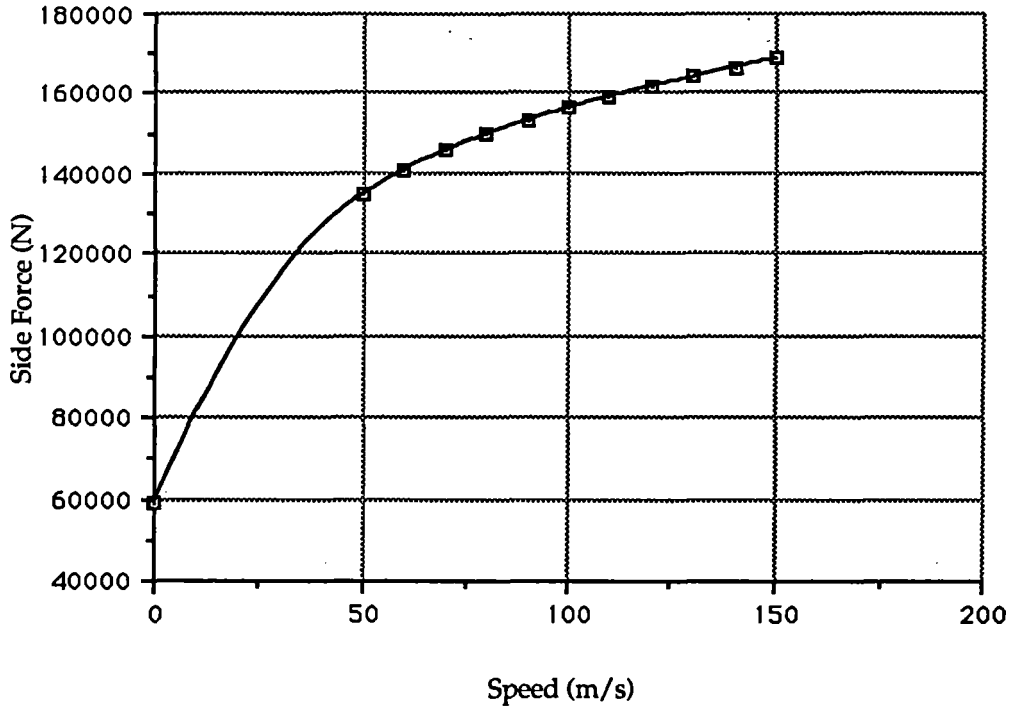

Figure C5-18 Side force vs speed adjusted for low speeds

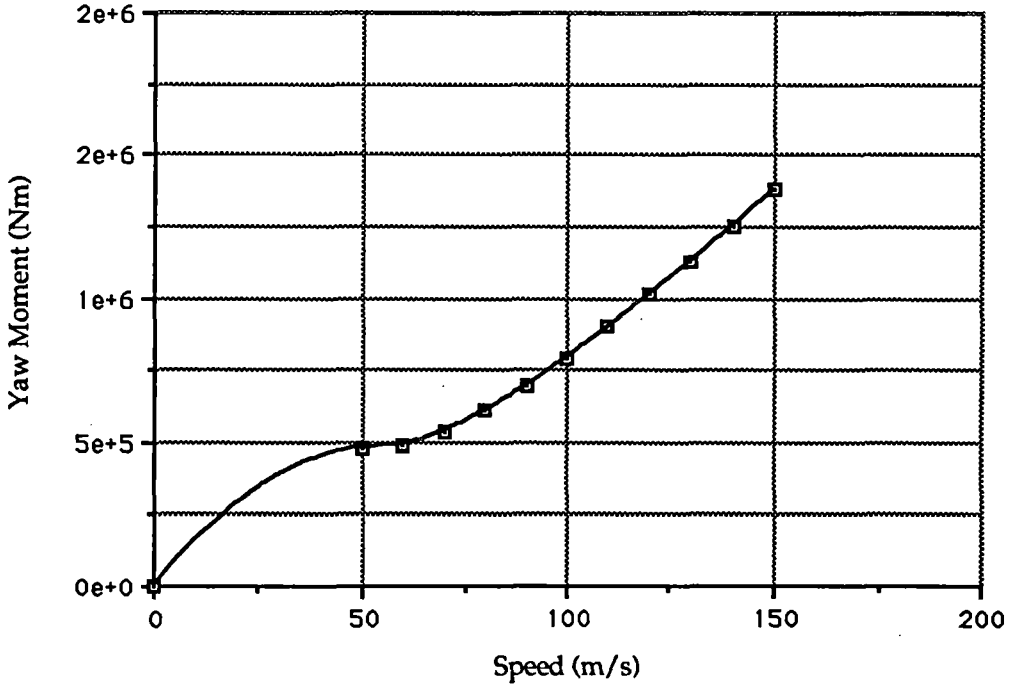

Figure C5-19 Yaw moment vs speed adjusted for low speeds

Roll Moments on the Strawman Vehicle in a Steady Crosswind

For estimating the roll moments, we refer to Reference 4. Here, roll moment, K, is defined as:

$$K = \frac{1}{2} q C_K b^3 \qquad (11)$$

Also the side force, Y, is defined as:

$$Y = q C_Y b^2 \qquad (12)$$

If $K = Y (r + 0.417)$

Then

$$r = \frac{C_K}{C_Y} \frac{b}{2} - 0.417 \qquad (13)$$

Here

$b \equiv$ Vehicle Width = 9 ft .

$h \equiv$ Vehicle Height = 15 ' 10"

$r \equiv$ Moment Arm from the centerline of the vehicle

And 0.417 is for the distance between the centerline and the reference point in Reference 4.

$$\frac{r}{h} = \frac{1}{2} \frac{C_K}{C_Y} \frac{b}{h} - \frac{0.417}{h} \qquad (14)$$

Figure C5-20 displays the measured values of C_K and C_Y as presented in Reference 4.
Figure C5-21 is the computed value of r/h (moment arm ratio) as represented in equation (14). We will use r/h = -0.05 as a conservative value for the moment arm ratio. Roll moments are computed by assuming that the side force is acting at a distance 0.05 x 5.275 = 0.26 m below the centerline of our vehicle.

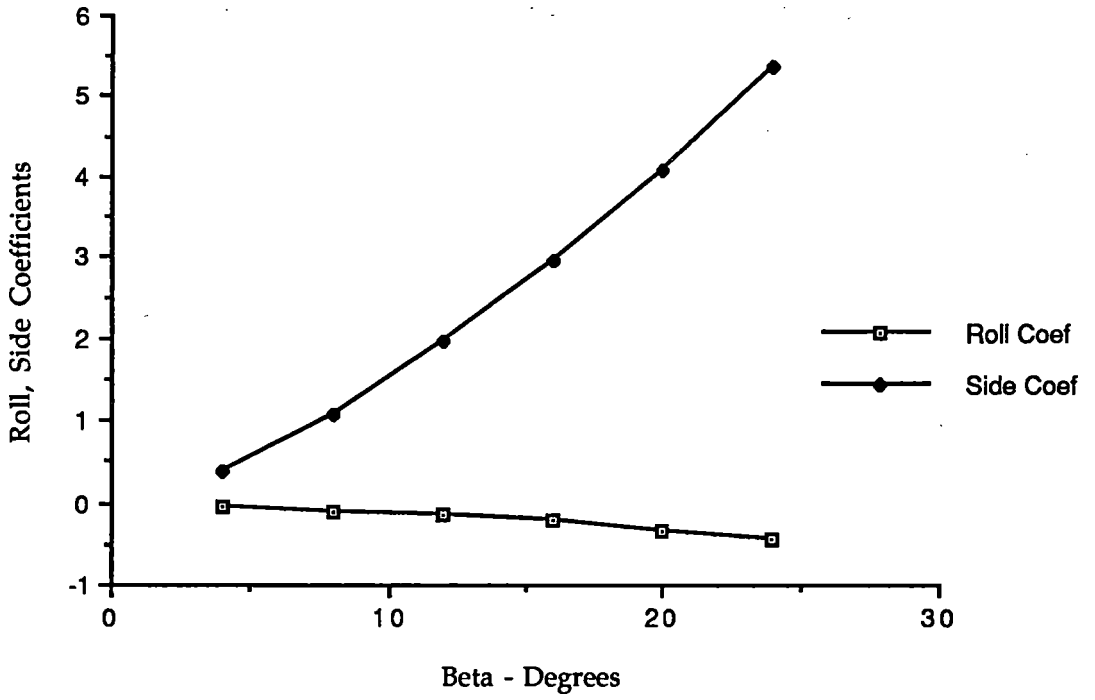

Figure C5-20 Measured values for roll coefficient (Ck) and side coefficient (Cy) [from Ref 4.]

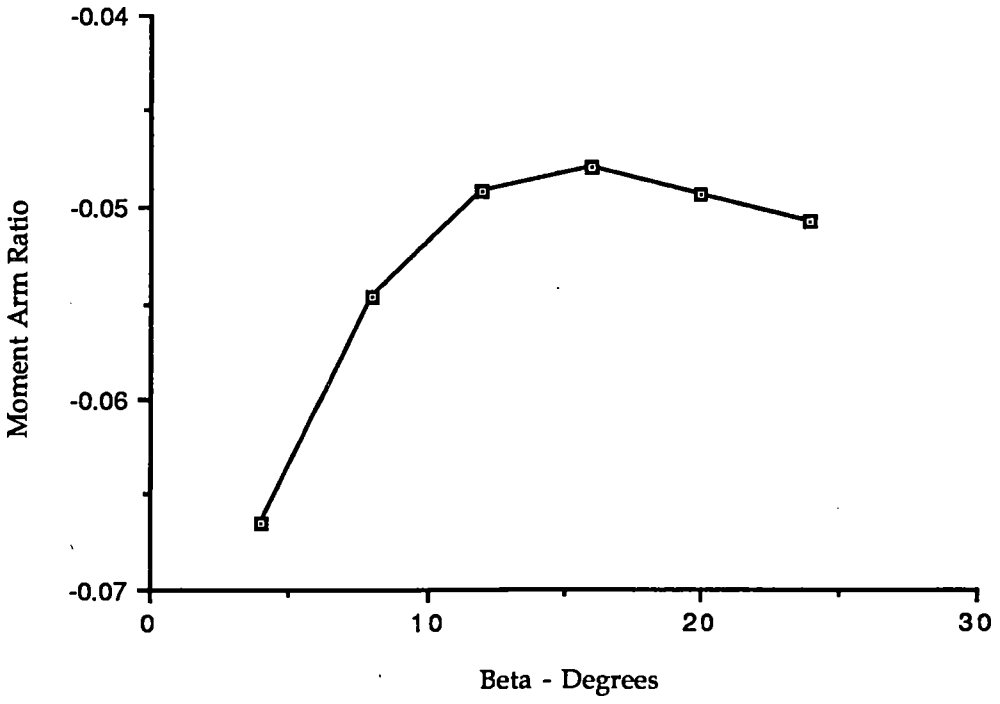

Figure C5-21 Computed moment arm ratio vs sideslip angle

Reduction of Crosswind Effects on Vehicle

The problem of crosswind forces can be alleviated by having a long tapered nose. This spreads out the crosswind force over the length of the nose region. One alternate configuration which takes advantage of this possibility is shown in Figure C5-22. This is a three-car consist carrying 200 passengers. The lead car is entirely devoted to baggage, hotel power collection, and other equipment. Since this car carries no passengers, it is shaped according to the dictates of aerodynamics. In effect, the entire lead car is the nose. This consist can operate with no restrictions in crosswinds up to 60 mph and is offered for consideration on future analyses.

Crosswind Forces on the Structure (Guideway)

Crosswind forces on the bare guideway (no vehicle) in a 89.4 m/s (200 mph) wind are computed. For this case, the classical square drag law is used.

$$Y = q\, C_D\, A_P$$

where, Y is the side force, q is the dynamic pressure (= 1/2 ρ v_c^2), A_P is the projected area, and C_D is the crossflow drag coefficient. ρ is the mass density of air and v_c is the wind velocity. Crossflow drag coefficient for a square beam is assumed to be 2.05. Reference 1 lists this value in Figure 33, 3-17. The projected area for the beam is A_p. For a q of 4,896 N/m^2 (102 psf), Y is 10,036 A_p (N), or 209 A_p (pounds).

References

1. Ruetenik, J. R., and Brooks, W. B., Transient Airloads on a Body of Revolution Due to Indicial Sinking at a Large Angle of Attack, MIT, ASRL TR 121-1, August 1964.

2. Ruetenik, J. R., and Zartarian, G., Development of Methods for Predicting Airloads on TACV Configurations Due to Strong Crosswind Gusts, Report DOT-TSC-171-1, March 1972.

3. Ruetenik, J. R., Correlation of Side-Force and Yawing-Moment Data for TACV Configurations at Large Angles of Sideslip, FRA-ORD&D-74-29, DOT, Washington D.C., January 1974.

4. Tracked Hovercraft Limited, A Cost Comparison of Three Tracked Air Cushion Vehicle Configurations, FRA-RT-71-68, NTIS PB 197 501, July 1970.

5. Hoerner S. F., Fluid-Dynamic Drag, 1965.

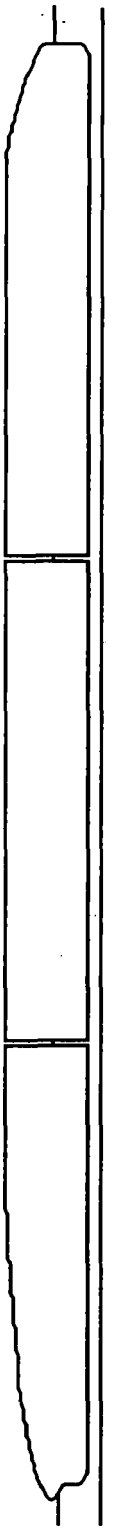

Figure C5-22 Aerodynamic profile of three-car consist

5.2.2 Windblown Sand and Track Debris

Brief Abstract

Any transportation system will be subjected to a variety of climatic forces. While some of these will depend on where the system is sited (e.g., thermal extremes), issues such as windblown sand and track debris will be common to a large number of commonly anticipated maglev sites. The discussion that follows explores the possible adverse effects associated with windblown sand, snow, ice, and guideway debris on a maglev system and mitigation approaches to reduce the adverse effects and extend the overall life of the system. Thermal effects on the guideway and attached equipment are covered elsewhere in this document.

Key Requirements

Design guidelines established for the maglev systems call for operation that is "compatible with all common U.S. weather conditions (e.g. wind, snow, rain, fog, icing, heat, lightning) with minimal degradation in system performance. In the region of operation, maglev should be the transportation mode least affected by adverse weather conditions."

Snow, ice, and accumulations of other forms of guideway debris may hinder maglev operation if they are too large for the vehicle to pass over without impact or if they alter the magnetic fields substantially. Removal with a plow-type device on the front of the vehicle, as has been historically done with lower speed trains, is inappropriate at the higher speeds of maglev both for the potential damage to the vehicle and because of wayside hazards associated with items pushed off the guideway. Thus, while debris removal is necessary for continued operation, it must be done safely and carefully.

Windblown sand can cause two types of problems: those resulting from pitting due to sand in motion and those occurring as a result of accumulated sand. Wherever possible, the system should be designed to reduce both. Where mitigation for one exacerbates the other, mitigation selection should be based on the least cost option that most contributes to overall system reliability and safety.

Approach Used

From an operational point of view, the critical criteria for debris removal is whether it might, if not removed, damage the vehicle or guideway, or pose a greater threat than leaving the debris in place.

Within the context of this report, debris is considered to be both manmade trash and natural accumulations of snow, ice, dirt, etc. except where otherwise noted.

There are a number of inherent benefits to maglev that minimize debris collection. The system consists for the most part of an isolated, elevated structure with little horizontal surface to accumulate debris. In addition, prevailing winds will, in many cases, blow most lightweight debris from the track before it accumulates. Nonmagnetic debris that is shorter than the clearance between vehicle and support beam should not be consequential to operations since there is no contact. Finally, the anticipated frequency of vehicles on the system means the guideway beam will not be vacant and collecting debris for long periods of time. Thus the real problem appears to come from debris that either accumulates rapidly or is sufficiently massive (size and weight) that it will not be blown away by local winds, is not easily run over or pushed out of the way by the vehicle, or might become a hazardous projectile if launched by an oncoming vehicle from the guideway.

Any maglev system is confined to operate along a fixed route and cannot dodge debris except to stop, so it is essential that potentially hazardous debris be cleared as quickly as it can be detected. Despite the relatively small cross section of the guideway beam, there are small collecting surfaces which could accumulate debris. The isolation and elevation of the guideway makes track clearance difficult except by dedicated vehicle.

Windblown sand can cause pitting of the vehicle exterior, reducing the aerodynamic smoothness of its shape and thereby reducing the overall system efficiency. The impact of windblown sand on the structural integrity of the guideway is expected to be minimal, if any, over the life of the structure. Impacts on guideway electronics, power cables, and magnet structures are largely unknown at this time, but all guideway attachments are mounted with a cover in our baseline concept as a precaution (as well as for noise attention).

Accumulated sand as a result of windstorms may adversely affect the operation of roadside and guideway based electronics if they are not adequately housed in a protective structure. Because there is no physical contact of the vehicle with the guideway, no frictional losses are anticipated as a result of sand accumulations. In general, accumulated sand should have little or no impact on the magnetic fields required for levitation, propulsion, or guidance of vehicles within the system since most sand is composed of only minor fractions of ferromagnetic material.

Description

We propose to follow the lead of other automated guided vehicles by having a dedicated vehicle that will run the full course of the system each day before full operations begin to clear the track of any accumulated debris. The dedicated vehicle will operate under its own power so that it can also be used to clear stranded vehicles from the track as needed at any time. By running the full length of the system (in segments between stations, using a fleet of dedicated vehicles) the continuity of the track can also be verified. A system of track monitors will provide additional surveillance of the track for debris accumulation and can signal the control system to halt an oncoming vehicle if hazardous debris appears on the track block ahead of the vehicle.

Proposed mitigation for windblown sand is in three forms: full enclosure of critical components, especially electronic systems; tough, sand resistant vehicle body coatings to maintain a smooth, aerodynamic shape; and an overall design to minimize areas where sand can accumulate sufficiently to adversely affect maglev system operations.

Benefits/Risks

The only way to avoid the effects of either debris or windblown sand completely would be to completely enclose the guideway/vehicle system. This is expected to be cost prohibitive over the extensive distances that must be travelled by maglev. Also such an enclosure could be particularly hazardous in case of an emergency or a system malfunction since it would hinder external access to the system. Therefore, enclosures should be constructed only where needed and at the smallest appropriate level to afford adequate protection for critical system elements (e.g., sealed boxes around electronic control components).

Debris clearance by a dedicated vehicle operating under its own power, as described above, provides a daily verification of track alignment and fitness, but requires the development of a separate vehicle with its own contained propulsion system. However, such a vehicle would be essential for evacuations in emergencies involving power failures. Slow speed debris clearance minimizes the risk that debris will affect system safety.

Sand barricades, if they are not complete enclosures, frequently become sand collectors somewhere else. If barricades are indicated, their design must consider where sand collection or accumulation will not adversely affect system operation. Overall the design of the system will consider minimizing the excessive accumulation of sand at any location. Either the system will be

designed to "self clean" (e.g., grates or meshes) or maintenance plans will facilitate/require the removal of any accumulated sand.

5.2.3 Vehicle Passing Effects And Optimum Guideway Separation

Vehicle Passing Design Criteria

The subject of vehicle passing should be considered in conjunction with crosswind effects. One design condition which is the subject of the following discussion is shown in Figure C5-23, which shows a two-lane guideway with maximum traffic in both directions with an 18 m/s crosswind. As the vehicles pass each other there are two effects. The first effect is called shielding: the upwind vehicle briefly shields the downwind vehicle from the crosswind force, producing a momentary loss of wind-induced side force and yawing moment, resulting in an acceleration in the upwind direction. The second effect is the passing pulse due to the disturbance of the oncoming vehicle which is present even if there is no crosswind. The criteria which is chosen for optimum guideway separation is to make both of these effects approximately equal. The justification for this criteria will now be explained.

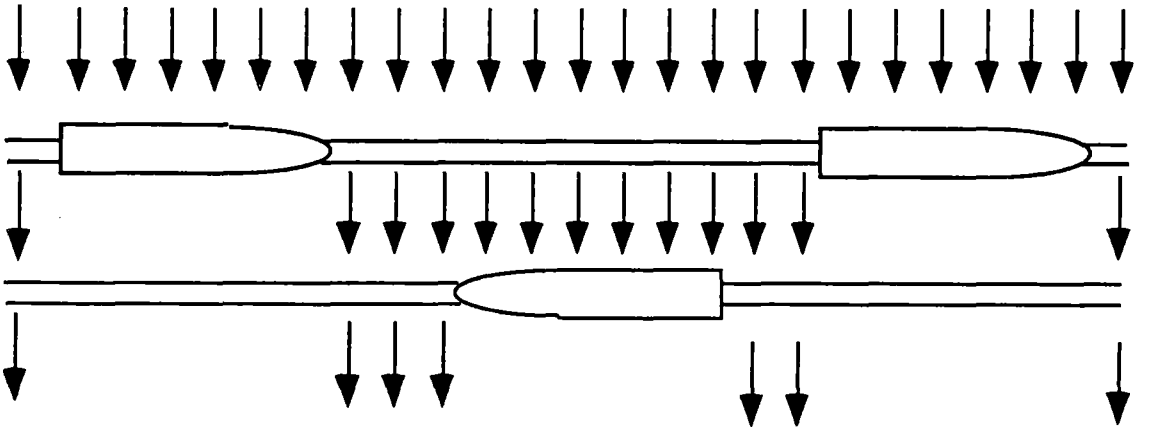

Figure C5-23 Shielding effect during crosswinds

At the maximum anticipated system capacity the headway is 40 seconds. This means that in the frame of reference of a moving vehicle, another vehicle is passed every 20 seconds. This is a short enough time span that the passing phenomena should be considered as part of the spectrum of ride roughness inputs rather than as isolated events. The passing pulse defined above drops off approximately inversely with the square of the separation between the guideways. In contrast, the shielding effect will not be diminished even by relatively large guideway separations. This is due to

the fact that during crosswinds the wake of the vehicle on the lee side of the guideway persists for a very large distance downstream (i.e., many vehicle diameters). If one chooses a small guideway separation, such that the passing effect is larger than the shielding effect, there will be large and undesirable accelerations on the vehicle. As the guideway separation is increased these undesirable accelerations will diminish. This is a cost effective tradeoff as long as the passing pulse is the dominant effect. The chosen separation, when both effects are equal, is the point beyond which the shielding effect becomes dominant and there is no longer much improvement from adding further separation between the guideways.

The design criteria is for the vehicle to meet ride quality constraints in an 18 m/s (40 mph) crosswind. Beyond this speed the ride quality will deteriorate. The operating plan is to decrease the vehicle speed if the crosswinds become greater than this. At 27 m/s (60 mph), all vehicles are brought to the nearest station where they wait until weather conditions improve. The following steps describe our team's approach to determining vehicle passing effects.

Side Force Transients Due to Shielding Effects from 18 m/s Crosswinds

These forces are computed similar to forces computed in Section 5.2.1. The steady-state values of the transient side force (Y) are computed. The strawman condition is the vehicle traveling at 150 m/s (336 mph) subject to a gust of 18 m/s (40 mph). This results in a sideslip angle of 0.12 radians (6.8 degrees) and the resultant Mach number is 0.44. For these strawman conditions, the side force coefficient (C_Y) for the vehicle is computed to be 0.25 (equation 9 of section 5.2.1). In order to be able to compare computations made in this subsection with the following subsections we assumed the vehicle to be 4 m high. The baseline vehicle is 4.1 m wide and 4.88 m high. For 4 m high vehicle, reference area is 12.57 m^2. The dynamic pressure (q) is 13,980 N/m^2, hence the side force on the vehicle is 43,932 N. The average pressure change, assuming 144.52 m^2 projected area for the vehicle (4 m X 36.129 m), due to shielding is 304 N/m^2. For the baseline vehicle, height is 4.88 m giving a reference area (A) of 18.7 m^2. For dynamic pressure (q) of 13,980 N/m^2, the side force on the vehicle is 65,357 N. The average pressure change, assuming 176 m^2 projected area for the vehicle, due to shielding is 371 N/m^2.

Open-Ground Passing Transients on Vehicles to Match the Shielding Perturbations

High-speed maglev vehicles will cause aerodynamic disturbances that effect other vehicles and objects along the guideway. When two vehicles pass, they create pressures and loads on each other. These pressures are unsteady and change relatively rapidly. A relatively simple solution to these pressures can be obtained by using a linearized theory. This could be appropriate as the

vehicle considered is slender. In this analysis, the oncoming vehicle is modeled as a line of moving sources. Perturbation in the velocity field depends primarily on the distribution of cross sectional area. For our case the line source is distributed over the nose length. The nose is assumed to be circular. The constraints due to the presence of a wall and/or another vehicle can be simulated using images of the vehicle in the wall plane, as shown in Figure C5-24. This is a crude approximation which is used in the industry and is not valid for nose-to-nose situation. It is assumed that Q, rate of change of cross section area, is constant throughout the nose region.

The pressure coefficient, C_p, for a single vehicle with and without a wall (another passing vehicle) a given distance away can be computed. Pressure at any point caused by a vehicle is given by (Ref 1):

$$C_p = \frac{1}{2\pi}\frac{A_t}{C}\left\{\frac{1}{(x^2 + y^2 + z^2)^{\frac{1}{2}}} - \frac{1}{((x - C)^2 + y^2 + z^2)^{\frac{1}{2}}}\right\}$$

Here, A_t is the cross section area of the vehicle, C is the nose-length, and x, y, z are the coordinates of a point where the pressure is desired. This coordinate system has its origin at the nose of the vehicle. We will again assume the vehicle cross section to be circular of 4 m diameter. Also assume C = 2.0 m (circular nose), and A_t = 12.57 m^2 (135.28 ft^2). For a nose shape with constant increase in area:

$$y = \sqrt{\frac{A_t x}{\pi C}}$$

C_p was first computed for a single vehicle with no wall plane effects and as a function of x. Next, we computed the perturbations on vehicle B. The maximum perturbations on vehicle B occur very near to the point closest to vehicle A, denoted by m in Figure C5-24. Here z=r and y=0. Pressure

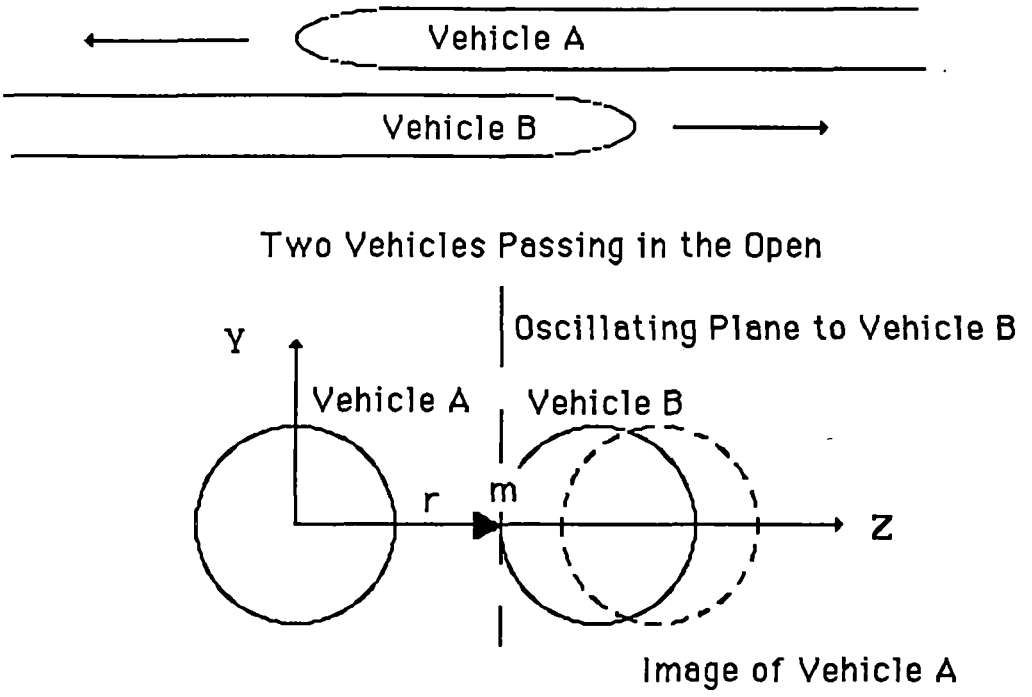

Figure C5-24 Vehicles and aerodynamic images

coefficients from the two bodies are computed and summed. The results for a guideway separation of 7 m (i.e., vehicle walls are only 3 m away) give a pressure perturbation of 1228 N/m^2 at point m. This value for the pressure perturbation is a peak value. This technique was not satisfactory so an alternate solution was sought. In this solution each of the passing trains is modeled as a combination of a moving source and a doublet. This model is displayed in Figure C5-25. Here again, vehicle is assumed to have a 4m diameter circular cross-section with sources and doublets located 1 m away from the nose which is also assumed circular.

First, the values for doublet position and strength are computed that give correct boundary conditions when sources are closest together. These parameters are computed for a given guideway separation. For a H of 3.5 m (7 m guideway separation) the doublet strength q is 4.428 at a distance b of 0.193 m from the source. For H of 3.0 m, q is calculated as 6.096 and b is 0.226 m.

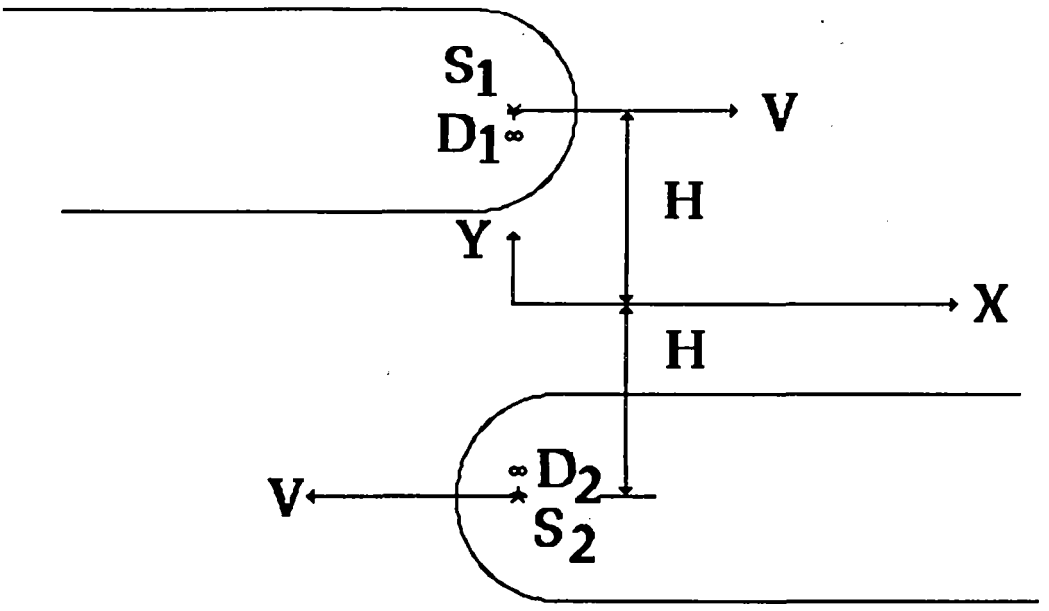

Figure C5-25 Vehicles modeled as pair of sources and doublets

Using these values, C_p can be computed at each location as a function of time as the vehicles approach each other. Each of the vehicles is traveling at 150 m/s . A typical example of such computation is presented in Figure C5-26. In order to obtain an average pressure perturbation at each cross section of the vehicle, following procedure is used.

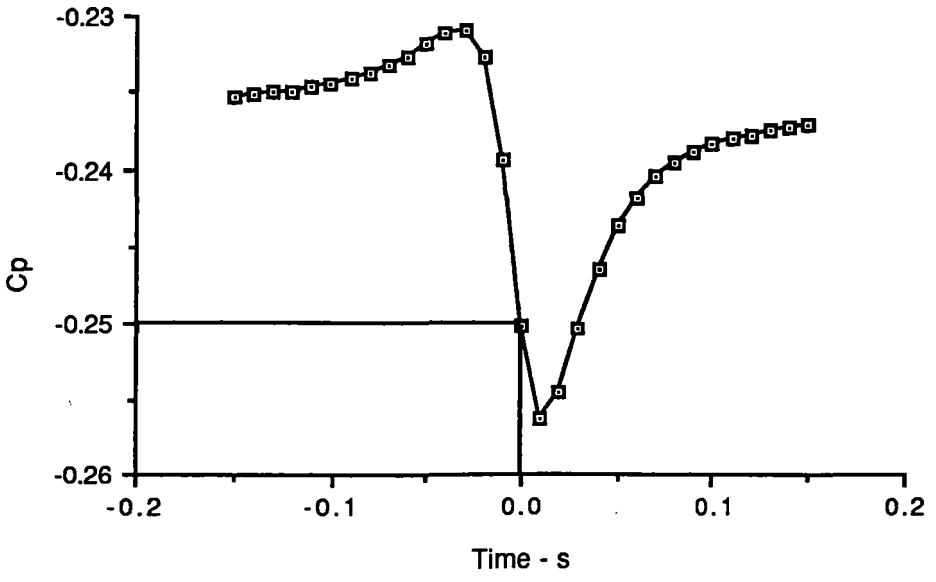

Figure C5-26 Pressure coefficient at a location on the vehicle

For each location on the vehicle, it is assumed that the pressure around the circular cross section of the vehicle is sinusoidal. The point closest to the oncoming vehicle has the maximum pressure and the point furthest away has the minimum pressure. In between points have pressures that vary as a sine wave. Hence, average force at a given location can be determined from two values of pressure. Using this technique we determined the side force F_y per unit length at various locations on the vehicle (nose backward) and for two guideway separations (6 m and 7 m) as a function of time as two vehicles pass each other. Figure C5-27 presents the side force per unit length as a function of time at cross sections 0.25 m, 0.50 m, and 1.0 m from the nose. These values are for a 7 m separation of the guideways (vehicle walls are only 3 m apart). Figure C5-28 presents similar results for cross sections 1 m, 1.5 m, 2 m, 3 m, and 5 m from the nose. Peak perturbations for each cross section are presented in Figure C5-29.

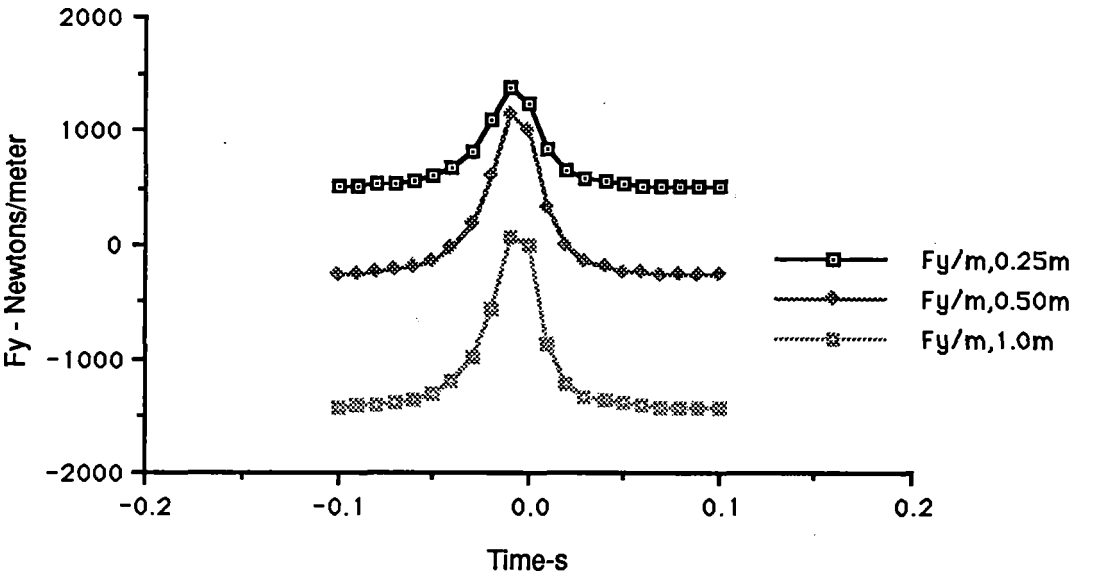

Figure C5-27 Side force per unit length at various locations on vehicle

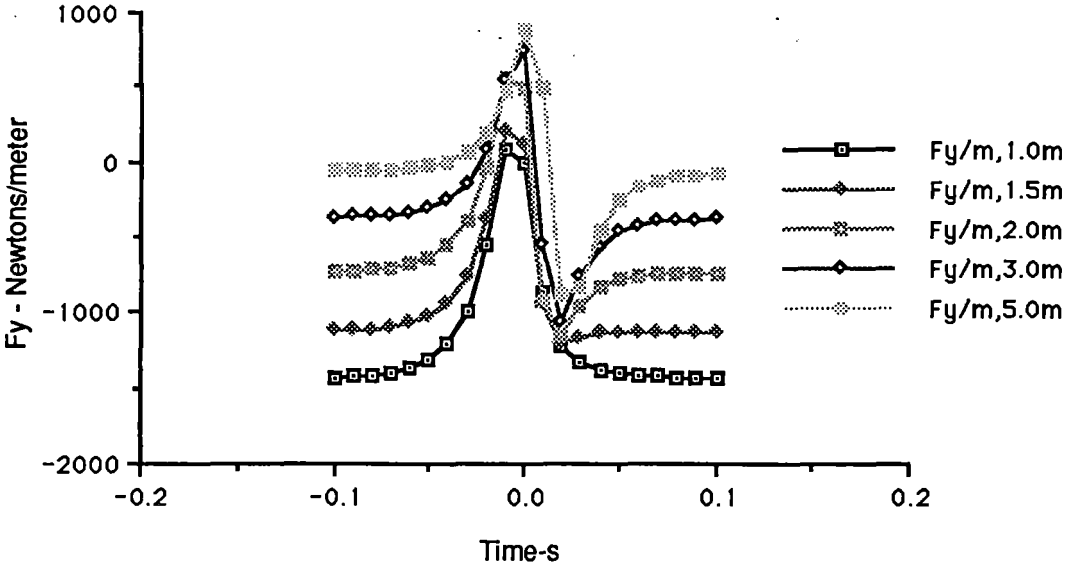

Figure C5-28 Side force per unit length at various locations on vehicle

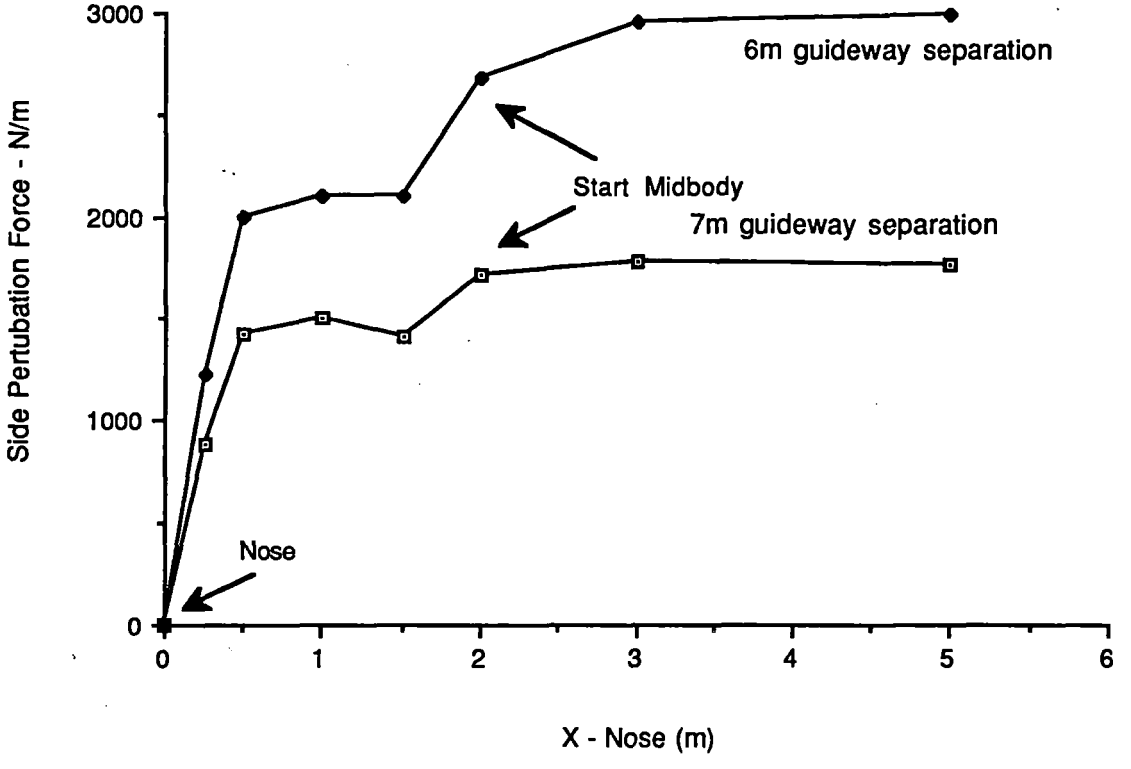

Figure C5-29 Side force perturbation for two guideway separations

Results for both 6m and 7m separations are presented. From this figure the average side perturbation pressure on 4m high vehicles traveling at 150m/s and at 7m guideway separation is computed to be 400 N/m^2.

Optimum Guideway Separation

Guideways are usually placed as close together as is practical, in order to decrease the size of the entire guideway system. The optimum separation will be computed from results of the above analysis, using those results to compute ride quality, and then examining any required increases in guideway separation and/or suspension stiffness needed to improve ride quality. For the present study the recommended guideway separation is 7m. This is a distance at which the shielding effects are equivalent in magnitude to the open ground passing effects.

References

1. Hammit, A. G., Aerodynamics of High Speed Ground Transportation, Western Periodicals Co., North Hollywood, CA, 1973.

5.2.4 Design of Active Aero Surfaces

Aerodynamic Forces on Control Surfaces

Control Surfaces as Wings

A conceptual design of four control surfaces on the maglev vehicle is displayed in Figure C5-30. The effective aspect ratio of each surface (including a reflection plane) is taken as the double geometric aspect ratio.

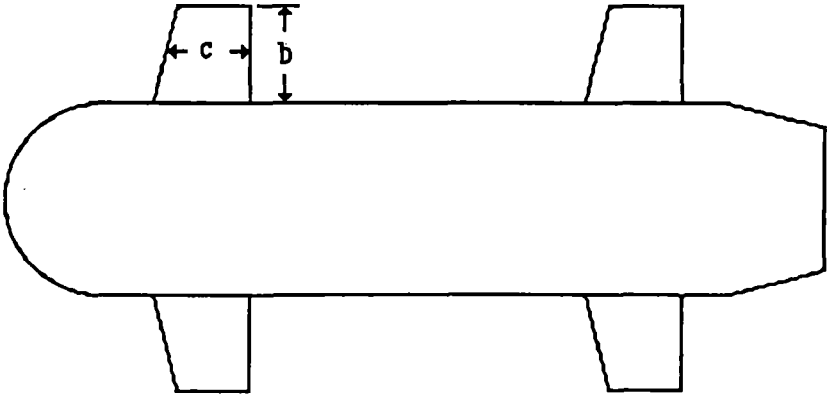

Figure C5-30 Control surfaces conceptual design

$$\text{Æ}R = 2\frac{b^2}{S}$$

ÆR ≡ Double geometric aspect ratio

b ≡ Span

S ≡ Planform area

Let;

$b = 1.12$ m

$\frac{S}{b} = c = 1.40$ m = Average Chord Length

$S = 1.57$ m^2

Æ$R = 1.60$

Lift force L is given by:

$$L = \frac{1}{2}\rho S C_L V^2$$

C_L ≡ Lift coefficient

V = Train speed

Drag force D is given by:

$$D = \frac{1}{2}\rho S C_D V^2$$

C_D ≡ Drag coefficient

In general, lift and drag forces and moments due to control surfaces have three components: forces and moments due to control surfaces alone; effects of vehicle-body on control surfaces; and effects of control surfaces on vehicle-body forces and moments. For the present system concept definition study only forces and moments due to control surfaces alone are considered.

Lift Coefficient

Using small aspect ratio theory, we have the linear and non-linear components of the lift coefficient.

$$C_L = C_{Ll} + C_{Ln}$$

For a sharp edged rectangular wing Reference 1 gives:

$$\frac{d\,C_{Ll}}{d\,\alpha} = \frac{180}{\pi}\,\frac{1}{\frac{36.5}{AR} + 2\,AR} \qquad \text{for } AR \le 2.5$$

$$= 2.20 \qquad \text{for } AR = 1.60$$

Here α is the angle of attack and,

$$C_{Ll} = \frac{d\,C_{Ll}}{d\,\alpha}\sin\alpha$$

Also, Reference 1 gives;

$$\frac{d\,C_{Ln}}{d\,\alpha} = 2.0\,|\sin\alpha|\cos\alpha$$

Hence;

$$C_L = \{2.20 + 2.0\,|\sin\alpha|\cos\alpha\}\sin\alpha$$

A plot of this equation is presented in Figure C5-31. In this figure the coefficient of lift increases with the angle of attack until stall occurs. Stall occurs at an angle of attack when the maximum lift coefficient has been achieved. Planform shape of the control surface is the dominant factor influencing this maximum. We will assume that the maximum allowable $C_L = 1.2$. This value corresponds to $\alpha_{max} = 0.42$ radians = 24 degrees. Linear curve fit to Figure 5.2.4-2 gives:

$$\frac{d\,C_L}{d\,\alpha} = 2.81 \text{ / radian}$$

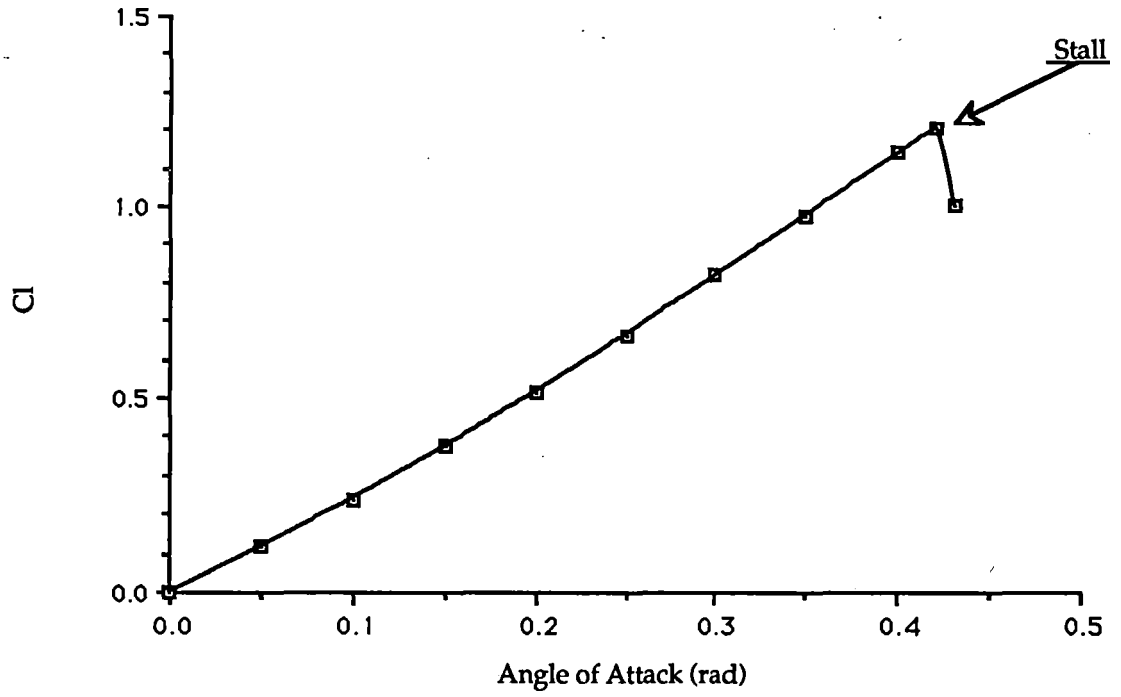

Figure C5-31 Lift coefficient vs. angle of attack

Drag Coefficient

Drag coefficient, C_D, is comprised of the profile drag, C_{DS}, and the lift-induced drag, C_{Di}.

$$C_D = C_{DS} + C_{Di}$$

Based on chord length;

$$R_c = \frac{Vl}{\nu}$$

$$\nu = \frac{1.56}{10^4}\frac{ft^2}{s} \qquad \text{where} \qquad l = 1.4\ m = 4.59\ ft$$

$$V_{max} = 150\ m/s = 492\ ft/s$$

$$R_{cmax} = 1.4 \times 10^7$$

Hence both laminar and turbulent boundary layer regions are encompassed. The profile drag is given by Reference 2.

$$C_{DS} = 2\,C_f\left(1 + \frac{t}{c}\right) + \left(\frac{t}{c}\right)^2 \qquad R_c < 10^4$$

$$C_{DS} = 2\,C_f\left[\,1 + 2\,\frac{t}{c} + 60\left(\frac{t}{c}\right)^4\,\right] \qquad R_c \geq 10^5$$

Here t/c is the thickness/chord of the control surface. C_f is the skin-friction coefficient (Ref. 2).

$$C_f = \frac{6.8}{R_c} \qquad R_c < 10$$

$$C_f = \frac{1.328}{\sqrt{R_c}} \qquad 10 \leq R_c \leq 4.21 \times 10^5$$

$$C_f = \frac{1}{(\,3.46 \log R_c - 5.6\,)^2} \qquad R_c > 5.7 \times 10^6$$

The induced drag given in Reference 2 is:

$$C_{Di} = \frac{C_L^2}{\pi\, AR}$$

Plots of L and D for various V's are presented in Figures C5-32 and C5-33. Control surface deflections of 0.1, 0.2, 0.3 and 0.4 radians are considered.

Computation of Average Drag

Let rms of α = 8 degrees. For a sine wave of amplitude = 11.32° (.20 rad), rms = 8°. We compute drag force for a fin-deflection of 0.20 sin ωt. Average of this force is presented in Figure C5-34. Another way of computing this drag force is to take 1/3 of the force generated by α_{max} (24 deg). This is also presented in Figure C5-34. Figure C5-35 presents drag forces of Figure C5-34 divided by V^2 to display respective drag constants.

Control Surfaces as Wings with Flaps

Lift force L is given by:

$$L = \frac{1}{2}\rho\, S\, C_L(\,\alpha, \delta\,)\, V^2$$

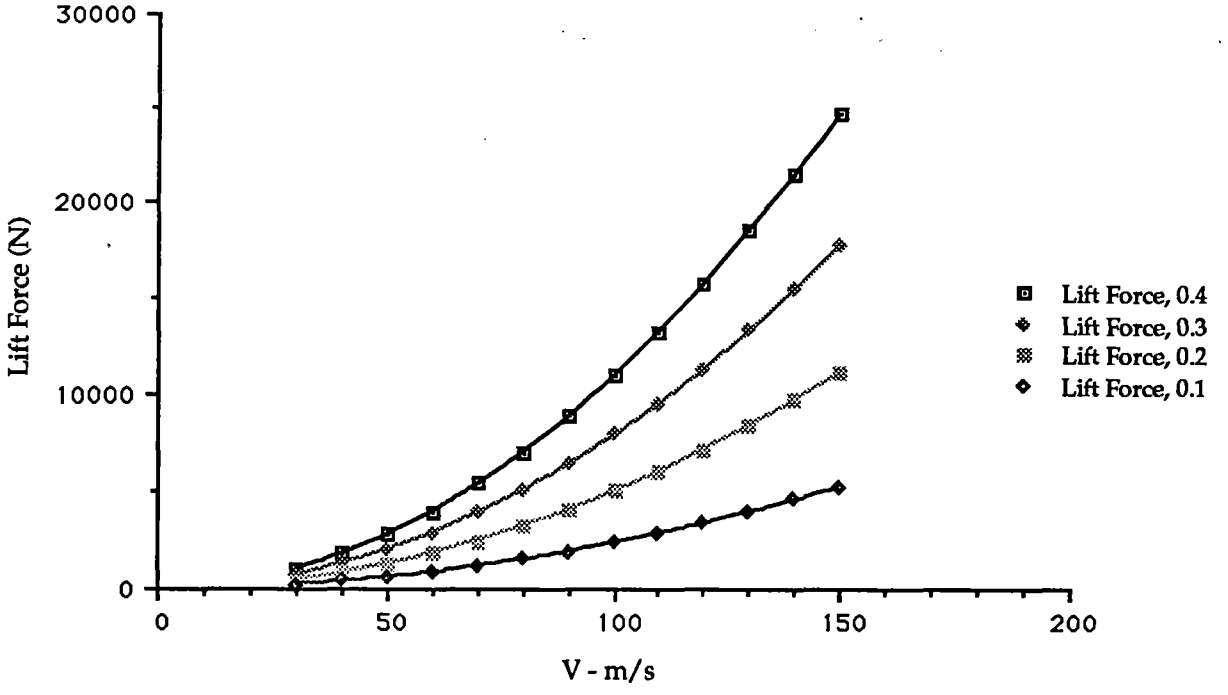

Figure C5-32 Lift force/foil for various angles of attack in radians

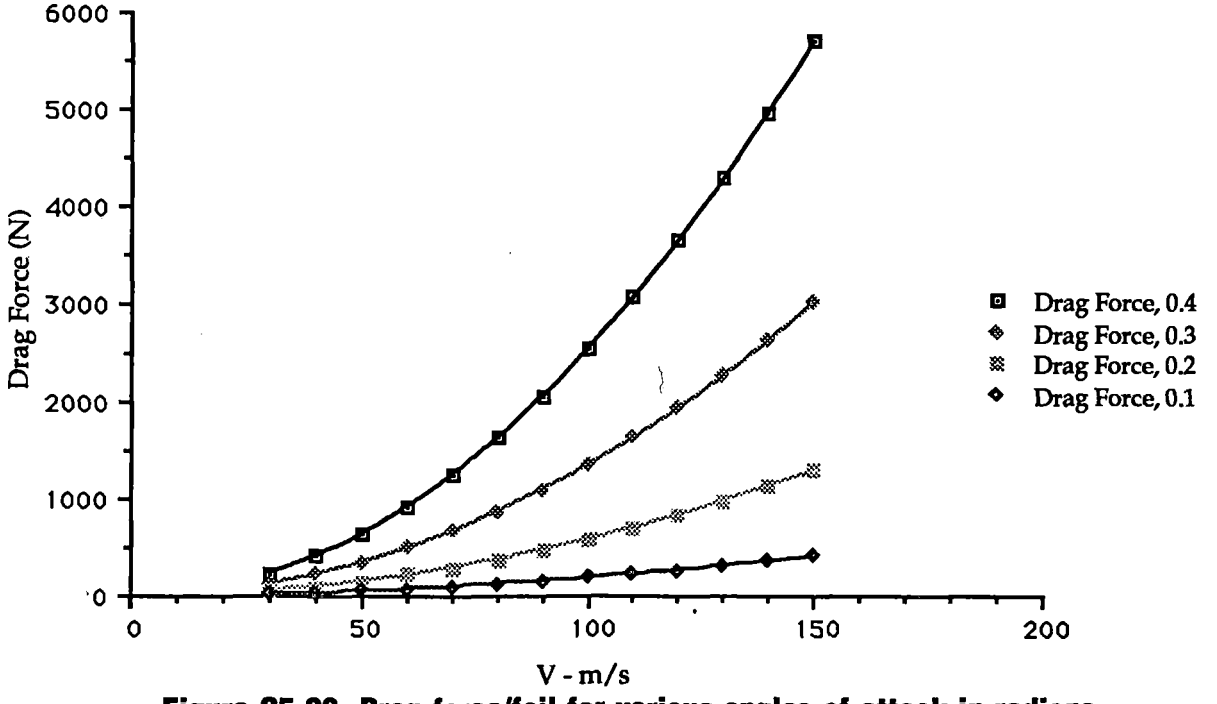

Figure C5-33 Drag force/foil for various angles of attack in radians

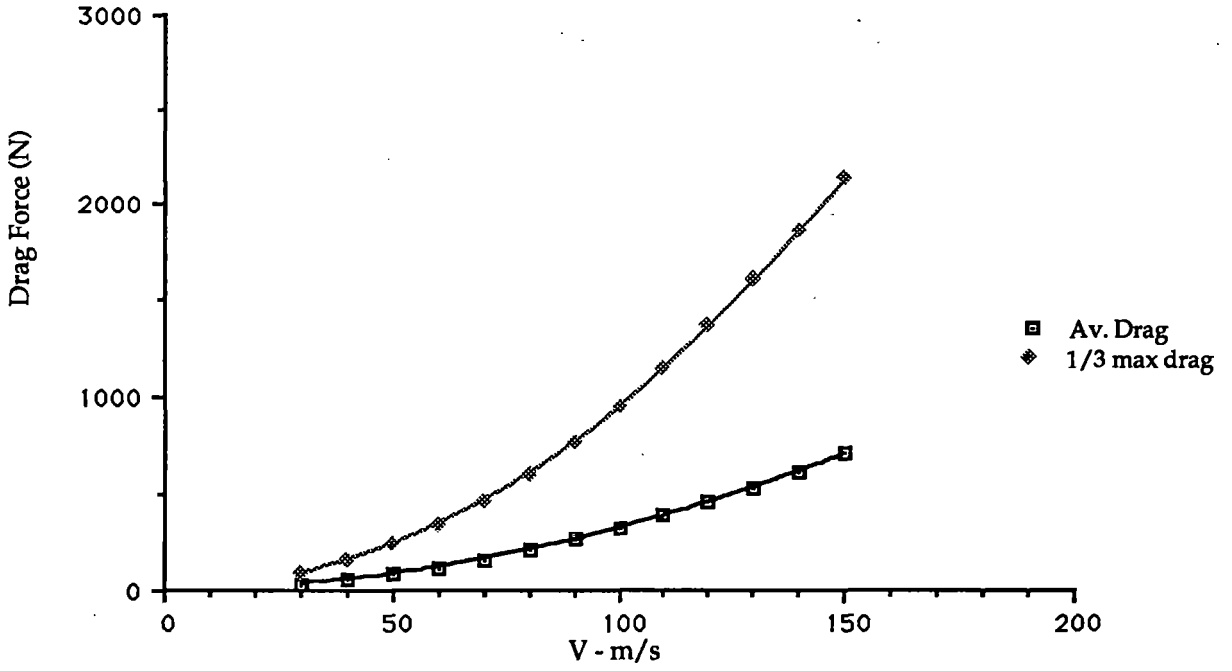

Figure C5-34 Drag force/foil for various drag constants

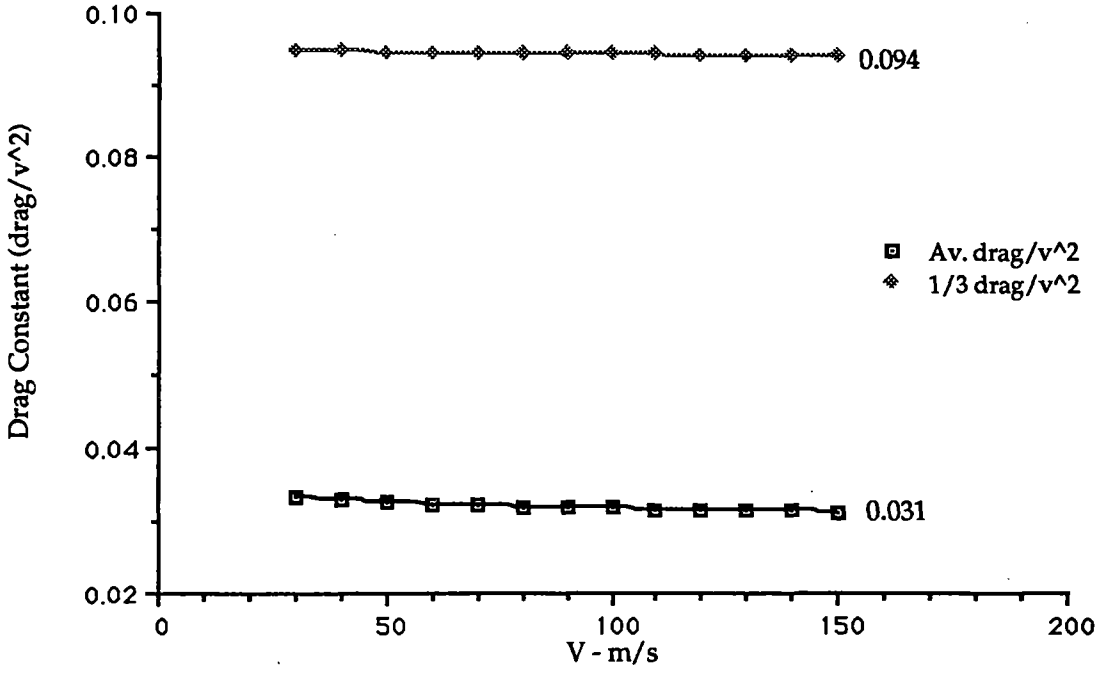

Figure C5-35 Drag constant vs speed

Linear Component of Lift Coefficient (a = 0)

$$C_L = \frac{d C_L}{d \alpha}\left[\frac{d \alpha}{d \delta} \sin \delta\right]$$

Again, for a sharp edged rectangular wing Reference 1 gives (for aspect ratios less than 2.5):

$$\frac{d C_L}{d \alpha} = \frac{180}{\pi} \frac{1}{\frac{36.5}{AR} + 2} \qquad AR \leq 2.5$$

For flap deflection, theoretical function given in Reference 1 is:

$$\frac{d \alpha}{d \delta} = \sqrt{\frac{C_f}{C}} \frac{4}{\pi}$$

Where;

$C_f \equiv$ Chord of the flap

$C \equiv$ Total wing chord

if $\frac{C_f}{C} = 0.3$

$\frac{d \alpha}{d \delta} = 0.697$ (Theoretical)

and

if $\frac{C_f}{C} = 0.5$

$\frac{d \alpha}{d \delta} = 0.9$ (Theoretical)

Experimental $d\alpha/d\delta$ have been found to be always smaller than the theoretical predictions. Realistic values are (Ref. 1):

30% $\frac{d \alpha}{d \delta} = 0.6$

$$50\% \qquad \frac{d\alpha}{d\delta} = 0.77$$

Combining and for 30% flap;

$$C_L = 2.20 \times 0.6 \sin \delta = 1.32 \sin \delta$$

Nonlinear Component of Lift Coefficient (a = 0)

$$C_L = 2.0 \left\{ \frac{C_f}{C} \left| \sin \delta \right| \sin \delta \cos \delta \right\}$$

Total C_L for 30% flap and $\alpha = 0$

$$C_L = \left[1.32 + 0.6 \left| \sin \delta \right| \cos \delta \right] \sin \delta$$

C_L is plotted as a function of δ in Figure C5-36. Assume that maximum $C_L = 0.7$ at which point stall occurs. At stall;

$\delta_{max} = 0.465$ radian for 30% flap and 0.355 radians for 50% flap.

Drag Coefficient

$$D = \frac{1}{2} \rho S C_D (\alpha, \delta) V^2$$

$$C_D = C_{DS} + C_{Di}$$

$C_{DS} \equiv$ Same as before

$$C_{Di} = 1.32 \sin \delta \sin \frac{\delta}{2} + 0.6 \sin^2 \delta \left| \sin \delta \right| \cos \delta$$

Figure C5-37 displays the lift and drag forces for maximum deflection of the 30 percent flap (0.465 radians). Vehicle speed is varied between 30 and 150 m/s. For our basline concept, in this context, we will assume the control surfaces to be wings with 30 percent flaps.

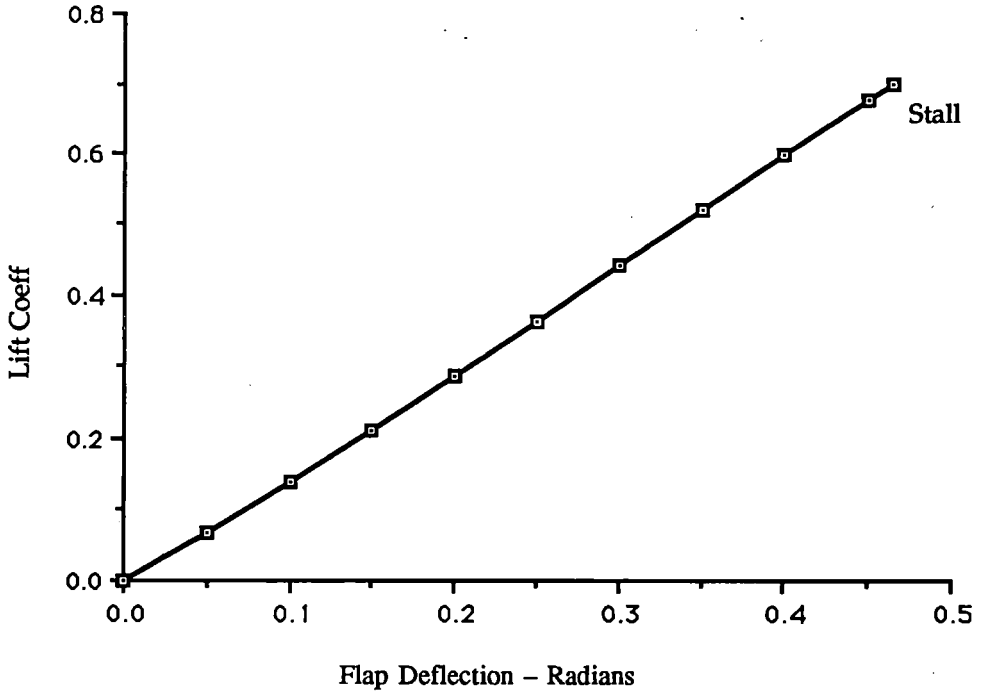

Figure C5-36 Lift coefficient vs. flap deflection

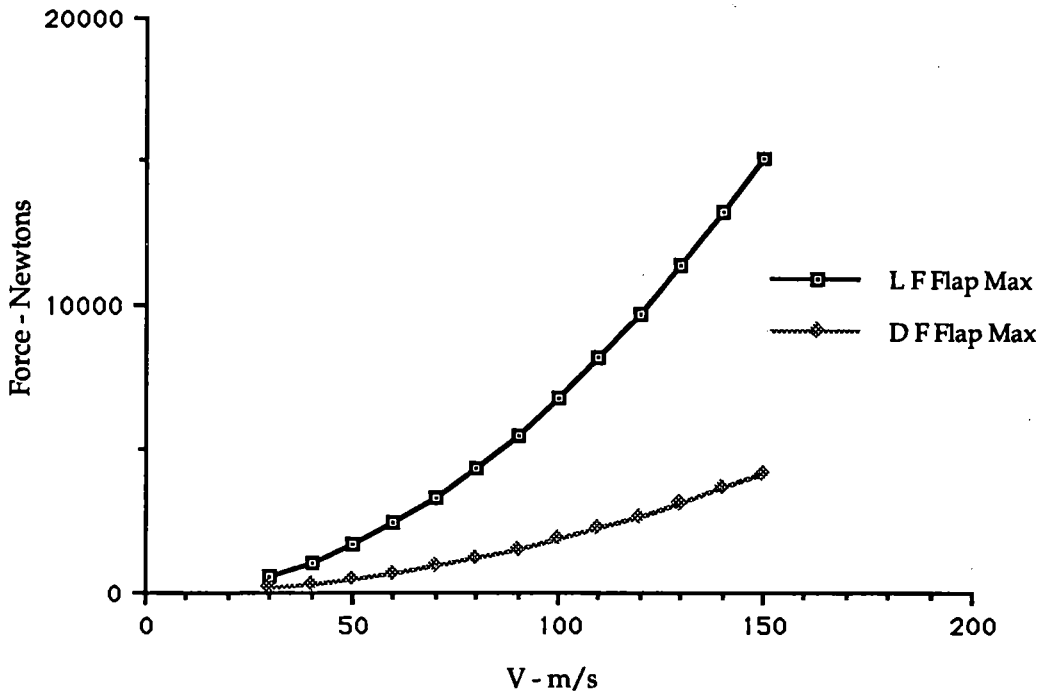

Figure C5-37 Lift force vs. speed

References

1. Hoerner, S. F. and H. V. Borst, Fluid-Dynamic Lift, 1975.

2. Hoerner, S. F., Fluid-Dynamic Drag, 1965.

6. Vehicle Dynamics

6. VEHICLE DYNAMICS

6.1 DRAPER FIVE-DEGREE-OF-FREEDOM MODEL

6.1.1 Model Development

6.1.1.1 Introduction and Outline

We modeled the vehicle supported by two bogies with an electrodynamic suspension (EDS) primary suspension, active secondary suspension, and aerodynamic control surfaces mounted on the vehicle and/or bogie. This chapter describes the general five degree-of-freedom model developed for maglev vehicles.

The chapter consists of 11 sections. The first 10 provide a description of the general model developed. The final section describes the extra assumptions and adaptations that were made in using this model to simulate the SCD baseline vehicle. The chapter begins with an overview of the model's assumptions and a description of the axis conventions. Detailed descriptions of the vehicle, suspension, and disturbance models are presented subsequently.

The vehicle-suspension model includes the following components:

- Passenger compartment (vehicle), including vehicle aerodynamic effects (wind, aerodynamic yaw-stability derivatives)
- Suspension bogies
- Secondary suspension elements, including actuators used for active suspension control
- Primary suspension elements (the magnetic suspension)
- Aerodynamic control surfaces (wings)

Sections 6.1.1.3 through 6.1.1.7 follow this outline, presenting models for each of these components.

Equations describing vehicle accelerations due to aerodynamic and secondary suspension forces are derived in Section 6.1.1.3. Included in this section is an aerodynamic model that includes aero-stability effects and forces on the vehicle caused by crosswinds. Section 6.1.1.4 presents the bogie model and equations for bogie acceleration due to forces from the primary and secondary suspension elements. Detailed equations for the forces due to the primary and secondary suspensions are described in Sections 6.1.1.5 and 6.1.1.6. Section 6.1.1.7 presents models of the aerodynamic control surfaces investigated.

The vehicle-suspension system modeled in Sections 6.1.1.2 through 6.1.1.7 is driven by two types of inputs:

- Controllable inputs due to the secondary suspension actuators and aerodynamic flaps
- Disturbance inputs due to the guideway position and wind velocity

Models for the guideway position and wind velocity disturbances are derived in Sections 6.1.1.8 and 6.1.1.9, respectively. In Section 6.1.1.10, these disturbance models are combined with the vehicle-suspension model – and, for the active secondary suspension, control laws for the secondary and aerodynamic flaps – to yield a complete model of the vehicle-suspension system and its disturbances. This model takes the form of a linear system driven by white noise and constant terms. This form is desirable because it permits the development of closed-form analytic solutions for the system outputs. The constant wind force and torque inputs are ignored for the analysis of the RMS values of the outputs. However, the constant forces are considered when determining the aerodynamic stability derivatives and yaw angle about which the vehicle's non-linear aerodynamic response will be linearized.

6.1.2.2 Overview of Assumptions and Definition of Axes

Assumptions

The vehicle-suspension system is modeled as a two-bogie vehicle with an EDS primary suspension (see Figure C6-1). Linear lumped elements are used to model the vehicle, bogies, and suspension elements. The model includes:

- Vehicle rotation and rotation rates in three dimensions
- Vehicle and bogie displacements and velocities perpendicular to the velocity vector
- Rotation of the bogies about the velocity vector (roll)

Thus, the vehicle has five degrees of freedom, while the bogies are each limited to three. The bogie yaw and pitch modes are omitted, since these modes can be made stable with a passive suspension system[1] and do not significantly impact the rigid vehicle's dynamics.

---

[1]Guenther, Christian R.; Leonides, Cornelius T., "Synthesis of a High-Speed Tracked Vehicle Suspension System - Part I: Problem Statement, Suspension Structure, and Decomposition" IEEE Transactions on Automatic Control, vol. AC-22, No. 2, April 1977.

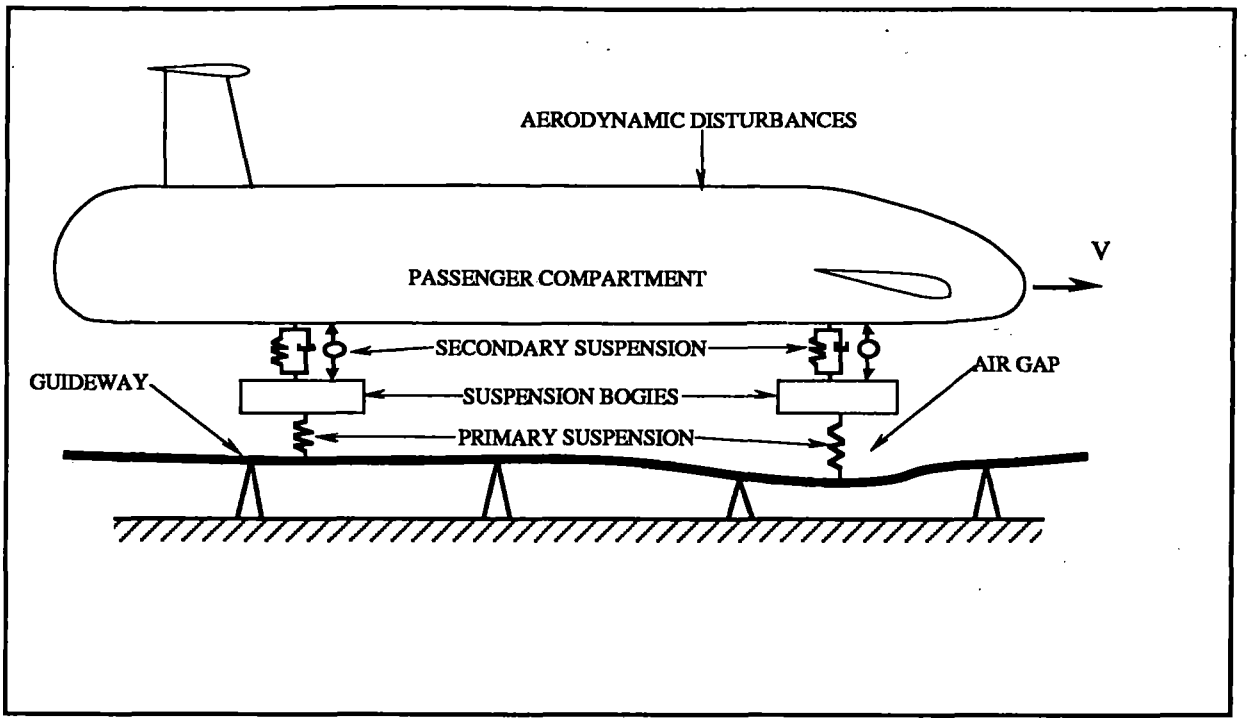

Figure C6-1 Overview of vehicle model with aero-surfaces - side view

We made the following assumptions in developing the model:

1. General

- The vehicle velocity changes slowly relative to the other dynamics of the system so that velocity can be modeled as constant
- There is no coupling between propulsion and levitation (no time-varying lift contributed by the propulsion system)
- Non-linear equations of motion are used to obtain a linear model, linearized appropriate operating points where necessary
- Although not inherent assumptions in the model, for this analysis, both the primary and secondary suspension stiffnesses are the same at the front and rear, and the center of gravity (cg) is located at the midpoint between the front and rear bogies
- When active control is implemented, full state feedback is assumed

2. Vehicle

- The vehicle (including passengers and baggage) is completely rigid
- The vehicle center of mass is in the vertical plane bisecting the vehicle
- Angular rotation rates of the vehicle are small (Coriolis accelerations or gyroscopic effects are ignored)

3. Bogie

- The bogies have "zero length" (no guideway filtering, no bogie pitch or yaw dynamics)
- The bogies (including cryogenic subsystems) are perfectly rigid
- Each bogie is axi-symmetric, with center of mass in the vertical plane bisecting the bogie
- The relative displacements of the bogies with respect to the vehicle are small

4. Primary suspension

- The primary suspension is an EDS, and has no damping
- Crosswind forces act only on the vehicle (no wind forces on bogies)

5. Hydraulic actuators

- The active secondary suspension forces are perfectly controllable without time delays

6. Aerodynamic actuators

- The flap angles are perfectly controllable without time delays

7. Guideway

- Guideway roughness is a random process with zero mean and stationary statistics (i.e., statistics do not vary with time or vehicle location)

8. Wind

- The time-varying component of the wind is a random process with zero mean and stationary statistics

Definition of Axes

Displacements and rotations of the vehicle and bogies are defined relative to a right-handed Cartesian reference frame (see Figure C6-2). The frame conventions are:

- X-axis parallel to the vehicle's instantaneous Earth-relative velocity vector, and positive in the forward direction
- Z-axis vertical, positive upwards
- Y-axis perpendicular to X and Z, completing the right-handed coordinate frame
- ϕ (roll) is rotation about the +X axis
- θ (pitch) is rotation about the +Y axis
- ψ (yaw) is rotation about the +Z axis

In all cases, vehicle and bogie displacements and rotations are measured from their no-load equilibrium positions.

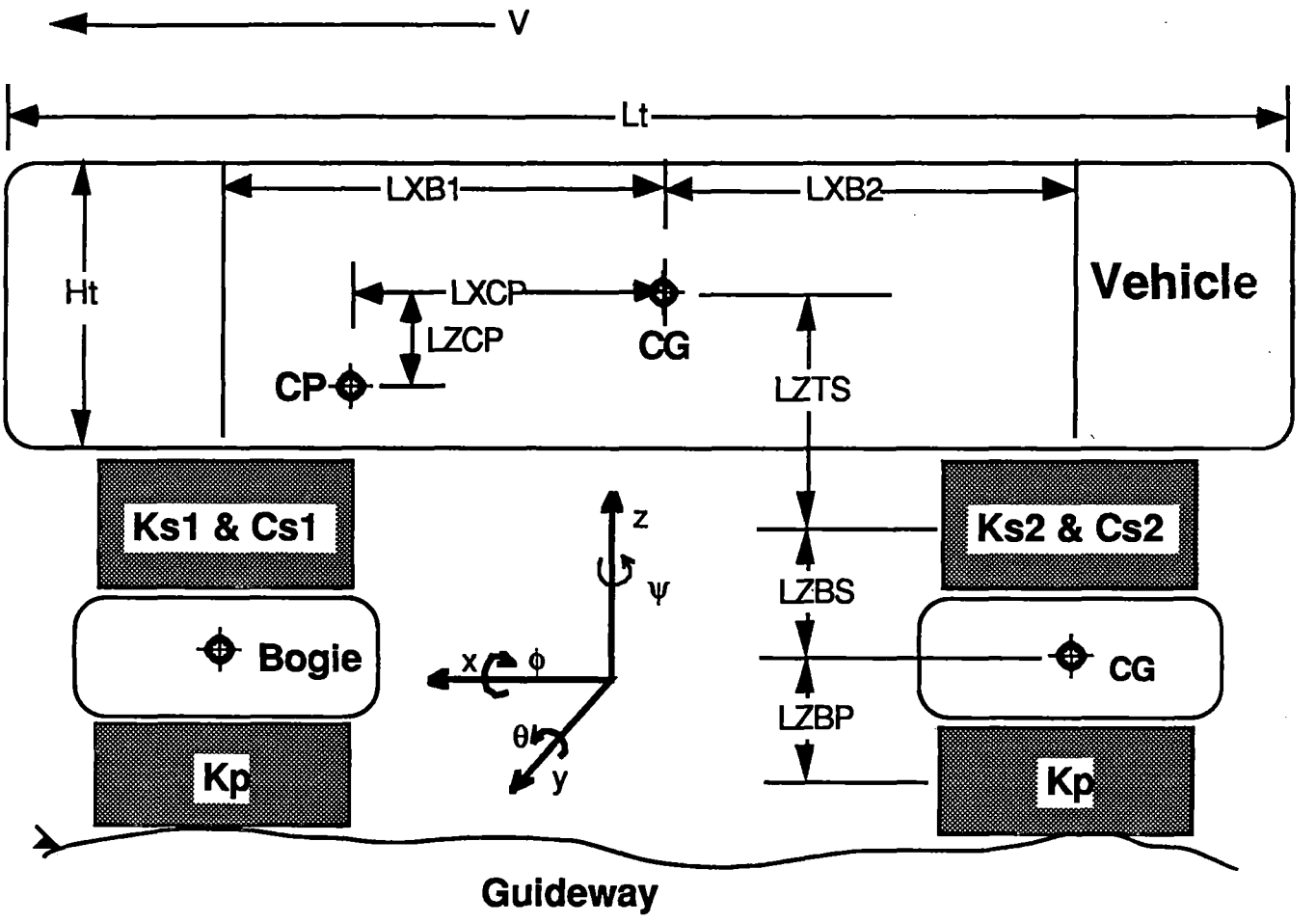

Figure C6-2 Side view of vehicle model

6.1.1.3 Vehicle

The vehicle is modeled as a rigid mass, with a center of mass in the vertical plane bisecting the vehicle (see Figure C6-3). The vehicle is allowed to rotate about any axis and translate in the Y and Z directions, but is assumed to move at a constant velocity in the positive X direction. The vehicle state is defined by a vector[2] of linear and angular vehicle displacements

$$\mathbf{x}_t = [y_t \quad z_t \quad \phi_t \quad \theta_t \quad \psi_t]^T \tag{C6.1}$$

and their derivatives $\dot{\mathbf{x}}_t$.

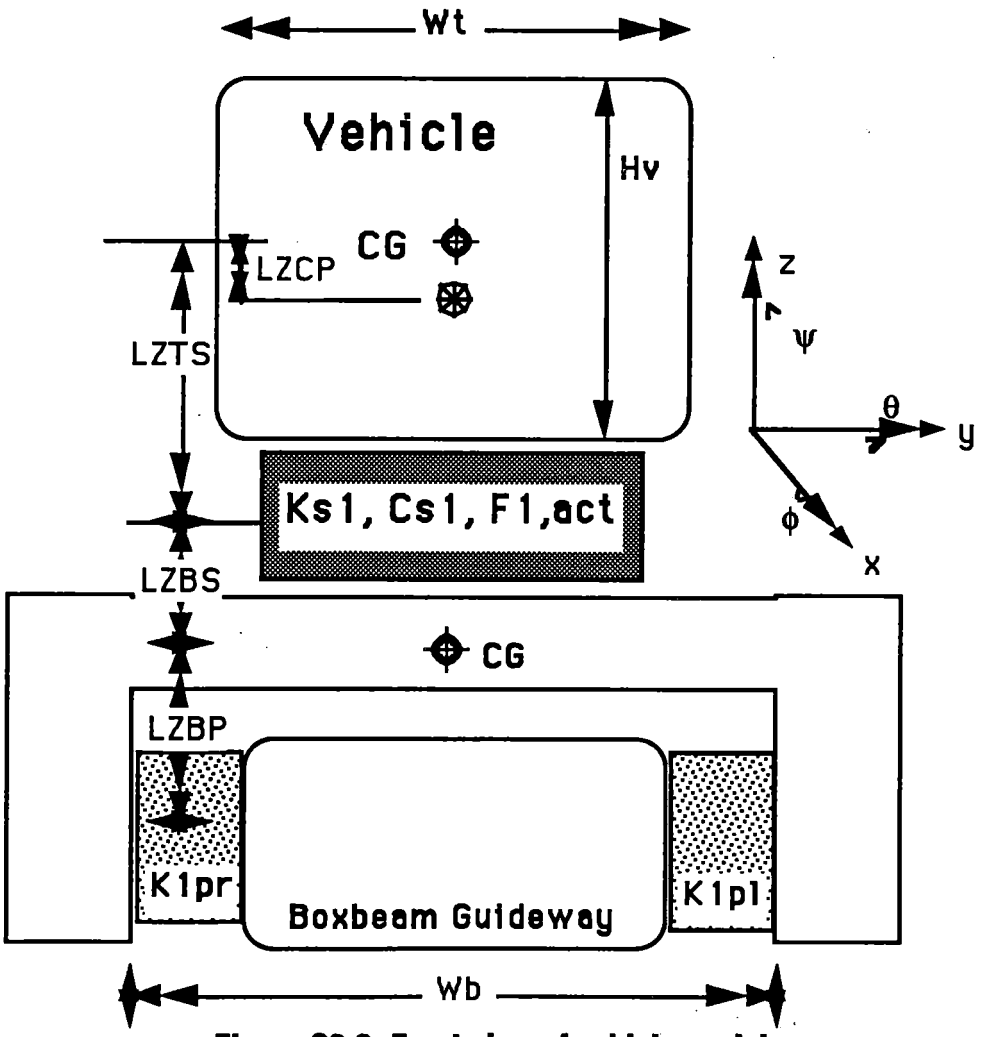

Figure C6-3 Front view of vehicle model

[2] Vectors will be identified by **bold** face print.

The vehicle is characterized in term of its length (L_t), width (W_t), height (H_t), cross-sectional area (A_t), mass (m_t), inertia matrix (I_{xx}, etc.) and aerodynamic force and torque coefficients (C_y, C_n). The vehicle parameter values used in our study are listed in Section 6.1.1.4.

Three sets of forces[3] act on the vehicle: forces due to the secondary suspension elements (both active and passive); forces due to wind and aerodynamic stability effects; and forces due to aerodynamic actuators. Thus, under the assumption of very small vehicle rotation rates, the vehicle accelerations are given by:

$$\ddot{\mathbf{x}}_t = \mathbf{I}_t^{-1} \cdot \left(\mathbf{T}_{s1\text{-}t}^{f} \cdot \mathbf{F}_{s1} + \mathbf{T}_{s2\text{-}t}^{f} \cdot \mathbf{F}_{s2} + \mathbf{T}_{aero\text{-}t}^{f} \cdot \mathbf{F}_{aero} + \mathbf{T}_{flap\text{-}t}^{f} \cdot \mathbf{F}_{flap} \right) \tag{C6.2}$$

$$\mathbf{I}_t^{-1} = \begin{bmatrix} 1/m_t & 0 & 0 \\ 0 & 1/m_t & 0 \\ 0 & 0 & \begin{bmatrix} I_{xx} & I_{xy} & I_{xz} \\ I_{yx} & I_{yy} & I_{yz} \\ I_{zx} & I_{zy} & I_{zz} \end{bmatrix}^{-1} \end{bmatrix} \tag{C6.3}$$

where

m_t = mass of vehicle
I_{xy}, etc. = moments of inertia for vehicle (defined about the vehicle cg)
F_{s1} = force across the front secondary suspension
F_{s2} = force across the rear secondary suspension
F_{aero} = force on the vehicle due to wind and aero-stability effects
F_{flap} = force on the vehicle due to aerodynamic flaps

---

[3] Throughout this chapter, "forces" refers to a vector of both forces and torques.

$T^f_{s1\text{-}t}$ = transformation from forces at front secondary suspension to forces at the vehicle cg

$T^f_{s2\text{-}t}$ = transformation from forces at rear secondary suspension to forces at the vehicle cg

$T^f_{aero\text{-}t}$ = transformation from forces at the aerodynamic center of pressure at the vehicle cg

$T^f_{flap\text{-}t}$ = transformation from forces at the aerodynamic flaps to forces at the vehicle cg

The transformation matrices (T) are included to transform forces and torques from their points of application to forces and torques acting at the vehicle center of mass[4] .

Accelerations Due to Secondary Suspension Forces

Forces across each of the two secondary suspensions are given by a roll torque and vertical and lateral forces:

$$\mathbf{F}_{si} = \left[F_y \quad F_z \quad T_\phi\right]_{si}^{T} \quad (i=1,2) \tag{C6.4}$$

These forces act at points LXB1 and LXB2 fore and aft, and LZTS below, the vehicle center of mass, as shown in Figure C6-1. Thus, the transformation from forces at the front secondary suspension to the vehicle's cg is given by:

$$T^f_{s1-t} = \begin{bmatrix} 1 & 0 & 0 \\ 0 & 1 & 0 \\ LZTS & 0 & 1 \\ 0 & -LXB1 & 0 \\ LXB1 & 0 & 0 \end{bmatrix} \tag{C6.5}$$

so that

---

[4] We use transformation matrices so that the model can describe forces and torques acting at arbitrary points on the vehicle and bogie. This approach allows the model to be modified quickly to reflect changes in vehicle configuration (vehicle dimensions, bogie locations, etc.).

$$\begin{bmatrix} F_y \\ F_z \\ T_\phi \\ T_\theta \\ T_\psi \end{bmatrix}_{\text{train c.g.}} = \mathbf{T}^{f}_{s1-t} \begin{bmatrix} F_y \\ F_z \\ T_\phi \end{bmatrix}_{s1} \tag{C6.6}$$

The transformation matrix $\mathbf{T}^{f}_{s2-t}$ is similar.

Wind and Aerodynamic Stability Effects

Crosswind forces on the vehicle are modeled as a side force[5] acting in the +Y direction (perpendicular to velocity) at the center of pressure, denoted cp (see Figure C6-4). Since the center of pressure is LXCP ahead of, and LZCP above, the vehicle's cg, the transformation from force at this point to force at the vehicle cg is:

$$\mathbf{T}^{f}_{aero-t} = \begin{bmatrix} 1 \\ 0 \\ -LZCP \\ 0 \\ LXCP \end{bmatrix} \tag{C6.7}$$

$$\begin{bmatrix} F_y \\ F_z \\ T_\phi \\ T_\theta \\ T_\psi \end{bmatrix}_{\text{train c.g.}} = \mathbf{T}^{f}_{aero-t} \left[F_y\right]_{aero} \tag{C6.8}$$

---

[5] Since drag acts parallel to the train's velocity, it can be excluded from our model. Lift forces are assumed small.

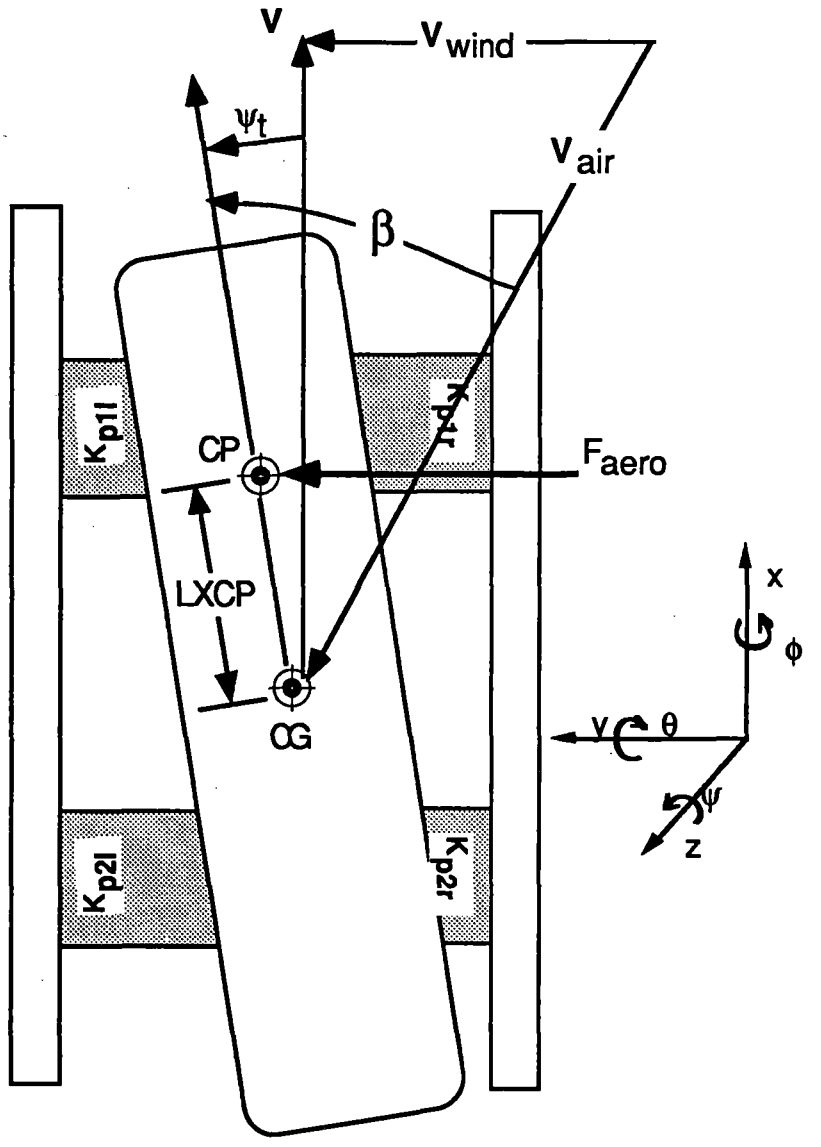

Figure C6-4. - Top view of vehicle model

The aerodynamic side force is dependent on the wind and vehicle velocities, vehicle cross-sectional area, and aerodynamic side force coefficient:

$$[F_y]_{aero} = \frac{1}{2}\rho\, |V_{air}|^2 A_t\ C_y(\beta) \qquad \text{(C6.9)}$$

where

ρ = density of air
$|V_{air}|$ = magnitude of air-relative vehicle velocity
A_t = cross-sectional area of the vehicle
$C_y(\beta)$ = coefficient of side force

The air-relative vehicle velocity is a vector sum of the vehicle's earth-relative velocity and the applied wind. For our work, we model all winds as perpendicular to the vehicle's velocity, so:

$$|V_{air}|^2 = |V|^2 + |V_{wind}|^2 \qquad \text{(C6.10)}$$

The aerodynamic coefficient, $C_y(\beta)$, is non-linearly dependent on the sideslip angle, β:

$$\beta = \psi_t + \arctan\left(\frac{|V_{wind}|}{|V|}\right) \qquad \text{(C6.11)}$$

For this research, $C_y(\beta)$ is described by a curve fit to data generated as described in Section 5.1.1:

$$C_y(\beta) = C_{y0} + C_{y1}\,\beta + C_{y2}\,\beta^2 + C_{y3}\,\beta^3 \qquad \text{(C6.12)}$$

It is desirable to form a single linear state space representation describing the dynamics of the system. To do this, a linear model of the wind force is required. A state space description of this wind model may then be appended to the state space description of the vehicle's dynamics.

We begin by noting that the wind model consists of two parts, a steady (DC) term and a random, time-varying component:

$$V_{wind} = \overline{V}_{wind} + V_{wind}(t) \qquad \text{(C6.13)}$$

Similarly, the vehicle yaw angle will have two parts:

$$\psi_t = \overline{\psi}_t + \psi_t(t) \tag{C6.14}$$

Thus, the sideslip angle consists of two components:

$$\beta = \beta_0 + \delta\beta(t) \tag{C6.15}$$

We apply a first-order approximation to obtain a linear equation for $C_y(\beta)$:

$$C_y(\beta) \approx C_y(\beta_0) + \left(\frac{dC_y}{d\beta}\right)_{\beta_0} \delta\beta(t) \tag{C6.16}$$

$$\left(\frac{dC_y}{d\beta}\right)_{\beta_0} = C_{y1} + 2C_{y2} \cdot \beta_0 + 3C_{y3} \cdot \beta_0{}^2$$

Note that $C_{y\beta}$ is calculated based on β_0.

We continue the linearization by assuming that the $V_{wind}(t)$ is small relative to the vehicle's Earth-relative velocity. This assumption yields a small angle approximation for sideslip as:

$$\delta\beta(t) \approx \psi_t(t) + \frac{|V_{wind}(t)|}{|V|} \tag{C6.17}$$

and an approximation for the air-relative vehicle velocity

$$|V_{air}|^2 \approx |V|^2 \tag{C6.18}$$

Combining the equations above yields the desired linear approximation for aerodynamic side-force:

$$\left[F_y\right]_{aero} \approx \frac{1}{2}\rho\,|V|A_t\left(C_y(\beta_0)+\left(\frac{dC_y}{d\beta}\right)_{\beta_0}\left(V\psi_t(t)+V_{wind}(t)\right)\right) \qquad \text{(C6.19)}$$

We rewrite this equation in terms of the vehicle state vector as:

$$\left[F_y\right]_{aero} \approx \frac{1}{2}\rho\,|V|A_t\left(C_y(\beta_0)+\left(\frac{dC_y}{d\beta}\right)_{\beta_0}\left(V\mathbf{T}^{x}_{t-\psi_t}\mathbf{x}_t+V_{wind}(t)\right)\right) \qquad \text{(C6.20)}$$

The location of the center of pressure, denoted by LZCP (distance from cg in the +Z direction) and LXCP (distance in the +X direction) must now be determined. Here we assume LZCP to be such that the cp 0.24 meters below a point midway between the top and bottom of the vehicle (the assumed value of LZCP is listed in Section 6.1.4). LXCP is calculating by noting that:

$$\left[T_\psi\right]_{aero} = \left[F_y\right]_{aero} LXCP \qquad \text{(C6.21)}$$

$\left[T_\psi\right]_{aero}$ is also given by[6] :

$$\left[T_\psi\right]_{aero} = \frac{1}{2}\rho\,|V_{air}|^2 A_t\;L_t\;C_n(\beta) \qquad \text{(C6.22)}$$

$$C_n(\beta) = C_{n0} + C_{n1}\,\beta + C_{n2}\,\beta^2 + C_{n3}\,\beta^3 \qquad \text{(C6.23)}$$

Algebraic manipulation yields:

$$LXCP = L_t\frac{C_n(\beta)}{C_y(\beta)} \qquad \text{(C6.24)}$$

---

[6] Again determined from a curve fit to data [C5.b.1].

Since C_{n0} and C_{y0} are zero for a symmetric vehicle, equation EQN can be reduced to:

$$LXCP = L_t \frac{C_{n1} + C_{n2} \cdot \beta + C_{n3} \cdot \beta^2}{C_{y1} + C_{y2} \cdot \beta + C_{y3} \cdot \beta^2} \tag{C6.25}$$

which is non-singular for zero sideslip. To linearize the model, we calculate LXCP assuming:

$$\beta = \beta_0 \tag{C6.26}$$

Accelerations Due to Vehicle-Mounted Aerodynamic Actuators

Aerodynamic actuators can be mounted in many places on the vehicle. We describe the location of each actuator relative to the vehicle cg via the parameters:

$$[LXFi \quad LYFi \quad LZFi]^T$$

Note that these parameters may be positive or negative.

A force is exerted on each aero-surface at its center of pressure; by definition there is no torque exerted on the control surface at this point. The force due to a flap on the vehicle is described by the vector:

$$\mathbf{F}_{flapi} = \begin{bmatrix} F_y \\ F_z \end{bmatrix}_{flapi}$$

The transformation of a flap's forces to forces and torques at the vehicle cg is given by:

$$\mathbf{T}^f_{flapi-t} = \begin{bmatrix} 1 & 0 \\ 0 & 1 \\ -LZFi & -LYFi \\ 0 & -LXFi \\ LXFi & 0 \end{bmatrix} \tag{C6.27}$$

$$\begin{bmatrix} F_y \\ F_z \\ T_\phi \\ T_\theta \\ T_\psi \end{bmatrix}_{\text{train c.g.}} = T^f_{\text{flap}i-t} F_{\text{flap}i} \qquad \text{(C6.28)}$$

6.1.1.4 Suspension Bogies

Both suspension bogies in our two-bogie vehicle are assumed to be identical. Each is modeled as a rigid mass, with center of mass in the vertical plane bisecting the bogie (see Figure C6.2). Bogies are assumed to translate in the Y and Z directions and roll about the X axis – however, rotations about the Y axis (pitch) and Z axis (yaw) are neglected. Each bogie's state is defined by a vector of its positions

$$x_{bi} = \begin{bmatrix} y_{bi} & z_{bi} & \phi_{bi} \end{bmatrix}^T \qquad \text{(C6.29)}$$

and their derivatives $\dot{x}_{bi}$.

The bogies are characterized by their width (W_b), mass (m_b), and roll moment of inertia (I_{xx}). The bogie parameter values used in our study are listed in Section 6.1.4.

The secondary suspension, primary suspension, and aerodynamic actuators act on each bogie (we assume that wind forces do not affect the bogie). Thus, under the assumption of small rotation rates, the bogie accelerations are given by:

$$\ddot{x}_{bi} = I_b^{-1} \cdot \left(T^f_{si\text{-}bi} \cdot F_{si} + T^f_{pil\text{-}bi} \cdot F_{pil} + T^f_{pir\text{-}bi} \cdot F_{pir} + T^f_{gef\text{-}bi} \cdot F_{gef} \right) \qquad \text{(C6.30)}$$

$$\mathbf{I}_b^{-1} = \begin{bmatrix} 1/m_b & 0 & 0 \\ 0 & 1/m_b & 0 \\ 0 & 0 & I_{xx}^{-1} \end{bmatrix} \qquad \text{(C6.31)}$$

where

$\mathbf{I}_{xx}$ = roll moment of inertia for bogie (defined about bogie cg)

$\mathbf{F}_{pi\,l}$ = force across the left side of the primary suspension (at bogie *i*)

$\mathbf{F}_{pi\,r}$ = force across the right side primary suspension (at bogie *i*)

$\mathbf{F}_{si}$ = force across the secondary suspension (at bogie *i*)

$\mathbf{F}_{gef}$ = force due to ground-effect flaps mounted on the bogie

$\mathbf{T}^f_{pil\text{-}bi}$ = transformation from forces at left side of *i*-th primary suspension to bogie cg

$\mathbf{T}^f_{pir\text{-}bi}$ = transformation from forces at right side of *i*-th primary suspension to bogie cg

$\mathbf{T}^f_{si\text{-}bi}$ = transformation from forces at *i*-th secondary suspension to forces at bogie cg

$\mathbf{T}^f_{gef-bi}$ = transformation from forces at ground effect flaps to forces at bogie cg

Accelerations Due to Secondary Suspension Forces

The secondary suspension force acts on the bogie at a point LZBS above the bogie center of mass, as shown in Figure C6-2. Thus, for each bogie, the transformation from forces and torques at the secondary suspension to the bogie's cg is given by:

$$\mathbf{T}^f_{si-bi} = \begin{bmatrix} -1 & 0 & 0 \\ 0 & -1 & 0 \\ \text{LZBS} & 0 & -1 \end{bmatrix} \qquad \text{(C6.32)}$$

so that

$$\begin{bmatrix} F_y \\ F_z \\ T_\phi \end{bmatrix}_{\text{bogie}-i\ \text{c.g.}} = \mathbf{T}^f_{si-bi} \begin{bmatrix} F_y \\ F_z \\ T_\phi \end{bmatrix}_{si} \qquad \text{(C6.33)}$$

Accelerations due to primary suspension forces

Forces at each of the four corners of the primary suspension are given by vertical and lateral forces. There is no roll stiffness of the primary suspension at each corner as it is defined, so any torques about each bogie's cg are due to the fact that the vertical and lateral forces do not act at the cg. These torques naturally arise from the application of transformation matrices described below. Nevertheless, the forces at each corner of the primary suspension can be described by:

$$\mathbf{F}_{pij} = \left[F_y \quad F_z \quad T_\phi \right]_{pij}^{T} \quad (j = l, r) \tag{C6.34}$$

These forces act at points LZBP below, and $\frac{W_b}{2}$ to the left or right of, the bogie center of mass (see Figure C6-2). The transformations from forces and torques at these points to forces and torques about the bogie's cg are given by:

$$\mathbf{T}^{f}_{pil-bi} = \begin{bmatrix} 1 & 0 & 0 \\ 0 & 1 & 0 \\ LZBP & \frac{W_b}{2} & 1 \end{bmatrix} \tag{C6.35}$$

$$\mathbf{T}^{f}_{pir-bi} = \begin{bmatrix} -1 & 0 & 0 \\ 0 & 1 & 0 \\ -LZBP & -\frac{W_b}{2} & 1 \end{bmatrix} \tag{C6.36}$$

6.1.1.5 Secondary Suspension

Each secondary suspension (front and rear) is modeled as an element that exerts equal and opposite forces on the vehicle and bogie (see Figure C6-5). These forces can be dependent on displacements, velocites, or a combination of the states, and so can represent springs, dampers, and active elements. The location of these "elements," as described in Sections 6.1.1.3 and 6.1.1.4, are shown in Figures C6-2 and C6-3. The forces across each secondary suspension are a combination of the forces due to its active and passive elements:

$$\mathbf{F}_{si} = \mathbf{F}_{si,act} + \mathbf{F}_{si,pass} \tag{C6.37}$$

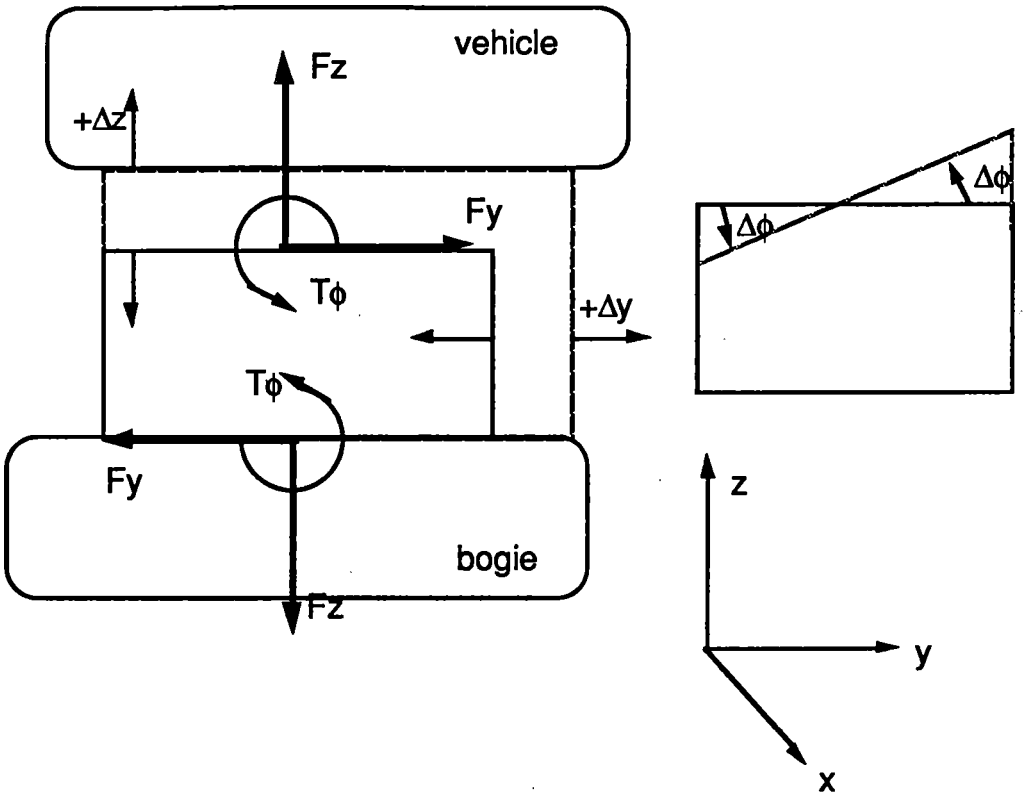

Figure C6-5 Secondary suspension model

In this report, actuator dynamics are ignored so that $\mathbf{F}_{act}$ is a perfectly controllable input (control laws are discussed in Chapter CC). Passive forces are given by a combination of linear stiffness and linear damping:

$$\mathbf{F}_{si,pass} = \mathbf{K}_{si} \cdot \Delta \mathbf{x}_{si} + \mathbf{C}_{si} \cdot \Delta \dot{\mathbf{x}}_{si} \qquad \text{(C6.38)}$$

where

$$\mathbf{K}_{si} = \frac{\delta \mathbf{F}_{si}}{\delta \Delta \mathbf{x}_{si}} \text{ (negative for a stable spring)} \qquad \text{(C6.39)}$$

$$\mathbf{C}_{si} = \frac{\delta \mathbf{F}_{si}}{\delta \Delta \dot{\mathbf{x}}_{si}} \text{ (negative for a stable damper)} \qquad \text{(C6.40)}$$

and Δx_{si} is the deflection across the secondary suspension element (positive when the deflection of the secondary increases):

$$\Delta \mathbf{x}_{si} = \begin{bmatrix} \Delta y \\ \Delta z \\ \Delta \phi \end{bmatrix}_{si} \tag{C6.41}$$

Δx_{si}, in terms of displacements of the vehicle and bogie states is:

$$\begin{bmatrix} \Delta y \\ \Delta z \\ \Delta \phi \end{bmatrix}_{s1} = \begin{bmatrix} -y_{b1} + LZBS \cdot \phi_{b1} + y_t + LZTS \cdot \phi_t + LXB1 \cdot \psi_t \\ -z_{b1} + z_t - LXB1 \cdot \theta_t \\ -\phi_{b1} + \phi_t \end{bmatrix} \tag{C6.42}$$

$$\begin{bmatrix} \Delta y \\ \Delta z \\ \Delta \phi \end{bmatrix}_{s2} = \begin{bmatrix} -y_{b2} + LZBS \cdot \phi_{b2} + y_t + LZTS \cdot \phi_t - LXB2 \cdot \psi_t \\ -z_{b2} + z_t + LXB2 \cdot \theta_t \\ -\phi_{b2} + \phi_t \end{bmatrix} \tag{C6.43}$$

which can be written using transformation matrices:

$$\Delta \mathbf{x}_{si} = \mathbf{T}^{x}_{t-si}\, \mathbf{x}_t + \mathbf{T}^{x}_{bi-si}\, \mathbf{x}_{bi} \tag{C6.44}$$

Similarly,

$$\Delta \dot{\mathbf{x}}_{si} = \mathbf{T}^{x}_{t-si}\, \dot{\mathbf{x}}_t + \mathbf{T}^{x}_{bi-si}\, \dot{\mathbf{x}}_{bi} \tag{C6.45}$$

Combining the equations above yields an equation for secondary suspension force in terms of system states and control inputs:

$$\mathbf{F}_{si} = \mathbf{F}_{si,act} + \mathbf{K}_{si}\left(\mathbf{T}^{x}_{t-si}\, \mathbf{x}_t + \mathbf{T}^{x}_{bi-si}\, \mathbf{x}_{bi}\right) + \mathbf{C}_{si}\left(\mathbf{T}^{x}_{t-si}\, \dot{\mathbf{x}}_t + \mathbf{T}^{x}_{bi-si}\, \dot{\mathbf{x}}_{bi}\right) \tag{C6.46}$$

In this report, we assume that the secondary suspension stiffness ($\mathbf{K}_s$) and damping ($\mathbf{C}_s$) are free design parameters. Generally, we chose diagonal stiffness and damping matrices, thereby implying that we are defining these values at the roll center of the suspension (note that transformations yield off-diagonal terms). The non-zero terms in the stiffness matrix describing the stiffness in the vertical and lateral directions are determined by specifying a natural frequency:

$$\omega_n = \sqrt{\frac{2k_{si}}{m_t}} \tag{C6.47}$$

or

$$\omega_n = \sqrt{\frac{2k_{si}}{I_t}} \tag{C6.48}$$

Terms on the diagonal of the damping matrix are determined by specifying a damping ratio:

$$\xi = b_{si}\sqrt{\frac{1}{2k_{si}m_t}} \tag{C6.49}$$

or

$$\xi = b_{si}\sqrt{\frac{1}{2k_{si}I_t}} \tag{C6.50}$$

These frequencies and damping ratios are for mode shapes of pure vehicle translation above fixed bogies. While these modes are not necessarily actual modes of the system, they are easy to visualize and therefore useful for communicating suspension parameter values. The roll stiffness and roll damping were determined by the particular vehicle geometry, with a provision for fine-tuning these parameters via the addition of extra stiffness and damping. This extra stiffness and damping would be provided in practice by additional suspension elements (such as a swaybar on an automobile).

6.6. PRIMARY SUSPENSIONS

We assumed an EDS primary suspension. Because damping is very low in these types of suspension, the primary was modeled as linear stiffnesses without damping.

We considered a box-beam type guideway configuration, where the bogie is suspended over a box-beam element as shown in Figure C6-3. In this configuration, the primary suspension at each of the two bogies is considered to consist of two box-shaped elements (left and right). Each element exerts equal forces at opposing sides in response to deflections across the element (see Figure C6-6). For our analysis, we assumed that the stiffness is the same in all the elements. These box-shaped elements are a representation of the primary suspension stiffness at each of the four corners of the vehicle. Thus, this is how the primary suspension was modelled, as mentioned in Section 6.1.1.4 *(Accelerations due to primary suspension forces).*

The forces across a side of a primary suspension are given by the equation

$$\mathbf{F}_{pil} = \mathbf{K}_p \cdot \Delta \mathbf{x}_{pi,l} \qquad \text{(C6.51)}$$

$$\mathbf{F}_{pir} = \mathbf{K}_p \cdot \Delta \mathbf{x}_{pi,r} \qquad \text{(C6.52)}$$

where

$$\mathbf{K}_p = \frac{\delta \mathbf{F}_{pi(l,r)}}{\delta \Delta \mathbf{x}_{pi(l,r)}} \text{ (negative for a stable spring)} \qquad \text{(C6.53)}$$

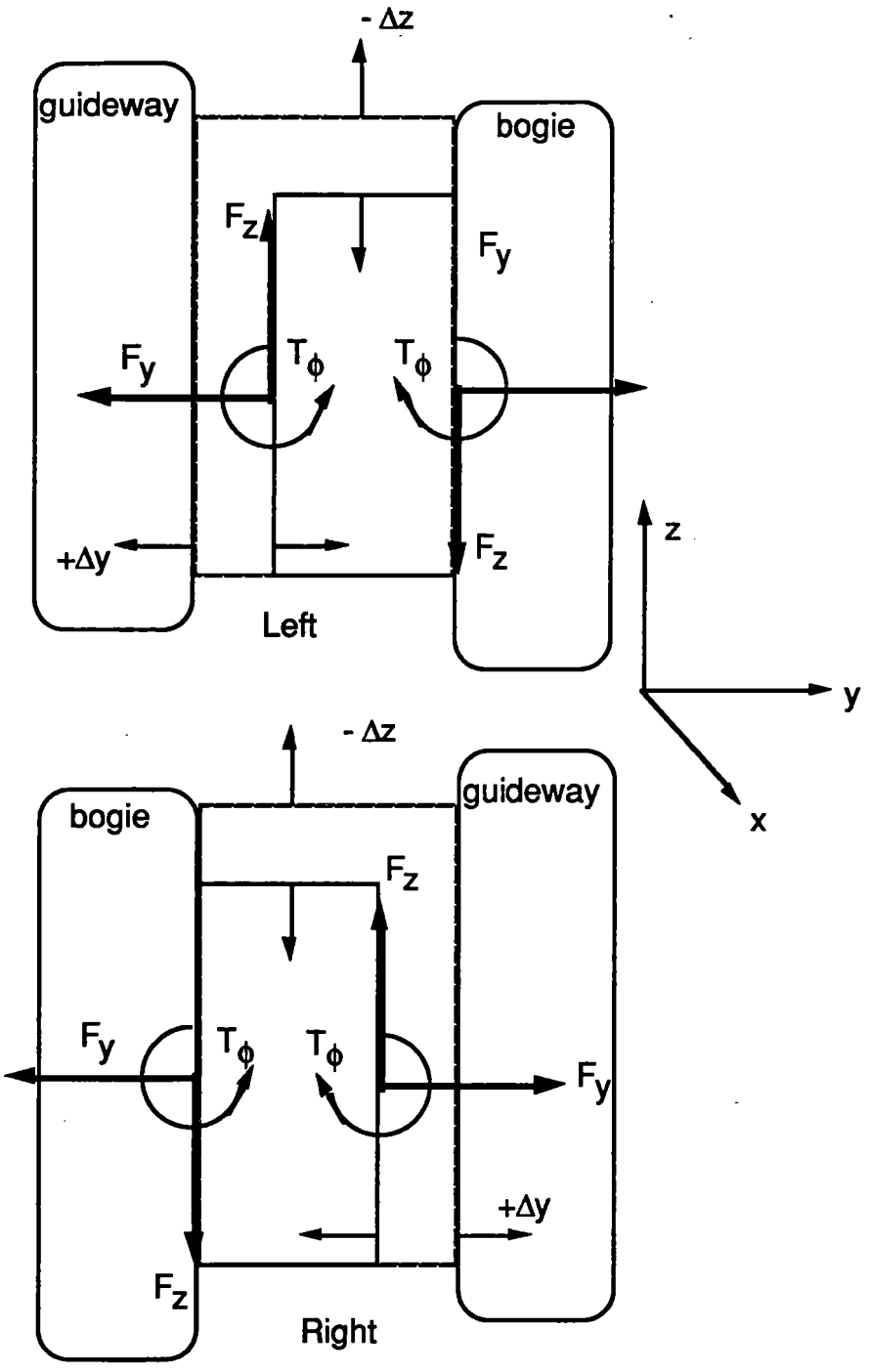

Figure C6-6 Primary suspension model

and $D\mathbf{x}_{pi(l,r)}$ are the deflections across the primary suspension elements:

$$\Delta \mathbf{x}_{pi(l,r)} = \begin{bmatrix} \Delta y \\ \Delta z \\ \Delta \phi \end{bmatrix}_{pi(l,r)} \tag{C6.54}$$

The primary suspension deflections can be written in terms of guideway position and the displacement of the bogie center of mass:

$$\Delta \mathbf{x}_{pil} = \begin{bmatrix} y_{bi} + \phi_{bi} LZBP - y_{gi} \\ z_{bi} - z_{gi} + \dfrac{W_b}{2}\left(\phi_{bi} - \phi_{gi}\right) \\ \phi_{bi} - \phi_{gi} \end{bmatrix} \tag{C6.55}$$

$$\Delta \mathbf{x}_{pir} = \begin{bmatrix} -y_{bi} - \phi_{bi} LZBP + y_{gi} \\ z_{bi} - z_{gi} - \dfrac{W_b}{2}\left(\phi_{bi} - \phi_{gi}\right) \\ -\phi_{bi} + \phi_{gi} \end{bmatrix} \tag{C6.56}$$

Using transformation matrices, the primary deflections can be written as:

$$\Delta \mathbf{x}_{p1l} = \mathbf{T}^{x}_{b1-p1l}\,\mathbf{x}_{b1} + \mathbf{T}^{x}_{g1-p1l}\,\mathbf{x}_{g1} \tag{C6.57}$$

$$\Delta \mathbf{x}_{p1r} = \mathbf{T}^{x}_{b1-p1r}\,\mathbf{x}_{b1} + \mathbf{T}^{x}_{g1-p1r}\,\mathbf{x}_{g1} \tag{C6.58}$$

$$\Delta \mathbf{x}_{p2l} = \mathbf{T}^{x}_{b2-p2l}\,\mathbf{x}_{b2} + \mathbf{T}^{x}_{g2-p2l}\,\mathbf{x}_{g2} \tag{C6.59}$$

$$\Delta \mathbf{x}_{p2r} = \mathbf{T}^{x}_{b2-p2r}\,\mathbf{x}_{b2} + \mathbf{T}^{x}_{g2-p2r}\,\mathbf{x}_{g2} \tag{C6.60}$$

where

x_{g1} = the guideway position at the front bogie

x_{g2} = the guideway position at the rear bogie

The guideway position at each bogie[7] is specified by a vector:

$$\mathbf{x}_{gi} = \begin{bmatrix} y \\ z \\ \phi \end{bmatrix}_{gi} \tag{C6.61}$$

Combining the above equations yields an equation for the force due to a primary suspension element in terms of system states:

$$\mathbf{F}_{pi(l,r)} = \mathbf{K}_p \left(\mathbf{T}^{x}_{bi-pi(l,r)} \mathbf{x}_{bi} + \mathbf{T}^{x}_{gi-pi(l,r)} \mathbf{x}_{gi} \right) \tag{C6.62}$$

In an EDS system, the primary stiffness is dependent on vehicle speed (in addition to the suspension design). We input stiffness terms into the model using stiffness vs. speed data from the MIT Plasma Fusion Center and linear extrapolation.

6.1.1.7 Aerodynamic Actuators

Vehicle-mounted actuators operate in "free-stream," and are modeled as simple flaps with one degree of freedom. The lift and induced drag for a flap in free-stream are given by:

$$F_{L_{flap}} = \frac{1}{2} \rho \, |V_{air}|^2 A_{flap} C_L(\alpha) \tag{C6.63}$$

$$F_{D_{flap}} = \frac{1}{2} \rho \, |V_{air}|^2 A_{flap} C_D(\alpha) \sin(\alpha) \tag{C6.64}$$

---

[7] Although the guideway position is not constant along the length of the bogie, we model the bogie as having zero-length. Thus, we ignore "finite length filtering" effects which tend to smooth high frequency (closely spaced) guideway variations. Disregarding these effects makes our analysis slightly conservative. However, this conservatism is somewhat negated by our assumption of a two-bogie vehicle, as a vehicle with many bogies will have a smoother ride than one with two bogies.

where

a = flap angle of attack

C_y (b) = coefficient of lift

In modeling the vehicle dynamics, we considered only the lift component of the flap forces. The induced drag of the flaps is calculated to determine the drawbacks of aerodynamic control, but its effects on vehicle accelerations are not considered[8].

The lift coefficient was obtained from the curve shown in Figure C6-7. An explanation of the aerodynamic surfaces can be found in Section C5 of this report.

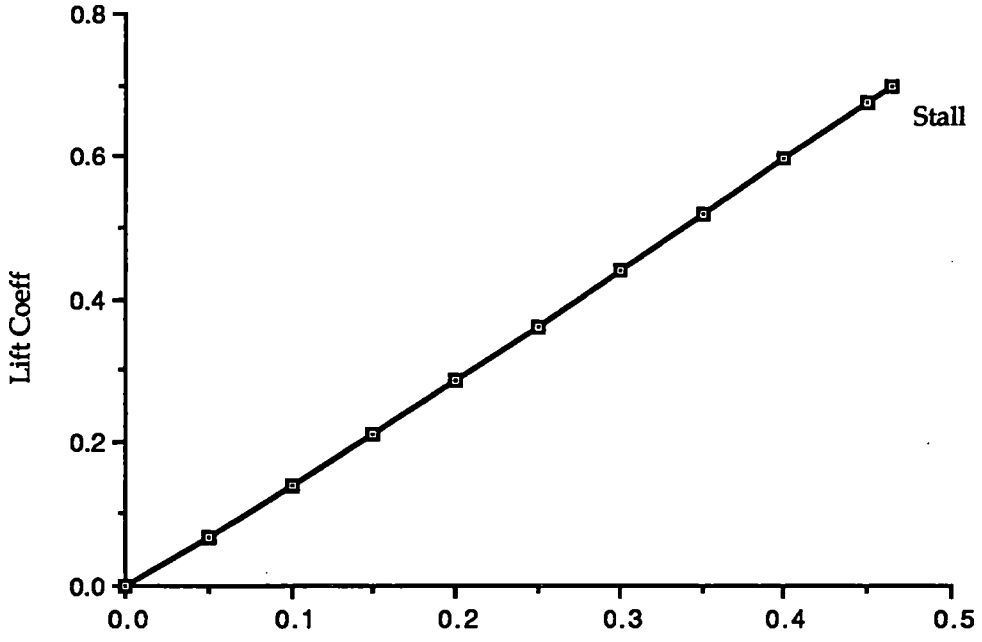

Figure C6-7 Flap deflection – radius

Since this curve is nearly linear for small alpha's, a linear equation for $C_L(a)$ results:

$$C_L(\alpha) \approx C_{L\alpha}\,\alpha \qquad \text{(C6.65)}$$

[8] Since induced drag acts parallel to the velocity vector, drag forces act in a direction not included in our model. Induced drag also creates torques when the drag force is transformed to the train c.g.; but these torques are small compared to other torques on the vehicle. Also, the drag is in the same direction, regardless of the sign of the deflection of the aero-surface's angle. Therefore this effect cannot be included in a linear model.

where

$$C_{L\alpha} = \frac{\partial C_L}{\partial \alpha}(\alpha)\Big|_{\alpha_0} \qquad \text{(C6.66)}$$

As in Section 6.1.1.3 *(Wind and aerodynamic stability effects)*, we approximate $|V_{air}|$ as equal to the vehicle's velocity. In addition, we ignore the effects of wind and vehicle rotation and, using a small angle approximation for α, model the lift force (normal to the wing) as perpendicular to the velocity vector. Thus, the final equation for the magnitude of the flap force is:

$$|\mathbf{F}_{flapi}| = \frac{1}{2}\rho\, |V|^2 A_{flap}\, C_{L\alpha}\, \alpha_{flapi} \qquad \text{(C6.67)}$$

The direction of this force depends on the mounting point and orientation of the flap, so that

$$\mathbf{F}_{flapi} = \begin{bmatrix} F_y \\ F_z \end{bmatrix}_{flapi} = \mathbf{T}\,|\mathbf{F}_{flapi}| \qquad \text{(C6.68)}$$

The dynamics of the actuators controlling the flap angles are ignored so that each α_{flapi} is assumed to be perfectly controllable.

Note that if the flap rotates about its center of pressure, the aerodynamic torques across the flap rotation joint are small compared to the forces generated by the flap. Thus, a very large aerodynamic force can be obtained for relatively little actuator torque. However, the actual force required in a hydraulic system which drives the wing can still be large, due to physical constraints and practical considerations, as explained in addition, the dynamics of the system dictate a high actuator bandwidth (based upon LQR Optimal control designs), so that actuator power requirements are dominated by the flap moment of inertia.

6.1.1.8 Wind inputs

Since, for suspension performance, the worst-case wind is perpendicular to the vehicle, we model all wind as cross-winds. Cross-wind is modeled as a random process with two components:

$$V_{wind} = \overline{V}_{wind} + V_{wind}(t) \qquad \text{(C6.69)}$$

where

$\overline{V}_{wind}$ = mean cross-wind velocity (steady component of wind)
$V_{wind}(t)$ = time-varying wind component

The random component is modeled as a first-order Markov process with power-spectral-density:

$$\Phi_{wind}(\omega) = \frac{2\sigma_w^2 \nu}{\omega^2 + \nu^2} \qquad \text{(C6.70)}$$

where

F_{wind} = power spectral density of time-varying cross-wind
n = break frequency of wind spectrum (rad/s)
s_w = RMS of time-varying wind component (m/s)
w = frequency (rad/s)

The break frequency (n) depends on weather conditions and terrain features. We assumed a value of 1 (rad/s). s_w and $\overline{V}_{wind}$ also depend on weather and terrain. We assumed a relationship between s_w, $\overline{V}_{wind}$ and the peak wind:

$$(V_{wind})_{max} = \overline{V}_{wind} + 3\, s_w \qquad \text{(C6.71)}$$

$$(V_{wind})_{min} = \overline{V}_{wind} + 3\, s_w = 0 \qquad \text{(C6.72)}$$

Thus, the peak wind is equal to twice the mean wind, with a minimum wind speed of zero.

Several different levels of maximum wind were considered.

For our analysis, we desire a model for the time-varying wind in the form of a linear system driven by white noise. A linear system that has an output with the appropriate power spectral density (PSD) is straightforward to derive. The PSD of the output of a linear system is given by:

$$\Phi_{wind}(\omega) = \Phi_{yy}(\omega) = g(j\omega)\, g(-j\omega)\Phi_{uu}(\omega) \qquad \text{(C6.73)}$$

If we choose unfiltered white noise as the system input, its PSD is:

$$\Phi_{uu}(\omega) = 1 \qquad \text{(C6.74)}$$

A system with the desired output is:

$$g(j\omega) = \frac{\sigma_w\sqrt{2\nu}}{j\omega + \nu} \qquad \text{(C6.75)}$$

$$g(s) = \frac{\sigma_w\sqrt{2\nu}}{s + \nu} \qquad \text{(C6.76)}$$

We use a state-space representation of this system for our covariance analysis, i.e.:

$$\dot{\mathbf{x}}_w = \mathbf{A}_w\mathbf{x}_w + \mathbf{B}_w\xi_w \qquad \text{(C6.77)}$$

$$\mathbf{V}_{wind}(t) = \mathbf{C}_w\, \mathbf{x}_w \qquad \text{(C6.78)}$$

where

x_w = white noise input to wind model

The mean component of the wind is accounted for in the mean sideslip angle b_0 (see the wind force equations in Section 3.2). System responses to sharp discontinuities in the wind profile,

such as might occur when the vehicle exits a tunnel or passes a terrain feature, can be evaluated by employing appropriate time functions for $V_{wind}(t)$.

6.1.1.9 Guideway inputs

The guideway is modeled as a time-varying vector of positional and rotational inputs to the front and rear primary suspensions:

$$\mathbf{x}_{gi} = \begin{bmatrix} y \\ z \\ \phi \end{bmatrix}_{gi} \tag{C6.79}$$

Since the guideway position is constant at a given point on the guideway, the input to the rear bogie is a time delay of the input to the front:

$$\mathbf{x}_{g1} = e^{-s\tau}\,\mathbf{x}_{g2} \tag{C6.80}$$

where τ is the time it takes the vehicle to travel the distance between the two bogies:

$$\tau = \frac{LXB1 + LXB2}{V}$$

To obtain a linear approximation of the time delay, we used a Pade approximation :

$$e^{-s\tau} \approx \frac{2 + (-s\tau) + \frac{(-s\tau)^2}{2!} + \cdots + \frac{(-s\tau)^n}{n!}}{2 + (s\tau) + \frac{(s\tau)^2}{2!} + \cdots + \frac{(s\tau)^n}{n!}} \tag{C6.81}$$

where

n = the order of approximation[9]

For covariance analysis, a state-space form of equation EQN is used:

$$\dot{\mathbf{x}}_d = \mathbf{A}_d \mathbf{x}_d + \mathbf{B}_d \mathbf{x}_{g1} \tag{C6.82}$$

$$\mathbf{x}_{g2} = \mathbf{C}_d \mathbf{x}_d + \mathbf{D}_d \mathbf{x}_{g1} \tag{C6.83}$$

Guideway inputs to the front bogie are a sum of known inputs (curves, inclinations, etc.) and random guideway roughness:

$$\mathbf{x}_{g1} = \left(\mathbf{x}_{g1}\right)_{known} + \mathbf{x}_{g1}(t) \tag{C6.84}$$

Known inputs are modeled by summing simple waveforms (steps, ramps, sinusoids), where a position-dependent guideway position, $\mathbf{x}_g(x)$, is transformed to a time-dependent input by:

$$x = V\,t \tag{C6.85}$$

To describe guideway roughness, we adapted a commonly applied model (see C.6.1.5) which describes each roughness component as a power-spectral density function of the form:

$$\Phi_{guideway}(\omega) = \frac{A_r V}{\omega^2} \tag{C6.86}$$

where

A_r = roughness parameter

---

[9] We primarily used 10th order approximations to generate the results presented in this report.

The appropriate roughness parameter is dependent on the characteristics of the guideway variation. A discussion of roughness parameters used for our work is in Section 6.1.5. Note that our present analysis excludes guideway flexibility and periodic guideway variations due to such factors as static guideway sag. In addition to this, none of the known inputs (curves, inclinations, etc.) are included for our analysis.

For our analysis, we desire a model of the guideway input in the form of a linear system driven by white noise. Derivation of the guideway model is similar to derivation of the wind model.

When driven by white noise, a linear system has the desired output statistics:

$$g(s) = \frac{\sqrt{A_r V}}{s} \tag{C6.87}$$

We use a state-space representation of this system:

$$\dot{\mathbf{x}}_{gm} = \mathbf{A}_{gm}\,\mathbf{x}_{gm} + \mathbf{B}_{gm}\,\xi_g \tag{C6.88}$$

$$\mathbf{x}_{gl}(t) = \mathbf{C}_{gm}\,\mathbf{x}_{gm} \tag{C6.89}$$

where

x_g = white noise input to guideway model

6.1.1.10 Forming the Complete Model

At this point, having presented models for all components of the vehicle-suspension system, we can form a complete model of the system. Combining equations yields the vehicle accelerations in terms of the system inputs and the vehicle states as:

$$\ddot{\mathbf{x}}_t = \mathbf{I}_t^{-1} \cdot \begin{pmatrix} \left(\mathbf{T}^f_{s1\text{-}t}\,\mathbf{K}_s\,\mathbf{T}^x_{t\text{-}s1} + \mathbf{T}^f_{s2\text{-}t}\,\mathbf{K}_s\,\mathbf{T}^x_{t\text{-}s2} + \mathbf{T}^f_{aero\text{-}t}\,q\,A_t\,C_{y\beta}\,V\,\mathbf{T}^x_{t\text{-}\psi_t}\right)\mathbf{x}_t \\ +\left(\mathbf{T}^f_{s1\text{-}t}\,\mathbf{C}_s\,\mathbf{T}^x_{t\text{-}s1} + \mathbf{T}^f_{s2\text{-}t}\,\mathbf{C}_s\,\mathbf{T}^x_{t\text{-}s2}\right)\dot{\mathbf{x}}_t \\ +\mathbf{T}^f_{s1\text{-}t}\,\mathbf{K}_s\,\mathbf{T}^x_{b1\text{-}s1}\,\mathbf{x}_{b1} + \mathbf{T}^f_{s2\text{-}t}\,\mathbf{K}_s\,\mathbf{T}^x_{b2\text{-}s1}\,\mathbf{x}_{b2} \\ +\mathbf{T}^f_{s1\text{-}t}\,\mathbf{C}_s\,\mathbf{T}^x_{b1\text{-}s1}\,\dot{\mathbf{x}}_{b1} + \mathbf{T}^f_{s2\text{-}t}\,\mathbf{C}_s\,\mathbf{T}^x_{b2\text{-}s1}\,\dot{\mathbf{x}}_{b2} \\ +\mathbf{T}^f_{aero\text{-}t}\,q\,A_t\,C_{y\beta}\,V_{wind} + \mathbf{T}^f_{aero\text{-}t}\,q\,A_t\,C_\beta(\beta_0) \\ +\mathbf{T}^f_{s1\text{-}t}\mathbf{F}_{s1,act} + \mathbf{T}^f_{s2\text{-}t}\mathbf{F}_{s2,act} + \sum_i \mathbf{T}^f_{flapi-t}\,q\,A_{flapi}\,C_{y\alpha}\alpha_i \end{pmatrix} \tag{C6.90}$$

$$\ddot{\mathbf{x}}_{b1} = \mathbf{I}_{b1}^{-1} \cdot \begin{pmatrix} \mathbf{T}^f_{s1\text{-}b1}\,\mathbf{K}_s\,\mathbf{T}^x_{t\text{-}s1}\,\mathbf{x}_t + \mathbf{T}^f_{s1\text{-}b1}\,\mathbf{C}_s\,\mathbf{T}^x_{t\text{-}s1}\dot{\mathbf{x}}_t \\ +\left(\mathbf{T}^f_{s1\text{-}b1}\,\mathbf{K}_s\,\mathbf{T}^x_{b1\text{-}s1} + \sum_i \mathbf{T}^f_{gefi-b1}\,q\,A_{flapi}\,C_{y\varepsilon}\mathbf{T}^x_{b1\text{-}gefi}\right)\mathbf{x}_{b1} \\ +\mathbf{T}^f_{s1\text{-}b1}\,\mathbf{C}_s\,\mathbf{T}^x_{b1\text{-}s1}\,\dot{\mathbf{x}}_{b1} \\ +\sum_i \mathbf{T}^f_{gefi-b1}\,q\,A_{flapi}\,C_{y\varepsilon}\mathbf{T}^x_{g1\text{-}gefi}\,\mathbf{x}_{g1} \\ +\mathbf{T}^f_{s1\text{-}b1}\mathbf{F}_{s1,act} + \sum_i \mathbf{T}^f_{gefi-b1}\,q\,A_{flapi}\,C_{y\alpha}\alpha_{gefi} \end{pmatrix} \tag{C6.91}$$

$$\ddot{\mathbf{x}}_{b2} = \mathbf{I}_{b2}^{-1} \cdot \begin{pmatrix} \mathbf{T}^{f}_{s2\text{-}b2}\,\mathbf{K}_s\,\mathbf{T}^{x}_{t\text{-}s2}\,\mathbf{x}_t + \mathbf{T}^{f}_{s2\text{-}b2}\,\mathbf{C}_s\,\mathbf{T}^{x}_{t\text{-}s2}\dot{\mathbf{x}}_t \\ + \left(\mathbf{T}^{f}_{s2\text{-}b2}\,\mathbf{K}_s\,\mathbf{T}^{x}_{b2\text{-}s2} + \sum_i \mathbf{T}^{f}_{gefi-b2}\,q\,A_{flapi}\,\mathbf{C}_{y\varepsilon}\mathbf{T}^{x}_{b2\text{-}gefi} \right)\mathbf{x}_{b2} \\ + \mathbf{T}^{f}_{s2\text{-}b2}\,\mathbf{C}_s\,\mathbf{T}^{x}_{b2\text{-}s2}\,\dot{\mathbf{x}}_{b2} \\ + \sum_i \mathbf{T}^{f}_{gefi-b2}\,q\,A_{flapi}\,\mathbf{C}_{y\varepsilon}\mathbf{T}^{x}_{g2\text{-}gefi}\,\mathbf{x}_{g2} \\ + \mathbf{T}^{f}_{s2\text{-}b2}\mathbf{F}_{s2,act} + \sum_i \mathbf{T}^{f}_{gefi-b2}\,q\,A_{flapi}\,\mathbf{C}_{y\alpha}\alpha_{gefi} \end{pmatrix} \tag{C6.92}$$

If we define a state vector **x**, control input vector **u**, and disturbance input vector **d**, a state-space equation for the system can be derived:

$$\dot{\mathbf{x}} = \mathbf{A}\,\mathbf{x} + \mathbf{B}_u\,\mathbf{u} + \mathbf{B}_d\,\mathbf{d} \tag{C6.93}$$

where

$$\mathbf{x} = \begin{bmatrix} \mathbf{x}_t & \mathbf{x}_{b1} & \mathbf{x}_{b2} & \dot{\mathbf{x}}_t & \dot{\mathbf{x}}_{b1} & \dot{\mathbf{x}}_{b2} \end{bmatrix}^T \tag{C6.94}$$

$$\mathbf{u} = \begin{bmatrix} \mathbf{F}_{s1,act} \\ \mathbf{F}_{s2,act} \\ \alpha_{flapi} \\ \vdots \\ \alpha_{gefi} \\ \vdots \end{bmatrix} \tag{C6.95}$$

$$\mathbf{d} = \begin{bmatrix} x_{g1} \\ x_{g2} \\ V_{wind}(t) \\ \frac{\rho V^2}{2} A_t C_{y\beta}(\beta_0) \end{bmatrix} \qquad \text{(C6.96)}$$

Equations for system outputs of interest in terms of system states, disturbance inputs, and controls are:

$$\mathbf{z} = \mathbf{C}\mathbf{x} + \mathbf{D}_u \mathbf{u} + \mathbf{D}_d \mathbf{d} \qquad \text{(C6.97)}$$

The system outputs (z) are vehicle accelerations and rotation rates, primary suspension air gap changes, and secondary suspension strokes.

A system model in the form of a linear system driven by white noise is desired for covariance analyses. To obtain such a model, we combine the equations above with control laws for the active secondary and aerodynamic actuators and equations derived in Sections 6.1.1.8 and 6.1.1.9 for guideway and wind disturbance inputs.

The guideway model is added first to yield a new system model of the form:

$$\dot{\mathbf{x}} = \mathbf{A}\mathbf{x} + \mathbf{B}_u \mathbf{u} + \mathbf{B}_d \xi_g + \mathbf{L} \begin{bmatrix} V_{wind}(t) \\ \frac{\rho V^2}{2} A_t C_{y\beta}(\beta_0) \end{bmatrix} \qquad \text{(C6.98)}$$

$$\mathbf{y} = \mathbf{C}\mathbf{x} + \mathbf{D}_u \mathbf{u} + \mathbf{D}_d \begin{bmatrix} V_{wind}(t) \\ \frac{\rho V^2}{2} A_t C_{y\beta}(\beta_0) \end{bmatrix} \qquad \text{(C6.99)}$$

When driven by the white noise input, this system will have non-stationary random outputs due to the integrators in the guideway model. As a result, closed-form covariance analyses cannot be performed to determine system response to the random guideway and wind inputs.

This problem can be overcome by executing a change of variables for the entire vehicle-suspension system. First, observe that the integrator portion of the guideway model is present to determine the position of the guideway relative to some Earth-fixed reference frame. Since the output variables of interest (air gaps, secondary suspension strokes, etc.) do not depend on Earth-relative position, this part of the model is not needed. Thus, any state transformation that removes the integrator modes from the system model while retaining all other modes retains all the information required for our analysis. This can be performed because the integrator modes of the system are unobservable in the outputs of interest. We derived such a transformation:

$$\mathbf{x}' = \mathbf{T}\,\mathbf{x} \tag{C6.100}$$

where $\mathbf{x}'$ is the transformed state. This transformation was applied to redefine our system:

$$\dot{\mathbf{x}} = \mathbf{T}\mathbf{A}\mathbf{T}^{-1}\mathbf{x} + \mathbf{T}\mathbf{B}_u\mathbf{u} + \mathbf{T}\mathbf{B}_d\xi_g + \mathbf{T}\mathbf{L}\begin{bmatrix} V_{wind}(t) \\ \frac{\rho V^2}{2} A_t C_{y\beta}(\beta_0) \end{bmatrix} \tag{C6.101}$$

$$\mathbf{z} = \mathbf{C}\,\mathbf{T}\mathbf{x} + \mathbf{D}_u\mathbf{u} + \mathbf{D}_d\begin{bmatrix} V_{wind}(t) \\ \frac{\rho V^2}{2} A_t C_{y\beta}(\beta_0) \end{bmatrix} \tag{C6.102}$$

Note that, for convenience, the superscript (') has been dropped from the state vector in the above equations. Also for convenience, we redefine the system matrices as their transformed versions:

$$\mathbf{A} \leftarrow \mathbf{T}\,\mathbf{A}\,\mathbf{T}^{-1}$$

$$\mathbf{B}_u \leftarrow \mathbf{T}\,\mathbf{B}_u$$

$$\mathbf{B}_d \leftarrow \mathbf{T}\,\mathbf{B}_d$$

$$\mathbf{C} \leftarrow \mathbf{C}\,\mathbf{T}$$

We continue by introducing equations to describe the control inputs **u**. Full-state feedback is assumed, yielding an equation for the control inputs in terms of the states of the transformed system[10] :

$$\mathbf{u} = -\mathbf{G}\,\mathbf{x} \tag{C6.103}$$

Note that the full-state feedback assumption implies availability of noise-free measurements of the system states, including the primary suspension air gaps and their changes in response to guideway position inputs. This is because our transformed states do not contain the absolute position of the guideway, so we only know the relative positions of each in terms of the air gap in each direction. Thus, when we perform feedback on these states, which of course must be controllable to do so, we assume that the air gap can be controlled by changing the position of the bogie and measuring perfectly the position of the guideway. Also observe that the dimensions of **u** and **G** depend on the specific actuator configuration chosen. For the case of an all-passive system, **u** and **G** are zero.

Redefining **A** and **C** as:

$$\mathbf{A}_{cl} = \mathbf{A} - \mathbf{B}_u\,\mathbf{G} \tag{C6.104}$$

$$\mathbf{C}_{cl} = \mathbf{C} - \mathbf{D}_u\,\mathbf{G} \tag{C6.105}$$

yields:

$$\dot{\mathbf{x}} = \mathbf{A}_{cl}\,\mathbf{x} + \mathbf{B}_d\,\xi_g + \mathbf{L}\left[\frac{\rho V^2}{2} A_t\, C_{y\beta}(\beta_0)\right] \quad V_{wind}(t) \tag{C6.106}$$

$$\mathbf{z} = \mathbf{C}_{cl}\,\mathbf{x} + \mathbf{D}_d\left[\frac{\rho V^2}{2} A_t\, C_{y\beta}(\beta_0)\right] \quad V_{wind}(t) \tag{C6.107}$$

---

[10] A description of how the gain matrix G is derived appears in Chapter CC.

Finally, the model for the time-varying wind component is appended to yield the system equations used to calculate the output response:

$$\dot{\mathbf{x}} = \mathbf{A}_{cl}\,\mathbf{x} + \mathbf{B}_d \begin{bmatrix} \xi_g \\ \xi_w \end{bmatrix} + \mathbf{L}\left(\frac{\rho V^2}{2} A_t\, C_{y\beta}(\beta_0)\right) \qquad \text{(C6.108)}$$

$$\mathbf{z} = \mathbf{C}_{cl}\,\mathbf{x} + \mathbf{D}_d\left(\frac{\rho V^2}{2} A_t\, C_{y\beta}(\beta_0)\right) \qquad \text{(C6.109)}$$

The last term in these system equations is the force that results when the steady wind component ($\overline{V}_{wind}$) is applied. In our research, we solve for response to this component separately, thus determining the DC components of the system outputs and the mean sideslip angle (β_0) used for system linearization. The aerodynamic stability derivative $C_{y\beta}(\beta)$ and center of pressure position (LXCP) are then determined as described in Section 6.1.1.3 (*Wind and aerodynamic stability effects*), and the steady wind term set to zero, yielding a linear system driven by white noise:

$$\dot{\mathbf{x}} = \mathbf{A}_{cl}\,\mathbf{x} + \mathbf{B}_d \begin{bmatrix} \xi_g \\ \xi_w \end{bmatrix} \qquad \text{(C6.110)}$$

$$\mathbf{z} = \mathbf{C}_{cl}\,\mathbf{x} \qquad \text{(C6.111)}$$

6.1.1.11 Adaptation of 5 DOF Model for SCD Vehicle Analysis

The roll center of the secondary suspension was assumed to be at a point 1.486 meters below the cg of the sprung mass. Also, the analysis inherently assumes that the secondary suspension is linear, and that the roll center remains stationary as the suspension deflects. All of these assumptions would have to be checked if the analysis is pursued beyond the concept definition stage.

In an attempt to more closely model the primary suspension, an off-diagonal term was added. This term provided the effect of giving a roll torque on each bogie when it was displaced laterally. This effect occurs because the lift force on each side of the bogie is sensitive to the lateral air gap.

In other words, if the bogie is displaced to the right, the lift force on the right side increases, while the lift force on the left side decreases, resulting in a roll torque exerted on the bogie. Numbers to model this effect were obtained from data provided by MIT Plasma Fusion Center.

6.1.2 Control Law Description

6.1.2.1 Derivation of Control Gains

Active control was applied to the vehicle through the use of so-called Linear Quadratic Optimal Control methods, using full state feedback. The suspension design criteria remain the same: minimize passenger accelerations without exceeding limits on air gap variations and secondary suspension strokes. The active suspension must meet these goals while maintaining reasonable actuator requirements.

In deriving the control law, we begin with the equations (C6.104) to (C6.107) of the previous section.

$$\dot{\mathbf{x}} = \mathbf{T}\mathbf{A}\mathbf{T}^{-1}\mathbf{x} + \mathbf{T}\mathbf{B}_u\mathbf{u} + \mathbf{T}\mathbf{B}_d\xi_g + \mathbf{T}\mathbf{L}\begin{bmatrix} V_{wind}(t) \\ \frac{\rho V^2}{2} A_t C_{y\beta}(\beta_0) \end{bmatrix} \qquad \text{(C6.112)}$$

$$\mathbf{z} = \mathbf{C}\,\mathbf{T}^{-1}\mathbf{x} + \mathbf{D}_u\mathbf{u} + \mathbf{D}_d\begin{bmatrix} V_{wind}(t) \\ \frac{\rho V^2}{2} A_t C_{y\beta}(\beta_0) \end{bmatrix} \qquad \text{(C6.113)}$$

Because, under this study, we use the same control law for all wind conditions, it is appropriate to linearize the equations describing these conditions about the steady state sideslip angle. In addition, since the time-varying wind ($V_{wind}(t)$) cannot be measured, it is excluded from the state vector for feedback purposes. The resultant system model used for designing the control law (the so-called design plant model) is:

$$\dot{\mathbf{x}} = \mathbf{T}\mathbf{A}\mathbf{T}^{-1}\mathbf{x} + \mathbf{T}\mathbf{B}_u\mathbf{u} + \mathbf{T}\mathbf{B}_d\xi_g \qquad \text{(C6.114)}$$

$$\mathbf{z} = \mathbf{C}\,\mathbf{T}^{-1}\mathbf{x} + \mathbf{D}_u\mathbf{u} \qquad \text{(C6.115)}$$

6.1.2.2 Control Law Derivation

To apply state-feedback optimal control, three key assumptions must be made.

1) All of the model states[11] are available for feedback. (This assumes we can make noise-free measurements of all the model states)
2) The system [**A**, $\mathbf{B_u}$] is stabilizable. That is, all unstable modes of the system are controllable. Our system is open-loop stable, so these criteria are met
3) The system [**A**, $\mathbf{B_u}$] is detectable. That is, all unstable modes of the system are observable in the output. Again, since our system is open loop stable, these criteria are met.

Making these assumptions, we now apply so-called Linear Quadratic Optimal Control Theory to obtain a control law. The result is a control law for the system of the form:

$$\mathbf{u} = -\mathbf{G}\,\mathbf{x} \tag{C6.116}$$

The gain matrix **G** is selected to minimize a quadratic cost function that includes both the performance variables of interest and the control effort, thereby giving an optimum trade-off between the actuator effort and the performance of the system. The cost function that is minimized is:

$$J = \lim_{T\to\infty} E\left\{\int_0^T \left(\mathbf{z}(t)^T \mathbf{Q}\,\mathbf{z}(t) + \mathbf{u}(t)^T \mathbf{R}\,\mathbf{u}(t)\right) dt\right\} \tag{C6.117}$$

where **Q** is a weighting matrix used to vary the relative importance of the system outputs and **R** is a weighting matrix applied to ensure that the gain matrix yields reasonable controls (**u**). **z**(t), the time varying portion of the performance variables, is described by:

$$\mathbf{z}(t) = \mathbf{C}\,\mathbf{x}(t) + \mathbf{D_u}\,\mathbf{u}(t) \tag{C6.118}$$

---

[11] The states in the design plant include the primary and secondary suspension gaps and the absolute velocities of the vehicle and bogies. The wind model is not included, so wind measurements are not assumed available.

Thus, the cost function to be minimized becomes:

$$J = \lim_{T\to\infty} E\left\{\int_0^T \left(\mathbf{x}(t)^T \mathbf{C}^T \mathbf{Q}\mathbf{C}\mathbf{x}(t) + 2\mathbf{x}(t)^T \mathbf{C}^T \mathbf{Q}\mathbf{D}_u \mathbf{u}(t) + \mathbf{u}(t)^T \left(\mathbf{D}_u{}^T \mathbf{Q}\mathbf{D}_u + \mathbf{R}\right)\mathbf{u}(t)\right)dt\right\} \quad \text{(C6.119)}$$

The gain matrix **G** that minimizes this cost function is described by:

$$G = R^{-1}\left[D_u^T QC + B_u^T K\right] \quad \text{(C6.120)}$$

with **K** determined from the solution to the following algebraic Riccati equation:

$$0 = \mathbf{KA} + \mathbf{A}^T\mathbf{K} + \mathbf{C}^T\mathbf{QC} - [\mathbf{KB_u} + \mathbf{C}^T\mathbf{QD_u}]\,\mathbf{R}^{-1}\,[\mathbf{B_u}^T\mathbf{K} + \mathbf{D_u}\,\mathbf{QC}] \quad \text{(C6.121)}$$

6.1.2.3 Choice of Weights in Cost Function

The choice of the weighting matrices (**Q**, **R**) in the cost functional determines the relative performance of the system in terms of the output variables and the control effort. The weights were chosen with emphasis on the Pepler index, which includes the vertical and lateral accelerations and the roll rate. This minimization was performed while maintaining acceptable air gap variations and secondary suspension strokes.

Three different suspension systems were developed and compared. The first was an optimized passive system (the choice of suspension parameters is described in detail elsewhere). These optimized passive parameters were used to develop two actively controlled systems:

- A system with active secondary suspension (hydraulic actuators acting between the bogie and the vehicle)
- A system with an active secondary suspension including both hydraulic actuators and active aerodynamic flaps on the vehicle

The limits imposed on the air gap variations and secondary suspension strokes are described in Section 6.1.3.

6.1.2.4 Active Suspension Design Trade-offs

The use of optimal control laws in the implementation of an active secondary system using hydraulic actuators assures an optimum trade-off (in a linear quadratic sense) between the ride comfort and the suspension displacements. This was achieved by making the control weighting

matrix R small compared to the performance variable weighting matrix Q, so that the cost functional would be dominated by the performance variables. This allowed the air gap variations and secondary suspension stroke lengths to be traded off against passenger accelerations.

Thus, no limitations were imposed on the forces applicable by the hydraulic actuators except to verify that the forces of the final system were obtainable with currently available hydraulic systems. Nevertheless, there is still a fundamental limitation in system performance because any force exerted on the vehicle by the hydraulic actuator in an attempt to reduce passenger accelerations will also act on the bogie, tending to decrease the primary air gap. In the case of the aero-surfaces, a limitation on the available control force was imposed by limiting the RMS value of the flap or wing angle, having sized these actuators as described in Section C.5.2.

The primary advantage of the active aerodynamic surfaces mounted on the vehicle is that forces can be applied between the vehicle and an inertial reference frame. Thus, the forces act directly on the vehicle, but do not directly act on the bogies. Because of this, passenger accelerations can be reduced with no deleterious effects on air gap variations. Crosswind forces that act on the vehicle can be directly cancelled, as can forces from the secondary suspension elements, whether passive or active, that are exerted on the vehicle. This effectively allows the vehicle to act as though it has more mass, thus emulating a system with a lower unsprung mass to total mass ratio, which results in both improved guideway tracking and reduced passenger accelerations.

6.1.3 Evaluation Methodology

6.1.3.1 Suspension Requirements

The maglev vehicle's suspension system is required to:

1) Maintain the primary suspension air gaps (prevent the bogies from striking the guideway)
2) Ensure that the secondary suspension stroke does not exceed stroke limits
3) Maximize passenger comfort

These performance requirements can be quantified in terms of the performance output vector **z**. The system outputs are driven by both a DC component due to steady wind and zero-mean random inputs (modeled as a vector of white noise) due to guideway roughness and time-varying winds. Thus, the components of the output vector **z** are each the sum of a steady component and a zero-mean, randomly varying component.

$$\mathbf{z}(t) = \bar{\mathbf{z}} + \tilde{\mathbf{z}}(t) \qquad \text{(C6.3 122)}$$

where:

$\mathbf{z}(t)$ = performance output vector, including air gaps and secondary suspension strokes

$\bar{\mathbf{z}}$ = steady state, DC component of outputs

$\tilde{\mathbf{z}}(t)$ = time varying portion of outputs

The suspension requirements are written in terms of these two components.

1. Air Gap Variations and Secondary Stroke

The primary suspension air gap requirements are described by limits on the maximum primary suspension strokes:

$$\Delta x_{pi(l,r)} < \left(\Delta x_{pi(l,r)}\right)_{max} \qquad \text{(C6.123)}$$

where:

$\Delta x_{pi(l,r)}$ = change in primary air gap, on either the left or right side of the bogie

The limits on air gap variations are determined by the available nominal air gap between the bogies and the guideway, minus the gap used up by steady crosswinds. The resulting limits on peak air gap variations were assumed to be 10 cm in the vertical direction and 5 cm in the lateral direction.

The limit imposed on RMS variations of the primary air gap was:

$$\Delta\bar{x}_{pi(l,r)} + 5\sigma_{\Delta x_{pi(l,r)}} < \left(\Delta x_{pi(l,r)}\right)_{max} \qquad \text{(C6.124)}$$

where:

$\Delta\bar{x}_{pi(l,r)}$ = change in primary air gap, on either the left or right side of the bogie, due to DC input(s)

$\sigma_{\Delta x_{pi(l,r)}}$ = RMS variation in primary air gap, on either the left or right side of the bogie

At any given instant in time, there is a probability of 2.87×10^{-7} that the random component of the air gap will be greater than five times its RMS value. Therefore, we judge these criteria to be conservative.

The requirement of satisfying the secondary suspension stroke limits was quantified as:

$$\Delta x_{si} < \left(\Delta x_{si}\right)_{max} \qquad \text{(C6 125)}$$

where:

Δx_{si} = the change in the gap between the bogies and the vehicle; i.e., the secondary suspension stroke

The criteria we used were:

$$\Delta\bar{x}_{si} + 3\sigma_{\Delta x_{si}} < \left(\Delta x_{si}\right)_{max} \qquad \text{(C6.126)}$$

where:

$\Delta\bar{x}_{si}$ = change in the gap between the bogies and the vehicle due to DC input(s)

$\sigma_{\Delta x_{si}}$ = RMS variation in the gap between the bogies and the vehicle

There is a probability of 0.00135 that the secondary stroke will be greater than this three-sigma variation at any given instant in time. These less stringent criteria (three-sigma versus five-sigma peaks) were applied for the secondary suspension stroke because the (still rare) event of hitting the

secondary suspension stops is not judged to be a critical failure of the suspension, as touchdown on the guideway is. (If the secondary suspension stroke limit is exceeded, the likely outcome is a slight "bump" felt in the passenger compartment as the suspension bottoms out). The maximum secondary suspension stroke was assumed to be 11 cm in the vertical direction and 19.5 cm in the lateral direction.

2. Ride Quality

Two measures of ride quality are commonly used for maglev vehicles, the International Standardization Organization (ISO) ride quality criteria and the Pepler ride quality criteria.[12] Both measures are dependent on vehicle accelerations. In addition, the Pepler index includes the effects of roll and noise. Vehicle accelerations and vehicle rotation rates are variables in the output vector **z**.

The Pepler ride quality index is a scalar sum of statistics of system variables:

$$P.I. = 1.0 + 0.5\sigma_{\dot{\phi}} + 17\sigma_{\ddot{z}} + 17\sigma_{\ddot{y}} + 0.1(dB(N) - 65) \qquad \text{(C6.127)}$$

where

$\sigma_{\dot{\phi}}$ = RMS passenger roll rate (deg/s)

$\sigma_{\ddot{z}}$ = RMS passenger acceleration in the Z direction (g's)

$\sigma_{\ddot{y}}$ = RMS passenger acceleration in the Y direction (g's)

dB(N) = passenger compartment noise level (decibels)

This research did not include the effect of noise on ride quality, so the formula used for Pepler index was:

$$P.I. = 1.0 + 0.5\sigma_{\dot{\phi}} + 17\sigma_{\ddot{z}} + 17\sigma_{\ddot{y}} \qquad \text{(C6.128)}$$

---

[12] Dunlap and Associates, Inc., "Development of Techniques and Data for Evaluating Ride Quality, Volume II: Ride Quality Research," Report No. DOT-TSC-RSPD-77-1,II for U.S. Dept. of Transportation, February, 1978.

which depends only on RMS values of the system outputs.

The ISO ride quality criteria specify limits on RMS vertical and lateral vehicle accelerations in one-third octave bands over a specified range of frequencies. (See the plots of system performance versus ISO 1 hour reduced comfort specifications in the results section.) The limits are different for the lateral and vertical directions.

$$(\ddot{y}_t)_{rms} = \left\{ \int_{\omega_l}^{\omega_u} S_{\ddot{y}_t}(\omega) d\omega \right\}^{\frac{1}{2}} \tag{C6.129}$$

Given each center frequency ω_c, the upper and lower bounds for the one-third octave band are determined by:

$$\omega_u = \omega_c \exp\left(\frac{1}{6}\ln 2\right) = 1.122\omega_c \tag{C6.130}$$

$$\omega_l = \omega_c \exp\left(-\frac{1}{6}\ln 2\right) = 0.891\omega_c \tag{C6.131}$$

Note that the steady component of the system output vector does not contribute to either ride quality measure. Thus, only the time-varying portions of the system outputs affect ride quality, and only the system response to the white noise input needs to be considered in ride quality evaluations. Ride quality measures were calculated at the "worst seat in the vehicle," typically a front or rear corner of the passenger compartment.

6.1.3.2 Calculations

As stated previously, the output variable **z** can be written as the sum of a DC (mean) component and a random, time-varying component.

$$\mathbf{z}(t) = \bar{\mathbf{z}} + \tilde{\mathbf{z}}(t) \tag{C6.132}$$

The mean and random components of the output are calculated separately and then added to determine system performance.

1. Determining the Mean of the Outputs

We first set the time-varying disturbances to zero and solve the remaining non-linear equations. This requires the solution to:

$$\dot{\mathbf{x}} = \mathbf{A}\mathbf{x} + \mathbf{B}_{dc}\left(\frac{\rho}{2}|V|^2 C_y(\beta_0)\right) = 0 \qquad \text{(C6.133)}$$

$$\bar{\mathbf{z}} = \mathbf{C}\mathbf{x} + \mathbf{D}_{dc}\left(\frac{\rho}{2}|V|^2 C_y(\beta_0)\right) \qquad \text{(C6.134)}$$

for the mean sideslip angle (β_0) and the steady component of the system outputs ($\bar{\mathbf{z}}$). The resultant value for β_0 is then used to calculate the aerodynamic terms which depend on β ($C_{y\beta}$, LXCP). Dropping the steady disturbance term from the system equations then yields a system model that is linear and driven by white noise:

$$\dot{\mathbf{x}} = \mathbf{A}\mathbf{x} + \mathbf{B}_d\,\xi \qquad \text{(C6.135)}$$

$$\mathbf{z} = \mathbf{C}\mathbf{x} + \mathbf{D}_d\,\xi \qquad \text{(C6.136)}$$

These equations are used to calculate RMS values of the time-varying outputs ($\mathbf{z}(t)$). RMS values could be calculated in two ways: numerical integration of the transfer functions describing the PSD Power Spectral Density (PSD), through a steady-state covariance analysis which involves solution of Lyapunov equations.

2. Determining RMS Outputs via Numerical Integration

RMS acceleration in a given frequency band can be calculated by numerically integrating the power-spectral density function over the desired range of frequencies:

$$(z)_{rms} = \left\{\int_{\omega_1}^{\omega_2} S_z(\omega)\,d\omega\right\}^{\frac{1}{2}} \qquad \text{(C6.137)}$$

Since the time-varying output is driven by two random inputs (guideway and wind), the RMS response to each input is calculated separately. The two results are combined to yield the total RMS system output:

$$(z)_{rms} = \sqrt{(z_g)_{rms}^2 + (z_w)_{rms}^2} \qquad \text{(C6.138)}$$

These components are given by:

$$\Phi_{z_g} = |G_g(j\omega)|^2 \Phi_{\xi_g}(\omega) \qquad \text{(C6.139)}$$

$$\Phi_{z_w} = |G_w(j\omega)|^2 \Phi_{\xi_w}(\omega) \qquad \text{(C6140)}$$

where

$$\mathbf{G_g}(j\omega) = \mathbf{C}(j\omega\mathbf{I} - \mathbf{A})^{-1}\mathbf{B_g} + \mathbf{D_g} \qquad \text{(C6.141)}$$

$$\mathbf{G_w}(j\omega) = \mathbf{C}(j\omega\mathbf{I} - \mathbf{A})^{-1}\mathbf{B_w} + \mathbf{D_w} \qquad \text{(C6.142)}$$

and, since the input in each case is white noise:

$$\Phi_{\xi_g} = \Phi_{\xi_w} = 1 \qquad \text{(C6.143)}$$

Integrating the PSD from 0 to infinity (or some frequency range that captures all the system's dynamics) yields the total RMS of the system outputs.

Note that if we use the form of the system that has wind and guideway positions as inputs, we can input the wind and guideway PSDs directly. The result of the RMS calculations is identical to results of the procedure described above, except that an exact description of the guideway time delay can be used:

$$\Phi_{z_g} = |G_{g1}(j\omega) + G_{g2}(j\omega)e^{-j\omega\tau}|^2 \Phi_g(\omega) \qquad \text{(C6.144)}$$

By comparing RMS calculations from this representation to that which employs the Pade approximation of the time delay, the accuracy of the Pade approximation can be determined. We found no significant loss of accuracy in RMS calculations when a 10th order Pade approximation is used.

3. *Determining RMS Outputs Analytically*

Although generally the most accurate method, calculating RMS values via numerical integration of PSDs requires relatively large amounts of computation time. An alternate procedure is to calculate output covariances analytically via the solution of an appropriate Lyapunov equation. This method requires much less computation than integration of PSDs, but necessitates a vehicle description in the form of a linear system driven by white noise.

For the linear system driven by white noise:

$$\dot{\mathbf{x}} = \mathbf{A}\mathbf{x} + \mathbf{B}_d \xi \tag{C6.145}$$

$$\mathbf{z} = \mathbf{C}\mathbf{x} \tag{C6.146}$$

the state covariance obeys the equation:

$$\dot{\Sigma}_{xx} = \mathbf{A}\Sigma_{xx} + \Sigma_{xx}\mathbf{A}^T + \mathbf{B}_d \Xi_{\xi\xi} \mathbf{B}_d{}^T \tag{C6.147}$$

$$\Xi_{\xi\xi} = \mathbf{I} \tag{C6.148}$$

where

$\Xi_{\xi\xi}$ = intensity matrix for the white noise inputs

Σ_{xx} = covariance matrix for the state vector **x**

In steady state, the covariance equation becomes:

$$0 = \mathbf{A}\Sigma_{xx} + \Sigma_{xx}\mathbf{A}^T + \mathbf{B}_d \mathbf{B}_d{}^T \tag{C6.149}$$

which is a Lyapunov equation that can be solved algebraically for Σ_{xx}. The output covariance matrix, in terms of the state covariance matrix, is:

$$\Sigma_{zz} = \mathbf{C}\Sigma_{xx}\mathbf{C}^T \tag{C6.150}$$

The RMS components of the output vector (**z**) is the square-root of the terms along the diagonal of Σ_{yy}.

The results obtained from both a Lyapunov analysis and direct integration of the PSDs were compared to verify the software tools developed for this research. Results can be obtained via either method; however, a covarience analysis was performed, both because it is guaranteed to be accurate[13] , and because it is much faster on a computer.

6.1.4 Vehicle Parameters

Vehicle parameters are as follows:

6.1.4.1 Mass Parameters

Total Mass = 6.44e4 kg
Mass Ratio = 0.366

where the mass ratio is defined as the unsprung mass over the total mass

$I_{vehicle\ (roll)}$ = 8.587e4 kg-m^2
$I_{vehicle\ (pitch)}$ = 4.18e6 kg-m^2
$I_{vehicle\ (yaw)}$ = 4.18e6 kg-m^2
$I_{bogies\ (roll)}$ = 3.61e3 kg-m^2 (per bogie, assuming two bogies total)

6.1.4.2 Distances

lateral distance from vehicle cg to average passenger's heart = 1.564 m

vertical distance from vehicle cg up to average passenger's heart = 0.251 m

longitudinal distance between vehicle cg and each bogie, assuming two-bogie system equivalent to six-bogie design = 8.539 m

distance from vehicle cg up to assumed roll center of secondary suspension = 1.486 m

vertical distance from bogie cg up to assumed roll center of secondary suspension = 0.661 m

vertical distance from bogie cg down to point of force application by primary suspension = 0.014 m

---

[13] The accuracy of numerical integration is dependent on the frequency interval chosen, while solution of a lyaponov equation yields directly the state covarience.

lateral distance between the two points on the bogie that are subjected to lift forces	= 1.720 m
decimal percent to multiply lateral stiffness by to obtain roll torque stiffness term due to lateral displacement in primary suspension	= 0.954
longitudinal distance from vehicle cg forward to center of pressure for crosswind forces (for V= 134 m/s)	= 13.4359 m
vertical distance from vehicle cg up to center of pressure for crosswind forces (speed independent)	= -0.681 m
lift versus angle of attack for aerodynamic control surfaces	= 0.02635447 CL/deg

where CL stands for coefficient of lift

width of each aerodynamic control surface	= 1.12 m
geometric aspect ratio for each aerodynamic control surface	= 0.8
lateral distance between centers of pressure of each pair of aerodynamic control surfaces	= 2.435 m

6.1.5 Stochastic Input Parameters

6.1.5.1 Guideway Stochastic Model

We use the following guideway input spectrum

$$\Phi_{guideway}(\omega) = \frac{A_r v}{\omega^2} \qquad \text{(C6.151)}$$

$\Phi_{guideway}$ = Power Spectral Density of Guideway Irregularities

A_r = Roughness Parameter

v = Vehicle Velocity

A roughness parameter A_r corresponding to welded steel rail was used in defining the guideway PSD, which was then used to form a linear system driven by a white noise input to descibe the guideway position variations. While our guideway will not be welded steel rail and its roughness as seen by the vehicle will be dominated by the alignment of the guideway's coils, the PSD of the guideway is expected to be similar. In other words, the stochastics should be the same for both cases, so the use of a roughness parameter corresponding to welded steel rail is valid. However, the results of this analysis can be applied generally, knowing the equivalent roughness parameter of the actual guideway. The results scale linearly with the square root of the roughness parameter.

The same roughness was assumed in both the vertical and lateral directions. The roughness parameter used to model the guideway roll variations was determined by comparing our situation to railroad measures of this parameter.[14] Again, the stochastics were assumed to be similar for a maglev guideway, and so the relationship between cross-level[15] and profile[16] for rail of gage 4 to 6 was determined. This relation was then assumed to apply equally to the maglev guideway, and an angular roll disturbance was computed based on the roughness in the vertical direction. A guideway width of 1.2 meters was used for this calculation.

The resulting roughness parameters were:

$$A_r(\text{vertical}) = 2\pi \times 6.1\pi \times 10^{-8}$$
$$A_r(\text{lateral}) = 2\pi \times 6.1\pi \times 10^{-8}$$
$$A_r(\text{roll}) = 2\pi \times 6.1\pi \times 10^{-8}/(1.75\text{x}1.2)$$

Wind Stochastic Model

$$\Phi_{wind}(\omega) = \frac{2\sigma_w^2 \nu}{\omega^2 + \nu^2} \qquad \text{(C6.152)}$$

Φ_{wind} = Power Spectral Density of Wind
ν = break frequency of wind spectrum (rad/s)
σ_w = rms wind (m/s)
ω = frequency (rad/s)

---

14 Garg, Vijay K.; Dukkipati, Rao V., "Dynamics of Railway Vehicle Systems," Academic Press, 1984.
15 The difference between the elevation of two rails (railroad terminology).
16 Vertical surface profile is the average elevation of the two rails (railroad terminology).

when Power Spectral Density is defined as:

$$\Phi(\omega) = \frac{2\sigma_w^2 \nu}{\omega^2 + \nu^2} = \int_{-\infty}^{+\infty} \underbrace{\sigma_w^2 e^{-\nu|\tau|}}_{\psi(\tau)} e^{-j\omega\tau} d\tau \qquad \text{(C6.153)}$$

with $\psi(\tau)$ = the Auto-Correlation Function for the disturbance

The guideway and wind models described in this report are developed using this relationship between Power Spectral Densities and Auto-Correlation Functions.

Using this definition for Power Spectral Density, $A_r = 2\pi \times 6.1\pi \times 10^{-8}$ for Welded Steel Rail, as shown above. Note the extra 2π factor multiplying the roughness parameter which is found elsewhere[17] for Welded Steel Rail. This factor is needed to account for the different definition of the relationship between Power Spectral Density and Auto-Correlation Function found in those other places.

6.2 RIDE QUALITY RESULTS

6.2.1 Introduction

Ride comfort is expected to be an important determinant of public acceptance of maglev transportation systems. While it appears that ride quality better than the Government-specified design goals may not divert passengers from alternative modes, like air and highway travel which are known to be quite comfortable, it is likely that significantly poorer ride quality will certainly deter use of a maglev system. Consequently, the design of the vehicle, primary and secondary suspensions, and the guideway were carefully integrated to ensure superior passenger ride quality, with the intention of attracting passengers from competing modes.

At the high operating speeds of maglev vehicles, any imperfections in the guideway and fluctuations in the winds impinging on the vehicle can result in significant suspension force variations, resulting in vehicle vibrations. Studies have shown that if sufficiently large, these vibrations can cause passenger discomfort and even motion sickness, resulting in dissatisfaction

---

17 Wormley, D.N.; Young, J.W., "Optimization of Linear Vehicle Suspensions Subjected to Simultaneous Guideway and External Force Disturbances," Journal of Dynamic Systems, Measurement, and Control: Transactions of the ASME, Paper No. 73-Aut-H, March 16,1973.

with the quality of the ride. The suspension force variations also produce dynamic stresses in the guideway and the suspension components mounted on the guideway, as well as in the vehicle. The guideway imperfections and wind fluctuations also cause variations in the clearance between the vehicle and the guideway; if sufficiently large, these variations can result in vehicle-to guideway contact which can result in damage. The cost of constructing a guideway without these minor imperfections and in such a way as to shield the vehicle from wind would be prohibitive. For this reason, the discomfort resulting from guideway roughness and wind fluctuations is minimized in our baseline vehicle concept by the use of an actively controlled secondary suspension.

Studies have developed criteria and standards for evaluating ride quality [1 and 2]. It is thus necessary to evaluate the passenger accelerations, secondary suspension actuator strokes, and primary suspension air gap variations of the vehicle/active secondary suspension controller/guideway combination to determine satisfactory design and establish that it provides adequate ride comfort. Generally, there is a trade-off between the conflicting requirements of minimizing passenger accelerations, maintaining adequate vehicle-guideway clearances and providing reasonable actuator strokes.

6.2.2 Approach

Dynamic models of vehicle suspensions and guideways have been developed at MIT and Draper and have been applied to our vehicle, suspension, and guideway design to determine ride comfort along the "Severe Segment Test" route provided by DOT/FRA and as specified in Contract Modification 0002. Ride comfort in the vibration regime was determined both by calculating the Peplar index in the 1.0 to 25 Hz frequency band for a passenger located at the roll center of the vehicle and by comparison of the vertical and lateral accelerations (in the local coordinate system) at the worst passenger seat in the vehicle (for the baseline vehicle, this is a window seat at the front of the vehicle) with the ISO 1 hour reduced comfort curves over the 0.1 to 80 Hz frequency band. Ride comfort in the Motion Sickness regime (0.1 to 1.0 Hz) was determined by comparing the vertical acceleration with the extended ISO one hour reduced comfort curve set forth in Figure 2 of the contract modification.

Ride comfort in the curving regime was to be determined by comparing the vertical, lateral, and longitudinal accelerations and jerk and/or jolt with the design goal values set forth in the contract modification. However, in our simulations of vehicle performance over the Severe Segment Test route, the vehicle was constrained to observe these limits at all times; hence, it was unnecessary to

compare these parameters with the desired values, since they were guaranteed to be observed. These simulations were performed by Hughes using the Maglev Performance Simulator program. The simulations provided a vehicle velocity profile for the entire Severe Segment Test route; the velocities through the specified ride comfort evaluation segments of the route were examined and the maximum velocity was determined to be 134 meters/second through segment #4, both on a straight section and around a 1 kilometer radius curve. Ride comfort parameters for this report were evaluated for a maximum vehicle speed of 134 meters/second.

Although the ride comfort and air gap variations generally tend to be poorer at the highest vehicle speeds, the vehicle inputs from guideway roughness and wind variations do depend upon the vehicle speed, and the primary suspension stiffnesses and drag also are speed dependent. Accordingly, the ride comfort and air gap variations were also evaluated at a selected lower speed to ensure that satisfactory ride comfort was maintained over the range of operating speeds. Since the lower speeds through the ride comfort evaluation sections of the Severe Segment Test route occurred during curve negotiation, the quasi-static lateral accelerations of the vehicle due to centrifugal force were included in the calculation of air gap variations. The reduced speeds were 72 meters/second in ride quality evaluation segment 1, while negotiating a 1 km radius curve, and 65 meters/second in segment 2 while negotiating an 800-meter radius curve (the centrifugal force on the vehicle was the same in both cases).

In the calculation of the Pepler ride comfort index, the vehicle interior noise was estimated as 65 db(A); a noise level of 65 db(A) or lower does not affect the value of the Pepler index. Although the Proposal stated that ride comfort would be evaluated for entrance to/exit from tunnels, the ride comfort evaluation zones of the Severe Segment Test route do not include the single tunnel on the route, so the effect of these inputs were not evaluated. The vehicle accelerations resulting from passing vehicles also were not included in this study. It should be noted that, whereas the contract specified that the Pepler index be calculated using RMS accelerations in a 1 Hz to 25 Hz bandwidth, the values presented here were calculated over a very wide frequency range; this was inherent in the calculation method and results in slightly pessimistic Pepler index values.

Ride comfort models

A number of models have been developed for assessing the impact on ride quality of vehicle vibrations resulting from guideway roughness and wind forces. These range from simple single degree-of-freedom heave models [3 and 4] to more complex models incorporating multiple degrees of freedom and a multiplicity of primary suspension modules [5 and 3, respectively].

Figure C-6-8 depicts several of the simple models [4] and Figure C6-9 shows a more complicated model which, while analyzing only two degrees of freedom of the passenger compartment (heave and pitch), incorporates a larger number of suspension modules like our baseline vehicle concept.

The results presented in this report were all obtained from an improved model, the Five-Degree-of-Freedom model, which was completed at Draper during this study under an internally funded Corporate Sponsored Research project. This model is more comprehensive than any appearing in the open literature to date and, in simulating inputs from guideway roughness, includes the real world situations in which both the front and rear bogies pass sequentially over the same guideway imperfections and roll effects due to unequal inputs from the left and right sides of the guideway. Inputs to the vehicle from impinging wind forces are simulated, including both vibrational inputs

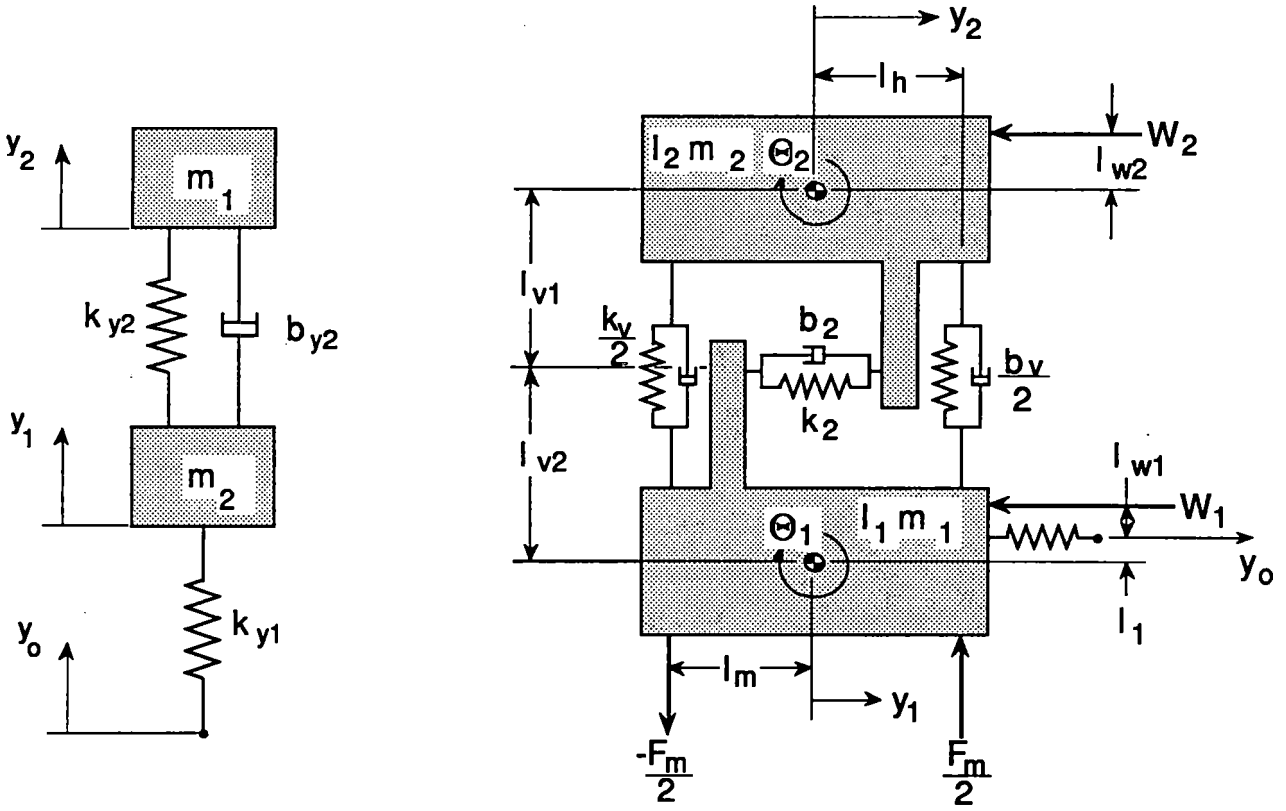

Figure C6-8 Draper simple dynamic models

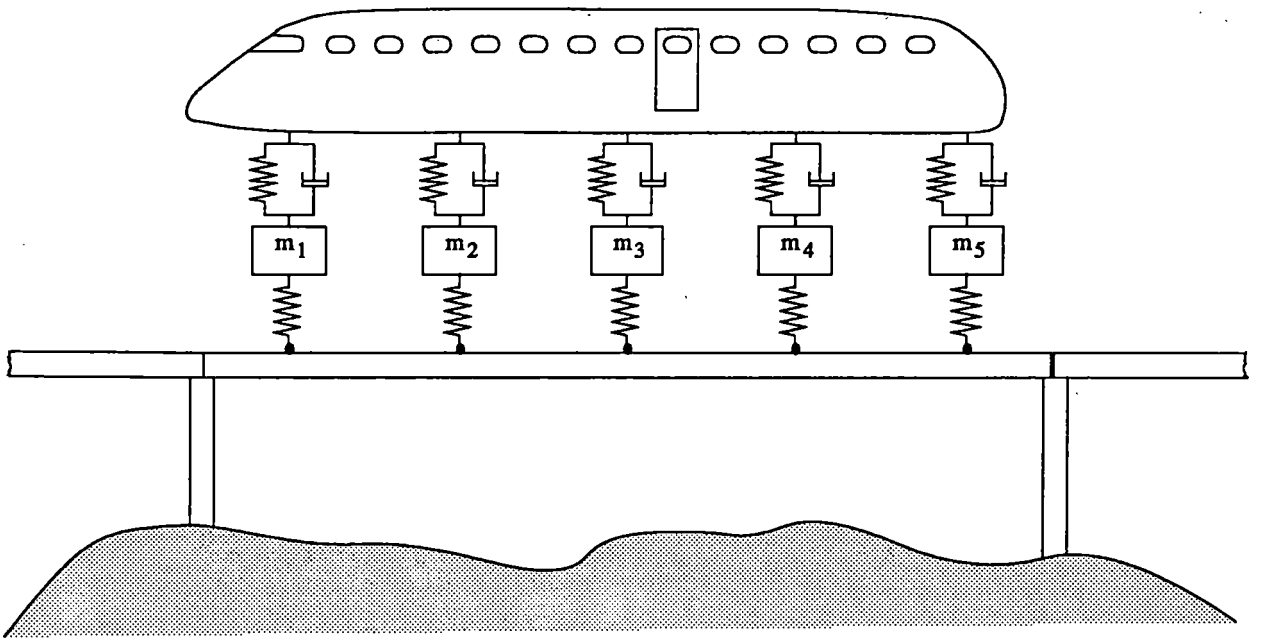

Figure C6-9 MIT multi-bogey dynamic model

due to fluctuations and the effects of the destabilizing yaw moments resulting from the aerodynamic forces acting on the vehicle. Importantly, the model contains the capability to implement an optimal active control strategy to minimize passenger accelerations while at the same time consvehicleing vehicle-to-guideway clearance variations within acceptable values. The model is fully described earlier in Section C.6.1.

Many of the existing models simulate guideway roughness and fluctuating wind inputs by driving the system transfer function with a temporal Power Spectral Density function obtained from a guideway roughness spatial PSD and vehicle velocity. The resulting passenger compartment vertical and lateral acceleration PSDs are then used in one of two ways, depending upon whether the performance is being compared with the ISO standards or the Peplar index. In the former case, the output PSD is used to calculate RMS vibration amplitudes in one-third octave wide bands, while in the latter the RMS vibration over the entire applicable frequency range is calculated. The Draper five-degree-of-freedom model (Figure 6-10) uses a somewhat different approach, as described in Section C.6.1

Recent work [6] addresses the dynamic interaction between the vehicle, its suspensions and the guideway structure as the moving vehicle passes over it. While it provides many valuable insights into the effects of these interactions, its generality and consideration of only simple passive

secondary suspensions prevents its use here in making meaningful quantitative assessments of the behavior of the vehicle defined in this concept study. In this study, the assessment of the dynamic guideway interaction effects on passenger accelerations and gap variations was limited to inclusion of the effects of the vehicle passing over the dynamically deflected guideway. This was done by multiplying the transfer function (relating acceleration or gap variation to guideway disturbance magnitude) by the dynamic guideway deflection caused by the passage of the vehicle over the guideway described by Wormley, et al.

6.2.3 Results

As mentioned above, the passenger accelerations and gap variations were calculated for a vehicle speed of 134 m/s, corresponding to the highest speed attained over the ride comfort evaluation zones of the Severe Segment Test route. Passenger accelerations resulting from curve negotiation and cresting and bottoming of hills were not included, since the specified values were guaranteed not to be exceeded by the consvehiclets placed on the simulation; these consvehiclets were the Design Goal values for the results presented here.

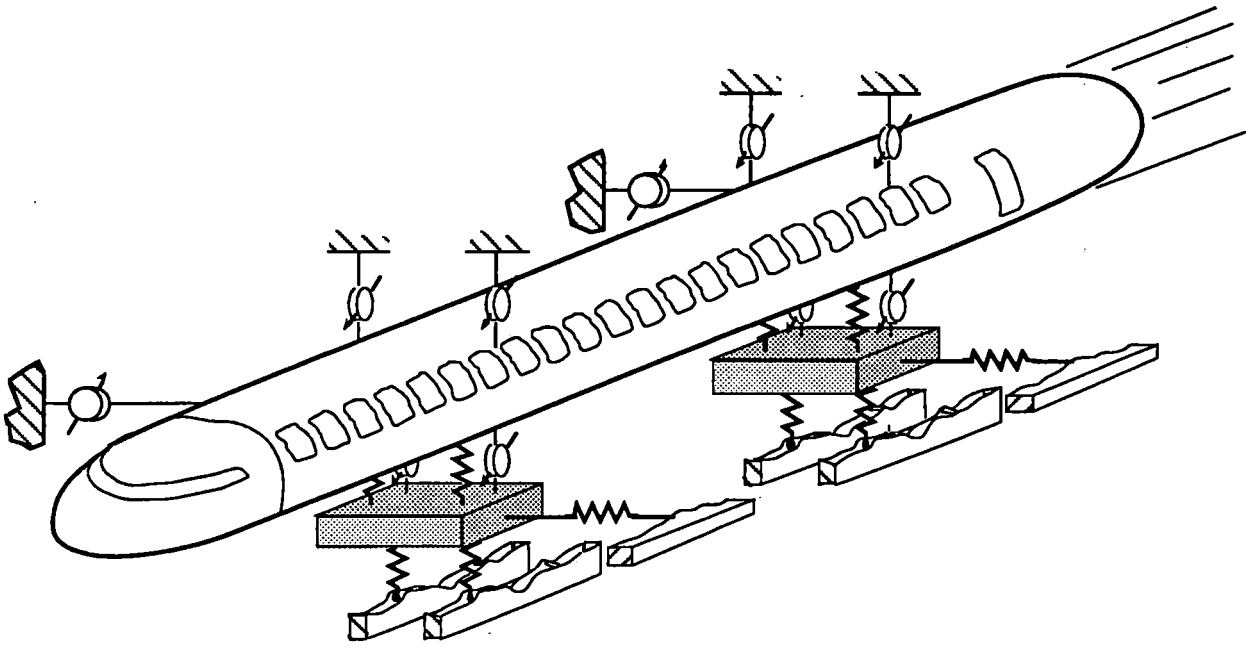

Figure C6-10 Draper 5-degree of freedom dynamic model

Of the many cases analyzed in this study, results from only two are presented here: these are for an optimized passive secondary suspension system and for the baseline configuration consisting of an active secondary suspension system with optimal controller and horizontal aerodynamic control surfaces. The data presented are for the vehicle location with the highest values; generally, this is at the front of the vehicle, while the values in the rear are smaller than in the front and values in the center of the vehicle are lowest of all. For a two-bogey vehicle, Wormley, et al [3 and 6] have shown that the vertical passenger accelerations and air gap variations are generally higher in the front of the vehicle than in the rear; their results show that for a six-bogey vehicle the accelerations are lower overall than for the two-bogie vehicle and are slightly larger in the rear than in the front, with lowest values also in the center of the vehicle.

6.2.3.1 Passive Secondary Suspension

Table C6-1 shows the Pepler index and passenger compartment accelerations in both the vertical and lateral directions which result from guideway roughness, interaction with the guideway dynamic deflection (vertical only), and wind fluctuations for the baseline vehicle with an optimized passive secondary suspension.

Table C6-1
Passenger Accelerations, Passive Secondary Suspension

Speed	Guideway Roughness		Wind Fluctuations		G/W Interac	Total			Pepler Index
	Vertical	Lateral	Vertical	Lateral	Vertical	Vertical	Lateral	Roll	
(m/s)	(g)	(g)	(g)	(g)	(g)	(g)	(g)	(°/s)	
134	0.0658	0.0673	0.1126	0.0336	0.0006	0.1304	0.0752	2.12	5.56
90	0.0438	0.0408	0.0827	0.0324	0.0008	0.0936	0.0521	1.66	4.31

Note that the Pepler index values are quite high, in the somewhat uncomfortable range of 5 to 6 for the maximum speed of 134 meters/second. Even at the lower speed of 90 meters/second the ride quality is in the neutral range between 4 and 5. As can be seen from the table, the major contributors to the poor ride quality are the large vertical acceleration due to the wind fluctuation input and, to a lesser extent, the large roll rate. Throughout the results reported here, it will be noted that there are substantial vertical responses from the horizontal winds. This is a result of the location of the effective point of application of the wind forces, which is somewhat above the primary suspension and fairly near the front of the vehicle so that horizontal wind forces produce

roll moments which must be reacted by the vertical suspension. A further aerodynamic contributor to large accelerations at the front of the vehicle is the yaw moment which results when the relative wind (vector sum of the mean crosswind and vehicle velocity) is not parallel to the longitudinal axis of the vehicle. The magnitude of this yaw moment increases with increasing yaw angle and has the effect of a negative (unstable) spring stiffness for yaw motions which has the undesirable effect of increasing the yaw responses to applied forces.

Figure C6-11 depicts the horizontal (lateral) accelerations at the front, center, and rear of the vehicle in comparison to the ISO one hour reduced comfort profile. The accelerations at the front and rear of the vehicle are noticeably above the ISO profile and the center not very much below it. The effect of the aerodynamic effects to increase accelerations at the front are clearly evident.

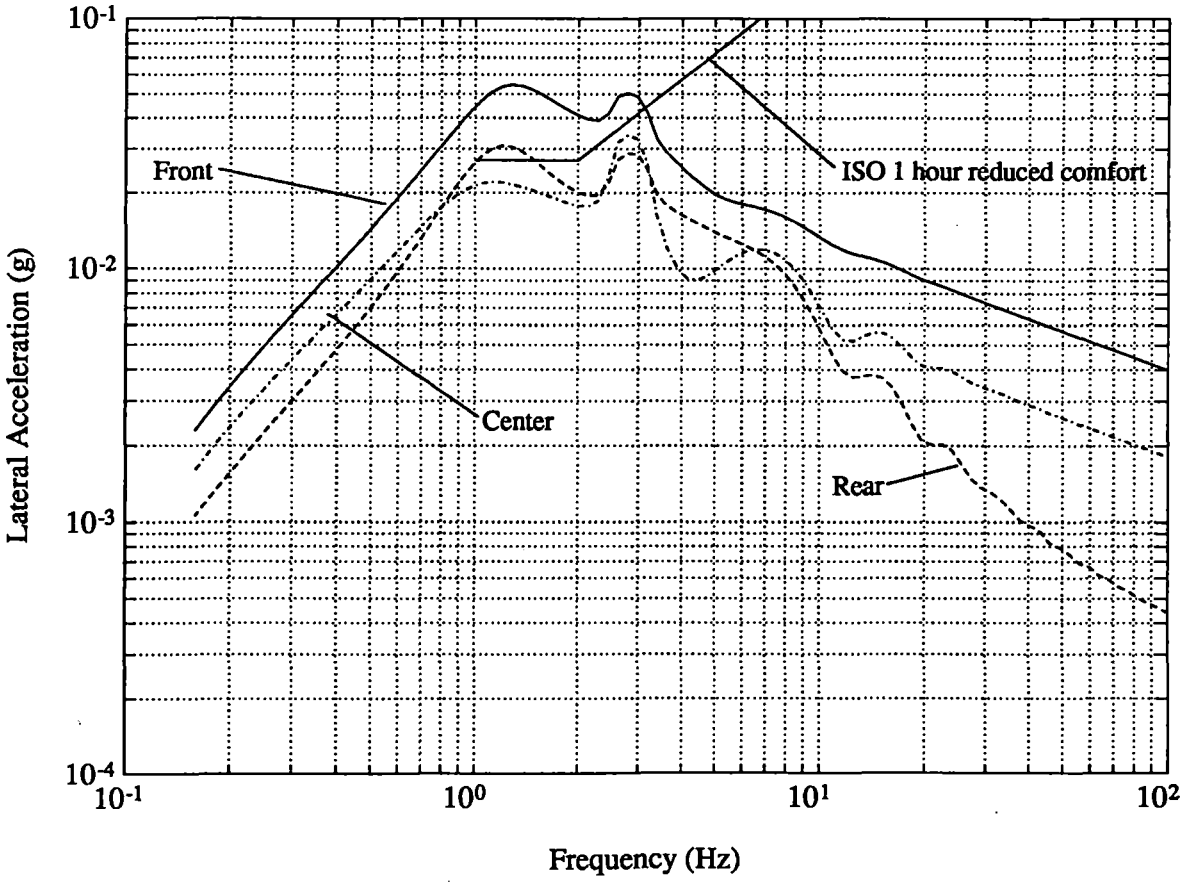

Figure C6-11 Lateral accelerations, optimized passive secondary suspension

Figure C6-12 shows the vertical accelerations at the front, center and rear of the vehicle in comparison to the ISO one hour reduced comfort profile. The accelerations at all locations in the vehicle are slightly above the ISO profile and the effect of the aerodynamic effects in increasing accelerations at the front of the vehicle are not nearly as pronounced as for the lateral direction.

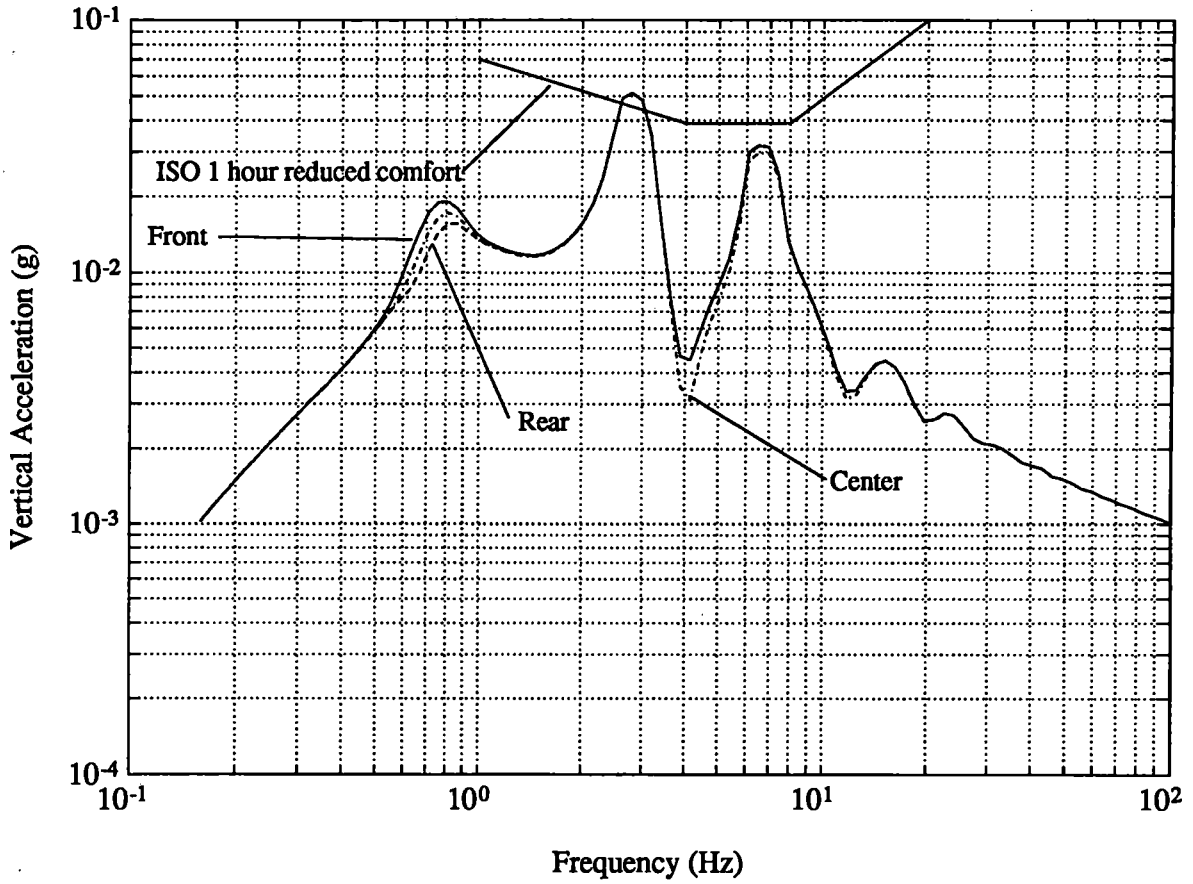

Figure C6-12 Vertical accelerations, optimized passive secondary suspension

Table C6-2 shows the maximum air gap variations resulting from guideway roughness, steady wind and fluctuating wind components, and centrifugal force due to curve negotiation for the optimized passive secondary suspension. Values for the four most severe conditions occurring in the four ride comfort evaluation zones of the Severe Segment Test Route are shown. Although only the maximum values calculated are included, it is noted that the largest values for all but centrifugal force occur at the front suspension bogie of the vehicle. Note that the RMS variations and steady wind values are those calculated for 90 meters/second and are thus somewhat conservative. The last two columns show the maximum expected gap variations expressed as a fraction of the nominal suspension physical gaps (0.1 meter for the vertical suspension and 0.05 meters for the lateral suspension). These totals include five times the standard deviation (RMS for

a Gaussian distribution) of the variations due to guideway roughness and wind fluctuations; the probability of exceeding 5σ is 2.87×10^{-7}. It can be seen that, in spite of penalizing poor ride comfort in the optimization, the air gap variations are unsatisfactory in the lateral direction, although for the vertical primary suspension they are quite satisfactory. Various factors, discussed in the conclusions, render the predicted gap variations quite pessimistic and the indicated variations may not, in fact, be unacceptable. Also discussed later are simple vehicle design modifications which can minimize, or eliminate, the previously mentioned deleterious aerodynamic effects, and this could make even these pessimistic predictions acceptable.

Table C6-2 Gap Variations, Passive Secondary Suspension

Speed	Curve Radius	Centrifugal Force		RMS Roughness & Wind Variation		Dyn. G/W Interac	DC Wind		Total, w/5s wind& roughness	
		Vertical	Lateral	Vertical	Lateral	Vertical	Vertical	Lateral	Vertical	Lateral
(m/s)	(m)	(m)	(m)	(m)	(m)	(m)	(m)	(m)	(% gap)	(% gap)
65	800	.0084	.0122	.0052	.0095	.0011	.0017	.0060	36%	131%
72	1,000	.0084	.0122	.0052	.0095	.0011	.0017	.0060	36%	131%
129	•	.0000	.0000	.0065	.0124	.0006	.0021	.0083	35%	141%
134	8,000	.0004	.0000	.0065	.0124	.0006	.0021	.0083	35%	141%

6.2.3.2 Fully Active Secondary Suspension With Aerodynamic Control Surfaces

Table C6-3 shows the Pepler index and passenger compartment accelerations in both the vertical and lateral directions which result from guideway roughness, interaction with the guideway dynamic deflection (vertical only), and wind fluctuations for the baseline configuration consisting of fully active secondary suspension with optimal controller and aerodynamic control surfaces. The benefits to ride comfort of this configuration, as compared to the passive secondary suspension, are dramatically evident; the value of the Pepler index is reduced from 5.56 to 1.88 at 134 meters/second, and is now in the very comfortable to comfortable range. At 90 meters/second, the ride comfort is slightly better still. (It should be remembered that the Pepler index is 1.0 for zero accelerations, zero roll rate and noise below 65 db(A)).

Table C6-3 Passenger Accelerations, Active Secondary Suspension with Aerodynamic Control Surfaces

Speed	Guideway Roughness		Wind Fluctuations		G/W Interac	Total			Pepler Index
	vertical	lateral	vertical	lateral	vertical	vertical	lateral	Roll	
(m/s)	(g)	(g)	(g)	(g)	(g)	(g)	(g)	(°/s)	
134	0.0185	0.0439	0.0272	0.0492	0.0013	0.0292	0.0659	0.55	1.88
90	0.0154	0.0078	0.0187	0.0050	0.0013	0.0242	0.0093	0.45	1.79

Figure C6-13 depicts the horizontal (lateral) accelerations at the front, center, and rear of the vehicle in comparison to the ISO one-hour reduced comfort profile. In contrast to the passive secondary suspension, the accelerations at all locations in the vehicle are noticeably below the ISO one-hour reduced comfort profile, indicating a very comfortable ride by that standard. The action of the aerodynamic effects to increase accelerations at the front are still clearly evident.

Figure C6-14 shows the vertical accelerations at the front, center, and rear of the vehicle in comparison to the ISO one-hour reduced comfort profile. The accelerations at all locations in the vehicle are more than an order of magnitude below the ISO profile indicating, like the lateral plot, a very comfortable ride by the ISO standards as well as by the Pepler index. In this case, the influence of the aerodynamic effects in increasing accelerations at the front of the vehicle is barely perceptible. The contribution to vertical acceleration of the disturbance resulting from the dynamic guideway deformation due to the passage of the vehicle is not included in the ISO plot; it is sufficiently small in magnitude that its effect would be barely perceptible on the plot.

The motion sickness limits in the region of 0.1 to 1.0 Hz, added to the ISO one-hour reduced comfort standard by the contract modification, are not shown on this plot. It is obvious, however, that the vertical accelerations in that frequency range are more than an order of magnitude below the minimum value ($\approx$0.035 g at $\approx$0.2 Hz) of that added segment.

Table C6-4 shows the vertical and lateral air gap variations which result from guideway roughness, steady wind, and wind fluctuations for the baseline configuration consisting of active secondary suspension with optimal controller and aerodynamic control surfaces. These results indicate that, in spite of the dramatically improved ride comfort provided by the active secondary suspension and aerodynamic control surfaces, the air gap variations are not significantly improved from the

passive suspension case. A major reason for this is that the aerodynamic control surfaces cannot provide any lateral forces with which to reduce the lateral air gap variations, while the concentration of the lateral wind force at the front of the vehicle and the effect of the unstable aerodynamic yaw moment cannot be adequately counteracted by trading off increased lateral acceleration (i.e., reduced ride comfort) for reduced gap variations. It is again emphasized that the projections presented here, as in the case of the passive suspension, are very conservative and this predicted worst case lateral air gap variation of ≈140 percent may not, in fact, be unacceptable. This point is further discussed in the summary.

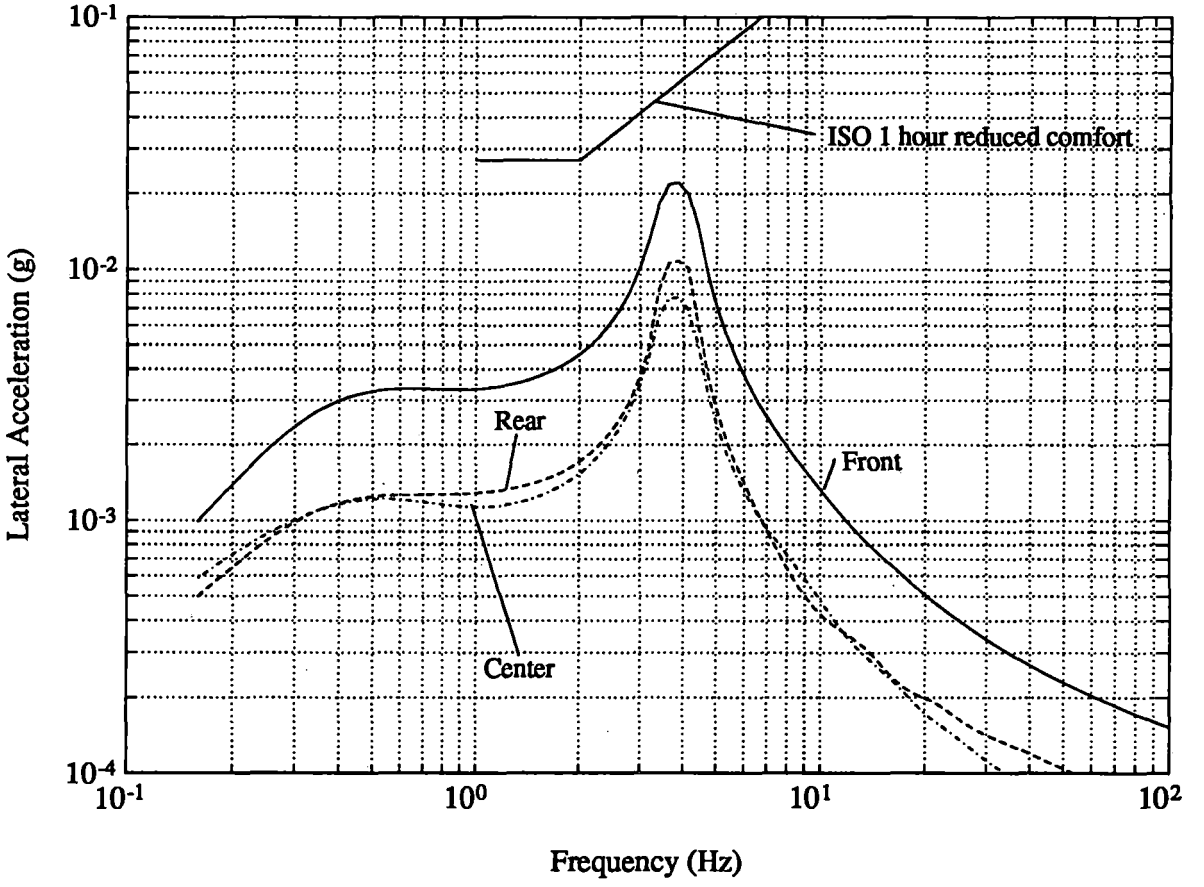

Figure C6-13 Lateral accelerations, active secondary suspension with aerodynamic actuators

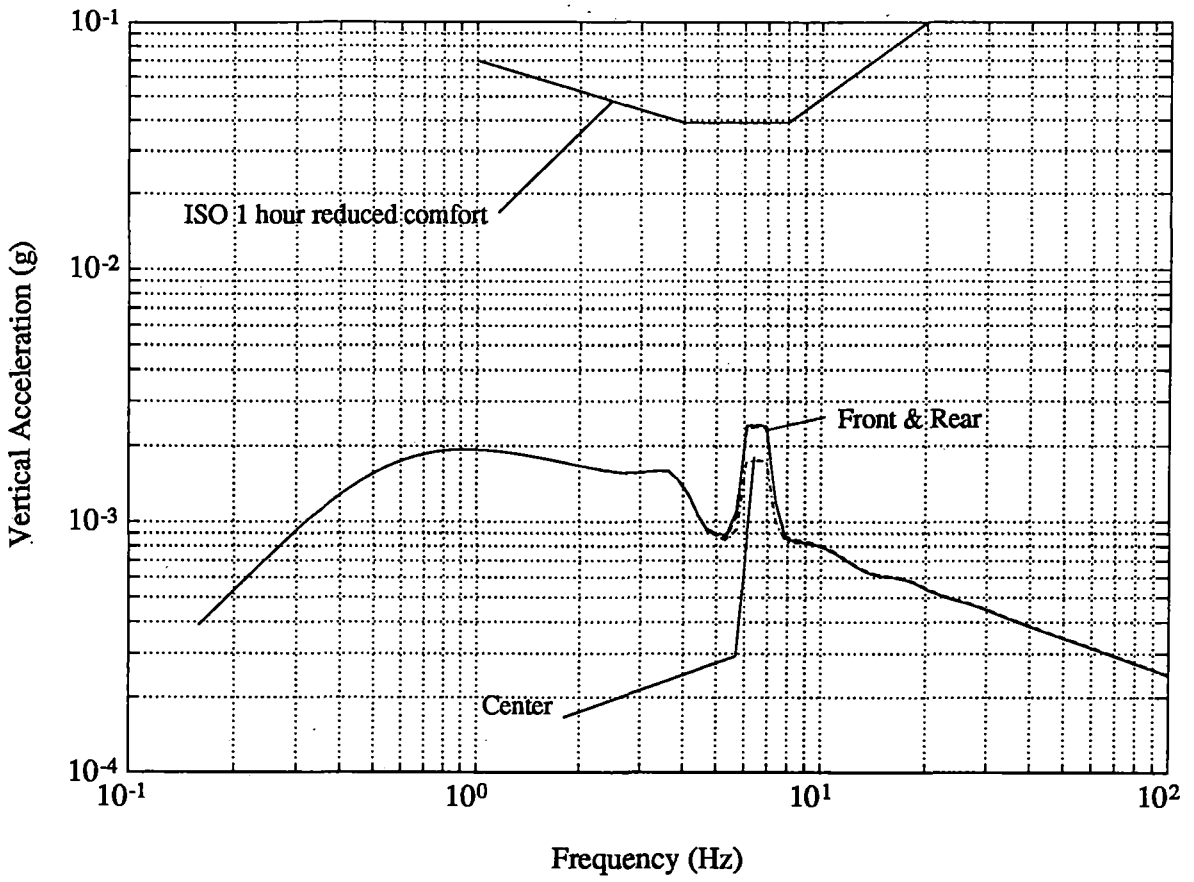

Figure C6-14 Vertical accelerations, active secondary suspension with aerodynamic actuators

Table C6-4
Gap Variations, Active Secondary Suspension with Aerodynamic Control Surfaces

Speed	Curve Radius	Centrifugal Force		RMS Roughness & Wind Variation		Dyn. G/W Interac	DC Wind		Total, w/5s wind& roughness	
		Vertical	Lateral	Vertical	Lateral	Vertical	Vertical	Lateral	Vertical	Lateral
(m/s)	(m)	(m)	(m)	(m)	(m)	(m)	(m)	(m)	(% gap)	(% gap)
65	800	.0084	.0122	.0132	.0096	.0058	.0017	.0060	79%	132%
72	1,000	.0084	.0122	.0132	.0096	.0058	.0017	.0060	79%	132%
129	•	.0000	.0000	.0127	.0122	.0063	.0021	.0083	69%	139%
134	8,000	.0004	.0000	.0127	.0122	.0063	.0021	.0083	70%	139%

6.2.4 Summary

These results have shown that the baseline vehicle concept should be capable of providing a very comfortable ride to passengers. To achieve this comfortable ride required the use of a fully active secondary suspension with an optimal controller and aerodynamic control surfaces, because the optimized passive secondary suspension could not provide an acceptable comfortable ride quality.

Although the results indicate substantial likelihood of guideway-suspension contact, a number of considerations strongly suggest that this is not likely to be a problem in an actual vehicle of this design. These considerations are described in the following paragraphs:

First, the primary suspension was assumed to be strictly linear; in fact, the suspension forces increase more rapidly with larger displacements, tending to reduce the maximum air gap variations, compared with those predicted using the linear assumption.

Second, the active controller was assumed to be perfectly linear, without any provision for applying more control effort when the primary suspension approached contact with the guideway. If necessary, such provisions could be made, further reducing the probability of contact.

Third, the baseline system configuration envisions post-installation alignment of the guideway suspension components to a tolerance of approximately ±0.5mm. If this were implemented, the magnitude of the guideway roughness with spatial wavelengths of between 0.33 meters and 25 meters (1 span length) could be reduced below that of the assumed welded steel rail values. This would reduce the vehicle excitation by the guideway in this bandwidth, reducing both the passenger accelerations and air gap variations (note, however, that this alone may not provide adequate relief since, in the lateral direction at 134 meters/second, the contribution of wind variations to gap variation is more than twice that of the guideway roughness).

Fourth, the baseline vehicle has six primary suspension bogies, whereas the five-degree-of-freedom model which provided the performance estimates has two bogies. Wormley, et al [3, 6] have shown that, for the range of parameter values they studied, a six-bogie vehicle exhibits lower passenger accelerations with smaller air gap variations than a two-bogie vehicle. In the case of guideway roughness excitations, the RMS accelerations at front and rear of a six-bogie vehicle were from 35 to 45 percent of those of a comparable two bogie vehicle. In the case of vehicle motions resulting from dynamic vehicle-guideway interactions, the air gap variations of a six-bogie vehicle were ≈55 percent of those of a two-bogie vehicle for a span crossing frequency ratio

of 0.75 (134 meters/second for our vehicle) and ≈80 percent for a span crossing frequency ratio of 0.4 (90 meters/second for our vehicle). Passenger accelerations for a six-bogie vehicle were 25 to 30 percent of those for a two-bogie vehicle at a crossing frequency ratio of 0.75 and 40 to 70 percent for a crossing frequency ratio of 0.4.

Fifth, it was assumed in the five-degree-of-freedom dynamic model that the damping in the primary suspension is zero; this is the assumption commonly made for electrodynamic suspensions and is undoubtedly reasonable for image flux configurations such as Magneplane. However, it appears that this assumption may not be strictly correct for the suspension configuration used in our concept, and approximate calculations have been made which indicate the possibility of significant damping. Further work will be required to accurately quantify the level of damping present, but it is clear that even a small amount of damping can substantially decrease the passenger accelerations and air gap variations resulting from guideway roughness and probably from wind fluctuations as well. Figure C6-15 shows the substantial improvement a small amount of damping produces in the vertical accelerations and air gap variations caused by guideway roughness; the data is from the Draper simple heave model shown in Figure C6-8 having a 1 Hz, ζ_s=0.25 passive secondary suspension with other parameters corresponding to our baseline vehicle concept.

Finally, it was mentioned earlier that the concentration of the aerodynamic force from crosswinds at the front of the vehicle and the unstable yaw moment due to aerodynamic forces both result in larger passenger accelerations and primary suspension air gap variations at the front of the vehicle than would otherwise be the case. As a result, although excellent ride comfort is available from the baseline vehicle with active secondary suspension, the air gap variations calculated at the front of the vehicle are larger than would be desirable. Both of these deleterious effects can be very substantially reduced, or perhaps even eliminated, by the simple addition of a vertical aerodynamic surface at the rear of the vehicle to bring the center of pressure nearer to the center of the vehicle (note that the baseline vehicle already has actively controlled horizontal aerodynamic surfaces at both the front and rear). Still further improvement in the air gap variation/passenger acceleration tradeoff can be obtained by actively controlling such a vertical surface. This can be very advantageous because the forces required to decrease passenger accelerations can then be applied directly to the vehicle where they are most effective. By contrast, with a hydraulic actuator in an active secondary suspension, these forces are accompanied by equal and opposite forces on the bogey which tends to increase the air gap variations. Moreover, to the extent permitted by available control force capability, the aero actuator forces can be made to counteract hydraulic actuator forces intended to reduce gap variations so that, overall, increased passenger accelerations

are not traded for reduction of gap variations. This simple design addition can potentially, in itself, reduce the lateral air gap variations to a satisfactory level while retaining the excellent ride comfort provided by the baseline vehicle concept.

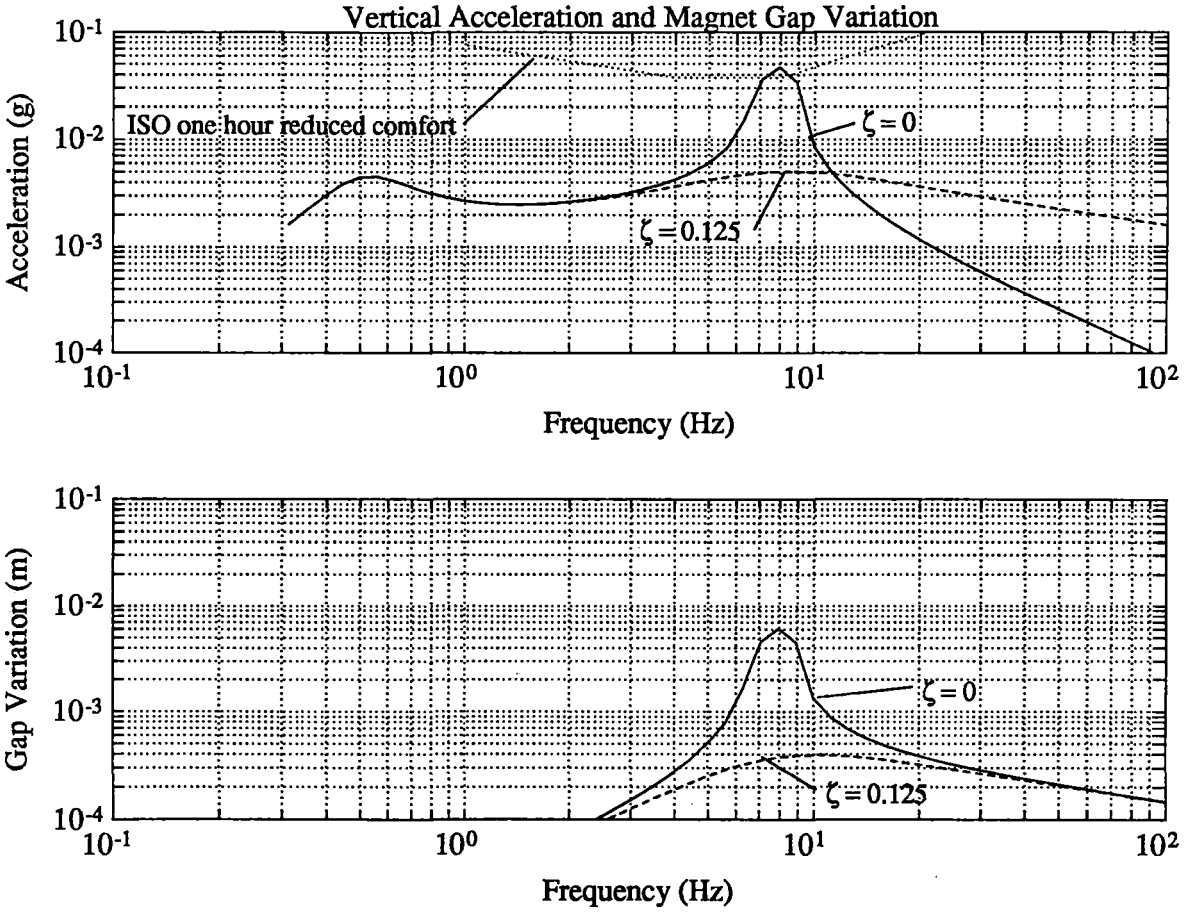

Figure C6-15 Vertical accelerations and air gap variations Draper simple heave model with passive secondary suspension

REFERENCES

1. Peplar, R.D., et al, "Development of Techniques and Data for Evaluating Ride Quality, Vol. II: Ride Quality Research," Report No. DOT-TSC-RSPD-77-1, II.

2. "Guide for the Evaluation of Human Exposure to Wholebody Vibration," ISO Standard 2631/1 International Organization for Standardization, 1985.

3. "Magnetic Levitation Vehicle-Suspension Guideway Interaction," D. N. Wormley, R. D. Thornton, S. H. Yu, and S. Cheng, Technical Memorandum No. TBD, Center for Transportation Studies, Massachusetts Institute of Technology, January, 1992.

4. "Final Report, Comparison of Major Parameters in Electrodynamic and Electromagnetic Levitation Transportation Systems," (Maglev BAA #24), S. Brown, C. R. Dauwalter, F. Heger and M. Weinberg, Report R-2420, Charles S. Draper Laboratory, Inc., July, 1992.

5. "Title TBD," D. C. McCallum, et al, Report C-TBD, Charles S. Draper Laboratory, Inc., TBD, 1992.

6. "Interactions Between Magnetically Levitated Vehicles and Elevated Guideway Structures," D. N. Wormley, R. D. Thornton, S.-H. Yu and S. Cheng, Draft Final Report (Maglev BAA #204), Center for Transportation Studies, Massachusetts Institute of Technology, July, 1992.

7. SYSTEM RELIABILITY ISSUES

7.1 INTRODUCTION

Beyond technical feasibility, any maglev concept must be safe, environmentally sensitive, cost effective, and reliable. Safety is discussed in greater detail in Part J; environmental issues in Part H; and cost issues are examined in Parts K and L (Part L being dedicated to system development considerations and costs in the "external benefits" sense). System reliability is examined here with special consideration given to quantifiable measures of reliability where possible.

There is a key distinction between safety and reliability. Reliability is the probability of successfully completing a mission without mishap; in this case, it means getting from origin to destination. Safety is the probability of successfully completing a mission without mishap, but it also allows for a failure as long as safety is maintained.

7.2 KEY REQUIREMENTS

The maglev system must meet or exceed the reliability of current transportation technologies if it is to gain widespread public acceptance. Specifically, the maglev must provide improved reliability when compared to current short and medium haul aircraft operations. To measure this reliability, we have selected an overall reliability value of 10^{-6} per hour; i.e., deviations from perfect operation in terms of ability to complete a trip from one identified point to another must not exceed one failure in a million for every hour of operation. By contrast, system safety requirements call for an upper bound of 10^{-9} per hour.

7.3 APPROACH USED

The overall system reliability is comprised of numerous possible failure points, each having a quantifiable probability of occurring. The discussion below identifies some of the key areas where system reliability may be affected and assigns upper bounds on the probability of these events occuring. In most cases these values are either derived from design characteristics or assigned to indicate areas where design must be focused on minimizing failures. The overall reliability of the system is a mathematical combination of the relevant probabilities: where one probability is contingent upon another, the final probability is the product of its constituents; where they are mutually unrelated, the final probability is the greatest of all the possible values.

7.4 DESCRIPTION

In developing a rational set of reliability requirements for a maglev architecture we assumed 200 passengers per vehicle (average assuming some mix of single vehicle and multi-vehicle consist dispatching, as distinct from our baseline concept of single vehicle operation), and an average between 2,000 and 6,000 passengers per direction (one-half of peak) over the 24-hour period. This results in a total of 4,000 to 12,000 trips per day for the entire region.

Using as a guideline the basic assumptions in the data for the the Hypothetical Route, we assumed the region covered by the maglev system would be approximately (for this analysis) 800 kilometers in length. Further assuming a 5-kilometer average guideway zone, the 800-kilometer system there would comprise a total of 320 zones, or 160 in each of two directions of travel. The average trip time between stations is assumed to be one hour. Using these assumptions as a baseline, preliminary reliability figures of merit have been tentatively assigned for several of the top level design elements.

****

NOTATION: For visual clarity in discussing assigned probabilities that closely approach 1.0, the following notation is adopted:

.999 is indicated by .9(3)

.9999 is indicated by .9(4)

.99934 is indicated by .9(3)34

etc.

****

Vehicle Allocations

The probability that a vehicle is dispatch-ready at the completion of a trip, given that it began the trip with a full complement of operational equipment. >.9(3)

A .9(3) probability of being dispatch-ready indicates that the typical vehicle will fail to be dispatch-ready approximately once in every 1,000 trips. This is an order of magnitude better than current airline experience, but is expected to be achievable with a mature maglev design.

The probability that a vehicle will arrive at its destination station without delays due to vehicle component failure, given that it was dispatch-ready at the start of the journey.	> .9(5)

A total of 4,000 to 12,000 trips are expected to occur daily within the region. A probability of .9(5) allows one of every 100,000 trips to experience a delay due to higher than normal levels of vehicle failures. A delayed trip may occur somewhere within the region once every 8 to 25 days.

The probability that a vehicle will achieve its destination without stopping on the guideway between stations due to vehicle equipment failures.	>.9(7)

One vehicle will become stuck on the guideway due to catastrophic vehicle failures once in every ten million journeys. The fleet assigned to the region may experience a vehicle caused guideway blockage once every 2.3 to 6.9 years.

Zone Allocations

A zone consists of a section of guideway, its associated power distribution and power conversion equipment, and a zone controller which provides the wayside processing for the zone and controls the power equipment, causing it to supply the guideway windings with appropriate levels of power for the desired vehicle speed. The zone provides six-phase power to drive the vehicle. Two independent (but synchronized) three-phase power conversions are supplied to the windings. As a result, the zone has two modes of operation: full power mode and half power mode. Vehicle operation at half power implies normal operations at reduced speed (about 10-15 percent less than full power speed). Full power mode, by definition, includes the ability to perform half power mode if desired or necessary. If the substation providing power to the zone fails, the vehicle can maintain levitation using power from the inverter station batteries as it coasts through the zone.

Many of the maglev zones are in areas distant from the passenger or maintenance stations and their associated repair facilities. As a result, an average repair time of four hours has been assumed in the allocations which follow.

Full Power Inherent Availability	>.9(4)
Half Power Inherent Availability	>.9(4)33

This results in an inability to supply full power operation once every 40,000 hours, or 4.5 years. A complete loss of capability would be allowed to occur once every 60,000 hours or 6.8 years.

Station Allocations

The vehicle stations provide physical facilities for the vehicles and passengers along with processing to support vehicle control and to provide needed passenger-related information. Facility construction is expected to follow best current practice for public facilities in the region in which the system is installed so the probability of structural failures at stations is considered negligible. If stations are unavailable for some reason, they can be bypassed because loading and unloading areas will be off-line. Therefore, stations cannot by themselves affect overall measures of system reliability except for those trips originating or completing at the given station. The processing functions supplied by each station must be capable of providing continuous operation, covering for adjacent stations if necessary, with infrequent outages. Since maintenance personnel are expected to be resident at each station location, a 1-hour repair time is assumed in the allocations given below.

Vehicle Control Function Availability	>.9(5)	(1)
Passenger Information Function Availability	>.9(4)	(2)

1. Loss of station provided vehicle control functions that do not cause a safety hazard but may affect overall reliability. Vehicle control functions in the vehicle and wayside zone can safely compensate for functionality loss.

2. Ticketing, arrival and departure displays, etc.; these do not directly affect system reliability, but may directly influence the passengers' perception of the reliability.

Thus, nuisance interruptions of passenger information functions are allowed to occur once every year. Interruption of vehicle control function, thus loss of station usability is limited to no more often than once every 11.4 years.

While the control system is specifically designed to prevent entry of vehicles except within designated clear slots (if a vehicle misses its assigned slot it must wait for the next available slot),

there is a non-zero chance that a vehicle could arrive into the system unscheduled. However, the probability of this happening is considered negligible.

Central Control Allocations

The Central Control facility provides centralized traffic scheduling and control along with a variety of services which impact all the stations. In order to establish reliability requirements for Central Control, specific service levels associated with the availability requirements must be defined. For the regional control, three levels or modes of operations are defined. In increasing order of level of service, they are: emergency mode processing, degraded mode processing, and full-service processing.

For allocation purposes, emergency mode processing is defined to include all the central control processing needed to ensure automated vehicle separation and headway control. Loss of this processing will not cause a safety incident to occur. However, control of the movement of vehicles will be assumed to be the station controllers with some reduction in the frequency of movements. Additionally, the computer center system operator's functional capability is defined as a part of emergency mode processing. This functionality will be needed to allow recovery to higher modes of operation.

Degraded service mode consists of the emergency mode processing plus all processing associated with health and status monitoring of vehicles, zone controllers, and stations. The maglev system operator's displays and control processing are also a part of degraded mode operations.

Full service mode processing consists of all degraded mode processing functions plus all scheduling functions. The scheduling functions include traffic schedule preparation and updating, all ticketing and reservation functions, and maintenance tracking.

The following availabilities are defined for each mode:

Emergency Mode Processing	> .9(6)
Degraded Mode Processing	> .9(5)
Full Service Mode Processing	> .9(4)5

If we consider a 4-hour repair as typical for the facility, these availabilities allow nuisance interruption of passenger services such as ticketing once every 80,000 hours or 9 years. Processing, which supports operations monitoring of all system activity, is constrained to fail no more often than once every 400,000 hours or 45.6 years on the average. Loss of vehicle separation services with subsequent regional shutdown is constrained to occur no more often than once every 4 million hours on the average. Shutdown of a central control facility due to equipment failure is effectively prohibited throughout the life span of the central facility.

Communications Allocations

Communications links are essential to the ongoing performance of the maglev command and control design. Loss of any individual communications link will not cause a loss of system functionality for our concept definition. However, outages of multiple communications links can cause unplanned system outages. Thus, the reliability of the individual communications links must be high to ensure that the probability of failures in multiple, independent links, is acceptably remote.

Communications Availability (per link) > .9(4)

7.5 BENEFITS/RISKS SUMMARY

Allocation of reliability requirements to individual architectural elements allows the design of specific, detailed architectures for the various system elements to proceed. Requiring reliabilities which are high enough to ensure system acceptance without becoming so difficult that high risk and high cost approaches are needed ensures that a robust design can be achieved with an acceptable level of risk.

8. HUMAN FACTORS

The Human Factors Engineering Program is directed toward a safe, effective equipment and software user-system interface design. The human engineering objectives are: to ensure passenger comfort and safety; simplify operator and maintainer tasks; ensure operator effectiveness; and enhance operator and maintainer performance through efficient display, control, and software analysis and design. Working continually toward these objectives will ensure maximum system effectiveness.

The Human Engineering (HE) Program approach ensures the integration of human performance skill consideration and design constraints, according to the criteria of MIL-STD-1472D and the criteria determined by the Safety Research Division of the Association of American Railroads, into the design and development of the maglev equipment, software, procedures, and documentation as well as into the design of the maglev initiative architecture. The HE program that is an integral part of the C3 system design, permitting the early analysis and identification of operator and maintainer system interface requirements, that will be followed by a comprehensive series of analytic studies, design efforts, and tests.

The details of the HE program approach will be presented in the Human Factors Program Plan (HFPP). The HFPP will describe the approach used in conformance with MIL-STD-1472D, RFP DTFR53-91-R-00021 and will identify compliance with HF specifications and contractual requirements. The HFPP will describe, at a minimum: (1) organization of the HF effort as an integral part of the system engineering, mechanical engineering, and design efforts, (2) HF development of operator/maintainer task and skill analysis, integrating data with the hardware and software personnel assigned, the development of supporting rationale identifying functional and operator/system requirements affecting design decisions and the conduct of workload analysis, (3) HF participation in verification and evaluation of maglev hardware and software to verify that human/system requirements meet DTFR53-91-R-00021 and the HFPP, and (4) HF participation in the system engineering, safety, and test efforts to define operator/user performance.

Three major activities characterize the human engineering program; analysis, design, and test and evaluation. Figure C8-1 shows the Human Factors Engineering Program process. This phase of the maglev effort concentrates on the effort leading to a complete system analysis. A thorough HF program will contain the following elements:

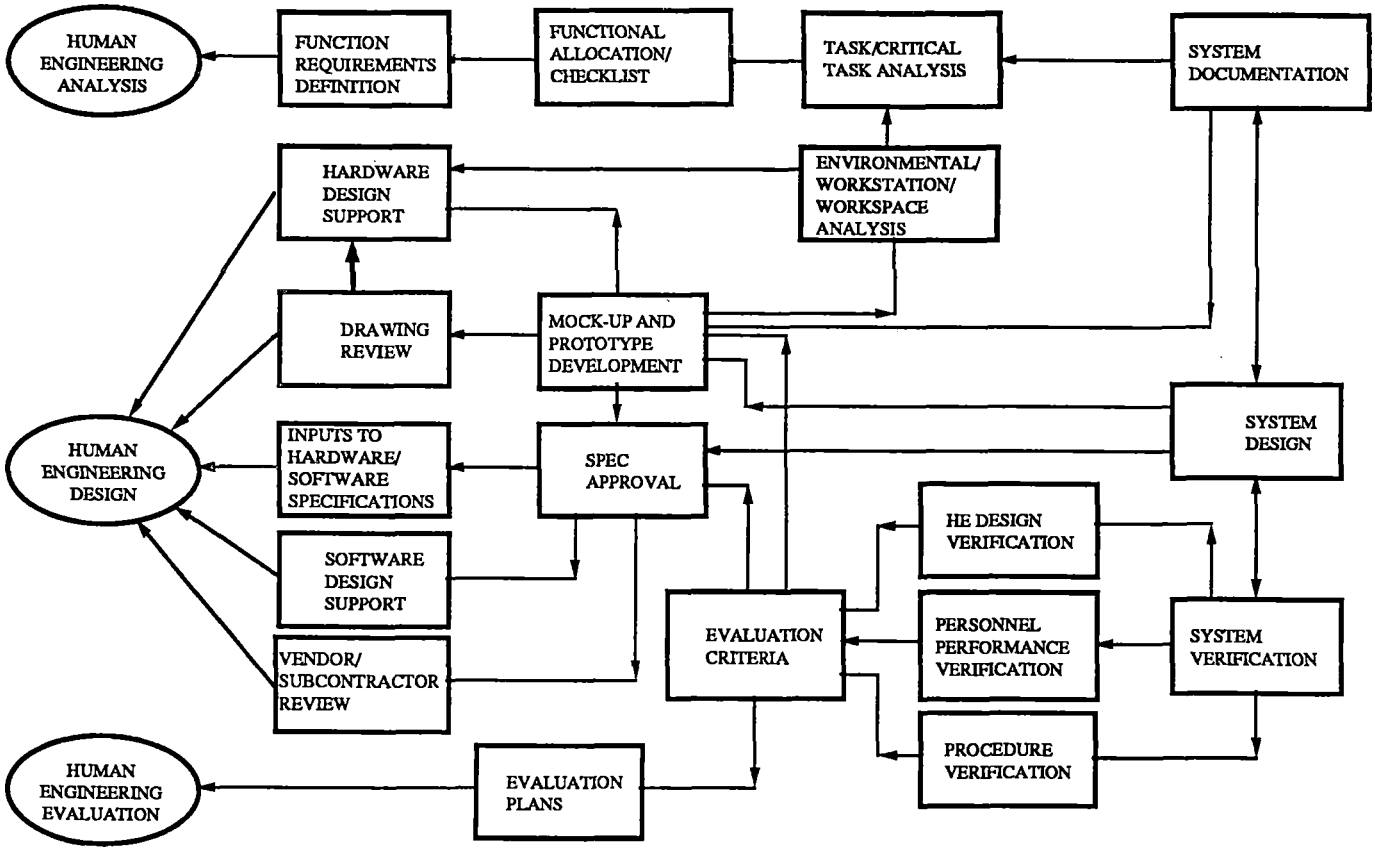

Figure C8-1 Human engineering design process for the maglev system

Human Engineering Analysis: HE analysis of system and operator functions leads to the identification of critical tasks and to workload analysis. The early analysis, provided by prior work efforts in the human performance and design contributions to C3 and ATC programs, will provide insight into operator/attendant factors within the train cab as well as within command and control facilities. To further define operator and display/auditory control requirements for an effective man-machine interface, the human factors analysis conducted and implemented for air traffic control systems are being used as a base. ATC systems utilize color displays for command and control and require extensive computer/human interface analysis and design. Data available from the Society of Automotive Engineers and the University of Michigan Transportation Institute provide guidelines for passenger seating and comfort. Further refinement will involve the development of operator and passenger scenarios that will allow the conduct of a function analysis. Areas for functional investigation include: scheduling system, location system, planning system, passenger loading and offloading systems, crisis management system. Operator functional allocation will be documented to show the flow of information and events from the initial start-up identification/transmission through each system input and output device, as well as between system controllers. During trade-off and comparative analyses, these data will contribute to an operator/workload evaluation of the maglev design using the Automated Interactive Simulation Model (AISIM) dynamic workload program.

The subsystems for detection, operation, identification and communication tasks will be analyzed to identify critical operator/maintainer tasks. Critical tasks are defined as those that, if performed incorrectly, lead to significant operation performance degradation, cause hazardous situations, cause undue delay in reaction time, result in system failure, exceed maintenance time requirements, cause damage to equipment, cause injury to personnel, or compromise system operation. In addition, human operator requirements and action times will be updated from prior analysis for use in software development and to assess operator and controller workload and display-station layouts. A Critical Task Analysis Listing developed in accordance with the human factors program plan will summate the task analysis effort.

Human Factors Engineering Design: Human engineering design entails the review of all prototypes, drawings, documents, reports, models for compliance with HE standards and system specifications. This activity also ensures subcontractor and supplier compliance with HF and system requirements. This activity is coordinated and integrated with the maglev working group activities. For command, control, and communication facilities as well as for vehicle and station facilities, human engineering guidelines will be used to establish system requirements. Operational and maintainability requirements, including maintenance access to Maglev equipment,

will be reviewed during the development of soft mockups and test bench design of the equipment and coordinated with the system engineering manager. Other prime areas for investigation in the maglev control facilities include rapid menu selection, minimum operator/controller entry, standardization of display segments, standardization of voice and/or tone outputs and easily identified hazard/fault nomenclature. US1 maglev Team's prior experience provides insight to areas of design enhancement such as user-hardware interaction, display formatting, color selection, icon/symbol development and software menu development.

During analysis and design, human factors specialists will support design efforts related to system panel layouts, control panel layouts, equipment arrangements, display formats, auditory alarms/alerts, accessibility, lighting, display legibility, noise limits, and other human factors related to system performance. The objective is to minimize operator or maintainer workloads which, in turn, decrease skill requirements. Human factors specialists, as part of the system engineering functions, participate in design reviews and review all data and drawings that have significant impact on the man-machine interface and environment.

Human factors personnel will provide engineering notebook documentation that will describe the layout, detail design, and arrangement of all maglev equipment with an operator/controller interface. The documentation will also describe operator tasks associated with the equipment and describe the extent to which the human performance requirements, and other applicable human engineering documents specified in the contract have been incorporated into the layout, design, and arrangement of equipment having a user interface. Operator task analysis results will support the improvement features of display selection, formatting, color selection, symbol selection, layout design, and integration of the maglev design into selected test subsystems.

Additionally, a major focus of the design effort of the maglev operator-system interface is to identify those human performance limits that could negatively impact overall system performance. Environmental conditions, such as vibration and noise, can also lead to perceptual limitations. Noise, volume control, and communication interdiction is a current concern featured for analysis during the design phase. The AAR Safety Research Division's Ergonomic Guide, designed to provide background information, evaluation techniques, and control strategies for the railroad operating environment, will provide additional areas for design considerations. Special consideration will be given to the capabilities and limitations of an older population, since the reported average age of railroad employees is 45 years (Human Factors Society Bulletin, March, 1991).

Human Factors Engineering Evaluation: The final effort of the maglev initiative concept study phase of the HF program is HF evaluation to validate the operational procedures or equipments, and to validate design conformance to HE criteria and system requirements. HE evaluations will be performed during design development and during vehicle, guideway, and facility evaluation. To validate effective operator-system interface definition and design, a checklist of functional capabilities is used to help match system interface requirements with the implemented design. The HE evaluation process will verify the achievement of minimum skill requirements, operator effectiveness, and performance for all age groupings.

Based on prior command, control, communication, and vehicle design experience, display development experience, and the requirements of DTFR53-91-R-00021, appropriate human engineering evaluation techniques will be applied to ensure design conformance and compatibility as well as effective hardware and software integration. These techniques include checklists, mockups, and dynamic simulation of the operator-system displays and controls, and design tests, as necessary. Personnel subsystem requirements (such as hardware and interface compliance, symbol legibility, obstructions, access, and layout) have been identified for evaluation. HE verification and evaluation are conducted concurrently with various aspects of systems integration and checkout and/or during maintainability testing in order to minimize redundant effort and cost. The objective, therefore, is to make sure that detailed operations and maintenance of the maglev can be performed effectively, reliably, and safely by a wide range of operators and that hazards are accurately recognized and safely avoided. A Human Factors Engineering Evaluation Report will identify the results and conclusions of the maglev human factors evaluation.

8.1 MOCKUP GUIDELINES FOR DISPLAY AND CONSOLE DESIGN

Computer-assisted design techniques are employed to explore design features and configurations prior to the construction of "soft" mockups. An existing design program, GEOMOD, will be applied to the maglev control workstations and equipment. GEOMOD allows engineers to manipulate individual components of models, assemble them into complete structural systems, and perform interference checking, inertia property calculations, packaging, and kinematics. It offers exceptional human engineering benefits in that human anthropometrics can be presented in working positions at correct-scaled drawings of equipment, and the combination of the operator and equipment can be rotated, or viewed from any desired angle to permit comprehensive evaluation. In this manner, the number of candidate designs committed to soft mockups can be limited to the most promising ones.

During the Human Engineering Program, GEOMOD is planned to be used for the modeling of individual control workstations, station facilities, and vehicle passenger accommodation. The GEOMOD model will be used to evaluate various configurations with respect to viewing envelopes, display parallax, and operator access to communications large screen displays. Figure C8-2 shows human dimensions used for workstation mockups and design.

Soft mockups will be built by human factors engineers to provide three-dimensional full-scale design help in assessing equipment configurations and sizes of human fit. These mockups of the workstations are inexpensive structures that represent accurately the dimensions and configuration of equipment but are not permanent and do not contain functioning control or display hardware. US1 maglev Team uses foamcore sheets for these mockups, cut to accurate sizes and shapes, and joined at seams or edges with hot glue and wood blocking. Keyboards, switch panels, display surfaces, and other control devices are represented in these soft mockups by dummy components, drawings, or photographs. These mockups permit evaluation of change recommendations and multiple designs, layouts and arrangements prior to the selection of a configuration. Soft mockups will be used to aid in the integration of position entry devices (PEDs), keyboards, and operator comfort features into the workstations. Soft mockups of the local and central control worksurfaces, including keyboards, PEDs, and communication controls and displays will be constructed in order to evaluate multiple worksurface layouts with regard to required functionality, allocation of workspace, reach and view envelopes, and operator comfort.

Dynamic simulation is a tool used to evaluate design features affecting human performance. The process permits analysis of the effectiveness of controls (and control panels) requiring complex operation sequences, displays that present large amounts of data in complex formats, and user-computer interactions for complex tasks. The use of the selected hardware and display demonstration equipment will facilitate dynamic simulation of a limited set of task action sequences during program design and development.

The multiple functions performed and the large volume of information that can be generated, exchanged, and maintained at the various control, station, and supervisory positions present a unique problem in human factors design features. The variety of required operator interactions necessitates rapid and accurate access to differing information types to support these specific functions. This can include vehicle time-spacing, number of vehicles active, number of vehicles being maintained, routing information, passengers and baggage quantification, etc. Supervisors may be required to control up to 2 or 3 different way stations and any number of vehicles that may

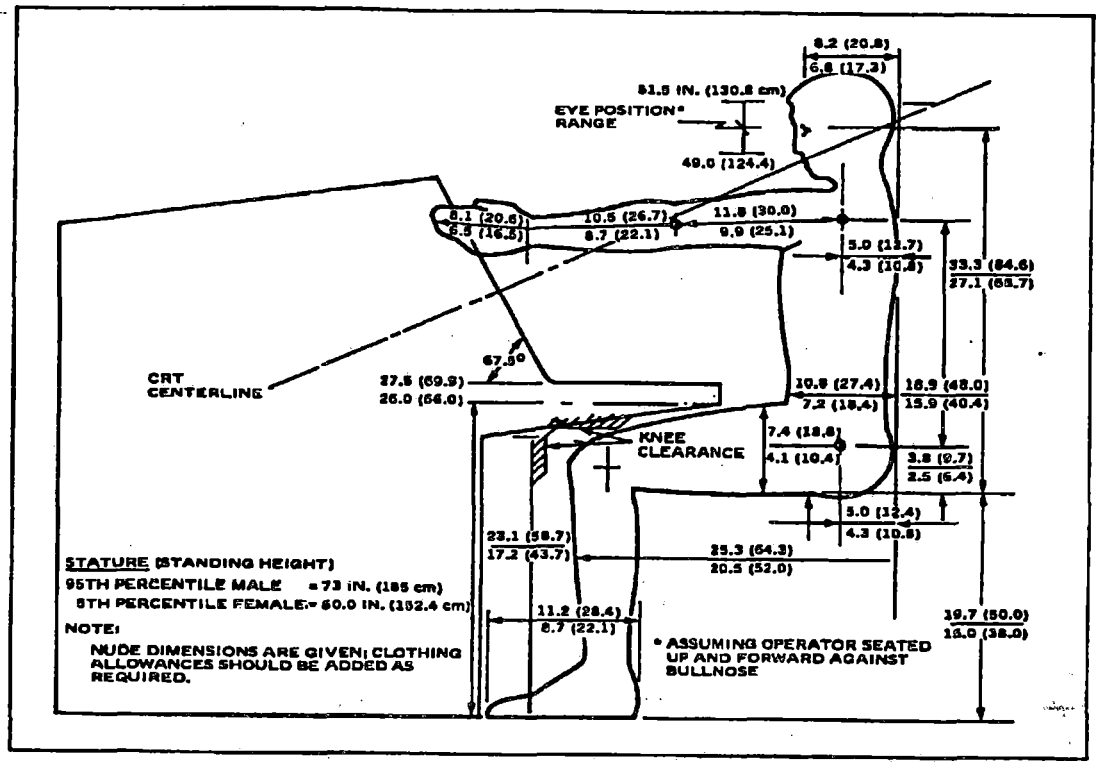

Figure C8-2 Range of critical body dimensions to be used for maglev control console design. Top numbers are body dimensions for large male operators; lower number of dimensions of small female operators. Dimensions are given as "inches" (cm).

be performing to different operating doctrines. The operator work stations incorporate design, display, and automated features which facilitate changes in configuration options, based on the standard deployment or holiday scenario, as well as the technical support requirements associated with the overall system.

The operator workstation is configured to allow ease of operator access to displays and controls, with all controls within a 36-inch reach envelope from the front edge of the bullnose. The anthropometric requirements of potential operators, ranging in stature from 5'0" to 6'1" (5th to 95th percentiles), drives the sizing of the workstation. Critical body dimensions (functional reach, eye height, etc.) that must be considered in the workstation's design is obtained from MIL-STD-1472D. The workstation design provides sufficient clearance from the bottom of the shelf to the knee of a large operator, even when seated all the way forward against the shelf. The displays are situated directly in front of the operator, with the lower display sloped back at an angle to provide optimum visual interface for the size range of the expected users (15-30 degrees downward). The

projection of the upper display's centerline is just above the eye position of the small operator when seated in an erect position. This means that in a normal working position (operator's body slumped and head slightly forward) the average operator's line of sight is nearly perpendicular to the displays for the majority of the user population. In effect, angle and location of the displays result in minimum required operator movement to achieve good viewing and less operator fatigue.

The multi-purpose operator keyboard is on the work shelf, directly below and in front of the displays. A MIL-STD-1280 QWERTY-style keyboard is recommended to facilitate rapid data input. Through the use of a combination of fixed function control and an alphanumeric keyboard, operator speed is maximized and operator error and skill requirement minimized.

Switch controls are placed alongside the displays and are compatible with, and clearly related to, their associated displays. Through the use of a track ball cursor capability, operator selection and entry control are unambiguous and allow the operator to respond quickly to the functional situation.

The display allows different formats to be shown on the screen, permitting call-up of needed information while maintaining essential data on the primary portion of the screen. Windowing capability also allows the operator to display essential data while maintaining his monitoring vigilance. The establishment of a menu directory allows quick operator access to a required display without processing through layers of menus. The user-system interface, windowing capability, and trackball, provide a rapid data exchange for the operator.

Additionally, a major focus of the design effort of the maglev user-system interface is to identify those human performance limits that could negatively impact the overall system performance. Human performance limits can be grouped into three broad areas: Sensory/perceptual, motor, and information processing. Sensory and perceptual performance limitations arise when information is presented at or near threshold levels. Environmental conditions, such as vibration and high ambient light, can also lead to perceptual limitations. Data storage and replay features in the software subsystems, will resolve much of these limitations for many of the pattern identification/classification, set-up planning and even operating doctrine control for operator tasks.

Color also provides advantages of speed and accuracy for operator task performance. For the workstation, color is used to differentiate between specific levels of capacities and conditions. If all capacities and conditions are within specified accepted range, all information will be displayed in green. If any parameter, such as the number of passengers delayed (requiring the addition of

another vehicle to a route), exceed a certain maximum, it is displayed in a different color. Several levels of criticality can be displayed in a standard color of green, yellow or red. For example, the color red can indicate equipment that is non-operational or off-line, yellow indicates equipment that has limited operational capability, and green, operational equipment.

8.2 COMMAND, CONTROL, AND COMMUNICATIONS

It is essential that control and operations personnel work in a system environment in which human factors design criteria have been applied to all user-system interfaces. Successful performance throughout the control centers is dependent upon the quality of the user-system interface. The eventual system will have a high degree of automation, sophisticated traffic management and sensor algorithms, and a variety of support software modules. Highly automated systems often are intended to reduce manual operations. In reality, such systems are able to handle more data at higher rates and place different kinds of performance demands on system operators. Instead of a great number of mechanistic manual operations, operators are faced with monitoring complex processes and the need to engage in higher order decision-making tasks.

When user-system interfaces are carelessly designed, the resulting designs have been shown to be problematic in terms of operator workload, cumbersome procedures, discomfort at the workstation, job dissatisfaction, fatigue, and the potential for design-induced error. Therefore, the general objective of the human factors program is to ensure that maglev and its control operations are totally compatible with the capabilities and limitations of the personnel who will operate and maintain the elements of the system. To that end, human factors specialists will engage in analyses, hardware and software design, as well as the test and evaluation phases of the program. Where criteria data are lacking, the human factors specialist will conduct special studies to obtain the required information.

The human factors analysis and design effort includes the workstations; integration of communication devices with other controls and displays; display formats; seating; hardware accessibility for maintenance; software functionality relative to operating procedures; job aids; training requirements; the layout of the control center considering personnel interactions, personnel flow, visibility to any group displays, emergency egress, operational modes, and its internal environmental factors such as lighting and noise control.

The primary user-system interface exists at the workstation in the centers. It is here that the software and its databases are translated into display formats with which the maglev personnel

must interact by means of a variety of potential control devices. Human factors engineering criteria will be applied to the design and/or selection of hardware and display equipment. Each workstation must be a functional integration of the individual pieces. The 5th to 95th percentile anthropometric range of the user population will be used to arrange the display monitors, keyboards (or any other data entry devices such as trackballs or touchscreens), and work surface size and height. Seating will be selected that is ergonomically sound and compatible with the controls and displays. Requirements for adjustability of workstation components will be determined. The communication gear will be integrated with the rest of the workstation rather than merely tacked on. Figure C8-3 shows alternative workstation designs that permit effective integration of equipment for control operators and C3 task performance.

The function analysis and task analysis efforts will help determine whether or not a need exists for a commonly shared group display, a large screen display (LSD). LSDs currently are used in automotive and railroad traffic management control centers. If shown to be necessary or highly desirable for task performance, a determination of its characteristics (in terms of resolution, brightness, size, location, front vs rear projection, etc.) will be made. The presence of an LSD would have significant implications for control center arrangement.

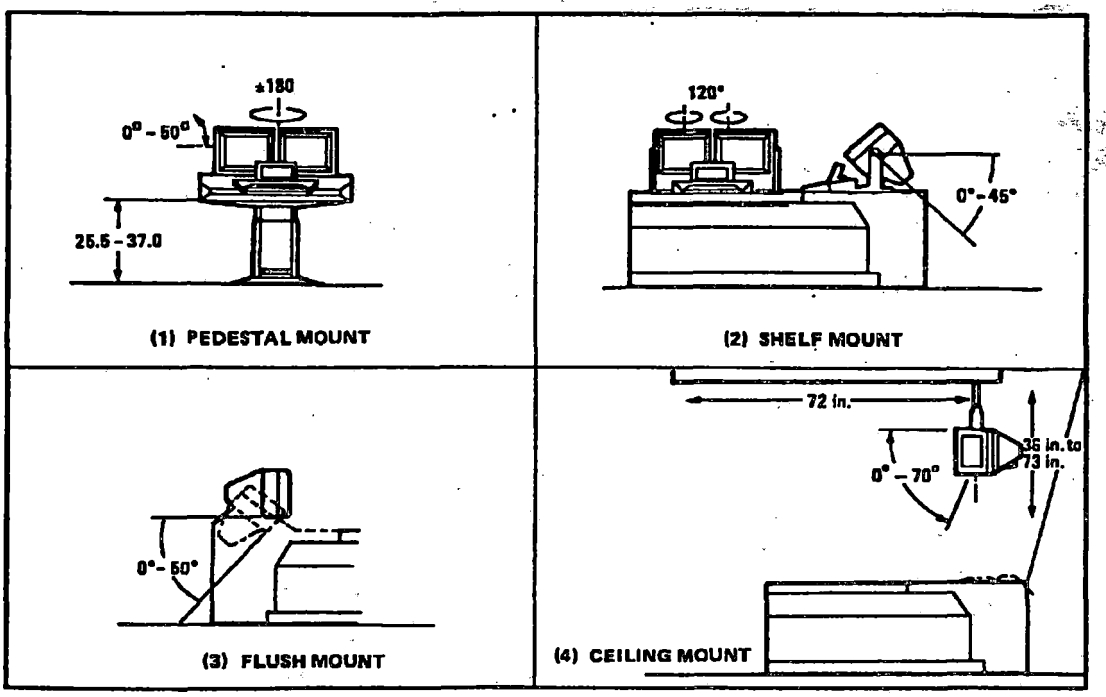

Figure C8-3 Examples of alternative maglev console mounting methods

Human factors considerations will be a key factor in determining command/control center layout/arrangement, based on the mission, function, and task analyses which evolve to an operations concept. When the concept is defined, it is then possible to arrange the major functional areas, for operations in different loading situations, routing, training, crisis management, maintenance, storage, etc. Other factors such as personnel flow, personnel interaction, maintenance access, visibility requirements, and others then dictate the detailed placement of all major and support pieces of equipment.

Human factors affecting field items such as CCTV, passenger message/routing signs, call boxes, etc., involve concern with placement, visibility, accessibility, security, labeling, and basic control/display requirements.